RESEARCH PERFORMANCE FINAL REPORT

Federal Agency and Organization Element to Which Report is Submitted	Office of Fossil Energy U.S. Department of Energy National Energy Technology Laboratory
Federal Grant or Other Identifying Number Assigned by Agency	DE-FE0027035
Project Title	Pilot-Scale Testing of an Integrated Circuit for the Extraction of Rare Earth Minerals and Elements from Coal and Coal Byproducts Using Advanced Separation Technologies
PD/PI Name, Title and Contact Information (e-mail address and phone number)	Rick Q. Honaker, Ph.D., Professor University of Kentucky 230 MMRB, 504 Rose Street Lexington, Kentucky, 40506-0107 Phone: (859) 257-1108 (Work) Phone: (859) 333-0189 (Mobile) Email: rick.honaker@uky.edu
Name of Submitting Official, Title, and Contact Information (e-mail address and phone number), if other than PD/PI	Rick Q. Honaker, Ph.D., Professor University of Kentucky 230 MMRB, 504 Rose Street Lexington, Kentucky, 40506-0107 Phone: (859) 257-1108 (Work) Phone: (859) 333-0189 (Mobile) Email: rick.honaker@uky.edu
Submission Date	6/27/2021
DUNS Number	93-901-7877
Recipient Organization (Name and Address)	University of Kentucky Research Foundation 109 Kinkead Hall 500 South Limestone Street Lexington, Kentucky, 40526-0001
Project/Grant Period (Start Date, End Date)	1/1/2016 – 3/31/2020
Reporting Period End Date	12/31/2020
Report Term or Frequency (annual, semi-annual, quarterly, other)	Final
Signature of Submitting Official (electronic signatures are acceptable)	Rick Honaker Digitally signed by Rick Honaker Date: 2021.06.27 11:13:52 -04'00'

TABLE OF CONTENTS

TABLE OF CONTENTS ii
TABLE OF FIGURES v
TABLE OF TABLES xvii
EXECUTIVE SUMMARY 21
1.0 INTRODUCTION 24
1.1 Objectives 24
1.2 Approach 24
2.0 MAJOR ACCOMPLISHMENTS 26
2.1 Pilot plant construction 26
2.2 Detailed engineering testing 27
2.2.1 Environmental Monitoring & Management 27
2.2.2 Feedstock Collection & Preparation 28
2.2.3 Exploratory Testing 28
2.2.4 Test Plan Revision 31
2.2.5 Detailed Parametric Testing 32
2.2.6 Optimization & Validation 33
2.2.7 Provide Split Samples 34
2.2.8 Secondary Feedstock Testing 34
2.2.9 Modeling & Simulation 35
2.2.10 Technical & Economic Analyses 35
3.0 RESULTS AND DISCUSSION 36
3.1 Project Management & Planning (PB2& PB3) 36
3.2 Pilot plant construction (PB2) 37
3.2.1 Host Site Agreements 37
3.2.2 Detailed Systems Engineering 37
3.2.3 Environmental Controls Assessment 52
3.2.4 Site Rehabilitation 55
3.2.5 Bidding & Procurement 59
3.2.6 Fabrication & Construction 62
3.2.7 Installation & Assembly 63
3.2.8 Systems Safety Analysis & Training 70
3.2.9 Startup & Shakedown 70
3.3 Environmental Monitoring & Management (PB3-Task2) 70
3.3.1 Materials and Sample Preparation 70
3.3.2 Experimental and Results 71
3.3.3 Conceptual Process Flowsheet Development 133
3.4 Feedstock Collection & Preparation (PB3-Task3) 135
3.4.1 West Kentucky No. 13 Source 135
3.4.2 Fire Clay Source 137

3.5 Exploratory Testing (PB3-Task4) 138
3.5.1 X-ray Sorter 138
3.5.2 Roasting and pretreatment 148
3.5.3 Pilot Scale Leaching Circuit 157
3.5.4 Solvent extraction feed reduction 161
3.5.5 Pilot scale continuous leaching and SX circuit testing 164
3.5.6 Pilot Scale Solvent Extraction Circuit 175
3.5.7 Selective precipitation 185
3.5.8 Pilot Scale Leaching and Multi-stage Precipitation Circuit Testing 194
3.5.9 Rare earth mineral concentration (HHS) 211
3.6 Test Plan Revision (PB3-Task5) 233
3.6.1 Hydrometallurgical circuit 233
3.6.2 Mobile HSS Unit 234
3.7 Detailed Parametric Testing (PB3-Task6) 234
3.7.1 West Kentucky No. 13 Source 234
3.7.2 Fire Clay Source Parametric Testing 274
3.8 Optimization & Validation (PB3-Task7) 289
3.8.1 Modelling and optimization 290
3.8.2 Validation Tests 296
3.8.3 Chemical cost analysis and validation 307
3.9 Provide Split Samples (PB3-Task8) 308
3.10 Secondary Feedstock Testing (PB3-Task9) 311
3.10.1 Heap leach REE extraction 311
3.10.2 Will Scarlet Acid Mine Drainage 321
3.10.3 West Kentucky No. 13 Acid mine drainage 330
3.11 Analytical Lab Construction & Operation (PB3-Task10) 342
3.12 Modeling & Simulation (PB3-Task11) 343
3.13 Sample Analyses (PB3-Task12) 355
3.13.1 Solid sample analysis 356
3.13.2 Liquid sample analysis 356
3.13.3 Process mass balancing 357
3.14 Technical & Economic Analyses (PB3-Task13) 362
3.14.1 Approach and Task Objectives 362
3.14.2 Global Economic Assumptions 363
3.14.3 Scale-Up and Cost Estimation Procedures 364
3.14.4 Process Descriptions 368
3.14.5 Scenario Matrix and Descriptions 372
3.14.6 Results and Discussion 376
3.14.7 Conclusions and Recommendations 405
3.15 Commercialization Analyses (PB3-Task14) 406

3.15.1 Market Assessment 406
3.15.2 PESTLE analysis 407
3.15.3 Technology Readiness Level Assessment 407
3.16 Decommissioning & Disposition (PB3-Task15) 409
4.0 PRODUCTS 410
4.1 Journal Articles 410
4.2 Peer-Reviewed Conference Articles 412
4.3 Non-Reviewed Conference Articles 412
4.4 Abstract & Conference Presentation 413
4.5 Other Publication Products 415
4.6 Patents & Patent Applications 415
5.0 PARTICIPANTS & COLLABORATING ORGANIZATIONS 415
6.0 CHANGES/PROBLEMS 416
APPENDIX A - PROJECT MANAGEMENT PLAN 424
APPENDIX B - HEALTH, SAFETY & ENVIRONMENTAL PLAN 444
APPENDIX C- SYSTEM TESTING, OPERATION & SAMPLING/ANALYSIS PLAN 451
APPENDIX D – Environmental monitoring and management supplementary data 468
APPENDIX E: WKY No. 13 Core Hole Analysis Results 485

TABLE OF FIGURES

Figure 3.2.1 Generalized flow diagram for the rare earth element production system. 38
Figure 3.2.2 Scaled layout schematic for Process Train 1.00 – Preconcentration, which incorporates mobile unit operations for sizing, sorting and on-site materials handling. (a - top) Operational configuration at mine site. (b - bottom) Transportation configuration during transportation..... 40
Figure 3.2.3. Photograph of the completed Process Train 1.0 – Preconcentration. 40
Figure 3.2.4 Scaled layout schematic for Process Train 2.00 – Size Reduction & Liberation, which incorporates unit operations for crushing, grinding and micronizing of solid feedstocks. 41
Figure 3.2.5 Scaled layout schematic for Process Train 3.00 – Physical Separation, which incorporates unit operations for feedstock decarbonization, dealkalinization and dewatering. 42
Figure 3.2.6 Scaled layout schematic for Process Train 4.00 – Acid Leaching, which incorporates unit operations for multi-stage solids digestion and thickening. 43
Figure 3.2.7 Updated/revised process flowsheet utilized within Process Train 4.00 – Acid Leaching. 43
Figure 3.2.8 Generalized 3D layout of Process Train 4.00 – Acid Leaching. 44
Figure 3.2.9 Scaled layout schematics for Process Train 5.00 – Solvent Extraction & Precipitation, which incorporate mixer/settler tanks for solvent extraction (a – front view, b – back view). 45
Figure 3.2.10 Generalized 3D layout of Process Train 5.00 – Solvent Extraction & Precipitation..... 46
Figure 3.2.11. Pilot plant flowsheet being used for construction purposes. 48
Figure 3.2.12. Proposed pilot plant SX flowsheet for construction 50
Figure 3.2.13. Proposed REE precipitation and recovery step. 50
Figure 3.2.14. Concept P&ID leach circuit drawing (provided by SX Kinetics). 51
Figure 3.2.15 Solvent extraction system as shown in Figure 15 with ventilation system highlighted. 52
Figure 3.2.16 Leaching circuit showing tanks which will be ventilated. 53
Figure 3.2.17 Hydrometallurgy flowsheet showing sumps. 53
Figure 3.2.18 Proposed banking with sump layout. 54
Figure 3.2.19. Floor plan for the REE extraction facility at the Dotiki Portal No. 1 mine site. 56
Figure 3.2.20 Exterior photograph of the REE pilot plant building. 56
Figure 3.2.21 Interior wide-angle photograph of the two-story high-bay area prior to process train installation (Note: Solvent extraction train already sit in place). 57
Figure 3.2.22 Photograph of upgrades to the facility electrical services. 57
Figure 3.2.23 Installation of spill containment beams within the test facility. 58
Figure 3.2.24 Installation of pump-away containment tanks/beams/liners outside the test facility for water management and disposal. 58
Figure 3.2.25 Photograph of Process Train 2.00 – Size Reduction & Liberation as installed at the Dotiki pilot plant test site in western Kentucky. The train includes (left to right) jaw crusher module, cone crusher module, primary ball mill/sieve screen, and micronizer. 64
Figure 3.2.26 Photograph of Process Train 3.00 – Physical Separation as installed at the Dotiki pilot plant test site in western Kentucky. The train includes (left to right) decarbonization flotation column, coal product disc filter, decarbonization thickener, dealkalinization flotation column, dealkalinization thickener, and filter press. 64
Figure 3.2.27 Photograph of Process Train 4.00 – Acid Leaching as installed at the Dotiki pilot plant test site in western Kentucky. The train includes primary leach tanks and thickener (rear) and secondary leach tanks and thickener (front). 65
Figure 3.2.28 Photograph of Process Train 5.00 – Solvent Extraction & Precipitation as installed at the Dotiki pilot plant test site in western Kentucky. The train includes eight individual mixer-settler tanks along the length of the processing unit. 65
Figure 3.2.29. Equipment from older proof of concept HHS process. 66

Figure 3.2.30. Mobile HHS process under construction. 66
Figure 3.2.31. Construction of the building that is housing the non-explosion proof equipment. 67
Figure 3.2.32. Fire-resistant wall design 68
Figure 3.2.33. Feed side of the HHS process 69
Figure 3.2.34. Product side of HHS Process 69
Figure 3.3.1 Pictures illustrating the experimental procedures of selective precipitation tests. (A) pH measurement, (B) Settling after precipitation. 72
Figure 3.3.2 Experimental flowsheet followed during selective precipitation tests. 73
Figure 3.3.3 Cumulative precipitation of total rare earths, thorium, and uranium 73
Figure 3.3.4 Cumulative precipitation of total, heavy, light, critical, and uncritical rare earths at various pH values. 74
Figure 3.3.5 Experimental flowsheet followed during exploratory solvent extraction tests. 76
Figure 3.3.6 Separation between aqueous and organic phases during solvent extraction tests. 76
Figure 3.3.7 Recovery of total rare earths, thorium, and uranium into the REE product stream of both the one-stage and two-stage solvent extraction process. 78
Figure 3.3.8 Recovery of individual rare earth, thorium, and uranium into the REE product stream of both the one-stage and two-stage solvent extraction process. 78
Figure 3.3.9 Recovery of the total, heavy, light, critical, and uncritical REEs from both the one-stage and two-stage solvent extraction process. 79
Figure 3.3.10 A modified experimental protocol developed for enhanced separation of thorium, uranium, and rare earth elements. 82
Figure 3.3.11 Precipitation of total REEs, Th, U, and major metals at the pH value of 4.85. Error bars represent one standard deviation of three replicate tests. 83
Figure 3.3.12 Precipitation of total, heavy, light, critical, and uncritical rare earths at the pH value of 4.85. Error bars represent one standard deviation of three replicate tests. 84
Figure 3.3.13 XRD pattern of the solids samples obtained from selective precipitation tests at a pH value of 4.85. 85
Figure 3.3.14 Elemental identification of the solids samples obtained from selective precipitation at a pH of 4.85 using SEM-EDX analysis. 86
Figure 3.3.15 SEM images of precipitated solids (at a pH of 4.85) observed under various magnifications. 86
Figure 3.3.16 Species distribution diagram of Th-HCl system. 87
Figure 3.3.17 Species distribution diagram of U-HCl system. 88
Figure 3.3.18 Eh-pH diagram of Th-Cl-Na-Ca-H_2O system. 89
Figure 3.3.19 Eh-pH diagram of U-Cl-Na-Ca-H_2O system 90
Figure 3.3.20 Species distribution diagrams of REEs-HCl system. A) Cerium, B) Neodymium, C) Gadolinium, D) Lanthanum, E) Yttrium 92
Figure 3.3.21 Species distribution diagram of Fe-HCl system. 93
Figure 3.3.22 Species distribution diagram of Al-HCl system. 93
Figure 3.3.23 Experimental designs for uranium separation using TBP as the extractant: (A) DI water as the strippant; (B) H_2SO_4 as the strippant. 95
Figure 3.3.24 Experimental procedure and the operating conditions followed the first subset of solvent extraction tests. 97
Figure 3.3.25 Recovery of total rare earths and uranium into the final REE product stream based solely on solvent extraction circuit. Error bars represent one standard deviation of three replicate tests. 98
Figure 3.3.26 Overall recovery of total rare earths and uranium with respect to the overall experimental flowsheet. Error bars represent one standard deviation of three replicate tests. 99

Figure 3.3.27 3D surface response graphs and 2D contour plots obtained from the statistical analysis using Design-Expert. 101
Figure 3.3.28 Experimental procedure and the operating conditions followed the second subset of solvent extraction tests. 102
Figure 3.3.29 Recovery of total rare earth elements and uranium into the final rare earth product stream based solely on the solvent extraction circuit. Error bars represent one standard deviation of three replicate tests. 103
Figure 3.3.30 Overall recovery of total rare earth elements and uranium with respect to the whole experimental flowsheet. Error bars represent one standard deviation of three replicate tests. 104
Figure 3.3.31 Distribution ratio of total rare earth elements in the two extraction stages. Error bars represent one standard deviation of three replicate tests. 106
Figure 3.3.32 Distribution ratio of uranium in the two extraction stages. Error bars represent one standard deviation of three replicate tests. 106
Figure 3.3.33 Separation factor between total rare earth elements and uranium. Error bars represent one standard deviation of three replicate tests. 107
Figure 3.3.34 3D surface response graphs obtained for the statistical model predicting uranium recovery. 110
Figure 3.3.35 Experimental flowsheet followed for rare earth oxalate sample. 112
Figure 3.3.36 Precipitation of total rare earth elements and thorium at various pH values. Error bars represent one standard deviation. 113
Figure 3.3.37 The SEM image of the rare earth oxide feed sample. 113
Figure 3.3.38 The SEM image of precipitated solids at pH 4.6. 114
Figure 3.3.39 Particle size distribution of three zeolite samples. (A) Coarsest sample, P_{80}=1490 µm, (B) Middle-sized sample, P_{80}=200 µm, (C) Finest sample, P_{80}=12 µm. 117
Figure 3.3.40 X-ray diffraction pattern of the initial zeolite samples. 118
Figure 3.3.41 Elemental identification of the zeolite samples obtained from the ED 119
Figure 3.3.42 SEM images of the zeolite samples under various magnification. (A) the coarsest sample, (B) medium size sample, (C) the finest sample. 120
Figure 3.3.43 The Brunauer–Emmett–Teller (BET) Nitrogen adsorption isotherm of middle-sized zeolite sample 121
Figure 3.3.44 Classification of (A) physisorption isotherms, (B) classification of hysteresis (Thommes et al., 2015) 122
Figure 3.3.45 Pore size distribution of the middle-sized zeolite sample 122
Figure 3.3.46 Adsorption recoveries into the solid phase. (A) total rare earths, (B) thorium, (C) uranium. Error bars represent one standard deviation of multiple replicate test. 123
Figure 3.3.47 SEM image showing the fractures and cracks formed after adsorption. 125
Figure 3.3.48 Diagnostic plots obtained based on the statistical model developed for the adsorption recovery of rare earths. 127
Figure 3.3.49 XRD pattern of the solid samples generated with Test 11. 128
Figure 3.3.50 SEM images of the solid samples generated after adsorption. Bright areas highlighted in the red boxes indicating the deposition of heavy elements. 129
Figure 3.3.51 EDX pattern of the solid sample generated after Test 11. (A) Full EDX pattern indicating high-intensity elements. (B) Close-up view showing the detection of rare earth elements and thorium. 129
Figure 3.3.52 Adsorption recoveries of total rare earth elements, thorium, and uranium as a function of contact time. Error bars represent one standard deviation of multiple replicate tests. 131

Figure 3.3.53 Distribution coefficient values of (A) total rare earth elements and (B) thorium as a function of contact time. Error bars represent one standard deviation of multiple replicate tests. 131
Figure 3.3.54 Freundlich adsorption isotherms of the elements onto zeolite. (A) total rare earths (B) thorium..... 132
Figure 3.3.55 D-R adsorption isotherms of the elements onto zeolite. (A) total rare earths (B) thorium. 133
Figure 3.3.56 Conceptual flowsheet designed for the removal of thorium and uranium from rare earth elements. 135
Figure 3.4.1. Rare earth element distribution in the high ash content segments along the portion of the vertical profile of a drill cores intersecting the West Kentucky No. 13 coal seam..... 137
Figure 3.5.1. REE and thorium concentrations in feed, concentrate and tail samples obtained from the x-ray sorter when processing Dotiki coarse reject material. 140
Figure 3.5.2 X-ray scans of eject and pass through material from x-ray sorter. 140
Figure 3.5.3. Calibration of sorter cut point used for parametric study. 141
Figure 3.5.4. Ash content of Feed, pass through and eject streams at Rougher stage. 142
Figure 3.5.5. REE analysis of Rougher eject and pass through samples. 143
Figure 3.5.6. Leaching characterization of the density fractionated sorter product and tailing material within size range of 1x0.05 inch. (Leaching condition: 1.2M sulfuric acid, 10 g/L solid concentration, 75 °C. Particle size: 80 mesh) 146
Figure 3.5.7. Sorter Eject 2.0 Float (80 mesh, Muffle Furnace Roast at 600C 2 hour) 146
Figure 3.5.8. Sorter Eject 2.0 Sink (80 mesh, Muffle Furnace Roast at 600C 2 hour) 147
Figure 3.5.9. Sorter Pass 2.0 Float (80 mesh, Muffle Furnace Roast at 600C 2 hour) 147
Figure 3.5.10. Sorter Pass 2.0 Sink (80 mesh, Muffle Furnace Roast at 600C 2 hour) 148
Figure 3.5.11. Roaster setup at the pilot plant including feeder system (left), controlling system (middle), and dust collection system (right). 149
Figure 3.5.12. Rare earth concentration on whole basis before and after roasting. 150
Figure 3.5.13. Leaching recovery improvement before and after roasting. (1M H_2SO_4, S/L=1/5, room temperature, retention =15 min) 151
Figure 3.5.14. Individual REE concentration on whole mass basis in the roasted feed material. 152
Figure 3.5.15. XRD analysis of the fire clay feed material before (top) and after (bottom) roasting at 600 C for 2 hours using a blast furnace. (I-illite, M-muscovite, K-kaolinite, Q-quartz, P-pyrite.) 152
Figure 3.5.16. Correlation between set point temperature and measured inner tube heat zone temperature. 153
Figure 3.5.17. Effect of roasting temperature on leaching performance of different elements. (Leaching condition: 1M sulfuric acid, S/L=200 g/L, room temperature, 15 minutes)..... 155
Figure 3.5.18. Effect of roasting time on leaching performance of TREE. (Leaching condition: 1M sulfuric acid, S/L=200 g/L, room temperature, 15 minutes) 156
Figure 3.5.19. Schematic of the roaster heat zone and discharge overflow weir. 156
Figure 3.5.20. Schematics of the entire circuit and the locations of the sampling points. 157
Figure 3.5.21. The change of pH during leaching under different initial acid concentrations..... 159
Figure 3.5.22. Individual element recovery at different acid concentration level after 2 hours of leaching. (Temperature = 75 °C, solid concentration = 100g/L)..... 160
Figure 3.5.23. Leaching recovery of (a) TREEs, (b) Al, (c) Ca, and (d) Fe using 0.1M, 0.5M, and 1.2M sulfuric acid leaching in batch and continuous mode. 161
Figure 3.5.24. Effect of Ascorbic Acid addition on the pH and ORP of Dotiki mine water 162
Figure 3.5.25. The visual change of the mine water as incremental amount of ascorbic acid was added.163
Figure 3.5.26. Extraction curves for REE and contaminant elements from exploratory shakeout tests performed on Dotiki mine water..... 163

Figure 3.5.27. Results of TREE concentration in tank 6 and tank 7 with time. 166
Figure 3.5.28. Theoretical solid concentration in tank 6. (Starting with 100-gallon liquid, continuously feeding in 50 lbs. per hour of solid and 1 gallon per minute of liquid). 166
Figure 3.5.29. Solid feeder calibration (left) and sulfuric acid feeder calibration (right). 168
Figure 3.5.30. Leach tank overflow solid concentration monitoring in the continuous operation. 170
Figure 3.5.31. Leaching recovery of total rare earth elements in the continuous operation. 170
Figure 3.5.32. Leaching recovery of individual rare earth elements in the continuous operation. 171
Figure 3.5.33. Leaching recovery of Al in the continuous operation. 171
Figure 3.5.34. Leaching recovery of Ca in the continuous operation. 171
Figure 3.5.35. Leaching recovery of Fe in the continuous operation. 172
Figure 3.5.36. Baseline evaluation for acid and base cost to adjust the pH of water to 1, 2, and 3, and neutralize to 8. 173
Figure 3.5.37. pH comparison between pH maintained at 2 (DTKCR-B5) and pH free drifted (DTKCR-B3) test with initial acid concentration of 0.01M. 174
Figure 3.5.38. TREE recovery comparison between pH maintained at 2 (DTKCR-B5) and pH free drifted (DTKCR-B3) test with initial acid concentration of 0.01M. 174
Figure 3.5.39. Individual RE recovery comparison between pH maintained at 2 (DTKCR-B5) and pH free drifted (DTKCR-B3) test with initial acid concentration of 0.01M. 175
Figure 3.5.40. Accumulative acid consumption to maintain a pH of 2 for test DTKCR-B5. 175
Figure 3.5.41. SE Rougher Circuit Flowsheet. 177
Figure 3.5.42. Parameters tested during scoping study. 178
Figure 3.5.43. Typical Feed and Raffinate Concentration. 179
Figure 3.5.44. Result of scoping study. 179
Figure 3.5.45. Percent extraction of individual REEs at DEHPA dosage of 25%. 180
Figure 3.5.46. TREE in Raffinate. 181
Figure 3.5.47. TREE in Feed. 181
Figure 3.5.48. TREE in Strip Bleed. 182
Figure 3.5.49. Loading Rate. 182
Figure 3.5.50. Contaminants Concentration in Feed (ppm). 183
Figure 3.5.51. Contaminants Concentration in Raffinate (ppm). 184
Figure 3.5.52. Experimental apparatus used for the precipitation tests. 185
Figure 3.5.53. Sum of operational and capital costs of using the current solvent extraction system to produce a rare earth product as a function of total REE concentration in the leachate. 187
Figure 3.5.54. Recovery of total REEs, Fe, Al and some individual REEs to the precipitate as a function of solution pH. 187
Figure 3.5.55. Pictures of the original filtrate (left) and the filtrate with some hydrogen peroxide added (right). 188
Figure 3.5.56. Sodium hydroxide costs to produce 1 kilogram of rare earth oxide by increasing the solution pH to different values. 188
Figure 3.5.57. A comparison of the laboratory test results and the results obtained using a 100-gallon tank with a mixing speed of 37 Hz. 190
Figure 3.5.58. A comparison of the laboratory test results and the results obtained using a 100-gallon tank with a mixing speed of 10 Hz. 191
Figure 3.5.59. A comparison of the laboratory test results and the results obtained using a 100-gallon tank with a mixing speed of 20 Hz. 191
Figure 3.5.61. Re-dissolution of the precipitate in 50 ml digestion tubes. 192

Figure 3.5.62. Concentrations of major elements (Al and Ca) in leachate obtained by leaching perlite under different solution pH values. 194
Figure 3.5.63. Effect of acid concentration on TREE leaching recovery at 75°C (bench scale). 195
Figure 3.5.64. Leaching recovery of TREE and individual elements in leaching stage using 0.05M sulfuric acid at 75 °C with solid/liquid ratio of 1/10 (w/v) (pilot scale). (Retention time 2 hours) 196
Figure 3.5.65. Precipitation efficiency of TREEs and major contaminants in the leachate solution using 1M NaOH (bench scale). 197
Figure 3.5.66. REEs and major contaminant precipitation efficiency values at pH 6.5. The values represent average values obtained for samples collected every two hours of a 20 hour operating period in the pilot plant. 197
Figure 3.5.67 Sequential precipitation characteristics of REEs, Al, and Fe in the re-dissolved solution. 198
Figure 3.5.68. Precipitation characteristics of REEs, Al, and Fe from the re-dissolved solution when using sodium phosphate as the precipitant. 199
Figure 3.5.69. Redissolution efficiency of REEs, Al, Ca and Fe at various pH (bench scale test). 200
Figure 3.5.70. Redissolution efficiency of rare earth elements and major contaminants from the pilot-plant circuit using a solution pH value of 2.5 201
Figure 3.5.71. Effect of oxalic acid dosage in rare earth oxalate precipitation. (Retention time = 20minutes, Reaction pH =2.5) 203
Figure 3.5.72. Effect of pH on rare earth and contaminate ion oxalate precipitation (Retention time = 20minutes, oxalic acid dosage = 12.8 g/L). 203
Figure 3.5.73. Oxalic precipitation efficiency of individual rare earth elements and contaminant ions (Oxalic acid dosage 12.8g/L at pH 2.5 regulated using 4M NaOH, pilot scale). 204
Figure 3.5.74. Flowsheet of REO production from the Dotiki coarse refuse material (Test C2). 206
Figure 3.5.75 The relative concentration of the contaminants in the wash solution at different acid and solid concentrations. 208
Figure 3.5.76 Rejection of different metals for different solids concentration using a range of acid concentrations. 209
Figure 3.5.77 Elemental composition of the wash liquid at 20 g/L solids concentration using 0.5 M HCl solution 210
Figure 3.5.78. Large agglomerates 211
Figure 3.5.79. New flotation launder design 213
Figure 3.5.80. HHS Trailer was set up in the storage shed at Virginia Tech facilities (b) 214
Figure 3.5.81. Exhaust fan installed on the side of the shed. 215
Figure 3.5.82. Heating ductwork was installed from the main building into the shed. The open side of the shed was covered with a clear plastic tarp for heat insulation. 215
Figure 3.5.83 Recovery of combustible matter to the clean product and REEs to the REE product (high-ash tails). 218
Figure 3.5.84 Ash contents of the clean product and REE product (high-ash tails). 218
Figure 3.5.85 Element concentration versus ash content for selected elements. 219
Figure 3.5.86. Element concentration versus ash content for selected elements. 220
Figure 3.5.87. Element concentration versus ash content for selected elements. 221
Figure 3.5.88. Element-by-element recoveries achieved during decarbonization testing. 222
Figure 3.5.89. Experimental Apparatus used in laboratory-scale HHS testing. 223
Figure 3.5.90. HHS flowsheet used for laboratory-scale testing. 223
Figure 3.5.91. Effect of grind size on REE recovery and grade in laboratory-scale HHS process. 224
Figure 3.5.92. Effective of sodium metallicate dosage on REE recovery and grade in laboratory-scale HHS process. 224

Figure 3.5.93. Effect of sorbitan monooleate (SMO) dosage on recovery and grade in laboratory-scale HHS process. 225
Figure 3.5.94. Effect of sample aging on recovery and grade of laboratory-scale HHS process. 225
Figure 3.5.95. Comparison between column flotation, conventional flotation, and the HHS process on REE recovery. 225
Figure 3.5.96. Summary of all laboratory-scale HHS trials 226
Figure 3.5.97. SEM micrograph of high grade REM product from HHS concentration tests. Lighter areas are indicative of higher atomic numbers 227
Figure 3.5.98. SEM micrograph and corresponding EDX spectra for high grade REM product from HHS concentration tests. 227
Figure 3.5.99. TEM and diffraction analysis for high grade REM product from HHS concentration tests. 228
Figure 3.5.100. HHS flowsheet for the recovery of REMs 230
Figure 3.5.101. Flowsheet of the HHS batch scale process 232
Figure 3.7.1. Effect of acid dosage on TREE recovery. 236
Figure 3.7.2. Effect of leaching acid dosages on NaOH consumption during RE precipitation. 236
Figure 3.7.3. Effect of leaching acid dosages on HCl consumption during RE redissolution. 237
Figure 3.7.4. Effect of acid concentration on major REE and contaminants leaching recovery. 238
Figure 3.7.5. Effect of solid concentration on major REE and contaminants leaching recovery. 238
Figure 3.7.6. Effect of acid dosage in terms of kg acid/ton feed a) 45.42 kg acid/ton of feed; b) 22.71 kg acid/ton of feed. 239
Figure 3.7.7. Precipitation efficiency of RE, major contaminants, and some critical elements at pH 6.5 using NaOH. 240
Figure 3.7.8. Redissolution efficiency of RE, major contaminants, and some critical elements at pH 2.5 using HCl. 241
Figure 3.7.9. Effect of solid concentration in initial leaching process on RE redissolution efficiency. 241
Figure 3.7.10: Schematic of Oxalic precipitation circuit 243
Figure 3.7.11: Concentration of individual REE in C4 and C5 244
Figure 3.7.12: Concentration of major contaminants 244
Figure 3.7.13: Recovery of REE and Contaminants from C4 245
Figure 3.7.14: Recovery of REE and Contaminants from C5 245
Figure 3.7.15: Press and frame filter 246
Figure 3.7.16: Recovery of TREE and Contaminants from C6 248
Figure 3.7.17: Recovery of TREE and Contaminants from C7-Split-1 248
Figure 3.7.18: Recovery of TREE and Contaminants from C7-Split-2 249
Figure 3.7.19: Recovery of TREE and Contaminants from C8 249
Figure 3.7.20. La species distribution in solution at equilibrium and La oxalate precipitation efficiency at a) 1 ppm La; b) 10 ppm La; c) 100 ppm La; d) 1000 ppm La with 0.01 M oxalate 25 °C simulated using Visual MINTEQ software. (The $La(C_2O_4)_3^{3-}$ and $LaOH^{2+}$ species are calculated to be less than 0.1% in these four systems, therefore not included in the plots.) 251
Figure 3.7.21. Fe species distribution in the precipitation system at equilibrium with 0.035M $C_2O_4^{2-}$, 0.1M Cl^-, 150 ppm Fe^{3+}, 60 ppm Al^{3+}, 130 ppm Ca^{2+}, and 35 La^{3+} at 25 °C simulated using Visual MINTEQ software. (Species less than 0.01% were included in the calculation but not plotted) 252
Figure 3.7.22. Effect of Fe concentration on La oxalate precipitation pH and efficiency. (0.035M $C_2O_4^{2-}$, 0.1M Cl^-, 60 ppm Al^{3+}, 130 ppm Ca^{2+}, and 35 La^{3+} at 25 °C calculated using Visual MINTEQ software). 254

Figure 3.7.23. Effect of Fe concentration on La oxalate precipitation pH and efficiency. (0.035M $C_2O_4^{2-}$, 0.1M Cl^-, 150 ppm Fe^{3+}, 60 ppm Al^{3+}, 130 ppm Ca^{2+}, and 35 La^{3+} at 25 °C simulated using Visual MINTEQ software.) 254
Figure 3.7.24. Comparison of Al, Ca and Fe to TREE ratio in the acid leaching RE pregnant leachate solution with and without prewash. 257
Figure 3.7.25. Precipitation behavior of RE and major contaminants in PLS solution by increasing pH. (DTK-C4) 258
Figure 3.7.26 Precipitation behavior of RE and major contaminants in PLS solution by increasing pH. (DTK-C11) 258
Figure 3.7.27. Precipitation behavior of element of interest at pH 4.5 in the continuous pilot plant operation. 259
Figure 3.7.28. Schematic flowsheet of leachate recirculation to optimize leaching circuit. 260
Figure 3.7.29. Concentration of TREE in leaching (L1), acid preparation (AP1), and recirculation tank (RC1). 262
Figure 3.7.30. Concentration of TREE and major impurities in the leaching tank (L1). 262
Figure 3.7.31 Comparison of leaching performance before (hour 4) and after (hour 16) leachate recirculation. 264
Figure 3.7.32. Precipitation efficiency of RE and major contaminants in PLS solution with increasing pH (DTK-C13). 264
Figure 3.7.33 Al precipitation (PT0) efficiency of major RE and elements of interest (pilot scale, feed rate 1 GPM, pH 4.5 automatically adjusted using 2M NaOH). 265
Figure 3.7.34. RE precipitation (PT1) efficiency of major RE and elements of interest (pilot scale, feed rate 1 GPM, pH 6.5 automatically adjusted using 2M NaOH). 265
Figure 3.7.35. Redissolution (L2) efficiency of major RE and elements of interest (pilot scale, 200 Gallons, HCl 9ml/L, pH 2.5). 266
Figure 3.7.36. Oxalate precipitation (OXP) efficiency of major RE and elements of interest (pilot scale, feed rate 2 GPM, oxalic acid 6.4 g/L, pH 1.5, 20 min retention time). 266
Figure 3.7.37. DTK-C13 RE production flowsheet. 267
Figure 3.7.38. The bi-hourly leaching recovery of REEs, CMs and major elements of interest. (pilot scale continuous operation, 50lb/hr feed, 50kg/ton sulfuric acid, 50% leachate recirculation.) 269
Figure 3.7.39. Recorded pH of three PLS streams in leaching circuit. 269
Figure 3.7.40 . Precipitation efficiency curve of the DTK-C14 PLS. 270
Figure 3.7.41. Recorded pH of Al precipitation and RE precipitation operation. 270
Figure 3.7.42. Precipitation efficiency of REEs and elements of interest. (DTK-C14-PT0 Al precipitation at pH 4.2, residence time 1 hour.)) 271
Figure 3.7.43. Precipitation efficiency of REEs and elements of interest. (DTK-C14-PT1 RE precipitation at pH 6.5, residence time 2 hour.) 271
Figure 3.7.44. Redissolution curve of TREE and element of interests. (DTK-C14) 273
Figure 3.7.45. Redissolution efficiency of REEs and elements of interest. (DTK-C14-L2, pH2.0, HCl dosage 6.9 ml of 36% pure HCl per Liter of blended slurry.) 273
Figure 3.7.46. Oxalate precipitation recovery of REEs and elements of interest. (DTK-C14-OXP, pH 1.5 automatic control, oxalic acid dosage = 6.4 g/L of feed, oxalic acid fed in as 80g/L concentration solution.) 274
Figure 3.7.47. RE concentration on whole mass basis in the roasted fire clay material that feed into the hydrometallurgical circuit. 275
Figure 3.7.48. Schematic of flowsheet used in Fire Clay parametric testing. 277

Figure 3.7.49. PLS Concentration at 0.1M acid leaching. Left: Concentration of TREE in leaching (L1), acid preparation (AP1), and recirculation tank (RC1). Right: Concentration of major impurities in the leaching tank (L1). 280
Figure 3.7.50. PLS Concentration at 0.5M acid leaching. Leaching Left: Concentration of TREE in leaching (L1), acid preparation (AP1), and recirculation tank (RC1). Right: Concentration of major impurities in the leaching tank (L1). 281
Figure 3.7.51. PLS Concentration at 0.05M acid leaching. Left: Concentration of TREE in leaching (L1), acid preparation (AP1), and recirculation tank (RC1). Right: Concentration of major impurities in the leaching tank (L1). 281
Figure 3.7.52. Leaching recovery of RE and other elements of interest at the end of continuous run in pilot scale operation (FC-C4: 0.1M, FC-C5: 0.5M, FC-C6: 0.05M Sulfuric acid, 75 ºC). 282
Figure 3.7.53. Precipitation efficiency of RE and major contaminants in PLS solution with increasing pH (FC-C4). 283
Figure 3.7.54. Precipitation efficiency of RE and major contaminants in PLS solution with increasing pH (FC-C5). 283
Figure 3.7.55. Precipitation efficiency of RE and major contaminants in PLS solution with increasing pH (FC-C6). 284
Figure 3.7.56. Al precipitation (PT0) efficiency of major RE and elements of interest (pilot scale, feed rate 2 GPM, 1 h retention time, pH 4.5 automatically adjusted using 2M NaOH). 284
Figure 3.7.57. Redissolution efficiency of RE and major contaminants from PT1 cake using 36% HCl (FC-C4). 285
Figure 3.7.58. Redissolution efficiency of RE and major contaminants from PT1 cake using 36% HCl (FC-C5). 286
Figure 3.7.59. Redissolution efficiency of RE and major contaminants from PT1 cake using 36% HCl (FC-C6). 286
Figure 3.7.60. Dosage of HCl used to adjust the pH in RE redissolution stage. 287
Figure 3.7.61. RE redissolution (L2) efficiency of major RE and elements of interest (pilot scale, pH adjusted using HCl, C4-200 gallon, C5-200 gallon, C6-100 gallon). 287
Figure 3.7.62. Oxalic precipitation efficiency (OXP) of major RE and elements of interest (pilot scale, feed rate 1 gpm, pH 1.5, Oxalic Dosage: 6.4g/L for FC-C6 and FC-C4, 12.8 g/L for FC-C5). 288
Figure 3.8.1. Leaching recovery and contamination level as function of acid dose. (West Kentucky 13 coarse refuse material, roasted, leaching with 0.001M, 0.01M, 0.1M, and 1M sulfuric acid, S/L 200g/L at 75°C.) 291
Figure 3.8.2. Correlation of TREE leaching recovery to acid dose (kg/ton feed). 291
Figure 3.8.3. Correlation of leaching recovery of Al and Fe to acid dose (kg/ton feed). 292
Figure 3.8.4. Precipitation curve of Al and Fe in three different solution with different solution chemistry. 293
Figure 3.8.5. Correlation of NaOH dosage to precipitation pH in WKY13 AMD (Al 330 ppm, Fe 720ppm). 294
Figure 3.8.6. Acid dosage needed to achieve targeted pH of the liquified RE precipitate cake under different dilution ratio (left). And the ending concentration of Al, Ca, and Fe in the redissolved RE solution as a function of the acid dosage used (right). 295
Figure 3.8.7. Leaching recovery of RE and other elements of interest over the continuous run in pilot scale operation (Test code DTK-C16:50kg H_2SO_4 per ton of feed, 75lb/hour feed solid, 75 ºC, with 50% recirculation). 298
Figure 3.8.8. Precipitation efficiency of REEs and elements of interest. (DTK-C16-PT0 Al precipitation at pH 4.5, residence time 1 hour.) 299

Figure 3.8.9. Precipitation efficiency of REEs and elements of interest. (DTK-C16-PT1 RE precipitation at pH 6.8, residence time 2 hour.) 300
Figure 3.8.10. Redissolution efficiency of REEs and elements of interest. (DTK-C16-L2, pH2.3, HCl dosage 6.5 ml of 36% pure HCl per Liter of blended slurry, residence time 30 min) 301
Figure 3.8.11. Oxalate precipitation efficiency of REs and other elements of interest. (pH 1.5, oxalic acid dosage 6.21 g/L of concentrated PLS, residence time 20 min) 301
Figure 3.8.12. Leaching recovery of RE and other elements of interest over the continuous run in pilot 303
Figure 3.8.13. Precipitation efficiency of REEs and elements of interest. (FC-C8-PT0 Al precipitation at pH 4.2, residence time 1 hour.) 304
Figure 3.8.14. Precipitation efficiency of REEs and elements of interest. (FC-C8-PT1 RE precipitation at pH 6.8, residence time 2 hour.) 305
Figure 3.8.15. Redissolution efficiency of REEs and elements of interest. (FC-C8-L2, pH2.2, HCl dosage 12 ml of 36% pure HCl per Liter of blended slurry, residence time 30 min) 306
Figure 3.8.16. Oxalate precipitation efficiency of REs and other elements of interest. (pH 1.5, oxalic acid dosage 9.85 g/L of concentrated PLS, residence time 20 min) 307
Figure 3.10.1. SX Flowsheet for REE Recovery in the Pilot Plant 313
Figure 3.10.2. Recovery of REEs present in the feed in the rougher circuit of with respect to running time 314
Figure 3.10.3. Concentration buildup of REEs in the stripping solution with running time and different stripping flow rates 314
Figure 3.10.4. Concentration buildup of calcium in the stripped solution with running time and the effect of bleed of scrubbing solution 315
Figure 3.10.5. Concentration buildup of iron in the stripped solution with running time and the effect of corresponding ascorbic acid dosage 316
Figure 3.10.6. Concentration buildup of calcium in the scrubbing solution with running time and the effect of bleed of scrubbing solution 317
Figure 3.10.7. Setup for cleaner stage for SX circuit in the continuous plant. 318
Figure 3.10.8. Extraction curves of REEs and Iron with pH of the feed solution for cleaner circuit and HREE/LREE ratio for different pH solutions. 319
Figure 3.10.9. Concentration buildup of REEs and contaminants in the stripped solution of cleaner circuit with running time and the effect of flow rates of stripped solutions. 320
Figure 3.10.10. Recovery of REEs in the cleaner circuit and the effect of stripped solution flowrates. .. 320
Figure 3.10.11. Separation curves of TREEs, Fe, Al, and Ca during selective precipitation over a range of pH. 323
Figure 3.10.12. The recorded pH of continuous process of REEs and contamination precipitation over 20 hours of operation. 323
Figure 3.10.13, Precipitation efficiency of individual REEs compare to Al, Ca, and Fe in two stage precipitation at pH 4.5 and pH 7.5 during the continuous process over an operation period of 20 hours. 324
Figure 3.10.14. REE precipitate re-dissolved at various pH value after centrifuge. 325
Figure 3.10.15. Rare earth redissolution efficiency as the solution pH value is reduced using hydrochloric acid. 325
Figure 3.10.16. Redissolution efficiency of individual REE and major contaminants at pH of 3.5, 3.0, and 2.5. 326
Figure 3.10.17. Precipitation efficiency of TREEs and major contaminants at various pH values using NaOH. 327

Figure 3.10.18. Extraction efficiency of iron from the re-dissolved precipitate solution using 5% DEHPA solution at different dosages of 200 g/L solution of ascorbic acid. 328
Figure 3.10.19. Stripping efficiency of REE with different volumes of 6M HCl on a 5% DEHPA solution loaded with the re-dissolved precipitate solution at pH 2.0. 329
Figure 3.10.20. Precipitation efficiency curve of the DTK-AMD2020. 332
Figure 3.10.21. Recorded pH of feed and effluent solution in the Fe precipitation operation over time period of 48 hours (left). Recorded 2M NaOH solution consumption to fulfill the targeted pH in the Fe precipitation operation over 48 hours (right). 333
Figure 3.10.22. Precipitation efficiency of REEs and other element of interest at Fe precipitation. (DTK-AMD-PT0, pH 3.2, NaOH dosage 0.62g/L AMD solution, pump automatic controlled, residence time 1 hour.) 333
Figure 3.10.23. Recorded pH of feed and effluent solution in the Al precipitation operation over time period of 33 hours (left). Recorded 2M NaOH solution consumption to fulfill the targeted pH in the Al precipitation operation over 33 hours (right). 334
Figure 3.10.24. Precipitation efficiency of REEs and other element of interest at Al precipitation step. (DTK-AMD-PTAl, pH 4.5, NaOH dosage 0.79 g/L of AMD, automatic controlled, residence time 1 hour). 334
Figure 3.10.25. Redissolution curve of Sc from the Al precipitation cake using HCl. 335
Figure 3.10.26. Recorded pH of feed and effluent solution in the Al precipitation operation over time period of 32 hours (left). Recorded 2M NaOH solution consumption to fulfill the targeted pH in the Al precipitation operation over 32 hours (right). 335
Figure 3.10.27. Precipitation efficiency of REEs and other element of interest at RE precipitation step. (DTK-AMD-PT1, pH6.5, NaOH dosage 0.19 g/L AMD, automatic controlled, residence time 1 hour). 336
Figure 3.10.28. Redissolution curves of select elements in the DTK-AMD20 rare earth hydroxide cake at a 50-gallon dilution. Hydrochloric acid aliquots were added to the slurry to induce redissolution, and samples were taken and analyzed at 0.5 pH intervals. 337
Figure 3.10.29. Redissolution curves of select elements in DTK-AMD20 rare earth hydroxide cake at 100-gallon (top) and 200-gallon dilutions (bottom) dilutions. Samples were analyzed at 0.5 pH intervals. 339
Figure 3.10.30. Redissolution efficiency of REEs and other elements of interest at pH 3.0, HCl dosage 39 ml/L of blended slurry. 340
Figure 3.10.31. Oxalate precipitation efficiency of REs and other elements of interest. (pH 1.5, oxalic acid dosage 20 g/L of concentrated PLS, NaOH dosage 10.4 g/L of concentrated PLS) 341
Figure 3.11.1. Photograph of the onsite laboratory equipped with an ICP-OES, fume hoop and sink that is supplied with high quality deionized water. 342
Figure 3.12.1. Overview worksheet that lists the types of calculation worksheets for different unit operations that are current available in the REESim simulation tool. 345
Figure 3.12.2. "Reagents" worksheet listing reagents type, concentration and density. 347
Figure 3.12.3. Sample flowsheet pasted into REESim. 347
Figure 3.12.4. "Nodes" worksheet example. 347
Figure 3.12.5. Illustration of the pages utilized by the "Feed" computational worksheet. 349
Figure 3.12.6. Page 1 (Feed Data) contained within the "Feed" computational worksheet. 350
Figure 3.12.7. Page 2 (User Tools) contained within the "Feed" computational worksheet. 350
Figure 3.12.8. Page 3 (Feed Blend) contained within the "Feed" computational worksheet. 353
Figure 3.12.9. Page 4 (Assays) contained within the "Feed" computational worksheet. 353
Figure 3.12.10. Illustration of typical pages for "Unit Operation" computational worksheets. 354

Figure 3.12.11. Drop-down menu for selecting unit operation worksheets. 355
Figure 3.12.12. Drop-down menu for selecting process stream for a chosen unit operation. 355
Figure 3.13.1. Mass balance Megasheet output. (First sheet) 359
Figure 3.13.2. Megasheet mass balance calculation sheet. (Second sheet) 360
Figure 3.13.3. Megasheet results output page. (Third sheet) 361
Figure 3.14.1. Relationship between REE recovery and capital intensity (defined as $ of capital cost per kg per year of REE production capacity) for 10 scenarios evaluated in this study. 378
Figure 3.14.2. Relationship between REE recovery and total operating cost ($/kg REE) for 10 scenarios evaluated in this study. 378
Figure 3.14.3. Relationship between project NPV and product basket price ($/kg REE) for 10 scenarios evaluated in this study. 379
Figure 3.14.4. Reagent utilization correlations determined from multiple pilot-scale trials. All data is shown as mass of reagent normalized to overall plant feed mass. 381
Figure 3.14.5. Mass, water, and reagent balance for PM1: Feed Preparation. 384
Figure 3.14.6. Mass, water, and reagent balance for PM2: Roasting. 385
Figure 3.14.7. Mass, water, and reagent balance for PM3: Leaching. 386
Figure 3.14.8. Mass, water, and reagent balance for PM4: Leachate Precipitation. 387
Figure 3.14.9. Mass, water, and reagent balance for PM5: REE Re-Dissolution. 388
Figure 3.14.10. Mass, water, and reagent balance for PM6: REOx Precipitation. 389
Figure 3.14.11. Sensitivity analysis showing the effect of key technical parameters on total operating cost for Scenario ID2. Limits of tornado graph indicate +/- 30% change in the input value. 393
Figure 3.14.12. Sensitivity analysis showing the effect of plant feed rate on total plant capital costs for Scenario ID2. 393
Figure 3.14.13. Sensitivity analysis showing the effect of plant feed rate on total plant operating costs for Scenario ID2 394
Figure 3.14.14. Sensitivity analysis showing the combined effect of plant feed rate and leach percent solids on capital intensity for Scenario ID2. Here capital intensity is defined as $ of capital cost per kg/yr of REE production. 395
Figure 3.14.15. Sensitivity analysis showing the combined effect of plant feed grade and acid consumption/cost on capital intensity for Scenario ID2. 396
Figure 3.14.16. Sensitivity analysis showing the impact of leaching retention time on net present value, REE recovery, plant capital costs, and plant operating costs for Scenario ID 6. Leaching data based on laboratory testing at the designated leaching times. 398
Figure 3.14.17. Sensitivity analysis showing the combined effect of scandium oxide price and overall REE recovery on project net present value for Scenario ID6. 399
Figure 3.14.18. Sensitivity analysis showing the impact of leaching retention time on net present value, REE recovery, plant capital costs, and plant operating costs for Scenario ID 8. Leaching data based on laboratory testing at the designated leaching times. 400
Figure 3.14.19. Sensitivity analysis showing the combined effect of scandium oxide price and overall REE recovery on project net present value for Scenario ID8. 400
Figure 3.14.20. Sensitivity analysis showing the combined effect of scandium oxide price and overall REE recovery on project net present value for Scenario ID10. 401

TABLE OF TABLES

Table 3.2.1University of Kentucky equipment list. 59
Table 3.2.2 Virginia Tech equipment list and order status. 60
Table 3.3.1 Elemental composition of synthetic feedstock solution. 71
Table 3.3.2 Operating conditions for exploratory solvent extraction tests. 75
Table 3.3.3 Individual rare earth, thorium, and uranium concentrations (ppm) in the rare earth product stream obtained from both the one-stage and two-stage solvent extraction process. 79
Table 3.3.4 Individual rare earth, thorium, and uranium concentration (mg/L) of the filtrate obtained at the pH value of 4.85. 83
Table 3.3.5 Redox potential measurements at various pH values. 89
Table 3.3.6 Gibbs free energy and enthalpy and entropy values of rare earths under standard operating conditions (1 atm and 25 °C). 91
Table 3.3.7 Test order and conditions of the first subset of solvent extraction following the modified experimental protocol. 95
Table 3.3.8 Test order and conditions of the second subset solvent extraction following the modified experimental protocol. 95
Table 3.3.9 Elemental composition of individual rare earth and uranium (mg/L) in the final REE product stream obtained from Test 8. 98
Table 3.3.10 ANOVA analysis of the quadratic model for the prediction of uranium recovery. 100
Table 3.3.11 Elemental composition of individual rare earth and uranium (mg/L) in the final REE product stream obtained from Test 8. 104
Table 3.3.12 ANOVA analysis of the quadratic model for the prediction of uranium recovery. 108
Table 3.3.13 Elemental composition of the rare earth oxalate sample. 111
Table 3.3.14 Test order and conditions of zeolite adsorption tests. 116
Table 3.3.15 ANOVA analysis of the quadratic model for predicting rare earth recovery. 126
Table 3.4.1. Rare earth content distribution in the high ash content segments of a drill core associated with the West Kentucky No. 13 coal seam; core was extracted in October 2018. 136
Table 3.4.2. Size by density fractionation characterization of Fire Clay coarse refuse. 138
Table 3.5.1 Float-sink analysis results of sorter re-cleaner step 144
Table 3.5.2. Sorter products density separation on 1x0.05 inch size fraction. 144
Table 3.5.3. Rare earth concentration in X-ray sorted Fireclay coarse refuse material feed to hydromet circuit. 145
Table 3.5.4. Effect of roasting temperature and flow rate on leaching recovery. 150
Table 3.5.5. Parametric study on roasting conditions corresponding to leaching recovery. 154
Table 3.5.6. Calculation of heat zone and tube holding capacity at varies material bed depth. 156
Table 3.5.7. Test FCR-B2 test: Roasted leatherwood material leaching with 0.1 M sulfuric acid. 158
Table 3.5.8. Test FCR-B3 test: Roasted leatherwood material leaching with 0.5 M sulfuric acid. 158
Table 3.5.9. Test FCR-B1: Roasted leatherwood material leaching with 1.2M sulfuric acid. 158
Table 3.5.10. Pilot run FCR-C1 continuous test leaching sample pH (maintained) and solid concentration. 164
Table 3.5.11. Chemical consumption of operating 10 hours leaching with 1.2 M sulfuric acid solution. 167
Table 3.5.12. Timeline of the continuous operation. 168
Table 3.5.13. Make-up acid solution adjustment based on various recycle rate of raffinate. 170
Table 3.5.14. Chemical cost per one kilogram of REE in pregnant solution of the hydrometallurgical circuit. 173
Table 3.5.15. Correlation between Feed and Raffinate Concentration. 183

Table 3.5.16. REE and major elements concentrations in the leachate generated using an initial pH of 2.0. 186
Table 3.5.17. Experimental parameters for the re-dissolution tests. 192
Table 3.5.18. Major element concentration in the solution obtained by re-dissolving the precipitate. 193
Table 3.5.19. Rare earth element and major contaminant concentrations in the re-dissolved solution of the rare earth preconcentrate. 198
Table 3.5.20. Preliminary test results on REEs precipitation using oxalic acid. 202
Table 3.5.21. REO product purity produced from Dotiki coarse refuse material in pilot plant. 204
Table 3.5.22. Chemical cost per kg of REO produced from Dotiki coarse refuse material. 205
Table 3.5.23 Elemental composition of the washed product in terms of REEs and REOs by weight 210
Table 3.5.24. Decarbonization data from five series of detailed HHS test runs. 217
Table 3.5.25. REE concentration data from five series of detailed HHS test runs. 218
Table 3.5.26. Decarbonization data from the HHS test run using Leatherwood thickener underflow samples 229
Table 3.5.27. Batch HHS REM Concentration Test Results 233
Table 3.7.1. Leaching conditions in parametric study with responding leaching pH. 235
Table 3.7.2. Chemical consumption per gram of RE recovered under various leaching conditions. 235
Table 3.7.3. The ratio of contaminants to RE in leaching, precipitation and redissolution stage showing the elements association and migration in the flowsheet. 242
Table 3.7.4: Operating condition for C4 and C5 244
Table 3.7.5: Operating Condition for C4, C5 and C6 246
Table 3.7.6: Concentration of individual REE and Contaminants in feed 247
Table 3.7.7. The percentage distribution of oxalate species in solution with various amounts of Fe. 253
Table 3.7.8 The equilibrium constants of REEs and other contaminants obtained from (Zhang et al. 2020) and (Watts and Leong 2020) 254
Table 3.7.9. Circuit optimization test conditions and subjects. 256
Table 3.7.10. Solid feed and solid residue analysis before and after water wash. 256
Table 3.7.11. DTK-C13 operation log on leaching and leachate recirculation. 261
Table 3.7.12. Comparison of cost break down in percentage for DTK-C12 and DTK-C14 in terms of $ per kg of RE produced in final product REO mix. 274
Table 3.7.13. Test conditions for fireclay continuous run (pilot scale). 275
Table 3.7.14. Two-shift operation schedule on each continuous run. 276
Table 3.7.15. Operation log of FC-C4 test leaching and recirculation circuit. 278
Table 3.7.16. Operation log of FC-C5 test leaching and recirculation circuit. 279
Table 3.7.17. Operation log of FC-C6 test leaching and recirculation circuit. 280
Table 3.7.18. RE and major composition of the solution achieved from RE redissolution. 288
Table 3.7.19. RE grade in terms of %REO produced from Fireclay coarse refuse material. 289
Table 3.7.20. Cost comparison of 3 Fireclay continuous run under various condition. 289
Table 3.8.1. Circuit performance prediction and case analysis for west Kentucky No. 13 coarse refuse material. 296
Table 3.8.2. Circuit performance prediction and case analysis for Fire Clay coarse refuse material. 296
Table 3.8.3. Operation log of Dotiki validation test leaching circuit. 297
Table 3.8.4. Operation log of Dotiki validation test Al precipitation circuit. 298
Table 3.8.5. Operation log of Dotiki validation test RE precipitation circuit. 299
Table 3.8.6. Operation log of Dotiki validation test RE oxalate precipitation circuit. 301
Table 3.8.7. Operation log of Fire Clay validation test leaching circuit. 302
Table 3.8.8. Operation log of Fire Clay validation test Al precipitation circuit. 304

Table 3.8.9. Operation log of Fire Clay validation test RE precipitation circuit. 304
Table 3.8.10. Operation log of Fire Clay validation test RE oxalate precipitation circuit. 306
Table 3.8.11. RE recovery and REO grade of each pilot scale test run performed on west Kentucky No. 13 coarse refuse material. 307
Table 3.8.12. Break down of chemical cost per run on individual stage of the circuit. 307
Table 3.8.13. Chemical prices used to evaluate the chemical cost of each run. 308
Table 3.9.1. Grade of REOs produced from West Kentucky No. 13 coarse refuse. (analyzed using ICP-OES at UK and ICP-MS at VT) 308
Table 3.9.2. Grade of REOs produced from Fire Clay coarse refuse. (analyzed using ICP-OES at UK and ICP-MS at VT) 309
Table 3.9.3. Grade of REOs produced from West Kentucky No. 13 Acid Mine Drainage. (analyzed using ICP-OES at UK) 310
Table 3.10.1. Rare earth element analysis results obtained for a pregnant solution produced from the oxidation and acid generation of West Kentucky No. 13 coal coarse refuse using ICP-OES. 311
Table 3.10.2. Trace element analysis results obtained for a pregnant solution produced from the oxidation and acid generation of West Kentucky No. 13 coal coarse refuse using ICP-OES. 311
Table 3.10.3. Will Scarlet mine water composition and concentration. 321
Table 3.10.4. Concentration of total REEs and major contaminants remained in solution at different pH. 322
Table 3.10.5. REEs and contaminants redissolution using HCl at various pH (1-Liter of slurry). 325
Table 3.10.6. Cost of reagents used for the contaminant removal using the staged precipitation method. The cost is calculated per liter of the re-dissolved precipitate solution treated. 330
Table 3.10.7.Cost of reagents used for contaminant removal for the SX process method. The cost is collected per liter of the re-dissolved precipitate solution treated. 330
Table 3.10.8. Composition of RE and other major elements in the WKY No. 13 AMD. 331
Table 3.10.9. Product grade and composition of the REO mix produced from the Dotiki AMD solution. 341
Table 3.14.1. Worksheet Descriptions for REE-Econ Software 363
Table 3.14.2. Scale-up criteria used in techno-economic analysis 365
Table 3.14.3. Capital cost model parameters used in techno-economic analysis. 366
Table 3.14.4. Lang factor estimation for commercial-scale installation. 367
Table 3.14.5. Labor Cateogry Descriptions. 367
Table 3.14.6. REE Price deck used for commercial-scale economic analysis 368
Table 3.14.7. Listing of process modules used in economic analysis. 369
Table 3.14.8. List of Scenarios Evaluated in Techno-Economic Analysis 372
Table 3.14.9. Summarized Technical Results from 10 TEA Scenarios 377
Table 3.14.10. Summarized Economic Results from 10 TEA Scenarios 377
Table 3.14.11. REE Grade for West Kentucky No. 13 Coarse Refuse material considered in techno-economic analysis. 382
Table 3.14.12. Element-by-element recovery values by unit operation used in techno-economic analysis 383
Table 3.14.13. Module-level capital cost for commercial scale plant, Scenario ID 2 (500 st./hr). 390
Table 3.14.14. Total operating cost breakdown for commercial-scale plant, Scenario ID2 (500 st/hr.). . 391
Table 3.14.15. Power cost summary by process module for commercial-scale plant, Scenario ID2 (500 st/hr.). 391
Table 3.14.16. Chemical cost summary by process module for commercial-scale plant, Scenario ID2 (500 st/hr.). 391

Table 3.14.17. Final Economic Summary for Scenario ID2. 392
Table 3.14.18. Final Economic Summary for Favorable Economic Scenarios. ID6 = ammonium sulfate leaching of 1.4 float material; ID8 = acid leaching of roasted middlings; ID10 = acid leaching of FBC ash. 397
Table 3.14.19. Technical and Economic Input Parameters for Analysis of FBC Energy Production System. 404
Table 3.14.20. Technical and Economic Output Data for Analysis of FBC Energy Production System. 405
Table 5.1. Listing of key project personnel. 416

EXECUTIVE SUMMARY

The primary objective of this project was to develop and demonstrate an integrated pilot-scale circuitry for recovering high-value rare earth elements (REEs) from coal and coal byproducts. The target performance was to produce a mixed REE product with content of at least two percent by weight on a dry mass basis in a cost-effective and environmentally benign manner. During the first nine months of the project period (Phase 2 Budget Period 2), pilot plant construction was completed including all field site startup activities such as permitting, engineering design, procurement/bidding, unit fabrication, site construction, equipment installation, module assembly, safety training, and circuit shakedown. During the remaining 21 months of project period (Phase 2 Budget Period 3), detailed field-testing activities were performed including feedstock sample collection and preparation, exploratory testing, circuit modification, detailed parametric study, and performance optimization. A detailed techno-economic analysis was performed based on the pilot plant testing findings which provided various scenarios for REE production.

The project successfully accomplished the proposed target performance by producing mixed rare earth oxide (REO) with greater than 90% purity by weight in a continuous pilot scale operation from two distinctly different coarse refuse materials (i.e., West Kentucky No. 13 and Fire Clay coal seams), and at least three secondary sources (i.e., heap leach process and naturally formed acid mine drainage system). Project partners included the University of Kentucky, Virginia Tech, West Virginia University, Alliance Coal, Blackhawk Mining, Mineral Refining Company, and Mineral Separation Technologies.

The pilot scale test facility was constructed at a former mining complex owned by Alliance Natural Resource Partners (Alliance Coal). The site was rehabilitated to accommodate the equipment installation, construction and fabrication, electrical power requirement, water line management and containment. The process units constructed and installed included X-ray sorting unit, crushing and grinding unit, physical separation unit, acid leaching unit, solvent extraction unit, and wastewater management unit. A rare earth mineral concentration unit was constructed as a standalone unit for flexible operation.

A detailed environmental assessment and control plan was carried out to identify and quantify any potential impacts of the pilot-scale processing circuitry on the human and eco-system health and well-being. Corresponding mitigation strategies and control measures were provided. A conceptual flowsheet was developed to effectively remove thorium and uranium from high purity rare earth oxide mix or any potential radionuclide enriched stream.

The two distinct feedstock materials were secured from the Blackhawk Mining Complex in eastern Kentucky where the Fire Clay (Hazard No. 4) seam is processed. The West Kentucky No. 13 (Baker) coarse refuse material was collected from an active process stream at an Alliance coal preparation plant located in western Kentucky. Characterization analysis indicated that both of feed materials generated from the two sources contained >300 ppm of TREEs on a dry whole mass basis which met the requirements for a qualified feed stock. The two feedstocks were further upgraded using a dual x-ray sorter to prepare the feed material for hydrometallurgical circuit.

Thermal treatment on feed material prior to leaching was found to: 1) improve the leaching recovery of REEs, 2) increase the leaching kinetics, and 3) allow the leaching reaction to occur at lower acidity. Roasting at 600°C was selected as the pre-treatment condition for both West Kentucky No. 13 and Fire Clay coarse refuse material. Over 40% of leaching recovery was achieved by roasting West Kentucky No. 13 material having a top particle size of 3 mm in the pilot scale operation using 1.2M sulfuric acid leaching at 75°C.

Initial pilot scale testing involved continuous operation of the pilot plant for 94 hours. The leaching unit was operated at solid-to-liquid ratio of 1 to 10 (w/v) using 0.5M sulfuric acid solution at a temperature of 75°C. The continuous solvent extraction circuit utilized rougher and cleaner units with DEHPA and TBP as the extractants. An innovative stripping circuit was developed to accumulate the REE concentration in the stripping solution to a level above 600 ppm. A bleed stream from the recycled strip solution was treated using oxalic acid precipitation which produced a high grade rare earth oxalate. The oxalate product was roasted to remove the oxalate which produced a rare earth oxide product having a purity greater 90%.

Due to high concentrations of contaminant ions in the pregnant leach solution (PLS), a modified flowsheet was developed that involved pre-concentration of the REEs using multiple stages of precipitation and redissolution. The advantage of this process was improved removal of contamination before the downstream purification process and a significant cost reduction relative to the circuit that utilized the solvent extraction process. The modified circuitry included processes involving leaching, multistage precipitation, redissolution, and oxalate precipitation followed by roasting of the oxalate product. The circuit produced a mixed REO that was 92.96% pure from the initial test.

A detailed parametric test plan was carried out which involved varying key parameters including solids feed rate, acid flowrate, acid concentration, multistage precipitation pH, redissolution pH, oxalate precipitation dosage and pH. The response variables included REE recovery, contaminant recovery, REO product grade and overall chemical consumption. Test results indicated that the acid-to-solid ratio is the key parameter to leaching efficiency as performance deteriorated with an increase in solids concentration. The optimal pH determined for REE precipitation and redissolution was 6.5 and 2.5, respectively. Additional tests were conducted to further improve the flowsheet. Recirculating a portion of the PLS to the feed of the leach tanks improved the leaching performance by lowering the pH of the leaching system and reducing the contamination recovery by shortening the residence time. Moreover, the removal of Al prior to REE precipitation significantly reduced the oxalic acid consumption in the oxalate precipitation circuit. The modified circuit produced over 90% grade REO by weight from both West Kentucky No. 13 and Fire Clay coarse refuse material in pilot scale continuous test programs.

A case analysis model was developed to project the REE and major contaminants concentration in each PLS stream based on the leaching condition, pH cut point, and oxalic acid dosage. A correlation was established using empirical and semi-empirical models. Using the models, chemical consumption required for each stage was predicted based on the projected performance of the hydrometallurgy circuit. After identifying the optimum conditions, validation tests were carried out for the treatment of both West Kentucky No. 13 and Fire Clay coarse refuse materials

in the pilot plant. The actual circuit performance and chemical consumptions were very close to the model predictions.

Other than the two coarse refuse sources, several secondary feedstocks were also tested in the pilot plant facility. A “heap leach” system was constructed using the coarse refuse material generated from cleaning the West Kentucky No. 13 seam coal. Using the two stage SX rougher and cleaner circuit, a concentrate with a grade >90% REO was produced while recovering >97% of the REEs from the heap leach PLS. Naturally generated acid mine drainage (AMD) from West Kentucky No.13 mine was processed using the multistage precipitation circuit in the pilot plant in a test conducted for a period of 32 hours. The final grade of the mix RE oxide produced from the AMD was 90.84% with an overall circuit recovery of 64%. The primary source of REE was the selective precipitation steps involving iron and aluminum rejection.

The hydrophobic-hydrophilic separation (HHS) process was proven to effectively recover coal from fine waste materials. For REM recovery, the HHS process was able to produce concentrates at grades of approximately 1.8% REE on an ash basis; however, recovery values were typically low, <10%, under the optimal conditions determined in the laboratory-scale testing. Staged testing of the pilot-scale HHS process for coal recovery and semi-continuous laboratory testing for REM testing showed that a total concentration ratio of more than 15x was observed for the REM recovery process.

A circuit simulation package was developed for REE extraction and purification using a spreadsheet-based platform (Microsoft Excel). The REESim circuit simulation package is configured to track the mass and volume flows of components passing through a series of unit operations specified and configured by the user. The mass rates can then be utilized by the user to determine important performance indicators such as product mass yields, concentrate purity levels, element-by-element recoveries, and so forth.

The techno-economic analysis showed that the roasting and leaching operations were the most expensive capital items, each contributing approximately 30% to the total capital cost. One notable contributor to the high production costs was the low REE recovery observed in the pilot scale trials. The product basket price was shown to have a strong influence on the economic viability of the scenarios, with the scandium price being the most significant influencer. Operating cost was shown to be extremely sensitive to REE recovery, REE feed grade, and leaching acid consumption. An analysis of ten different scenarios for a 500 t/h commercial operation revealed that three were economically favorable, producing internal rates of return varying from 27.7% to 33.1% and payback periods of 4 to 5 years.

The project successfully developed and demonstrated a process to recover REEs from coal and coal byproducts in a pilot-plant operation which consistently produced over 90% grade REO mix from varies types of feedstocks. Commercialization analysis showed that the technology readiness level successfully achieved TRL 6 at the end of the project and demonstrated the need and the potential for scaling the process to further advance the technologies toward the goal of providing a domestic supply of REEs at a commercial scale.

1.0 INTRODUCTION

1.1 Objectives

The primary objective of this project was to successfully complete the engineering development and field demonstration of pilot-scale circuitry for recovering high-value rare earth elements (REEs) from coal and coal byproducts in a cost effective and environmentally benign manner. The pilot-scale circuitry was demonstrated at a U.S. coal processing site at a dry solids feed rate of 1⁄4 ton per hour. For management purposes, the project workflow was subdivided into two distinct periods of work. The specific objective of the first period of work was the successful completion of field startup activities required to commission the pilot-scale facility. This portion of the project included work related to site permitting, engineering design, procurement/bidding, unit fabrication, site construction, equipment installation, module assembly, safety training, and circuit shakedown. After commissioning, a second period of work was initiated with the specific objective of demonstrating the capabilities of the pilot-plant circuitry for producing REEs. This portion of the project included experimental work related to sample collection, sample preparation, exploratory testing, detailed parametric testing, and optimization testing. This period also included wrap-up engineering analyses (i.e., technical, economic, commercialization) and close-out work (i.e., reporting, decommissioning, technology transfer).

1.2 Approach

A wide range of work activities were undertaken to meet the required project deliverables. The first period of work had a duration of 9 months and included 10 different project tasks. These tasks were undertaken to:

- formally prepare and obtain signed site host agreements granting access to all project participants, including DOE representatives, to the partner owned facilities housing the proposed test circuits;
- prepare a detailed system engineering package based on the revised engineering design package that specifies in sufficient detail the equipment, components and systems needed to finalize the construction of the proposed pilot-scale facility.
- conduct an assessment of environmental controls that identifies and quantifies potential adverse impacts of the proposed processing strategies on human and eco-system health and well-being;
- perform detailed engineering of process systems, based on the Phase I design report, that are required to produce REEs concentrates at recovery, purity and cost levels sufficient to be commercially viable for each of the proposed coal and coal byproduct samples;
- carry out administrative functions associated with the bidding and procurement necessary to obtain the equipment, materials and services necessary to build the pilot-scale facility;
- fabricate, construct, assemble and install the primary process equipment and ancillary support services and structure necessary to bring on-line the proposed pilot-scale process circuitry at two different industrial test sites;
- perform a detailed systems safety analysis, and associated health and safety training, required to ensure proper startup, operation and shutdown of the pilot-scale facility; and

- initiate the sequential startup and shakedown of each process bay within the pilot-scale facility to confirm facility operability and suitability for continued testing and evaluation.

Upon successfully completing the activities described above, a second period of work was undertaken. This addition period of work, which ran from facility testing through project completion, had a duration of 24 months and incorporated 16 different project tasks. These tasks were undertaken to:

- representatively collect, characterize and prepare sufficient quantities of feedstocks of coal and coal byproducts from at least two industrial coal production sites for use in the proposed experimental pilot-scale testing program;
- establish success criteria for the proposed pilot-scale facility that incorporates quantitative metrics for technical, economic and environmental performance in accordance with the spirit of the DOE initiative;
- perform three levels of pilot-scale testing at each of the two proposed industrial field sites that will, at a minimum, include initial exploratory tests, detailed parametric tests (based on a statistical design of experiments), and long-duration optimization/performance validation tests;
- conduct additional pilot-scale testing using one or more of the pilot-scale process bays to evaluate the extraction of rare earth elements from alternate feedstocks, such as mine influenced waters (MIW) and refuse acid drainage (RAD), available at each of the two industrial test sites;
- provide NETL with a single sample that reflects the highest achieved REE concentration generated during conduct of project effort. The quantity of material to be provided to NETL shall be no less than 5 grams. Material Safety Data Sheets (MSDS) are required to accompany material supplied to NETL. NETL reserves the right for DOE/NETL employees or agents to witness the sampling and splitting. Results of any analysis arranged by DOE/NETL will be documented in a Publicly Releasable Report accessible on the NETL website;
- perform detailed environmental monitoring of the pilot-scale facility to establish mitigation strategies and emission controls necessary to fully protect water/air resources and ensure no new solid wastes are generated beyond those already present at the industrial mining sites;
- develop mathematical process models and flowsheet simulation routines that can be used to optimize existing process plant performance and design new/improved plant flowsheets for future installations of commercial rare earth recovery systems; and
- perform detailed technical, economic, commercialization and market analyses required to promote the effective transfer of technology and know-how related to the recovery of rare element elements from coal-based sources to the industrial partners supporting this initiative.

2.0 MAJOR ACCOMPLISHMENTS

This section of the report highlights major accomplishments for each of the major tasks through a series of abbreviated bullet points.

2.1 Pilot plant construction

- A Host Site Agreement was executed between the University of Kentucky and Alliance Coal who provided the test site for the project in December 2017. The pilot scale test facility was located in western Kentucky at the corner intersection of Corinth Church Road and Kentucky State Route 120. This site is formerly known as Dotiki No. 3, which was a mining complex that included administration offices, mine management offices, large workshop area, bathhouse, hoist house and storage areas. The site is owned by Alliance Natural Resource Partners (Alliance Coal) and operated by Webster County Coal Company, LLC.
- The site was rehabilitated during the second quarter of year 2018, including 1) removal of equipment and supplies located in the building; 2) installation of floor sumps and pumps for water/spill containment; 3) acid resistant floor coating; 4) installation of wastewater management system; 5) upgrading of the electrical feed/panels.
- Bidding and procurement of the major equipment, instrumentation, and key components for module construction was completed in the second quarter of the year 2018. Fabrication and construction work was performed upon receiving the units, including fabrication of the support structures and storage system for material transportation, mechanical and electrical system for equipment installation, and automation control system for circuitry operation and control.
- Seven process trains were constructed to accommodate the flowsheet for each type of feedstock. The process units included: 1) Pre-concentration duel X-Ray sorter; 2) size reduction and liberation; 3) physical separation; 4) acid leaching; 5) solvent extraction and precipitation; and 6) rare earth mineral concentration HHS mobile unit. The seven units were designed and constructed to have the flexibility to operate continuously or solo.
- A detailed environmental control assessment and control plan was conducted with identifying potential environmental risks and properly addressed with regards to 1) feed material processing dust control; 2) radionuclide concentration monitoring; 3) chemical reagents release and control; 4) water quality and air quality monitoring and control. A ventilation system was properly designed and installed to emit gas and vapor release from the hydro met circuit.
- A detailed *Health, Safety and Environmental Plan* (appendix B) for the test site was prepared and submitted on June 15, 2018. All personnel involved with the on-site installation and operation attended and successfully completed formal Mining Safety and Health Administration (MSHA) training.
- System startup and shakedown were performed successfully upon the completion of installation activities, which examined the circuit electrical and mechanical integrity, pumping capacities, pipe sizes, control systems, and instrumentation, etc. A *System Testing, Operation and Sampling/Analysis Plan* (Appendix C) was submitted.

2.2 Detailed engineering testing

2.2.1 Environmental Monitoring & Management

- Experimental data obtained from initial selective precipitation and solvent extraction tests indicated that selective precipitation is effective for the removal of thorium, while solvent extraction has superior performance for selectively separating uranium from rare earths. A two-stage solvent extraction process proved to be more efficient than a single-stage process. During the former process, approximately 97%, 94%, and 43% of REEs, thorium, and uranium were recovered into the circuit product stream, respectively.
- A modified experimental protocol was developed which aimed to efficiently separate thorium and uranium using selective precipitation and solvent extraction, separately. Nearly 100% of the thorium precipitated out at a solution pH value of 4.8 with 19.3% of the rare earths, 47.9% of the uranium, 65.6% of the iron, 38.5% of the aluminum, 17.1% of the calcium, and 14.2% of magnesium were co- precipitated at the same pH.
- Thermodynamic studies showed that the precipitation behavior of thorium, uranium, and rare earths was found to be spontaneous with a negative ΔG value. Also, the enthalpy change of the reactions further indicates that the processes are all exothermic.
- Characterization studies of solid samples generated from precipitation tests were performed using both X-ray Diffraction (XRD) and Scanning Electron Microscopy-Energy Dispersive X-ray Spectroscopy (SEM-EDX). Results indicated that precipitated solids are predominantly comprised of sodium chloride and iron oxide. Roughly spherical crystallites originating from the nucleation of nanosized particles that initially precipitated out from the saturated solutions were also observed through morphological image analysis.
- The majority of the uranium can be separated from the rare earth elements via double-stage solvent extraction. The optimum separation was obtained under the following operating condition: one-stage precipitation at a pH value of 4.8, solvent extraction feed pH of 3.5, 50 v% TBP, O/A ratio at 3:1, which corresponded to overall rare earth, thorium, and uranium recovery of 79.6%, 0%, and 3.1%, separately.
- Efforts were made to investigate an adsorption method using zeolite for its potential to remove thorium and uranium from rare earth elements. Test results indicated that zeolite adsorption is an effective technique for thorium removal. Nearly 100 wt.% thorium removal was achieved with approximately 20 wt.% total rare earth loss using 2.5 grams of 12-µm zeolite at a solution pH of 3 for a contact period of 2 hrs,
- The statistical model developed to predict the adsorption recovery of rare earths indicates that the initial solution pH, particle size, and zeolite amount are the key operating parameters that impact the adsorption recovery of rare earths. Kinetic studies suggest a fast adsorption rate for thorium in contrast to total rare earths and uranium. Multilayer physisorption was determined for total rare earths and thorium.
- Chemical compositions obtained from the XRF analysis show that the samples mainly consist of silicon and aluminum. A small portion of iron, calcium, magnesium, and potassium was also detected. Mineralogical compositions obtained by the XRD analysis indicate that all three adsorbent samples are the clinoptilolite-type zeolite.
- Rough, heterogeneous, and porous surfaces were observed during the SEM studies. BET nitrogen analyses indicate that the coarse, middle-sized, and fine zeolite samples

had a specific surface area of 16.1, 15.7, and 20.2 m2/g, respectively. The pore diameters of the coarse, middle-sized, and fine zeolite samples were determined as 12.6, 9.9, and 8.7 nm, separately.

- A conceptual flowsheet was developed to effectively remove thorium and uranium from high purity rare earth oxide mix. The proposed process flowsheet comprised of three major modules: (1) leaching of the rare earth oxide product and thorium removal by selective precipitation, (2) uranium removal by solvent extraction, and (3) rare earth precipitation and production.

2.2.2 Feedstock Collection & Preparation

- Feed samples were collected from the coarse waste streams at the Leatherwood and Dotiki coal preparation facilities. The Leatherwood sample was secured from the Blackhawk Mining Complex in eastern Kentucky which cleans coal from the Fire Clay (Hazard No. 4) seam. The Dotiki sample was secured from the Alliance Mining Complex in western Kentucky where the West Kentucky No. 13 seam was processed.
- A drill core sample from the West Kentucky No. 13 coal seam was provided by Alliance Coal in October 2018 which was extracted in the area that was mined during the performance period of this project. A 2.44-inch parting was found to contain 828 ppm which was comprised of nearly 50% cerium. Another parting contained 511 ppm and the immediate seat rock had 669 ppm on a dry, whole mass basis. The higher REE content segments typically contain elevated amounts of light REEs which the most notable being neodymium accounted for between 15% - 20% of the total REEs. The overall average REE content of the segment that likely reported to coarse refuse was 349 ppm on a dry, whole mass basis. As such, the source met the requirements for a qualified feed stock.
- Several 20-ton loads of Fire Clay coarse refuse material were collected from the Leatherwood coal preparation plant and transported to the Dotiki mine site. Size and density fractionation analysis showed that the 1.8 to 2.0 density fraction contained the highest rare earth content on a whole mass basis. The 2.0 specific gravity float material contained 604 ppm of total rare earth on a dry ash basis. The overall total rare earth content of the Fire Clay coarse refuse was 323 ppm on a whole mass basis.
- Each sample of coarse refuse was collected, sized using a portable vibrating screen, and pre-concentrated using a dual x-ray transmission sorter. The upgraded feedstocks were then sequentially passed through a jaw crusher and hammer mill to reduce the top size to around 1 mm. The pulverized feedstocks were then stored in 55-gallon drums until needed in the project test program.

2.2.3 Exploratory Testing

- A generalized flow diagram for the rare earth element (REE) extraction and recovery system was developed to accommodate a wide variety of feedstock sources as either solid or effluent streams.
- The x-ray sorter system was operated throughout the duration of this project to prepare a large stockpile of feed for pilot-plant testing. Testing showed that the sorter was best suited for treating dry material in the size range of 2 x ½ inch. It was discovered that the X-ray sorter system efficiency is sensitive to material moisture content. Wet/fine material would accumulate on the x-ray source over time and would cause false

readings on the sensor that results in less-than-optimal sorting results. It was also recommended to avoid sorter operation in freezing conditions since that the air nozzles would clog up due to ice building up inside the orifices.

- Each 20-ton increment of Fire Clay material was processed through the dual X-ray sorter from which 13 barrels were obtained for feed to the REE pilot plant. The average ash content of the material was 75.8%. The average concentration of total rare earth elements (TREEs) was 427 ppm +/- 36 ppm on a dry ash basis, and 323 ppm +/-18 ppm on a whole mass basis.
- Representative samples of the sorter product and tailing material were sent to an SGS lab for density separation at 2.0 s.g. to evaluate the leaching characteristics associated with each stream. The leaching characteristic indicated that Sc and Y in the 2.0 s.g. float fraction showed considerably higher leaching recovery than those contained in the 2.0 s.g. sink material. Therefore, effective density separation was proven to the beneficial to maximize the final product value.
- Thermal treatment of the feed material prior to leaching was found to significantly improve the leaching recovery of REEs, increase the leaching kinetics, and allow the leaching reaction to occur at lower acidity. A tube furnace roaster was purchased and refurbished to realize an in-house continuous roasting operation for feed preparation.
- A series of preliminary tests conducted on West Kentucky No. 13 material showed that roasting at 600°C provided the best improvement in REE leaching characteristics. The REE leaching recovery was improved from 9% to 34% after roasting using 1M sulfuric acid leaching at room temperature for 15 minutes. The improvement in leaching performance was primarily associated with the light REEs that are bonded in the aluminum silicate mineral structures.
- The second 20-ton Fire Clay material was roasted in-house at the pilot plant. The XRD plots showed that the kaolinite peaks disappeared after roasting. After roasting at 600 °C, the kaolinite mineral structure was decomposed through dehydration. Carbonate minerals, such as $CaCO_3$ and $MgCO_3$, were decomposed to metal oxide and released carbon dioxide, which benefits the leaching process by reducing acid consumption. Pyrite was oxidized to iron oxides (i.e. hematite and magnetite).
- Initial batch leaching tests in the pilot plant on the West Kentucky No.13 material examined the impact of solution acidity using 0.1M, 0.5M, and 1.2M sulfuric acid. The total REE recovery values after 2 hours of leaching time in the batch tests were 23%, 32.3%, and 40.4%, respectively.
- First continuous pilot scale trial test was conducted using Fire Clay coarse refuse through the leach and SX circuits continuously over 12-hour period. Test results concluded that the use of 1.2M H_2SO_4 was cost prohibitive due to excessive chemical consumption.
- In the second trial, the pilot scale leaching, solvent extraction, and wastewater treatment circuit was operated continuously for 94 hours over three weeks of time period. The leaching unit was operated at a solid-to-liquid ratio of 1 to 10 (w/v) using 0.5M sulfuric acid solution at a temperature of 75 ℃. The pregnant leachate solution was reduced and neutralized before feeding into the SX circuit.
- To reduce the fresh acid consumption, the raffinate that discharged from the solvent extraction loading stage was recycled to the leaching tank from 48 hours to 94 hours in a continuous run. With 25% raffinate recycle which occurred between the 48th and 75th

hours of operation, the amount of fresh acid consumption reduced by 7.8%; however, REE recovery slightly decreased from 30% to 27% due to the elevated concentration of contaminants in the raffinate. Also, the loading pH of the SX had to be elevated as well to maintain the loading efficiency at the cost of extra base solution.

- Continuous solvent extraction process was tested using two circuit configurations. The rougher circuit aimed to recover maximum REEs in the liquid, and the cleaner circuit treated the product generated from rougher circuit as a means of purifying the REEs. The rougher circuit consisted of two loading stages, one scrubbing stage and two stripping stages utilizing total 5-mixer settler units. The loading stage used an organic mixture containing DEHPA, TBP and Orfom in a proportion of 5, 10 and 15 percent v/v at phase A:O ratio of 1:1. Hydrochloric (HCL) acid of concentration 0.1 M was used as scrubbing agent and stripping was performed using 6 M HCl.
- A scoping study indicated that the maximum percent extraction achievable was 65.93 percent at pH 2.5 and 25 % v/v DEHPA. Increasing pH or extractant dosage any further causes operational problems: 1) localized precipitation and 2) elevated viscosity of the organic. As such, these conditions were not pursued at this stage. The stripping stream was recirculating within the stage to accumulate the REE concentration before extracting a bleed stream from the SX cleaner unit, which represented the final SX product. After 27 hours of operation, rare earth concentration in the stripping solution was built up to greater than 600 ppm. Over 90% grade rare earth oxide was produced from the cleaner circuit after oxalate precipitation and roasting.
- Considering the high concentration of contaminants in the leachate solution, a staged-precipitation process was developed in the lab which was able to generate a rare earth pre-concentrate containing several thousand ppm of REEs. The process utilized elevation of pH to about 4.5 to remove iron and aluminum followed by an additional increase in pH nearly a neutral condition to precipitate REEs. The advantage of this process included: 1) the removal of contamination before downstream purification processes; and 2) cost minimization given the fact that upward pH adjusted of the PLS is already required to discharge process water.
- The multi-stage precipitation process was studied in the pilot scale operation and the results showed that, by adding the same amount of sodium hydroxide, the recoveries of Al, REEs, and Fe in the tank precipitation test were reproducible relative to the laboratory-scale test results. The mixing condition was found to be critical for pilot scale testing due to the oxidation of various metals in solution. By re-dissolving the REE precipitate in dilute HCl solution, REEs concentration in solution can be as high as 675 ppm thereby allowing purification in an oxalate precipitation circuit.
- A pilot scale continuous test run was perforemd using the modified flowsheet consisting of leaching, multistage precipitation, redissolution, and oxalate precipitation. Leaching conditions included 0.05M sulfuric acid with a S/L ratio of 1/10 (w/v) at 75 Celsius degree. Over 99% of REEs were precipitate at pH value of 6.5 using diluted NaOH. Subsequently, over 90% of the REEs in the filter cake were redissolved using HCl at a pH value of 2.5 and enriched in a much smaller volumetric stream. Oxalate precipitation was carried out to produce a rare earth oxalate followed by roasting to produce a REO at a purity level of 92.96% grade by weight.

- A mobile pilot-scale HHS unit was designed, constructed, and operated. The unit accepted slurried feedstocks, such as thickener underflow, pond fines, or ground middlings and produced clean, dry coal at a nominal product capacity of 50 lb/hr.
- The HHS process was proven to effectively recover coal from fine waste materials. After startup and shakedown, parametric testing of the pilot process was shown to consistently produce a low ash (<10%), low moisture (<10%) saleable coal product, while also concentrating REEs into the tailings stream. REE contents of the tailings stream routinely assayed greater than 300 ppm on a whole sample basis.
- Laboratory-scale testing of the HHS process for REM recovery showed the influence of grind size, dispersing agents, hydrophobicity enhancing agents, and sample aging on the grade and recovery of the REE product. Under optimal conditions, the HHS process was able to produce concentrates at grades of approximately 1.8% REE on an ash basis; however, recovery values were typically low, <10%. Processing of fresh samples greatly increased grade and recovery.
- Microscopic analysis of the HHS concentrates confirmed a high population of well-liberated REM particles, typically identified as phosphates. A TEM-diffraction study of a single REM particle confirmed the mineralogy to be svanbergite, $SrAl_3(PO_4)(SO_4)(OH)_6$
- Staged testing of the pilot-scale HHS process for coal recovery and semi-continuous laboratory testing for REM testing showed that the combined approach can effectively concentrate the REEs. A total concentration ratio of more than 15x was observed for this process.

2.2.4 Test Plan Revision

- The initially proposed hydrometallurgical circuit consisted of co-current leaching circuits. The pregnant leachate solution was then subject to reduction and neutralization before reporting to the solvent extraction circuit for REE extraction. An innovative SX circuit was developed to improve the REEs stripping efficiency by recirculating the stripping solution.
- A modified flowsheet was designed and optimized to produce high purity REO from coal preparation plant waste material. The process consists of material roasting, acid leaching, REE precipitation, REE redissolution, and REE oxalate precipitation stages. The roasting process was optimized to increase the leaching recovery of REEs by five times and allows leaching to take place using milder acid conditions (i.e., pH 2.5-3.0). The REE content in pregnant leachate solution (PLS) was concentrated more than 10 times by first precipitate at pH 6.5 and redissolved at pH 2.5. The concentrated REE bearing solution was directly subject to RE oxalate precipitation and produced over 90% pure rare earth oxide by weight.
- A detailed test plan was modified based on the updated circuit design with varying key parameters including solid feed rate, acid flowrate, acid concentration, multistage precipitation pH, redissolution pH, oxalate precipitation dosage and pH. Response variables included REE recovery, contaminant recovery, REO product grade and the overall chemical consumption.

2.2.5 Detailed Parametric Testing

- The effect of acid concentration and solid concentration on REE recovery was examined over a range of testing conditions. At a 1:10 solid-to-liquid ratio, REE recovery did not increase proportionally with elevated acid concentrations. However, the recovery of Al, Ca, and Fe increased stoichiometrically. Using the same acid concentration, the leaching recovery decreased with increasing solid concentration. With the same acid-to-solid ratio, increasing solid concentration resulted in higher ionic strength in solution, which suppressed the hydrogen ion activity. The results showed that the solid concentration has a significant impact on Ca recovery. As such, the formation of calcium sulfate was observed during the leaching process, which suppressed REE recovery as a result of an exchange of three calcium ions with two rare earth ions in the gypsum structure.
- The leaching and precipitation processes were fully continuous during the pilot plant test programs. The pH values used for each precipitation stage were held constant from test to test. At a solution pH of 6.5, greater than 97% of the REEs were precipitated regardless of the leaching condition. A great amount of Co and Ni also precipitated with REEs at pH value of 6.5, whereas Li and Mn required higher solution pH values.
- The redissolution of the REE filter cake after the precipitation process was achieved using a HCl solution to achieve a redissolved cake solution value of 2.5. The amount of HCl needed to achieve the required solution pH varied based on the contents of the REE cake. The results showed that the TREE redissolution efficiency is strongly correlated with Al content. Over 80% of TREEs were recovered from the precipitate cake produced from low solid concentration leaching. Lower recovery values were realized from tests performed using high solid concentrations in the leaching process. The leachate generated from high solid concentration leaching contained more ions that need to be redissolved in a more diluted system.
- A parametric study on oxalate precipitation showed that the oxalic acid dosage and reaction pH are significant factors for rare earth oxalate precipitation recovery and purity. Higher pH values increased RE oxalate precipitation recovery but reduced the product purity due to the elevated calcium oxalate precipitation. Iron and aluminum concentrations play an important role in the required dosage of oxalic acid. Iron and aluminum are major consumers of oxalate ions in solution even without forming a precipitate. Interestingly, an increase in Fe(III) contamination also influences the precipitation pH of Ca-oxalate resulting in a relatively pure product.
- Based on the parametric study results, several additional pilot scale continuous tests were conducted to 1) examine the pre-wash effect prior to leaching circuit with a goal of reducing calcium content in the fresh leachate solution that is carried over to the downstream process; 2) implement leachate recirculation around the first stage leaching unit to reuse the un-consumed acid; and 3) evaluate the benefit on downstream chemical consumption reduction by removal of Al before rare earth precipitation. The results showed that the pre-wash process reduced the Ca concentration in the leaching circuit; however, Al and Fe concentrations were elevated due to the extention leaching time. The recirculation of PLS at higher acid concentrations resulted in a lower pH in the leaching system, which increased leaching recovery significantly. In addition, shortening the retention time reduced the ratio of impurities-to-REEs in the PLS. The removal of Al prior to REE precipitation significantly reduced the oxalate consumption

in the final precipitation circuit. The results show that 86% of Al can be removed from the leachate by precipitation with about 10% RE loss at pH 4.5.

- Parametric tests were conducted on the Fire Clay coarse refuse material based on the findings obtained from the results obtained on the West Kentucky No. 13 sources. Due to the intensive acidity required for Fire Clay material, the concentration of Al in the PLS is much higher than that of the West Kentucky 13 material. However, the modified circuit managed to reject more than 80% of Al in the precipitation circuit along with nearly 100% of the Ca removed in RE precipitation. Over 90% of the Fe was removed in the redissolution stage. The major contamination in the concentrated solution feeds to the oxalatic acid circuit was Al, which is a major consumer of the oxalic acid.
- A chemical cost analysis indicated that the highest cost of the circuit is the sulfuric acid consumption. The total chemical cost was almost linear to the acid concentration used in the leaching process. The modified circuit was capable of producing over 90% grade of REO by weight from both West Kentucky No. 13 and Fire Clay coarse refuse material in the pilot scale continuous operation.

2.2.6 Optimization & Validation

- A comprehensive analysis of the entire circuit using empirical and semi-empirical models were developed to optimize the entire circuit by employing different approach for model development. Three criteria were considered in the optimization process: 1) recovery efficiency; 2) product grade and composition; 3) chemical consumption/cost (economic analysis).
- Leaching efficiency can be predicted by varying the acid dose in terms of kg of acid per ton of solid feed. The concentration of major contaminants (Al, Ca, and Fe) leached in the PLS is a function of acid dose, which has an adverse impact on the downstream process efficiency and chemical consumption.
- The pH cut point in the Al precipitation stage determines the Al removal efficiency and the RE loss with the Al precipitate. The consumption of base can be calculated based on the stoichiometric ratio of Al^{3+} and Fe^{3+} to OH^{-}. Subsequently, the pH cut point for RE precipitation affects the RE precipitation efficiency. The chemical consumption at a selected pH cut point can be predicted with the projection of precipitation efficiency.
- The redissolution efficiency and acid dosage needed to redissolve the TREE into a concentrated solution can be modelled based on the amount of Al, Ca, and Fe concentration expected in the redissolved solution and the projected concentration of REEs. The oxalate precipitation efficiency was established based on the experimental data collected in each run with various concentration of Al and Fe at pH 1.5. The correlation of the Al and Fe concentration with oxalic acid dosage was established for a pH 1.5 precipitation system.
- A case analysis model was developed using the abovementioned methodology to predict the chemical dosage required for each stage based on the projected performance of the hydrometallurgy circuit. The model offered the option of varying the operation condition (pH cut point) of each stage and a prediction of the chemical consumption as a response of the contaminant concentration in each stream.
- Based on the optimized condition, validation tests were carried out for the West Kentucky No. 13 and Fire Clay coarse refuse materials in the pilot plant with preselected leaching condition. The actual chemical consumptions for DTK and FC

validation tests were within 91% and 83% of the projected (modeled) consumption and $18.32, respectively. The grades of REO produced from the West Kentucky No. 13 and Fire Clay coarse refuse sources were 92.7% and 79.5%, respectively. The grade difference was due to the varying leachate compositions in the PLS.

2.2.7 Provide Split Samples

- The REO samples produced from the pilot plant were submitted to NETL according to the original statement of work. The three samples included REO concentrates from the West Kentucky No. 13 coarse refuse validation test run, the Fire Clay coarse refuse validation test run, and a West Kentucky No. 13 acid mine drainage test.

2.2.8 Secondary Feedstock Testing

- Three types of secondary feedstock were tested in the pilot plant continuous operation including 1) REE extracted from a heap leach circuit; 2) acid mine drainage (AMD) collected from a well-known AMD site in southern Illinois; and 3) AMD collected from West Kentucky No. 13 operation.
- In 2018, a simple 'heap leach' system was constructed using the coarse refuse material generated from the West Kentucky No. 13 seam coal. The heap leach PLS was processed utilizing a pretreatment circuit, SX rougher circuit, SX cleaner circuit, wastewater treatment system and oxalate selective precipitation circuit. All components of the circuits were operated continuously for 240 hours. The heap leach PLS was first subject to a reduction process to convert ferric ion to ferrous ion. It was then fed into the SX circuit consisting of two loading and stripping stages, and one scrubbing stage, saponification and reprotonation. The results showed that, with recirculating the strip solution, the REE concentration accumulated and stabilized at around 250 ppm. The circuit produced a final REO concentrate having a grade >90% REO by weight while recovering >97% of the REEs present in the feed.
- In 2019 summer, acid mine water shipped from the former Will Scarlet mine site (Williamson County, Illinois) was treated using the selective precipitation circuit. The pH was regulated to 4.5 using 1M NaOH solution to remove Fe and Al, and then the effluent was sent to REE precipitation in which the pH was further elevated to a value of 7.5. The REE precipitate cake was then dissolved using HCl resulting in a final solution pH of 2.5. Solvent extraction procss and multi-stage precipitation process options were compared for the extraction of the REEs from the given AMD source. The results showed that multi-stage precipitation circuit was more economical to process a REE bearing solution that contained 2-3 orders of magnitude higher quantities of contamination ions relative to REEs.
- During summer 2020, acid mine drainage collected from West Kentucky No.13 mine was processed using the most updated modified flowsheet. The AMD was processed in the pilot plant for over 32 hours using Fe precipitation, Al precipitation, REE precipitation, redissolution and oxalate precipitation circuit. The AMD contained an average of 5.57 ±0.24 ppm of total rare earth, 796 ±98 ppm Fe, 348.5 ±15 ppm Al, 504.5 ±42 ppm Ca. The final grade of the mix RE oxide produced from AMD was 90.84% with an overall circuit REE recovery of 64%.

2.2.9 Modeling & Simulation

- A circuit simulation package was developed for REE extraction and concentration using a spreadsheet-based platform (Microsoft Excel). The simulation routine, which has been designated as "REESim" by the programming team, utilizes as separate worksheet "tab" for each unit operation included within a process flowsheet.
- The REESim circuit simulation package is configured to track the mass and volume flows of components passing through a series of unit operations specified and configured by the user. Tracked components include the mass flow rates of organic matter, ash, rare earth elements and other elemental impurities (e.g., Si, Al, Ca, etc.). The mass rates can then be utilized by the user to determine important performance indicators such as product mass yields, concentrate purity levels, element-by-element recoveries, and so forth.
- The REESim circuit simulation tool utilizes as separate computational worksheet "tab" for each unit operation included within a process flowsheet. The interconnection of streams between the various unit operations (spreadsheet tabs) is handled using Excel's built-in dropdown menus that specify which streams within a process circuit are fed/recirculated to a particular unit operation.
- To facilitate transfer of process stream data, a standard input/output matrix was incorporated into each unit's computational worksheet describing the various unit operations. The input/output matrix provides an interface for entering and reporting values for dry solids mass rate, volumetric slurry flow rate, chemical/reagent addition rates and species/component assay values.

2.2.10 Technical & Economic Analyses

- A robust techno-economic modeling software was developed and implemented during this project. The model was deployed on a Microsoft Excel platform and provides the flexibility for scenario and sensitivity analysis of various REE production approaches.
- Data collected from the operation of the pilot plant showed that across 18 production runs, chemical consumption costs varied from $381 to $2,200 per kg of REE produced, with superior results observed in latter runs. The optimal case providing a cost of $381 per kg was modeled at commercial scale. The overall operating cost for the commercial system was estimated to be $570 per kg.
- One notable contributor to the high production costs was the low REE recovery observed in the pilot scale trials. Sequential laboratory testing of each unit operation under similar chemical conditions indicated that further process improvement is possible resulting in a reduction in the operating costs to $281 per kg with no major changes to the process circuitry.
- For the baseline case, the roasting and leaching operations were shown to be the most expensive capital items, each contributing approximately 30% to the total capital cost. Likewise, reagents were shown to be the most expensive operating cost category, representing nearly 70% of the total. Leaching acid was the single largest line item.
- In addition to the raw plant data and the optimized plant data, eight additional scenarios were evaluated for a 500 t/h operation using the techno-economic model. Capital costs for these scenarios varied from $23.78 million to $252 million, while operating costs varied from $100 per kg REE to $570 per kg REE.

- Of the ten scenarios, three were found to be economically favorable, producing internal rates of return varying from 27.7% to 33.1% and payback periods of 4 to 5 years. Likewise, the capital intensity (dollars of capital per kg/yr. of REE production) for these favorable scenarios varied from $136 to $630 /(kg/yr.).
- The product basket price was shown to have a strong influence on the economic viability of the scenarios. All three favorable cases included a dedicated scandium recovery circuit, which prompted higher product basket prices relative to those without scandium recovery. Increased REE market prices or price guarantees for critical REEs may also prompt basket prices sufficient for economic viability.
- Capital intensity was shown to be extremely sensitive to plant feed rate and leaching percent solids up to approximately 20%. Above 20% solids, only modest reductions in capital intensity were observed.
- Operating cost was shown to be extremely sensitive to REE recovery, REE feed grade, and leaching acid consumption.
- Roasting was shown to be essential from a technical and economic standpoint. Despite the high relative cost of this operation, the improvements to leaching efficiency and acid consumption are notable. Overall, the incremental payback period of the roasting unit was shown to be less than one year.
- X-ray sorting and operating under a per ton lease agreement was shown to be a cost-effective approach to pre-concentration, prompting a 12% improvement to capital intensity and operating cost for the case studied.
- Roasted middlings as well as from a fluidized bed combustion system both showed robust economic favorability, owing to their increased leachability and increased REE content.
- One innovative scenario investigated the co-production of energy and REEs from a middling or waste coal. In this approach, the middling coal is combusted in a fluidized bed combustor (FBC) at a modest temperature. By avoiding high temperatures above 800° C, the REE leachability of the resultant ash is greatly enhanced, nearly matching that of material roasted under ideal conditions. Moreover, the off gas from the FBC unit can be collected and used to generate acid for the REE production system. Economic analyses of the energy production and REE production systems showed that both were independently viable with payback periods of 4 to 5 years.

3.0 RESULTS AND DISCUSSION

3.1 Project Management & Planning (PB2& PB3)

A detailed Project Management Plan was submitted to U.S. Department of Energy, National Energy Technology Laboratory in October 2017. A copy of the PMP is attached in Appendix A The official signing of the project award by DOE and subcontracts to key project participants was completed. An electronic filing system was setup under for storage and backup of project

management documents, technical reports, and experimental data files. An official kick-off meeting for the project was held on November 2, 2017.

Host site agreement was established with the management of Alliance Coal at the Dotiki mining operation. A tour of the proposed location of the pilot plant was conducted and the required modifications identified. The facility was modified and available in April 2018 when the equipment began to arrive on-site.

A MSHA safety training session was held on January 10 - 12, 2018 for researchers and engineers at the University of Kentucky involved in the pilot-scale plant testing. The training was required for individuals working on the surface at MSHA permitted facilities.

3.2 Pilot plant construction (PB2)

3.2.1 Host Site Agreements

A Host Site Agreement was prepared and executed between the University of Kentucky and Alliance Coal who provided the test site for the project in December 2017. The agreement allows access for researchers associated with the project and DOE/NETL personnel to the facilities at the Alliance Coal Dotiki operation where project activities occurred. The pre-concentration activities using the MST sorting technology were accomplished at the Dotiki coal preparation plant while the REE pilot-plant is located at the Portal No. 1 office and warehouse complex.

3.2.2 Detailed Systems Engineering

A generalized flow diagram for the rare earth element (REE) extraction and recovery system is provided in Figure 3.2.1. As shown, the process was initially designed to accommodate a wide variety of feedstock sources as either solid or effluent streams. For solids feedstocks, the flow diagram incorporates unit operations for sorting, crushing/grinding, coal recovery and alkali rejection. A separate series of unit operations are also included to recover crack rare earth minerals (REMs) from the spent tails of the decarbonization step. After the decarbonization and de-alkalinization steps, the residual solids passed through a series of hydrometallurgical operations, including acid leaching, solvent extraction, and precipitation, to extract, recover and purify REEs. The hydrometallurgical circuitry was designed to accept various types of leachate solutions (natural, pile, pad) that may not require the upfront processing steps or acid leaching.

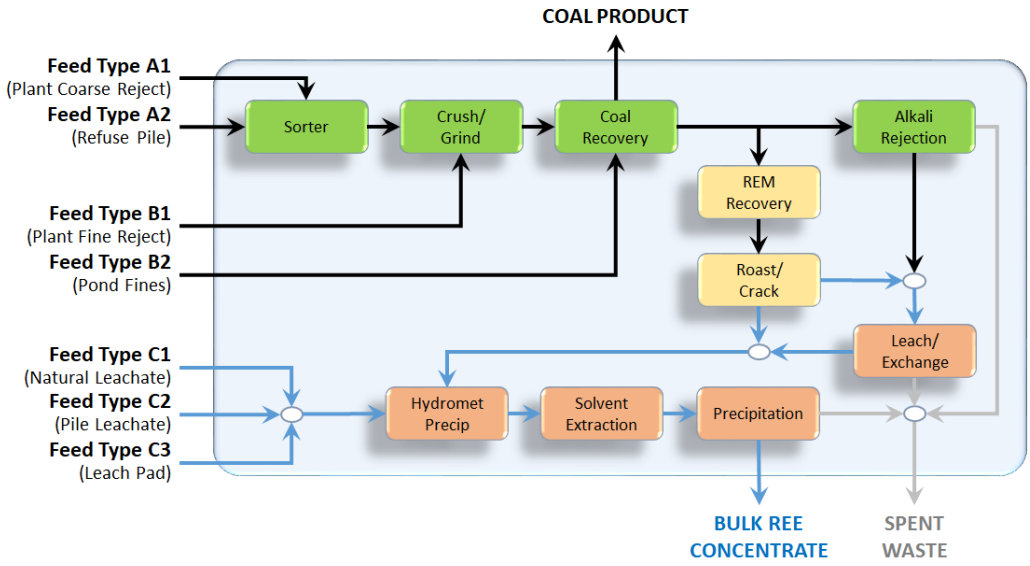

Figure 3.2.1 Generalized flow diagram for the rare earth element production system.

3.2.2.1 Facility construction

To accommodate the generalized flow diagram described above, a series of seven process trains were constructed. These include:

1.00 – Preconcentration (Mine Site)
2.00 – Size Reduction & Liberation
3.00 – Physical Separation
4.00 – Acid Leaching
5.00 – Solvent Extraction & Precipitation
6.00 – Rare Earth Mineral Concentration

The pre-concentration system, designated as Process Train 1.00, located onsite at the source of the refuse feed. This train utilizes dual scan x-ray sorting to partition 50x6 mm coarse refuse material into two streams, i.e., a high density/high ash component and a medium density/lower ash middlings component. The middlings materials were designed to be transferred to the process facility for size reduction and upgrading in Process Train 2.00 (Size Reduction/Liberation) and Process Train 3.00 (Physical Separation). Size reduction was designed for using four sequential steps of jaw crushing, cone crushing, ball milling and attrition micronizing (optional). The circuit was designed so that solids can be passed to either the physical separation for upgrading or directly to the leaching circuitry for digestion. The physical separation steps include an initial step of decarbonization froth flotation to remove carbonaceous matter followed by a subsequent step of de-alkalinization froth flotation to remove alkaline minerals ahead of acid leaching. The froth product from decarbonization is filtered and evaluated as a salable coal product. In Process Train 4.00, the non-floating tails product from decarbonization and de-alkalinization was subjected to acid leaching to extract rate earth elements (REEs) into solution and to reject insoluble solids to waste. The pregnant solution from this step passes to sequential stages of solvent extraction, stripping, and precipitation operations in Process Train 5.00

(Solvent Extraction & Precipitation). Process Train 7.00 provides an alternative pathway for recovering a dry clean coal product and rare earth minerals (REMs) from the feed prepared in Process Train 2.00 (Size Reduction/Liberation) using the Hydrophobic-Hydrophilic Separation (HHS) process. Bay 6.00 provides reagent mixing and dosage metering pumps for leaching, solvent extraction, and precipitation units.

i. *<u>Process Train 1.00 – Pre-Concentration</u>*

The flowsheet for Process Train 1.00 – Pre-concentration includes a vibrating screen, transfer conveyors and an electronic sorting unit. A scaled layout diagram for this train is provided in Figure 3.2.2a. The vibrating screen is used to reject undersize (<6 mm) and oversize (>50 mm) particles from the refuse feed stream prior to being fed at a controlled rate to an electronic sorting unit. The sorting unit incorporates a proprietary dual energy X-ray analyzer for sorting material based on atomic number. The process train for the sorter platform was designed and constructed as a portable/mobile unit that can be located onsite at the mine property. This minimizes material handling demands and also permits relocating the preconcentration units to accommodate different feedstocks sources and mine site properties. (see Figure 3.2.2b).

The Process Train 1.0 – Preconcentration was modified with installation of roofing over the materials handling systems used by the sorter. This modification was deemed necessary to fully protect the equipment electronics and other delicate mechanisms from harsh weather exposure at the industrial mine sites where the sorter was placed into service. The sheet metal roofing was installed onto a Unistrut frame assembled on the trailer. Also, expanded metal sheets were installed on each side of the frame to limit access to the processing area, thereby improving the overall safety of the modular system. Figure 3.2.3 provides a photograph of the finished sorter unit after the embedded feed conveyor assembly was sit in place.

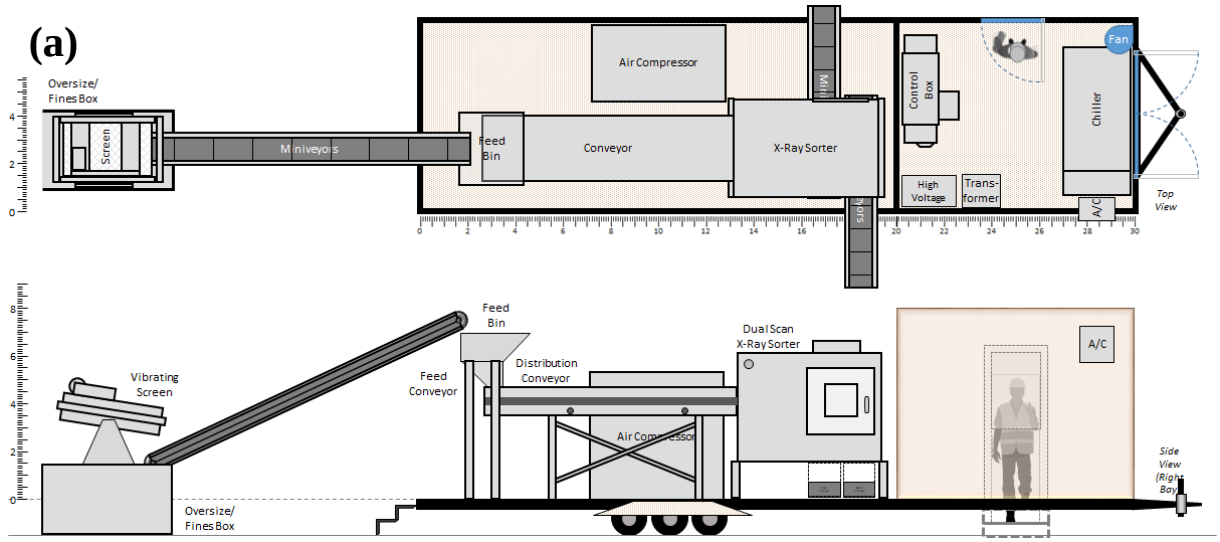

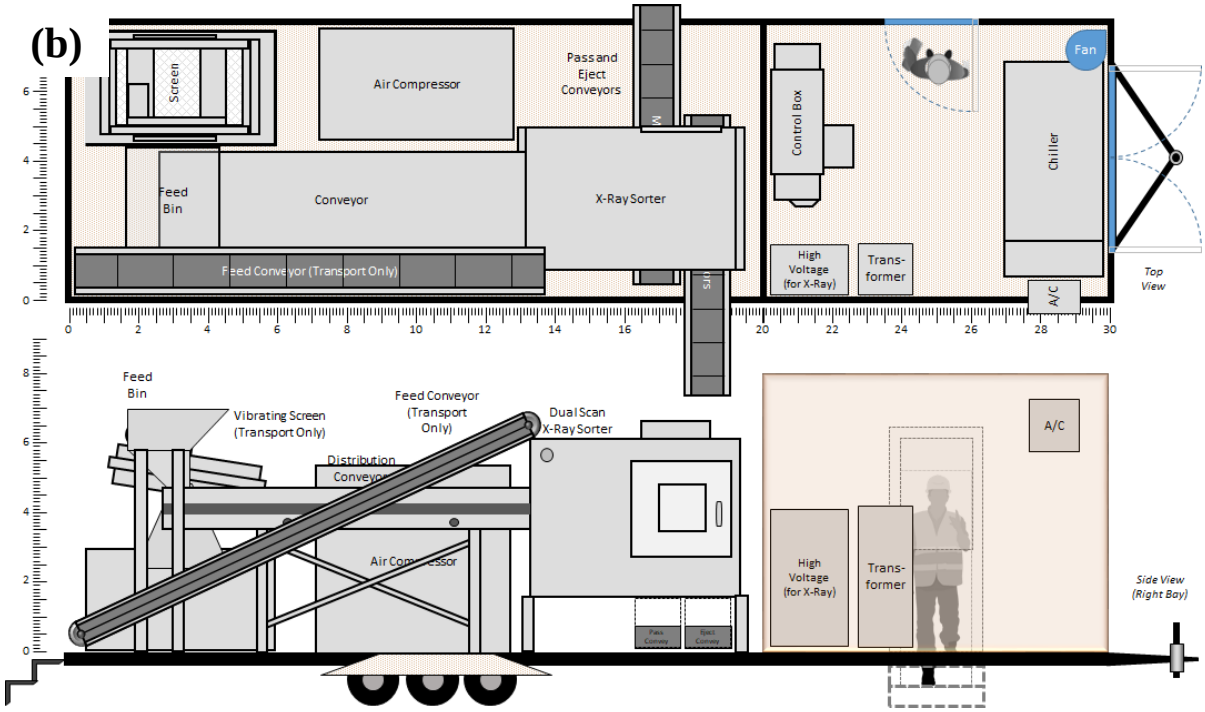

Figure 3.2.2 Scaled layout schematic for Process Train 1.00 – Preconcentration, which incorporates mobile unit operations for sizing, sorting and on-site materials handling. (a - top) Operational configuration at mine site. (b - bottom) Transportation configuration during transportation.

Figure 3.2.3. Photograph of the completed Process Train 1.0 – Preconcentration.

ii. <u>Process Train 2.00 - Size Reduction & Liberation</u>

The product from the first process train was designed to be transported in 55-gallon drums to the pilot plant facility. This material was fed to Process Train 2.00 – Size Reduction & Liberation. Figure 3.2.4 provides a scaled layout diagram for this process train. As shown, this train includes an initial stage of jaw crushing to reduce the top size from 50 to 12.5 mm (4:1 size reduction) followed by a second stage of cone crushing to reduce the top size from 12.5 to 2 mm (6.25:1 size reduction). These two stages of crushing were configured so that they can operate off-line to prepare granular feed for downstream operations. The minus 2 mm feed passes at a regulated rate via a vibratory feeder to a horizontal ball mill, which is designed to reduce the passing size to 80 mesh or finer. The mill operates in closed circuit with a sieve screen to provide flexibility in changing the grind size via a simple sieve panel change out. The process train for size reduction also includes an option to further reduce the particle size to single-digit micron sizes using an attrition micronizer (stirred ball mill), if deemed necessary for liberation of rare earth minerals.

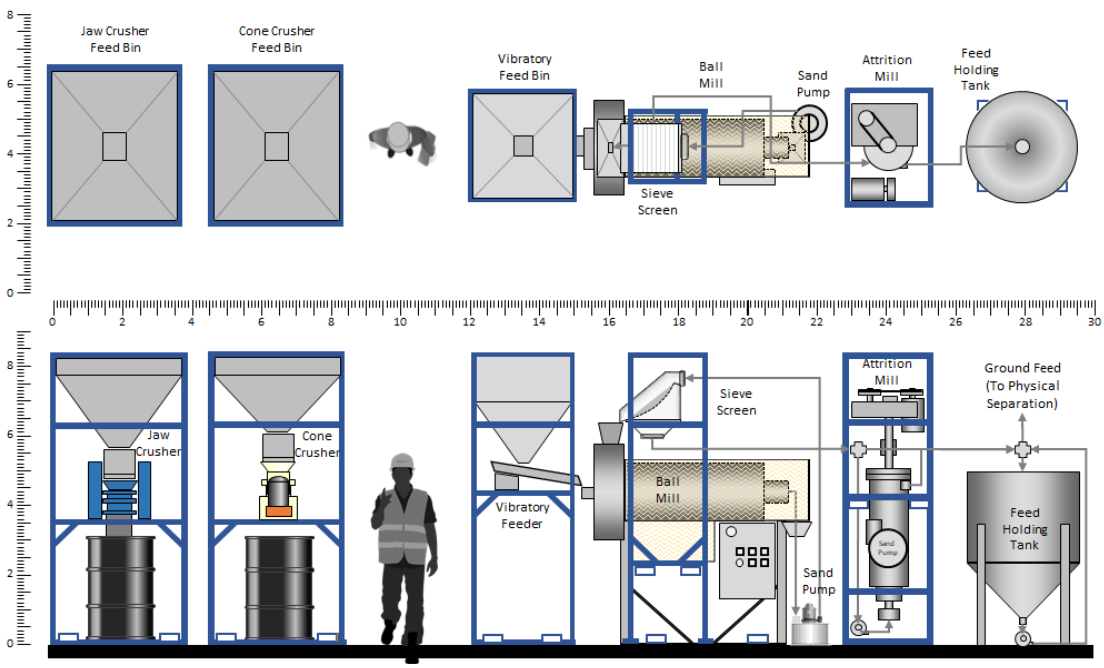

Figure 3.2.4 Scaled layout schematic for Process Train 2.00 – Size Reduction & Liberation, which incorporates unit operations for crushing, grinding and micronizing of solid feedstocks.

iii. <u>Process Train 3.00 – Physical Separation</u>

The next sequence of unit operations included in the REE extraction facility is Process Train 3.00 – Physical Separation. The scaled layout diagram for this particular process train is shown in Figure 3.2.5. This train is primarily designed to remove carbonaceous matter (coal) and alkali (acid consuming) minerals from the plant feedstock prior to hydrometallurgical processing using two-stages of column flotation technology. As shown, ground feed slurry from the grinding/mill is pumped to a conditioning tank located within the first column flotation module (decarbonization). The froth product from this operation is passed by gravity to a vacuum disc filter to remove unwanted surface moisture and produce a potentially saleable clean coal product.

The underflow from the decarbonization column flows to a thickener where clarified process water is recovered and recycled back to the grinding circuit and decarbonization operations.

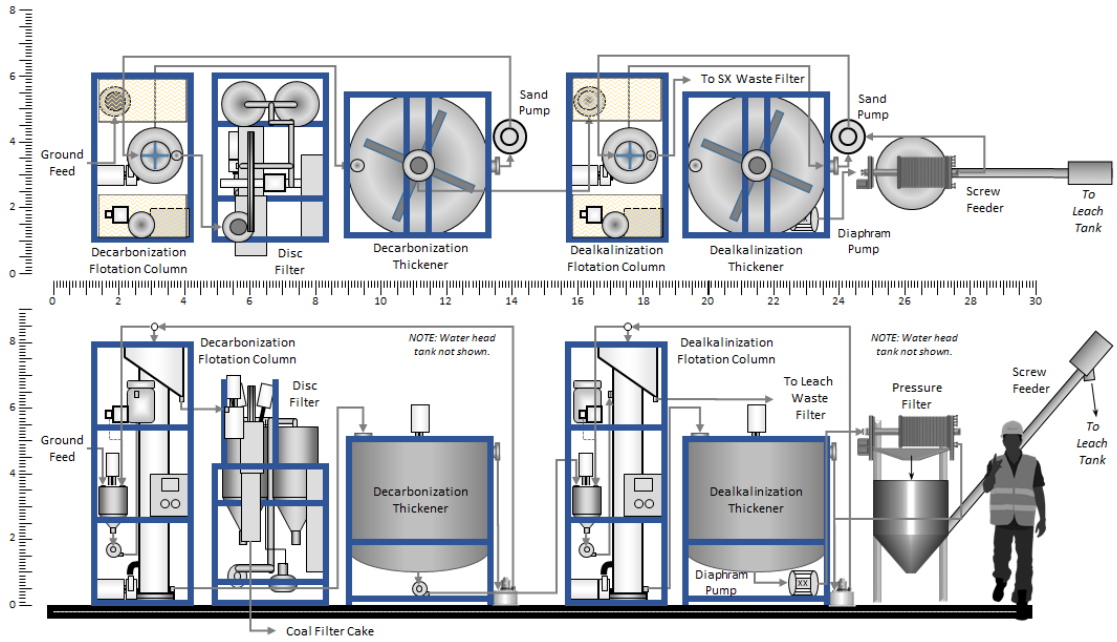

Figure 3.2.5 Scaled layout schematic for Process Train 3.00 – Physical Separation, which incorporates unit operations for feedstock decarbonization, dealkalinization and dewatering.

iv. Process Train 4.00 – Acid Leaching

The next set of unit operations in the REE recovery process are used to acid leach REEs from the upgraded feed material. This process module is being constructed off-site by SX-Kinetics, a well-known manufacturer of pilot-scale hydrometallurgy equipment. A scaled layout diagram for this process train is provided in Figure 3.2.6. The latest version of the revised material balance flowsheet for this key portion of the circuit is also provided in Figure 3.2.7. As shown, feed solids report to a multi-stage acid leaching and thickening circuit, which can be configured to circulate acid solutions and solids in a countercurrent fashion. A variety of reagents, including ascorbic acid, sodium hydroxide, acid makeup and spend scrub/raffinate, are added at various points throughout the circuit. The underflow from the last thickener is dewatered with a plate-and-frame pressure filter to provide a neutralized waste solids stream. The circuitry also includes a wide range of instrumentation to monitor and automatically control important operating variables such as chemical addition rates, solution pH and pulp temperatures. A three-dimensional rendition of the assembled module is provided in Figure 3.2.8.

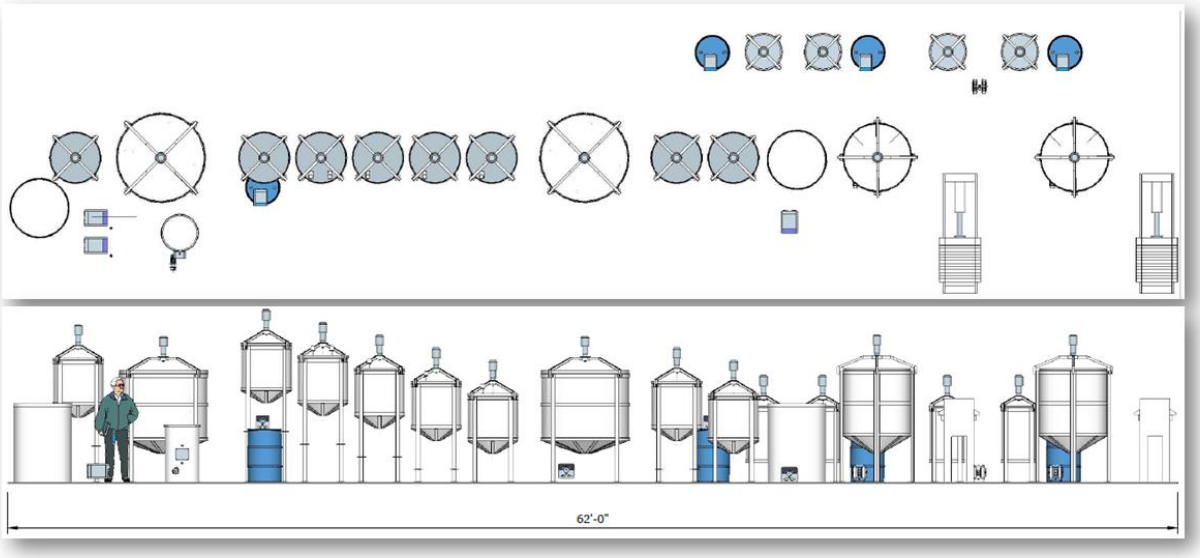

Figure 3.2.6 Scaled layout schematic for Process Train 4.00 – Acid Leaching, which incorporates unit operations for multi-stage solids digestion and thickening.

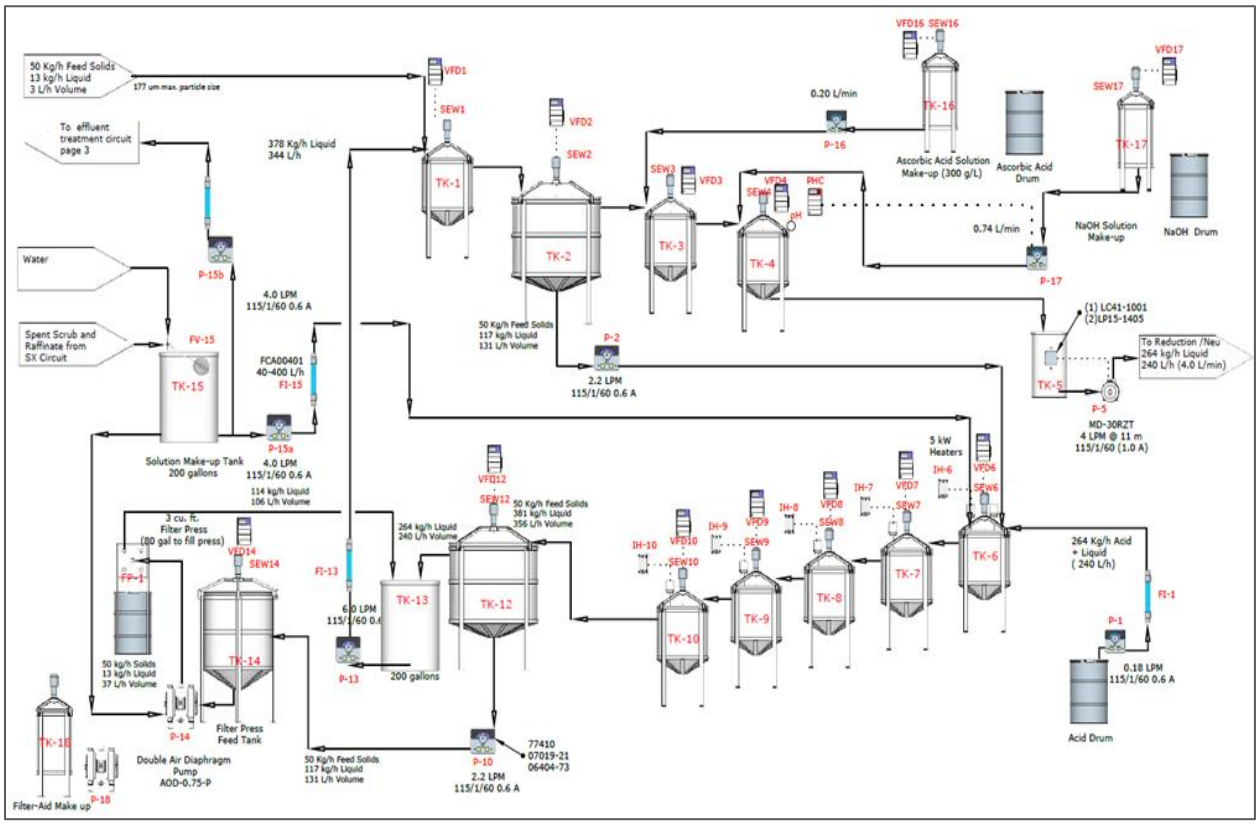

Figure 3.2.7 Updated/revised process flowsheet utilized within Process Train 4.00 – Acid Leaching.

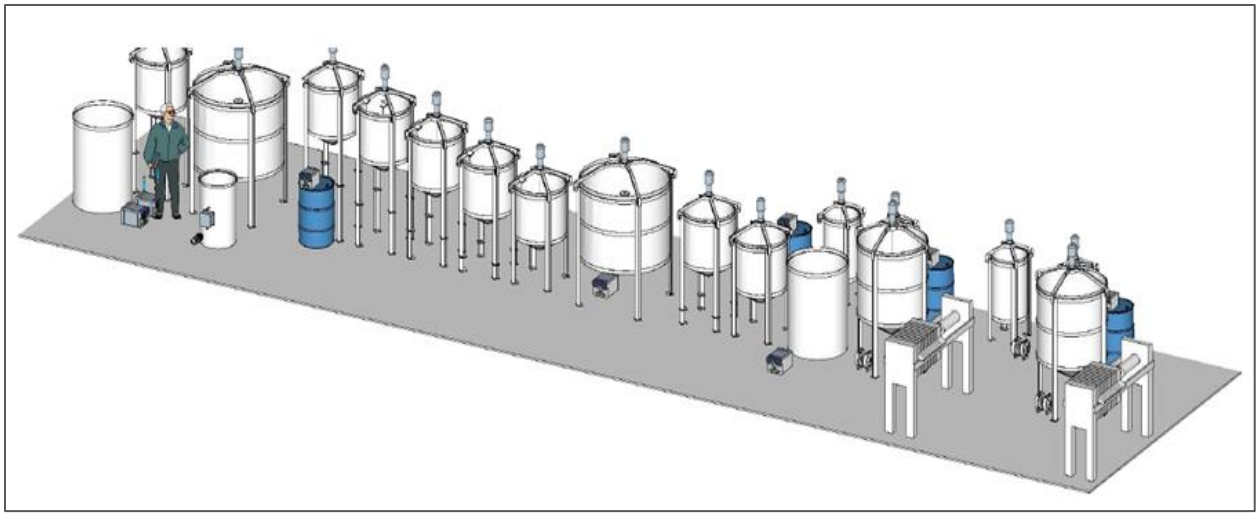

Figure 3.2.8 Generalized 3D layout of Process Train 4.00 – Acid Leaching.

v. <u>Process Train 5.00 - Solvent Extraction & Precipitation</u>

Process train 5.00 – Solvent Extraction & Precipitation incorporates standard mixer/settler technology that is well known in the hydrometallurgical processing industry. Figure 3.2.9 shows the scaled layout diagram for this particular process train. As shown, this segment of the circuitry includes a multi-stage, 10-tank solvent extraction module configured for two stages of extraction and stripping. Although not shown, this portion of the circuit also incorporates unit operations for selective precipitation and filtration of products and impurities. This process train is particularly important in that it provides the final upgrading of leachate solutions into products that meet or exceed DOE requirements on purity for this project. In addition, this final processing step is essential in ensuring that the proposed facility will have minimal impacts on the environment. A three-dimensional view of the assembled modules is provided in Figure 3.2.10.

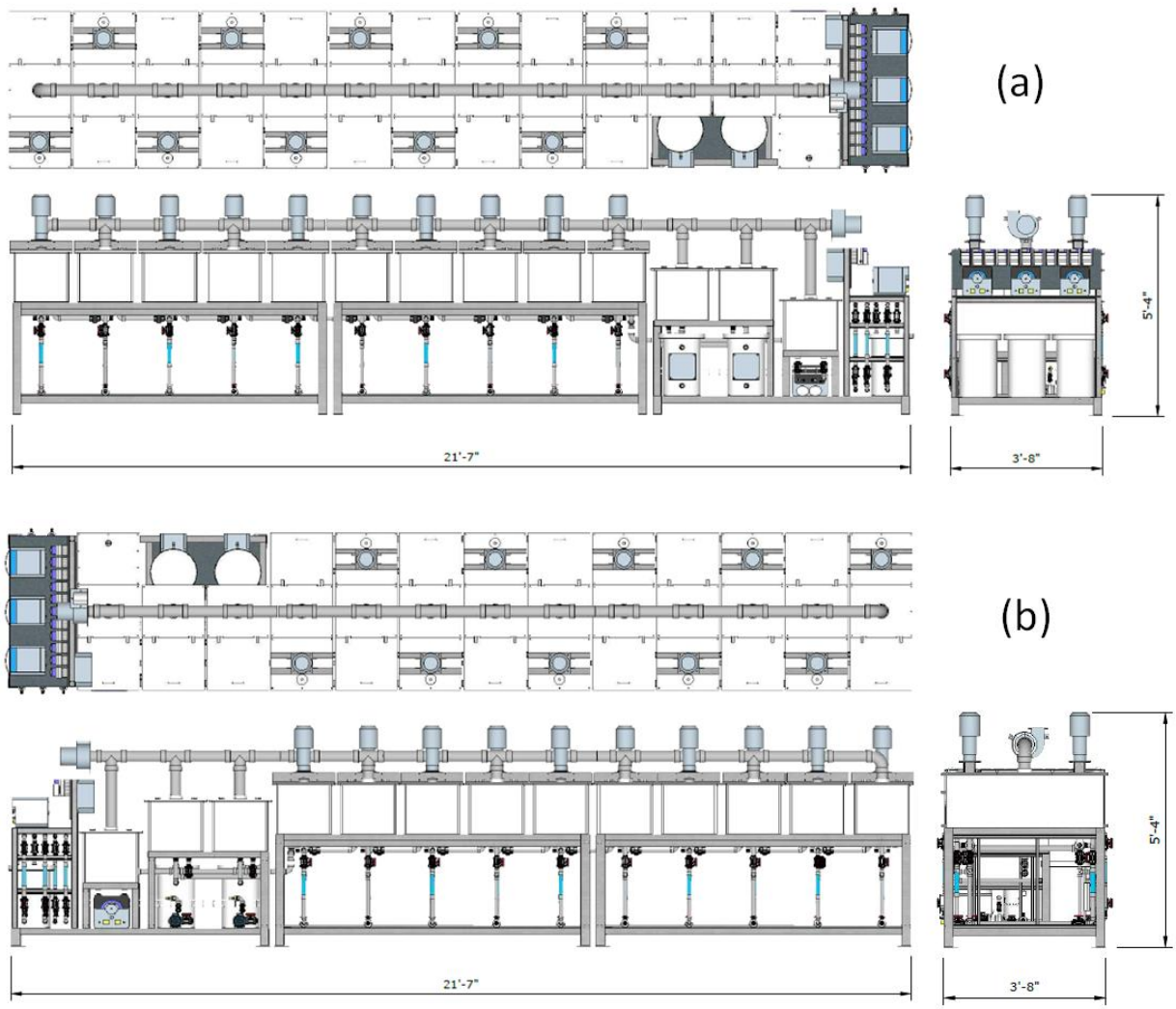

Figure 3.2.9 Scaled layout schematics for Process Train 5.00 – Solvent Extraction & Precipitation, which incorporate mixer/settler tanks for solvent extraction (a – front view, b – back view).

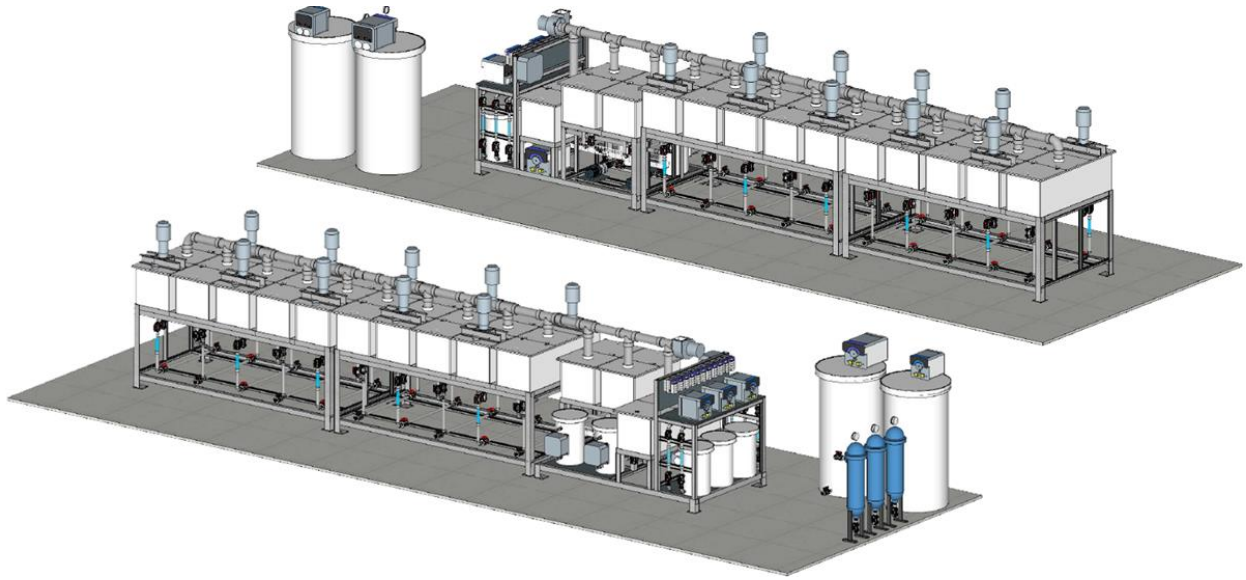

Figure 3.2.10 Generalized 3D layout of Process Train 5.00 – Solvent Extraction & Precipitation.

vi. Process Train 6.00 - Rare Earth Minerals Concentration

The final process train incorporated into the REE production facility is Process Train 6.00 – Rare Earth Mineral Concentration. The alternate processing pathway involves initial concentration of rare earth minerals (REMs) present in the feedstock prior to cracking/leaching, solvent extraction and precipitation of REEs. As outlined in the original proposal and subsequent progress reports, the physical concentration of rare earth minerals such as monazite require ultrafine grinding (<10 microns) to liberate the very small mineral grains containing valuable REEs. The subsequent separation of liberated minerals from the waste gangue also requires new technology since froth flotation is not efficient for particles finer than about 10 microns. Therefore, the current flowsheet for rare earth mineral (REM) concentration utilizes the Hydrophobic-Hydrophilic Separation (HHS) system developed commercially by Minerals Refining Company, Inc. (MRC). A scaled layout diagram for this process train was prepared by MRC for use in this project. The unit consists of an open-air, mobile platform that can be relocated to different mine sites. In the current project, the HHS process will be used to demonstrate the ability of this technology to provide an ultrafine clean (<2-5% ash) and dry (<4-8% moisture) coal product that can be sold into traditional energy markets to help offset processing costs for the REE extraction facility.

3.2.2.2 Flowsheet Development & Modifications

The proposed circuit consisted of two leach tanks that allows to operate in a counter current or co-current flow arrangement. The pregnant leaching solution reports to the reduction tank which reduces Fe^{3+} to Fe^{2+}. This an important step for two reasons. The first is the divalent iron loads under higher pH conditions thereby reducing iron recovery into the SX organic. The other reason is that Fe^{2+} is more soluble and thus does not precipitate during neutralization. This is an

important consideration as the next tank is neutralization which is needed to optimize pH conditions for selective loading of the REEs and the rejection of contaminant ions.

The layout in Figure 3.2.11 is largely symbolic where the operational detail of major units is hidden to allow for simplicity and more clearly show the major inflow and outflow portions of the hydrometallurgy circuit.

The leaching circuit is fed via an auger feeder from the physical separation circuit into the leaching circuit. The operator will be able to determine the pulp density, acid concentration and residence time for leaching. The tails will be recovered via filter press. The design allows for the filter cake to be mixed with concrete which provides options for tails immobilization and encapsulation if needed. The pregnant leaching solution is fed to the reduction and neutralization tanks. It is anticipated that less reagent will be needed in the neutralization circuit from findings derived from operating an SX circuit continuously which included saponification. As such, the recovery of the REEs by the SX circuit can be achieved at a lower pH.

The conditioned solution enters the SX circuit, where, after loading, the raffinate (barren leaching solution) is returned to the leaching circuit. A bleed stream is split from the raffinate stream and replaced with an equal amount of fresh acid solution. The bleed stream will prevent the buildup of contaminant ions in the leach circuit while significantly enhancing process economics. Increasing the amount of recycled raffinate is a major factor in the overall operating cost for the circuit.

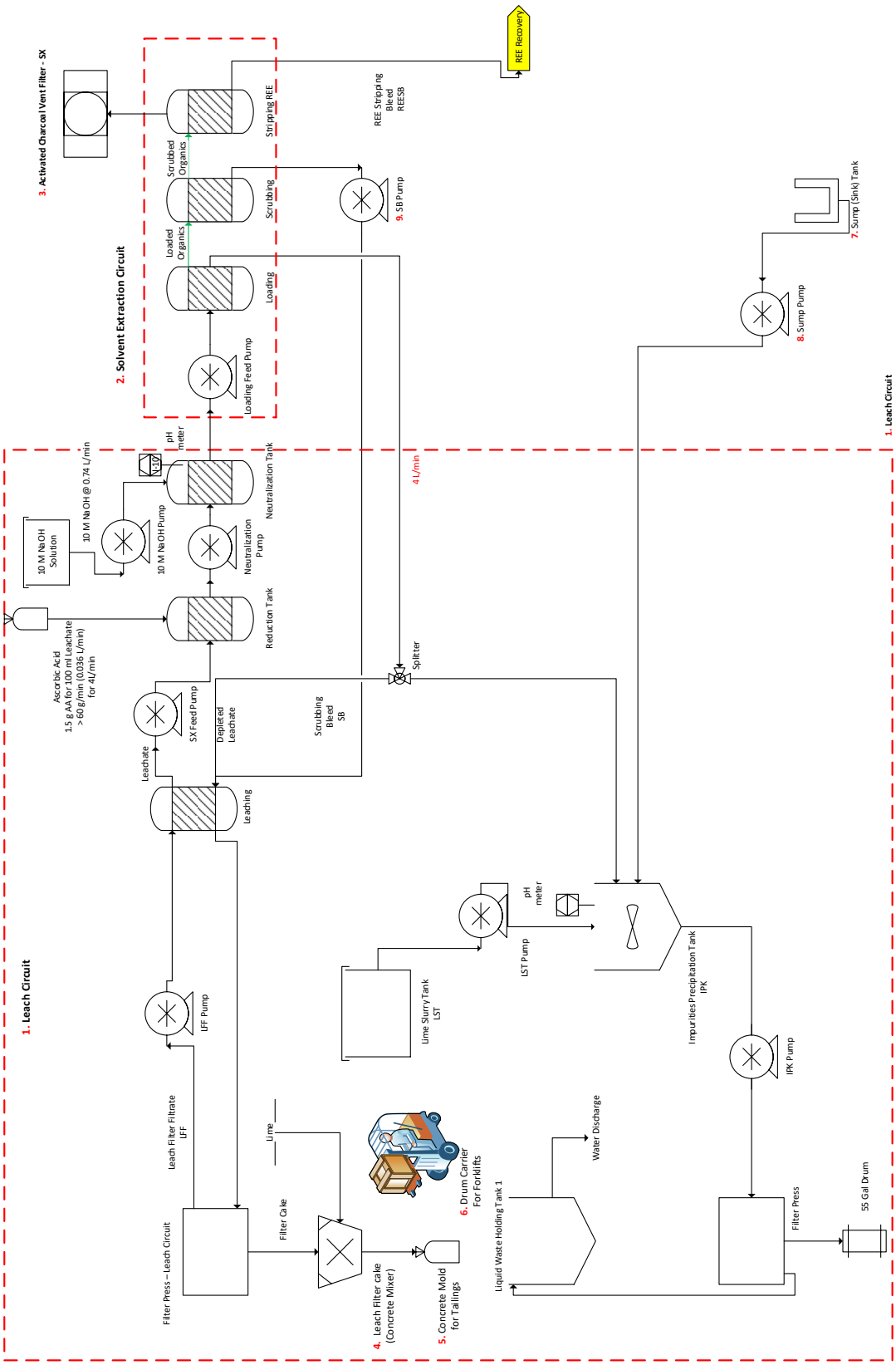

Figure 3.2.11. Pilot plant flowsheet being used for construction purposes.

In the original circuit the following ions were considered: contaminants (Fe^{3+}, Ca^{+}, Al^{3+}, Mn^{3+}); $REEs^{3+}$ and H^{+}. The loading stage exchanges H^{+} for both the contaminants and the REEs. Reduction prior to SX loading minimizes Fe^{3+} adsorption. In the scrubbing stage, the contaminant elements are significantly reduced. The REEs and remaining contaminants are exchanged for H^{+} allowing the REEs to be released into the aqueous stream to be reloaded to Stage 2. This process is repeated in Stage 2 to upgrade the aqueous solution.

The current flow sheet takes a different approach to achieve better results with less cost. The fundamental shift in design is to allow the organic phases to transport ions and not mix aqueous streams between functions. This single shift allows significant savings in reagent consumption. The current design makes uses of a single SX train where the aqueous solution is recycled. Ionic levels are maintained by utilizing a bleed stream. Thus, the equilibrium pH of the aqueous/organic reactions are maintained without the need for extra reagent for bulk pH adjustment of a flow stream.

The current circuit considers the following ions:

- Contaminants (Fe^{3+}, Ca^{+}, Al^{3+}, Mn^{3+})
- $REEs^{3+}$
- Sc^{3+}
- Na^{+}
- H^{+}

Figure 3.2.12 shows the current process with a scrubbing stage that utilizes a recycle of the mild acid to limit to amount of acid added. A bleed stream is taken from the recycle stream to maintain control on the number of contaminants in the recycle stream. The REE-rich organic stream from the scrubbing stage is directed to a stripping stage where 6M HCl solution is added to remove the REEs from the organic phase. A recycle of the REE-enriched aqueous stream is recycled to limit the amount of acid used and to load the stripping stage with REEs to improve selectivity. A REE-rich bleed stream is treated with oxalic acid to selectively precipitate the REEs and produce a final concentrate.

The current design utilizes SX as a roughing stage. The initial operation will maximize recovery of REEs by lowering grade. Initial operational data suggest that this ratio is 1:4 parts REEs to iron. Figure 3.2.12 shows the SX flow sheet layout as proposed. At this time, and per the scope of the project Oxalic acid will be utilized to produce a REE precipitate that will be roasted to achieve an oxide which is shown in Figure 3.2.13.

Further developments between Phases 1 and 2 were further insights into selective precipitation, including the development of intellectual property. The results have been encouraging with the laboratory results yielding over 98% pure REE oxide and semi-continuous operation yielding 95+% pure REE oxide. Based on the success of these discoveries, this technology will be considered for upgrading the aqueous REE concentrate.

Figure 3.2.14 shows the wastewater treatment. As the first site will be removing water back to the mine for disposal, the wastewater treatment consists of a mixing tank for neutralization

and a surge tank to feed a filter press. The water is then pumped to a holding tank for disposal to the mine.

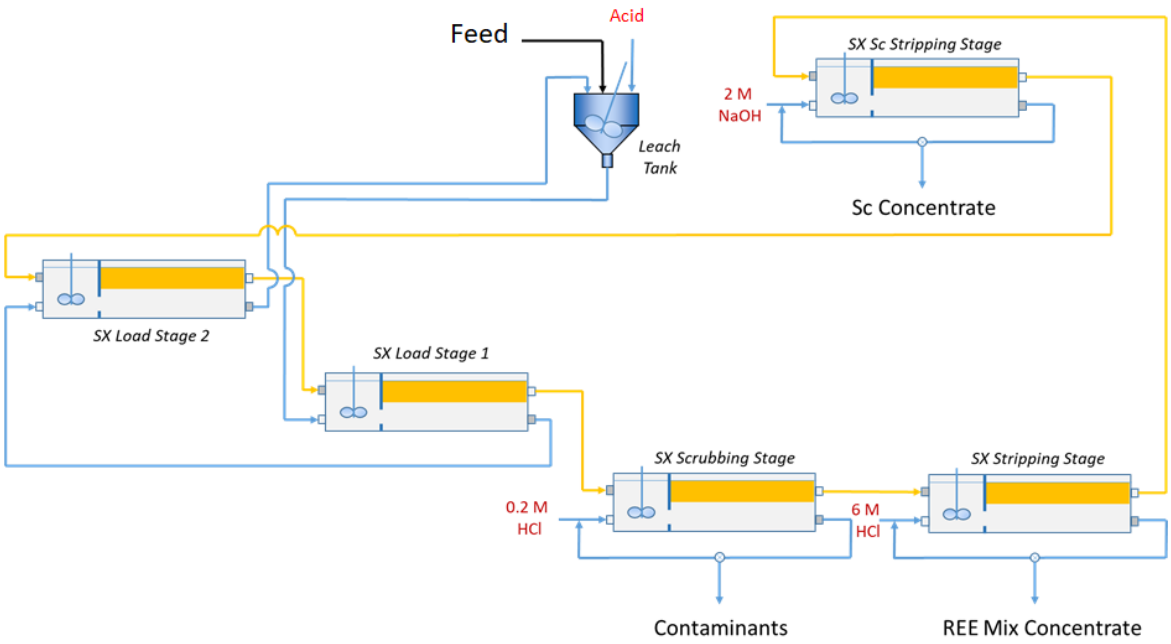

Figure 3.2.12. Proposed pilot plant SX flowsheet for construction

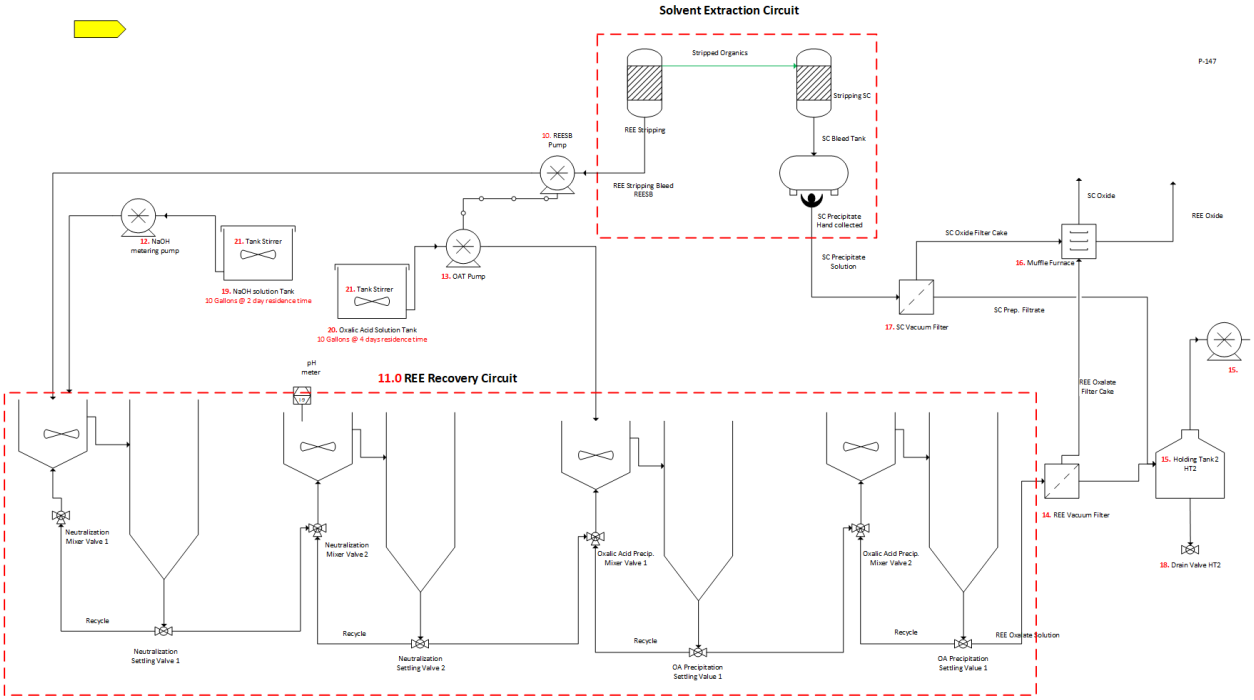

Figure 3.2.13. Proposed REE precipitation and recovery step.

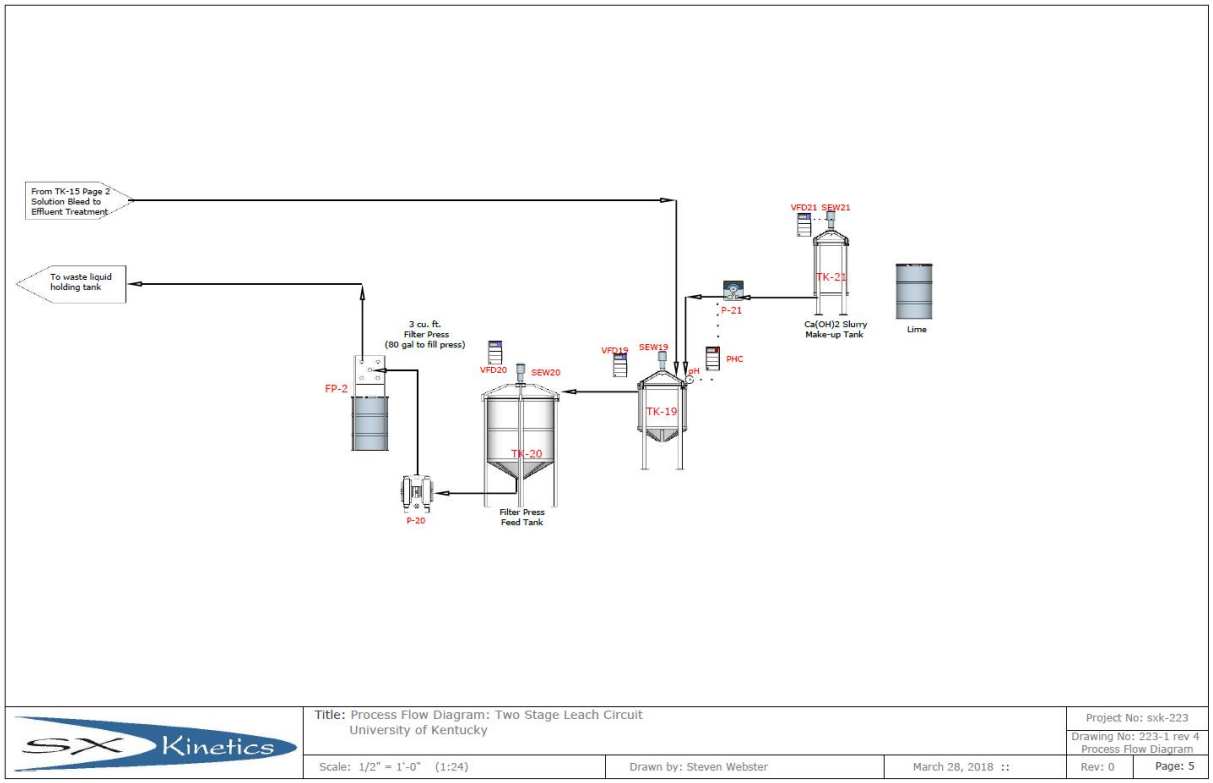

Figure 3.2.14. Concept P&ID leach circuit drawing (provided by SX Kinetics).

3.2.2.3 Techno-Economic Considerations:

The design and analysis of the flow sheet and economics for these systems are complex. At present, there are two apparent paths forward for the concentration of rare earth elements from coal sources as considered in our projects. These are solvent extraction and selective precipitation. Each one has their benefits as well as drawbacks.

The primary draw of the SX circuit is that is conventional and well known. Under current study it also has three benefits. The first is the rejection of most major contaminants during loading preferentially absorbing REEs. The second is the ability to return the barren leaching solution without neutralization. Thus, significant lixiviant savings may be realized by recycling leaching solution. The third benefit is that initial data shows the scandium reports to the organic which it tenaciously clings. Process methods were developed to remove scandium which is beneficial in creating a scandium hydroxide concentrate. The downside is the capital costs associated with acquiring and process loss of the organic extractant. Depending on the operation of the circuit, multi-stage processing is required involving roughing and subsequent concentrate upgrading in a cleaning stage. This is beneficial as the volume of processing effluent is significantly reduced making possible the utilization of stronger reagents. This upgrading may include solvent extraction or selective precipitation which has proven to be effective at concentrating REEs.

The second option is selective precipitation. The primary draw with this process is simplicity and purity. This option is utilized where the leaching solution is neutralized after bearing with REEs. Thus, this is a logical choice where acid mine drainage, or wastewater treatment occurs because the reagent costs are covered by the current operation economics. The downside to this process is the apparent increase of the equipment footprint and perhaps capital costs due to the number of tanks required. The project evaluated both options and produced >90% grade mixed REO product in continuous operation from both processes.

3.2.3 Environmental Controls Assessment

There are several items with regards to operator safety that have been incorporated. The first is the ventilation of the SX circuit. The SX circuit is designed to have negative pressure and includes exhaust fan as shown on top of the unit and further highlighted in Figure 3.2.15. Based on the nature of the exhaust air an activated carbon filter was installed on sited and then vented externally. The leaching circuit generates limited acid mist and water vapor which was also included in ventilation system to maintain negative pressure in the leaching tanks. This will be exhausted to the outside. These ventilation points are shown by Figure 3.2.16. Further sumps and banks are being installed by the mine site to allow for safe and easy cleanup of wash water and if any spills occur containment. Figure 3.2.17 shows the highlighted sumps. These sumps are designed to report to wastewater for neutralization. Figure 3.2.18 shows the anticipated layout with banking. This arrangement allows for the safe and efficient double containment and spill mitigation should it occur.

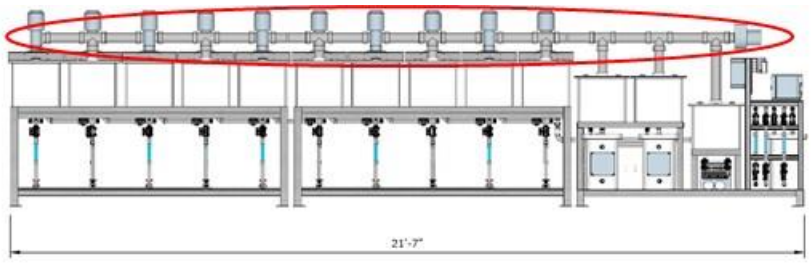

Figure 3.2.15 Solvent extraction system as shown in Figure 15 with ventilation system highlighted.

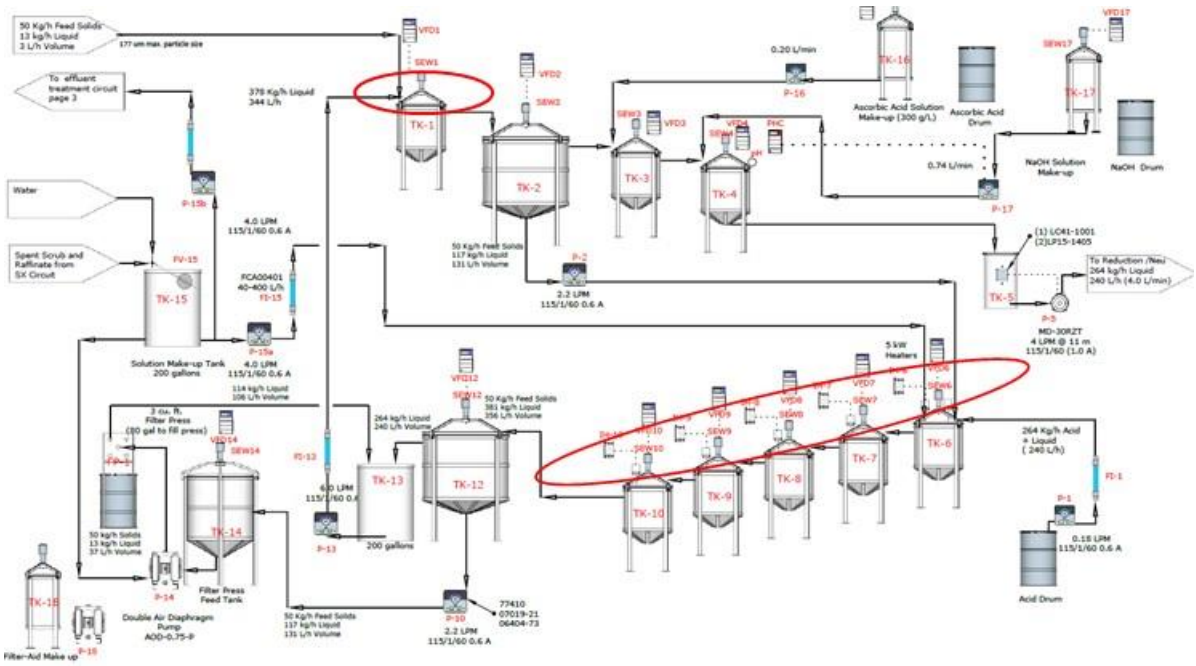

Figure 3.2.16 Leaching circuit showing tanks which will be ventilated.

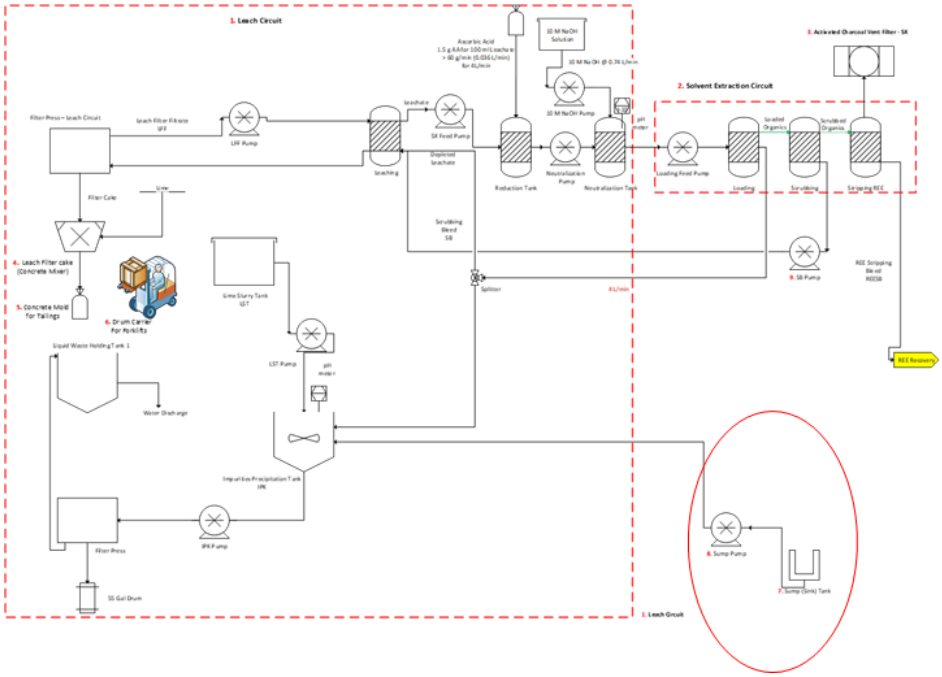

Figure 3.2.17 Hydrometallurgy flowsheet showing sumps.

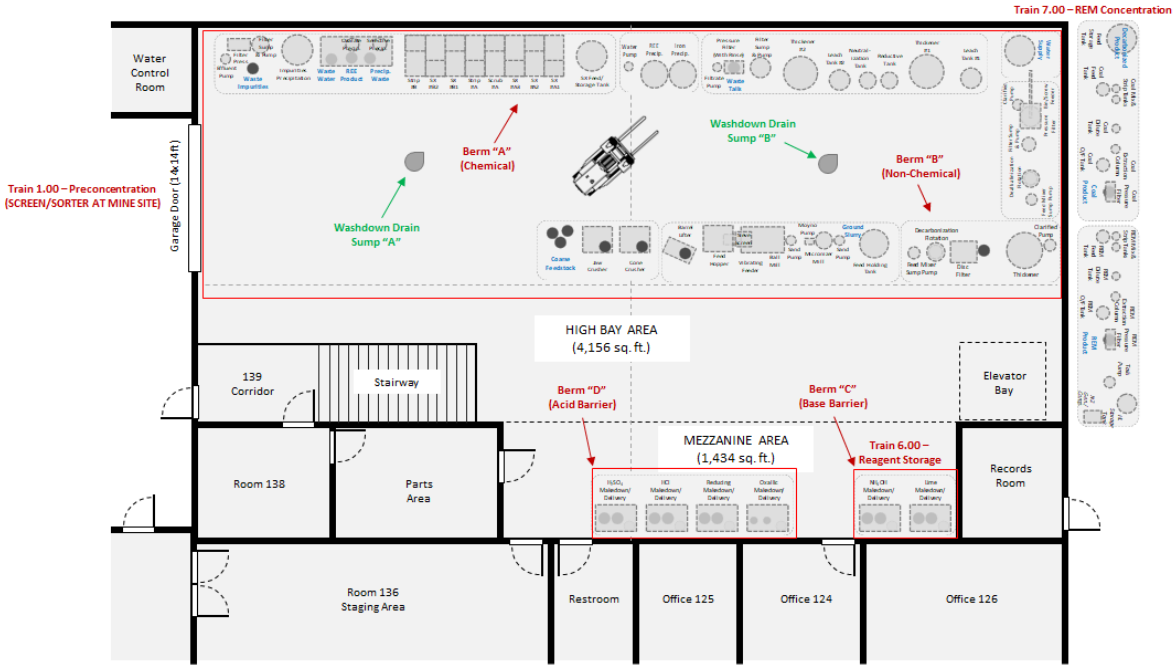

Figure 3.2.18 Proposed banking with sump layout.

Regarding uranium and thorium, the strategy focused on the prevention of leaching after disposal and the removal of radionuclides from concentrated RE products. As most thorium reports with mineral forms that tend to be difficult to leach, majority of the Th remains in solid residue. Solid and liquid samples were taken randomly by a contracted environmental analyses lab to be analyzed for potential hazards throughout the project. If selective precipitation is considered, the uranium and thorium tend to report to precipitates. A detailed study on removal of radionuclides from enriched stream was carried out and reports in the following sections.

The potential risks identified from the environmental control's assessment were used to prepare the Health, Safety and Environmental Plan for the test site. A copy of the plan is attached to this report as Appendix B. The plan outlines the major components necessary to execute the project while avoiding any environmental excursions or injuries. As such, the plan represents a significant statement of project policy to ensure good environmental and social stewardship. The major categorical sources of environmental risk identified in the plan include:

- Modification of Feed Materials
- Concentration of Radioactive Materials
- Release of Reagents
- Water Quality Impact
- Air Quality Impact

3.2.4 Site Rehabilitation

The pilot scale test facility is located in western Kentucky at the corner intersection of Corinth Church Road and Kentucky State Route 120, is part of the Dotiki mining complex owned by Alliance Natural Resource Partners (Alliance Coal) and operated by Webster County Coal Company, LLC. The general layout of the facility is shown in Figure 3.2.19. The facility provides sufficient space for installation of all of the necessary pilot-plant equipment as well as accommodations for setup of laboratory instrumentation, work rooms and personnel quarters. The working area for the pilot-scale equipment encompasses approximate 4,156 square feet of open bay space along with 1,434 square feet of second floor mezzanine space.

The site rehabilitation work included (i) the removal of all equipment and supplies owned by the participating mining company from the metal building, (ii) the excavation and addition of two large concrete floor sumps for internal water/spill containment, (iii) the coating of all concrete floor surfaces with acid-resistant epoxy paint, (iv) the installation of two large water holding tanks outside the main building structure for water management, and (v) several upgrades to the electrical distribution feeds/panels to meet the power requirements of the pilot plant facility. Most of these rehabilitation activities were performed directly or with major assistance by Alliance Coal personnel as part of their cost-sharing commitment to the project.

Figure 3.2.20 shows an exterior photograph of the facility provided by Alliance Coal for the installation of the REE pilot plant. The industrial property consists of a metal building that encloses various office, shop and garage areas. Most importantly, the facility includes a large two-story high-bay area that is fully dedicated for this project and ideally suited for the installation of pilot-scale process equipment. Figure 3.2.21 shows a wide-view photograph of the two-story high-bay area after rehabilitation and just prior to installation of the process trains for REE extraction, recovery and concentration.

The rehabilitation activities also required considerable modifications to the electrical infrastructure within the test facility (see Figure 3.2.22). The work included sourcing new 480/220/120-volt power distribution panels, running new electrical wiring to predetermined points within the pilot plant area to provide power for all the new process equipment, and completing final electrical wiring for secondary motors, drives, instrumentation, etc. The work was performed by electrical personnel from Alliance Coal as part of their cost-sharing commitment to this project.

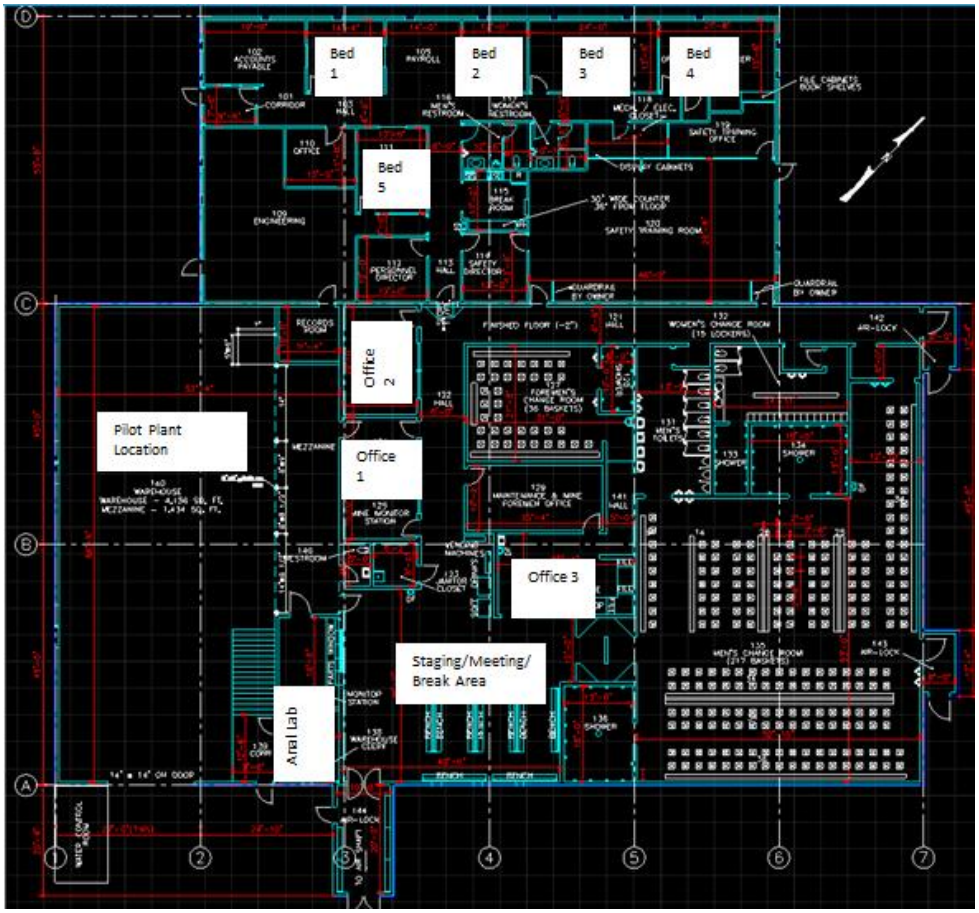

Figure 3.2.19. Floor plan for the REE extraction facility at the Dotiki Portal No. 1 mine site.

Figure 3.2.20 Exterior photograph of the REE pilot plant building.

Figure 3.2.21 Interior wide-angle photograph of the two-story high-bay area prior to process train installation (Note: Solvent extraction train already sit in place).

Figure 3.2.22 Photograph of upgrades to the facility electrical services.

Another major rehabilitation activity was the installation of containment systems for planned equipment wash-downs and unplanned spills, leaks or other unexpected outflows of liquids or solids from the various process trains installed in the pilot plant. These systems required the excavation and installation of two large concrete floor sumps located near the front and back ends of the pilot plant area. The sump located near the front end was largely designed to handle discharges of non-hazardous liquid and solids from the process trains incorporating equipment for size reduction (jaw crusher, cone crusher, ball mill, micronizer) and physical separation (decarbonization flotation, dealkalinization flotation) and water clarification (decarbonization

thickener, dealkalinization thickener, plate-and-frame pressure filter). The sump located near the back end of the facility was designed to manage more hazardous discharges of chemicals (acids/bases) used in the hydrometallurgical operations (leaching tanks, solvent extraction tanks, plate-and-frame pressure filter). To effectively isolate this area, the portions of the plant housing the hydrometallurgical operations were enclosed by spill containment berms (see Figure 3.2.23). Also, two large tanks for water management/disposal were placed outside the building (see Figure 3.2.24). These tanks were also isolated from the environment by constructing gravel berms around the tanks and covering the enclosed area with impermeable liners.

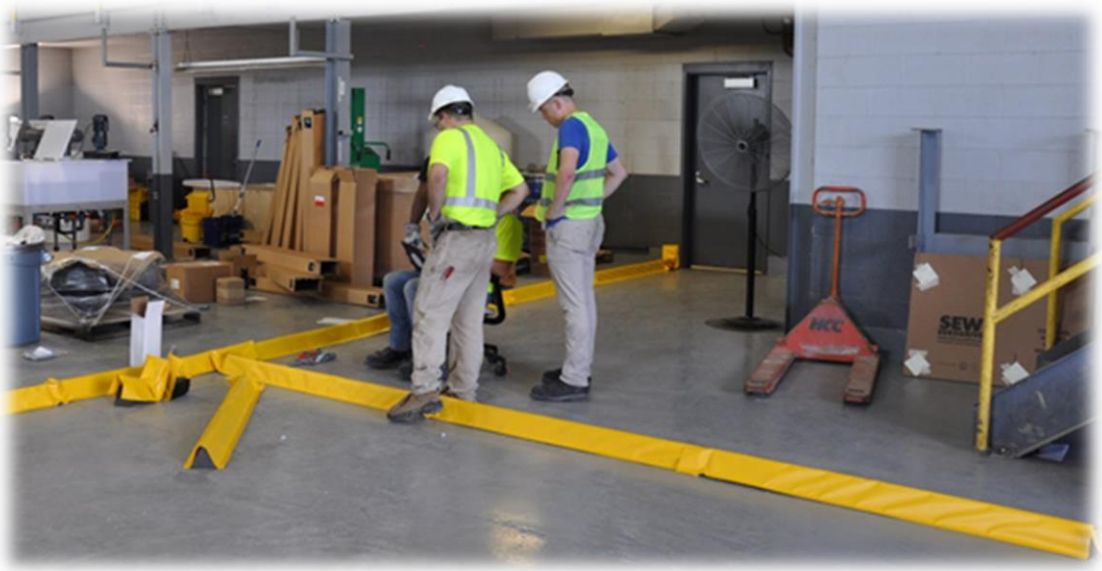

Figure 3.2.23 Installation of spill containment beams within the test facility.

Figure 3.2.24 Installation of pump-away containment tanks/beams/liners outside the test facility for water management and disposal.

3.2.5 Bidding & Procurement

A detailed procurement list was created for use in managing the purchases of key components used in equipment fabrication and module construction (Table 3.2.1 and Table 3.2.2). The bidding and procurement protocols used to purchase these items met or exceeded all state and federal regulations for such transactions. Details related to the purchasing policies can be obtained from the University of Kentucky's Office of Central Purchasing, 322 Peterson Service Building, 411 Limestone, Lexington, Kentucky (Phone: 859-257-9100). Likewise, information regarding the purchasing policies of Virginia Tech, a major subcontractor heavily involved in this project, can be obtained from Virginia Tech's Office of Procurement, North End Center, Suite 2100, 300 Turner Street NW, Blacksburg, Virginia (Phone: 540-231-6221). Some procurement activities were continued throughout the project to accommodate process circuit improvements, instrumentation for circuit automation and control, and equipment repairs/replacements.

Table 3.2.1University of Kentucky equipment list.

	Equipment	Quantity	Unit Cost	Total Cost
1	Leach Circuit	1	$469,800.00	$469,800.00
2	Solvent Extraction Circuit	1	$194,000.00	$194,000.00
3	55 Gallon Air General Activated Charcoal Vent Filter - SX	1	$ 525.00	$525.00
4	Leach Filter cake (Concrete Mixer)	1	$ 2,009.00	$2,009.00
5	Concrete Mold for Tailings	10	*$ 77.98*	$779.80
6	Drum Carrier For Forklifts	1	$ 964.00	$964.00
7	Sump (Sink) Tank	1	$ 2,000.00	$2,000.00
8	Sump Pump	1	$ 1,599.00	$1,599.00
9	SB Pump	1	$ 964.95	$964.95
10	REESB Pump Metering Pump	1	$ 964.95	$964.95
11	REE Recovery Circuit	1	$ 27,600.00	$27,600.00
12	NaOH metering pump	1	$ 964.95	$964.95
13	OAT pump	1	$ 964.95	$964.95
14	REE Vacuum Filter (Pump, Filter unit, gauge)	1	$ 2,058.93	$2,058.93
15	100 Gallons Holding Tank 2 HT2	1	$ 752.91	$752.91
16	Muffle Furnace (Digital)	1	*$ 2,702.85*	$2,702.85
17	SC Vacuum Filter (Pump, Ceramic Filter unit, gauge)	1	$ 2,058.93	$2,058.93
18	Drain Valve HT2 (automatic)	1	$ 200.00	$200.00
19	10 Gallons NaOH solution tank	1	$ 134.77	$134.77
20	10 Gallons Oxalic Acid solution tank	1	$ 134.77	$134.77
21	Tank Stirrers	2	$ 2,055.00	$4,110.00
22	Roller Stairs	1	$ 702.24	$702.24
23	Roaster	1	$ 30,000.00	$30,000.00
24	Kinematic Mill	1	$ 31,750.00	$31,750.00
Total Equipment Cost				**$777,742**

Table 3.2.2 Virginia Tech equipment list and order status.

	Qty	Unit Cost	Total Cost
Process Train 1 - Preconcentration			
Product Conveyor	2	$ 4,500	$ 9,000
Reject Conveyor	2	$ 4,500	$ 9,000
Skid Steer Loader	1	$ 8,500	$ 8,500
Skid Steer Forks	1	$ 500	$ 500
Sorter/Screen Framing	1	$ 1,000	$ 1,000
Skidsteer Barrel Handler			$ -
Transformer	1	$ 1,000	$ 1,000
Trailers	2	$ 10,000	$ 20,000
Air Accumulator	1	$ -	$ -
Air Compressor	1	$ 17,800	$ 17,800
Modified Cargo Container/Ctrl Room	1	$ 8,470	$ 8,470
Process Train 2 - Size Reduction			
Jaw Crusher			$ -
Jaw Crusher Feeder			$ -
Cone Crusher Feeder Controller	1	$ 261	$ 261
Jaw Crusher Frame	1	$ 1,700	$ 1,700
Jaw Crusher Hopper	1		$ -
Cone Crusher			$ -
Cone Crusher Feeder			$ -
Cone Crusher Feeder Controller	1	$ 261	$ 261
Cone Crusher Hopper	1	$ -	$ -
Ball Mill Feed Hopper	1	$ 1,000	$ 1,000
Ball Mill Sieve Screen			$ -
Ball Mill			$ -
Ball Mill Sand Pump			$ -
Vibrating Feeder			$ -
Micronizer Feed Moyno Pump			$ -
Micronizer Feed Tank	1	$ 654	$ 654
Micronizer Feed Tank Agitator	1	$ 2,360	$ 2,360
Micronizer Mill	1	$ 77,720	$ 77,720
Micronizer Frame	1	$ 1,000	$ 1,000
Product Sand Pump			$ -
Feed Holding Tank			$ -
Feed Holding Tank Moyno Pump	1	$ 1,755	$ 1,755
Feed Holding Tank Agitator	1	$ 2,360	$ 2,360
Fork Lift + Barrel Handler			
Process Train 3 - Physical Separation			
Flotation 1 Feed Tank	1	$ 310	$ 310
Flotation 1 Feed Tank Mixer			$ -
Flotation 1 Feed Tank Pump	1	$ 1,138	$ 1,138
Flotation 1 Column Pipe			$ -
Flotation 1 Column Launder Pipe			$ -
Flotation 1 Column Frame	1	$ 1,000	$ 1,000
Flotation 1 Disk Filter			$ -
Flotation 1 Disk Filtrate Pump	1	$ 2,709	$ 2,709
Flotation 1 Nash Vacuum Pump	1	$ 2,415	$ 2,415
Flotation 1 Level probes for disk filter	2	$ 525	$ 1,050
Flotation 1 1 " Automatic Ball valve	2	$ 427	$ 854
Flotation 1 Valve and motor controls	1	$ 500	$ 500
Flotaiton 1 Thickener	1	$ 24,600	$ 24,600
Flotation 1 Weir Tank	1	$ 654	$ 654
Flotation 1 Thickener UF Pump	1	$ 1,755	$ 1,755
Flotation 1 Thickener Overflow Tank	1	$ 266	$ 266
Flotation 1 Thickener Overflow Tank Stand	1	$ 519	$ 519

Flotation 1 Thickener Water Pump			$ -
Flotation 2 Feed Tank	1	$ 310	$ 310
Flotation 2 Feed Tank Mixer	1	$ 2,360	$ 2,360
Flotation 2 Feed Tank Pump	1	$ 1,138	$ 1,138
Flotation 2 Column Pipe	1	$ 800	$ 800
Flotation 2 Column Launder Pipe	1	$ 1,141	$ 1,141
Flotation 2 Column Frame	1	$ 1,000	$ 1,000
Flotation 2 Sparger Pump	1	$ 1,138	$ 1,138
Flotation 2 Thickener	1	$ 24,600	$ 24,600
Flotation 2 Weir Tank	1	$ 654	$ 654
Flotation 2 Thickener UF Pump	1	$ 1,755	$ 1,755
Flotation 2 Thickener Overflow Tank	1	$ 266	$ 266
Flotation 2 Thickener Overflow Tank Stand	1	$ 519	$ 519
Flotation 2 Thickener Water Pump	1	$ 1,138	$ 1,138
Flotation 2 Pressure Filter	1	$ 29,400	$ 29,400
Flotation 2 Pressure Filter Product Tank	1	$ 157	$ 157
Flotation 2 Pressure Filter Product Tank Stand	1	$ 119	$ 119
Flotation 2 Screw Conveyor, w/ hopper	1	$ 26,733	$ 26,733
Continuous weigh feeder	1	$ 12,457	$ 12,457
Process Train 7 - HHS			
1. Agglomeration Module			
Feed Pump	1	$ 1,755	$ 1,755
Pentane Feed pump	1	$ 3,000	$ 3,000
Silverson	1		$ -
High shear tank	1		$ -
Low shear motor	1	$ 2,200	$ 2,200
Low shear tank	1		$ -
Primary Float Phase Sep. (2 cell)	1		$ -
2. Morganizer/Filter			
Extraction Column	1		$ -
Filter Feed Pump	1	$ 1,013	$ 1,013
Filter Feed Pump Explosion Proof Motor	1	$ 832	$ 832
Pentane Recycle Pump	1	$ 3,000	$ 3,000
Drum Filter	1		$ -
Rotary filter dischage valve system	1		$ -
Vacuum pump	1		$ -
3. Dryer/Evaporator			
Holoflight Dryer	1		$ -
Holoflight dryer motor	1	$ 832	$ 832
Condenser	1		$ -
Dryer discharge system	1		$ -
Product screw Conveyor	1	$ 12,457	$ 12,457
Coal Discharge Condenser	1	$ 700	$ 700
4. Secondary Recovery			
Secondary Float cells (2 cell)	1		$ -
Tailings Pump	1	$ 6,987	$ 6,987
Tailings Sump	1	$ 83	$ 83
Tailings Sump Stand	1	$ 228	$ 228
Secondary cell condensor	1	$ 700	$ 700
Secondary Cell OF pump	1		$ -
5. Other/Utilities			
Solvent Tank	1		$ -
Oil Heater	1	$ 8,343	$ 8,343
Chiller	1	$ 22,000	$ 22,000
Nitrogen Generator	1		$ -
Air Compressor	1	$ 1,975	$ 1,975
Trailer	1	$ 10,000	$ 10,000
Control Room	1	$ 8,470	$ 8,470
Conspec Gas monitor	1		$ -

100' 1.5" rubber hose	1	$ 616	$ 616
1.5" ball valve	1	$ 118	$ 118
1.5" pinch valve	1	$ 225	$ 225
Lightnin mixer	1	$ 3,700	$ 3,700
Feed pump flowmeter	1	$ 1,260	$ 1,260
Diaphragm pump	2	$ 543	$ 1,086
Conductivity sensor	5	$ 860	$ 4,300
Primary agglomerate level probes	4	$ 520	$ 2,080
Ultrasonic level probe	1	$ 1,505	$ 1,505
Rotary valve that will handle cake	1	$ 3,500	$ 3,500
Rotary valve that will handle dry coal	1	$ 3,500	$ 3,500
Explosion proof vacuum pump for drum filter	1	$ 2,526	$ 2,526
Filter Feed Tank level probe	1	$ 1,055	$ 1,055
Flowmeter (0.05 - 0.15 GPM)	1	$ 1,640	$ 1,640
Flowmeter (1 - 5 GPM)	1	$ 2,345	$ 2,345
Miscellaneous			
Technical Assistance (Design, fabrication, programming, etc for Control and automation)	1	$ 40,000	$ 40,000
Automation and control (details below)	1	$ 44,167	$ 44,167
Total			
			$ 505,998

3.2.6 Fabrication & Construction

The majority of the fabrication and construction work performed is highlighted below.

- The construction of the Process Train 1.0 - The x-ray sorter unit supplied by Mineral Separation Technologies (MST) as a cost-sharing commitment to this project was placed on the mobile trailer platform along with other ancillary equipment (feed bin, feed conveyor, transfer conveyor, gas compressor, x-ray chiller, stepdown transformer, electronic controls, etc.) necessary to accommodate remote field operations and comply with MSHA regulations at the mine site.

- Fabrication of the components incorporated into Process Train 2.0 – Size Reduction and Liberation. Components specifically fabricated for this process module included support structures and storage bins for the required jaw and cone crushers, a feed hopper for the primary ball/grinding mill, and a fine-wire sieve screen for product sizing from the ball mill. Electrical control panels for each of the equipment components were also constructed prior to shipping for ease of field installation.

- Fabrication, construction, and refurbishment for the components required by Process Train 3.0 – Physical Separation. This work largely focused on mechanical and electrical upgrades to the decarbonization column flotation unit and coal product disc filtration system. In addition, a second column flotation unit for de-alkalinization of the underflow from the decarbonization step was also constructed as part of this effort.

- The hydrometallurgical equipment required by the project was purchased from SX Kinetics as completed assemblies that required on minor fabrication to be placed into service. For Process Train 4.0 - Acid Leaching, this work involved the fabrication of several sets of support stands that were necessary to accommodate the gravity flow of slurry though the

primary and secondary leach tanks. For Process Train 5.0, Solvent Extraction & Precipitation, no fabrication was required other than field mounting of the process module.

- Fabrication and construction work associated with Process Train 7.0 – REM Concentration was continued during this reporting period. Specific work involved refurbishment of existing process components and layout of operations for trailer mounting as a mobile test unit. Biweekly meetings with personnel from Minerals Refining Company (MRC) were held throughout the project to review progress in retrofitting their proof-of-concept (POC) plant with newer components necessary for feedstock decarbonization and REM concentration. The POC equipment was supplied by MRC at no cost to the project team as a cost-sharing contribution for the project.

3.2.7 Installation & Assembly

During this reporting period, all of the process trains required to pulverize (crush, grind, micronize and size), separate (decarbonize and dealkilize), dewater (thicken and clarify), extract (acid leach) and selectively concentrate (solvent extract and precipitate) coal-sourced feedstocks of REEs were assembled and installed at the Dotiki test site. This work included the installation of the following process trains:

- 2.00 – Size Reduction/Liberation
- 3.00 – Physical Separation
- 4.00 – Acid Leaching
- 5.00 – Solvent Extraction & Precipitation
- 6.00 – Chemical Storage
- 7.00 – HHS Mobile Unit

The primary unit operations required to place the REE pilot-plant into production mode were successfully installed by Summer 2018. Photographs of each of the key process trains are included in Figure 3.2.25 to Figure 3.2.28.

Figure 3.2.25 Photograph of Process Train 2.00 – Size Reduction & Liberation as installed at the Dotiki pilot plant test site in western Kentucky. The train includes (left to right) jaw crusher module, cone crusher module, primary ball mill/sieve screen, and micronizer.

Figure 3.2.26 Photograph of Process Train 3.00 – Physical Separation as installed at the Dotiki pilot plant test site in western Kentucky. The train includes (left to right) decarbonization flotation column, coal product disc filter, decarbonization thickener, dealkalinization flotation column, dealkalinization thickener, and filter press.

Figure 3.2.27 Photograph of Process Train 4.00 – Acid Leaching as installed at the Dotiki pilot plant test site in western Kentucky. The train includes primary leach tanks and thickener (rear) and secondary leach tanks and thickener (front).

Figure 3.2.28 Photograph of Process Train 5.00 – Solvent Extraction & Precipitation as installed at the Dotiki pilot plant test site in western Kentucky. The train includes eight individual mixer-settler tanks along the length of the processing unit.

The initial fabrication and construction work for the HHS mobile unit focused on the disassembly of an older process unit and the reassembly of the processing units onto a mobile trailer. Figure 3.2.29 shows the former unit, while Figure 3.2.30 shows the partially completed reassembly on the new mobile platform.

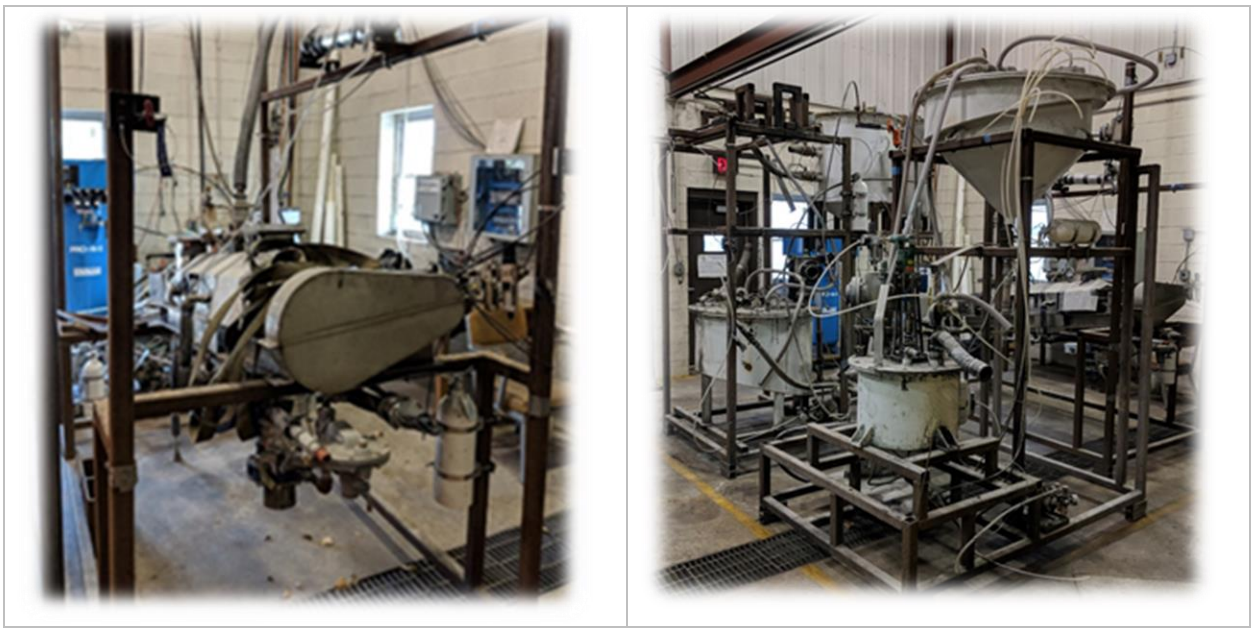

Figure 3.2.29. Equipment from older proof of concept HHS process.

Figure 3.2.30. Mobile HHS process under construction.

After mounting the main processing units, the building was framed using metal framing channels (unistrut) and plywood was used to construct the walls. Finally, metal roofing sheets were used to enclose the building (Figure 3.2.31).

Figure 3.2.31. Construction of the building that is housing the non-explosion proof equipment.

Personnel from Virginia Tech Environmental Health and Safety (EHS) that have experience in dealing with volatile hydrocarbons assisted the project team with designing a fire-resistant wall that would separate the processing area from the building. The wall was constructed based on the design given in Figure 3.2.32.

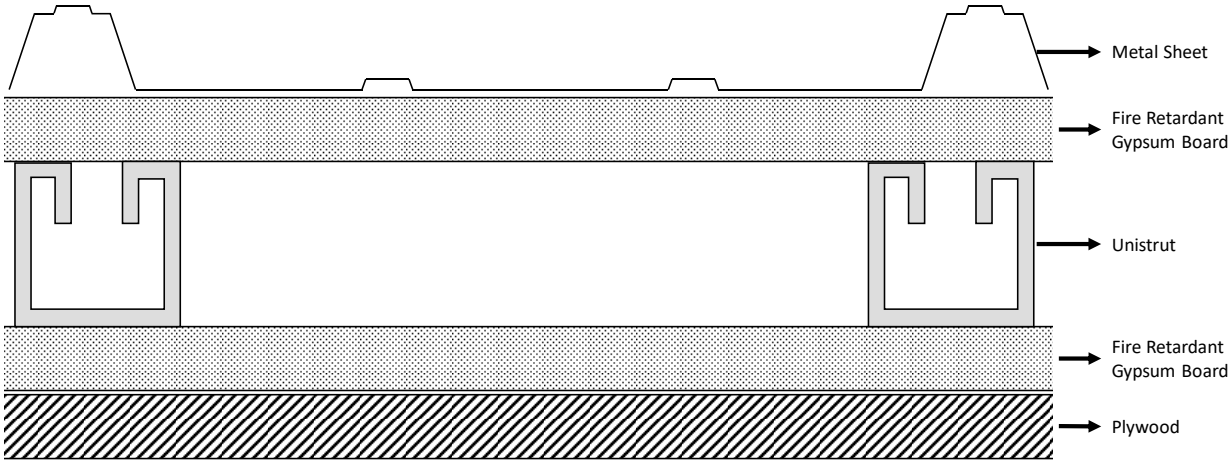

Figure 3.2.32. Fire-resistant wall design

The final assembly drawings for the mobile HHS process are shown in Figure 3.2.33 and Figure 3.2.34. As indicated, the plant can be delineated into two segments: a feed side and a product site. Based on the electrical limitations at the host facility, these segments were operated independently; however, the data can be combined to accurately depict a single process run.

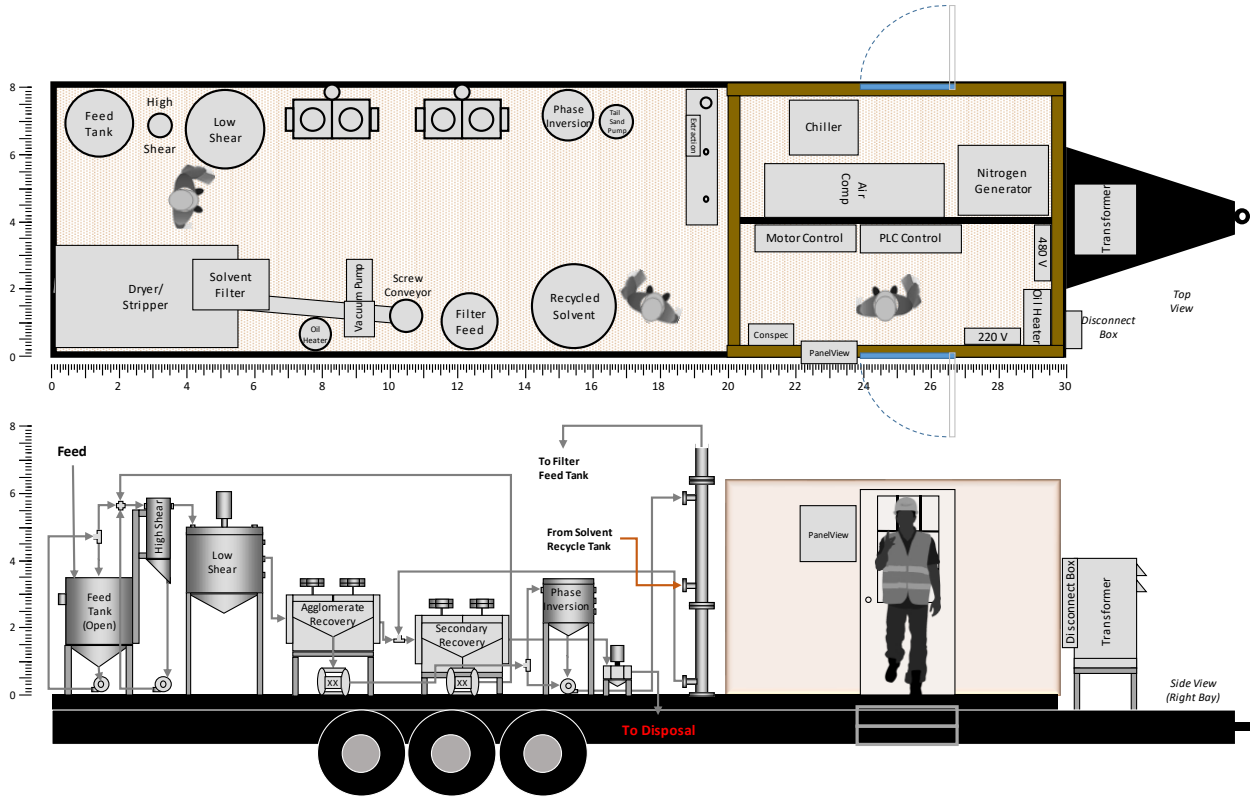

Figure 3.2.33. Feed side of the HHS process

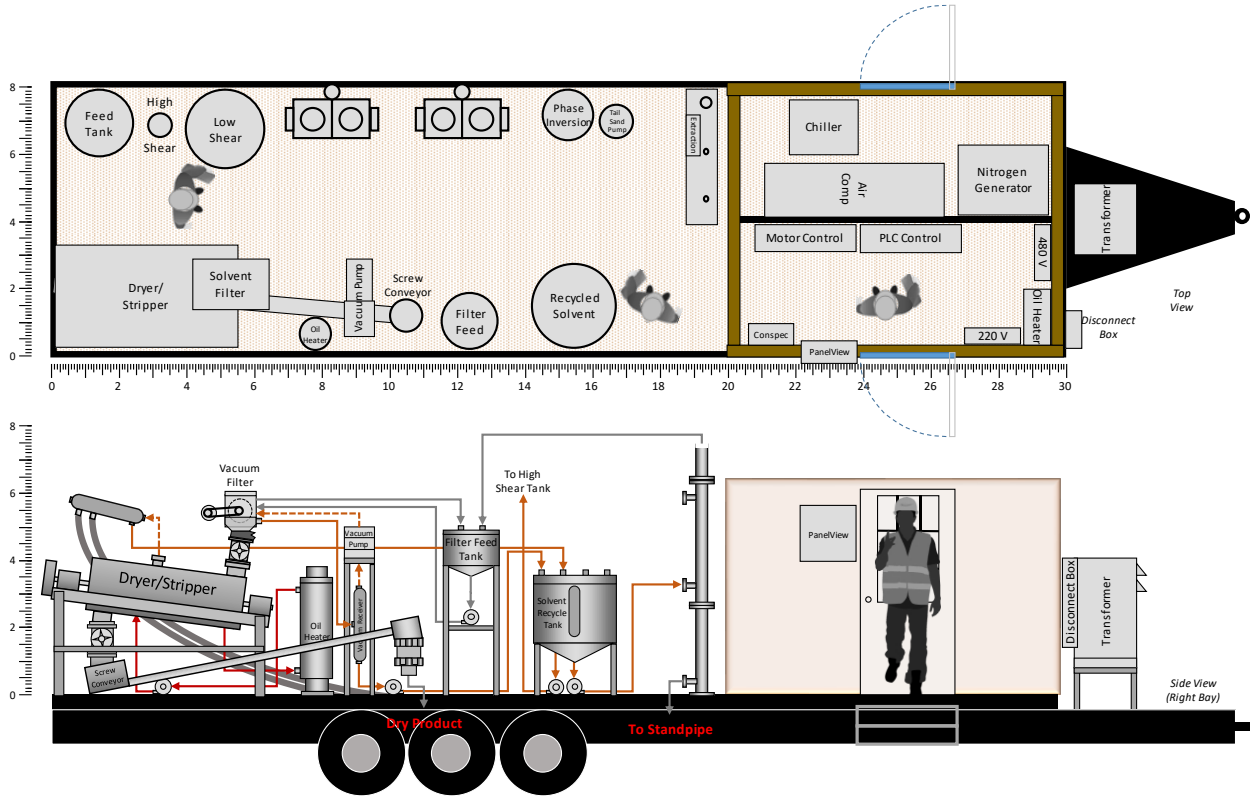

Figure 3.2.34. Product side of HHS Process

3.2.8 Systems Safety Analysis & Training

A *Safety Management Plan* was submitted on June 15, 2018 that details personnel training, task training and the operational management system employed to protect the safety of personnel and visitors at the pilot plant. A copy of the *Health, Safety & Environmental Plan* is attached to this report as Appendix B. All personnel involved with the on-site installation and operation of the REE pilot plant were required to attend and successfully complete formal health and safety training mandated by the federal Mining Safety and Health Administration (MSHA). Experienced personnel who participated in previous MSHA programs were required to successfully complete the 8-hour MSHA Part 46 Refresher course, while new employees without previous MSHA training were required to complete the 24-hour Part 46 New Miner course. In addition, a Safety Officer was designated by the project team to review and monitor safety protocols during all installation activities. This person was also responsible for posting safety signage throughout the facility to highlight potential health and safety notices, such as chemical hazard dangers.

3.2.9 Startup & Shakedown

System startup and shakedown activities were performed successfully upon the completion of installation activities at the Dotiki test site. The initial runs were performed (i) to evaluate the electrical and mechanical integrity of the installed circuitry and (ii) to ensure that pumping capacities, pipe sizes, electrical supplies, control systems, instrumentation, etc., were adequate for "water-only" test runs. No major operational issues were identified during the startup and shakedown tests. Closely monitored commissioning activities were carried out as a means of ensuring that all parties are familiar with standard operating and emergency shutdown procedures for the pilot plant facility. In addition, as part of the shakedown work, a revised *System Testing, Operation and Sampling/Analysis Plan* was submitted. A copy of this plan is attached to this report as Appendix C.

3.3 Environmental Monitoring & Management (PB3-Task2)

3.3.1 Materials and Sample Preparation

To conduct a detailed assessment of environmental controls that identifies and quantifies the potential impacts of the pilot-scale processing circuitry on the human and eco-system health and well-being, and provide corresponding mitigation strategies and control measures, laboratory testing was first initiated at the Mineral Processing Laboratories at WVU. To reduce the dependence on the feedstock samples generated at the pilot-scale facilities and improve the testing flexibility, synthetic solutions were prepared following the elemental composition of the strip solution produced at the pilot-scale plant resulting from acid leaching coarse coal refuses. The synthetic solution was prepared freshly before each test to avoid any sudden compositional change which may occur over time. Standard Inductively Coupled Plasma (ICP) solutions with 1000 mg/L of rare earths, thorium, uranium was purchased from Ricca Chemical, separately, while respective metal chlorides with a grade higher than 99% were purchased from Alfa Aesar. 6 mol/L hydrochloric acid was used as the acid medium throughout the synthetic feedstock preparation.

Various alkaline salts (i.e., sodium hydroxide (NaOH), potassium hydroxide (KOH), ammonia hydroxide (NH4OH)) were purchased from Merck and Fisher Scientific for selective precipitation tests. Hydrochloric acid (HCl) and sodium hydroxide with annular grade were used throughout the study for pH adjustment. The Oakton 450 pH meter was used to measure the solution pH which was calibrated using pH 4, 7, and 10 buffer solutions purchased from Ricca Chemical. Tri-butyl phosphate (TBP) and kerosene were purchased from Fisher Scientific and Sigma Aldrich, respectively, and used as extractant and diluent for the purpose of solvent extraction tests. Adsorption studies were performed as well during which zeolite samples with different particle sizes were purchased from both KMI Zeolite Inc. and Heiltropfen Lab LLP.

Deionized water was used at all stages of the study and all experiments were performed at room temperature unless otherwise noted. During each experiment, representative samples taken from the aqueous and solid samples that were generated from various stages were subjected to the rare earth element and major metal analyses using Inductively Coupled Plasma-Optical Emission Spectroscopy (ICP-OES), and thorium and uranium analysis using Inductively Coupled Plasma-Mass Spectroscopy (ICP-MS). ICP techniques were used due to their ability to detect trace elements with low detection limits and high sensitivity. While ICP-MS analyses were provided by West Virginia University National Research Center for Coal and Energy (WVU NRCCE), ICP-OES analyses were provided by the University of Kentucky. Except for X-ray fluorescence, particle size distribution, Brunauer–Emmett–Teller (BET) nitrogen adsorption analyses, and all other characterization testing was performed at WVU Shared Research Facility.

The elemental composition of the synthetic feedstock is provided in Table 3.3.1. As seen, the concentration of total REEs in the leachate is approximately 37 mg/L while the concentration of Th and U is 0.5 and 0.9 mg/L, separately. The content of major metals (i.e., Al, Ca, Fe, K, and Mg) is around 73.7 mg/L.

Table 3.3.1 Elemental composition of synthetic feedstock solution.

Element	Sc	Y	La	Ce	Pr	Nd	Sm	Eu
Concentration (mg/L)	0.00	3.09	1.91	14.47	1.90	9.03	2.67	0.47
Element	Gd	Tb	Dy	Ho	Er	Tm	Yb	Lu
Concentration (mg/L)	2.01	0.10	0.82	0.09	0.33	0.00	0.14	0.01
Element	Th	U	Al	Ca	Fe	K	Mg	
Concentration (mg/L)	0.50	0.86	1.99	55.20	12.85	0.82	2.86	

3.3.2 Experimental and Results

3.3.2.1 Exploratory Selective Precipitation Tests

To assess the potential of using different separation techniques to remove thorium and uranium from rare earth elements, several preliminary studies were performed. Selective precipitation tests were first conducted, which aimed to selectively precipitate out thorium, uranium, and REEs according to their distinctive precipitation behaviors at different pH values. Selective precipitation of elements by controlled pH is the most well-known method for the removal of certain elements from impure leach liquors. Besides, it is a simple and cost-effective operation (Monhemius, 1977; Zhou et al., 2018). The underlying mechanism of precipitation is reacting chemicals with ions to generate insoluble complexes which, then, can be separated from aqueous solutions by filtration (Hostetler and Garrels, 1962; Zhou et al., 2018).

A 200-ml feedstock solution with an initial pH value of less than zero was used for the experimental testing. 2 mol/L sodium hydroxide (NaOH), potassium hydroxide (KOH), and ammonium hydroxide (NH_4OH) were used to incrementally increase the pH, respectively. The pH value was elevated gradually by adding alkaline solution in a stepwise manner followed by three-min conditioning using a mechanical stirrer, and each addition of alkaline salt was monitored carefully to prevent sudden increments (Figure 3.3.1A). When significant precipitation was visually observed, the test was paused, and the solution was subjected to settling for enough time and subsequent filtration using 0.45μm pore-sized filter paper (Figure 3.3.1B). Afterward, precipitated solids were dried and weighed. A detailed flowsheet governing selective precipitation tests is shown in Figure 3.3.2.

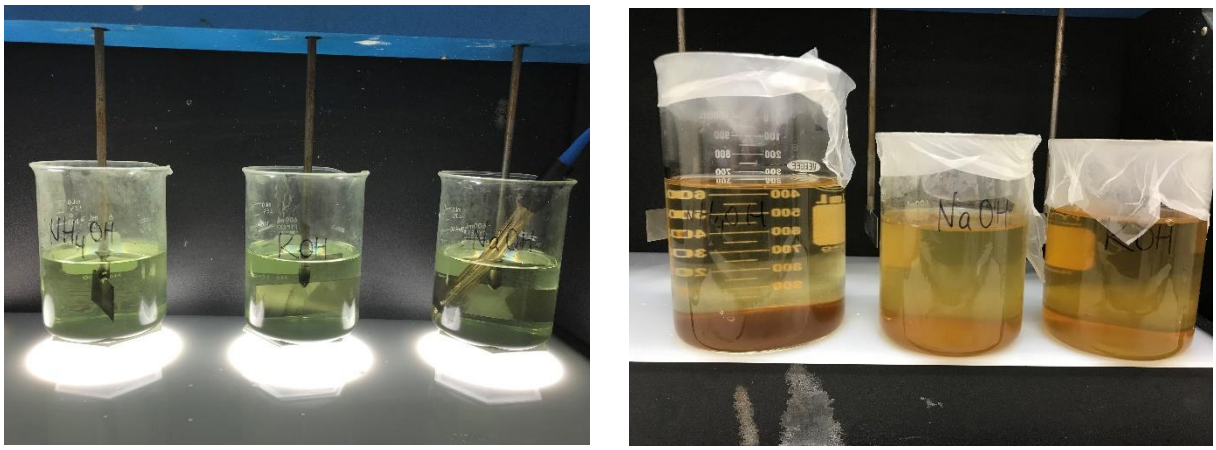

(A) (B)

Figure 3.3.1 Pictures illustrating the experimental procedures of selective precipitation tests. (A) pH measurement, (B) Settling after precipitation.

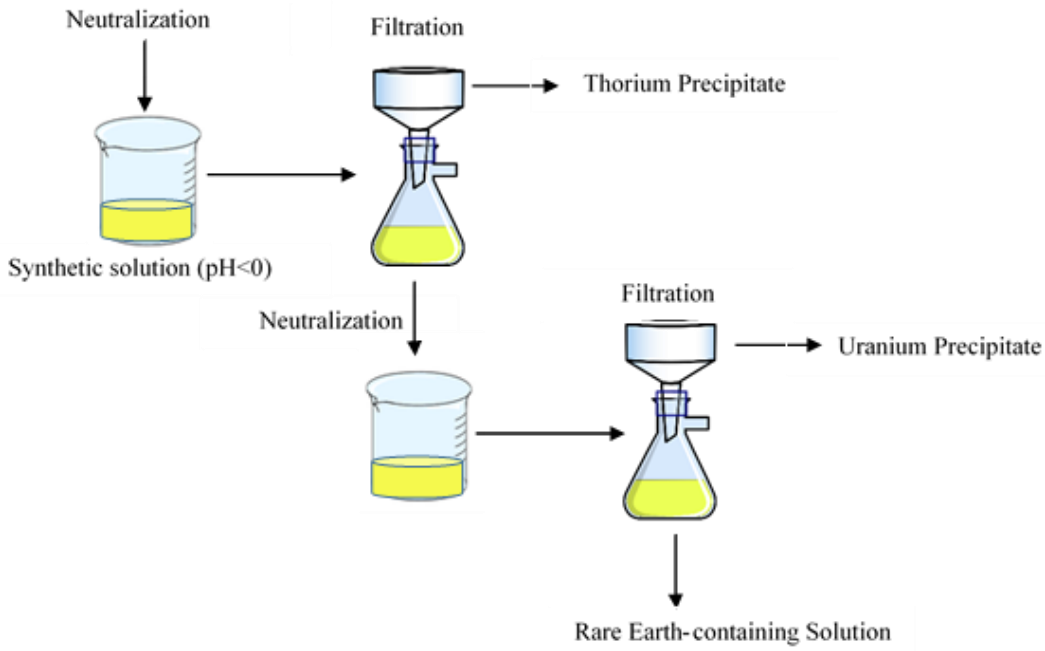

Figure 3.3.2 Experimental flowsheet followed during selective precipitation tests.

The initial precipitation data resulting from the addition of the three alkaline salts is shown in Figure 3.3.3. Test results indicate that there was no significant difference observed between various alkaline salts concerning the process separation efficiency. Therefore, the precipitation data obtained from all three pH adjustments were grouped and shown in Figure 3.3.3, and NaOH was chosen to be used for the subsequent experimental testing. It can be seen from Figure 3.3.3 that the first precipitation was observed in a pH range of 4 to 5. Under this condition, over 90% of thorium precipitated out while a small portion of uranium (i.e., 28.7%) and REEs (i.e., 16.3%) co-precipitated with thorium. As indicated in the study of Zhu et al. (2015), thorium's precipitation pH range is 2.5-5.5 which is consistent with the findings presented in this work. Thorium initially existed in the solution as Th^{4+} followed by being converted to thorium hydroxide with an increase in the solution pH. However, thorium hydroxide is unstable by nature and eventually transforms into thorium dioxide (Brookins, 1988). A further increase in the pH to a value of 6.2 resulted in higher thorium and uranium precipitation but also a significant amount of REEs' co-precipitation, which was approximately 34%. The observed phenomena can be attributed to the fact that the precipitation pH range of uranium (i.e., 5.5-7) and rare earths (i.e., 6.8-8.0) overlaps to some degree which leads to the co-precipitation of the two (Zhu et al., 2015). Detailed results for individual rare earth elements, thorium and uranium precipitation, and their concentrations in the filtrates at various pH values are given in the Appendix D.

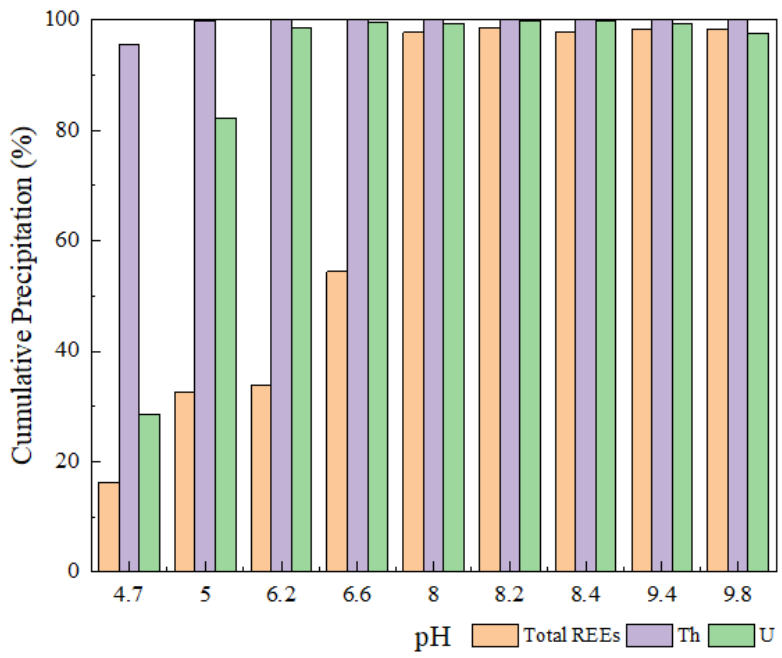

Figure 3.3.3 Cumulative precipitation of total rare earths, thorium, and uranium at various pH values.

It is known that most rare earths and uranium existed in the synthetic solution as $REEs^{3+}$ and U^{6+} along with Th^{4+} since standard ICP solutions had been used for the feedstock preparation. Chemical reactions governing the precipitation behavior of $REEs^{3+}$, Th^{4+}, and U^{6+} are given below

(Silva et al., 2018). As such, rare earth hydroxide, thorium oxide, and uranyl hydroxide are formed at their respective precipitation pH regions.

$$REEs^{3+}_{(aq)} + 3OH^{-}_{(aq)} = REEs(OH)_3 \quad (1)$$

$$Th^{4+}_{(aq)} + 4OH^{-}_{(aq)} = ThO_2 + 2H_2O \quad (2)$$

$$UO^{2+}_{2(aq)} + 2OH^{-}_{(aq)} = UO_2(OH)_2 \quad (3)$$

The precipitation behavior of total, heavy, light, critical, and uncritical rare earth elements are further examined and presented in Figure 3.3.4. As seen, the precipitation of heavy/light and critical/uncritical REEs was minimal at a pH value of 4.6. It also suggests that the precipitation of heavy REEs was relatively more significant in a pH range of 5 to 8 compared to light, critical, and uncritical REEs in the same pH region. Approximately 100% rare earth precipitation was achieved when the pH was above 8. The same trend and findings were observed in the studies carried out by Ponou et al. (2016) and Honaker et al. (2018) indicating that rare earths precipitation becomes significant when the pH value is beyond 5 and nearly 90% of rare earths precipitation occurs in a pH range of 5 to 10. Therefore, it can be concluded that selective precipitation is effective for the removal of thorium from rare earths and uranium at a pH value of less than 5. However, the fact that a further increase in the pH of the solution led to the co-precipitation of uranium and rare earths indicates an alternative technique ought to be evaluated to fully separate uranium from rare earths.

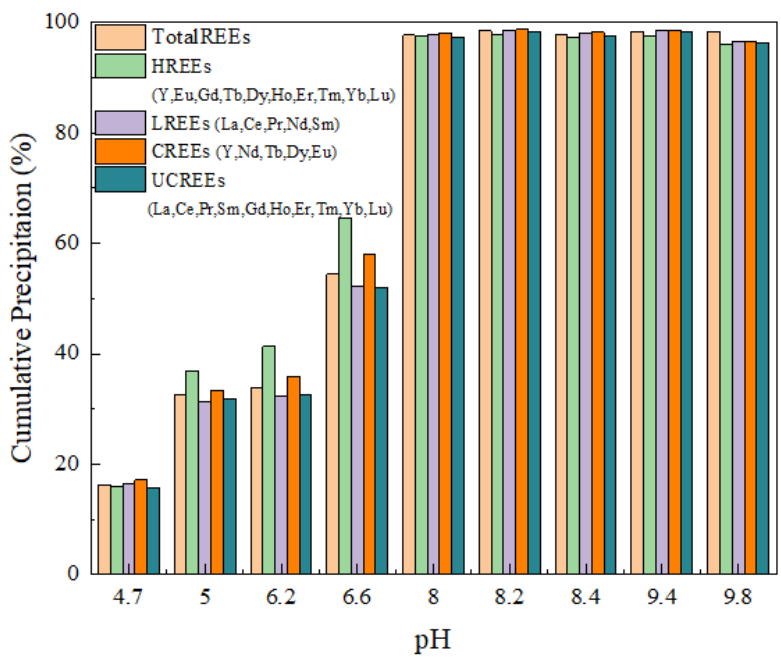

Figure 3.3.4 Cumulative precipitation of total, heavy, light, critical, and uncritical rare earths at various pH values.

3.3.2.2 Exploratory Solvent Extraction Tests

In addition to precipitation, solvent extraction tests were continued to explore its possibility of separating radioactive elements from rare earths. Solvent extraction has been the most extensively used method for purification purposes due to its capability to handle large volumes of aqueous solutions (Asselin et al., 1949; Hidayah and Abidin, 2017). It has been an effective technique to remove hazardous matters from rare earths (Brown and Sherrington, 1979). However, most of the extractants are also effective for the recovery of rare earths. Therefore, it is important to develop an experimental scheme for the desired selectivity and separation efficiency. Tri-butyl phosphate was selected for the study due to its capability to selectively extract thorium and uranium under controlled operating conditions (Palmieri, 1987; Habashi, 1997; Zhang et al., 2016). Two sets of exploratory solvent extraction tests were designed and performed during the study and the corresponding flowsheet is given in Figure 3.3.5.

Each test was conducted with a 50-ml synthetic feedstock solution at an initial pH value of 2.5. As seen from Figure 3.3.5, the solvent extraction test consisted of two parts with the first- and second-part targeting uranium and thorium removal, separately. To initially separate uranium, 5 v% TBP dispersed in a kerosene solution was used as the extracting organic phase. Kerosene was chosen as the diluent to enhance the extraction capability of TBP and also to reduce the emulsification of the extractant (Anitha et al., 2014). Mixing of the organic and aqueous phases was performed using a mechanical stirrer, then, the phases were separated using a separation funnel (Figure 3.3.6). 2 mol/L HNO_3 was used at both the scrubbing and stripping stages. A scrubbing circuit was engaged after the extraction phase to wash impurities from the organic phase before the final purification stage. The aqueous phase obtained from the uranium extraction step was subsequently sent for the thorium extraction and 40 v% TBP was used accordingly. Deionized water was used for the thorium stripping. Both sets of the solvent extraction tests were conducted under the same conditions except the number of stages applied to extraction, scrubbing, and stripping. For the first set of exploratory tests, each unit process (extraction, scrubbing, stripping) was conducted as a single-stage, while two stages were conducted for each of the aforementioned processes during the second set of tests. Test results obtained were used to compare the separation efficiencies resulting from various stages of extraction, scrubbing, and stripping. Detailed operating procedures for the exploratory solvent extraction tests are summarized in Table 3.3.2.

Table 3.3.2 Operating conditions for exploratory solvent extraction tests.

	Uranium Separation	Thorium Separation
pH	2.5	2.5
Extractant (v/v)	5% TBP	40% TBP
Scrubbing agent	2 M HNO_3	-
Stripping agent	2 M HNO_3	DI water
O/A ratio at	1:1	2:1
O/A ratio at	5:1	-
O/A ratio at stripping	2:1	2:1
Retention time (min)	20	20

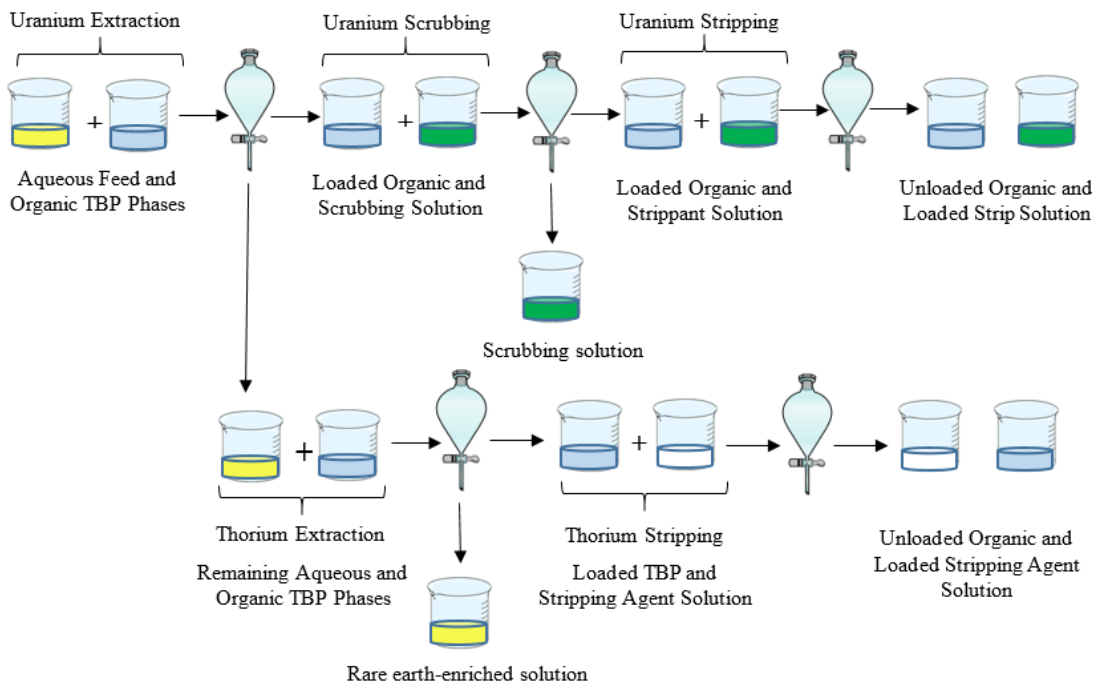

Figure 3.3.5 Experimental flowsheet followed during exploratory solvent extraction tests.

Figure 3.3.6 Separation between aqueous and organic phases during solvent extraction tests.

REE-enriched product, organic, and effluent streams were produced at the end of each set of solvent extraction tests. The content of individual rare earth, thorium, and uranium in the rare earth product stream for both the one-stage and two-stage process is provided in Table 3.3.3.

The results shown in Figure 3.3.7 indicate that approximately 97% of REEs and 94% of thorium were recovered into the circuit product stream of the two-stage process. Under the same operational conditions, 43% of uranium was recovered into the circuit product stream. For the one-

stage process, the recovery of rare earth elements, thorium, and uranium into the product stream was 90%, 93%, and 51% separately. Multiple contacts between aqueous and organic solutions may increase the extraction efficiency; however, the organic extractant tends to be lost into the aqueous phase after a long contact between aqueous and organic phases. Regardless of the number of stages conducted for the solvent extraction process (one-stage vs. two stages), the recovery of thorium did not fluctuate much; however, a noticeable difference was observed for the recovery of REEs and uranium. When the number of operating stages for extraction, scrubbing, and stripping was increased from one to two, the recovery of uranium was reduced from an initial value of 51% to 43% while the rare earth element recovery was increased from around 90% to 97%. Therefore, the efficiency of the multi-stage solvent extraction process was indicated as opposed to the single-stage process concerning the exaction of REEs and the removal of uranium.

However, no significant separation of thorium was observed compared to uranium, which may be explained by their distinct extraction behaviors in hydrochloric acid. Qi (2018) studied the extraction mechanism of thorium, uranium, and rare earths in the TBP-HCl system and stated that the order of extraction is $UO_2^{2+} > Th^{4+} > REE^{3+}$. When present with the three ion groups, TBP forms complexes with the ions in the solution according to their distinctive capabilities to bind with the extractant (Rand et al., 2008). The complexation reactions occurring between TBP and the three ion groups (i.e., U, Th, and REE) are given in Eqs. (4)– (6). Similarly, Nasab (2014) observed that the extraction of uranium is more feasible compared to thorium in a chloride medium, which is attributed to the species formed between uranium and hydrochloride that are readily extracted by TBP through forming organic soluble complexes. Another reason is that thorium purification by solvent extraction in nitric acid media is more favorable (Al-Areqi et al., 2014). On the other hand, nitrate is a preferred medium for enhanced extraction of thorium due to an associated increase in the hydration energy of the anions (Nasab, 2014; Lu et al., 2016).

The recovery of individual rare earths into the product stream shown in Figure 3.3.8 indicates that the majority of the elements achieved a recovery above 90% while a relatively lower recovery was noticed for scandium (<90%). The same phenomenon for scandium was also observed in Qi's (2018) study saying that in a high hydrochloric acid medium, the separation factor of scandium is much higher which results in transferring scandium into the organic phase. Moreover, Figure 3.3.9 suggests that no substantial difference was observed for the recovery of HREEs, LREEs, CREEs, and UCREEs for each of the two sets of solvent extraction tests with an improved recovery being obtained for the two-stage process. Detailed results are given in Table 21, Table 22 and Table 23 in the Appendix D.

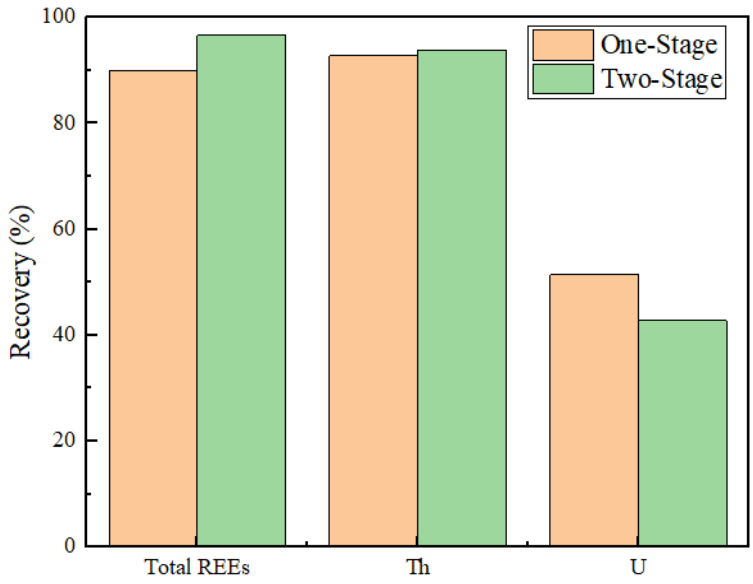

Figure 3.3.7 Recovery of total rare earths, thorium, and uranium into the REE product stream of both the one-stage and two-stage solvent extraction process.

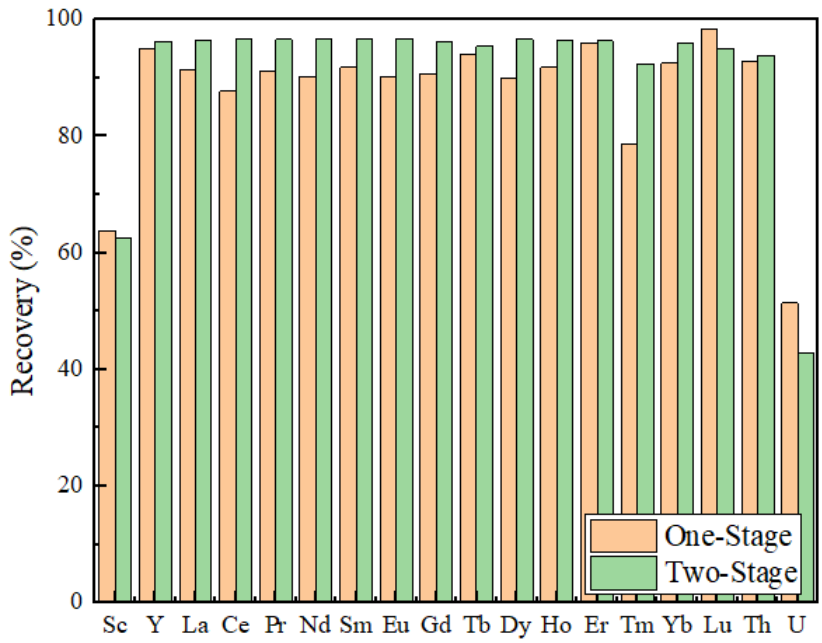

Figure 3.3.8 Recovery of individual rare earth, thorium, and uranium into the REE product stream of both the one-stage and two-stage solvent extraction process.

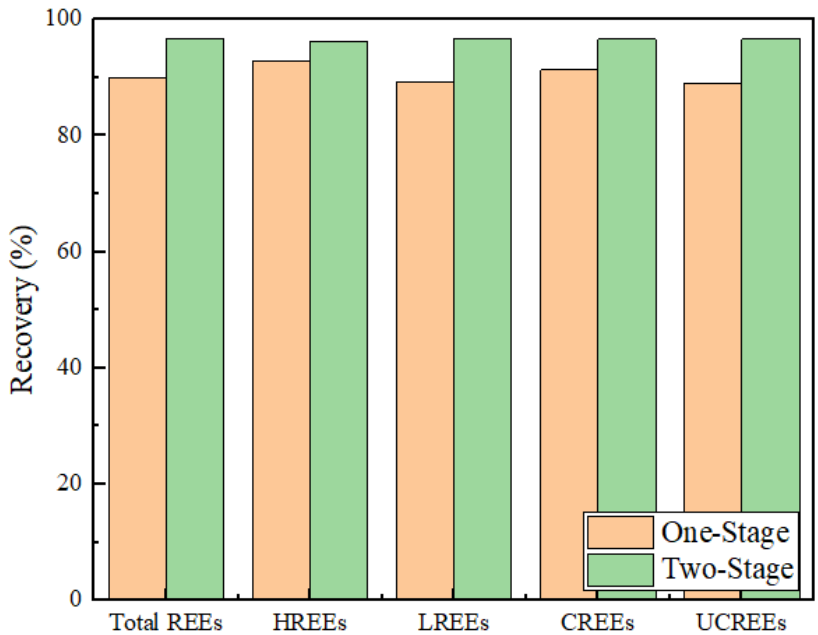

Figure 3.3.9 Recovery of the total, heavy, light, critical, and uncritical REEs from both the one-stage and two-stage solvent extraction process.

Table 3.3.3 Individual rare earth, thorium, and uranium concentrations (ppm) in the rare earth product stream obtained from both the one-stage and two-stage solvent extraction process.

Process	Sc	Y	La	Ce	Pr	Nd	Sm	Eu	Gd
One-Stage	0.00	1.49	0.85	6.17	0.84	3.95	1.18	0.20	0.88
Two-Stage	0.00	1.62	0.94	7.16	0.96	4.42	1.34	0.24	1.04

Process	Tb	Dy	Ho	Er	Tm	Yb	Lu	Th	U
One-Stage	0.04	0.36	0.04	0.156	0.00	0.06	0.01	0.21	0.20
Two-Stage	0.05	0.43	0.05	0.19	0.00	0.08	0.01	0.26	0.09

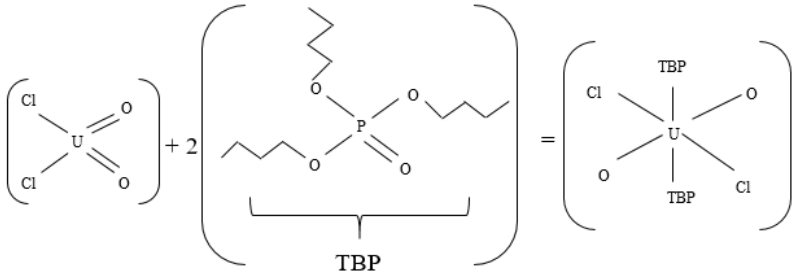

(4)

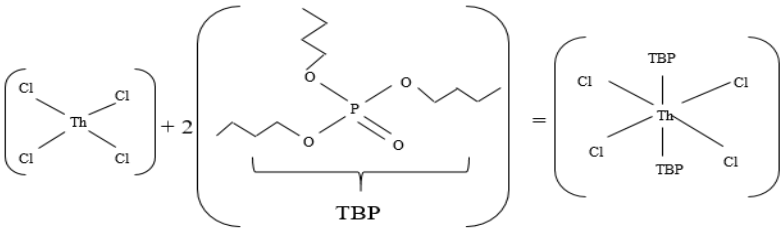

(5)

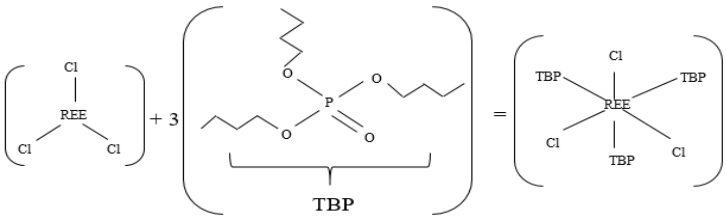

(6)

In addition, 2 mol/L HNO_3 was used as the scrubbing reagent to remove entrained REEs and Th from the U-laden organic phase following the reactions given in Eqs. (7) and (8). Afterward, DI water and 2 mol/L HNO_3 were applied as the stripping reagent for Th and U, separately, and the corresponding equations governing the complexation reactions are shown in Eqs. (9) and (10).

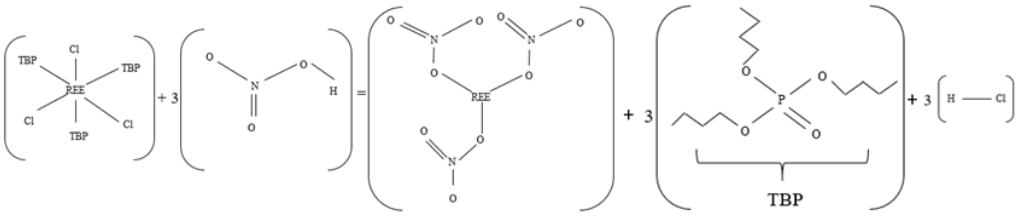

(7)

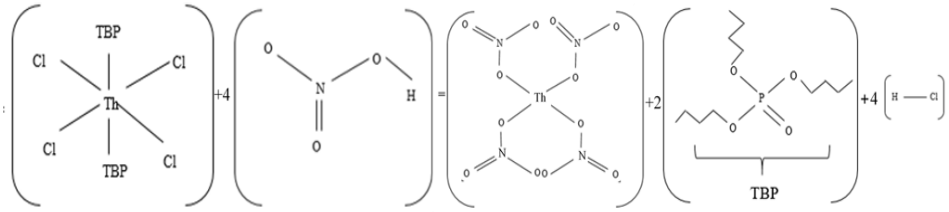

(8)

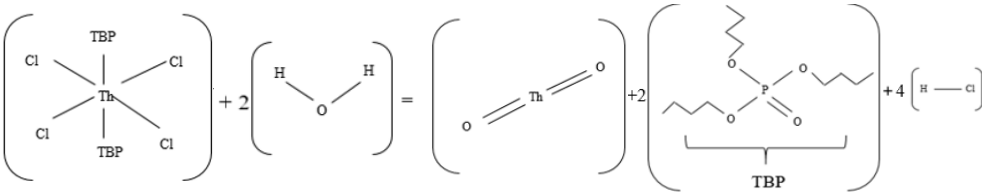

(9)

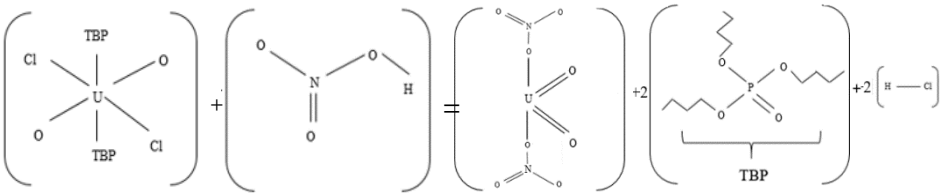

(10)

3.3.2.3 Modified Experimental Protocol

As seen from the results presented earlier, selective precipitation successfully precipitated out thorium, while solvent extraction was noticeably more effective in removing uranium from rare earth elements. Therefore, a modified experimental protocol consisting of one-stage precipitation and two-stage solvent extraction was developed, the procedure of which was strictly followed for improved separation of the radioactive elements from rare earth elements (Figure 3.3.10).

A 2 mol/L sodium hydroxide solution was used to gradually increase the pH to a value of around 4.85 that corresponded to a region under which solid precipitation was first observed. The tests were designed in a manner that precipitation aimed to selectively precipitate out thorium while the remaining filtrate loaded with uranium and rare earth elements were used as the feedstock for subsequent solvent extraction. Each solvent extraction test was performed with a 100-ml filtrate solution obtained from prior selective precipitation. Extraction and stripping were both carried out in two stages. Also, various parameters, such as the concentration of extractant, feed solution pH, organic to aqueous ratio (O/A), and type and concentration of strippant were evaluated to optimize the solvent extraction stage. At the end of each solvent extraction test, both REE-enriched (aqueous phase 2 in Figure 3.3.10) and uranium-enriched (aqueous phase 3 & 4 in Figure 3.3.10) streams were produced, and representative aqueous samples were taken from each step for rare earth, thorium, and uranium analysis using both ICP-MS and ICP-OES.

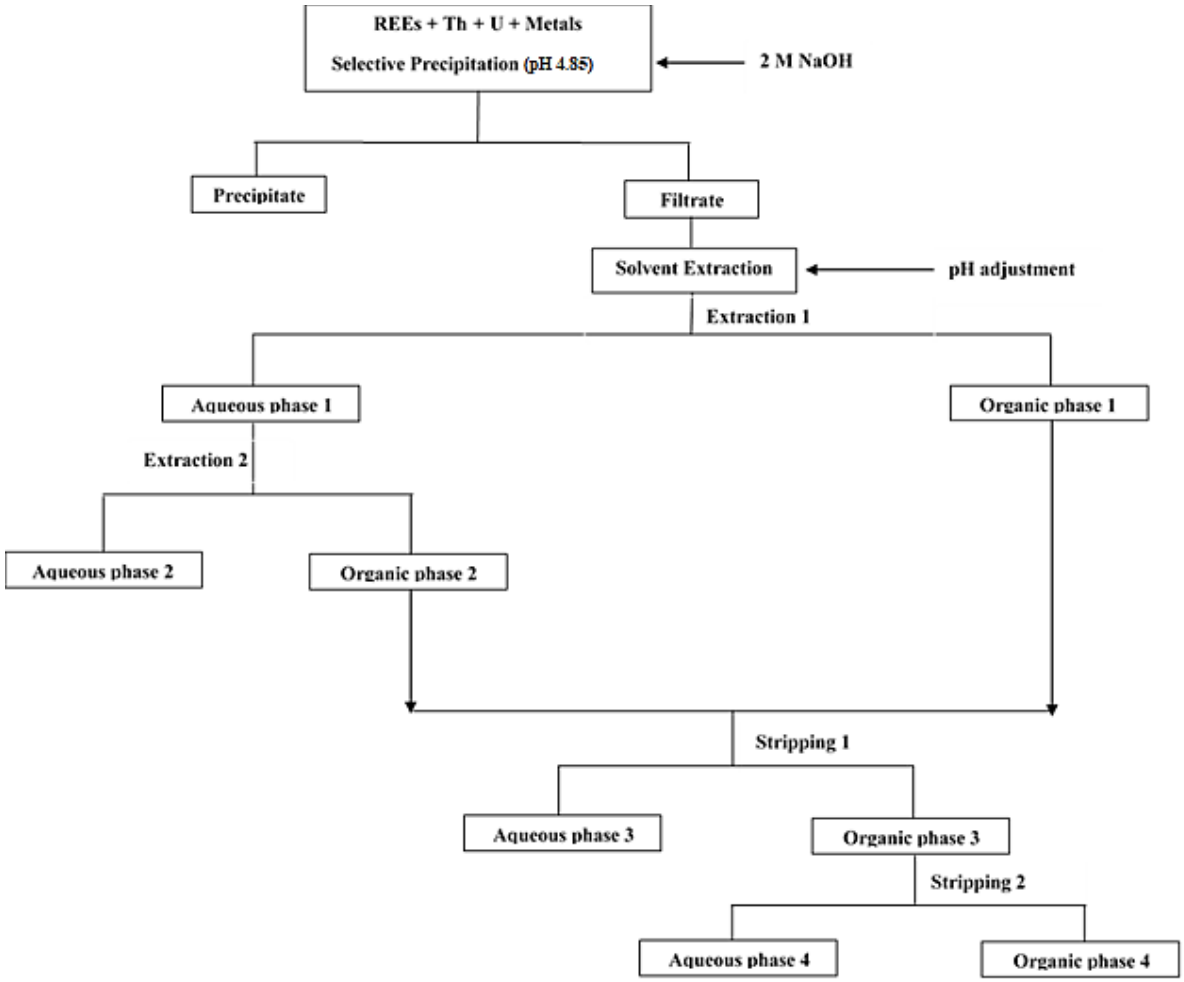

Figure 3.3.10 A modified experimental protocol developed for enhanced separation of thorium, uranium, and rare earth elements.

vii. <u>One-Stage Precipitation</u>

Individual REE content, as well as the concentration of thorium and uranium of the filtrate obtained at the precipitation pH of 4.85, are shown in Table 3.3.4. All the data reported are the average of three replicate selective precipitation tests. It can be seen from Table 3.3.4 that thorium present in the feedstock solution all precipitated out as solids and no content was detected in the remaining solution, which further confirms the findings previously discussed in selective precipitation. Besides, the amount of REEs, uranium, and major metals along with thorium precipitated at a pH of 4.85 was shown in Figure 3.3.11.

As seen, 100% of thorium precipitated out while approximately 19.32% of REEs and 47.98% of uranium co-precipitated at the same pH value. A similar result for uranium precipitation was also obtained by Tomazic et al. (1962). Furthermore, nearly 25% of major metals including aluminum, calcium, iron, and magnesium were transformed into solid forms under identical conditions. As for major metals, approximately 65.58% of iron precipitated followed by around 38.51% of

aluminum, 17.12% of calcium, and 14.17% of magnesium. The findings presented here are consistent with prior studies (Ladeira and Goncaves, 2007; Xie et al, 2014; Balintova and Petrilakova, 2011; Paul and Campbell, 2011). It is known that the precipitation of iron in the presence of oxygen starts at a pH value of 3.5, and $Fe(OH)_3$ is formed as a result of iron oxidization (Seo et al., 2017). In the present study, iron had existed in the solution as ferric iron, which was ready to precipitate with an increase in the pH, as seen in Eq. (11). On the other hand, the precipitation of aluminum typically initiates around a pH value of 5 (Balintova and Petrilakova, 2011), which results in the formation of $Al(OH)_3$ in the presence of OH^- ions following Eq. (12). Therefore, a substantially higher amount of iron precipitated out as opposed to aluminum, which also agrees well with the study carried out by Seo et al. (2017). High $Fe(OH)_3$ precipitation may partially contribute to the co-precipitation of rare earths due to its capability of absorbing particles onto the lattice sites of the iron crystals (Silva et al., 2018).

Supplemental information can be derived by further analyzing the rare earth precipitation data, as shown in Figure 3.3.12. It suggests again that heavy REEs tend to preferentially precipitate out compared to light REEs, which leads to a precipitation difference of approximately 4.5 percent. However, this difference is less than one standard deviation, which may not be statistically significant.

Table 3.3.4 Individual rare earth, thorium, and uranium concentration (mg/L) of the filtrate obtained at the pH value of 4.85.

Sc	Y	La	Ce	Pr	Nd	Sm	Eu	Gd	Tb	Dy	Ho	Er	Tm	Yb	Lu	Th	U
0	0.50	0.33	2.55	0.25	1.49	0.67	0.08	0.29	0.03	0.13	0.02	0.06	0.00	0.02	0.00	0.00	0.13

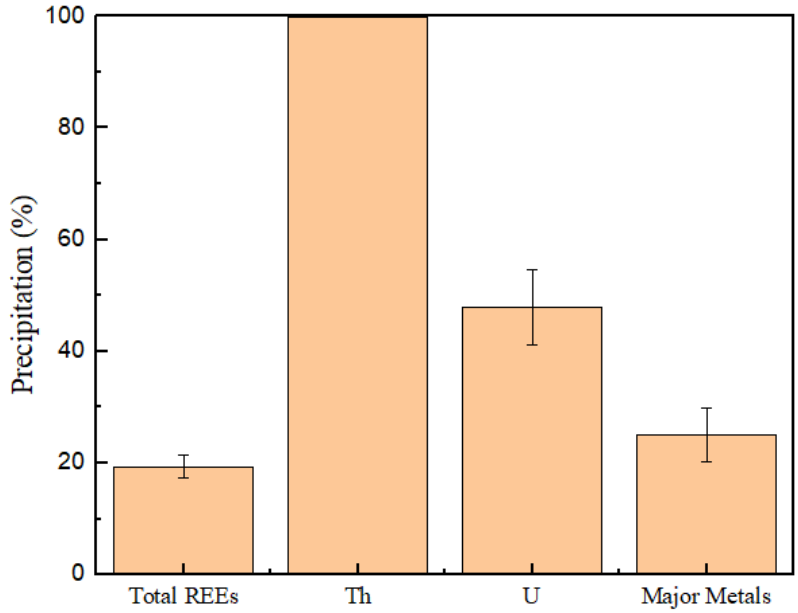

Figure 3.3.11 Precipitation of total REEs, Th, U, and major metals at the pH value of 4.85. Error bars represent one standard deviation of three replicate tests.

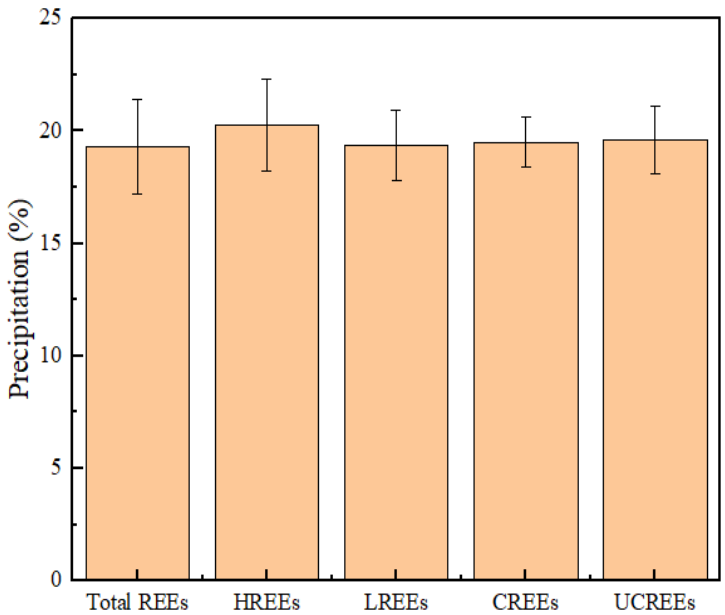

Figure 3.3.12 Precipitation of total, heavy, light, critical, and uncritical rare earths at the pH value of 4.85. Error bars represent one standard deviation of three replicate tests.

$$Fe^{3+}_{(aq)} + 3OH^{-}_{(aq)} = Fe(OH)_3 \quad (11)$$

$$Al^{3+}_{(aq)} + 3OH^{-}_{(aq)} = Al(OH)_3 \quad (12)$$

viii. *Characterization of Solids Generated from Selective Precipitation*

The dry solids produced from selective precipitation tests were subjected to X-ray Diffraction (XRD) and Scanning Electron Microscopy-Energy Dispersive X-ray Spectroscopy (SEM-EDX) analyses. XRD and SEM-EDX analytical techniques were applied to detect the mineralogy, morphology, and elemental compositions of the solid samples. Powdered samples were mounted in cavity mounts and XRD patterns were collected using a Malvern PANalytical X'Pert Pro diffractometer equipped with copper radiation and an X'Celerator parallel plate detector. The samples were scanned at 45 kV, 40 mA over a range of 10-85° two-theta in continuous mode. Evaluation and refinement of the diffraction pattern were carried out using the HighScore software. The Hitachi S4700 Scanning Electron Microscope was used for the SEM-EDX analysis. Prior to analysis, the sample was subjected to sputtering using both Denton Desk V Sputter and Carbon Coater to prevent charging and improve the quality of the image. Accelerating voltage and working distance was kept at 5 kV and 12 mm, respectively, during the analysis. The XRD instrument and the SEM and sample preparation instruments used during the characterization studies are seen in Figure 59 and Figure 60 in Appendix D.

The XRD pattern of the solid sample obtained from the one-stage precipitation is shown in Figure 3.3.13. It can be seen that precipitated solids predominantly consisted of halite (NaCl), which is attributed to the existence of sodium hydroxide and hydrochloric acid that were used to adjust the solution pH values according to various needs. In addition to halite, a relatively small amount of iron oxide was also detected which corroborates the prior finding that approximately 66% of iron

precipitated out from the feedstock solution and was transformed into iron oxide. Elemental identification of the solid sample was provided by SEM-EDX analysis as opposed to the qualitative analysis provided by XRD. As seen in Figure 3.3.14, the highest intensity peaks were observed for the elements of sodium (Na), oxygen (O), and chloride (Cl), which is consistent with the findings obtained from XRD analysis. In addition to the three elements, a portion of rare earth elements and Th were also detected in the EDX spectrum, however, the intensities are considerably low compared to Na, O, and Cl. The carbon peak seen in the EDX spectrum is due to the carbon tape substrate used during sample preparation. Moreover, SEM images presented in Figure 3.3.15 show the rough surfaces of the solid particles. The microscopic pictures observed under high magnifications further indicate that tiny nuclei in nanoscale initially precipitated out and deposited on top of the particles, which acted like the nucleating agents and led to the subsequent growth of the particles in the form of roughly spherical crystallites.

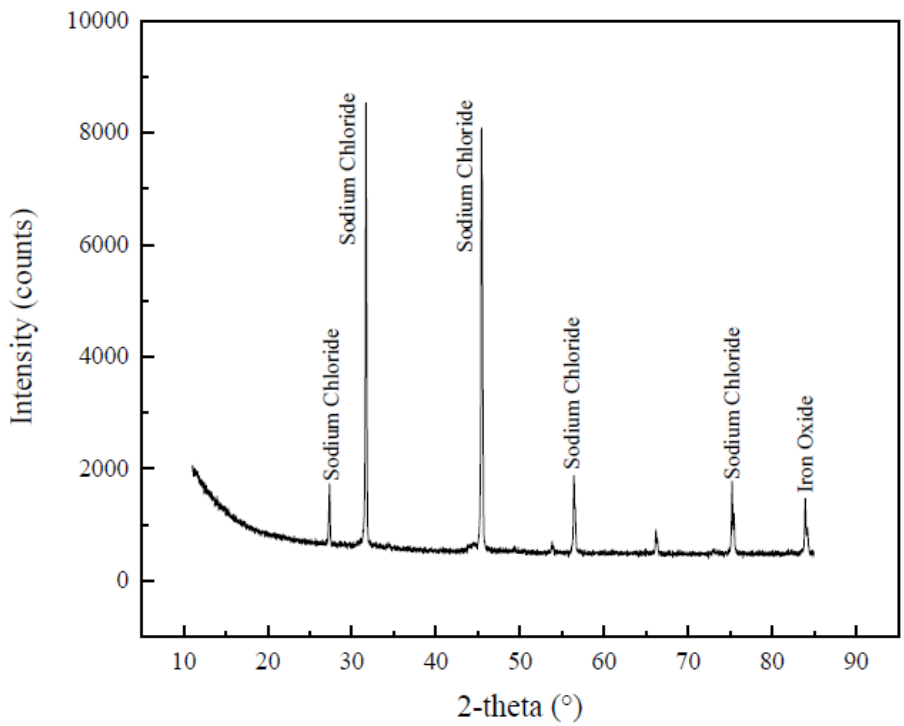

Figure 3.3.13 XRD pattern of the solids samples obtained from selective precipitation tests at a pH value of 4.85.

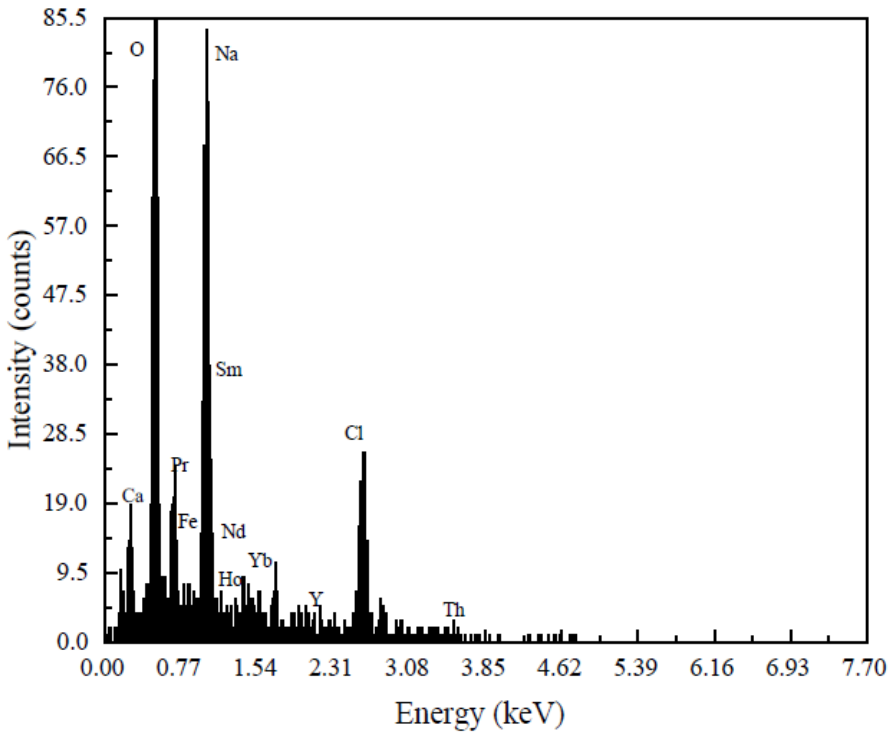

Figure 3.3.14 Elemental identification of the solids samples obtained from selective precipitation at a pH of 4.85 using SEM-EDX analysis.

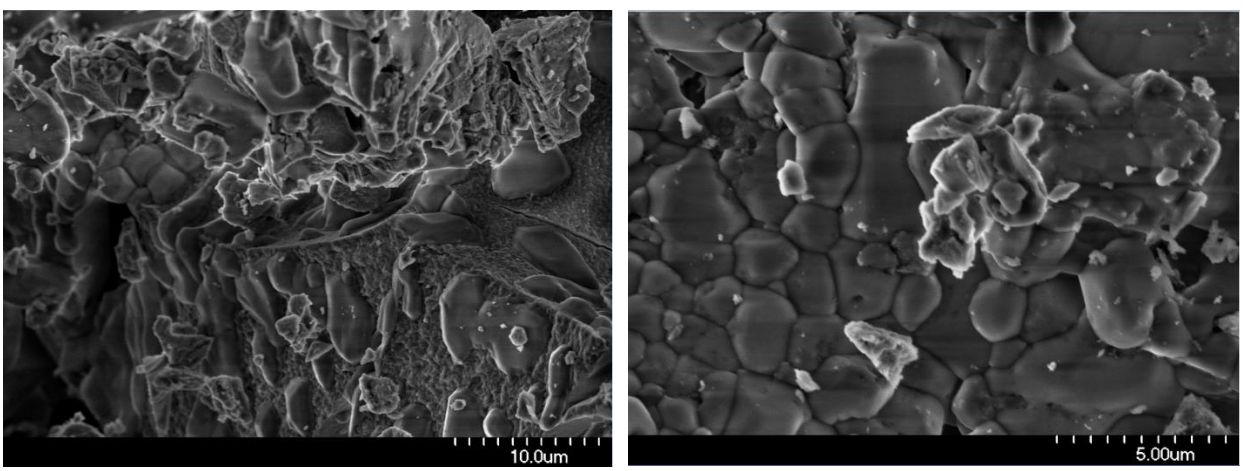

Figure 3.3.15 SEM images of precipitated solids (at a pH of 4.85) observed under various magnifications.

ix. <u>Equilibrium and Thermodynamic Evaluations of Selective Precipitation Tests</u>

The predominance and stabilities of ionic and non-ionic species in aqueous solutions are critical to understanding the concepts of dissolution, leaching, and selective precipitation. This information can be displayed graphically using speciation (species) distribution diagrams and Eh-pH (Pourbaix) diagrams. These diagrams are also helpful to identify major species existing at a certain pH value and provide the ability to predict the change in composition when there is a change in condition. Species distribution diagrams were constructed for selected rare earth elements, thorium, uranium, iron, and aluminum using the OLI Studio software based on their

initial concentrations in the synthetic solution. It was reported that the existence of various species is notably pH-dependent (Li et al., 2012; Liu et al., 2015; Li et al., 2018) since the pH value controls the ion activity (Monhemius, 1977; Hayes et al., 2002).

As seen in Figure 3.3.16, under acidic conditions, aqueous ions of Th^{4+} and $ThCl^{3+}$ are seen. The concentration of Th^{4+} starts to decrease around a pH value of 3, which is due to the OH^- ions liberated from NaOH that initiates thorium's precipitation by forming hydroxide complexes. Likewise, the concentration of $ThCl^{3+}$ starts to decrease at pH 3. Initially, $ThCl^{3+}$ is formed due to a reaction between Cl^- and Th^{4+} ions in the solution. However, when an alkaline is introduced to the solution, the reaction is reversed. It releases Cl^- ions back into the solution, and liberated Th^{4+} ions react with OH^- forming thorium precipitates. Meanwhile, a substantial increase of thorium hydroxide ($Th(OH)_4$) is seen with an elevation in the solution pH. $Th(OH)_4$ slowly transforms into thorium dioxide (ThO_2) which is stable in that form even in acidic conditions. The concentration of Th^{4+} and $Th(OH)_4$ reaches the same level at a pH value of 5, for which the precipitation of thorium is assumed to be completed (Zhu et al., 2015). A further increase in the pH does not change the concentrations of Th^{4+} and $Th(OH)_4$. The conclusions reached in this study are well correlated with the literature (Felmy et al., 1991). Thermodynamic studies were also performed following the precipitation equation shown in Eq. 13. The Gibbs free energy change of the reaction is -125.52 kJ/mol at the standard state conditions (1 atm and 25°C). The negative value of ΔG indicates the precipitation of thorium dioxide is thermodynamically favorable. The enthalpy value of -108.99 kJ/mol further supports and suggests that the reaction is exothermic. The entropy value of thorium precipitation is found to be 70 $J.mol^{-1}.K^{-1}$.

$$Th^{4+}_{(aq)} + 4OH^-_{(aq)} = ThO_2 + 2H_2O \tag{13}$$

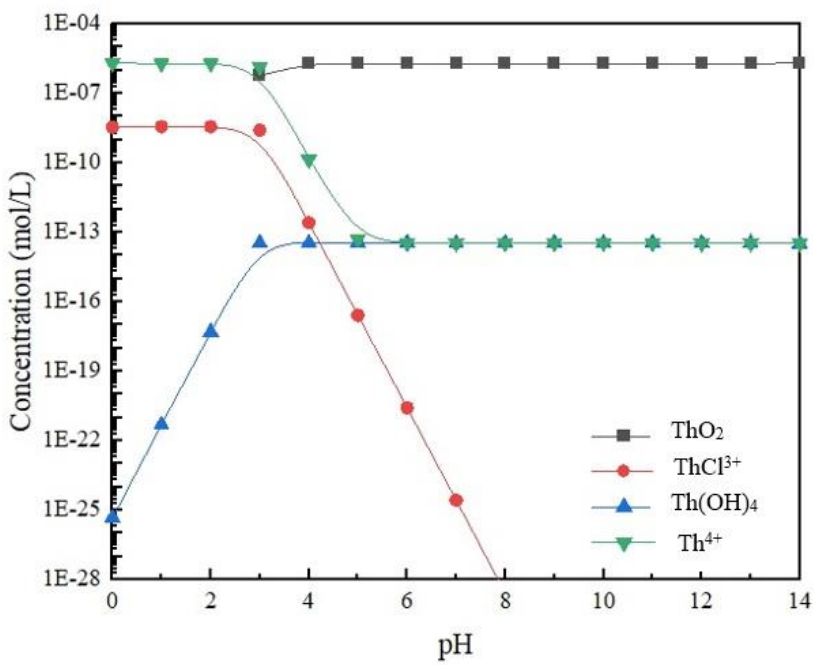

Figure 3.3.16 Species distribution diagram of Th-HCl system.

Thorium, with its only oxidation state, 4^+, is relatively easy to work with compared to other actinide elements, such as uranium, because of the simplicity of the species (Torapava et al., 2009). Uranium can be seen in many forms, such as U (III, IV, V, VI), and forms various complexes as oxides, phosphates, carbonates, etc. (Navrotsky et al., 2013). Among them, U (IV and VI) are the most common and stable states (Monji et al., 2016). The speciation of uranium in chloride media is given in Figure 3.3.17. Uranium initially exists in the solution with its 6^+ oxidation state as a uranyl cation. According to the literature data, the precipitation of uranium starts at a pH value of approximately 6 (Zhu et al., 2015), which means the solubility of the ions decreases, and the tendency to create insoluble complexes increases. Langmuir (1978) and Brookins (1988) performed comprehensive studies about the thermodynamic characteristics of aqueous and solid uranium species. Under oxidizing conditions (pH<4), uranium exists as UO_2^{2+} (U(VI)), which is well correlated with the results obtained in this study (Langmuir, 1978; Regenspurg et al., 2010; Abdel-Sabour, 2014; Monji et al., 2016). Starting from a pH value of 5, a sharp decrease in the UO_2^{2+} concentration is noticed. As the concentrations of U^{6+} and UO_2^{2+} are lessening, the aqueous state of uranyl hydroxide ($UO_2(OH)_2$) starts to be formed, which then transfers into a crystalline form around pH 7. Similarly, the precipitation of $UO_2(OH)_2$ is spontaneous and exothermic with ΔG and ΔH values of -65.69 kJ/mol and -53.93 kJ/mol, separately, at the standard state conditions. The entropy of the reaction was calculated to be 40 $J.mol^{-1}.K^{-1}$. Similar findings were also seen in Orabi's study (2013).

$$UO_{2(aq)}^{2+} + 2OH_{(aq)}^{-} = UO_2(OH)_2 \tag{14}$$

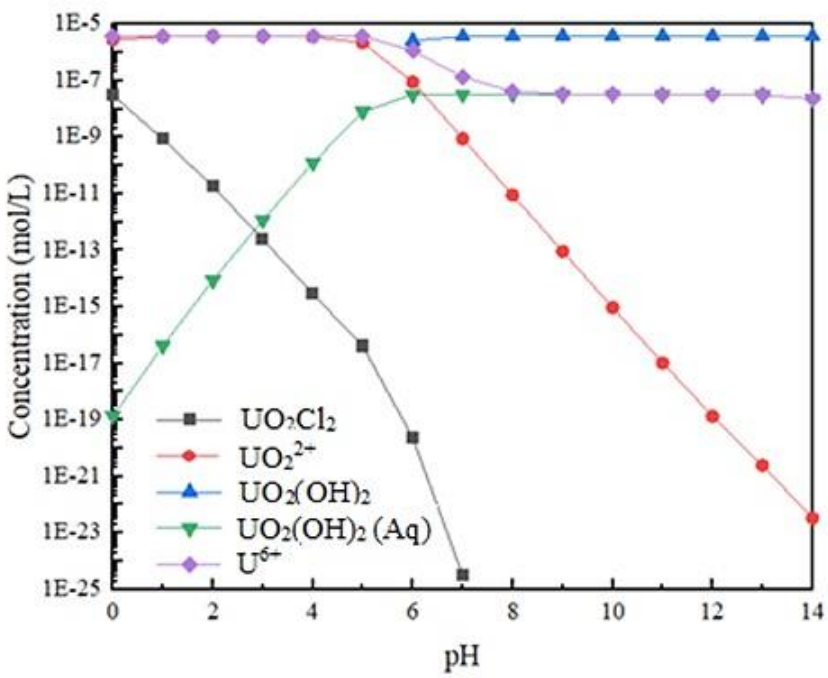

Figure 3.3.17 Species distribution diagram of U-HCl system.

Pourbaix diagrams of thorium and uranium systems were generated using HSC Chemistry Software, which is seen in Figure 3.3.18 and Figure 3.3.19, respectively. The elements with the most significant effect were selected to create a system that is as close as possible to the real system. In the diagrams, the dashed lines represent the stability area of water. Additionally, the redox potential measurements of the synthetic solution at various pH values are given in Table

3.3.5. Based on the redox potential readings, it is clear that at pH 4.8, thorium is stable in the form of ThO_2, which provides additional support of the experimental findings and previously presented species distribution diagrams. On the other hand, according to the redox readings, uranium may form a compound with sodium, which is expected due to the high concentration of sodium ions present in the solution.

Table 3.3.5 Redox potential measurements at various pH values.

pH	Eh (mV)
Initial pH <0	1030.6
0	927.0
0.25	794.8
0.50	687.5
1.00	597.9
1.50	590.5
2.50	564.9
3.00	551.4
3.50	434.4
4.00	389.3
4.50	338.8
4.80	331.7
5.00	296.4

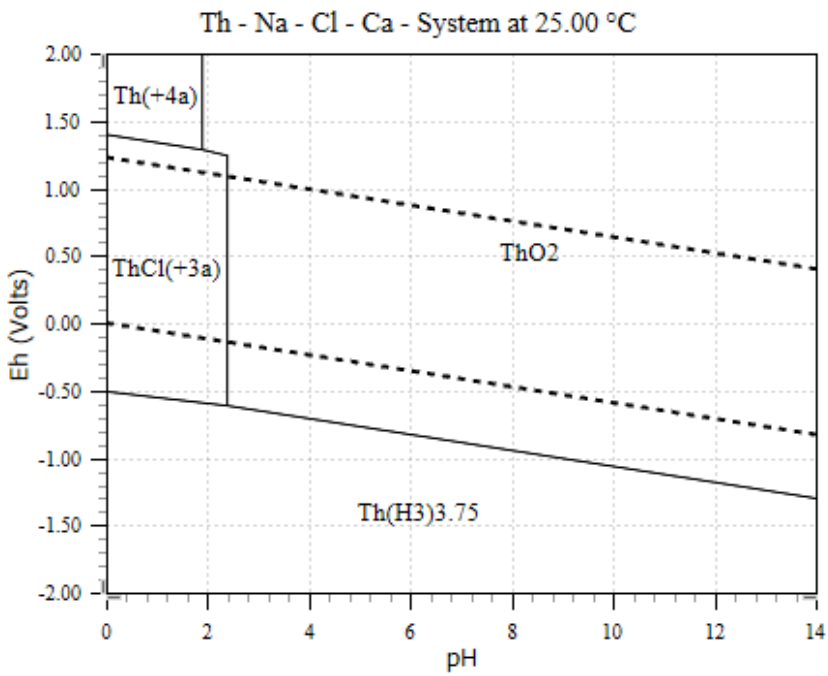

Figure 3.3.18 Eh-pH diagram of Th-Cl-Na-Ca-H_2O system.

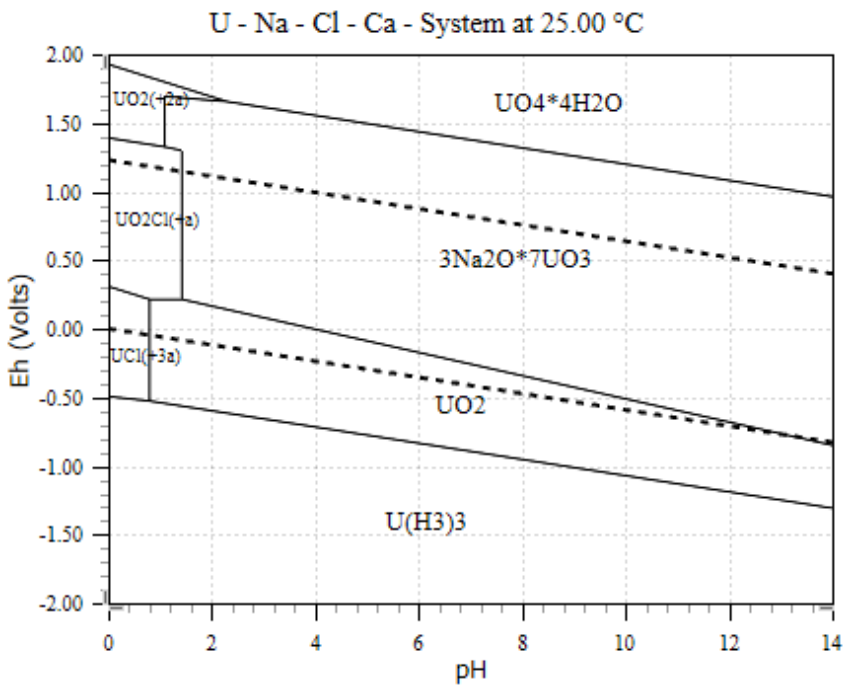

Figure 3.3.19 Eh-pH diagram of U-Cl-Na-Ca-H_2O system

The species distribution diagrams of selected rare earth elements are shown in Figure 21. Considering the concentration of individual rare earths in the synthetic feedstock solution, five rare earth elements, including cerium, neodymium, gadolinium, lanthanum, and yttrium, selected to represent different rare earth groups (i.e., heavy (Y, Eu, Gd, Tb, Dy, Ho, Er, Tm, Yb, Lu), light (La, Ce, Pr, Nd, Sm), critical (Y, Nd, Tb, Dy, Eu), and uncritical (La, Ce, Pr, Sm, Gd, Ho, Er, Tm, Yb, Lu) rare earth elements). It is known that most REEs existed in the synthetic solution as $REEs^{3+}$. However, cerium, praseodymium, and terbium may also be tetravalent and samarium, europium, and ytterbium can be in a divalent state, but these states of rare earths are not stable (Thakur, 2000). Rare earths become less soluble with increasing pH, and thermodynamically stable rare earth hydroxides can be obtained by treating aqueous solutions with a base. The precipitation of rare earths occurs between pH 6.8-8, where there is an overlap with uranium that leads to the co-precipitation of the two (Zhu et al., 2015). As seen in the diagrams (Figure 21), the precipitation behavior of rare earths is alike which reflects the similarity in their physical and chemical properties (Al-Nafai, 2015). Similar types of species tend to be formed approximately at the same pH regions. For all the rare earth elements examined, an increase in the concentration of the trivalent ion is observed starting from a pH value of 10. Thermodynamic values were also calculated for rare earths and can be seen in Table 3.3.6. Due to their similar characteristics, the thermodynamic values were considerably close to each other. The precipitation reaction of rare earths (Eq. 15) is favored according to the Gibbs free energy values. The enthalpy changes are suggesting that the processes are exothermic. Moreover, the thermodynamic findings shown in Table 9 indicate that heavy rare earth elements tend to precipitate as opposed to light elements. A more negative ΔG value is obtained for heavy rare earth elements (i.e., Gadolinium and Yttrium) compared to light rare earth elements (i.e., Cerium, Neodymium, and Lanthanum).

$$REEs^{3+}_{(aq)} + 3OH^{-}_{(aq)} = REEs(OH)_3 \quad (15)$$

Table 3.3.6 Gibbs free energy and enthalpy and entropy values of rare earths under standard operating conditions (1 atm and 25 °C).

Elements / Thermodynamic Parameter	ΔG (kJ/mol)	ΔH (kJ/mol)	ΔS ($J.mol^{-1}.K^{-1}$)
Cerium (Ce)	-130.5	-32.4	+330
Neodymium (Nd)	-136.9	-29.4	+360
Gadolinium (Gd)	-143.6	-32.9	+370
Lanthanum (La)	-124.6	-19.7	+350
Yttrium (Y)	-173.5	-59.3	+380

The speciation of iron and aluminum in the chloride media is presented in Figure 3.3.21 and Figure 3.3.22, respectively. Also, their precipitation reactions are given in Eqs. (16) and (17). In the synthetic feedstock solution, iron exists with its trivalent oxidation state, Fe^{3+}. The concentration of Fe^{+3} starts to decrease around a pH value of 3, which is consistent with the literature data (Balintova and Petrilakova, 2011; Seo et al., 2017). Due to the nature of the synthetic solution's medium, iron (III) chloride ($FeCl_3$) is also seen in the solution, and its concentration starts to decrease at the same pH value. While the concentrations of Fe^{+3} and $FeCl_3$ are reducing, the formation of iron hydroxide ($Fe(OH)_3$) is seen. Iron precipitation is found to be thermodynamically stable with a corresponding ΔG value of -317.13 kJ/mol and ΔH value of -229.43 kJ/mol. According to previous selective precipitation test results, approximately 66% Fe precipitated out at pH 4.85. Characterization studies also supported the presence of iron in the precipitates. The XRD pattern revealed the formation of iron oxide and the iron peak was detected in the EDX spectrum as well, which were all consistent with the distribution of iron species as indicated in Figure 3.3.21.

When an alkali is added to a solution containing aluminum, a precipitate is obtained in a hydroxide gel, $Al(OH)_3$. Generally, the formation of $Al(OH)_3$ starts to be seen at a pH value of 5 (Balintova and Petrilakova, 2011), which is supported by Figure 3.3.22. The original form of aluminum, Al^{3+}, gradually transforms into $Al(OH)_2^{+1}$. However, due to continuous reactions occurring between aluminum species and OH^-, the formed $Al(OH)_2^{+1}$ is not stable, and it decreases significantly at a pH value of 4. At that pH, the formation of $Al(OH)_3$ initiates. On the other hand, in the presence of sufficient alkaline solutions, aluminum decomposes water with the evolution of hydrogen, dissolving as aluminate ions AlO_2^- (Pourbaix, 1974). Although the stability is observed for $Al(OH)_3$ through a wide range of pH values, a decrease in its concentration starts when pH exceeds 10. Like iron, the aluminum precipitation mechanism is thermodynamically favorable with a standard energy change value of -540.03 kJ/mol. Moreover, the enthalpy change, -545.53 kJ/mol, suggests an exothermic reaction.

$$Fe^{3+}_{(aq)} + 3OH^-_{(aq)} = Fe(OH)_3 \tag{16}$$

$$Al^{3+}_{(aq)} + 3OH^-_{(aq)} = Al(OH)_3 \tag{17}$$

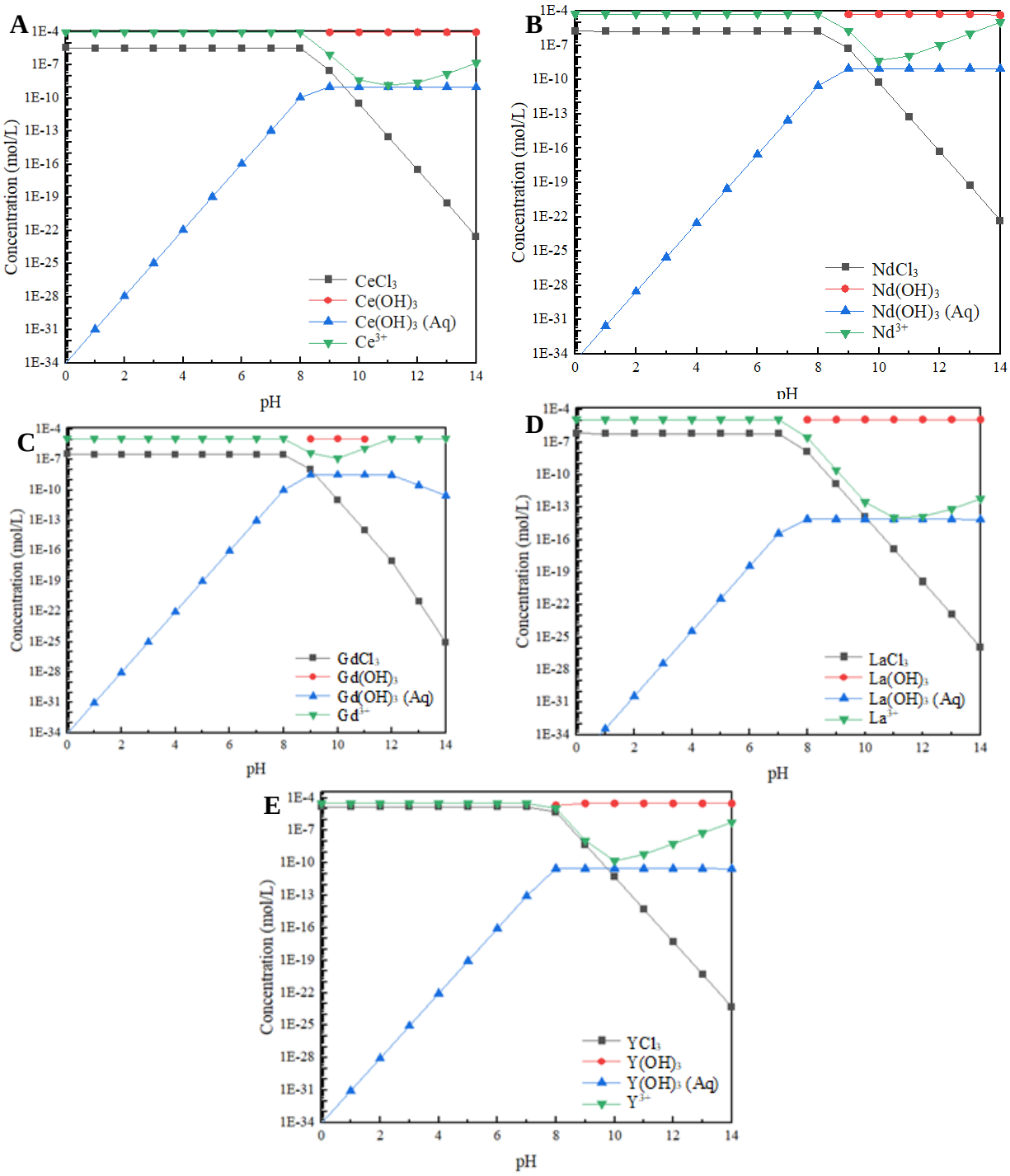

Figure 3.3.20 Species distribution diagrams of REEs-HCl system. A) Cerium, B) Neodymium, C) Gadolinium, D) Lanthanum, E) Yttrium

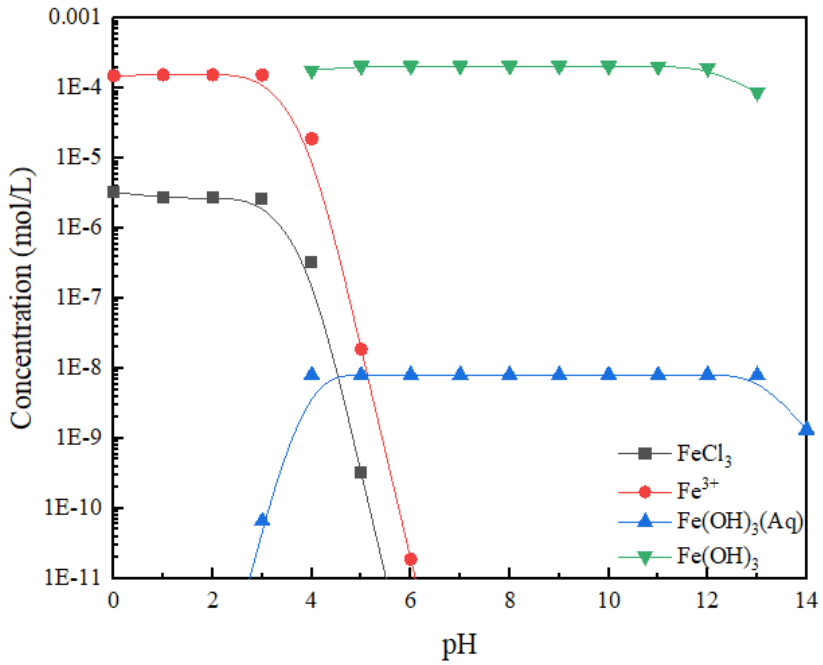

Figure 3.3.21 Species distribution diagram of Fe-HCl system.

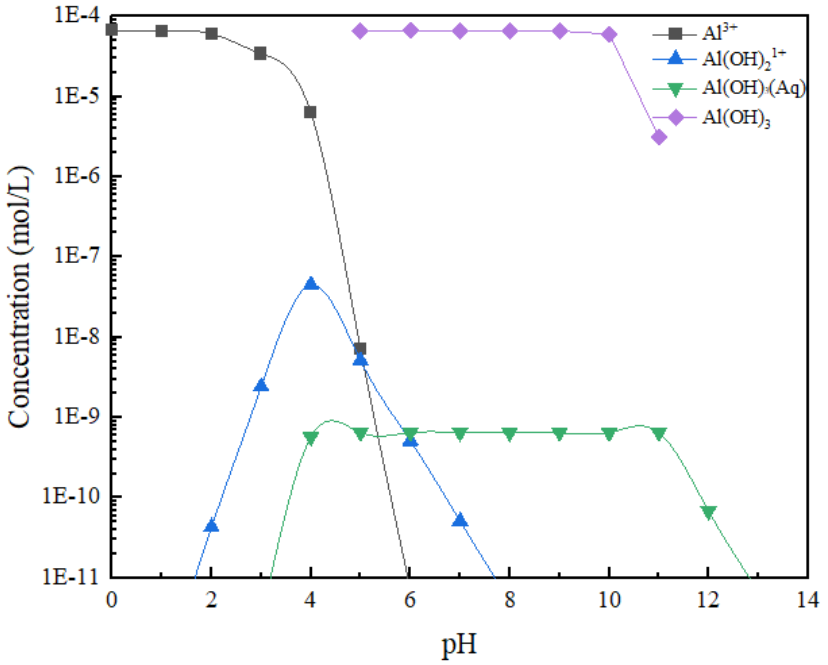

Figure 3.3.22 Species distribution diagram of Al-HCl system.

x. *<u>Experimental Design for the Solvent Extraction Stage of the Modified Experimental Protocol</u>*

Experimental design methodologies were used to guide the design of various separation techniques applied in this study. For this purpose, a Box-Behnken experimental design technique based on the response surface methodology (RSM) was used to determine the number of tests that need to be conducted. The design technique also ensures the tests to be performed are sufficient to evaluate the significance of every influential operating parameter.

The modified experimental protocol (Figure 3.3.10) was followed by two subsets of experimental design, with each subset having a fixed combination of extractant and strippant, as shown in Figure 3.3.23 (A) and (B), separately. It can be seen that three or four operating parameters, three levels of each, were investigated during each subset study. The levels of each parameter were determined based on prior studies conducted in a similar field (Menzies and Rigby, 1961; Nasab et al., 2011; Biswas et al., 2013; Xie et al., 2014; Jha et al., 2016). The retention time was fixed at 10 minutes. A total of 15 tests and 27 tests were conducted for the first and second subset, respectively, with the only difference being the stripping agent. The equation used to determine the number of test for each subset is:

$$N = 2k(k-1) + C_0 \tag{18}$$

where N is the number of tests required for the experimental design, k the number of variables to be studied (k=3), C_0 the number of center points (C_0=3). Detailed test order and conditions for the two subsets of experiments are shown in Table 3.3.7 and Table 3.3.8, respectively. A good separation is obtained in conditions of low extraction of one component and high extraction of the other, such that one component tends to stay in the organic phase, and the other in the aqueous phase. This is achieved when the chemical nature of the compounds is significantly different.

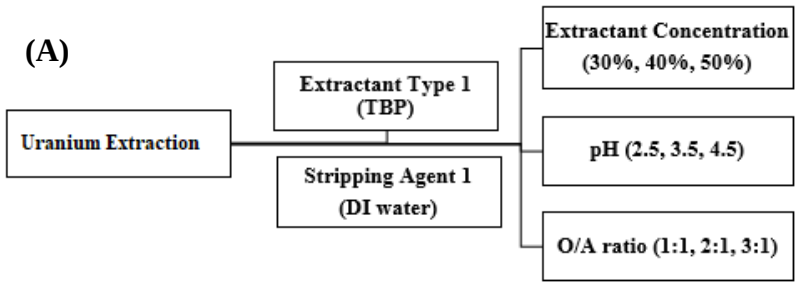

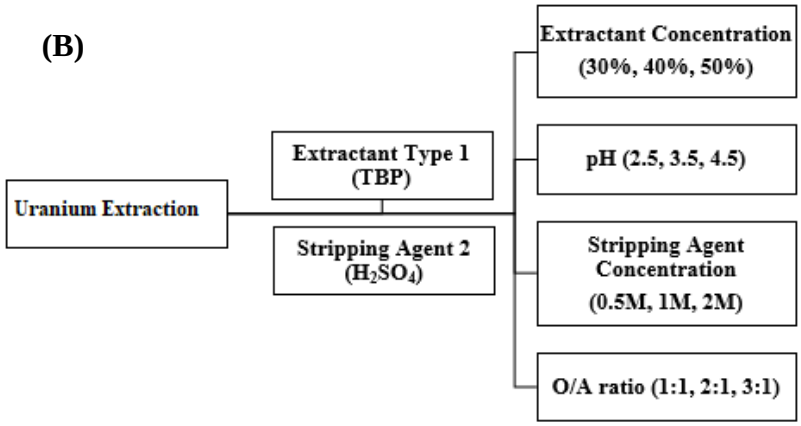

Figure 3.3.23 Experimental designs for uranium separation using TBP as the extractant: (A) DI water as the strippant; (B) H_2SO_4 as the strippant.

Table 3.3.7 Test order and conditions of the first subset of solvent extraction following the modified experimental protocol.

Test No.	Extractant Conc. (v% TBP)	pH	Organic/Aqueous Ratio
1	40	2.5	1
2		4.5	1
3		3.5	2
4		3.5	2
5		3.5	2
6		2.5	3
7		4.5	3
8	50	3.5	3
9		3.5	1
10		4.5	2
11		2.5	2
12	30	2.5	2
13		4.5	2
14		3.5	1
15		3.5	3

Table 3.3.8 Test order and conditions of the second subset solvent extraction following the modified experimental protocol.

Test No.	Strippant Conc., H_2SO_4 (mol/L)	Extractant Conc. (v% TBP)	pH	Organic/Aqueous Ratio
1	1	30	3.5	1
2		40	4.5	1
3		50	3.5	1
4		40	2.5	1

5		30	2.5	2
6		30	4.5	2
7		30	3.5	3
8		50	3.5	3
9		40	3.5	2
10		50	2.5	2
11		40	3.5	2
12		40	3.5	2
13		40	4.5	3
14		40	2.5	3
15		50	4.5	2
16	0.5	40	4.5	2
17		50	3.5	2
18		40	3.5	3
19		40	3.5	1
20		30	3.5	2
21		40	2.5	2
22	2	50	3.5	2
23		30	3.5	2
24		40	4.5	2
25		40	3.5	1
26		40	3.5	3
27		40	2.5	2

xi. *First Subset of Solvent Extraction Tests*

The experimental flowsheet containing the operational conditions is given in Figure 3.3.24. Recovery of rare earths and uranium into the final rare earth product stream, based solely on solvent extract circuit, as a result of the 15 tests are given in Figure 3.3.25. Likewise, the overall recovery of rare earths and uranium is shown in Figure 3.3.26, taking both selective precipitation and solvent extraction into account.

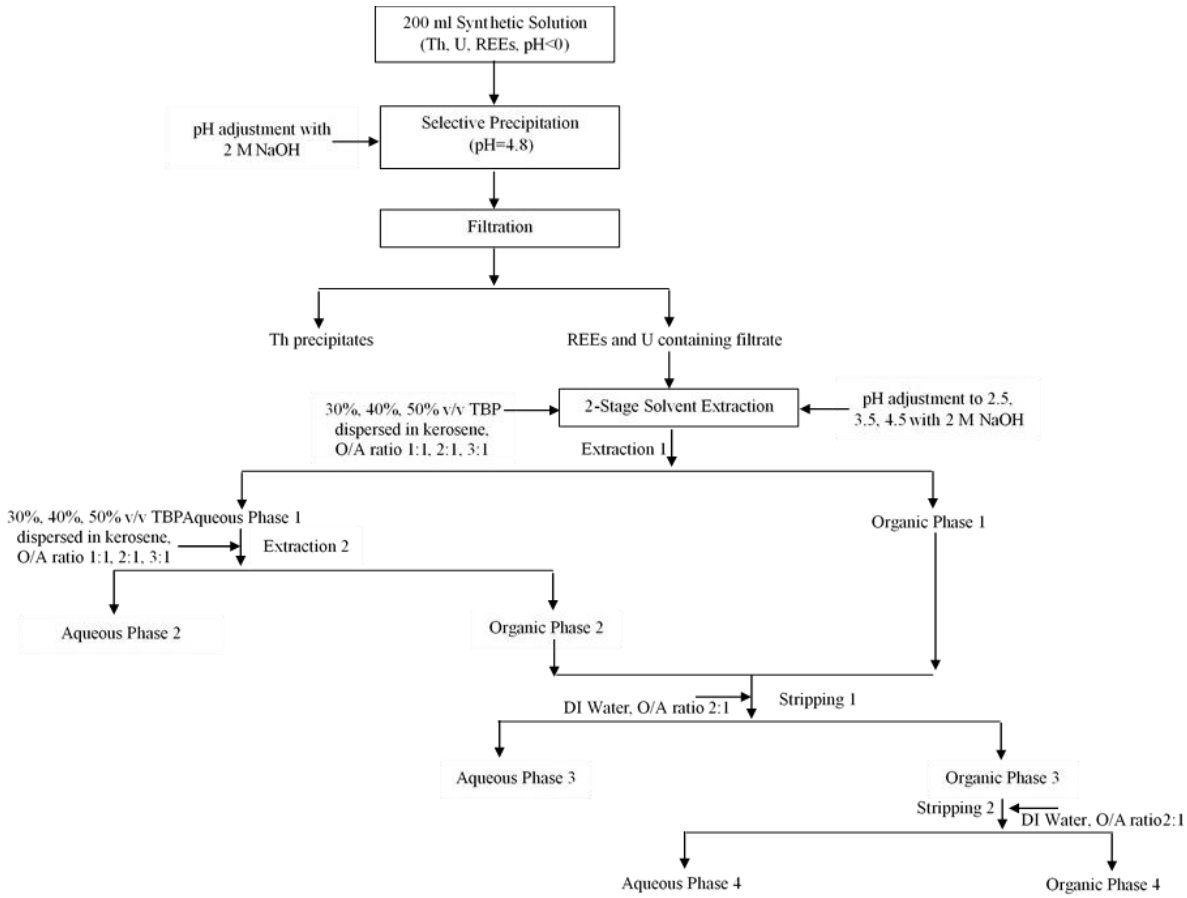

Figure 3.3.24 Experimental procedure and the operating conditions followed the first subset of solvent extraction tests.

As seen in Figure 3.3.25, the rare earth recovery obtained from the solvent extraction circuit varied from 90% to 98.9% while the corresponding uranium recovery changed between 5.9% to 89.4%. This noteworthy fluctuation in uranium recovery simply implies that the chosen variables had an impact on the removal of uranium. On the other hand, the rare earth recovery value close to each other suggests that the same variables had less profound or a minimal impact on the recovery of rare earths.

Figure 3.3.26 further indicates the overall recovery of rare earths and uranium based on the whole experimental route by incorporating the selective precipitation stage. After taking into account the amounts of rare earths and uranium that precipitated out as solid forms, the overall recovery of rare earths and uranium both decreased to a value varying between 72.6%-79.8% and 3.1%-46.5%, respectively. Data from Figure 3.3.25 and Figure 3.3.26 indicate the best results with respect to the recovery of rare earth and uranium were obtained by Test 8 under the following conditions: 50 v% TBP, feed pH value of 3.5, an O/A ratio at 3. An overall rare earth recovery of approximately 79.6% with a corresponding uranium recovery of 3.1% was produced under the same operating conditions. The elemental composition (i.e., individual rare earth and uranium) of the final REE product stream obtained from Test 8 is also given in Table 3.3.9. No thorium was reported since all the thorium precipitated out at a pH of approximately 4.8 prior to the solvent extraction tests.

It was also observed that a noticeable portion of uranium was reported to the organic stream instead of the uranium product stream. For example, for Test 8, on the basis of solvent extraction circuit, the recovery of uranium into the uranium product stream and final REE product stream was 52.1% and 5.9%, respectively, while the remaining uranium reported to the organic stream, which needs to be further extracted so that the organic can be reused for solvent extraction from the economic standpoint. One solution to purify TBP is treating the organic stream with sodium carbonate or sodium hydroxide solutions to neutralize and precipitate the organic impurities with high molecular weights (Geier, 1979; Srinivas et al., 1994; International Atomic Energy Agency, 2000). The quality of the organic phase must be periodically checked and maintained after recycling since TBP may be subject to hydrolyze in the aqueous phases (International Atomic Energy Agency, 2000). Among the 15 tests, the amount of rare earths reporting to the organic stream was >1% for eight tests with the highest value of 5.3% corresponding to Test 8. For the remaining seven tests, the non-selective recovery of rare earths into the organic stream is all less than 1%, which is negligible.

Detailed results of the individual rare earth elements and uranium extraction recoveries (%), their concentrations in the rare earth product stream, as well as the detailed overall extraction recoveries, are given in Table 25, Table 26 and Table 27, separately in the Appendix D.

Table 3.3.9 Elemental composition of individual rare earth and uranium (mg/L) in the final REE product stream obtained from Test 8.

Sc	Y	La	Ce	Pr	Nd	Sm	Eu	Gd	Tb	Dy	Ho	Er	Tm	Yb	Lu	U
0.0	0.6	0.3	2.9	0.2	1.7	0.7	0.1	0.3	0.0	0.1	0.0	0.0	0.0	0.0	0.0	0.0

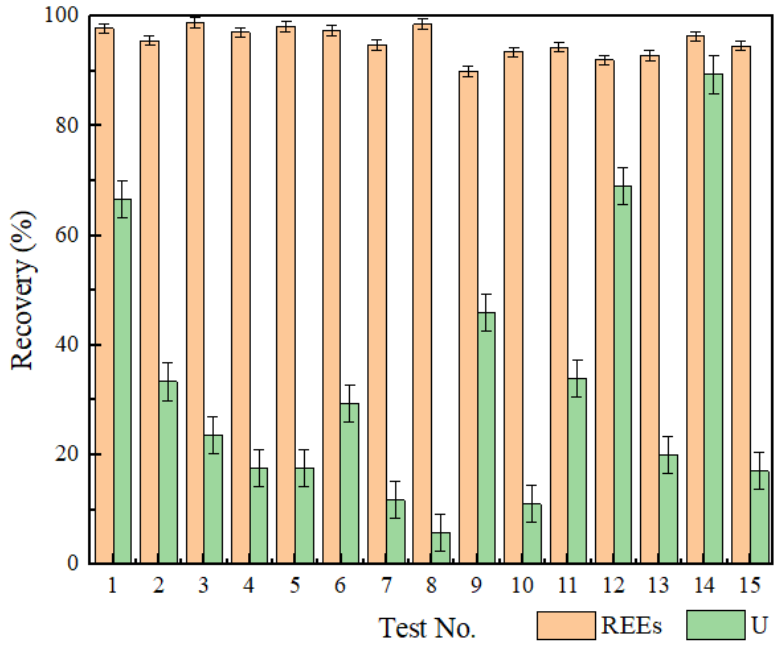

Figure 3.3.25 Recovery of total rare earths and uranium into the final REE product stream based solely on solvent extraction circuit. Error bars represent one standard deviation of three replicate tests.

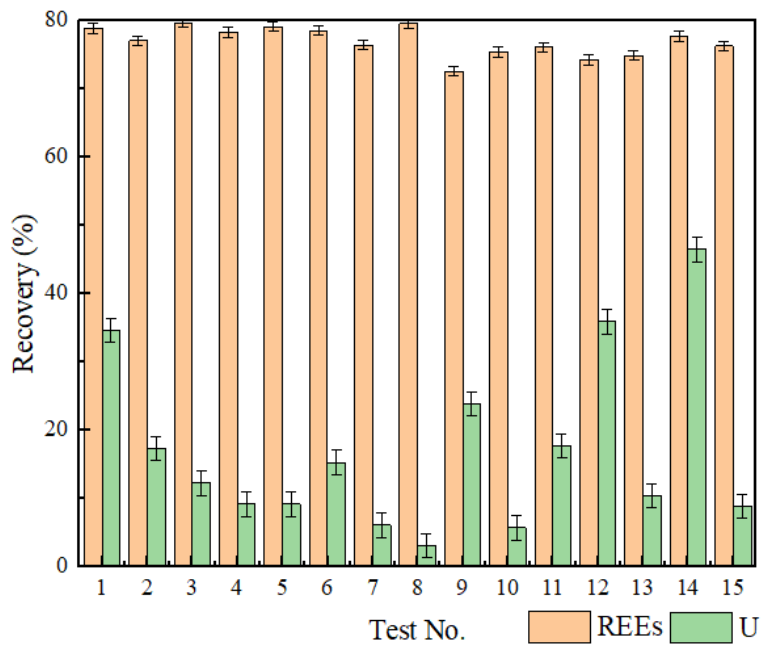

Figure 3.3.26 Overall recovery of total rare earths and uranium with respect to the overall experimental flowsheet. Error bars represent one standard deviation of three replicate tests.

Following data analysis, the impact of the operating variables (i.e., extractant concentration, feed solution pH, and O/A ratio) on the recovery of rare earth and uranium were analyzed using the Design Expert statistical analysis software. The statistical model developed to predict the recovery of uranium by considering the influential operating parameters is shown in Equation 19. It can be seen from the quadratic model that all three variables have a significant impact on the non-selective recovery of uranium into the REE product stream.

$$Uranium\ Recovery = +596.01 - 12.38 * A - 85.85 * B - 110.80 * C + 0.65 * AB + 0.80 * AC + 3.92 * BC + 0.09 * A^2 + 4.81 * B^2 + 10.88 * C^2 \quad (19)$$

where the uncoded model term A, B, and C is corresponding to extractant concentration, feed solution pH, and O/A ratio, respectively.

The Analysis of Variance (ANOVA) table provided detailed information on the significance of the model, as shown in Table 3.3.10. The Fischer variation ratio (F-value) is a statistically valid measure of how well the factors describe the variation in the data about its mean. In this model, an F-value of 9.84 implies the model is significant and the probability of an F-value to become this large is 1.07% (<5%, which is the critical P-value used to determine the significance). Model terms are considered as significant within a 95% confidence level or in other words, values of "prob>F" less than 0.05 indicate that terms are significant. Terms A (extractant concentration), B (pH), and C (O/A ratio) are all significant model terms according to the data obtained from ANOVA and they all have a profound impact on uranium recovery. The "lack-of-fit" model is insignificant based on a p-value greater than 5%, which further supports the statistical significance of the model. An R-squared value of 0.9466 and an adjusted R-squared value of 0.8503 again validate the model. Even though the coefficients associated with high-order terms are not high compared to that of the first-order terms, they are still needed to justify the significance of the model.

Table 3.3.10 ANOVA analysis of the quadratic model for the prediction of uranium recovery.

Source	Sum of	df	Mean	F Value	p-value Prob>	
Model	7992.72	9	888.08	9.84	0.0107	Significant
Lack of Fit	428.26	3	142.75	12.39	0.0756	Not significant
A-Extractant	1214.51	1	1214.51	13.46	0.0145	
Concentration	1890.82	1	1890.82	20.95	0.0060	
B-pH	3666.25	1	3666.25	40.62	0.0014	
C-O/A Ratio	169	1	169	1.87	0.2295	
AB	258.41	1	258.41	2.86	0.1514	
AC	61.54	1	61.54	0.68	0.4466	
BC	304.75	1	304.75	3.38	0.1256	
A^2	85.25	1	85.25	0.94	0.3758	
B^2	436.87	1	436.87	4.84	0.0791	
C^2						
R-Squared	0.9466					
Adj R-Squared	0.8503					
Pred R-Squared	0.1824					
Adeq Precision	10.172					

3D response surface and 2D contour plots shown in Figure 3.3.27 indicating the impact of two input variables on uranium recovery while the level of the third variable was fixed at the middle-range value. Figure 3.3.27 (A) first shows the effect of extractant concentration and feed solution pH on uranium recovery while the O/A ratio was maintained as a constant value of 2. As seen, a high pH value and high extractant concentration tend to generate enhanced separation results. It is corroborated by the experimental results that the lowest recovery of uranium into the rare earth product stream (i.e., 5.9%) was obtained with 50% TBP by volume. For the tests conducted with low TBP concentrations and low pH values, the amount of uranium reporting to the final product stream increased substantially. Similarly, the effect of extractant concentration and O/A ratio on uranium recovery was indicated in Figure 3.3.27 (C) with a constant feed solution pH value of 3.5. The uranium recovery decreases with an elevation in both extractant concentration and O/A ratio, which is supported by experimental results obtained from Test 8 (i.e., 50 v% TBP, O/A of 3) and Test 14 (i.e., 30 v% TBP, O/A of 1) where the lowest and highest uranium recovery was achieved, respectively. As the O/A ratio and pH increase, the recovery of uranium into the final product stream decreases, as reflected by Figure 3.3.27 (E). The shape of contour plots, on the other hand, suggests the degree of interaction between the variables taken into account. Elliptical contours indicate strong interaction, whereas circular contours display less significant or minimum interaction. It can be seen from Figure 3.3.27 (B), (D), and (F) that feed solution pH and extractant concentration are two variables strongly interacting with each other as indicated by the elliptical contour plot.

Following uranium, statistical analysis was also performed for the recovery of total rare earths and a model was first developed to predict the response parameter of interest. However, a scrutiny of the model, as reflected by the ANOVA table indicates the model is not statistically meaningful. However, the insignificance of this model is consistent with the experimental findings that the recovery of rare earths did not change much during the solvent extraction stage with the value varying between 90% and 98.9%.

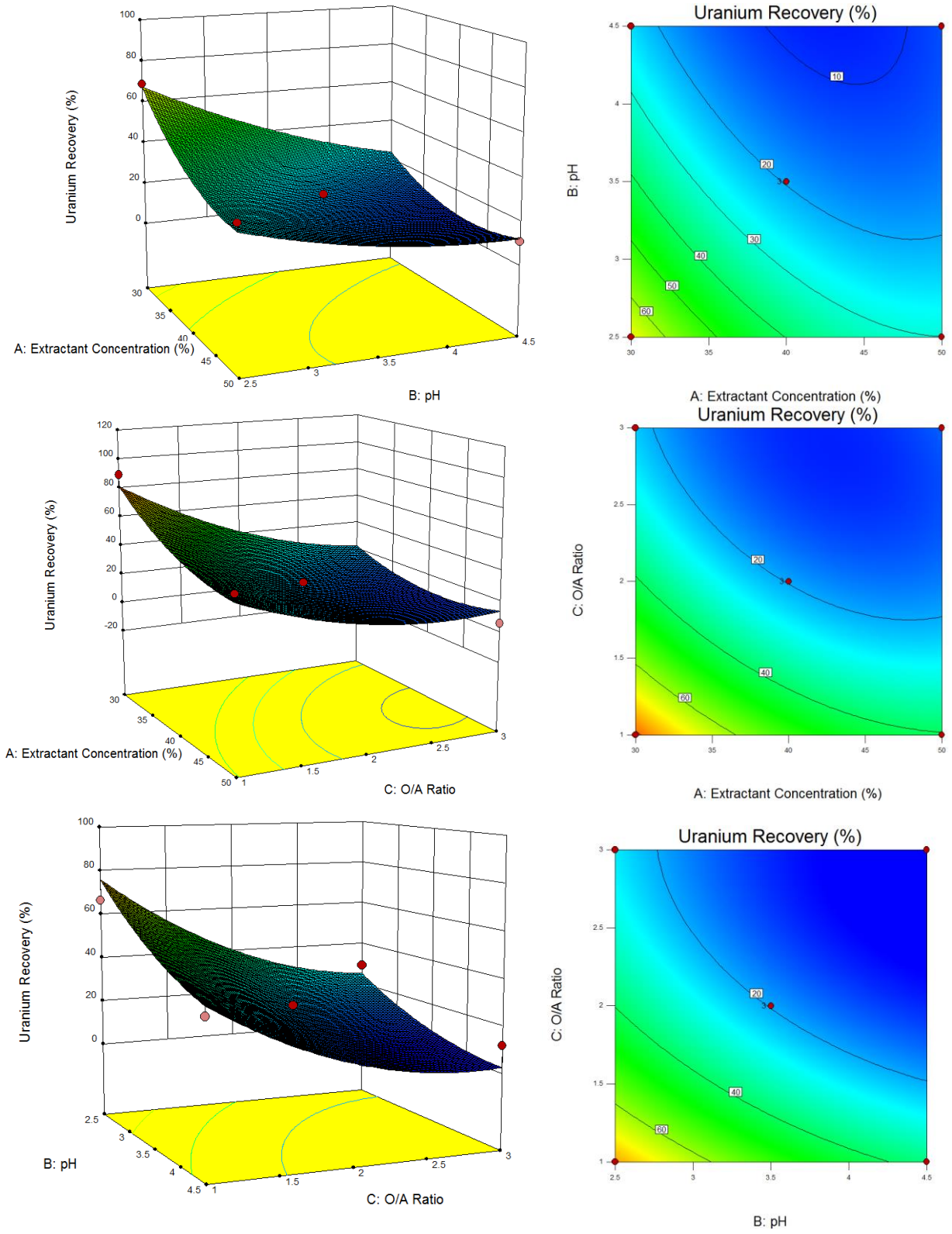

Figure 3.3.27 3D surface response graphs and 2D contour plots obtained from the statistical analysis using Design-Expert.

xii. Second Subset of Solvent Extraction Tests

The experimental procedure followed for the second subset of solvent extraction tests is given in Figure 3.3.28 with operating details. Recovery of rare earths and uranium into the final rare earth product stream, based solely on solvent extraction circuit, as a result of 27 tests are given in Figure 3.3.29. Likewise, the overall recovery of rare earths and uranium taking into account both selective precipitation and solvent extraction is shown in Figure 3.3.30.

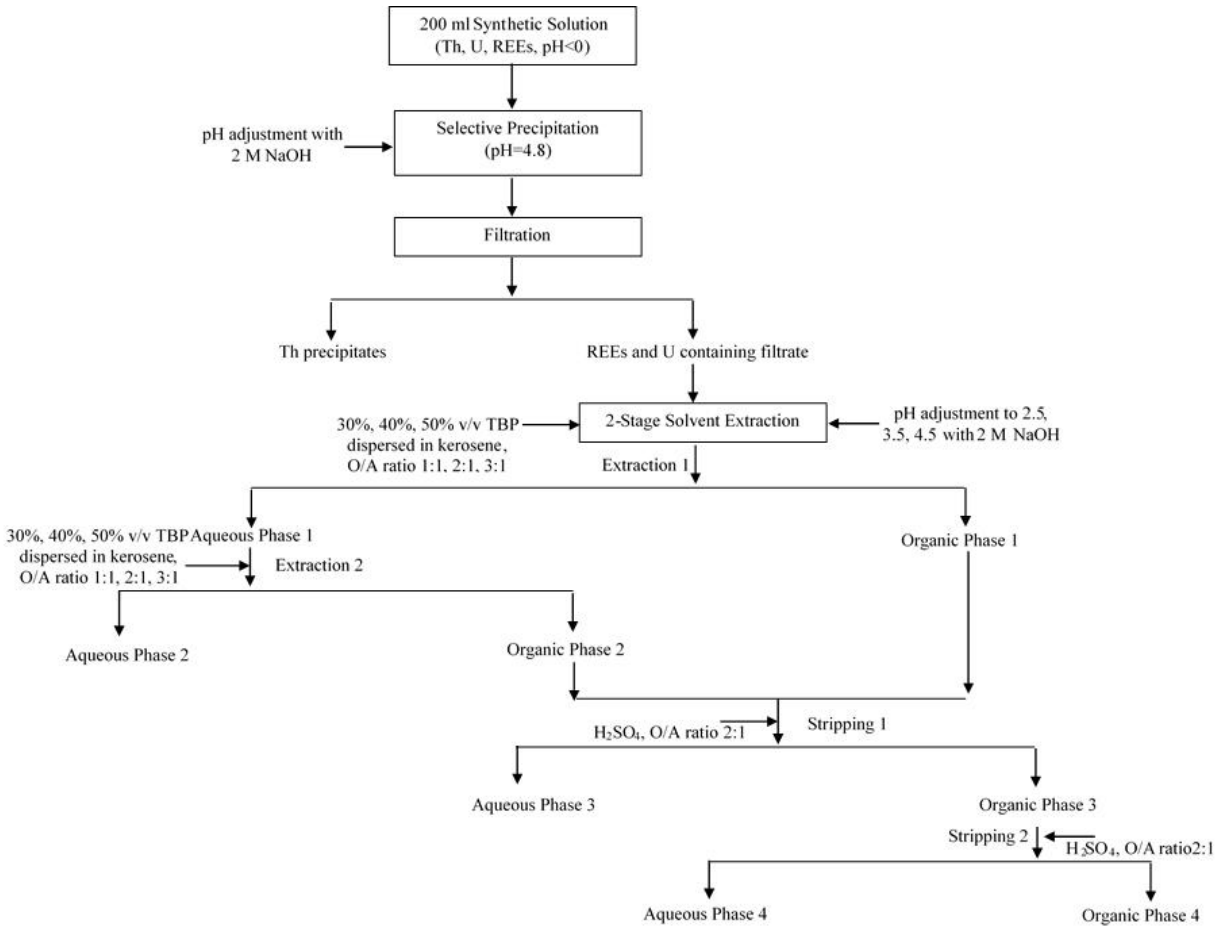

Figure 3.3.28 Experimental procedure and the operating conditions followed the second subset of solvent extraction tests.

As seen in Figure 3.3.29, the rare earth recovery obtained from the solvent extraction circuit varied from 80.2% to 97.6% while the corresponding uranium recovery changed between 3.4 to 62.5%. Similar fluctuation in uranium recovery was also observed in the first set of solvent extraction tests, which implies again the chosen variables had an impact on the uranium recovery. Moreover, compared to the results of the first set of tests, there is a noticeable reduction in the recovery range of uranium. During the first set of tests, the uranium recovery into the final product stream was varying between 5.9% to 89.4%. The narrowing recovery range shows that the strippant used in the second set of tests had a positive impact on the recovery of uranium since the only varying parameter between the first and second set is the strippant. On the other hand, there is a much smaller variation in the recovery of rare earths and the value close to each other indicates that the chosen variables had a less profound impact on the recovery of rare earths. A similar

phenomenon was also observed in the first set of tests. Although, this time, the recovery range of rare earths is slightly wider, which indicates that the new strippant (i.e., H_2SO_4) may have an impact on the recovery of rare earths as well.

Figure 3.3.30 further indicates the overall recovery of rare earth elements and uranium based on the whole experimental route by incorporating the selective precipitation stage. After taking into account the amount of rare earths and uranium previously precipitated out as solid forms, the overall recovery of rare earth elements and uranium both decreased which varied from 64.7% to 78.7% and 1.8% to 32.5%, respectively. Detailed results of the individual rare earth elements and uranium extraction recoveries (%), their concentrations in the rare earth product stream, as well as the detailed overall extraction recoveries, are given in Table 28, Table 29, and Table 30, separately in the Appendix D.

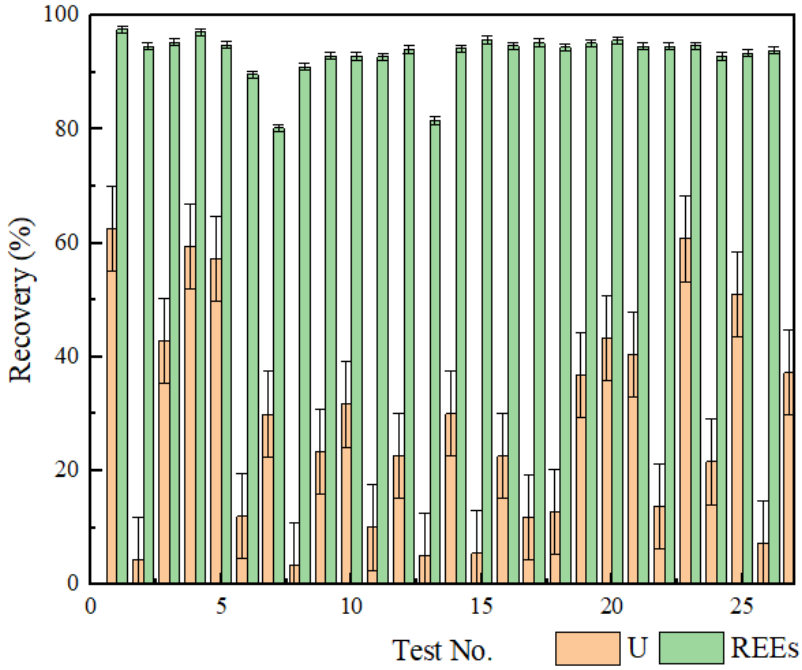

Figure 3.3.29 Recovery of total rare earth elements and uranium into the final rare earth product stream based solely on the solvent extraction circuit. Error bars represent one standard deviation of three replicate tests.

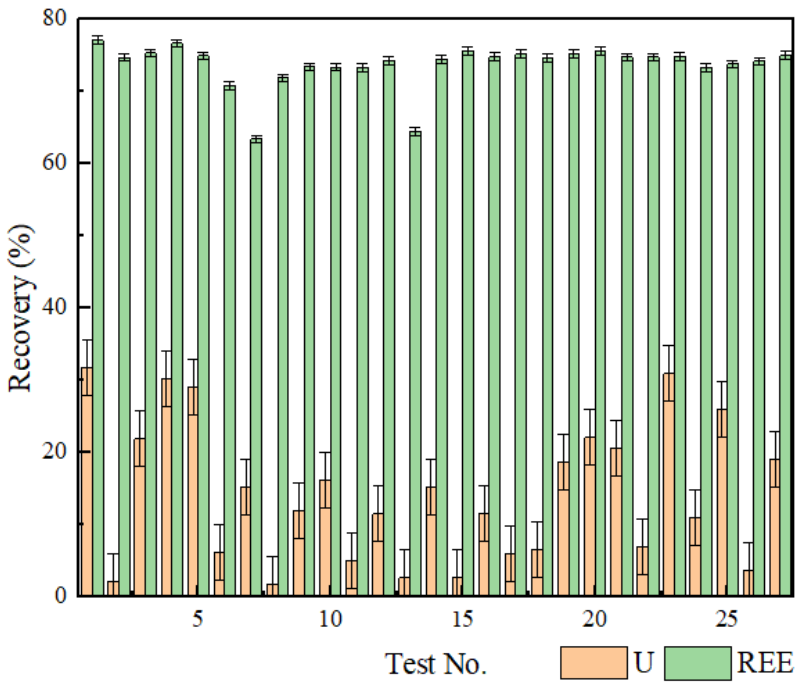

Figure 3.3.30 Overall recovery of total rare earth elements and uranium with respect to the whole experimental flowsheet. Error bars represent one standard deviation of three replicate tests.

During the first set of solvent extraction tests, it was observed that the test conditions that generated the highest rare earth recovery and the lowest uranium recovery were identical. However, the second set presented a different finding. Among all the 27 tests, the lowest uranium recovery (i.e., 3.42%, based solely on solvent extraction) into the rare earth product stream was produced by Test 8 with a corresponding rare earth recovery of 91%. On the other hand, the highest rare earth recovery (i.e., 97.57%, based solely on solvent extraction circuit) into the final product stream was generated by Test 1. However, the operating conditions of Test 1 resulted in a considerably higher uranium recovery of 62.47%. The elemental composition of the final REE product stream obtained from Test 8 is given as well in Table 3.3.11.

Table 3.3.11 Elemental composition of individual rare earth and uranium (mg/L) in the final REE product stream obtained from Test 8.

Sc	Y	La	Ce	Pr	Nd	Sm	Eu	Gd	Tb	Dy	Ho	Er	Tm	Yb	Lu	U
0.00	0.78	0.49	3.71	0.56	2.35	0.76	0.12	0.51	0.03	0.21	0.03	0.09	0.00	0.03	0.00	0.00

In the previous set of solvent extraction tests, it was noticed that a portion of uranium was reported to the organic stream. The amount of uranium reporting to the organic stream noticeably decreased in this set of tests which further supports the effect of the stripping agent. For example, for Test 8, on the basis of a solely solvent extraction circuit, no uranium was recovered into the organic stream. Under the same conditions, 3.42% of uranium reported to the rare earth product stream and the remaining uranium all reported to the uranium product stream, as expected. Besides, the amount of rare earth elements reporting to the organic stream was negligible (<1%) for most of the tests and the highest recovery of rare earths into the organic stream was seen as 5.96%.

Complexation reactions occurring during extraction and stripping stages are shown in Eqs. (19) -(21). The extraction ability of TBP is attributed to the phosphoryl group, which forms solvates with the metal ions in the solution (Giri and Nath, 2016). The extraction of rare earths increases proportionally to the atomic number (Peiro and Mendez, 2013). Figure 3.3.31 and Figure 3.3.32 show the distribution ratio of rare earth elements and uranium during extraction, respectively. Distribution ratios were calculated for total rare earth elements and uranium during each extraction step. D_1 represents the element concentration ratio of organic to aqueous phases during the first extraction, and similarly, D_2 shows that of the second extraction. Although the distribution ratio is not necessarily related to the extraction efficiency, it is an indicator of the necessity of multistage extraction. Generally, a decrease in the second distribution ratio was observed for rare earths. This may occur due to the completion of extraction during the first stage. However, there are a few exceptions for which the second step enhanced the extraction of rare earths, as seen in Figure 3.3.31. A similar trend was observed for uranium, although this time, the effect of the second extraction step is more profound. The distribution ratio of uranium under the best-operating conditions (Test 8) changed from 0.84 to 2, which resulted in the lowest uranium recovery into the final rare earth product stream. The separation factor between REEs/U is seen in Figure 3.3.33. The separation factor is a good measurement of the extractant's separation ability. The data indicate the effect of two-stage extraction on selectively removing uranium from rare earth elements.

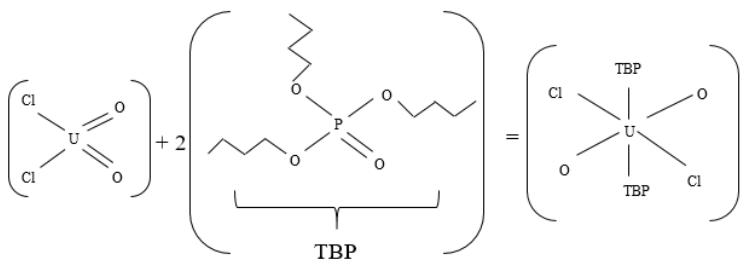

(19)

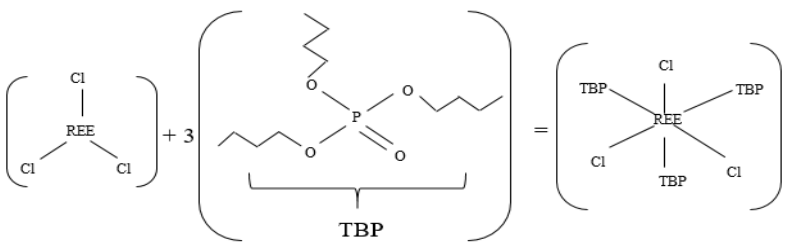

(20)

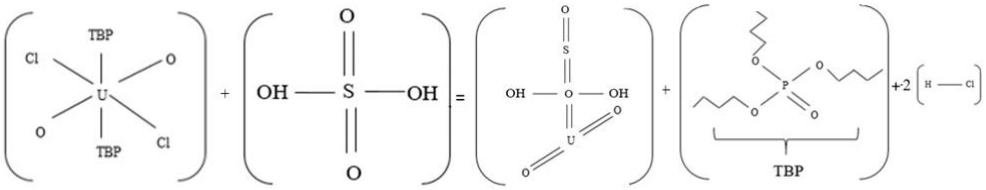

(21)

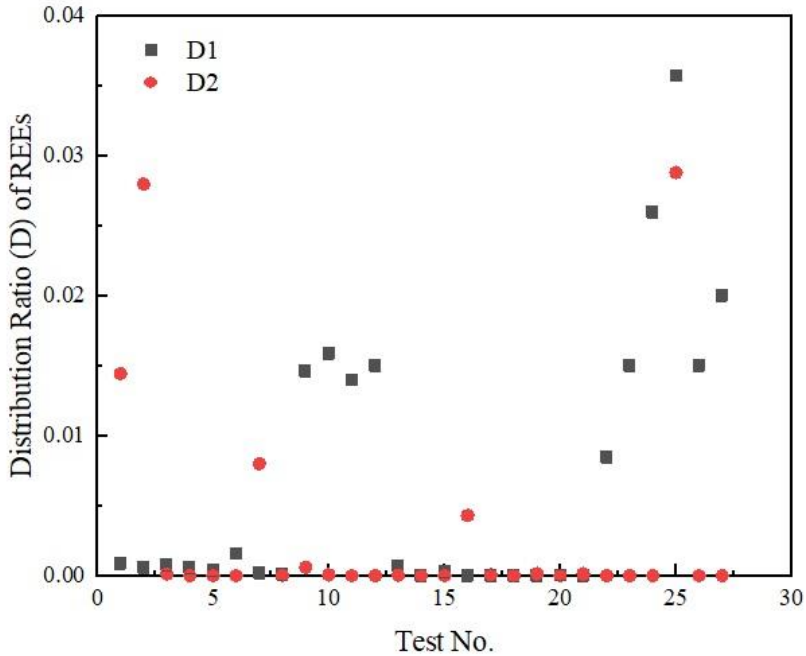

Figure 3.3.31 Distribution ratio of total rare earth elements in the two extraction stages. Error bars represent one standard deviation of three replicate tests.

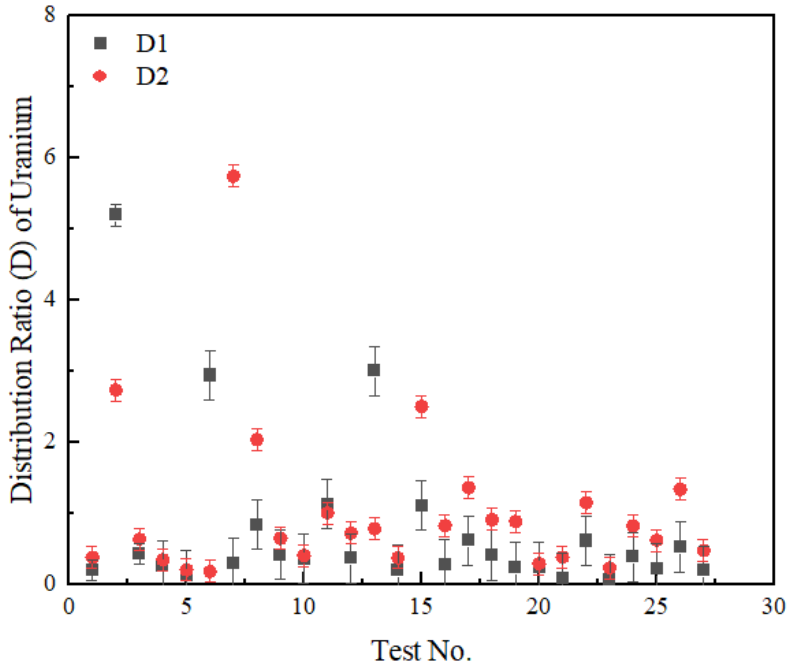

Figure 3.3.32 Distribution ratio of uranium in the two extraction stages. Error bars represent one standard deviation of three replicate tests.

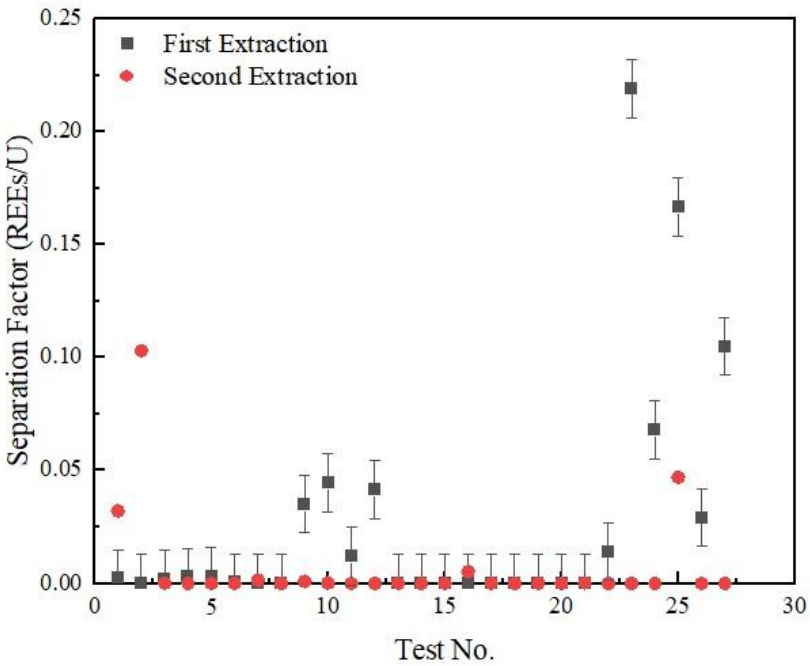

Figure 3.3.33 Separation factor between total rare earth elements and uranium. Error bars represent one standard deviation of three replicate tests.

The same methodology used during the first subset was followed and a statistical model was developed to predict the recovery of uranium by incorporating all the influential operating parameters, as shown in Equation 22. It can be seen from the quadratic model that all variables except the stripping agent concentration had a significant impact on the recovery of uranium.

$$Uranium\ Recovery = +18.64 - 13.06 * A - 15.41 * B + 1.99 * C - 14.02 * D + 4.75 * AB - 3.90 * AC - 1.74 * AD + 0.54 * BC + 7.55 * BD - 4.92 * CD + 8.24 * A^2 + 2.25 * B^2 + 6.29 * C^2 + 4.54 * D^2 \quad (22)$$

where the uncoded model term A, B, C, and D is corresponding to the extractant concentration, feed solution pH, strippant concentration, and O: A ratio, respectively.

The Analysis of Variance (ANOVA) table of this statistical model is shown in Table 3.3.12. The model F-value of 5.90 implies the model is significant and the probability of an F-value to become this large is 0.19%, which is noticeably lower than the critical P-value (5%). Model terms are considered as significant within a 95% confidence level, and in this case, terms A (extractant concentration), B (pH), and D (organic/aqueous ratio) are significant model terms with P-values less than 5%. The same conclusion was reached as of the first set of tests. On the other hand, the term D (strippant concentration) has a P-value of 0.5036, which is outside the confidence level and is considered an insignificant model term due to the same reason. Although the concentration of the strippant tested in the study did not generate a profound impact on the recovery of uranium, the data indicate a reduction in the uranium recoveries after using sulfuric acid as the strippant compared to deionized water. The concentration of the strippant may not contribute to the improved separation of uranium, but using a different strippant itself (i.e., H_2SO_4) can explain. The lack-of-fit value of 1.94 implies that there is a 38.79% chance that a lack-of-fit F-value can be this

high. R-squared values were also given in Table 3.3.12 to further evaluate the robustness of the developed model. As seen, an R-square value of 0.8731 and an adjusted R-squared value of 0.7250 confirms the significance of the model. The adequate precision value describes the signal to noise ratio, the value of which compares the range of predicted values at the design points to the average prediction error. In general, ratios greater than 4 are desirable and in this case, the adequate precision value is 8.03, which exceeds the desired ratio and indicates an adequate signal.

Table 3.3.12 ANOVA analysis of the quadratic model for the prediction of uranium recovery.

Source	Sum of	df	Mean	F Value	p-value	
Model	8250.39	14	589.31	5.90	0.0019	Significant
A- Extractant	2045.46	1	2045.46	20.46	0.0007	
B- pH	2849.62	1	2849.62	28.51	0.0002	
C- Strippant Concentration	47.52	1	47.52	0.48	0.5036	
D- O/A Ratio	2359.57	1	2359.57	23.61	0.0004	
AB	90.25	1	90.25	0.90	0.3608	
AC	60.76	1	60.76	0.61	0.4507	
AD	12.18	1	12.18	0.12	0.7331	
BC	1.17	1	1.17	0.012	0.9158	
BD	228.31	1	228.31	2.28	0.1566	
CD	96.73	1	96.73	0.97	0.3447	
A^2	361.72	1	361.72	3.62	0.0814	
B^2	27.10	1	27.10	0.27	0.6121	
C^2	211.29	1	211.29	2.11	0.1716	
D^2	110.07	1	110.07	1.10	0.3147	
R-Squared	0.8731					
Adj R-Squared	0.7250					
Pred R-Squared	0.3105					
Adeq Precision	8.029					

Like the first subset, here again, 3D response surface plots were given in Figure 35 to graphically represent the relation between the parameters and their subsequent effect on uranium recovery. It was observed from the experimental test results that an increase in the operational parameters produces a lower uranium recovery. However, when the interacting effect of the model terms was further analyzed, it was seen that any reduction in the uranium recovery into the final product stream does not depend solely on a single parameter. A simultaneous increase in the extractant concentration, O/A ratio, and solution pH generates the best separation performance. Figure 3.3.34 (A) shows the effect of extractant concentration and pH on uranium recovery while the O/A ratio and stripping agent concentration were fixed at 2 and 1 mol/L, respectively. One of the highest uranium recovery (57.22%) of this set of tests was observed when the feed solution pH and extractant concentrations were 2.5 and 30% by volume, respectively. A gradual increase in the pH and extractant concentration lowered the uranium recovery and the lowest uranium recovery (3.42%) into the rare earth product stream was obtained at a pH value of 3.5 with 50% TBP by volume. These findings prove that the pH of the feed solution and the extractant concentration are the two important factors impacting uranium recovery. A higher extractant concentration enhanced the process, and higher uranium removal from the aqueous phase to the organic phase was achieved. The same conclusion was reached in the previous set of tests with the lowest uranium

recovery being obtained under identical conditions (i.e., pH of 3.5 and 50 v% TBP). Figure 3.3.34 (B) shows the effect of extractant concentration and stripping agent concentration while the feed solution pH and O/A ratio were kept constant at 3.5 and 2, respectively. It can be seen that changing the stripping agent from DI water to sulfuric acid had an impact on uranium recovery. In both sets of the tests, the lowest uranium recovery was obtained under the same conditions (i.e., 50 v% TBP at pH 3.5 with O/A ratio 3) with the only difference being the stripping agent. The uranium recovery was reduced by approximately 2.5% after switching the strippant, which indicates the effect of sulfuric acid to some extent. However, the concentration of sulfuric acid tested in the study did not generate a significant impact on the separation results. In Figure 3.3.34(C), the effect of the O/A ratio and extractant concentration on uranium recovery can be seen. The uranium recovery into the final product stream decreases with an increase in both extractant concentration and O/A ratio. The highest uranium recovery of 62.47% was achieved with the lowest extractant concentration (30% TBP) and O/A ratio of 1. A low O/A ratio may not be sufficient to extract uranium ions from the aqueous phase for the separation purpose. Therefore, an increase in the O/A ratio results in an improved separation. Additionally, a high O/A ratio and pH produce noticeably enhanced separation results. Similar findings were also obtained in Jorjani and Shabazi's study (2012). Figure 3.3.34 (D) further shows the effect of feed pH value and stripping agent concentration while extractant concentration and O/A ratio were kept constant at 40% and 2, respectively. As it was indicated and statistically supported by the model, pH is an influential parameter and the best result was obtained at pH 3.5. The concentration of sulfuric acid tested in the study did not significantly impact the separation results. The lowest uranium recovery was generated using 1 mol/L sulfuric acid. Even though an increase in the concentration of the stripping agent from 0.5 mol/L to 1 mol/L lowered the uranium recovery, a further boost from 1 mol/L to 2 mol/L had a minimum impact on uranium recovery. This indicates that 1 mol/L H_2SO_4 solution was sufficient to break the uranium-TBP complex and strip uranium back into the aqueous phase. Figure 3.3.34 (E) displays the effect of O/A ratio and solution pH and it can be seen from the figure that a high O/A ratio and pH produce noticeably enhanced separation results. Moreover, a lower uranium recovery observed with an increase in the solution pH suggests that the higher pH favors creating more stable uranium-TBP complexes. Lastly, the plot in Figure 3.3.34 (F) shows the effect of the O/A ratio and stripping agent concentration on uranium recovery while keeping the extractant concentration and pH constant at 40% and 3.5, respectively.

Statistical analysis was also performed for the recovery of total rare earth elements, and a model was developed. Although a model was obtained, the ANOVA indicates the model is not statistically meaningful. However, the insignificance of this model is consistent with the experimental findings of both sets of tests. Considering the objective of this experimental design is to investigate the effect of different input operating variables on uranium recovery as opposed to rare earths recovery. Therefore, it is not surprising to see that the input variables had a minimum impact on the recovery of rare earth elements compared to uranium. In fact, this finding confirms the selectivity of the experimental design.

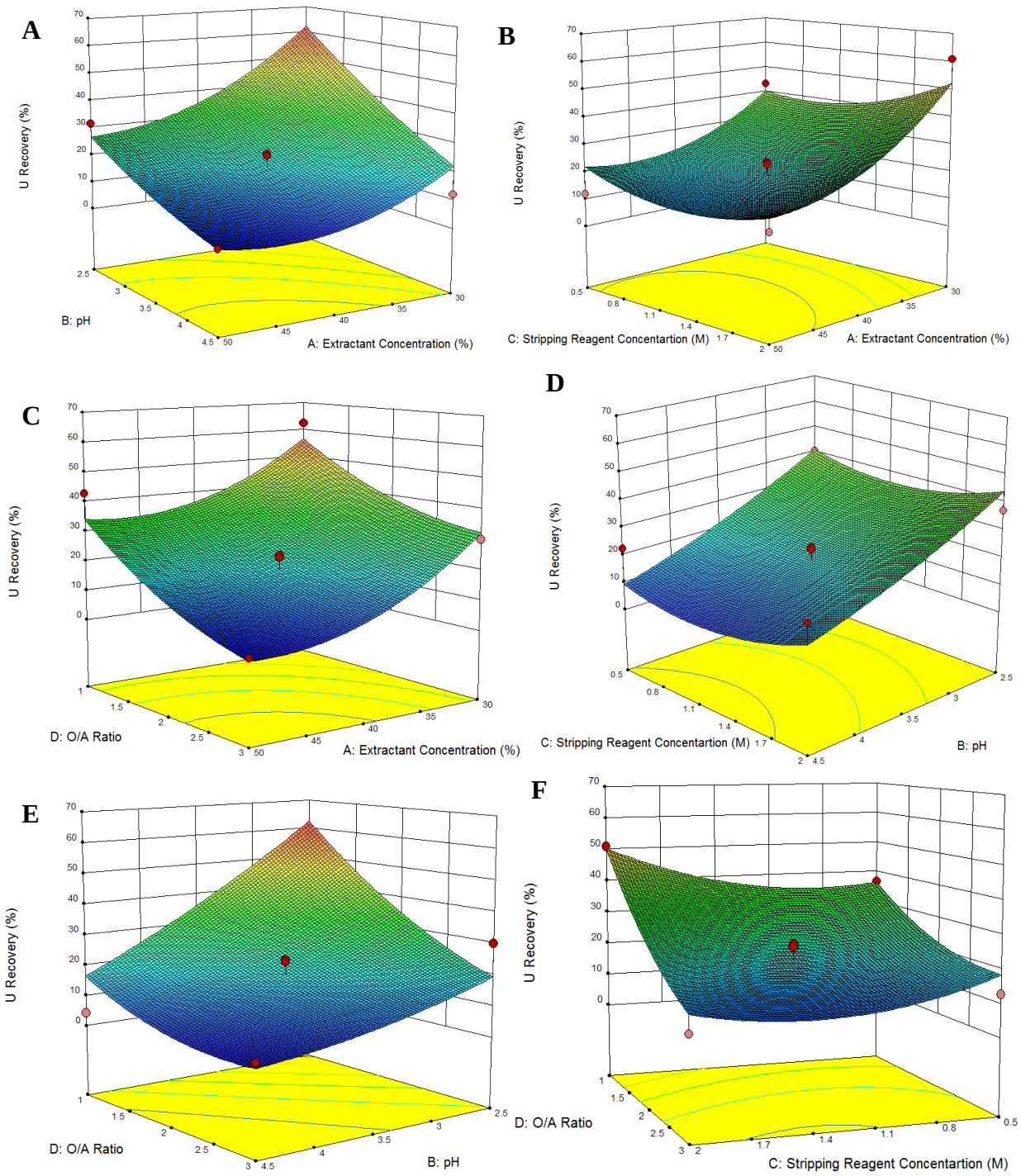

Figure 3.3.34 3D surface response graphs obtained for the statistical model predicting uranium recovery.

3.3.2.4 Rare Earth Oxalate Studies

Performance Validation tests were conducted with the rare earth oxalate sample provided by the project partner at the University of Kentucky. This sample was generated at the pilot-scale processing facilities and used to validate the developed experimental protocol. The elemental composition of the as-received rare earth oxalate sample is given in Table 3.3.13, and the process flowsheet followed for thorium removal is shown in Figure 3.3.35. As seen, the total rare earth elements concentration is around 37 wt%, and the light rare earth elements constitute the majority. While there was no uranium detected, thorium content is 0.12 mg/g.

Table 3.3.13 Elemental composition of the rare earth oxalate sample.

Element	Sc	Y	La	Ce	Pr	Nd	Sm	Eu
Concentration	0.14	14.42	66.20	144.80	17.78	72.42	12.46	2.20
Element	Gd	Tb	Dy	Ho	Er	Tm	Yb	Lu
Concentration	8.56	0.83	3.35	0.56	1.32	0.14	0.76	0.10
Element	Th	Ca	Fe					
Concentration	0.12	30.75	9.31					

Initially, a 10 g RE oxalate sample was roasted at 600 °C for 2 hours to produce rare earth oxide. After roasting, 5.7 g of solid was obtained. A representative sample of the solid residue was taken for the elemental analysis, while the remaining solid sample was washed with 0.5 mol/L hydrochloric acid to remove calcium. During the calcium wash step, the agitation was provided by a magnetic stirrer at a speed of approximately 525 rpm. After 15 minutes of washing, the solution was filtered using 0.45 µm pore size filter paper and the solid that had remained on filter paper was dried in the oven overnight. Solid, obtained after the Ca removal step, was weighed and a sample was taken for analysis. The sample was taken from the wash effluent as well.

Following the calcium removal step, leaching was performed at a solid concentration of 0.5 g/L using 6 mol/L hydrochloric acid (HCl) at 80 °C. Mixing was continued for 24 hours. After the leachate was generated, precipitation tests were conducted. To adjust the pH, 50% w/w NaOH was used. When the targeted pH value was achieved, the test was stopped. The solution was centrifuged for 15 min and then, it was subjected to filtration using 0.45 µm pore size filter paper. The sample was taken from the filtrate and the precipitated solid sample was dried in the oven overnight. All the stage-wise precipitation tests were conducted at room temperature and DI water was used at all steps.

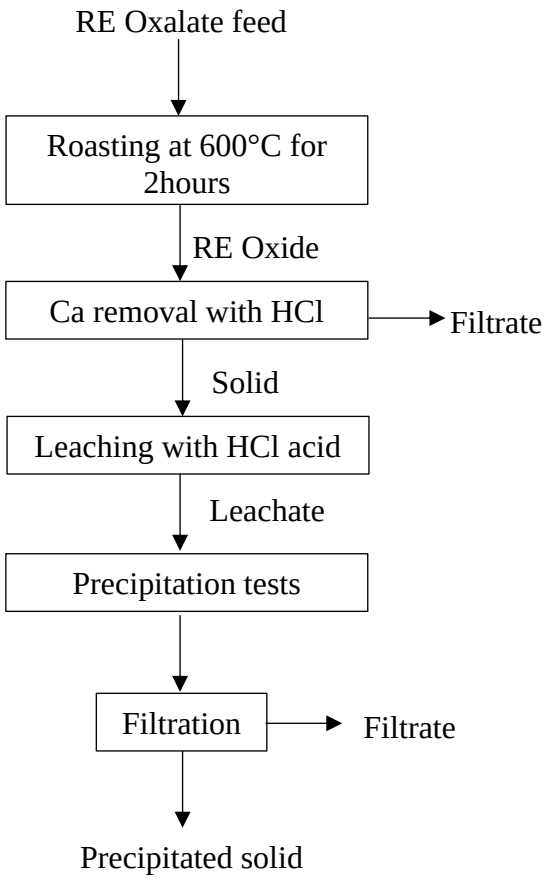

Figure 3.3.35 Experimental flowsheet followed for rare earth oxalate sample.

The results obtained from stage-wise precipitation tests are shown in Figure 3.3.36. The first color change and formation of particles were observed around pH 3.5 for all the tests. However, even after 45 minutes of settling and an additional 20 minutes of centrifuging, nothing precipitated or settled. Therefore, it is not suggested to pause at this pH value. The results are consistent with previous selective precipitation tests conducted with the synthetic solution. The desired selectivity was observed between thorium and rare earth elements at a pH value lower than 5. These findings coincide well with the results obtained with the synthetic solution. A continuous increase in rare earth precipitation was observed with an elevation in the solution pH, and it reached completion at pH 9.5. A significant increase in rare earth precipitation was seen between pH 7.5 and 8, which accounts for an incremental increase of 37%.

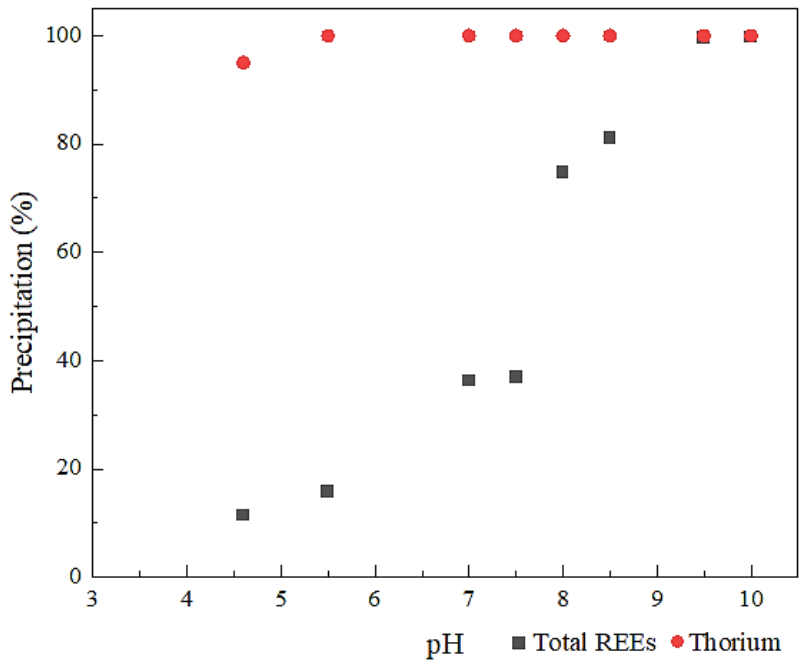

Figure 3.3.36 Precipitation of total rare earth elements and thorium at various pH values. Error bars represent one standard deviation.

The SEM images of the rare earth oxide sample used throughout the performance validation tests are given in Figure 3.3.37. As seen, the morphology is rough and heterogeneous. Also, the sample consists of various irregular-shaped particles. Besides, the presence of relatively big, rectangular prism-shaped particles is noticed. On the contrary, the SEM images (Figure 3.3.38) of solids obtained during stage-wise precipitation tests indicate that they have a very smooth surface with clearly identified cubic-shaped particles.

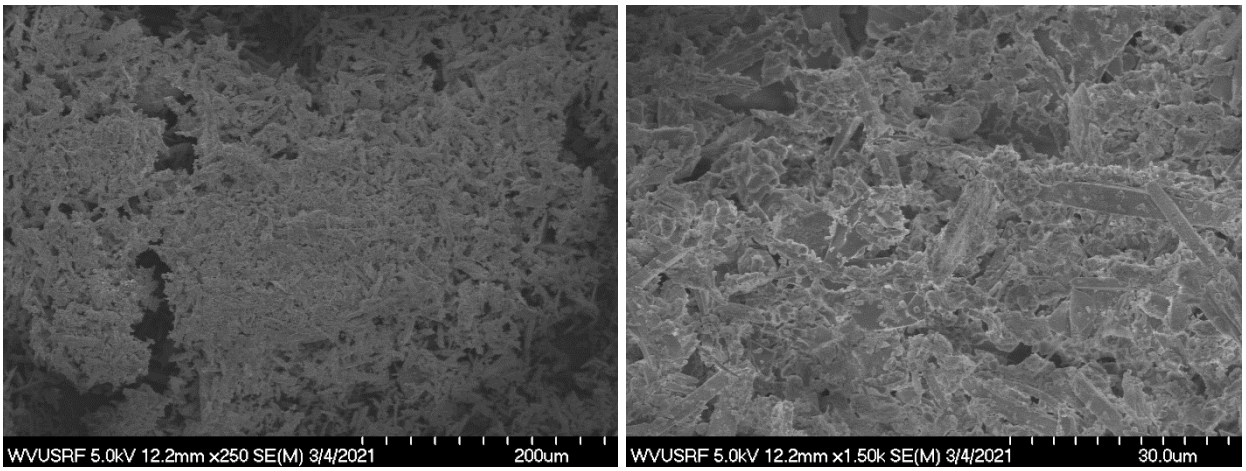

Figure 3.3.37 The SEM image of the rare earth oxide feed sample.

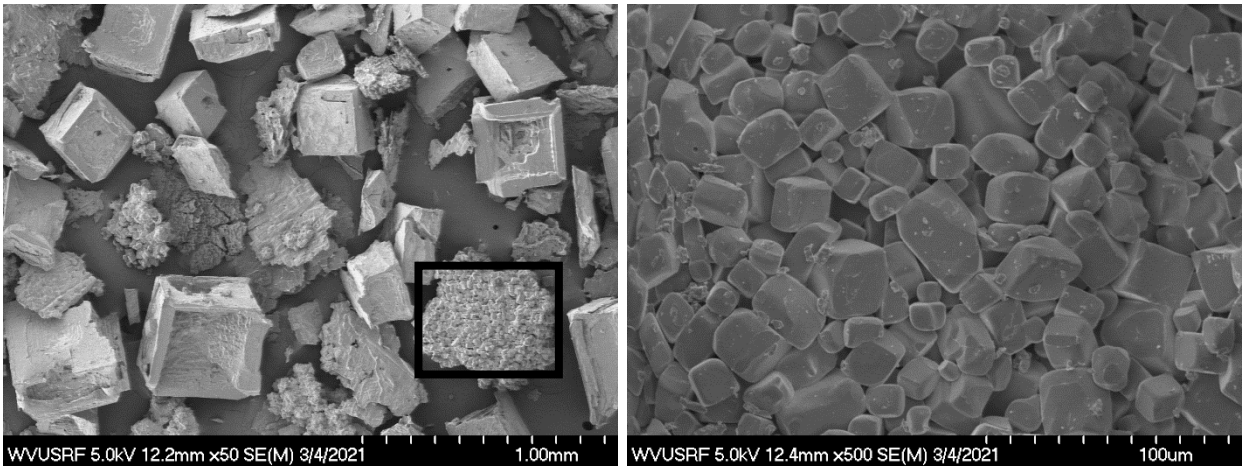

Figure 3.3.38 The SEM image of precipitated solids at pH 4.6.

3.3.2.5 Zeolite Adsorption Tests

Separation using solid materials is heavily used in metal separations, hydrometallurgy, water and wastewater treatment, removal, and recovery of metal ions (Sani et al., 2015). It has an advantage over the conventionally used solvent extraction mechanism by eliminating the consumption of organic extract and reducing environmental pollution those organic chemicals may create (Xiong et al., 2020). Sorbents are available in various material forms such as natural and synthetic organic, inorganic, or composite materials. Their surfaces are often heterogeneous, and bonding energies may vary from one site to another. Materials like zeolite, apatite, activated carbon, calcined phosphate, oxides, and hydroxides are examples of some highly abundant sorbents (Ladeira and Goncalves, 2007).

Therefore, in addition to selective precipitation and solvent extraction, the possibility of using sorbents to separate hazardous elements from rare earth was also evaluated. In this present study, zeolites, a group of crystalline alumina-silicates, were determined to be used for the adsorption tests due to their high chemical and radiation stability, unique physicochemical characteristics, high porosity, high sorption capacity, and many efficient applications to remove thorium and uranium from aqueous solutions by adsorption (Brindley and Bastovanov, 1982; Dyer and Jozefowicz, 1992; Misaelides et al., 1995; Kilincarslan and Akyil, 2005; Camacho et al., 2010). Zeolite's crystal lattice consists of two tetrahedral structures, SiO_4 and AlO_4, which are arranged to share each oxygen atom. The crystal structure of a zeolite has a net negative charge due to the charge difference between aluminum and silicon, and it is balanced with the exchangeable cations (Metaxas et al., 2003).

The adsorption process depends on the chemical nature of both fluid and solid. Also, it is highly affected by the available surface area and pore volume of the adsorbent (Couper et al., 2009). The effects of various operational parameters such as feed solution pH, adsorbent particle size, zeolite amount, and contact time on the removal of thorium and uranium were investigated during zeolite adsorption tests. The solution pH was decided to be varying between 2-4, according to earlier studies (Kaygun and Akyil 2007; Baybas and Ulusoy, 2011; Bertetti et al., 2011; Fasfous and Dawoud, 2012; Li et al., 2018). The pH plays an important role in sorption processes because it can influence the aqueous chemistry of the ions, determines the hydrolysis products, and the

properties of the active sites of the sorbent (Faghihian et al., 2004; Cheira et al., 2017). It also affects the external charge of the adsorbent which results in a change in the electrostatic interactions. It was seen that the capacity of uranium absorption increases with increasing pH and reaches a maximum value at a pH range of 2.0 to 3.5 (Cheira et al., 2017). A further increase in pH (above 4.5) typically leads to the precipitation of thorium, uranium, and rare earths which is the reason that experiments are not usually performed at pH values higher than 4 (Kutahyali and Eral, 2010; Cheira et al., 2017). Additionally, when pH is less than 2, the decomposition of zeolite is noticed, which will result in ineffective and lower adsorption capacity (Baybas and Ulusoy, 2011). 2 mol/L sodium hydroxide (NaOH) was used to adjust the solution chemistry to achieve different pH values as needed.

Particle size distribution is another critical factor due to its influence on the pressure loss upon passing the solvent through the sorbent. Besides, it affects mass transfer rates. Pressure loss increases with decreasing particle size, and mass exchange rates also increase with decreasing particle size because of shorter diffusion paths (Kammerer et al., 2011; Monji et al., 2016). An increase in adsorption capacity is expected when the particles are finer since the effective surface area increases as the size decreases (Zou et al., 2009). The pore size distribution also plays a significant role in the diffusion of the solutes into the sorbents. Following previously conducted studies, 1h, 2h, and 3h contact periods were determined for the tests (Kutahyali and Eral, 2010; Sani et al., 2015). Zeolite samples were used as received, without any pretreatment. The adsorption tests were carried out in a batch system by mixing the known volume of feedstock solution with a suitable amount of sorbent for a period of time at a controlled temperature to achieve equilibrium. Then, the sorbent was separated by filtration using 0.45 µm pore-sized filter paper and the representative supernatant was subjected to thorium, uranium, rare earths, and major metal analyses using ICP-MS and ICP-OES. An experimental design was generated with each parameter has three levels and a total of 27 tests were performed following the operational conditions seen in Table 3.3.14.

Following the test results, the amount of adsorbed thorium, uranium, and rare earth elements were calculated using the equation below:

$$Adsorption\ Recovery\ (\%) = \frac{C_i - C_f}{C_i}\ x\ 100 \tag{23}$$

where C_i and C_f are the concentration (mg/L) of the ions of interest in the aqueous solution before and after adsorption, separately. The results were also examined in terms of adsorption capacity and distribution coefficient according to the following equations:

$$Sorption\ Capacity\ (q) = (C_i - C_f)\ x\ \frac{V}{m} \tag{24}$$

$$Distribution\ Coefficient\ (K_d) = \frac{C_i - C_f}{C_i}\ x\ \frac{V}{m} \tag{25}$$

where V is the volume of the solution (L), m the weight of zeolite (g) used, and C_e the ion concentration (mg/L) when absorption equilibrium is reached. The distribution coefficient, which defines the ratio of ion of interest in the sorbent and the solution at equilibrium, is a direct indicator of the selectivity of the adsorbent towards the ions of interest (Metaxas et al., 2003).

Table 3.3.14 Test order and conditions of zeolite adsorption tests.

Test No.	Particle Size (µm)	pH	Adsorbent Amount (g)	Contact Time (hr.)
1	12	3	5.00	2
2	1490	2	3.75	2
3	200	4	3.75	1
4	12	4	3.75	2
5	1490	3	2.50	2
6	200	3	3.75	2
7	200	4	2.50	2
8	200	3	5.00	3
9	12	3	3.75	1
10	200	3	2.50	3
11	12	3	2.50	2
12	1490	3	3.75	1
13	1490	4	3.75	2
14	200	3	3.75	2
15	12	3	3.75	3
16	200	2	3.75	3
17	200	3	2.50	1
18	200	2	5.00	2
19	200	4	5.00	2
20	200	4	3.75	3
21	200	3	3.75	2
22	1490	3	3.75	3
23	12	2	3.75	2
24	200	3	2.50	1
25	1490	3	3.75	2
26	200	2	3.75	2
27	200	2	2.50	1

i. Characterization of Initial Zeolite Samples

A detailed characterization study was performed for the zeolite samples both before and after adsorption. First, the particle size analysis of each zeolite sample was performed using CILAS 1190 particle size analyzer. Following that, samples' mineralogical compositions were determined using the aforementioned PanAnalytical X'Pert Pro X-ray diffractometer. Samples were scanned at 45 kV and 40 mA over a 10-90° two-theta angle range in a continuous mode. As described previously, the evaluation and refinement of diffraction patterns were carried out using the HighScore software. The chemical composition of the samples was identified using the Olympus Vanta handheld X-ray fluorescence (XRF) analyzer. The same SEM-EDX instrument was utilized to analyze the samples' morphology. The accelerating voltage was varied between 5 and 15 kV, and the working distance was maintained at 12 mm during the SEM-EDX analysis. Similar to the other solid samples, before SEM-EDX analysis, zeolite samples were subjected to sputtering for 140 seconds using the Denton Desk V Sputter and Carbon Coater to enhance the image quality. SEM images taken under the lowest magnification were also analyzed with the ImageJ image processor for additional particle size measurement. The three zeolite feed samples were subjected to the Brunauer–Emmett–Teller (BET) nitrogen adsorption tests using the Micrometrics BET

instrument equipped with the ASAP 2020 Version 4.02 to identify the pore volume, pore size, and specific surface area.

The particle size distribution of these zeolite samples is provided in Figure 3.3.39. Figure 3.3.39 (A) shows the particle size dis tribution of the coarsest zeolite sample with a P_{80} passing value of 1490 µm whereas Figure 3.3.39 (B) displays the particle size distribution of the middle-sized zeolite sample with a P_{80} value of approximately 200 µm. Lastly, the particle size distribution of the finest sample is provided in Figure 3.3.39 (C). As seen, a P_{80} value of approximately 12 µm was found for this particular sample. Due to the limit of the particle size analyzer's capability, the particle size distribution of the coarsest zeolite sample was determined via sieve analysis while the rest two samples were subjected to the laser particle size analysis.

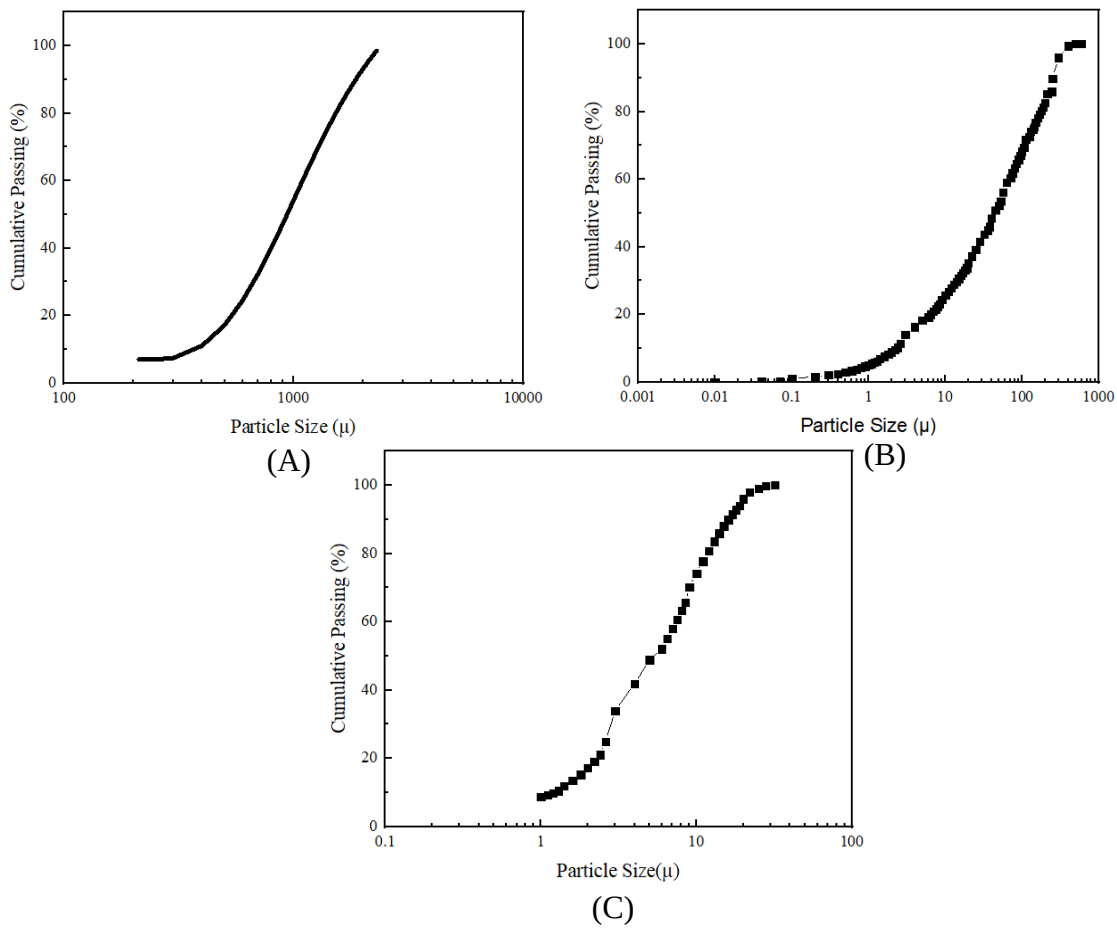

Figure 3.3.39 Particle size distribution of three zeolite samples. (A) Coarsest sample, P_{80}=1490 µm, (B) Middle-sized sample, P_{80}=200 µm, (C) Finest sample, P_{80}=12 µm.

Mineralogical compositions of the samples were identified using XRD. The combined XRD patterns of the three samples are provided in Figure 3.3.40. All samples displayed the same diffraction pattern, which refers to the single phase of clinoptilolite-type zeolite. It is the most commonly found zeolite type with the aluminum-silicate tetrahedral arrangement and Si/Al>4 (Godelitsas and Armbruster, 2003). This type of zeolite series has the complex chemical formula of $Na_6[Al_6Si_{30}O_{72}]_{24}H_2O$.

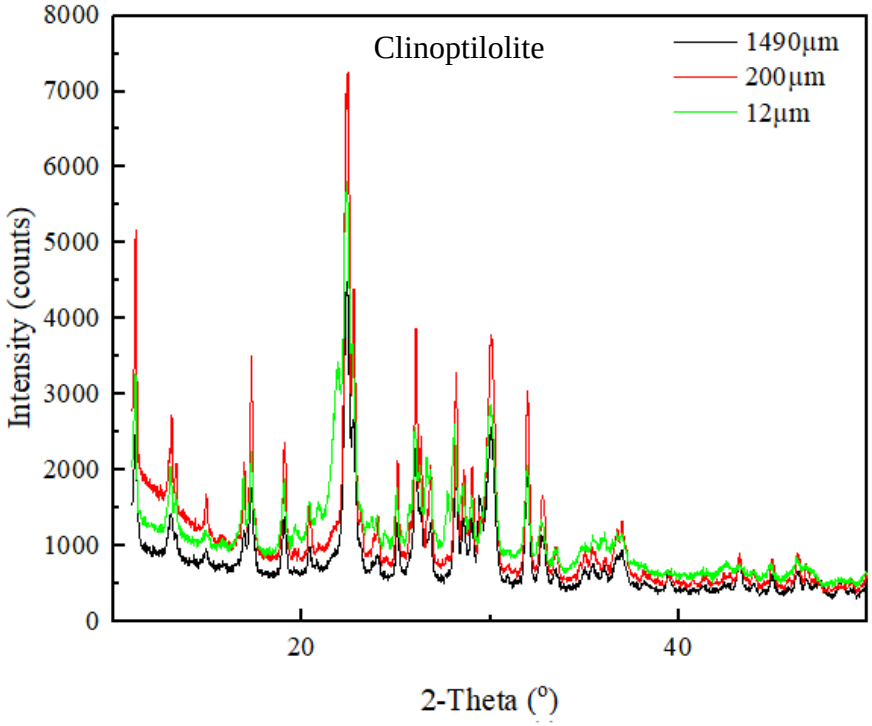

Figure 3.3.40 X-ray diffraction pattern of the initial zeolite samples.

XRD analysis was followed by identification of the chemical composition of the zeolite samples using Vanta handheld XRF analyzer. Test results indicate that the samples contain a high concentration of silicon and aluminum, which is typical for zeolites. The distinctive properties of zeolites result from their honeycomb structures with water molecules and exchange cations located in the cavities. Mostly, Ca^{2+}, Na^{+}, or K^{+} located in the cavities, are exchangeable with other ions depending on the Si/Al ratio and the position of the ion exchange sites. This ratio provides a relatively high negative charge for attracting positive ions from the solution, thus, an increase in aluminum concentration will also provide higher adsorption capacity. The SiO_2/Al_2O_3 ratio of the three zeolite samples was around 5.74%. In addition to these major components, 1.43 wt% Ca, 0.99 wt% Fe, 0.28 wt% Mg, and 2.10 wt% K were also detected in the samples as minor components. The framework structure containing cations and enclosing cavities, called super cage (Nandanwar et al, 2016).

EDX spectrums of three zeolite samples are presented in a combined graph (Figure 3.3.41). All three samples represent a similar EDX pattern which shows the presence of Si, O, and Al as the main peaks. Compared to coarse and middle-sized zeolite samples, the EDX pattern of the finest zeolite sample (12 µm) displays considerably high intensities for all element peaks. In addition to Si, Al, and O, a portion of Na was also detected. The findings obtained from EDX, XRF, and XRD analyses complete and support each other. The carbon peak seen in the EDX spectrum is due to the carbon tape substrate used during sample preparation.

The images obtained by SEM under various magnifications are seen in Figure 3.3.42. As seen, regardless of the sample size, the surface is heterogeneous and rough with noticeable porous structures. Also, particles all have flaky and irregular shapes, which are consistent with the observations provided in Zendelska and his co-workers' study (2015). Besides, The finest zeolite samples also tend to agglomerate due to an increased surface area, as seen in Figure 3.3.42 (C).

Lastly, the three zeolite feed samples with a P_{80} value of 1490 µm, 200 µm, and 12 µm, separately, were subjected to the BET nitrogen adsorption tests using Micrometrics BET instrument equipped with the ASAP 2020 Version 4.02 to identify the pore size and specific surface area. The Brunauer–Emmett–Teller (BET) method is most widely used for evaluating the surface area of porous materials. Nitrogen (at 77 K) is traditionally the adsorptive used to perform the analysis. While the coarsest zeolite had a pore diameter of 12.6 nm, the middle-sized and the finest zeolites had a pore diameter of 9.9 and 8.7 nm, respectively. According to the classification of pores established by the International Union of Pure and Applied Chemistry (IUPAC) in 1985 (Thommes et al., 2015), all zeolite samples have mesoporous structures due to pore widths less than 50 nm. The specific surface area of the coarsest sample was determined as 16.1 m^2/g. The middle-sized and the finest samples had a specific surface area of 15.7 and 20.2 m^2/g, respectively. As seen, with a decrease in the particle size, the corresponding specific surface area generally increased. Moreover, the pore volume distribution as a function of the pore size indicated a linear distribution for all three zeolite samples.

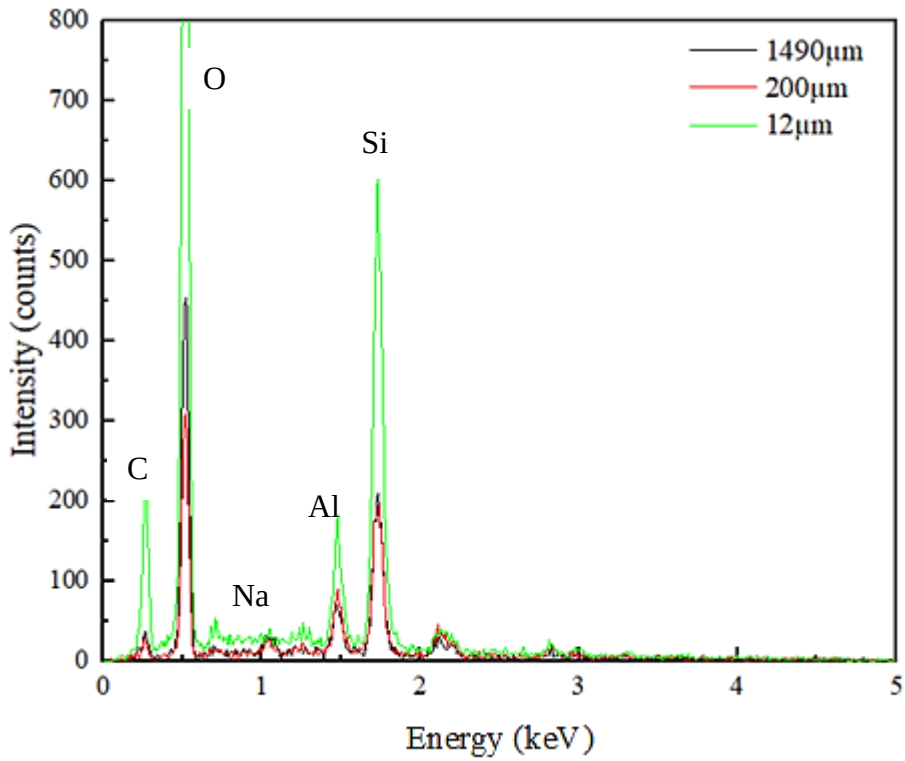

Figure 3.3.41 Elemental identification of the zeolite samples obtained from the ED

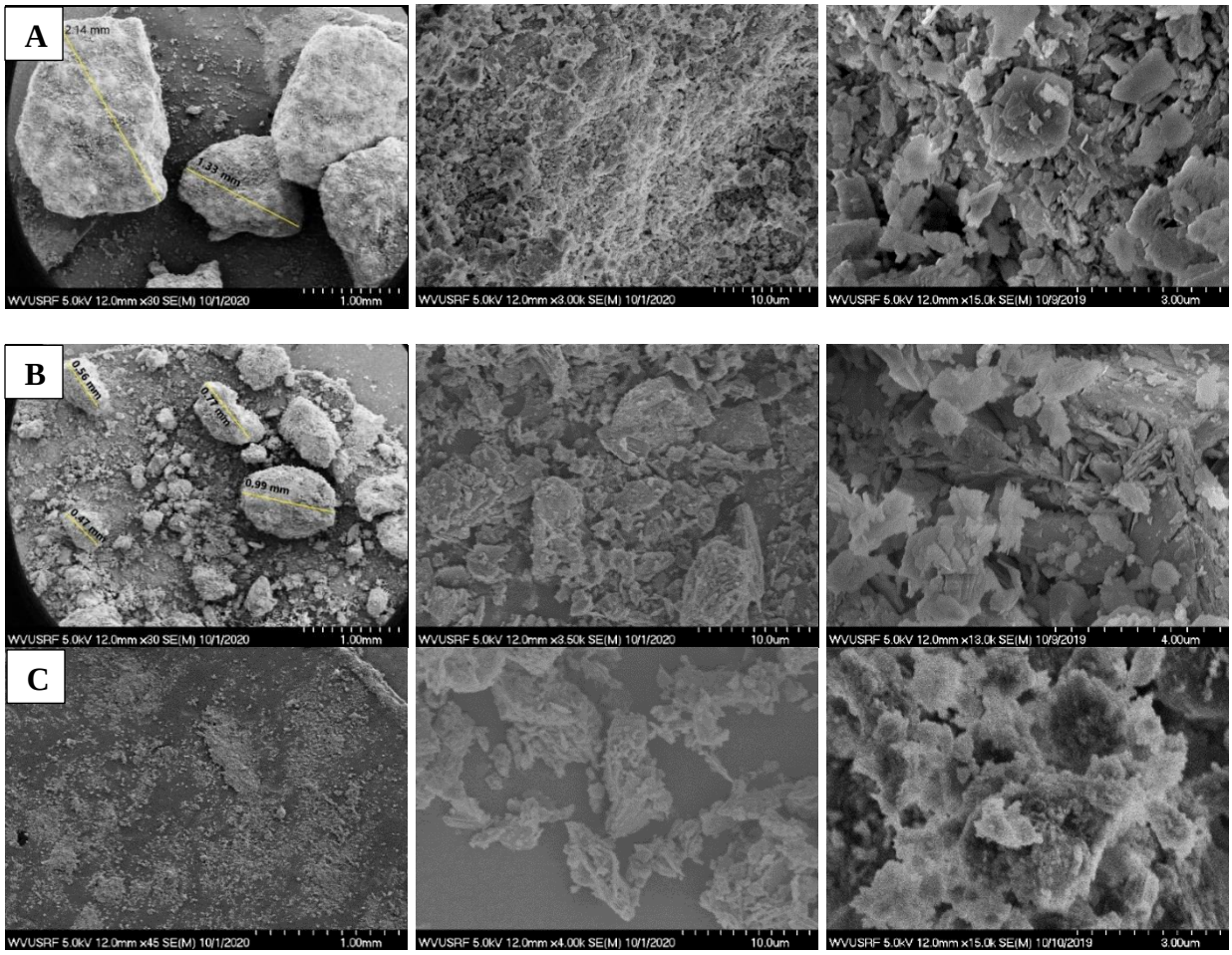

Figure 3.3.42 SEM images of the zeolite samples under various magnification. (A) the coarsest sample, (B) medium size sample, (C) the finest sample.

The adsorption isotherm of the three zeolite samples is given in Figure 3.3.43 and the classification of physisorption isotherms is shown in Figure 3.3.44 (A). According to the classification, the nitrogen adsorption on the zeolite sample is a Type IV (a) isotherm. Point B, the beginning of the near-linear section, usually corresponds to the completion of monolayer coverage. A more gradual curvature, for example, a less distinctive Point B, is an indication of significant overlap of the monolayer coverage and the multilayer adsorption. There existed a linear relationship between the absorbance and the relative pressure varying from 0.09 to approximately 0.7, which represents the predominant mesoporous region of the fraction. A near-vertical adsorption line appeared with a relative pressure beyond 0.9 indicates that the zeolites had a portion of macropores as well. Because, if a mesoporous adsorbent contains no macropores, its Type IV isotherm remains nearly horizontal over the upper range of p/p^0 (Thommes et al., 2015). In addition, the adsorption started at very low pressures, which may indicate the presence of some micropores (Ramesh et al., 2014). Besides, there existed a hysteresis between adsorption and desorption curves. This occurs when the pore width exceeds a certain critical width (i.e., pores wider than 4 nm) (Thommes et al., 2015). According to the hysteresis classification given in Figure 3.3.44 (B), it is an H3 type of hysteresis. Pore-size distribution is usually expressed in the form of

a pore volume distribution as the function of the pore size. As seen in Figure 3.3.45, the pore size distribution is linear. Overall, no difference was observed between the nitrogen adsorption behaviors of the three zeolite samples (i.e., coarse, middle-sized, and fine zeolite samples).

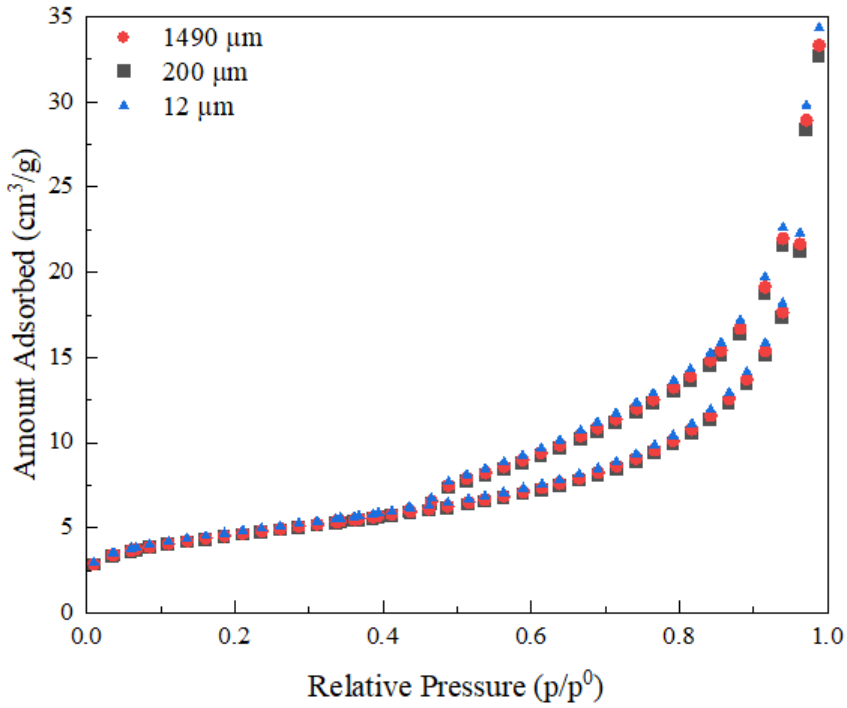

Figure 3.3.43 The Brunauer–Emmett–Teller (BET) Nitrogen adsorption isotherm of middle-sized zeolite sample

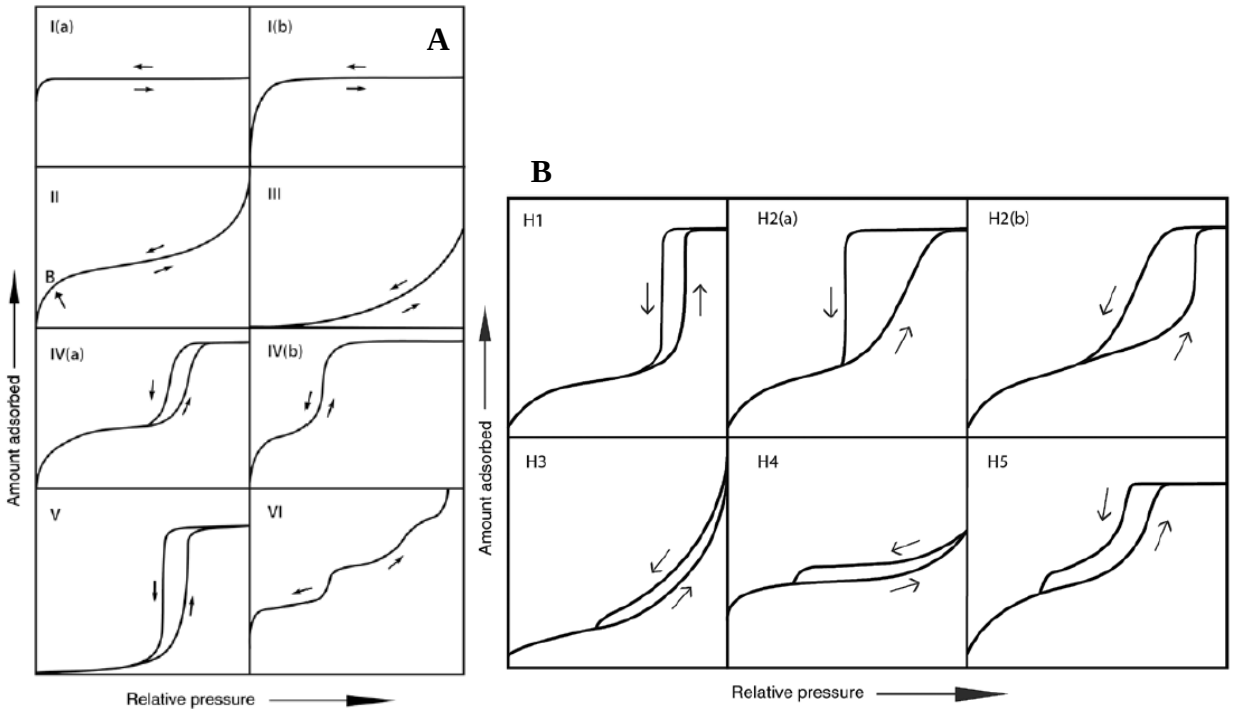

Figure 3.3.44 Classification of (A) physisorption isotherms, (B) classification of hysteresis (Thommes et al., 2015)

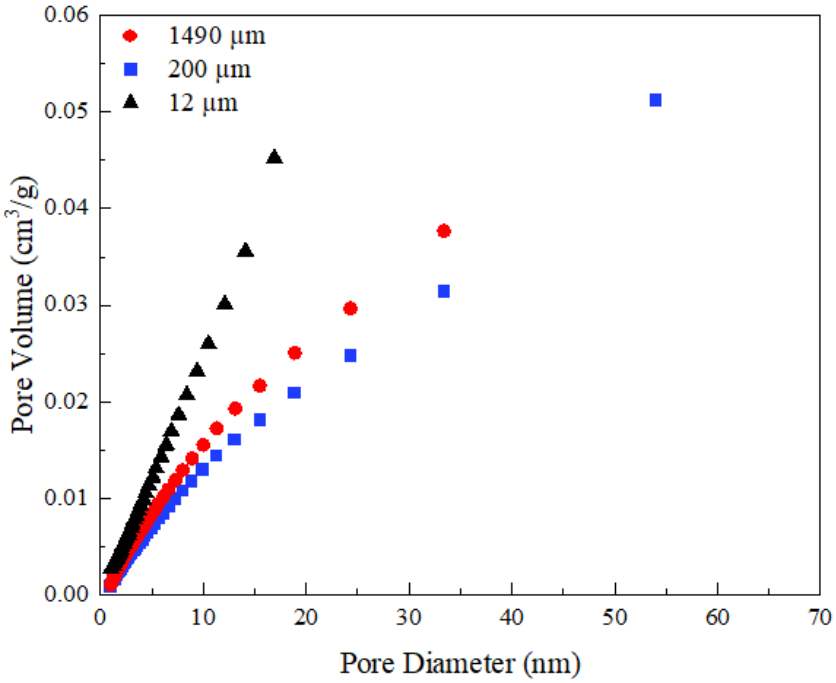

Figure 3.3.45 Pore size distribution of the middle-sized zeolite sample.

ii. *Adsorption Tests*

The recovery of total rare earths, thorium, and uranium into the solid phase was given in Figure 47. As seen in Figure 3.3.46 (A), the recovery of rare earth elements fluctuated between 0.03 wt% and 96.90 wt%. On the contrary, nearly 100 wt% thorium removal was achieved in every test condition except for Test 23, which yielded a 36.67 wt% of thorium adsorption (Figure 3.3.46(B)). Like rare earths, a significant variation was observed for uranium adsorption, as shown in Figure 3.3.46 (C). The adsorption recovery of uranium changed between 0.00 and 98.70 wt%.

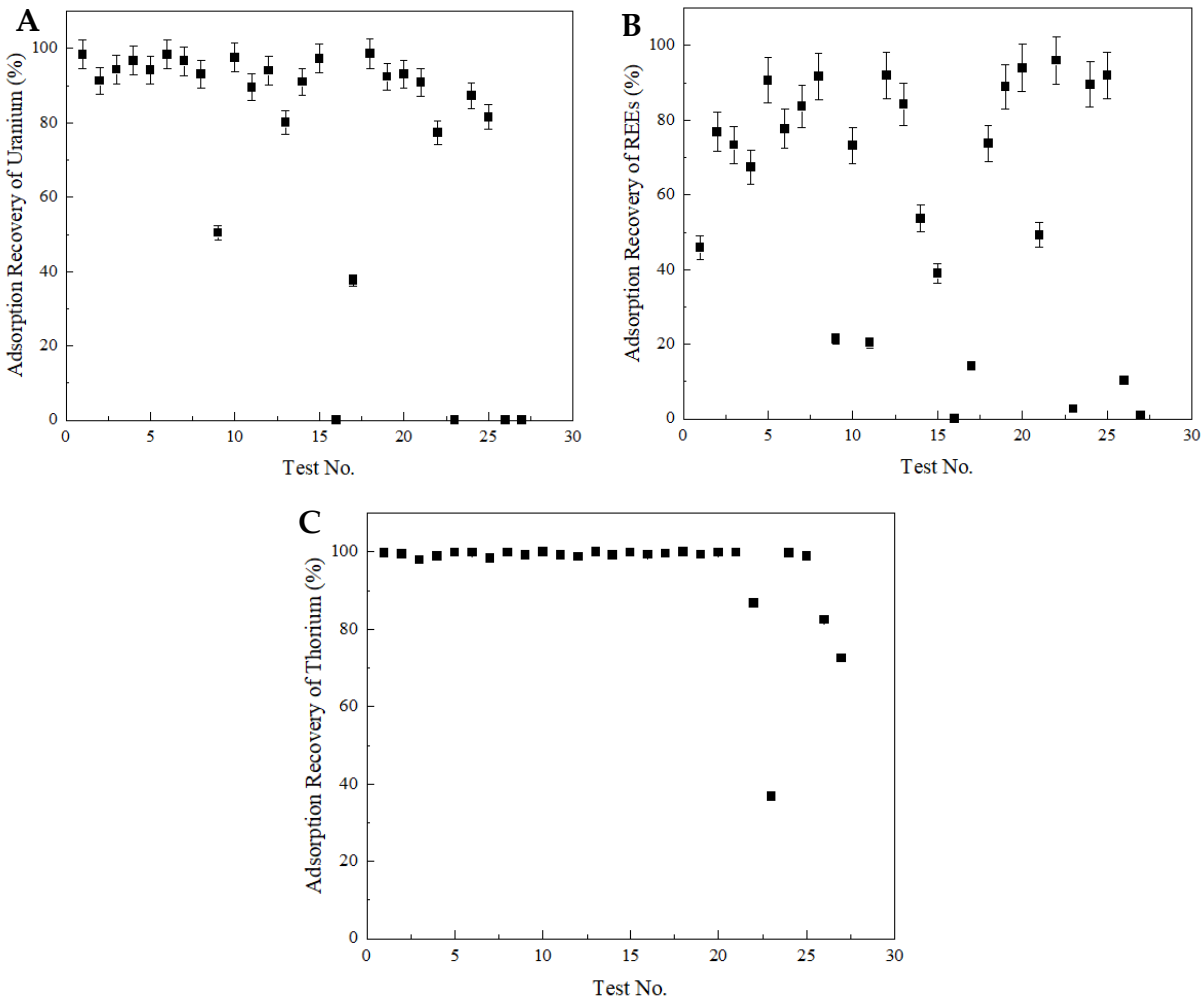

Figure 3.3.46 Adsorption recoveries into the solid phase. (A) total rare earths, (B) thorium, (C) uranium. Error bars represent one standard deviation of multiple replicate test.

The three lowest rare earth adsorption recoveries, namely 0.03 wt%, 1.01 wt%, and 2.67 wt%, were achieved with Test 16, 27, and 23, respectively, at the same pH value of 2. Additionally, Test 16 and Test 27 were conducted with zeolite samples of the same size (i.e., 200 µm). However, Test 23 was performed using the zeolite sample with a P_{80} value of 12 µm, which may indicate the impact of particle size on the adsorption mechanism. The retention time of Test 16, 27, and 23 was 3, 1, and 2 hours, respectively. As seen, Test 16 produced the lowest rare earth adsorption into the

solid phase (0.03 wt%), which corresponded to a 3-hour contact time. However, when the zeolite's size was reduced to 12 µm (Test 23), a retention time of 2 hours was sufficient to achieve a nearly equal low rare earth adsorption (2.67 wt%). Moreover, in a study conducted by Kini (2006), it was stated that different adsorption tests may take various contact times to equilibrate with the ions in the solution to complete the adsorption. Test 22 was conducted with a contact time of 3 h, which is longer than the contact time applied for Test 9, 11, and 17. A more complete absorption may be achieved for Test 22, which, therefore, led to the highest rare earth adsorption recovery (i.e., 97.4 wt%). Although these three tests generated the lowest rare earth adsorption recoveries into the solid phase, no separation was observed between uranium and rare earth elements under the same conditions. This may be due to the saturation of adsorption sites with other ions before uranium. Under all three test conditions, 0 wt% uranium was adsorbed by the zeolites. On the other hand, thorium adsorption recovery varied among these three test conditions. The thorium adsorption recovery at Test 16, 27, and 23 was 99.33 wt%, 72.52 wt%, and 36.67 wt%, respectively. It is known that thorium shows very little tendency to hydrolyze at low pH values, and the dominated ion at pH< 3 is Th^{4+}, which is the exchangeable ion between solution and the zeolite. When the solution pH increases, the formation of other species (i.e.$[ThOH]^{3+}$, $[Th(OH)_2]^{2+,}$ and $[Th(OH)_3]^{+}$) are seen due to hydrolysis. The hydroxyl group in these species increases with increasing pH (Faghihian et al., 2004).

The effect of particle size was expected since adsorption capacity is dependent on the effective surface area, which generally increases with decreasing particle size (Zou et al., 2009). Also, particles with a smaller diameter are characterized by a larger specific surface area, and thus the adsorption is enhanced and a shorter contact time is required to reach the equilibrium. However, an increase in the adsorption recovery of rare earth elements was observed while a coarser zeolite sample was used. For example, Test 5 and Test 11 were conducted under the same operating conditions, except for the zeolite particle size. While Test 5 was performed with the coarsest zeolite, 1490 µm, Test 11 was carried out with the finest size zeolite, 12 µm. The respective rare earth adsorption recoveries were found as 90.67% and 20.43%. The reason for this substantial increase in the adsorption recovery of rare earths may lie under the particle size reduction occurring during the mixing of solid and liquid phases throughout the adsorption process. The post adsorption SEM image provided in Figure 3.3.47 shows fractures and cracked surfaces, which may result from a reduction in the zeolite particle size. Later, the particle size analysis performed with post adsorption solid samples confirmed the size reduction. The particle size of the coarsest zeolite sample with an initial P_{80} value of 1490 µm was reduced to 45 µm after adsorption. Likewise, a reduction in the particle size of the middle-sized zeolite sample was also observed. After adsorption, the new P_{80} value of the middle-sized zeolite sample was found to be 60.5 µm as opposed to the initial value of 200 µm. However, no change in the particle size of the fine sample (i.e., 12 µm) was detected. The particle size reduction occurred for coarse and middle-sized zeolite samples during adsorption. It created fresh surfaces and new active sites ready for ion adsorption that may explain the elevated adsorption recovery with the increase in the nominal adsorbent particle size.

Overall, the best separation performance was achieved with Test 11 while using 2.50 grams of 12-µm zeolite sample at a pH value of 3 with a contact period of 2 hours. Under these conditions, the adsorption recovery of rare earth elements, thorium, and uranium into the solid phase was found to be 20.43 wt%, 99.20 wt%, and 89.60 wt%, respectively.

In terms of major metal adsorption, steady recovery results were observed for iron in comparison to aluminum and magnesium. Almost 100 wt% iron adsorption onto zeolite was seen

under every test condition. Similar selective iron adsorption over other metals was seen in Motsi and his coworkers' (2009) study on heavy metal adsorption from acid mine drainage by natural zeolite. Contrarily, adsorption recovery of aluminum changed between 12.49 wt% to 99.65 wt% where the lowest adsorption recovery was achieved with Test 11. The adsorption recovery of magnesium also varied. The lowest magnesium adsorption, 69.60 wt% was observed with Test 11, and the highest magnesium adsorption recovery seen was 99.87 wt%. Detailed results for the adsorption studies are provided in Table 32 and Table 33 in the Appendix D.

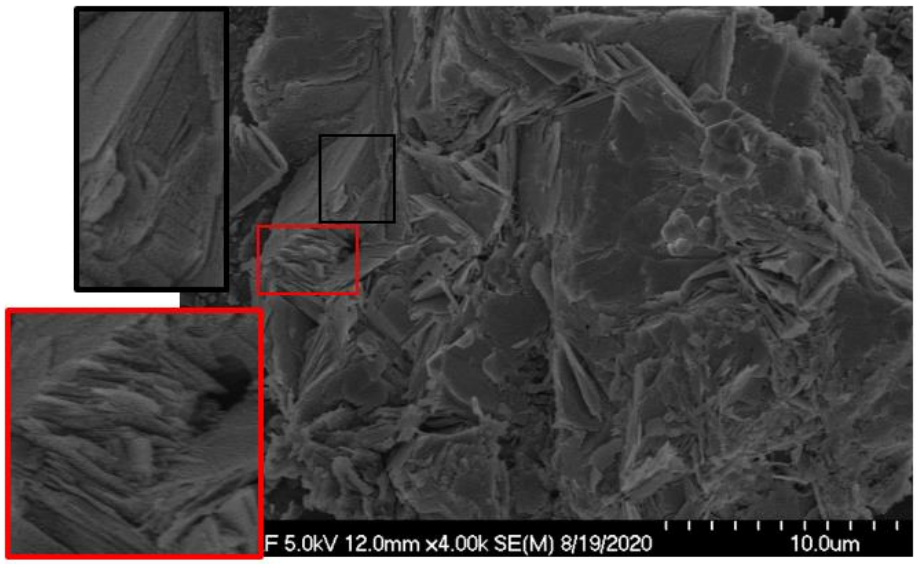

Figure 3.3.47 SEM image showing the fractures and cracks formed after adsorption.

Following the data analysis of the test results, the impact of four operating variables (i.e., zeolite particle size, feed solution pH, adsorbent amount, and contact time) on the recovery of total rare earths, thorium, and uranium was analyzed using the response surface methodology. The adsorption recovery values of rare earth elements, thorium, and uranium obtained from the full dataset were uploaded to the Design Expert Software following the Box Behnken experimental design. Statistical models were developed separately to determine the operational sensitivity with respect to the input parameters.

A statistical model was first developed as a tool to predict the recovery of rare earth elements by incorporating all the influential operating parameters, as shown in Eq. (26). It can be seen from the quadratic model that the variables, including the zeolite particle size, feed solution pH, and adsorbent amount, except the contact time, all had a significant impact on the recovery of rare earth elements.

$$REE\ Adsorption\ Recovery = +60.21 + 28.43 * A + 27.46 * B + 16.27 * C + 8.58 * D - 14.33 * AB - 5.08 * AC - 3.48 * AD - 14.13 * BC + 5.62 * BD - 14.23 * CD + 2.08 * A^2 - 7.39 * B^2 + 7.76 * C^2 - 3.68 * D^2 \quad (26)$$

where the uncoded model terms A, B, C, and D correspond to zeolite particle size, feed solution pH, adsorbent amount, and contact time, respectively. While a statistical model was generated for rare earths, a significant model was generated for neither thorium nor uranium.

The Analysis of Variance (ANOVA) table used to determine the significance of the statistical model generated for the estimation of rare earth adsorption recovery is shown in Table 3.3.15. As seen from the table, the model F-value of 6.90 implies the model is significant. The probability of an F-value becoming this large is 0.09% (<5%, which is the critical P-value used to determine the significance). Model terms are considered significant within a 95% confidence level, or in other words, values of "prob>F" less than 0.05 indicate that terms are significant. In this case, terms A, B, and C are significant model terms, whereas D is an insignificant model term. The lack-of-fit value of 1.21 implies a 53.50% chance that a lack-of-fit F-value can be this high. The lack-of-fit must be insignificant for a model to be fit. In the same table, R-squared values were also given to further evaluate the robustness of the developed model. As seen, the R-squared value of 0.8895, and an adjusted R-squared value of 0.7606 further confirm the model's significance.

Table 3.3.15 ANOVA analysis of the quadratic model for predicting rare earth recovery.

Source	Sum of	df	Mean Square	F Value	p-value Prob> F	
Model	26572.63	14	1898.05	6.90	0.0009	Significant
A- Particle Size	9696.90	1	9696.90	35.25	0.0001	
B- pH	9048.07	1	9048.07	32.89	0.0001	
C- Adsorbent	3177.21	1	3177.21	11.55	0.0053	
AB	821.68	1	821.68	2.99	0.1095	
AC	103.12	1	103.12	0.37	0.5518	
BC	798.06	1	798.06	2.90	0.1142	
A^2	23.08	1	23.08	0.084	0.7770	
B^2	290.94	1	290.94	1.06	0.3240	
C^2	320.78	1	320.78	1.17	0.3014	
Residual	3300.85	12	275.07			
Lack of Fit	2832.19	10	283.22	1.21	0.5350	Not significant
Pure Error	468.66	2	234.33			
Cor Total	29873.48	26				
R-Squared	0.8895					
Adj R-Squared	0.7606					
Pred R-Squared	0.4186					
Adeq Precision	10.110					

Three diagnostic plots developed based on the statistical model are given in Figure 49. In these plots, the relationship between two parameters was described while keeping the other two parameters constant at their middle values. In Figure 3.3.48 (A), the effect of particle size and pH is presented while keeping the adsorbent amount and contact time constant at 3.75 g and 2 hrs, respectively. It is well-known that pH is an important parameter in adsorption processes. As seen, rare earth recovery increases with an increase in the pH value. This could attribute to the competition between hydrogen ions and rare earth ionic species present in the solution at a given pH value (Faghihan et al., 2004). Typically, zeolite has a tendency to adsorb H^+ ions from the solution which creates a positive charge on the zeolite structure and other positively charged ions are repulsed due to the electrostatic interaction. When the solution pH increases, the amount of H^+ ions decreases, which results in the adsorption of other ions present in the solution (Motsi et al., 2009). However, freed negatively charged ions (i.e., Cl^-) may reverse the electrostatic repulsion and enhance adsorption. At the same time, depending on the concentration and conditions, it may

have an opposite effect and further reduce the adsorption by binding with metals and forming complexes that cannot be adsorbed. This could be the reason for the wide variation observed in the adsorption recovery of rare earths. Also, rare earth adsorption recovery rises with an increase in the particle size, which statistically supports the findings stated earlier that unexpected particle size reduction induced during mixing leads to enhanced adsorption due to freshly created surfaces for ion adsorption. The same trend was seen in Figure 3.3.48 (B), where the relationship between particle size and the adsorbent amount is given, while maintaining the pH and contact time constant at 2 and 2 hrs, respectively. In comparison to Figure 3.3.48 (A) and (C), Figure 3.3.48 (B) displays a relatively flat surface. A higher amount of adsorbent will result in more significant adsorption because the active adsorption sites will increase concurrently. Figure 3.3.48(C) further shows that rare earth recovery decreases at a lower pH value and a smaller adsorbent amount.

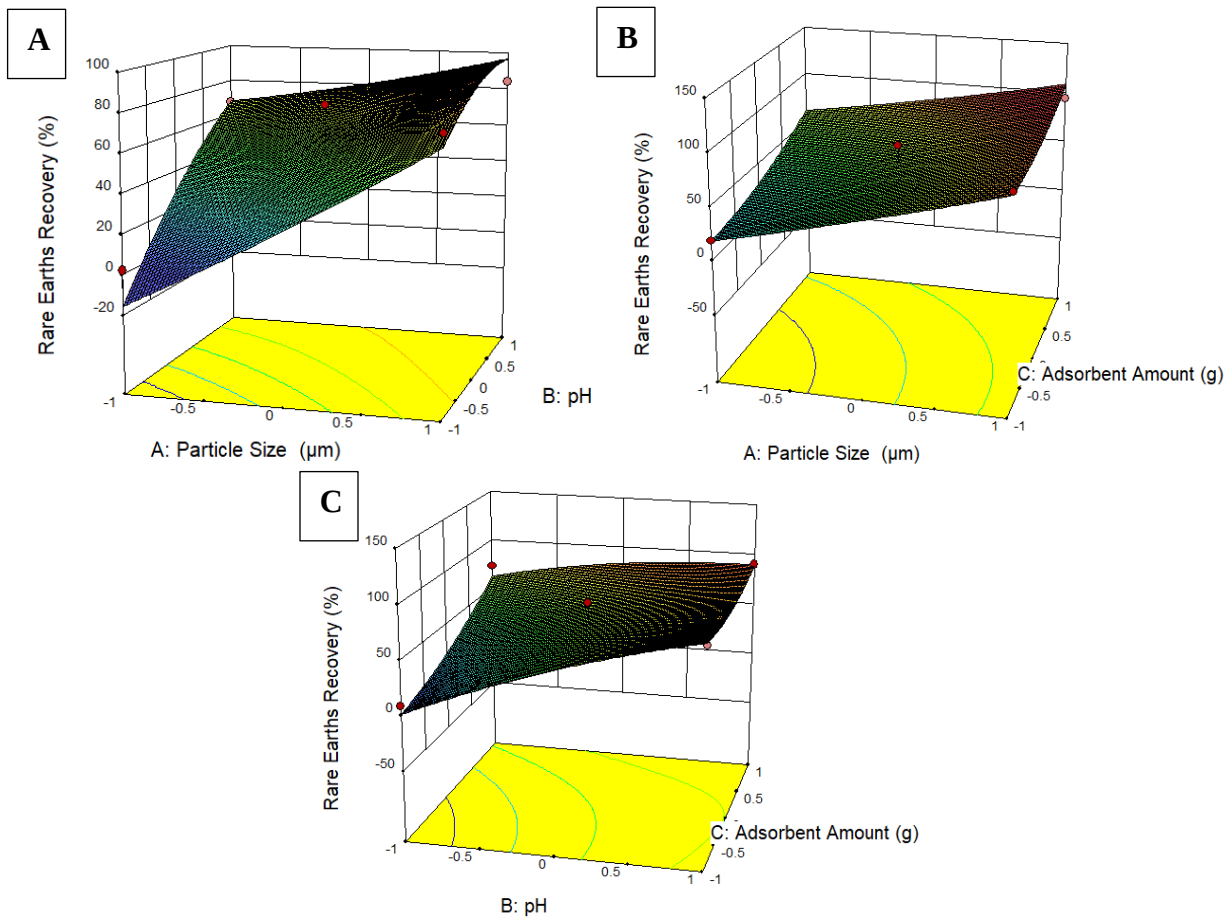

Figure 3.3.48 Diagnostic plots obtained based on the statistical model developed for the adsorption recovery of rare earths.

iii. Characterization of Post Adsorption Zeolite Samples

The solid sample used during Test 11 (12-µm zeolite), was subjected to XRD and SEM-EDX analyses to detect whether there was any change in the elemental and mineralogical compositions after adsorption. Results obtained from XRD revealed the formation of halite and

Perrierite-Ce in addition to clinoptilolite. Halite formation is probably due to the reaction between feedstock's medium, HCl, and the addition of pH regulator, NaOH. Also, the zeolite samples initially contained a small amount of sodium before the adsorption tests. Perrierite-Ce is a compound consisting of many elements and having a general formula of $A_4BC_2D_2Si_4O_{22}$, where A represents rare earth elements and thorium, B represents Fe, Mn, Mg, C refers to Fe, Mn, Mg, Al, Ti, Cr, and D corresponds to Ti (Muhling et al., 2014). Cerium and lanthanum are the most dominant rare earth elements. Perrierite-Ce is defined as radioactive according to the Code of Federal Regulations Title 49, which supports the high concentration of thorium in the zeolite post adsorption. The XRD pattern of the sample was given in Figure 3.3.49.

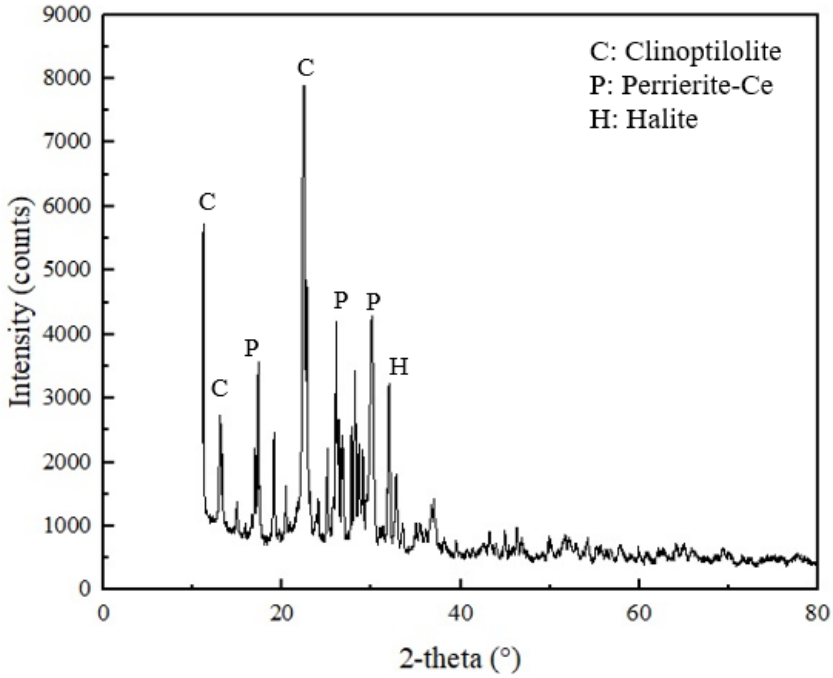

Figure 3.3.49 XRD pattern of the solid samples generated with Test 11.

Image analysis was performed using SEM to provide further information. As seen in Figure 3.3.50, the morphology remains rough, and the particles maintain irregular shapes. However, the formation of small prismatic crystal particles is seen. This finding is well correlated with the crystal structure of Perrierite-Ce (Chukanov et al., 2012). The bright areas highlighted in the image may refer to the accumulation of heavy elements such as the rare earth elements and thorium.

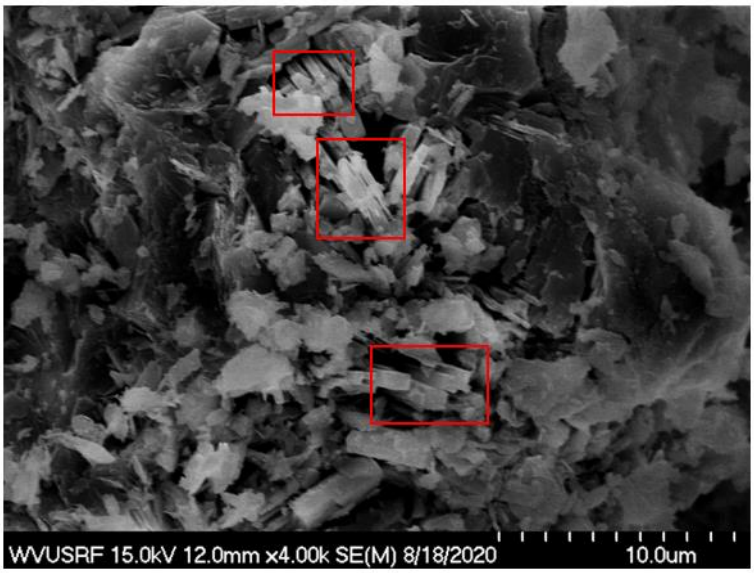

Figure 3.3.50 SEM images of the solid samples generated after adsorption. Bright areas highlighted in the red boxes indicating the deposition of heavy elements.

The EDX pattern of the solid sample generated from Test 11 is shown in Figure 3.3.51 (A). In comparison to the elemental concentration of the raw zeolite samples, after adsorption, a substantial decrease in the intensities of aluminum and silicon was observed. This finding suggests a reduction in both the aluminum and silicon concentration, attributed to the adsorption of external elements onto the zeolite structure. Like XRD, EDX was also able to detect thorium and most of the rare earth elements; however, their concentrations are considerably low compared to Al, Si, and O. Due to this fact, they are not clearly seen in the full pattern. However, as shown in the close-up view (Figure 3.3.51 (B)), most of the rare earth elements were observed in the energy level between 0.5 and 1.3 keV, and thorium was detected around 3 keV.

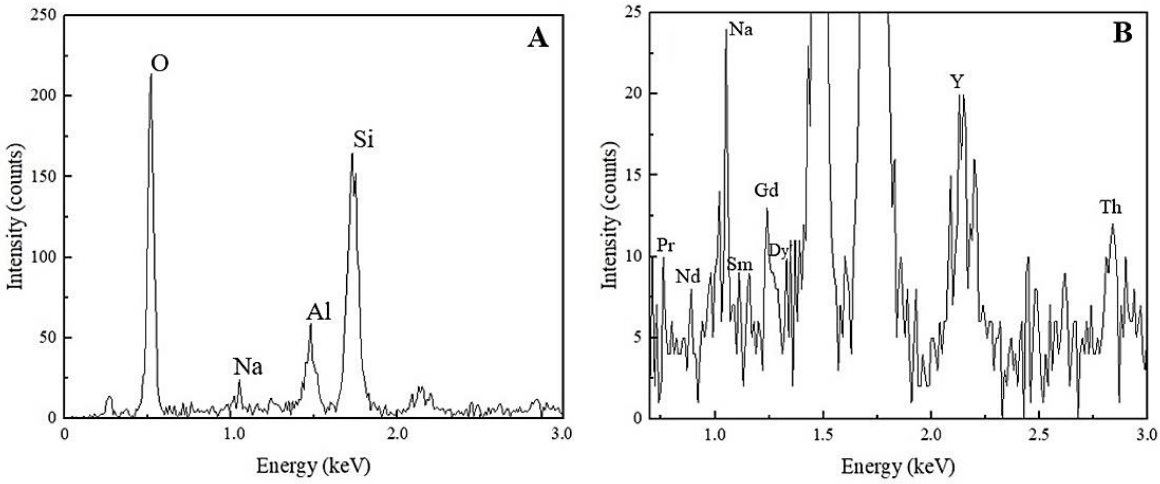

Figure 3.3.51 EDX pattern of the solid sample generated after Test 11. (A) Full EDX pattern indicating high-intensity elements. (B) Close-up view showing the detection of rare earth elements and thorium.

iv. *<u>Adsorption Kinetics and Isotherms</u>*

Kinetic adsorption test results shown in Figure 3.3.52 indicate fast adsorption for thorium as opposed to rare earths and uranium. Within the first 5 min, the adsorption recovery of thorium reached 86.5 wt%, which later continued to rise but with a small incremental increase. At the end of the 3-hr contact, the maximum thorium adsorption onto the zeolite was 93.4 wt%. On the other hand, rare earth elements and uranium followed a similar pattern jointly. A significant increase in the adsorption recovery of rare earths was first seen during the 10-15 min time interval. At the end of 10 min, the adsorption recovery of rare earths was 3.0 wt%, and at 15 min, it increased by 8.2 wt% and reached a new value of 11.3 wt%. Later, another 8.2 wt% increase was further observed during the 30-45 min time interval. Adsorption recovery of total rare earth elements reached 21.5 wt% at the end of the kinetic test. Data shown in Figure 3.3.53 further support the findings mentioned above. It can be seen from Figure 3.3.53 (A) that the distribution of rare earths in the solid phase increased significantly at both the 10-15 and 30-45 min time intervals. The distribution of thorium as a function of adsorption time is presented in Figure 3.3.53 (B), which again suggests that the most significant adsorption occurred during the first 5 min. Uranium exhibited a similar adsorption behavior as rare earth elements. Low uranium adsorption was also observed in Godelitsas and Armbsruster's study due to the complicated aqueous chemistry of uranium as well as the constant structural changes occurring in the mesoporous zeolite sample (Godelissas and Armbruster, 2003). In the same study, high thorium adsorption along with hydrogen ion adsorption at pH<3 was also observed, which shares similar findings presented here. The adsorption mechanism starts with the formation of complexes at the external surface. Later, the ions transport into the pores to form inner complexes via covalent or ionic bonding and become more stable. As the valence of a cation increases, the tendency of complexation also increases. Later the cation creates an outer-sphere complex in which at least one water molecule being in between the cation and the adsorbent. Sometimes, the cation which is surrounded by water molecules may locally neutralize the surface charge of the adsorbent instead of forming a complex. In that case, the ion lies in the diffusion layer. While the complexes on the Stern layer may have covalent or ionic bonding, the ions in the diffusion layer only have ionic bonds. Rapid thorium complexes formed on the external surface of the zeolite may block the formation of complexes with other ions. Afterward, the thorium molecules diffusing into the inner pores can hinder the adsorption of other ions. This may also be explained via the molecule sizes of rare earths, thorium, and uranium. While thorium has a molecule size of 0.24 nm, uranium has a molecule size of 0.23 nm. Although the molecule size of rare earth elements changes, it varies between 0.228 and 0.25 nm. If thorium is adsorbed first due to its easy nature, it may slow down the transport of other ions when the adsorbent has a narrow pore diameter (Malamis and Katsou, 2013). This also supports the identification of thorium-containing mineral phases in the XRD analysis conducted after adsorption. Moreover, Parzentny and Rog (2019) stated uranium is mainly concentrated on the surface of Al-Si porous structures, and thorium is concentrated in the Al-Si grains.

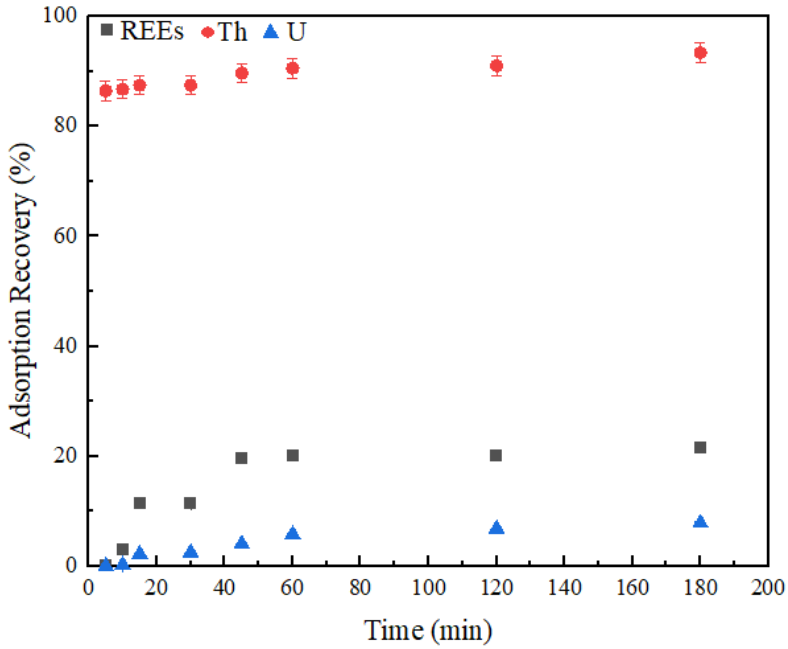

Figure 3.3.52 Adsorption recoveries of total rare earth elements, thorium, and uranium as a function of contact time. Error bars represent one standard deviation of multiple replicate tests.

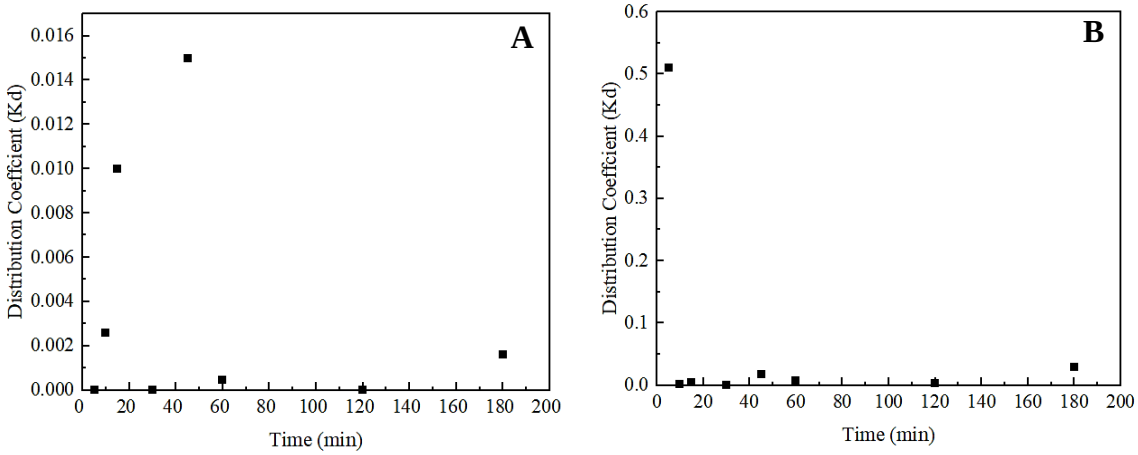

Figure 3.3.53 Distribution coefficient values of (A) total rare earth elements and (B) thorium as a function of contact time. Error bars represent one standard deviation of multiple replicate tests.

Adsorption isotherms were subsequently developed based on the kinetic adsorption data. To understand the adsorption capacity of the adsorbent, the absorption data and kinetics after reaching equilibrium must be evaluated using several classic adsorption isotherms. The isotherms indicate the distribution of molecules between the solid and liquid phases when the process reaches its equilibrium (Wang et al., 2012).

The Freundlich adsorption isotherm was found to be the best fit for both rare earths and thorium (Figure 3.3.54). Freundlich equation considers the adsorbent surface as heterogeneous (multilayer mode) and the amount absorbed at equilibrium is determined by the following equation (Liu et al., 2013):

$$q_e = K_F C_e^{1/n} \tag{27}$$

Where K_F is the Freundlich constant (L/g) and n is related to the adsorption density. The plots were generated following Eq. (27). Afterward, the slope and the intercept of the plots were used to calculate 1/n and K_f values. The high correlation coefficient (R^2) observed in both isotherms suggests a good model fit. The maximum adsorption capacity for rare earths and thorium was 2.05 and 0.24 mg/g, respectively. A negative slope observed for rare earths and thorium indicates a reverse correlation between the amount adsorbed (C_{ads}) and the equilibrium concentration (C_e), which corresponded well with the experimental findings that the amount adsorbed decreased as time increased. Moreover, the Freundlich isotherm indicates multilayer adsorption rather than monolayer and considers a heterogeneous surface.

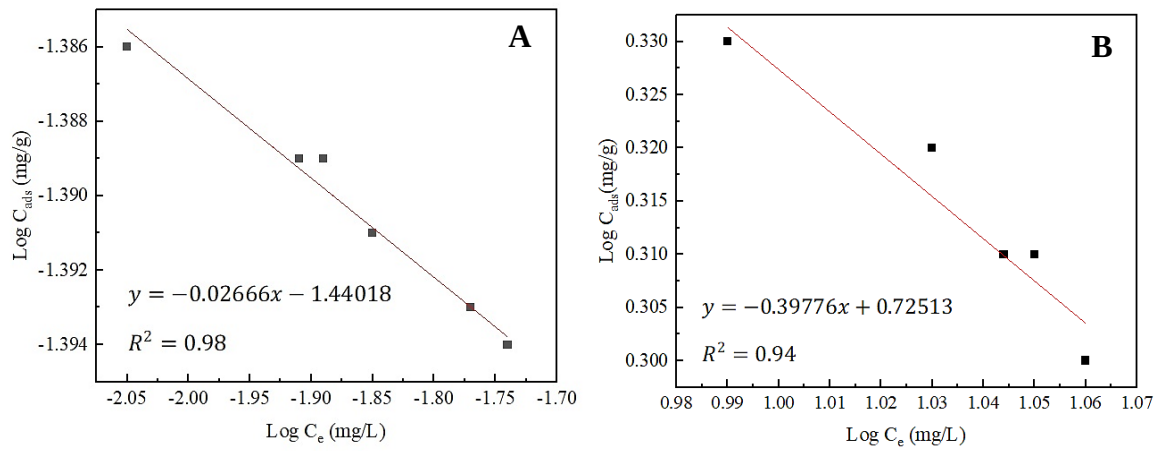

Figure 3.3.54 Freundlich adsorption isotherms of the elements onto zeolite. (A) total rare earths (B) thorium.

Dubinin-Raduskevich (D-R) adsorption isotherms of total rare earths and thorium are shown in Figure 3.3.55. The D-R isotherm is governed by the equation given below. It does not assume that the materials have homogeneous surfaces, either (Barkat et al., 2015).

$$lnq_e = lnq_{max} - K_{ads}\varepsilon^2 \tag{28}$$

Where q_{max} is the capacity of saturation theory (mg/g), K_{ads} is the adsorption energy constant (mol^2/kJ^2) and ε is the Polanyi potential which is defined as:

$$\varepsilon = RTlog(1 + \frac{1}{C_e}) \tag{29}$$

where R is gas constant (8.314 J/molK) and T is adsorption temperature (K). The mean adsorption energy calculated from the isotherms reveals supplemental information on adsorption behavior. If the mean adsorption energy value falls between 1 and 8 kJ/mol, it is considered physical adsorption. On the other hand, if the value varies between 9 and 16 kJ/mol, it represents chemical adsorption (Erden and Donat, 2016). The mean adsorption energy (E) values of rare earth elements and thorium were calculated as 5.8 kJ/mol and 1.80×10^{-3} kJ/mol, respectively. E<8 kJ/mol indicates that both rare earth and thorium adsorption is governed by reversible physisorption and

require less energy. Intermolecular forces are involved in accomplishing the adsorption. Moreover, the activity coefficient values were found to be -1.48x10^{6} mol^{2}/kJ^{2} and -1.54x10^{-5} mol^{2}/kJ^{2} for total rare earth elements and thorium, separately.

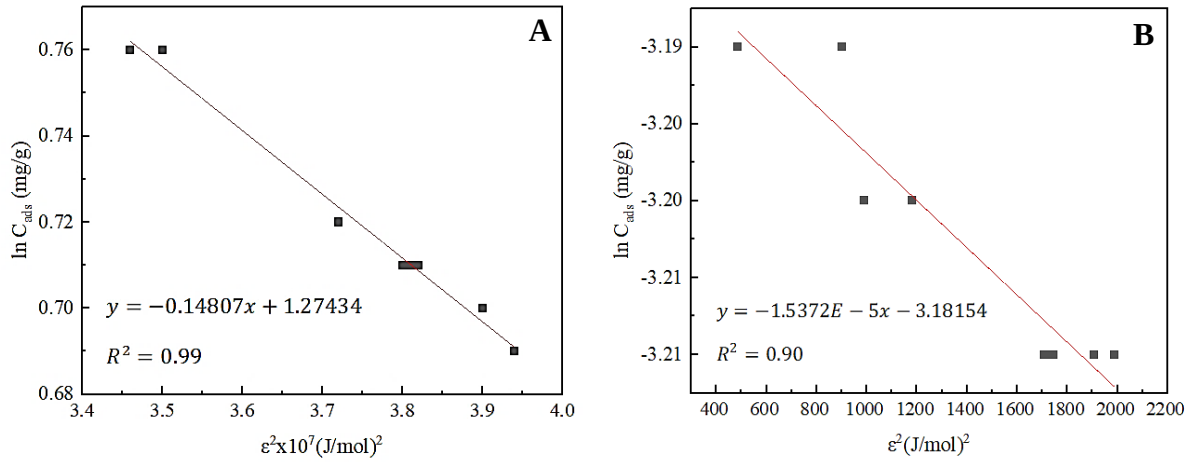

Figure 3.3.55 D-R adsorption isotherms of the elements onto zeolite. (A) total rare earths (B) thorium.

3.3.3 Conceptual Process Flowsheet Development

Based on the overall findings generated from the study, a conceptual flowsheet was developed to produce high purity rare earth oxide while removing thorium and uranium (Figure 3.3.56). The proposed process flowsheet was developed using metallurgical simulation software, METSIM, and comprised of three major modules. The unit operations in the flowsheet include: (1) leaching of the feedstock and thorium removal by selective precipitation, (2) uranium removal by solvent extraction, and (3) rare earth precipitation and production.

In the first module, a solid feedstock is introduced to the leaching tank, where the dissolution of the feedstock material with acid at an elevated temperature (80 °C) is achieved. After giving sufficient time, the resulting pregnant solution is subjected to filtration to remove undissolved residues. A press filter is recommended due to the fine particle sizes. While the undissolved leach residue is transported to the tailings pond, the loaded leach solution is subjected to one-stage precipitation in which selective thorium removal is targeted. Based on both experimental findings and literature review, it is recommended to keep the solution pH below 5 to prevent the loss of rare earth elements. When significant loss is observed, a re-dissolution-re-precipitation route can be followed to minimize the loss. According to the findings, there is no substantial difference between different alkaline salts for thorium removal; thus, sodium hydroxide (NaOH) is chosen as the alkaline used for pH adjustment due to its availability. After reaching the targeted pH, the solution is pumped to a second filter. Thorium is then separated from the rest of the solution and sent to the same tailing pond with the leach residue. The tailing pond materials can be utilized for mine backfilling since thorium concentration is diluted by mixing it with other residues.

The solution remained from precipitation is treated with solvent extraction (second module), where a two-stage extraction and a two-stage stripping are performed. In this study, the effect of scrubbing was found to be minimal. Therefore, no scrubbing unit is proposed in the conceptual flowsheet. After solvent extraction, the loaded aqueous phase, i.e., uranium product

stream, is transported to an evaporation tailing pond, and the sulfuric acid used during striping is recycled for reuse. The used extractant, TBP, is also sent to the recycling unit for purification and reuse. Ammonium nitrate solution and deionized hot water can be used to remove impurity elements, such as calcium, iron, magnesium, and phosphorus (Jorjani and Shahbazi, 2016).

On the other hand, the rare earth-containing aqueous stream is subjected to the third unit operation/module in which oxalic acid precipitation is performed to form rare earth oxalates. Precipitated rare earth oxalates are then filtered and roasted to produce sellable rare earth oxides. Afterward, the oxalic acid-containing stream is sent to the same evaporating tailing pond as the uranium product stream.

The technical feasibility of this flowsheet has been proven based on the data obtained from both laboratory parametric tests and performance validation testing using the samples generated from the pilot-scale facilities. However, this flowsheet only considers hydrometallurgical processing unit operations. Prior to this, other unit operations, such as sample preparation (e.g., crushing, grinding, sizing), pre-treatment (e.g., density-based separation, froth flotation), pre-roasting, may be needed to pretreat the feedstock and enhance the overall process efficiency as well as to reduce the amount of gangue materials entering the hydrometallurgical unit. For instance, significant improvements were observed in leaching several coal samples by calcinating before leaching. Due to coal power plants' high temperatures, mineralogical changes may occur in the coal samples and the rare earth recovery can be enhanced with an additional calcination step before leaching to enhance particles' liberation. (Honaker et al., 2019). Even though the application of traditional mineral processing techniques alone for rare earth recovery from coal-based materials is stated to be ineffective, they can still be utilized as a pre-treatment method.

Although a techno-economic analysis has not been performed, it is known that the majority of the cost is attributed to chemical reagents. Therefore, recycling and reuse are essential. Besides, all water must be recycled as much as possible and fed into the processing plant to reduce operational costs. However, since the developed flowsheet does not include additional unit operations other than typical rare earth extraction units, it is believed that no additional capital cost is induced for the removal of radioactive elements, i.e., thorium and uranium, from rare earths.

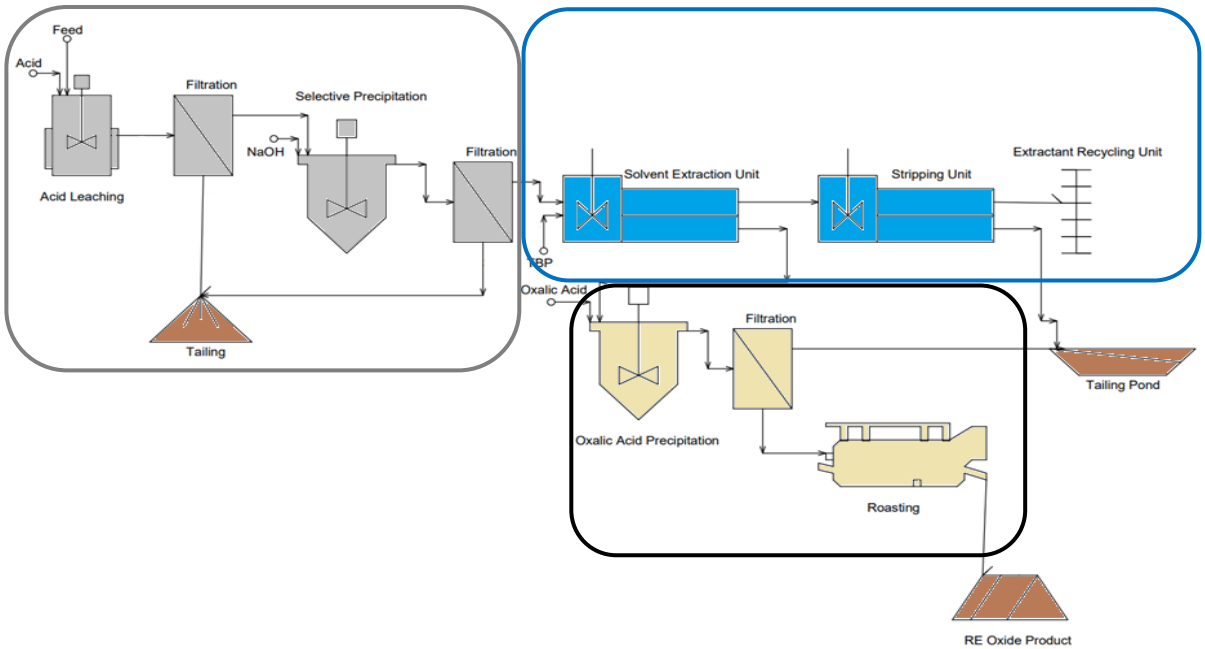

Figure 3.3.56 Conceptual flowsheet designed for the removal of thorium and uranium from rare earth elements.

3.4 Feedstock Collection & Preparation (PB3-Task3)

Bulk lots of feed sample were collected from the coarse waste streams at the Leatherwood and Dotiki coal preparation facilities. The Leatherwood sample was secured from the Blackhawk Mining Complex in eastern Kentucky where the Fire Clay (Hazard No. 4) seam is processed. The Dotiki sample was secured from the Alliance Mining Complex in western Kentucky where the West Kentucky No. 13 seam is processed. Characterization work showed that both feedstocks meet DOE's minimum TREE content of 300 ppm (dry, whole sample basis). Each sample of coarse refuse was collected, sized using a portable vibrating screen, and pre-concentrated using a dual scan x-ray sorter. The upgraded feedstocks were then sequentially passed through a jaw crusher and hammer mill to reduce the top size to below 1 mm. The pulverized feedstocks were then stored in 55-gallon drums until needed in the project test program. It should also be noted that portions of each pulverized feed was also subjected to low-temperature roasting using an off-site facility. Laboratory work conducted by the project team has shown that this additional preparation step substantially reduces acid consumption and greatly improves the extraction of REEs during leaching.

3.4.1 West Kentucky No. 13 Source

A new drill core sample was provided by Alliance Coal in October 2018 which was extracted in the area that was mined during the performance period of this project. Analysis of a new drill core was necessary due to a notification received by the company geologist and mine personnel that the characteristics of the seam were changing as the moved into a new area of the underground mine. Detailed analysis results are provided in Appendix E including petrographic information, proximate analysis results, mineralogical assessments, rare earth content analysis results and trace element results.

The target feed source for the REE pilot plant is the coarse refuse material generated from the cleaning of the extracted coal. The coarse refuse is likely generated from the immediate roof, floor and partings. Table 3.4.1 includes a list of the various segments in the core that likely contributes to the production of the coarse coal refuse material. There are a few interesting high-ash materials that contain a significant amount of REEs. A 2.44-inch parting was found to contain 828 ppm which was comprised of nearly 50% cerium. Another parting contained 511 ppm and the immediate seat rock has 669 ppm on a dry, whole mass basis. The higher REE content segments typically contain elevated amounts of light REEs which the most notable being neodymium which accounts for between 15% - 20% of the total REEs. The overall average REE content of the materials that could make up the coarse refuse is 349 ppm on a dry, whole mass basis. It is anticipated that the feed material generated from the West Kentucky No. 13 coal seam met the requirements for a qualified feed stock throughout the project.

The distributions of rare earth elements in the roof, partings and floor segments of the core are shown in Figure 3.4.1. The values represent the percentage of each REE with respect to the total REE content. The primary REE are cerium, lanthanum and neodymium. Considering its market value, scandium represents a respectable amount with the average being around 5%. The heavy elements yttrium and dysprosium have a higher percentage of the total in the middle partings. Praseodymium, gadolinium and samarium have concentration that could potential justify recovery and concentration.

Table 3.4.1. Rare earth content distribution in the high ash content segments of a drill core associated with the West Kentucky No. 13 coal seam; core was extracted in October 2018.

Lithology	Thickness (inches)	Estimated Sp. Gr.	Ash (%)	Total REE (whole basis)
Roof Shale	2.40	2.63	92.85	256.87
Roof Shale	4.20	2.21	75.15	243.17
Parting	2.16	2.42	85.40	321.25
Parting	2.28	2.20	72.47	511.52
Parting	6.00	2.55	89.93	325.69
Parting	6.00	2.59	91.63	264.02
Parting	6.00	2.61	92.01	277.49
Parting	6.00	2.62	92.81	281.72
Parting	7.80	2.62	92.75	344.70
Parting	5.16	2.58	91.44	282.22
Parting	2.40	2.54	90.02	828.22
Parting	1.20	1.83	40.14	53.39
Seat Rock	5.52	2.53	88.13	668.94
Seat Rock	4.80	2.64	93.39	272.99
AVERAGE	4.42	2.53	89.05	349.27

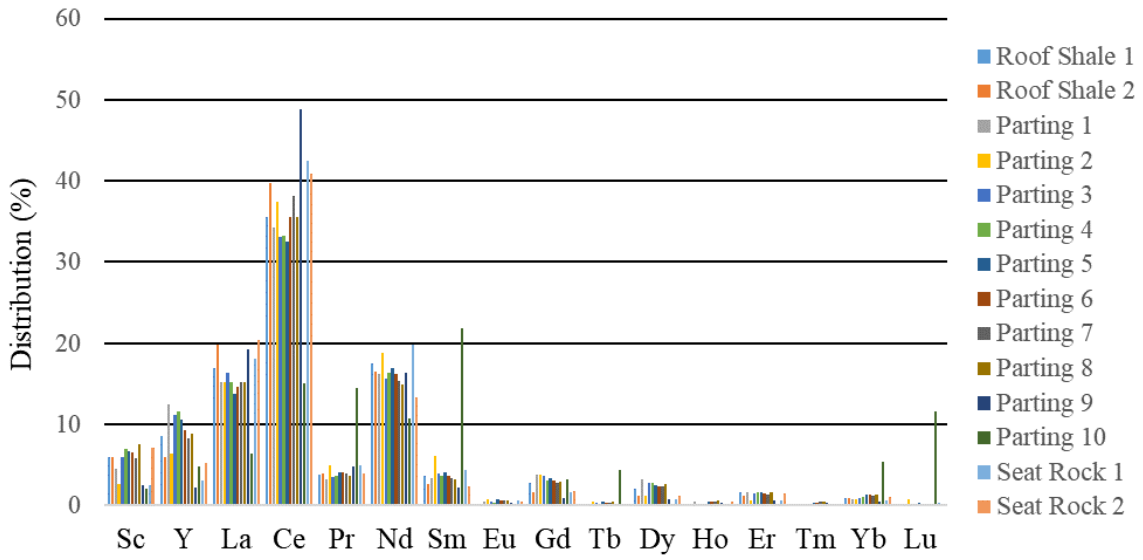

Figure 3.4.1. Rare earth element distribution in the high ash content segments along the portion of the vertical profile of a drill cores intersecting the West Kentucky No. 13 coal seam.

3.4.2 Fire Clay Source

20-ton of Fire Clay coarse refuse material was collected from the leatherwood coal preparation plant. The material was transported to the Dotiki mine site and sorted through the X-ray sorter. Size and density fractionation analysis was carried out on a representative sample of the bulk material as shown in Table 3.4.2. The results showed that the 1.8 to 2.0 density fraction contains highest rare earth content on a whole mass basis, and the combination of the density cut 2.0 material contains 604 ppm of total rare earth on a dry ash basis. Since after roasting, most of the carbon content burns off, the density 2.0 float material was targeted to be the feed material to the pilot plant hydromet circuit. X-ray sorter was used to separate the targeted density fraction through multiple rougher-cleaner-recleaner separation processes. The targeted 2.0 float fraction product yield is 12.5% based on the characterization data. The overall total rare earth content of the Fire Clay coarse refuse is 323 ppm on a whole mass basis. The 2.0 float fraction contains about 310 ppm on a whole mass basis with ash content of 51.2%, which yields to 604 ppm on dry ash basis.

In mid-2019, a new hydraulic gate was installed in the coarse reject line of the secondary dense medium vessel at the Leatherwood preparation plant to allow the collection of material finer than 2-inches and coarser than 3/8-inches. Approximately 20 tons of the Fire Clay waste material was collected from the gate valve and transported to the REE pilot plant in Providence, Kentucky. A representative sample was collected from the bulk and submitted for ash and REE analyses.

The Fire Clay coarse refuse material was processed through the X-ray sorter to achieve the light density fraction (S.G. 2.0 float) which contains elevated total REE concentration. The sorted material was crushed using a jaw crusher and passed through a hammer mill to achieve a top particle size of 1 mm. The detailed sorting and roasting process is presented in section 3.5. The Fire Clay feed stock was previously tested in quarter 1 and 2 in fiscal year 2019 using the original

flowsheet which included solvent extraction as the downstream purification method. Then the second 20-ton feed stock was tested in quarter 2 in fiscal year 2020 to evaluate the modified flowsheet using pilot plant roaster, leaching, multi-stage precipitation, redissolution and oxalate precipitation.

Table 3.4.2. Size by density fractionation characterization of Fire Clay coarse refuse.

Sample ID	Weight (%)	Ash (%), db		TREE on dry whole basis (ppm)		TREE on dry ash basis (ppm)	
		Incremental	Cumulative	Incremental	Cumulative	Incremental	Cumulative
1.6 Float	1.6	36.6	36.6	222.5	222.5	608.0	608.0
1.8 Float	7.5	49.1	46.9	248.8	244.3	507.0	520.7
2.0 Float	3.5	62.6	51.2	481.4	309.7	768.9	604.3
2.0 Sink	87.5	91.5	86.4	324.4	322.5	354.7	373.2
Total	100	86.4		323			

3.5 Exploratory Testing (PB3-Task4)

3.5.1 X-ray Sorter

The x-ray sorter system was operated throughout the duration of this project in order to prepare a large stockpile of feed for pilot-plant testing. For the first 22 tons of Fire Clay coarse refuse material, sized and upgraded product was produced with the sorter and roughly 6 tons of this material was sent out to an external contractor for roasting.

Operation of the x-ray sorter is straight forward on paper. Material to be sorted is fed to the machine via a high-speed belt and a portion of the material is ejected using air jets based on the separation parameters set using an onboard computer. In practice, however, the actual operation of the sorter has proven to be more challenging. Testing showed that the sorter is best suited for treating dry material in the size range of 2 x ½ inch. However, the coarse reject sample obtained from the coal processing plants contained a substantial amount of finer particles that tended to retain considerable moisture. The moisture made it exceed difficult to properly size the feed material due to solids sticking together and nearly impossible under freezing conditions where the material froze together and could not be separated. It was also discovered that wet/fine material would accumulate on the x-ray source over time and would cause false readings on the sensor that results in less-than-optimal sorting results. Therefore, the operation must be stopped regularly in order to clean the x-ray source inside the sorter. Another problem that surfaced during sorter operation in freezing conditions was that the air nozzles would clog up due to ice building up inside the orifices. This problem was mitigated by installing a heating unit inside the sorter near the array of air discharge nozzles during sub-freezing periods. Unfortunately, the heating unit eventually caused some of the airlines to melt and fuse together as a result of a thermostat setting that was too high. Consequently, these lines had to be replaced. Moreover, the small conveyors that are used to feed the high-speed conveyor belt also were prone to freezing and had to be sprayed with anti-freeze solution regularly in order keep them operating. All these issues point to the fact that any large-scale operation of the sorter should be performed within a heated building/structure

to avoid issues related to freezing conditions. Also, it is recommended that the feedstock to the sorter be secured directly from the well-sized and well-rinsed products of the existing drain-and-rinse screens within in the coal preparation plant. This setup would avoid issues associated with unwanted fines that get added to these streams prior to discharge of this material into the coarse refuse fill areas at the mine site.

It should be noted that, in the middle of the project period, the feed to the Dotiki coal preparation plant changed as a result of new geological conditions being mined by Alliance Coal. Prior to this geologic change, the preparation plant was operating at a relatively low specific gravity cutpoint and, therefore, a considerable amount of composite coal-rock "middlings" particles were being discarded with the reject material. Prior test work showed that some of the highest concentrations of rare earth minerals were intimately associated with these high-ash middlings. However, with the feed geology change, the preparation plant has now started operating at a much higher specific gravity cutpoint. Therefore, the reject material coming out of the processing plant now contains considerably less coal as middlings. Analysis of the new coarse reject material showed that it still qualifies as a rare earth feed stock for this project with a little over 300 ppm TREE content on a whole-sample basis. However, the coarse reject now contains so little organic matter that any attempts to recover a clean coal product from the waste is now impractical. Therefore, for this particular coal feedstock, it is now expected that no clean coal product will be recovered as part of this project.

The geologic change in the coal seam at the Dotiki site also made the operation of the x-ray sorter more challenging. Before the feed change, there was a significant difference between low-ash and high-ash material that could be easily exploited by the sorter. After the feed change, however, the separation is considerably more difficult since there is now less of a significant difference between particles to be separated. In order to evaluate the performance of the sorter under this new condition, representative samples from feed, concentrate and tail streams were taken and analyzed. The results of these analysis, which are summarized in Figure 3.5.1, show that the sorter was still able to concentrate REEs from the less favorable feed material. Samples taken from tailing and concentrate streams were also scanned using the x-ray scanner on site. In the two images given in

Figure 3.5.2, the top samples are the ejected "concentrate" samples, and the bottom ones are the pass-through or "tailing" samples. In these images, the orange particles are the lower density particles, whereas the dark green and blue particles are higher density particles. Lighter greens represent middlings particles containing various mixtures of organic and inorganic matter. As can be seen in the figure, there was a distinct difference between these two streams, which confirmed the analysis results.

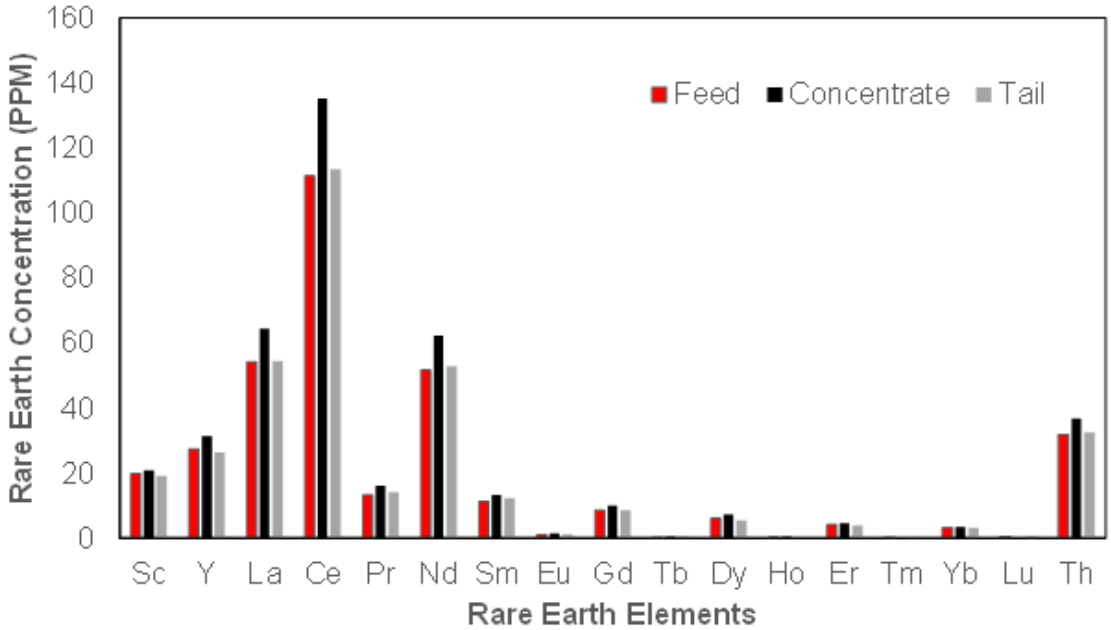

Figure 3.5.1. REE and thorium concentrations in feed, concentrate and tail samples obtained from the x-ray sorter when processing Dotiki coarse reject material.

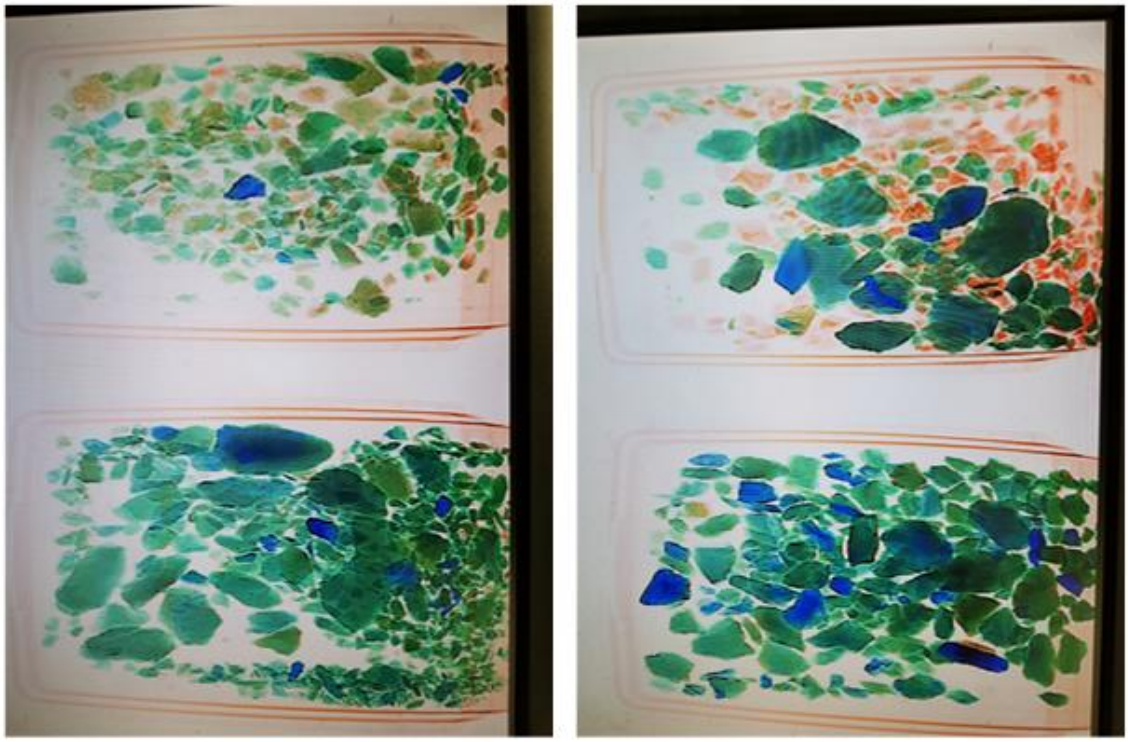

Figure 3.5.2 X-ray scans of eject and pass through material from x-ray sorter.

As the x-ray sorter products started accumulating, crushing and grinding activities were also initiated to covert this material into an appropriate size range for downstream processing in the physical separation and leaching circuits. During this particular reporting period, a total of more than 22 tons of material produced by the sorter was crushed with the jaw crusher module. Approximately 6 tons of the crushed material was also passed through the hammer mill module to prepare a minus 1 mm feed of pulverized material that was sent out to an external site for roasting.

Due to the issues observed when 20 tons of coarse reject obtained from the Leatherwood site was processed through the X-Ray sorter, a second 20-ton lot of coarse reject material was procured from the same site for further testing and processing. As before, a visual observation of the material indicated that it had a top size of approximately 2.5 inches and a bottom size of 3/8 inch, which is slightly out of the ideal size range recommended by the sorter vendor. Therefore, the material was screened using a shaker screen with a top size of 2 inches and a bottom size of ½ inches to obtain the ideal size fraction for sorting. The oversized material was collected and passed through a jaw mill to be rescreened and processed. The undersized material was discarded.

As this material was same as the material obtained from the Leatherwood site in the last reporting period, a detailed density fractionation analysis was not performed this time. Also, the same calibration curves given in Figure 3.5.3 from the last 20-ton run were utilized to process this material.

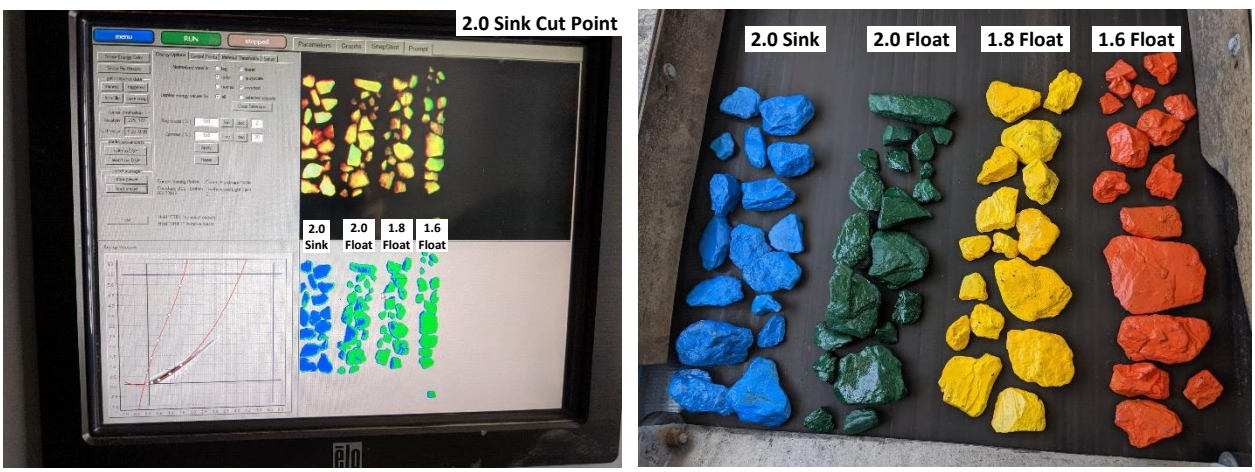

Figure 3.5.3. Calibration of sorter cut point used for parametric study.

To overcome the inefficiencies observed in the sorting run conducted in the last reporting period, both the pass through and eject products were reprocessed twice through the sorter with hopes of improving the separation performance. This would represent two processing circuits containing rougher→cleaner→recleaner and rougher→scavenger→scavenger-cleaner circuits. During the rougher run, several barrels of samples were collected over the course of the run to determine the sorting performance. A representative sample from each barrel was then analyzed for rare earth content. Results of these analyses given in Figure 3.5.5 show that the rougher run resulted in a poor separation performance as previous runs. Eject material, which was supposed to contain the lower density particles, had only slightly higher TREE content than the pass-through

material. Moreover, the ash content difference between the eject and the pass-through was not as large as it should have been based on the separation parameters given in Figure 3.5.3.

A float-sink analysis of products of the re-cleaner step given in Table 3.5.1 show that the reprocessing of rougher products did not improve the overall separation performance. As it was with the rougher run, calibration curves were adjusted to eject particles lighter than 2.0 SG. Based on the results, there was a low bypass of "lights" into the pass-through stream. This result indicates that the air jets accurately shot almost all of the "lights" into the eject stream. However, there was a significant bypass of "heavies" into the eject stream, which indicated that the air jets were not very precise. A close examination of air jets revealed that the area of influence of the jets was significantly larger than what it was supposed to be based on manufacturer's design.

To address the issue with air jets, MST personnel in conjunction with Virginia Tech personnel installed improvements to the air jets. The aperture on the original jets was found to be too large so a plate was fabricated to fit over the air jet nozzles. The plate was designed to reduce the aperture size without the need to have an entirely new nozzle block manufactured. The plate was able to reduce the air jet area of influence by approximately 50% from the original apertures. In addition to the plate, the hoses feeding the nozzles were cleaned out. Inside the hoses coal debris and other small particles began to collect and inhibited flow in some of the nozzles. This low flow in some of the jets was part of the reason the jets were not operating as deigned allowing bypass. The last modification made to the sorter was the calibration of the x-ray sensors and the control unit. Calibration had started on the unit but was not finished until this point due to restrictions on access to the unit imposed on MST personnel by MSHA.

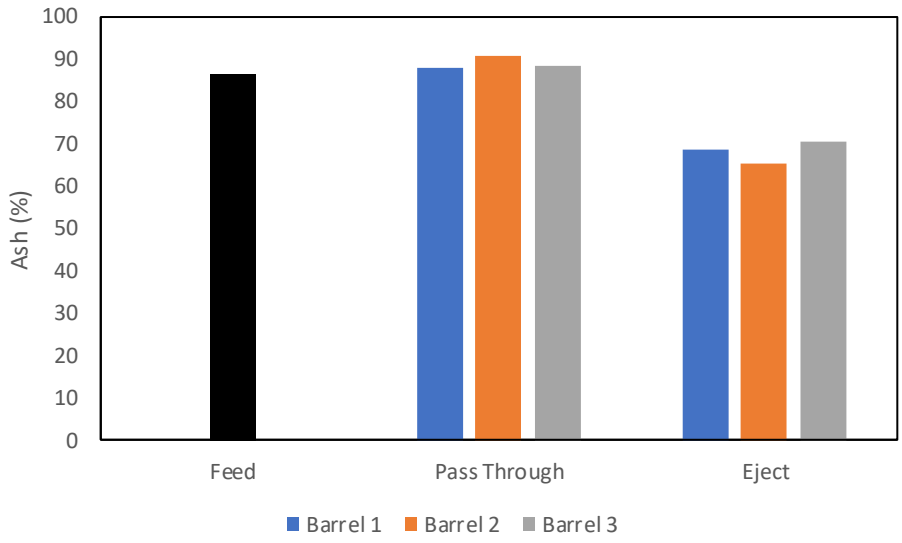

Figure 3.5.4. Ash content of Feed, pass through and eject streams at Rougher stage.

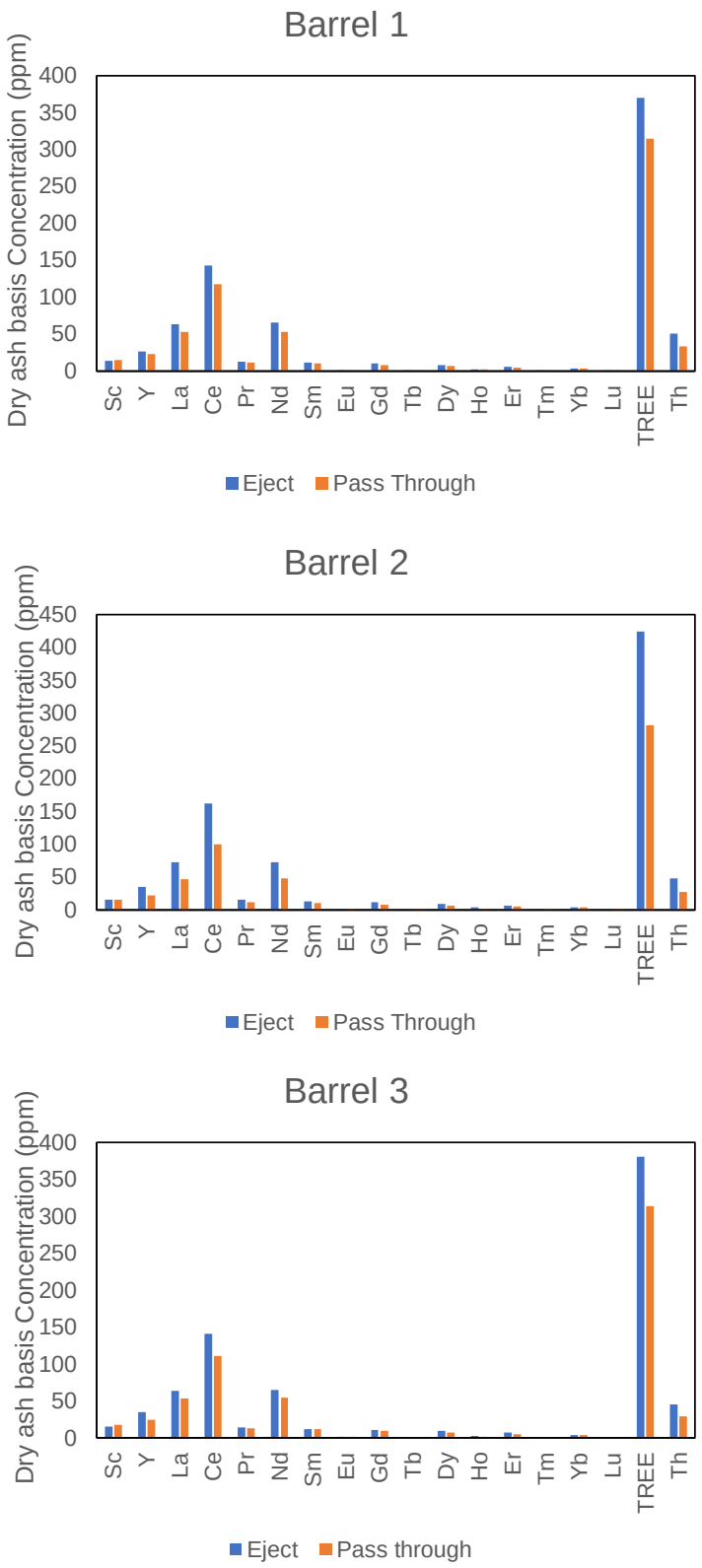

Figure 3.5.5. REE analysis of Rougher eject and pass through samples.

Table 3.5.1 Float-sink analysis results of sorter re-cleaner step

Sample	**Ash (%)**	**Mass (%)**
Eject – 2.0 Float	43.71	23.35
Eject – 2.0 Sink	88.54	76.65
Pass through – 2.0 Float	43.7	3.96
Pass through – 2.0 Sink	91.28	96.04

The 20-ton material was processed through the X-ray sorter and obtained 13 barrels of product. The assays of each barrel were analyzed. The average ash content of the material from 13 barrels is 75.8%. The average concentration of total rare earth elements (TREEs) is 427 ppm +/-36 ppm on a dry ash basis, and 323 ppm +/-18 ppm on a whole mass basis. The material contains most Ce, La, and Nd which are most likely associated with RE phosphate minerals such as monazite.

Representative sample of the sorter product and tailing material were sent to an SGS lab for density separation at 2.0 s.g. to evaluate the leaching characteristics associated with each stream. The light density fraction was ejected in the sorting process whereas the heavy density fraction passed through the sorter and report to the discharge port. The pass-through material that reports to the tailing stream from the sorter contains about 4% of the 2.0 s.g. float material as misplacement. Whereas the eject material contains 23% of the 2.0 s.g. float material that were correctly reported to the eject stream and 77% of the 2.0 s.g. sink material that were misplaced to the eject stream. The leaching characteristic shows that, after roasting, 60% of TREE can be extracted from either the eject product or pass-through tailing material regardless of the material density as shown in Figure 3.5.6. However, the difference occurs in the individual rare earth elements leaching characteristics especially for scandium and yttrium. As shown in Figure 3.5.7 through Figure 3.5.10, the individual rare earth element recovery was plotted for 2.0 float and sink fractions in eject and pass-through materials. The Sc leaching recovery reached 47% and 48% for the 2.0 float material in eject and pass-through streams, respectively. Whereas only 34% and 30% Sc were recovered by leaching from the 2.0 sink material in eject and pass-through streams, respectively. The yttrium leaching characteristic follows the same pattern that over 40% recovery achieved from the 2.0 float material and less than 30% was recovered from the 2.0 sink material. Considering the high value of Sc and Y, an effective density separation priory to roasting could potentially increase the final product value.

Table 3.5.2. Sorter products density separation on 1x0.05 inch size fraction.

Sample ID	Ash (%)	Wt. (%)	TREE Concentration on dry ash basis (ppm)
Sorter Eject 2.0 Float	43.71	23.35	636.0
Sorter Eject 2.0 Sink	88.54	76.65	284.7
Sorter Pass 2.0 Float	43.7	3.96	657.0
Sorter Pass 2.0 Sink	91.28	96.04	279.8

Table 3.5.3. Rare earth concentration in X-ray sorted Fireclay coarse refuse material feed to hydromet circuit.

Barrel ID	Element concentration on dry ash basis (ppm)																			Ash (%), ar	Total REEs (ppm, whole ash basis)
	Sc	Y	La	Ce	Pr	Nd	Sm	Eu	Gd	Tb	Dy	Ho	Er	Tm	Yb	Lu	Total	*Th*	*Li*		
LW1	15.6	31.3	74.2	178.8	17.6	71.7	15.2	2.0	13.2	0.6	8.9	2.4	6.6	0.8	3.7	0.2	**443.0**	*32.6*	*215.2*	77.4	342.9
LW2	18.7	33.1	75.4	176.3	17.8	72.5	15.3	2.2	13.1	0.7	9.4	2.4	6.5	0.9	4.1	0.5	**448.9**	*31.2*	*249.6*	77.2	346.7
LW3	15.5	30.4	69.4	156.9	16.7	67.2	14.3	1.9	12.7	0.6	8.3	2.2	6.5	0.8	3.7	0.4	**407.5**	*34.8*	*204.1*	77.0	313.6
LW4	16.5	29.6	66.3	157.2	16.5	67.5	13.8	2.0	12.7	0.9	8.2	2.2	6.5	0.8	3.7	0.3	**404.7**	*31.1*	*215.3*	76.5	309.7
LW5	16.9	33.2	74.5	172.2	17.9	71.9	15.4	2.1	13.5	0.8	9.1	2.3	6.7	0.8	4.0	0.4	**441.9**	*30.5*	*213.7*	73.9	326.5
LW6	17.5	34.3	75.6	177.7	18.3	73.6	15.2	2.1	13.9	0.6	9.5	2.4	6.6	0.9	4.1	0.3	**452.6**	*34.4*	*209.7*	72.7	329.0
LW7	17.7	35.7	81.2	195.1	20.2	79.5	16.9	2.3	14.9	0.5	10.2	2.6	7.0	0.9	4.2	0.3	**489.2**	*36.6*	*211.5*	70.0	342.2
LW8	18.2	34.7	74.8	173.9	18.1	74.0	15.5	2.4	13.8	0.6	9.4	2.3	6.6	0.9	4.0	0.4	**449.4**	*28.6*	*246.0*	73.4	330.0
LW9	16.9	33.4	74.1	178.4	17.9	73.6	15.4	2.2	13.9	0.6	9.7	2.3	6.6	0.9	4.0	0.3	**450.3**	*35.1*	*236.0*	75.1	338.1
LW10	17.1	31.6	70.5	152.5	17.6	68.5	14.4	2.0	12.8	0.9	7.9	1.9	6.1	0.8	4.1	0.6	**409.2**	*30.2*	*204.3*	75.7	309.8
LW11	17.4	32.0	71.6	163.4	16.8	68.6	14.4	2.0	13.1	0.9	9.1	2.3	6.6	0.8	4.0	0.4	**423.6**	*32.0*	*217.7*	74.7	316.4
LW12	19.6	28.4	58.7	126.6	14.6	55.7	12.7	2.1	11.2	1.0	6.5	1.4	5.5	0.6	4.0	0.9	**349.3**	*22.6*	*215.3*	83.5	291.5
LW13	16.0	29.9	61.8	146.0	15.6	63.3	13.9	1.9	12.1	0.9	7.9	2.0	6.1	0.8	3.8	0.5	**382.5**	*32.5*	*198.1*	78.1	298.7
Average	**17.2**	**32.1**	**71.4**	**165.8**	**17.4**	**69.8**	**14.8**	**2.1**	**13.1**	**0.7**	**8.8**	**2.2**	**6.5**	**0.8**	**4.0**	**0.4**	**427.1**	**31.7**	**218.2**	**75.8**	**322.7**
STD	**1.2**	**2.2**	**6.1**	**17.8**	**1.4**	**5.9**	**1.0**	**0.1**	**0.9**	**0.2**	**1.0**	**0.3**	**0.4**	**0.1**	**0.2**	**0.2**	**36.2**	**3.5**	**15.9**	**3.2**	**17.6**

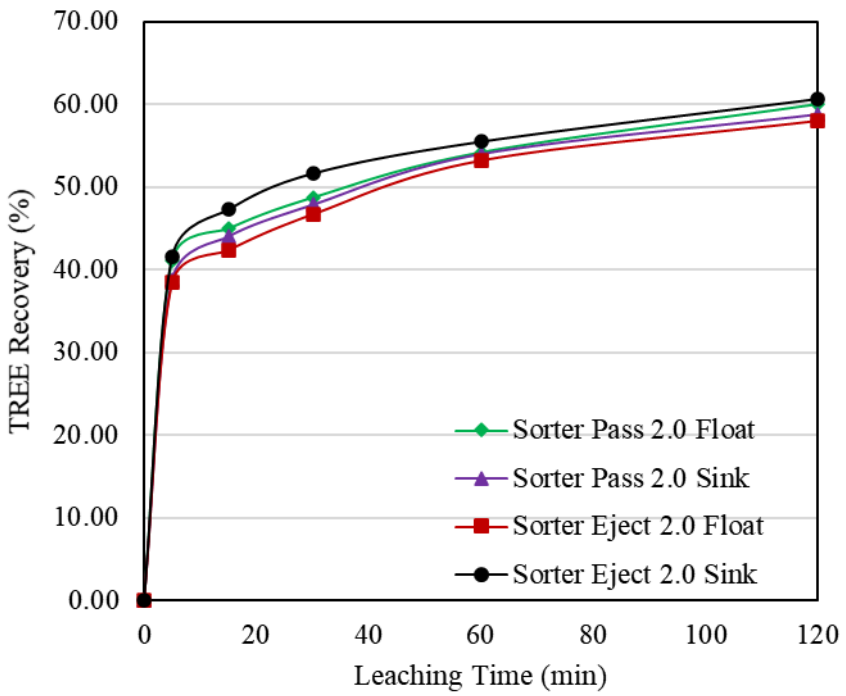

Figure 3.5.6. Leaching characterization of the density fractionated sorter product and tailing material within size range of 1x0.05 inch. (Leaching condition: 1.2M sulfuric acid, 10 g/L solid concentration, 75 °C. Particle size: 80 mesh)

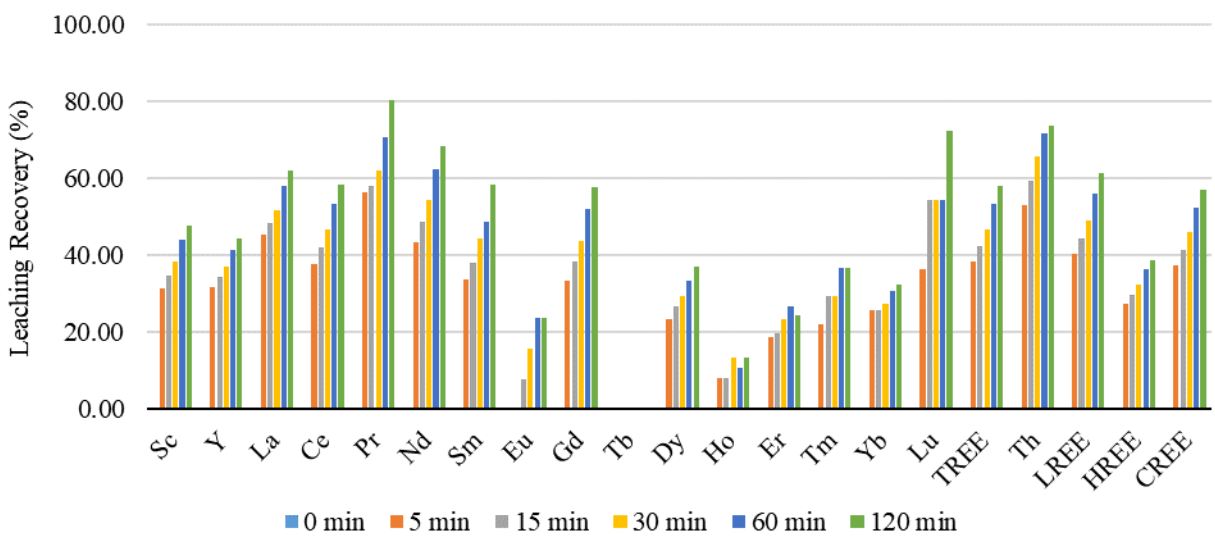

Figure 3.5.7. Sorter Eject 2.0 Float (80 mesh, Muffle Furnace Roast at 600C 2 hour)

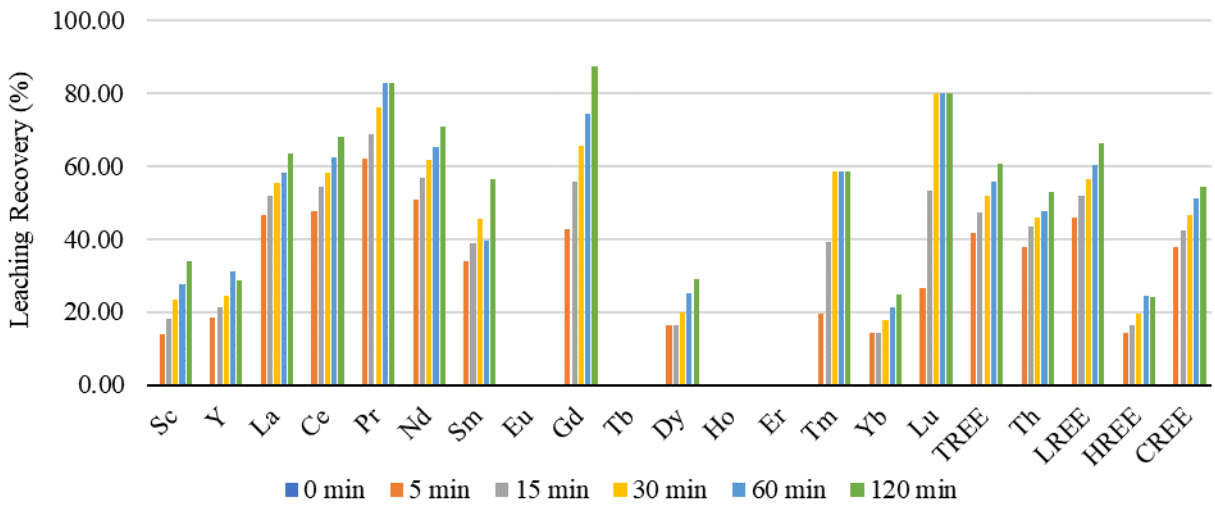

Figure 3.5.8. Sorter Eject 2.0 Sink (80 mesh, Muffle Furnace Roast at 600C 2 hour)

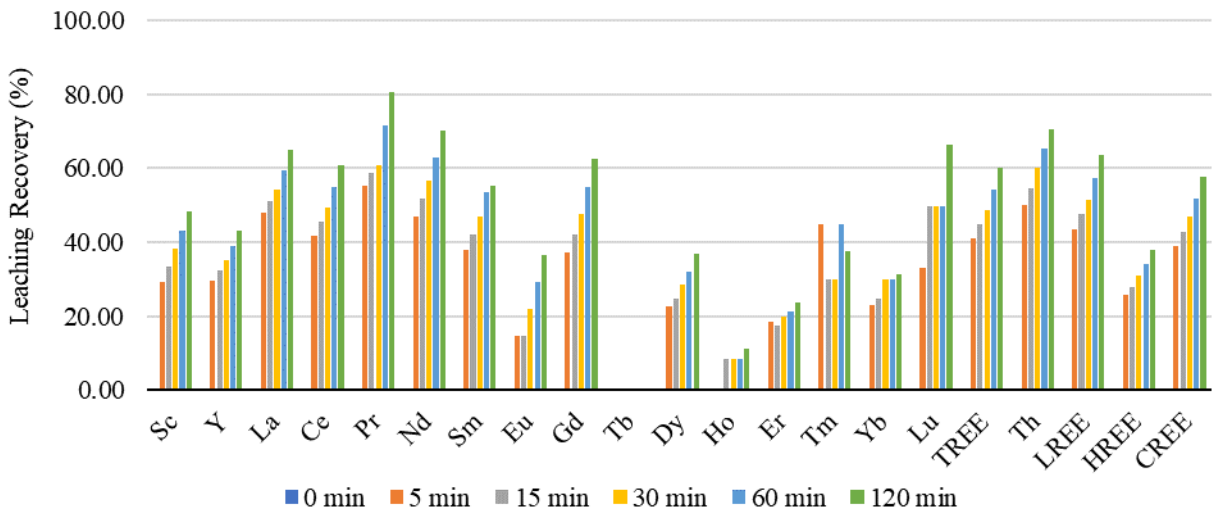

Figure 3.5.9. Sorter Pass 2.0 Float (80 mesh, Muffle Furnace Roast at 600C 2 hour)

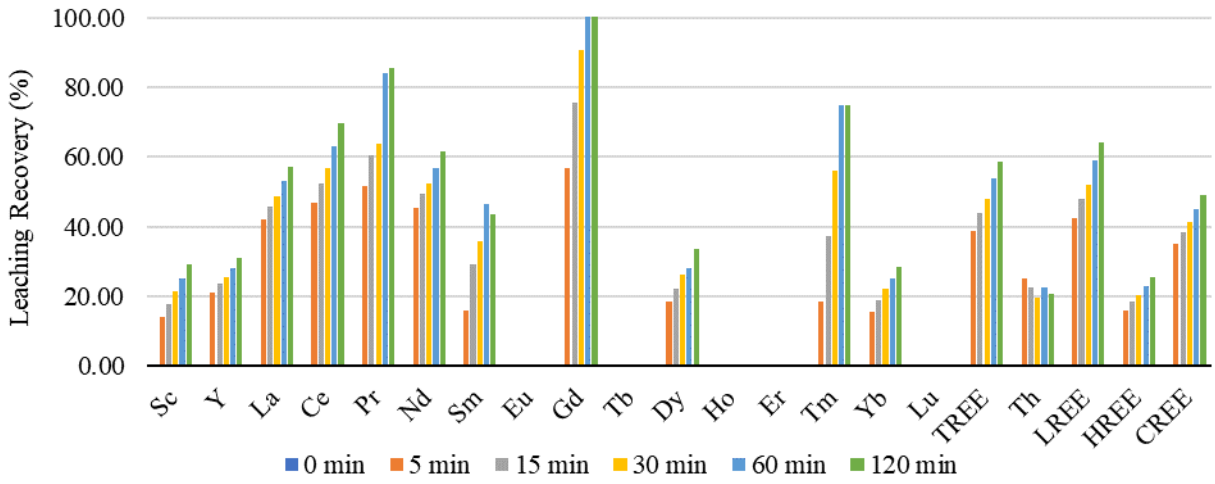

Figure 3.5.10. Sorter Pass 2.0 Sink (80 mesh, Muffle Furnace Roast at 600C 2 hour)

3.5.2 Roasting and pretreatment

In the past study, thermal treatment on feed material prior to leaching can significantly improve the leaching recovery of REEs, increase the leaching kinetics, and allow the leaching reaction to occur at lower acidity. A roaster was purchased and refurbished to be fully functional. The furnace provides heat from burning natural gas. The burner chamber temperature was controlled by automatically adjusting a butterfly valve that controls the air flow blew into the chamber. The roaster was inclined 10 degrees from the horizontal position to provide the desired material throughput and retention time.

The roaster system consists of three parts as shown in Figure 3.5.11. The feeding system consists of a 42-gallon hopper sitting on a screw feeder that was programed to provide 0 to 50 lb/hour feed rate. The conveying tube rotates at a constant speed that transfers material from the feeding point to the discharge point with a retention time of 20 minutes. The heating chamber provides approximately 20 inches of hot zone on the tube. In the initial test run, caking was observed inside of the tube as the material conveys from the hot zone to the cooling one due to moisture condensation from the atmosphere. An air operated knocker was installed and programed to strike on the tube every 10 seconds to knock off the caking material formed inside the tube during roasting. An infrared handheld thermometer was used to measure the inner tube temperature in the hot zone.

Figure 3.5.11. Roaster setup at the pilot plant including feeder system (left), controlling system (middle), and dust collection system (right).

3.5.2.1 West Kentucky No. 13 Feedstock Roasting

To study the effect of roasting temperature and flowrate on roaster performance, a series of preliminary tests was carried out on West Kentucky No. 13 material as shown in Table 3.5.4. Laboratory study showed that roasting at 600°C provided the best improvement in REE leaching characteristics. The roasting temperature within the roasting zone of the tube, which is two feet zone located within the middle of the five-foot tube, is a function of the outer chamber temperature and the mass flow rate. A standard leach test was established to quantify the pilot plant roaster performance in terms of the improvement on REE leaching recovery. The standard test was performed using 40 grams of solid and 200 ml of 1M sulfuric acid at room temperature for 15 minutes.

Using 600°C set point, the inside tube temperature was able to be maintained at 600°C in the roasting zone up to a product flow rate of about 4 lb/hr. The REE leaching recovery increased from 9.38% to 29.0% under this setting. To increase the throughput, the chamber temperature was adjusted to set point values between 700°C to 800°C to maintain the inner tube temperature above 600°C. However, when the product flowrate went above 10 lb/h, the inner tube was observed to be filled with smoke and the material discharged from the product end turned into charcoal black color instead of dark grey indicating incomplete roasting. The inner tube temperatures decreased to below 600°C due to overloading. The leaching recovery decreased due to the roasting environment.

The optimal roasting performance was observed to occur using a set point of 700°C with a mass throughput flow rate of 8 lb/hr. Under this condition, the material ash content increased from 85% to 97% on average. The individual rare earth concentration before and after roasting is provided in Figure 3.5.12. The REE leaching recovery was improved from 9% to 34% as shown in Figure 3.5.13. The improvement in leaching performance was primarily associated with the light REEs which validated the findings from the laboratory studies. Majority of the light REEs are bonded in mineral structure which are decomposed during proper roasting.

Table 3.5.4. Effect of roasting temperature and flow rate on leaching recovery.

Test	Product Flow Rate (lb/hr)	Temperature (°C)		TREE Leaching Recovery (%)
		Set Point	Inner Tube	
XTL 601	-	Raw		9.38
XTL 602	1.8	600	630	39.8
XTL 603	3.6	600	630	36.7
XTL 604	4.2	600	600	29.1
XTL 605	4.4	600	600	27.1
XTL 606	6.4	700	670	31.0
XTL 607	6.2	700	670	37.8
XTL 608	7.2	700	700	34.0
XTL 609	8.8	700	550	15.9
XTL 610	10.1	800	660	24.6
XTL 611	9.8	800	730	30.7
XTL 612	11.5	800	600	24.8

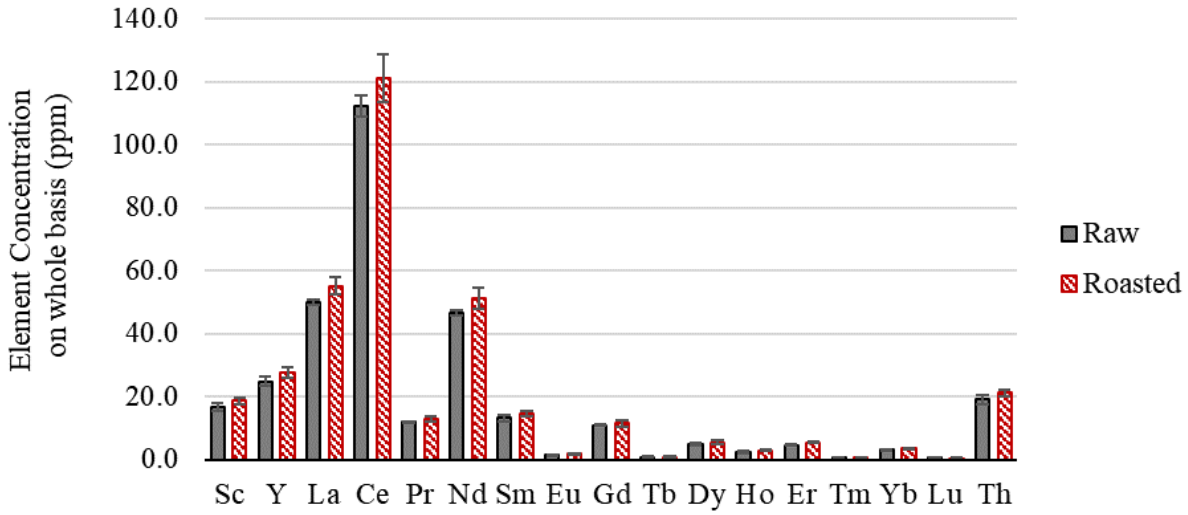

Figure 3.5.12. Rare earth concentration on whole basis before and after roasting.

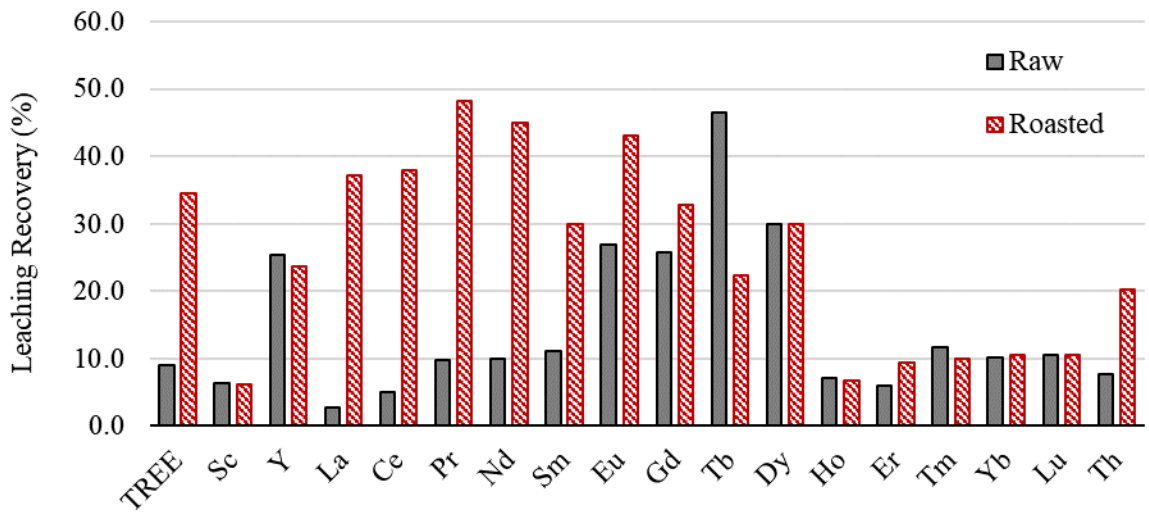

Figure 3.5.13. Leaching recovery improvement before and after roasting. (1M H_2SO_4, S/L=1/5, room temperature, retention =15 min)

3.5.2.2 Fire Clay Feedstock Roasting

The first 20-ton of Fire Clay coarse refuse material was sorted using the X-ray sorter, and then approximately 6 tons of light density fraction was transported to eastern Kentucky to be roasting at an offsite location. The second 20-ton Fire Clay material was roasted in-house at the pilot plant. The roasting performance was optimized to achieve the optimal leaching condition.

The feed material was collected in 55-gallon barrels from the coarse refuse stream produced at the Leatherwood coal prep plant which processes Fire Clay seam coal. The material was sorted using an X-ray sorter to produce a lighter density fraction which was previously found suitable for REE leaching. The material was air dried and crushed to a top particle size of 1 mm. The material was then roasted in a rotary drum calciner using an inner liner temperature of 600 °C. The ash content of the grounded material before and after roasting was 86% and 95%, respectively. After roasting, the total REEs content in the feed material was 356 ppm on a whole mass basis with 307 ppm of light REEs and 49 ppm of heavy REEs. The individual REE content of the roasted feed material is shown in Figure 3.5.14. Cerium accounts for 37% of the total REEs in feed.

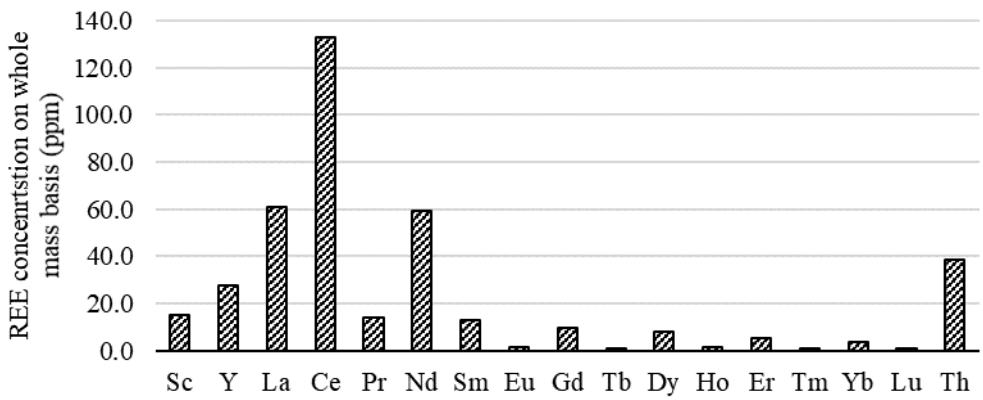

Figure 3.5.14. Individual REE concentration on whole mass basis in the roasted feed material.

The roasting process was expected to liberate the REE-containing minerals that were disseminated within the coal source and to decompose the mineral structures to create exposure of REEs to lixiviants during the leaching process. The major acid consuming minerals in the mine refuse system before roasting are mostly calcite, pyrite and clays, etc. An XRD analysis was performed on the sorted Leatherwood coarse refuse sample before and after roasting as shown in Figure 3.5.15. The XRD plots showed that the kaolinite peaks disappeared after roasting. After roasting at 600 °C, the kaolinite mineral structure was decomposed through dehydration. Carbonate minerals, such as $CaCO_3$ and $MgCO_3$, were decomposed to metal oxide and released carbon dioxide, which benefits the leaching process by reducing acid consumption. Pyrite was oxidized to iron oxides (i.e. hematite and magnetite).

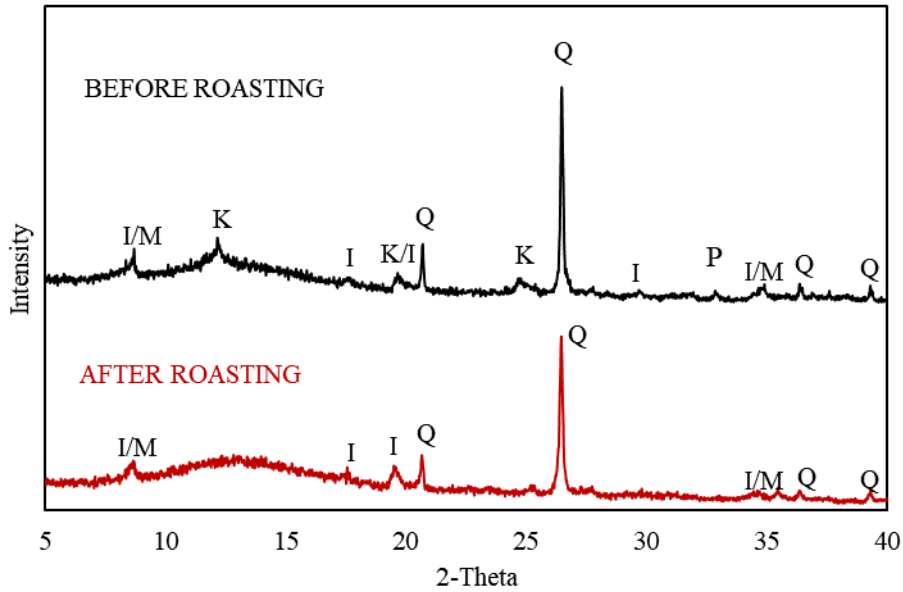

Figure 3.5.15. XRD analysis of the fire clay feed material before (top) and after (bottom) roasting at 600 °C for 2 hours using a blast furnace. (I-illite, M-muscovite, K-kaolinite, Q-quartz, P-pyrite.)

i. Fire Clay Roasting Performance Optimization

The Fire Clay coarse refuse material contains majority of rare earth elements exist in mineral form which is difficult to decompose. A test program was developed to optimize the roasting performance in terms of leaching recovery of the REEs in Fire Clay material. The critical factors in the roasting process include roasting material bed temperature and retention time. The material bed temperature is a function of temperature set point and the material mass flow rate. The retention time is a function of material bed depth and mass flow rate. The material feed rate in the pilot plant roaster is controlled by a screw feeder programmed to turn on and off at a preset time interval. Based on the previous study, the material bed temperature was targeted to be 600-700 °C to provide the optimal leaching performance. Table 3.5.5 shows a series of tests altering the feed rate and roasting temperature. The roaster product collected at varies settings were leached using 1M sulfuric acid with 200 g/L solid concentration at room temperature for 15 minutes to examine the leaching performance. The extracted TREE concentration in leachate solution is listed as a response for roasting performance evaluation.

The inner tube material bed temperature is slightly lower than the roasting temperature set point due to the energy consumption though the material mass flow. The results show approximately 100 °C deduction on the inner tube temperature from the set point as shown in Figure 3.5.16. The maximum leaching recovery of total rare earth occurred at the set point of 790 °C as shown in Figure 3.5.17. When the set point exceeded 800 °C, the leaching recovery reduced dramatically. The light rare earth group, such as Ce, appears to be very sensitive to the roasting temperature, whereas Sc and Y recovery showed very minimum sensitivity to roasting temperature.

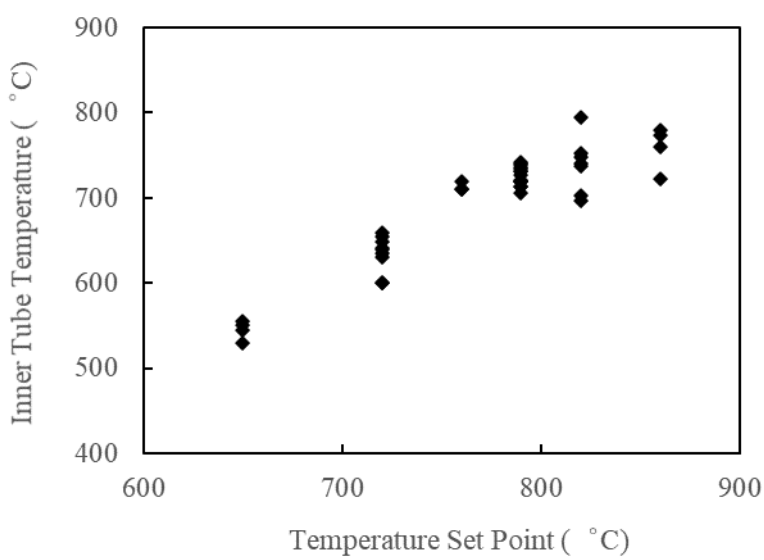

Figure 3.5.16. Correlation between set point temperature and measured inner tube heat zone temperature.

Table 3.5.5. Parametric study on roasting conditions corresponding to leaching recovery.

Test Number	Feed Time Settings		Feed Rate (lbs/hr)	Product Rate (lbs/hr)	Furnace Temperature (Celsius)	Maximum Inner Tube Temperature (Celsius)	Roaster Product TREE in Leachate (ppm)
	On	Off					
1	4	13	7.2	5.9	650	550	3.81
2	4	11	8.7	7.2	650	555	3.81
3	4	9	10.4	8.4	650	545	2.98
4	4	7	12.3	10.1	650	530	2.4
5	4	7	12.7	9.5	720	601	4.32
6	4	11	8.6	6.7	720	639	5.78
7	4	9	9.7	7.6	790	732	4.5
8	4	13	7.8	5.5	790	742	7.06
9	4	7	12.2	9.1	790	714	4.6
10	4	11	8.4	6.6	790	719	5.11
11	4	11	8.4	6.7	720	635	3.9
12	4	9	10.9	8.7	720	600	3.35
13	4	13	8.6	6.2	720	649	4.1
14	4	11	8.6	7.7	720	630	4.02
15	4	13	7.8	5.8	860	723	2.14
16	4	9	9.6	6.6	860	773	2.53
17	4	11	8.2	5.9	860	780	1.93
18	4	7	11.8	9	860	761	2.6
19	4	9	10.9	7.8	820	697	3.66
20	4	13	7.9	5.2	820	740	3.9
21	4	9	10.7	7.86	820	752	3.52
22	4	11	10.3	7.2	820	748	3.18
23	4	7	14.8	11.1	820	703	2.91
24	4	9	11.2	8.1	790	719	3.92
25	4	13	9	6.3	790	713	4.05
28	3	13	4.4	3.3	790	740	5.63
29	3	15	4.1	2.75	790	727	5.11
30	3	15	4.2	2.85	720	659	5.03
31	3	13	4.3	3.5	720	654	5.08
32	4	15	7.5	5	720	641	4.2
40	3	15	4.2	2.55	820	795	2.43
41	3	15	4.2	2.75	760	719	2.8
42	4	15	7.5	3.85	760	710	3.8
43	4	11	8.6	5.35	760	711	3.07
36	4	15	7.5	3.4	790	736	2.54
46	2	20	1.08	1.2	790	731	5.83
35	3	15	4.6	3.3	790	739	4.37

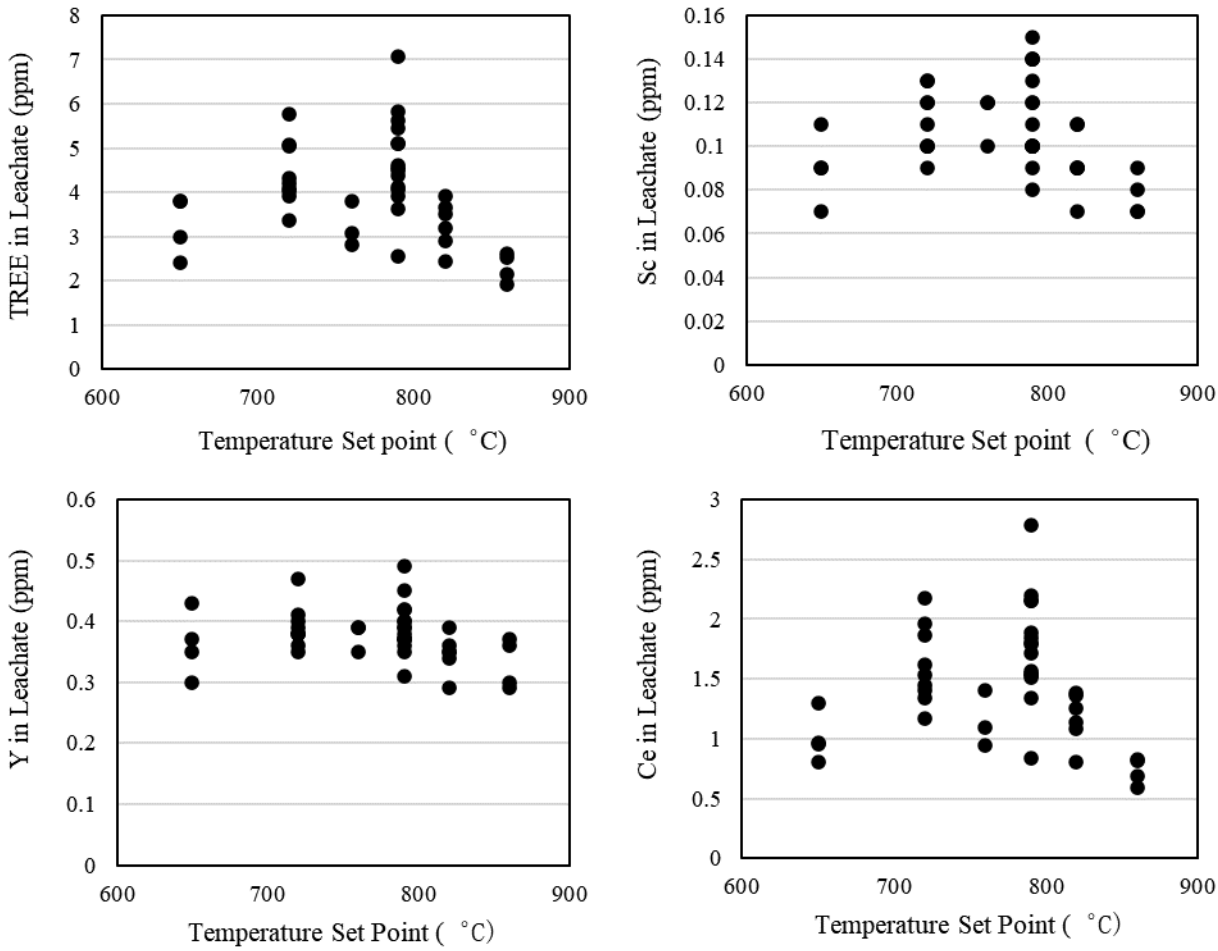

Figure 3.5.17. Effect of roasting temperature on leaching performance of different elements. (Leaching condition: 1M sulfuric acid, S/L=200 g/L, room temperature, 15 minutes)

ii. Fire Clay Roasting retention time

The retention time of the roaster is controlled by the material bed depth and the mass flow rate. The leaching results indicate that the optimal roasting retention time is 20-30 minutes as shown in Figure 3.5.18. To control the material retention time at the designated temperature, an overflow weir cap was installed on the discharge end of the roaster tube. The entire roaster tube length is 60-inch total, whereas the heating zone of the tube is estimated to be 20-inch long. Figure 3.5.19 shows a schematic of the roaster tube. By installing a ring cap at the discharge portal of the tube, the material can be sustained in the tube at a certain height before discharging. The calculation shows that by installing a ¾ inch cap, the roaster tube can hold 1.3 lbs of material in the heating zone and about 3.9 lbs of material in the entire tube (Table 3.5.6). To maintain a 20-30 minutes of retention time in the heat zone, the mass flow rate needs to be controlled within 2.6-3.9 lbs/hour.

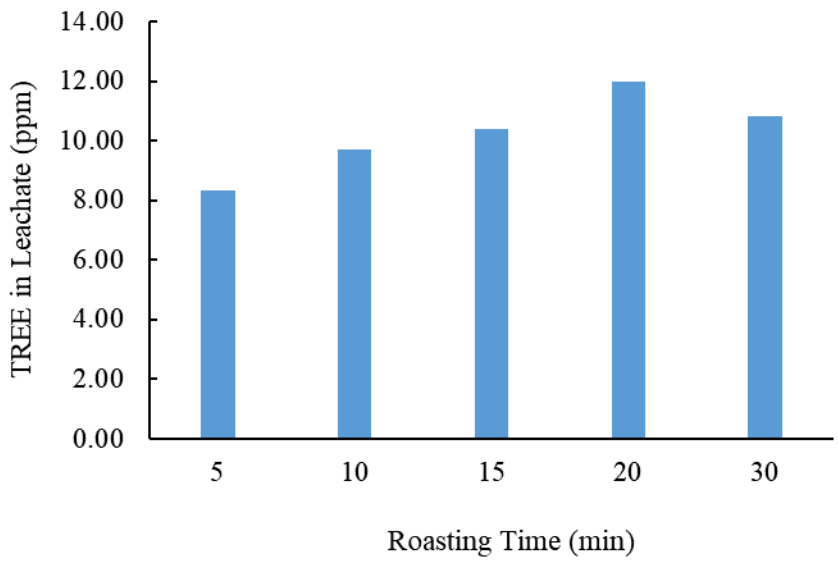

Figure 3.5.18. Effect of roasting time on leaching performance of TREE. (Leaching condition: 1M sulfuric acid, S/L=200 g/L, room temperature, 15 minutes)

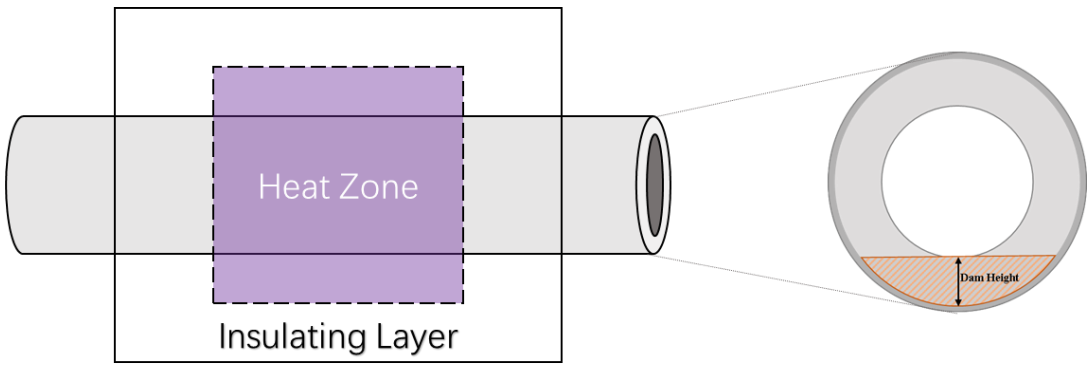

Figure 3.5.19. Schematic of the roaster heat zone and discharge overflow weir.

Table 3.5.6. Calculation of heat zone and tube holding capacity at varies material bed depth.

Dam Height (in)	Segment Area (in^2)	Heating Zone Volume		Tube Holding Volume		Product Powder Density	Heat Zone Mass	Tube Holding Mass
		cubic inch	ml	cubic inch	ml	g/ml	lbs.	lbs.
0.75	1.86	37.2	609.6	111.6	1828.8	0.97	1.3	3.9
0.5	1.03	20.6	337.6	61.8	1012.7	0.97	0.7	2.2
0.25	0.37	7.4	121.3	22.2	363.8	0.97	0.3	0.8

3.5.3 Pilot Scale Leaching Circuit

To identify the optimum acid concentration, three tests were designed to initiate the parametric study and investigate the effect of the larger scale system on leaching efficiency. In the batch test, 350 L of three different concentrations of sulfuric acid solution was prepared and preheated to 75 °C in reactor Tank 7 (Figure 3.5.20). In each batch, 35 kg of prepared solids feed was weighed and mixed into the acid solution. A slurry sample was collected from the leach reaction tank at 5, 15, 30, 60, and 120 mintes of leaching time. The slurry sample was filtered immediately using a lab vacuum filter. The leachate sample was collected and measured for pH. The solid sample was rinsed with 200 ml of water three times to wash off the acidic residues and dried in an oven. The dried solid weight was recorded for solid concentration calculations. The solid concentration and pH are listed in Table 3.5.7,

Table 3.5.8, and Table 3.5.9 for tests with 0.1M, 0.5M, and 1.2M sulfuric acid leaching, respectively.

Based on an initial test involving continuous operation of the leaching circuit, a decision was made to utilize Tank 6 as an acid preparation tank and Tank 7 as the reaction tank. A continuous test was conducted with 0.5M sulfuric acid starting which was started by first allowing the initial solids to be leached in Tank 7 for two hours before starting the continuous flow of solids and acid solution. A solids flow rate of 50 lbs/hr leached with 0.5M sulfuric acid solution were used during the continuous operation of the circuit. The fresh water feed rate influx rate was one gallon per minute. The sulfuric acid pump was calibrated and adjusted to pump 105 ml/min of pure sulfuric acid to generate the 0.5M sulfuric acid solution.

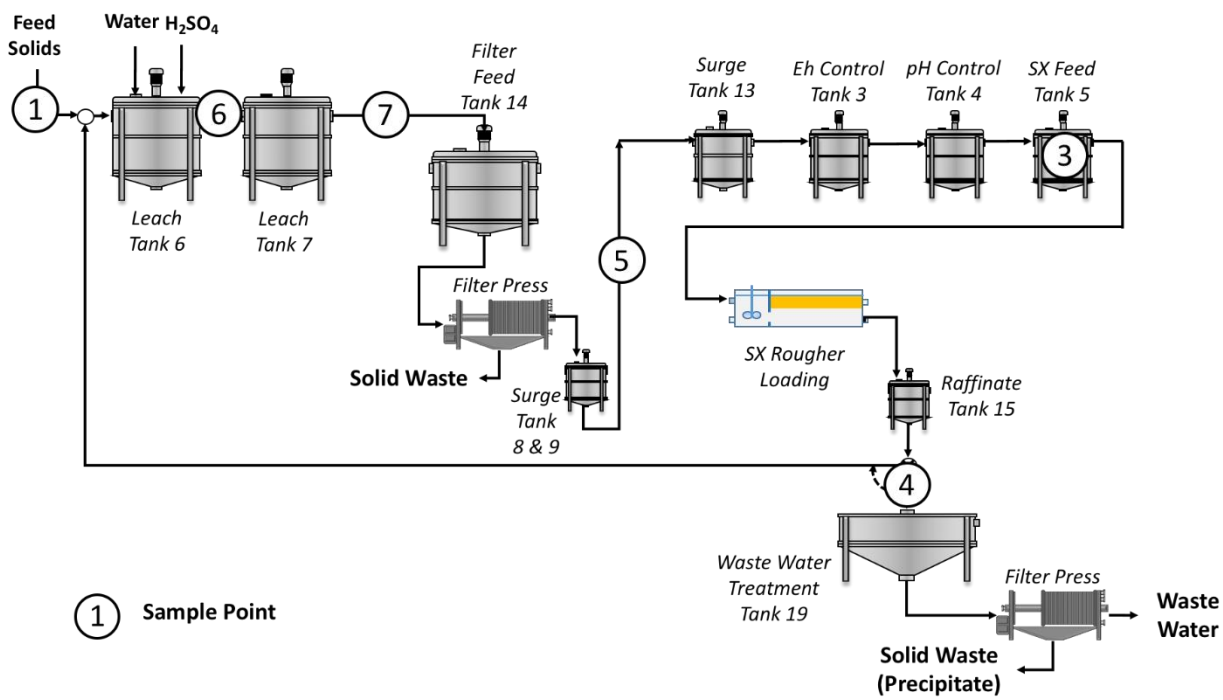

Figure 3.5.20. Schematics of the entire circuit and the locations of the sampling points.

Table 3.5.7. Test FCR-B2 test: Roasted leatherwood material leaching with 0.1 M sulfuric acid.

Time (min)	Temp (°C)	% Solid	pH
5	75	10.61	1.30
15	75	7.67	1.42
30	75	8.22	1.56
60	75	10.05	1.78
120	75	10.19	2.06
180	75	11.59	2.23
240	75	10.19	2.39
300	75	8.67	2.50

Table 3.5.8. Test FCR-B3 test: Roasted leatherwood material leaching with 0.5 M sulfuric acid.

Time (min)	Temp (°C)	% Solid	pH
5	75	9.20	0.49
15	75	4.88	0.53
30	75	7.03	0.56
60	75	3.68	0.60
120	75	6.32	0.68
180	75	9.57	0.73
240	75	10.64	0.74
300	75	11.00	0.78

Table 3.5.9. Test FCR-B1: Roasted leatherwood material leaching with 1.2M sulfuric acid.

Time (min)	Temp (°C)	% Solid	pH
5	77	4.12	0.15
15	77	7.97	0.16
30	76	9.04	0.18
60	76	8.09	0.21
120	76	7.00	0.22

The initial pH values at the start of the tests using 0.1M, 0.5M, and 1.2M sulfuric acid solutions were 0.97, 0.38, and 0.05, respectively. The pH increased with time which reflected the acid consumption during leaching of the solids. After 2 hours, the slurry pH increased to 2.06, 0.63, and 0.22 while leaching with 0.1M, 0.5M, and 1.2M of sulfuric acid solution, respectively. The pH drifting curves are shown plotted in Figure 3.5.21. The feed solution to the solvent extraction circuit was monitored and treated to maintain the pH value at 2.0. It is noted that when a 0.1M sulfuric acid solution is used, the pH does not need adjusted before solvent extraction which significantly reduces the amount of base solution needed. The lower acidity also has a significant effect in lowering the ascorbic acid usage due to the suppressed leaching of iron.

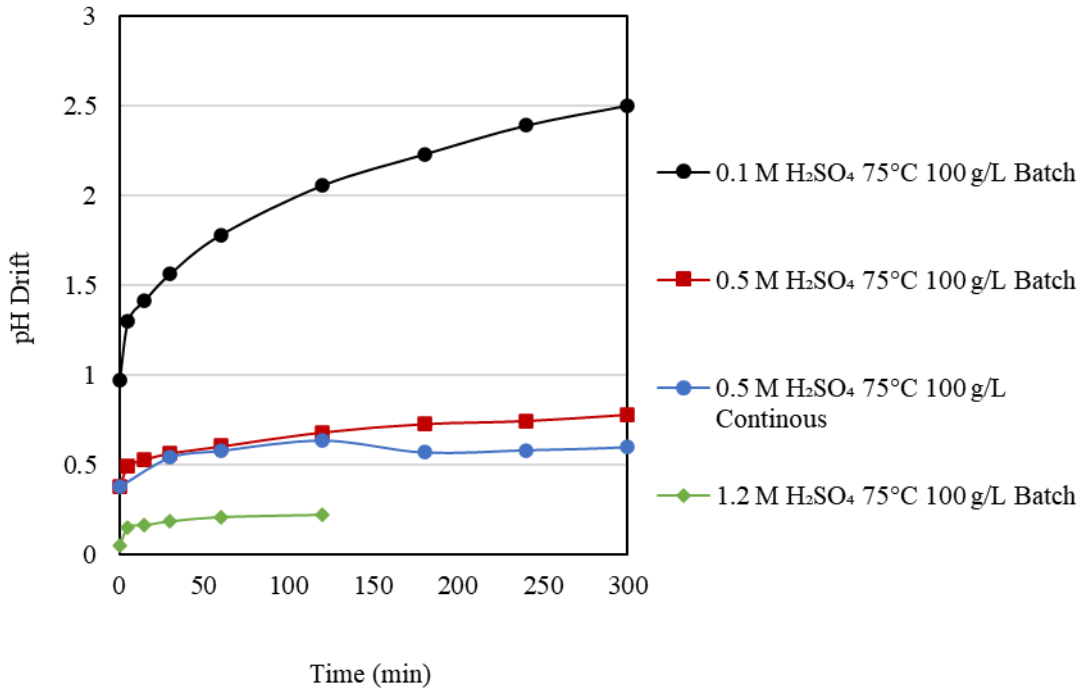

Figure 3.5.21. The change of pH during leaching under different initial acid concentrations.

The total REE recovery values after 2 hours of leaching time in the batch tests were 23%, 32.3%, and 40.4% using 0.1M, 0.5M, and 1.2M of sulfuric acid solution, respectively. Figure 3.5.22 shows that the recovery values obtained for praseodymium and gadolinium were the most impacted over the range of acid concentrations tested. Gadolinium recovery was nearly 90% using 1.2M H_2SO_4 solution. Recovery of the major light REEs such as cerium, lanthanum and neodymium nearly doubled over the range of acid concentrations; however, their values remained relatively low at around 42% which was largely reflected in the total REE recovery value. Scandium recovery is a major concern with a maximum value of 25% achieved using a 1.2M acid dosage.

The data in Figure 3.5.23 (a) shows that REE recovery as a function of time for both the batch and continuous tests. In the continuous test, fresh solid and acid solution were added after 2 hours of batch leaching which created a recovery drop. The recovery reduction may have been due to the effects of the perfect mixing conditions which result in short-circuiting of a portion of the solids. The mixing conditions may also explain the trend associated with the pH curve shown in Figure 3.5.21 for the continuous test. When the continuous process was initiated after two hours of batch leaching, the pH of the exiting stream from Tank 7 decreased from 0.63 to 0.57 which indicated a reduction in the reaction between the solids and lixivant. This likely contributed to a reduction in leaching efficiency and REE recovery.

The leaching recovery values for Al, Ca, and Fe, which are the major contaminants, are shown in Figure 3.5.23 (b), (c), and (d), respectively. Calcium recovery was almost 100% at each acid concentration level resulting approximately 200 ppm of Ca in leachate solution. The Fe recovery increased by 33 percentage points when the acid concentration was strengthened from

0.1M to 0.5M and raised another 16 percentage point when a 1.2M sulfuric acid solution was used. The Fe release into the leachate is a major factor that affects the ascorbic acid chemical consumption and the efficiency of solvent extraction. Aluminum recovery was relatively low and varied by only 10 percentage points between the different acid concentrations.

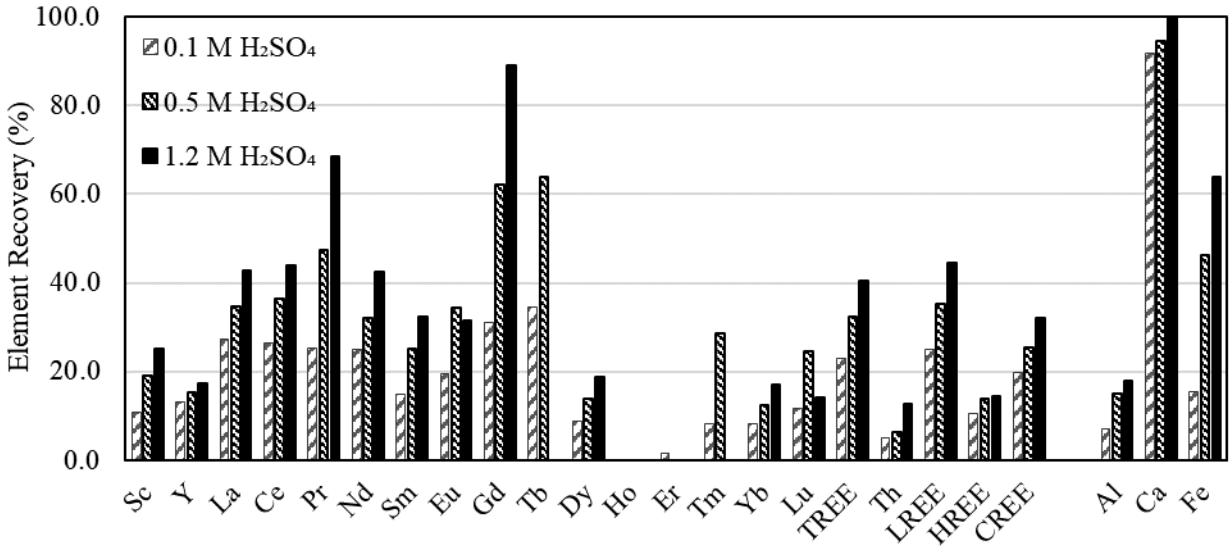

Figure 3.5.22. Individual element recovery at different acid concentration level after 2 hours of leaching. (Temperature = 75 °C, solid concentration = 100g/L)

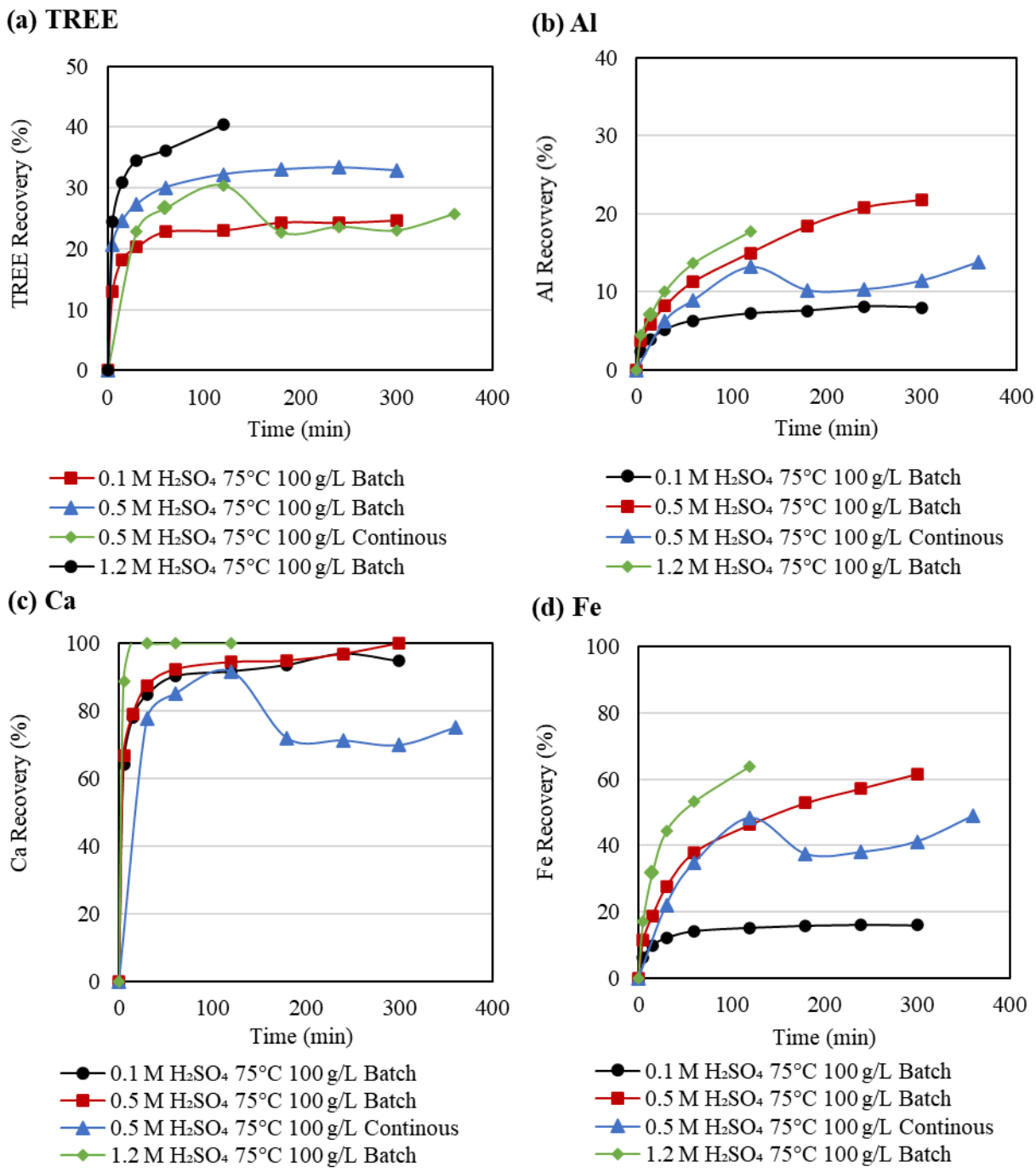

Figure 3.5.23. Leaching recovery of (a) TREEs, (b) Al, (c) Ca, and (d) Fe using 0.1M, 0.5M, and 1.2M sulfuric acid leaching in batch and continuous mode.

3.5.4 Solvent extraction feed reduction

Redox potential (Oxidation Reduction Potential or ORP) of a solution is the measure of the tendency of species present in the solution to be reduced i.e. acquire electrons in units of volts or millivolts. An increase in the ORP value indicates a greater tendency of species present in the system to be reduced. Iron has two stable valence states in solution, i.e., ferric (Fe^{3+}) and

ferrous (Fe^{2+}). Of these two states, Fe^{3+} has a higher tendency to become reduced than that of Fe^{2+}. In other words, a solution with a majority of iron in ferric state will have a higher ORP value, whereas a solution with majority of iron in ferrous state will have a lower ORP value.

The valence state of iron in the SX feed is pertinent for the separation efficiency of the REEs. The distribution coefficient of ferric species is orders of magnitude higher than the corresponding ferrous species. This is due to the trivalent nature of the ferric species and the higher affinity of the cation exchange extractant for the trivalent species. The iron in untreated SX feed is predominantly in ferric state and competes with REEs for extraction in the organic phase leading to contamination of the final product. For efficient separations, the iron can be reduced using a reducing agent to its ferrous state. For this test, ascorbic acid was used as a reducing agent. The ORP value of the solution was used as a control parameter to determine the optimum dosage rate for the continuous process.

The ascorbic acid solution was prepared by dissolving 10g of analytical grade ascorbic acid in 50 mL of deionized (DI) water. The mine water from the Dotiki coal mine was used as the test solution. The ascorbic acid solution was added to 50 mL of the leachate in incremental quantities using steps of 0.5 ml. The ORP and pH values of the solution were recorded. As shown in the Figure 3.5.24, the ORP value of the solution was reduced from 410 mV to 300 when incrementally treated with 2.4 ml ascorbic acid in 0.5 ml steps. Further addition of ascorbic did not have a significant impact on the ORP value. This indicated the concentration at which the majority of the iron was reduced to the ferrous state. The pH of the test solution also decreased from its natural pH of 2.35 to 1.91 upon addition of 2.4 ml of ascorbic acid. It was also observed, as shown in the Figure 3.5.25 that the color of the test solution changes color from deep red to pale green tinge due to the reduction of iron as the natural color of the ferric ion is reddish brown while the ferrous ion imparts a pale green color to the solution.

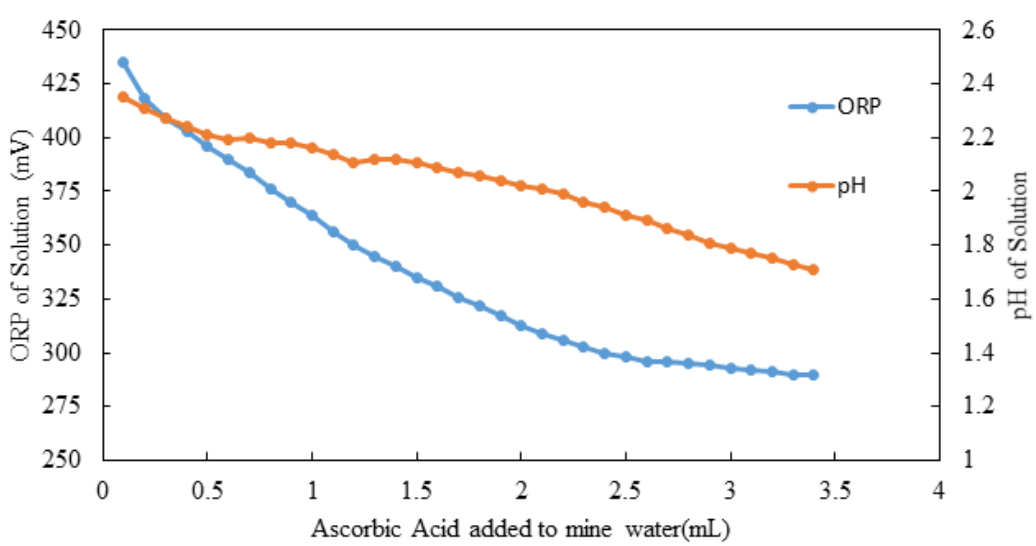

Figure 3.5.24. Effect of Ascorbic Acid addition on the pH and ORP of Dotiki mine water

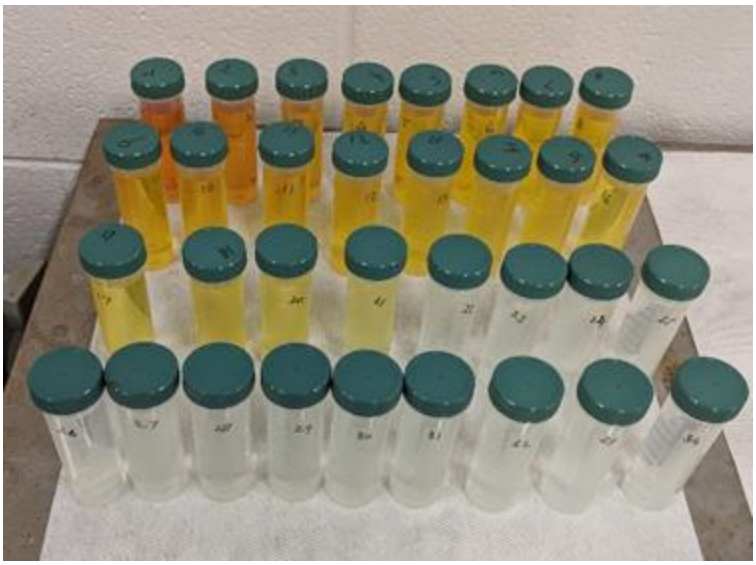

Figure 3.5.25. The visual change of the mine water as incremental amount of ascorbic acid was added.

For determining the optimum pH value for SX feed with Dotiki mine water as feed, exploratory shakeout tests for solvent extraction were conducted. 50 ml of pretreated solution was contacted with the organic extractant solution for 15 minutes at different pH values. The raffinate for each pH was analysed to develop the extraction equilibrium curves for both the REEs as well as major contaminants viz. iron, aluminum and calcium. It was concluded from the extraction curves developed from the test solution collected from the pilot plant under the given operating conditions indicated that the ideal operating pH for maximum recovery of REE while maintaining excellent selectivity was 2.0 as shown in Figure 3.5.26.

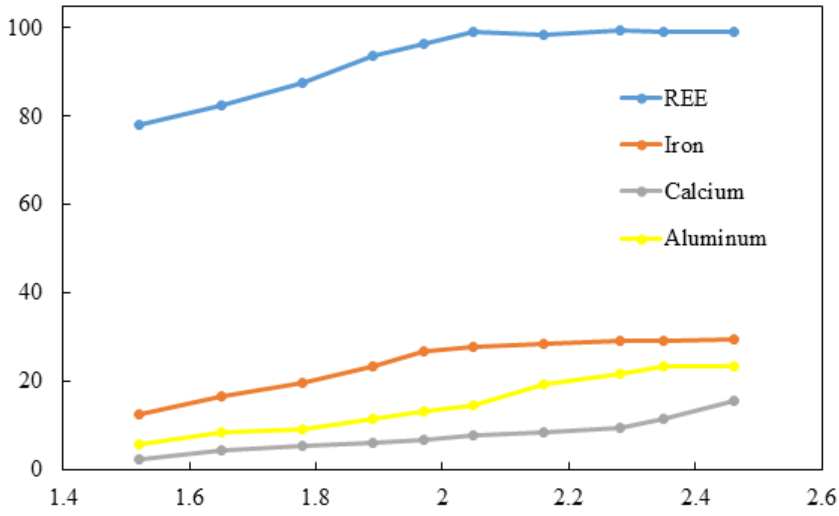

Figure 3.5.26. Extraction curves for REE and contaminant elements from exploratory shakeout tests performed on Dotiki mine water

3.5.5 Pilot scale continuous leaching and SX circuit testing

3.5.5.1 Continuous Leaching and SX Circuit Testing Trial 1

A trial test involving the processing of Fire Clay coarse refuse through the leach and SX circuits was conducted continuously over 12-hour period. In this test (code FCR-C1), two-stage co-current leaching was realized using reactor Tank 6 and Tank 7 to achieve the maximum leaching performance within a total 4 hours of retention time. The pH value of the solution in Tank 6 was controlled automatically with a calibrated pH probe and a pre-programmed peristaltic pump that fed the pure sulfuric acid to maintain the pH value constant at zero.

To start the test, Tank 6 and Tank 7 were each filled with 350 L of 1.2M sulfuric acid and heated to 75 °C. Solid feed was conveyed to the top of Tank 6 using a screw conveyor at a feed rate of 50 lbs per hour. Simultaneously, tap water was fed into Tank 6 with a controlled flow rate of 1 gallon per minute. Both tanks 6 and 7 have a volumetric capacity of 100 gallons. As such, the volumetric retention time was approximately 100 minutes. A slurry sample were collected from the overflow streams of Tank 6 and Tank 7 every 2 hours. The weight of the slurry sample was recorded as well as the pH value of the slurry as shown in Table 3.5.10.

The recovery of REEs and other elements were calculated based on the REE contents in the leachate and the maximum REEs that can be extracted from solid feed, i.e.:

$$\text{Recovery } \% = \frac{c_L * V_L}{c_f * m_f}$$

where, c_L is the element concentration in leachate (mg/L), V_L is the volume of leachate (L), c_f is the element concentration in feed solid (mg/kg), m_f is the weight of feed solid (kg).

Table 3.5.10. Pilot run FCR-C1 continuous test leaching sample pH (maintained) and solid concentration.

Sample Code	Retention (hour)	Slurry Wt. (g)	Temperature (°C)	Slurry pH	Solid Weight (g)	Solid Con (Wt %)
FCR-C1-Point 6-1	2	225.00	76.00	0.05	3.29	1.46
FCR-C1-Point 6-2	4	220.00	75.00	0.05	3.65	1.66
FCR-C1-Point 6-3	6	210.00	76.00	0.06	2.73	1.30
FCR-C1-Point 6-4	8	210.00	74.00	0.07	2.43	1.16
FCR-C1-Point 6-5	10	230.00	75.00	0.05	10.23	4.45
FCR-C1-Point 6-6	11	235.00	75.00	0.10	7.84	3.34
FCR-C1-Point 6-7	12	230.00	75.00	0.14	9.00	3.92
FCR-C1-Point 7-1	2	241.18	75.00	0.11	2.43	1.01
FCR-C1-Point 7-2	4	231.18	75.00	0.05	6.58	2.85
FCR-C1-Point 7-3	6	271.18	75.00	0.02	7.30	2.69
FCR-C1-Point 7-4	8	376.18	75.00	0.08	5.37	1.43
FCR-C1-Point 7-5	10	276.18	75.00	0.25	11.71	4.24
FCR-C1-Point 7-6	11	311.18	75.00	0.18	12.49	4.01
FCR-C1-Point 7-7	12	366.18	75.00	0.17	19.71	5.38

The previous investigation showed that the leaching reaction with roasted material was mostly completed within two hours of retention time in lab scale tests. Figure 3.5.27 shows the TREEs concentration that was leached into solution as a function of time. Since the tanks were filled with acid solutions at the beginning of the tests, a portion of the solid feed flows out of the system from the overflow discharge due to the continuous influx of 50 lbs/hr of solids and 1 gpm of solution. The theoretical solid concentration was modelled and plotted as shown in Figure 3.5.28. The solids concentration rises in the first few hours and reaches a plateau after 8 hours of continuous operation.

In two hours (one volumetric retention time), the TREE concentration in the first leaching tank (Tank 6) was 8.2 ppm, whereas the concentration in the second leach tank (Tank 7) was 4 ppm due to the low solid concentration at the beginning of the process. At 4 hours (2 retentions), the TREE concentration in Tank 7 elevated to 9.4 ppm which was approaching the level of the TREE concentration in Tank 6. The two curves in Figure 3.5.27 show that the TREEs concentration in Tank 6 and Tank 7 were approximately equal, except that Tank 7 has a time lag of 2 hours from Tank 6. It also indicated that 2 hours of retention time is adequate for the given feed material which led to the conclusion that one reactor tank was sufficient.

Chemical usages were recorded and tracked every two hours to monitor the process stability and the consumption over time. Chemicals were added at a total of six locations in the circuit. Each tank level was recorded as well as the refill volume of chemical solutions during the operation. Pure sulfuric acid was added into Tank 6 to initiate the acid leaching process. The slurry was filtered through the filter press to recover the pregnant leachate solution. To prevent precipitation during pH adjustment before solvent extraction circuit, ascorbic acid solution with a concentration of 100 g/L was added into Tank 3 to maintain the ORP level at 230 mV. Then, the solution pH was adjusted to a value of 2.0 in Tank 4 using 2M NaOH solution and pure sulfuric acid. In the solvent extraction circuit, 0.1M of HCl and 6M of HCl solution were used to scrub and strip the loaded organic solution, respectively. The raffinate solution discharged from the loading stage of solvent extraction circuit was neutralized in Tank 19 by adding 2M NaOH solution. The overall chemical consumptions are provided in Table 3.5.11. Leaching at 1.2M and maintaining the pH value of 0 required a formidable amount of acid. The strong acidic environment extracted a significant amount of contaminant ions which resulted in the use of an excessive amount of reducing agent and sodium hydroxide to neutralize the wastewater. The experience and the findings of this test led to the following conclusions:

1. The use of 1.2M H_2SO_4 is cost prohibitive due to the excessive chemical consumption.
2. The maintaining the pH at a target value in the leach vessel is not ideal due to the amount of acid needed and the ultimate cost of the chemicals; and
3. The leach circuit was modified to provide a leach solution preparation tank where the pH was adjusted. The solution naturally overflows into the leach tank where the solids are added, and the pH permitted to drift.

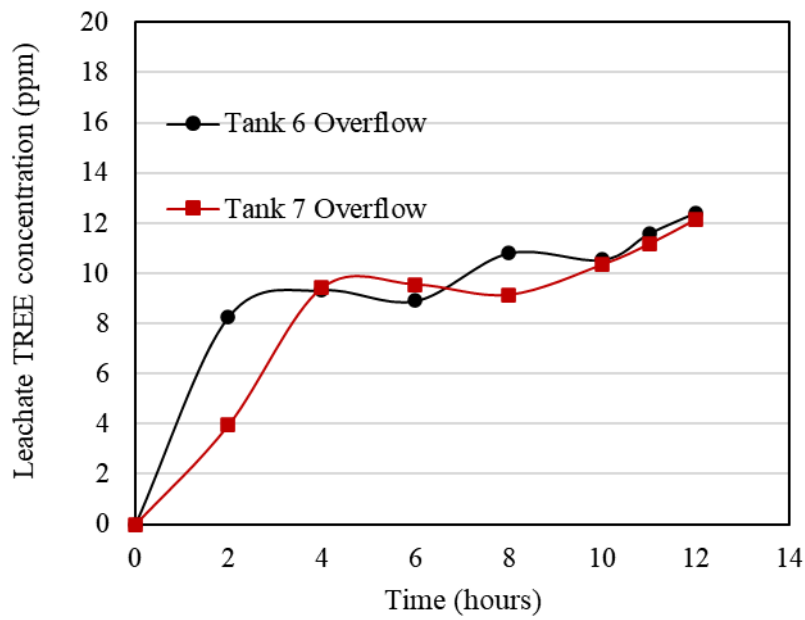

Figure 3.5.27. Results of TREE concentration in tank 6 and tank 7 with time.

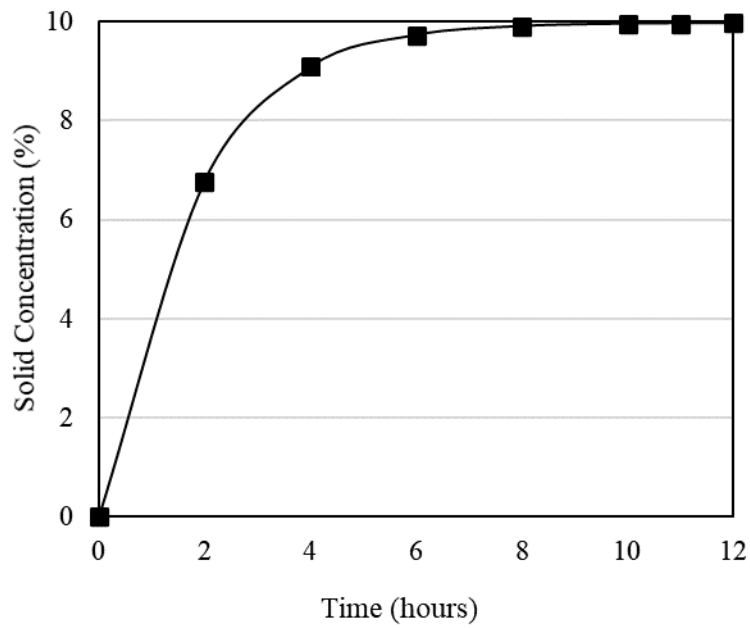

Figure 3.5.28. Theoretical solid concentration in tank 6. (Starting with 100-gallon liquid, continuously feeding in 50 lbs. per hour of solid and 1 gallon per minute of liquid).

Table 3.5.11. Chemical consumption of operating 10 hours leaching with 1.2 M sulfuric acid solution.

Tank Level	Leaching			Solvent Extraction		Water Treatment
	98% H_2SO_4 (Gallon)	2M NaOH (Gallon)	100 g/L Ascorbic Acid (Liter)	6M HCl (Gallon)	0.1M HCl (Gallon)	2M NaOH (Gallon)
START 9:00 AM	25.5	89.8	30.0	76.0	86.3	86.0
STOP 7:00 PM	31.5	15	43	14	59	28
Refills	75.0	80	520.0			80
Total Consumption	69.0	154.8	507.0	62.0	27.3	137.7

3.5.5.2 Continuous Leaching and SX Circuit Testing Trial 2

In the second trial, the pilot scale leaching, solvent extraction, and wastewater treatment circuit was operating continuously for 90 hours over three weeks of time period. Approximately 20000 L of pregnant leachate was generated and fed into the solvent extraction circuit to produce final rare earth oxide product. The chemical cost was evaluated over the entire hydrometallurgical circuit to analyze the economic feasibility of the current circuit. The analysis showed that the economics of the solvent extraction circuit was depending on the REE concentration in the pregnant solution, which was depending on the REE concentration in the feed material and the corresponding recovery. A baseline chemical cost evaluation was established to estimate the minimum cost of various pH values over a range of feed grade. The analysis showed that the circuit would be economical if leaching at pH of 2 or above. Therefore, an innovative circuit was designed to utilize selective precipitation and re-dissolution to preconcentrate the pregnant leachate solution.

Continuous Leaching Circuit:

The feed material was coarse refuse material collected from leatherwood plant which processes Fire Clay coal and roasted under 600 °C with approximately 30 minutes of retention time. The material was scrapped at 1mm using a vibration screen to discard all the over 1 mm size particles. To start the continuous leaching system, 350 L of 0.5M sulfuric acid solution was prepared and heated up to 75 ℃. 35 kg of solid feed was fed into the leaching tank and reacted for 2 hours. After 2 hours of reaction, 1 gallon per minute of water, 102 ml per minute of 93% pure sulfuric acid, and 50 lbs. per hour of solid feed were fed into the leaching tank simultaneously. The temperature was maintained at 75 ℃ during the whole process. The solid and acid feeders were calibrated as shown in Figure 3.5.29.

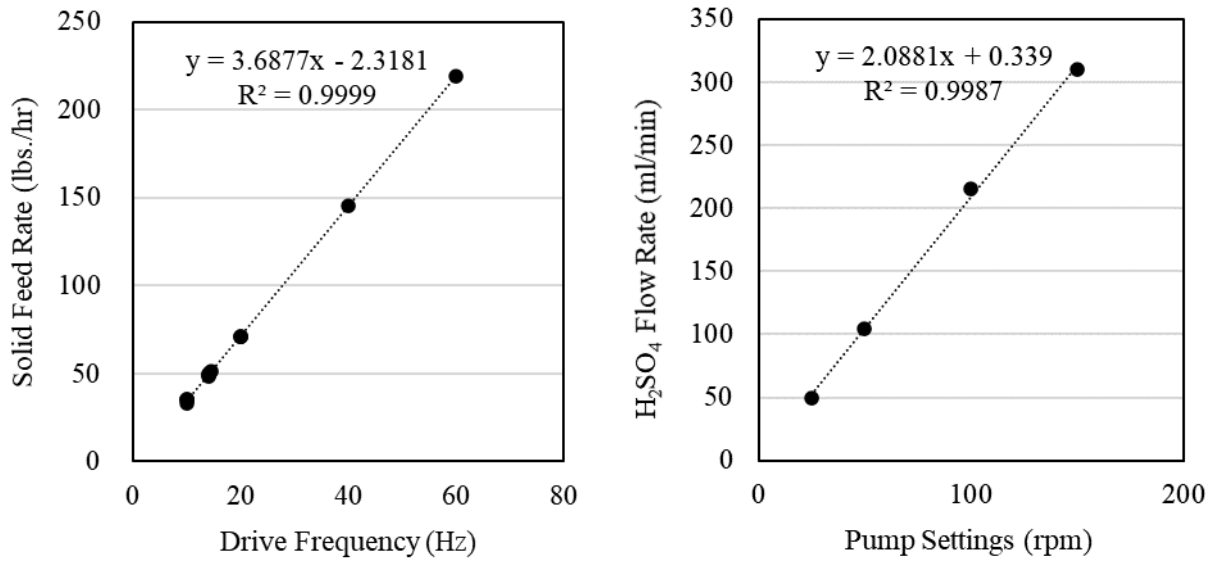

Figure 3.5.29. Solid feeder calibration (left) and sulfuric acid feeder calibration (right).

Table 3.5.12. Timeline of the continuous operation.

Time (h)	Notes
2	Solid/Acid feed starts
14	SX circuit start
24	Overflow Pump tubing changed
48	25% Raffinate start recycling
75	50% Raffinate start recycling
94	Stop

The timeline of the total 94 hours of continuous operation is listed in Table 3.5.12. The system started running continuously after the initial 2 hours. The leachate was produced at an approximate flow rate of 1 gallon per minutes, therefore, after 14 hours of operation, the volume of leachate was accumulated enough to start the solvent extraction (SX) system. The detailed experimental data for the SX circuit is presented in section 3.5.6. In the previous test run, the design of the leaching system was demonstrated where the leaching slurry was transferred to the filtration tank by gravity overflowing. During the continuous operation, a reduced solid concentration in the overflow material was observed which indicated a fluid bypass situation due to the inadequate mixing condition in the leaching reaction tank. The insufficient mixing created a solid concentration gradient vertically in the leaching reaction tank, where the bottom of the tank contained higher solid concentration and the top of the tank contained lower concentration of solid. With time, the solid particles remained in the leaching tank accumulated and the solid concentration increased which resulted in a higher solid-to-liquid ratio. To resolve this problem, the mixing speed was increased, and a pump was installed to withdraw slurry 10 inch below the liquid level. Figure 3.5.30 shows the solid concentration fluctuated before system debugging and stabilized after installing the overflow pump.

To reduce the fresh acid consumption, the raffinate that discharged from the solvent extraction loading stage was recycled to the leaching tank. Based on the pH value of the raffinate stream, the acid concentration was calculated using the correlation between acid concentration and corresponding pH values. As shown in Table 3.5.13, the raffinate pH was 0.835 after SX system stabilization, which corresponded to about 0.159 M sulfuric acid solution. For 25% recycling, 0.25 gpm of 0.159M raffinate was pump back to the make-up acid solution tank with 0.75 gpm of fresh water. In this case, 0.614M of fresh acid was required to make the acid solution to be 0.5M acid concentration. Therefore, only 94 ml/min of fresh sulfuric acid was needed instead of 102 ml/min which corresponds to about 7.8% of fresh acid reduction. However, the recycling of raffinate brought back a certain amount of contamination ions which loaded the solvent extraction system with time. The loading pH of the SX rougher stage increased from 2.0 to 2.5 in order to maintain the REE loading efficiency. This action caused the raffinate pH increased to 1.493 after the system stabilized. The increased pH of raffinate did not provide a significant change on fresh acid reduction. Even at 50% raffinate recycling rate, 98 ml/min of fresh acid was required to make 0.5M acid concentration solution which corresponded to only 4% of fresh acid reduction. The loading pH of the SX rougher stage had a great impact on both the REE loading efficiency and the fresh acid save-up.

Since the raffinate carried a certain amount of contamination ions, such as Ca, Fe, and Al, the leaching efficiency of REEs was impacted slightly due to the higher ionic concentration of the acid solution. The TREE recovery is plotted over time in Figure 3.5.31. At the first 24 hours of leaching, the system was not stabilized due to the solid concentration variation. From 24 hours to 48 hours, the leaching recovery in the continuous leaching system was stabilized to be in an average of 30%. From 48 hours to 75 hours, 25% of the raffinate was recycled back to the leaching tank, which brought down the TREE recovery to be about 27%. From 75 hours to 94 hours, 50% raffinate recycle was applied which further reduced the recovery to be about 22%. The individual RE recovery at stabilized condition under various recycling rate was compared in Figure 3.5.32. The impact on recovery was non-selective to any individual element. This phenomenon indicated that the recovery reduction was not due to selective leaching, but because of the co-precipitation and/or re-adsorption of REEs. To further evaluate the mechanism, the recovery of major contamination ions was plotted as shown in Figure 3.5.33, Figure 3.5.34, and Figure 3.5.35 for Al, Ca, and Fe, respectively. The results showed that the Ca recovery reduced significantly over time which could be a sign of $CaSO_4$ formation during leaching.

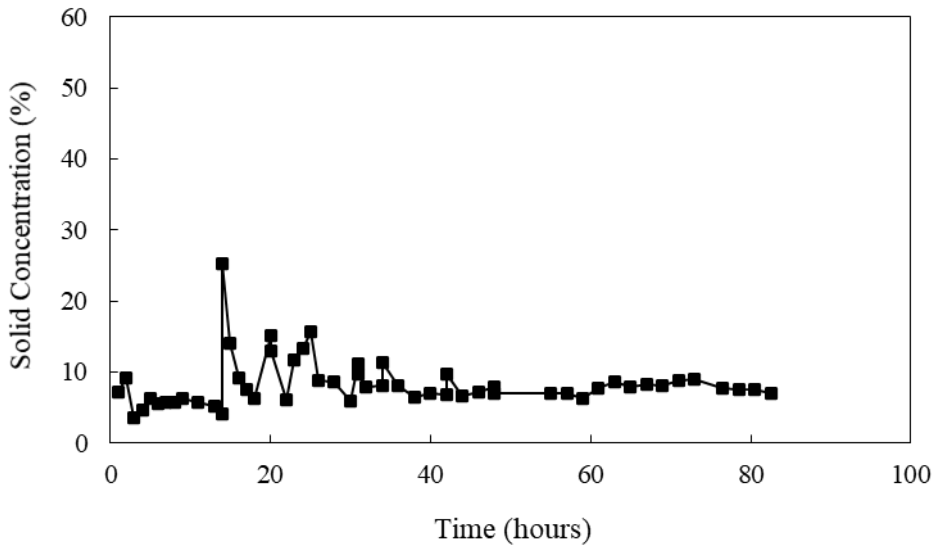

Figure 3.5.30. Leach tank overflow solid concentration monitoring in the continuous operation.

Table 3.5.13. Make-up acid solution adjustment based on various recycle rate of raffinate.

Input					Response			
Recycle Rate (%)	Raffinate pH	Raffinate $c(H^+)$ (M)	Target $c(H^+)$ (M)	Feed Rate (gpm)	Fresh Acid (M)	Tap Water (gpm)	Pure Acid (ml/min)	Pump Setting (rpm)
0	0.835	0.159	0.5	1	0.500	1	102	51
25	0.835	0.159	0.5	1	0.614	0.75	94	47
50	1.493	0.041	0.5	1	0.959	0.5	98	49

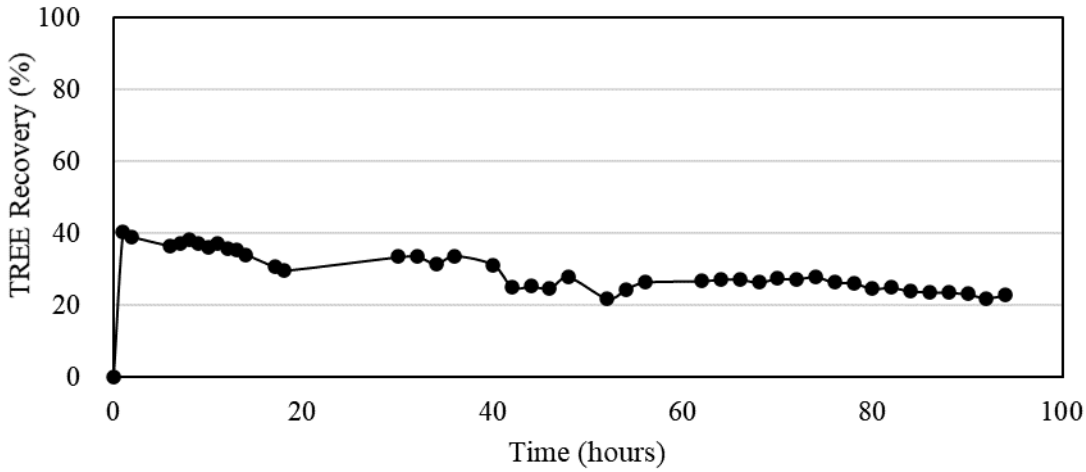

Figure 3.5.31. Leaching recovery of total rare earth elements in the continuous operation.

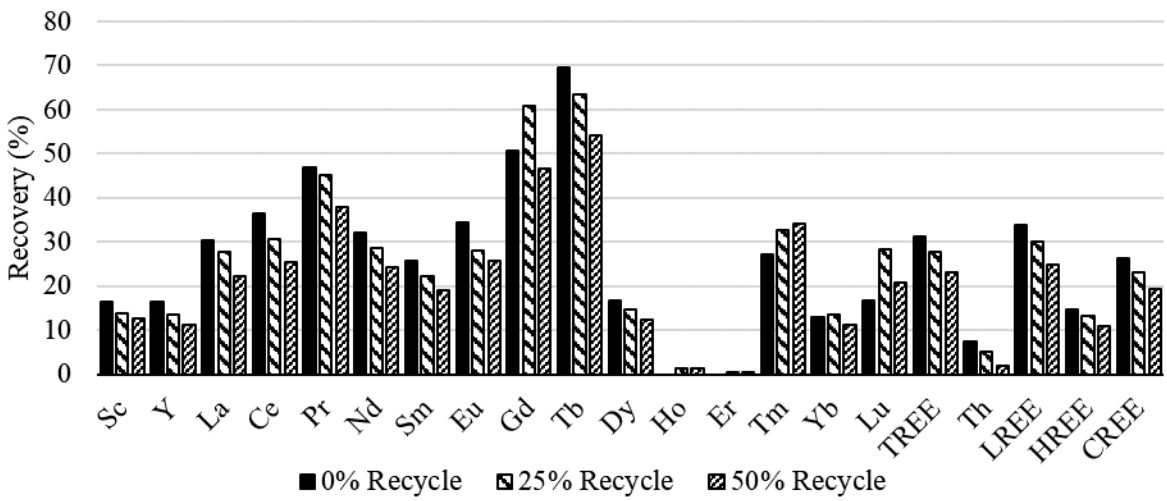

Figure 3.5.32. Leaching recovery of individual rare earth elements in the continuous operation.

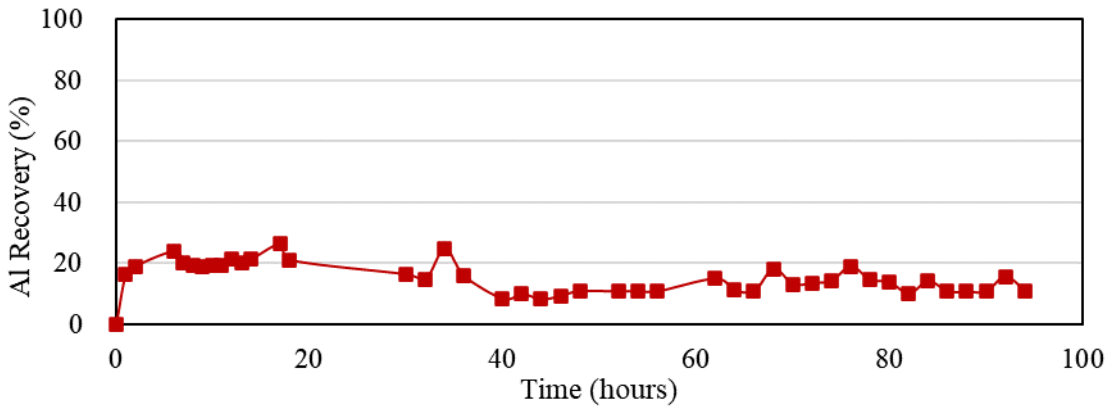

Figure 3.5.33. Leaching recovery of Al in the continuous operation.

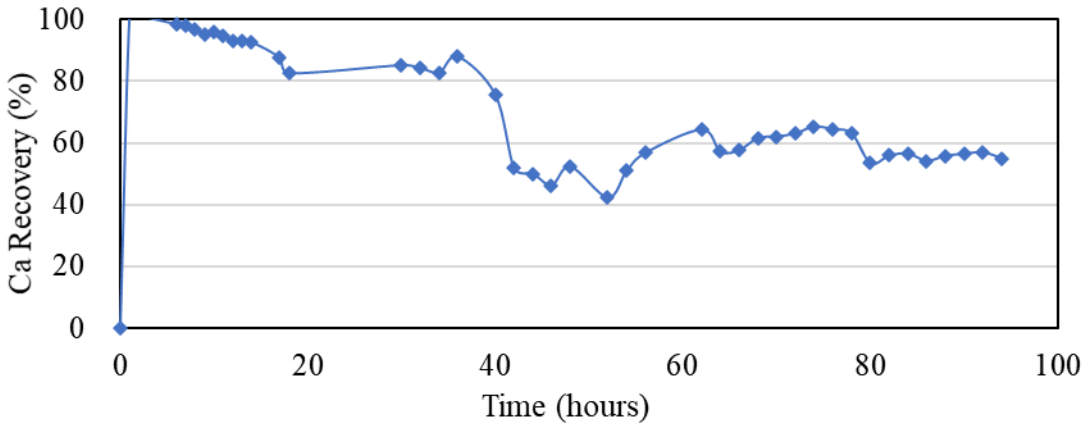

Figure 3.5.34. Leaching recovery of Ca in the continuous operation.

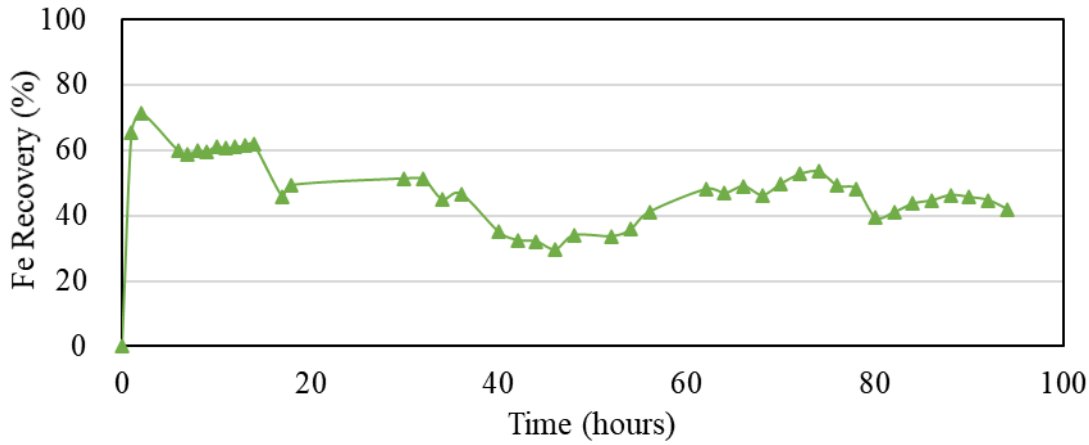

Figure 3.5.35. Leaching recovery of Fe in the continuous operation.

Chemical Cost Evaluation:

Over the entire hydrometallurgical circuit, chemicals were added in different locations for different purposes. The dosages were recorded for each individual stream of chemical addition as shown in Table 3.5.14. The price of each chemical reagent used in this evaluation process is based on the purchasing price of the bulk chemical solutions for the pilot plant. The cost of chemicals to produce and process each one kilogram of REE was calculated based on the average concentration of REE in pregnant leachate solution. During the 94 hours of continuous leaching, about 20000 L of leachate was produced which contained an average of 11 ppm of TREEs. The total cost to produce and process one kilogram of mixed REE is around $3910, which is unrealistically expensive. The table showed that most of the chemical cost came from the sulfuric acid, followed by the hydrochloric acid and sodium hydroxide.

The current circuit required many pH reduction and elevation points which consumed most of the acid and base solutions. Firstly, 0.5M of sulfuric acid was consumed to lower the pH to about 0.4 and extract REEs from solid to pregnant solution. Then, the pH was raised up to about 2.0~2.5 for SX circuit. The discarded raffinate solution was sent to a waste water treatment process which required to elevate the pH to 8.0~9.0. The series of pH adjustment cost over $3000 per kg of REEs regardless of the downstream refining process in SX circuit. Therefore, a baseline cost evaluation was established to estimate the minimum cost to simply bring the pH down to a designated pH value and raise it up to pH of 8. Designated pH value of 1, 2, and 3 were selected over a range of solid feed grade as shown in Figure 3.5.36. To control the cost to be less than 50$ per kilogram of REE, the ideal scenario is to increase the REE concentration in leachate with mild acid concentration. The circuit was modified based on this conclusion to pre-concentrate the REEs in leachate using selective precipitation and redissolution.

Table 3.5.14. Chemical cost per one kilogram of REE in pregnant solution of the hydrometallurgical circuit.

Chemical	Purpose	Dosage (per Liter of Leachate Produced)		Cost ($/kg REE)
H_2SO_4	Acid Leaching	26.30	mL 93% H_2SO_4	$1,845.03
NaOH	Waste water neutralization	10.85	mL 50% NaOH	$439.23
	SX Rougher feed pH adjusting	16.44	mL 50% NaOH	$665.13
	SX Cleaner feed pH adjusting	0.06	mL 50% NaOH	$2.37
	REEs Precipitation	0.00	mL 50% NaOH	$0.00
HCl	SX Rougher stripping & reprotonation	36.47	mL 37% HCl	$542.82
	SX Rougher scrubbing	0.22	mL 37% HCl	$3.28
	SX Cleaner stripping	0.00	mL 37% HCl	$0.00
Ascorbic Acid	SX Rougher reduction	1.44	g Ascorbic Acid	$411.10
	SX Cleaner reduction	0.00	g Ascorbic Acid	$0.00
Oxalic Acid	REEs Precipitation	0.01	g Oxalic Acid	$0.68
Total				$3,909.63

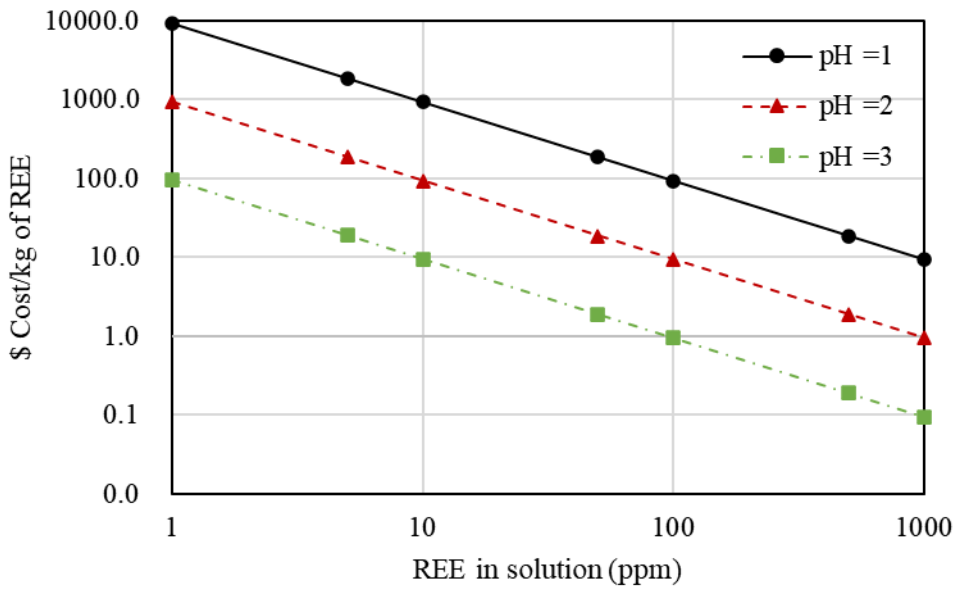

Figure 3.5.36. Baseline evaluation for acid and base cost to adjust the pH of water to 1, 2, and 3, and neutralize to 8.

Modification of Leaching Circuit:

Based on the previous section, an initial acid concentration of 0.01 M was selected to initialize the circuit modification. Leaching performance under a controlled pH and a free drifted pH were compared. In the controlled pH test, automation pH control system was applied where

the acid pump speed was recorded to calculate the volume of acid pumped over time. At the beginning of the test, 200 ml of 93% sulfuric acid was added to 350L of water to create a 0.01M acid solution. The initial pH of the solution was 1.936. Slurry samples were collected at 5, 10, 20, 30, 60, and 120 min to measure the pH and subject to solid-liquid separation to collect the leachate solution. The change of pH throughout both leaching tests were plotted in Figure 3.5.37. The corresponding TREE recovery for both tests are plotted in Figure 3.5.38 with individual RE recovery at leaching time of 2 hours plotted in Figure 3.5.39. The results showed that with maintaining the pH at 1, the TREE recovery reached nearly 50% after 2 hours of leaching, whereas without additional acid, the recovery of TREE was about 14%. However, the total acid addition required to maintain the pH at 2 is almost 10 times of the initial amount of acid as shown in Figure 3.5.40. Therefore, justifications need to be carried out to evaluate the value of REEs that was gained comparing to the cost for additional acid requirement.

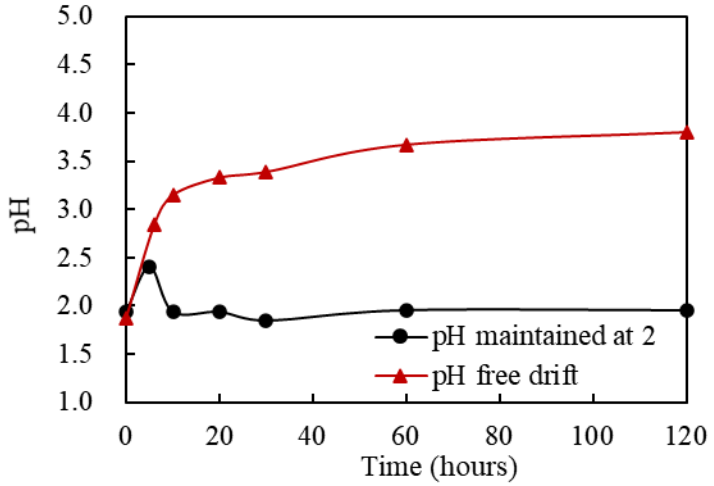

Figure 3.5.37. pH comparison between pH maintained at 2 (DTKCR-B5) and pH free drifted (DTKCR-B3) test with initial acid concentration of 0.01M.

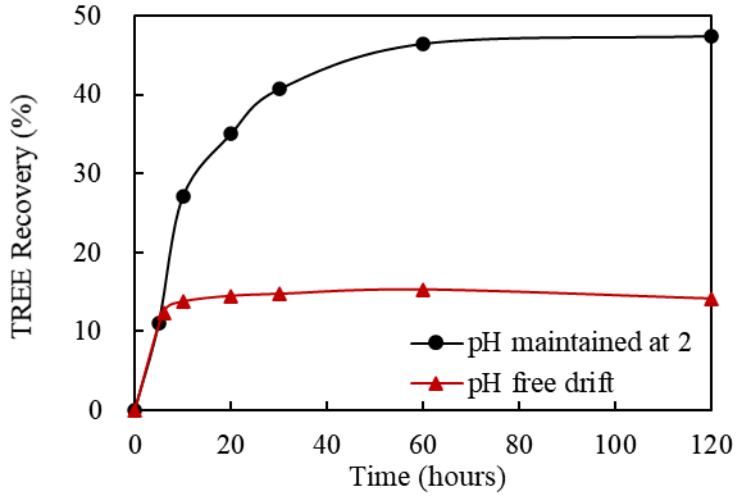

Figure 3.5.38. TREE recovery comparison between pH maintained at 2 (DTKCR-B5) and pH free drifted (DTKCR-B3) test with initial acid concentration of 0.01M.

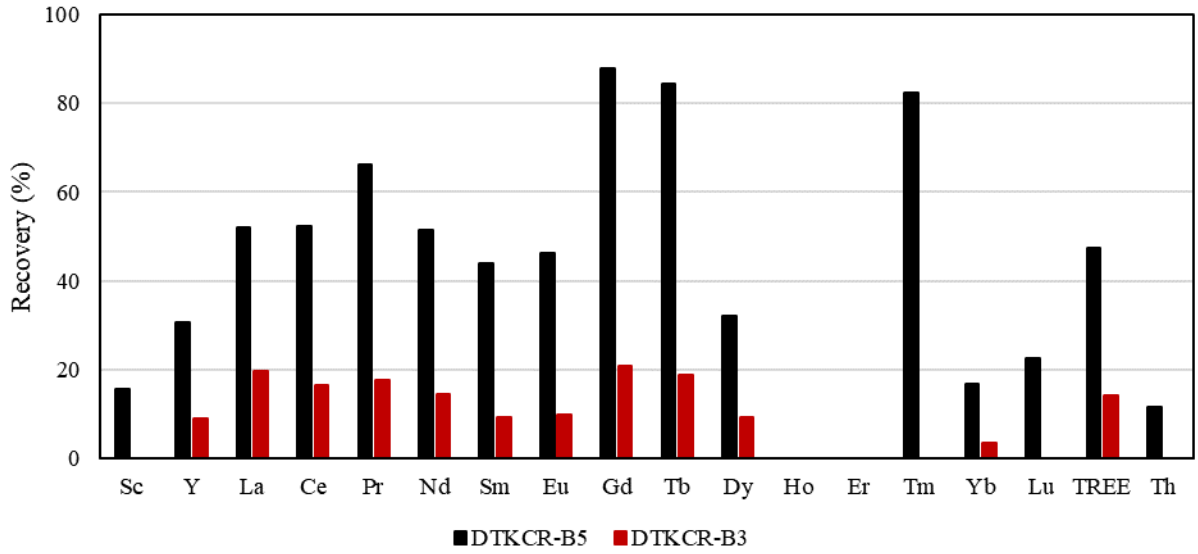

Figure 3.5.39. Individual RE recovery comparison between pH maintained at 2 (DTKCR-B5) and pH free drifted (DTKCR-B3) test with initial acid concentration of 0.01M.

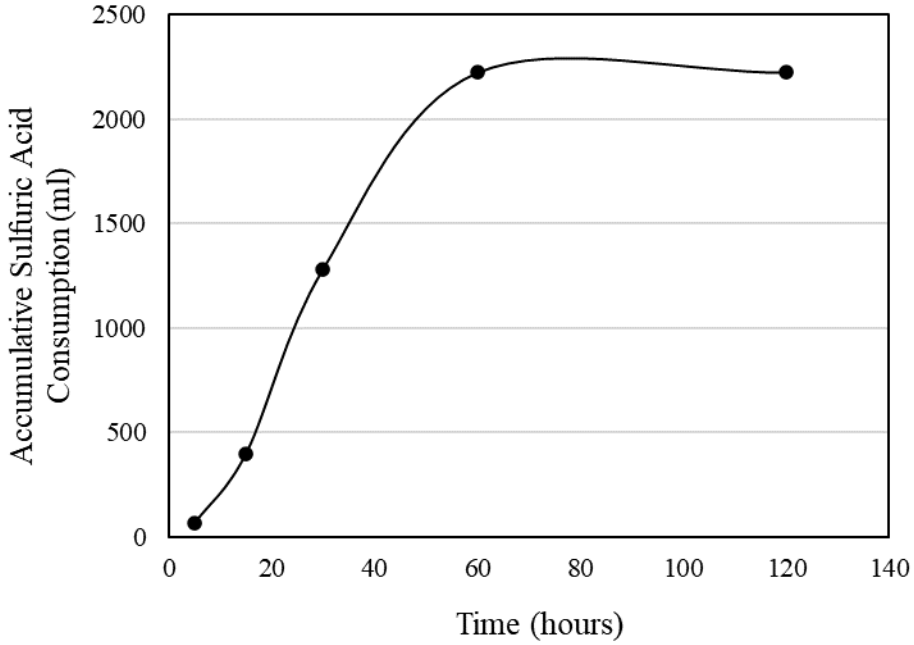

Figure 3.5.40. Accumulative acid consumption to maintain a pH of 2 for test DTKCR-B5.

3.5.6 Pilot Scale Solvent Extraction Circuit

The leachate generated from the roasted coal was treated by the continuous solvent extraction (SE) process to enrich the rare earths in the liquid phase for precipitation. This was achieved in two circuit configurations. The first circuit was called rougher circuit which aimed to recover maximum REEs in the liquid. The second circuit was called cleaner circuit which treated the product generated from rougher circuit to improve the quality. The rougher circuit consisted

of 10-mixer settler units of which 5 units were utilized at this stage of operation. The units were configured to have two loading stages, one scrubbing stage and two stripping stage.
Figure 3.5.41 shows a schematic of the rougher circuit. Aqueous feed after pre-treatment with ascorbic acid and pH adjustment was introduced to circuit at first loading stage. The feed volumetric flowrate was kept constant to a value of 1 L/min. The organic mixture containing DEHPA, TBP and Orfom in a proportion of 5, 10 and 15 percent v/v were introduced at the second loading stage. The purpose of loading was to extract rare earths to the organic phase. The DEHPA was the extractant in process, TBP was used as phase modifier and Orfom was used as the diluent to improve the flow properties of the organic extractant. The aqueous to organic volumetric flow ratio was kept to 1:1 during the course the operation. The organic from the loading stage containing extracted rare earth was sent to scrubbing unit to remove entrained impurities whereas, tailings known as raffinate was sent to waste water circuit. Hydrochloric (HCL) acid of concentration 0.1 M was used as scrubbing agent. The scrub spent was then sent back to reduction tank after treatment from the coalescer. Organic solution after scrubbing was sent to the stripping units for recovering the extracted rare earth back to the aqueous phase. Stripping was performed using 6 M HCl. The stripped bleed was sent to cleaner circuit for further treatment. The stripped organic was then recirculated back to the organic tank to be used again in the circuit. Apart from the above-mentioned unit, the circuit also consisted of raffinate coalescer. The purpose of the coalescer was to capture organics entrained in the aqueous phase from the raffinate.

The rougher circuit was operated continuously in synchronous with the leaching circuit for 8 hours every day from January 2019. The performance of the circuit was monitored by collecting the samples of the feed, raffinate, scrub bleed and strip bleed. The sample were collected at every two hour during the early stage of operation. The collected samples were then analyzed for the rare earth element concentration content using ICP-OES. After initial few days of operation of the circuit it was observed that the total rare earth (TREE) concentration in the raffinate of the rougher circuit was greater than 4 ppm. This number is significantly higher when compared to feed which had TREE concentration of 10.69 ppm. Higher concertation in the raffinate indicate the poor performance of the circuit and loss of REE to waste stream. At first it was sought that the poor performance was because the circuit did not reach the equilibrium. However, continued loss of rare earths during a day of operation eliminated that doubt as a typical SE circuit should not take more than a day to reach equilibrium. Hence a scoping study on the leachate generated from plant was initiated to identify the cause for poor extraction of the rare earths. The study was performed to see the effect of two different parameters, pH and extractant dosage. Laboratory scale SE test were performed in conical flask and magnetic stirrer. 50 ml of leachate was mixed with organic using a magnetic stirrer for 30 min. After mixing the liquid were transferred to a separatory funnel where organic and aqueous phase were allowed to disengage.

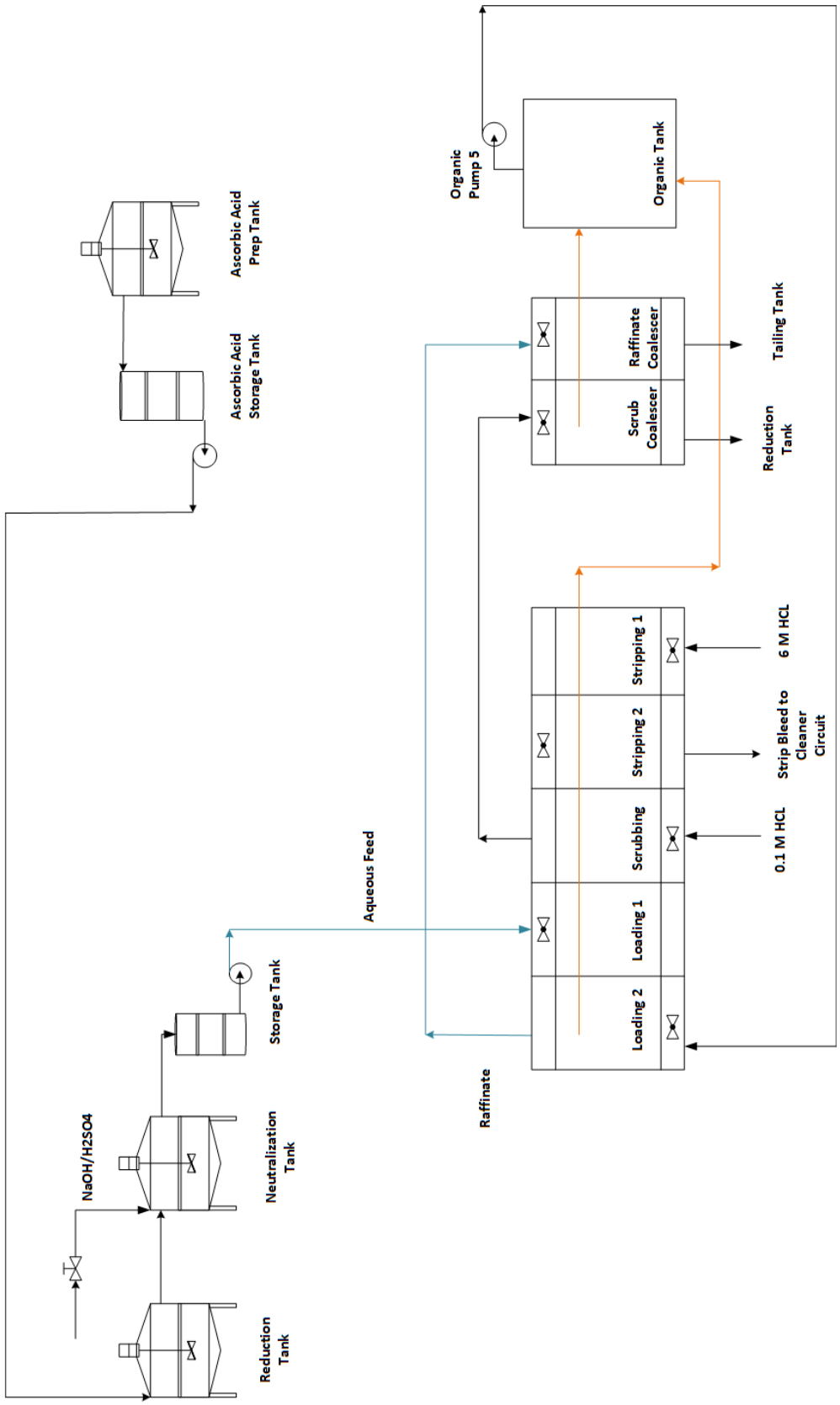

Figure 3.5.41. SE Rougher Circuit Flowsheet.

The aqueous was then collected and analyzed for the rare earth concentration. The amount of rare earth loaded in the organics was evaluated from the mass balance and percentage extraction of the experiment was calculated using the following equation:

$$\% \, E = \frac{([M^{3+}]_{Feed} - [M^{3+}]_{Raf}) * 100}{[M^{3+}]_{Feed}} \quad (1)$$

Where, $[M^{3+}]_{Feed}$, $[M^{3+}]_{Raf}$ are REEs in the feed and raffinate respectively. The experiment was repeated at different pH and extractant dosage. Figure 3.5.42 shows the different dosage and pH considered during the test.

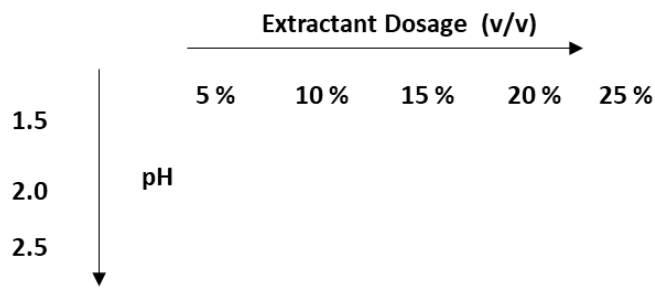

Figure 3.5.42. Parameters tested during scoping study.

i. *Effect of DEHPA Dosage and pH*

As shown in Figure 3.5.43, a typical feed and raffinate concentration of the samples collected during the early stage of operation of the circuit. It can be seen that the concentration of elements such as La, Ce, Pr, Nd and Gd in the raffinate accounts to almost 40% of the feed concentration indicating poor extraction. The results from extraction test conducted at pH 1.5, 2.0 and 2.5 are shown in Figure 3.5.44. It was found that increasing the pH of the extraction increased the percentage extraction significantly irrespective of extractant dosage. For the extractant dosage 5 % DEHPA v/v at which the rougher circuit was being operated the increase in percent extractant was about 20 percent with increase in pH. It was clear that to improve the performance of the circuit it should be operated at a pH of 2.5 which was previously operated at 1.5. However, increasing the pH more than 2.5 is not desirable as it results in localized precipitation of the contaminants and rare earths which may cause operational problem in SE circuit. Similarly, the study of the effect of extractant dosage showed that increasing the extractant dosage had a significant impact on the extraction. The maximum extraction of TREEs achieved was 65 % at DEHPA dosage of 20 and 25 % v/v at a pH of 2.5. Thus, it was decided to operate the circuit at DEHPA dosages of 25 % v/v. Despite of having same percent extraction at 20 % and 25 % of DEHPA dosage, the 25 % was preferred for circuit. The reason for higher dosage was the shape of the extraction curve which shows plateau at 25 % dosage indicating the equilibrium has been achieved which is not the case with 20 % DEHPA.

Figure 3.5.45 shows the extraction behavior for the major element in the feed at different pH when extracted with 25 % DEHPA. Plateau effect can be seen for all the elements except praseodymium (Pr).

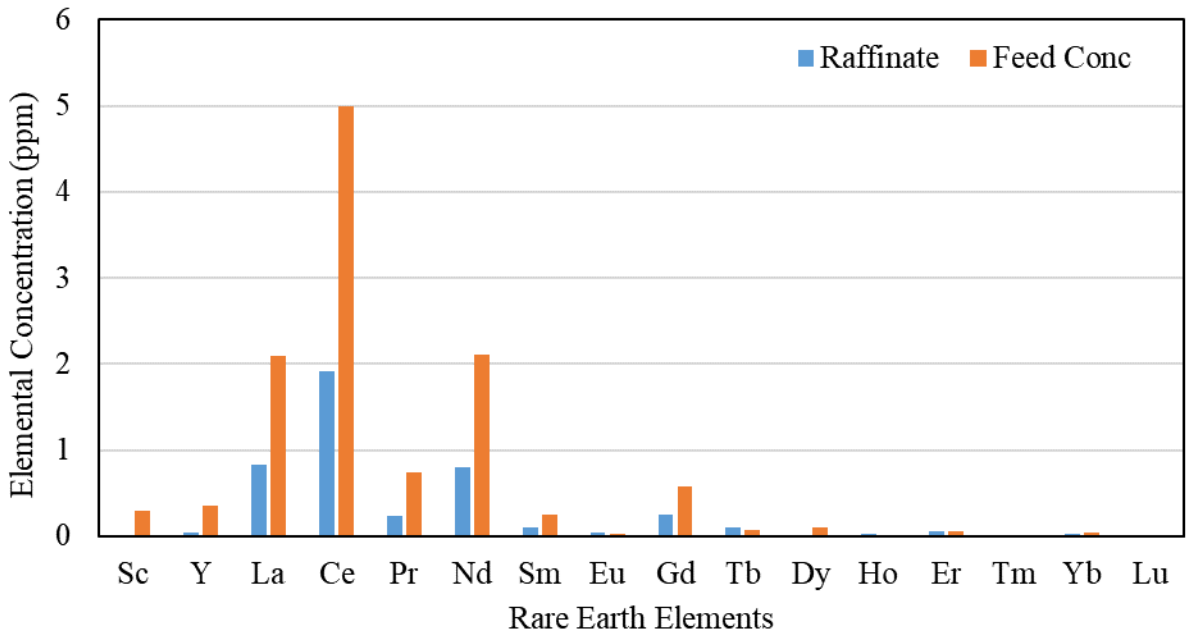

Figure 3.5.43. Typical Feed and Raffinate Concentration.

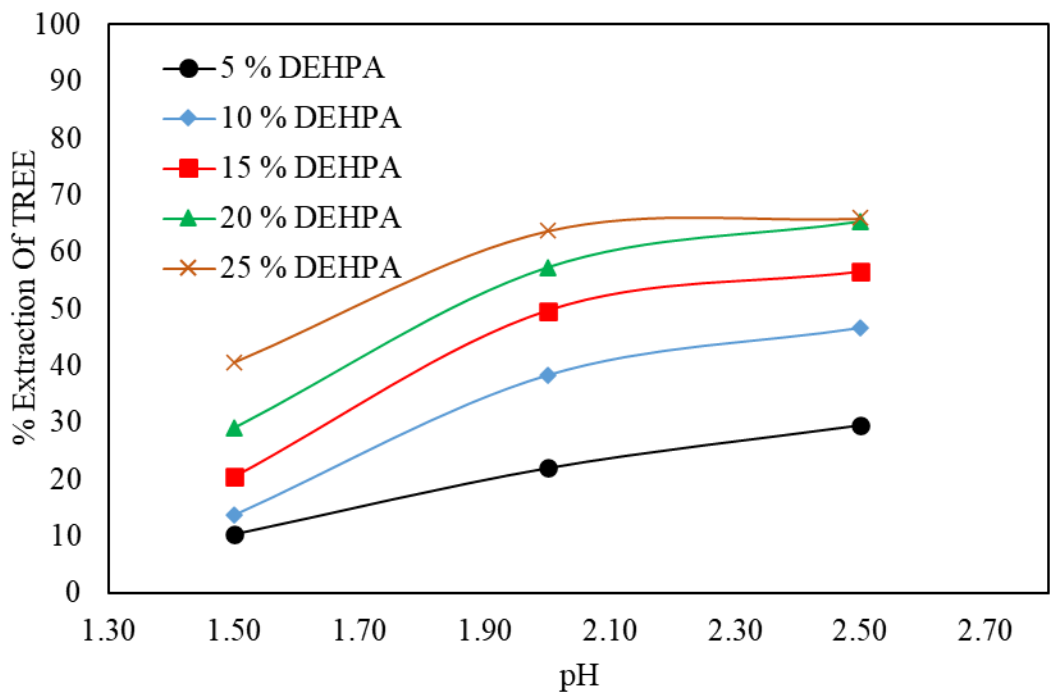

Figure 3.5.44. Result of scoping study.

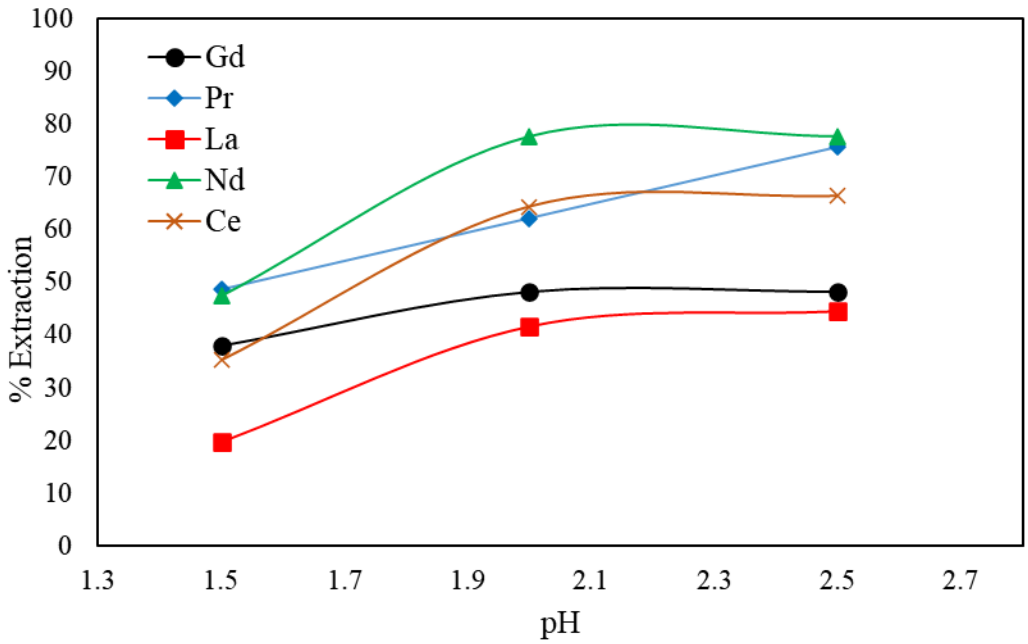

Figure 3.5.45. Percent extraction of individual REEs at DEHPA dosage of 25%.

ii. *Effect on TREEs Concentration:*

The changes in the circuit were then implemented. The set point for the feed pH was increased to 2.5. The extractant was added gradually at every 4 hour interval to increase the extractant content by 5 % till it reached to the value of 25 % v/v. It was observed that adding the extractant lead to the drop in the TREE concentration in the raffinate (Figure 3.5.46) while the concentration in feed was constant (Figure 3.5.47). A small rise at the end of the Figure 3.5.46 was observed. This was because of the buildup of TREEs in the organic. The strip bleed was reduced to the minimum value to allow the buildup of concentration of TREEs in the organic (Figure 3.5.48). The reason for building up the concentration was to produce a high concentration feed for the cleaner circuit. The concentration buildup process resulted in complete loading of the organic which had no further capacity to load any more rare earth causing increase in the raffinate. Loading rate was indirectly deduced by fitting a polynomial equation to the plot in Figure 3.5.48. A polynomial of order one reasonably explains the loading behavior. The equation obtained by fitting polynomial is given by:

$$y = -0.6995x^2 + 38.834x + 107.72 \quad (2)$$

Where y in above equation represent the change in concentration and x represent time in hours. Differentiating Eq (2) with time and equating it to zero will give the saturation time for the organic.

$$\frac{dy}{dt} = -1.399x + 38.834 = 0 \quad (3)$$

Solving for x using Eq (3) gives the value of 27.75 hours, which indicate that by 27 hours of operation the organic will be fully loaded and the loading system will reach equilibrium. The first difference in the TREEs concentration in the strip bleed (Figure 3.5.48) was also evaluated and plotted with hours of operation to estimate the rate of loading process from the measured data. Figure 3.5.49 shows the plot of loading rate evaluated from the data. The average value of loading rate was found to be 19.02 ppm/hr, if the negative values are omitted the average value comes out to be 27.35 ppm/hr which is close to the value obtained using Eq (3). After evaluating the loading rate, the strip bleed rate was increased and the bleed solution was collected and stored for further treatment in the cleaner circuit.

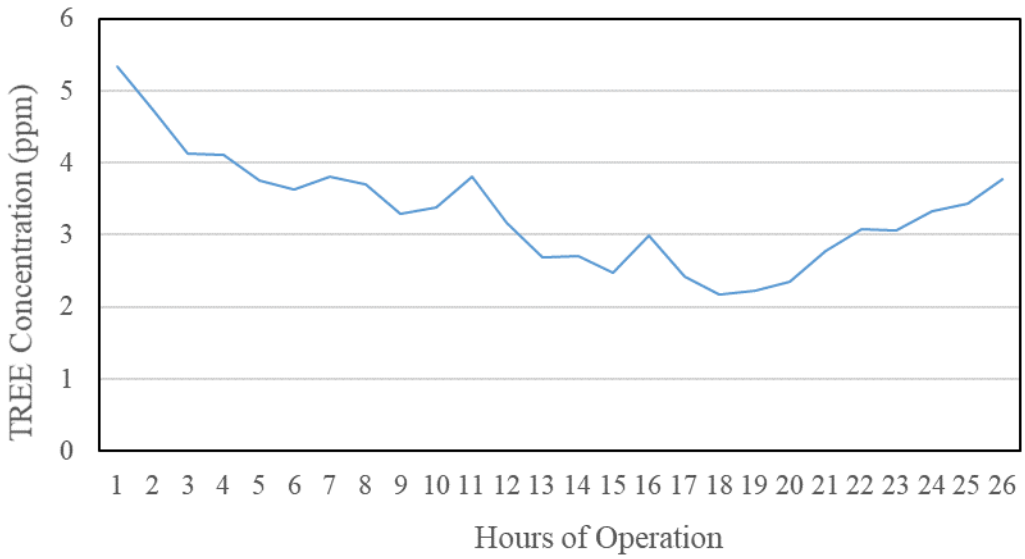

Figure 3.5.46. TREE in Raffinate.

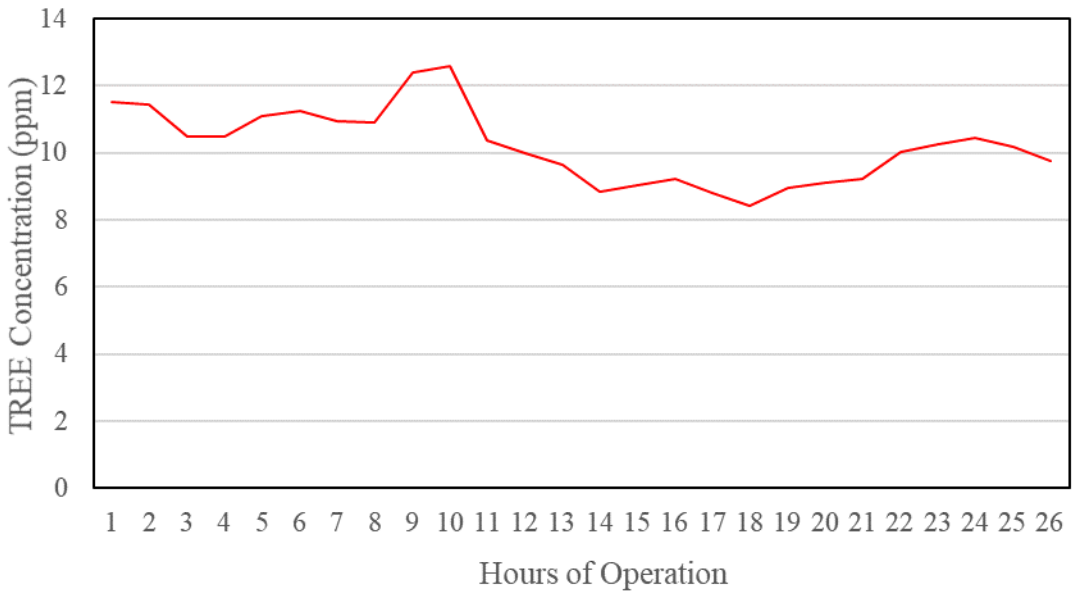

Figure 3.5.47. TREE in Feed.

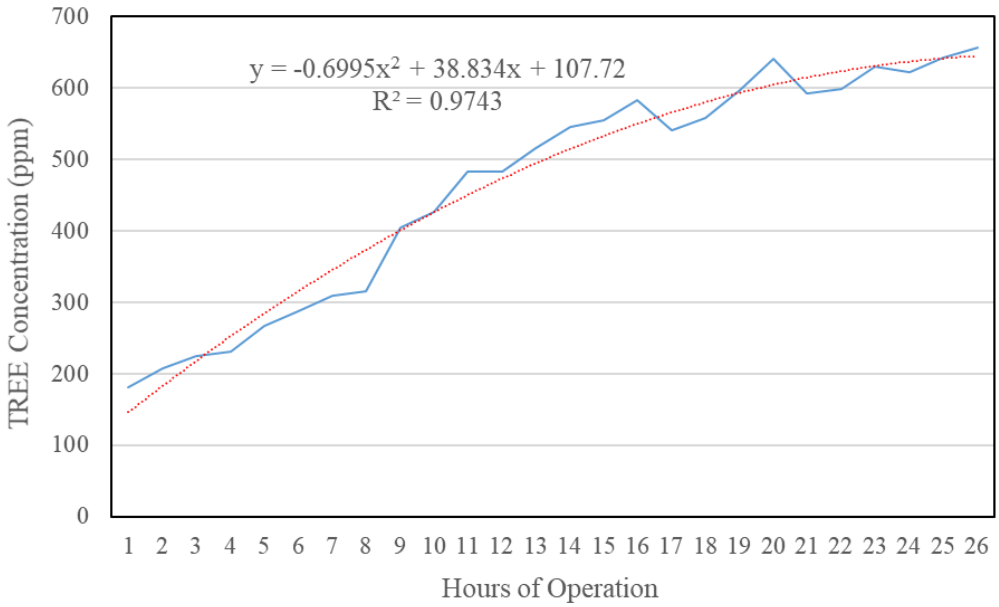

Figure 3.5.48. TREE in Strip Bleed.

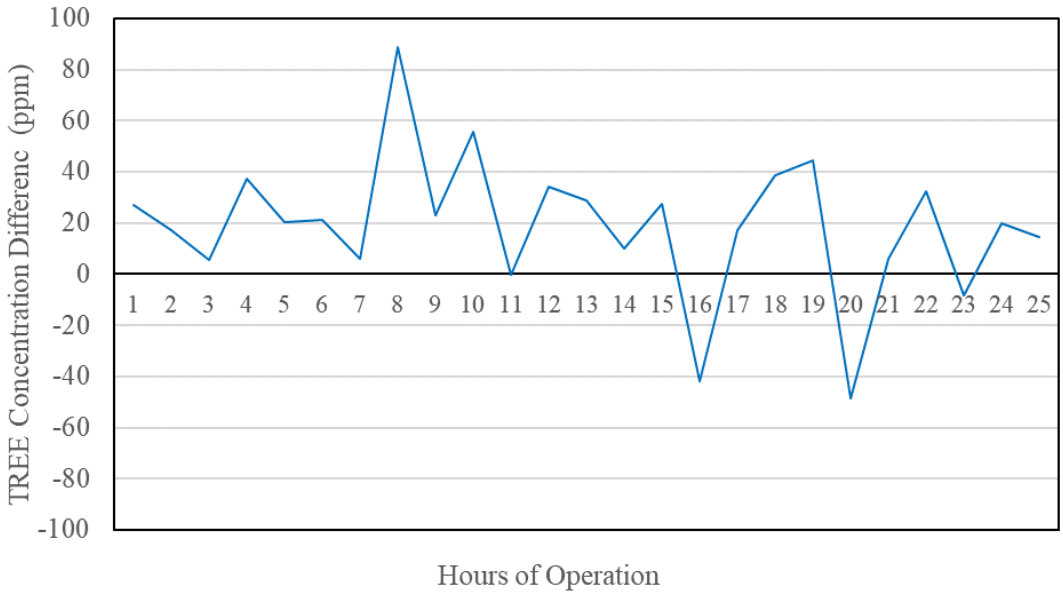

Figure 3.5.49. Loading Rate.

iii. <u>Effect on Contaminants:</u>

The concentration of few major contaminants which have extraction potential were also monitored. The major contaminants in feed consisted of Al, Fe, Mg and Ca. Figure 3.5.50 shows the contaminants concentration data in the feed measured with time. The average concentration for Al, Fe, Mg and Ca were 137.27, 138.72, 18.20 and 25.78 ppm respectively. The raffinate data collected at the same time instance confirmed that the contaminants were not extracted to the organic phase during the extraction process. Figure 3.5.51 shows the concentration of

contaminants in the raffinate. The correlation coefficient between feed and raffinate concentration was also evaluated to verify the fact. Table 3.5.15 shows the correlation coefficient value which indicates strong correlation between feed and raffinate concertation of major contaminants. This imply that the concentration of contaminants in the feed and raffinate follow the same behavior.

Table 3.5.15. Correlation between Feed and Raffinate Concentration.

Element	Al	Ca	Fe	Mg
Correlation between Feed-Raffinate concentration	0.87	0.69	0.90	0.91

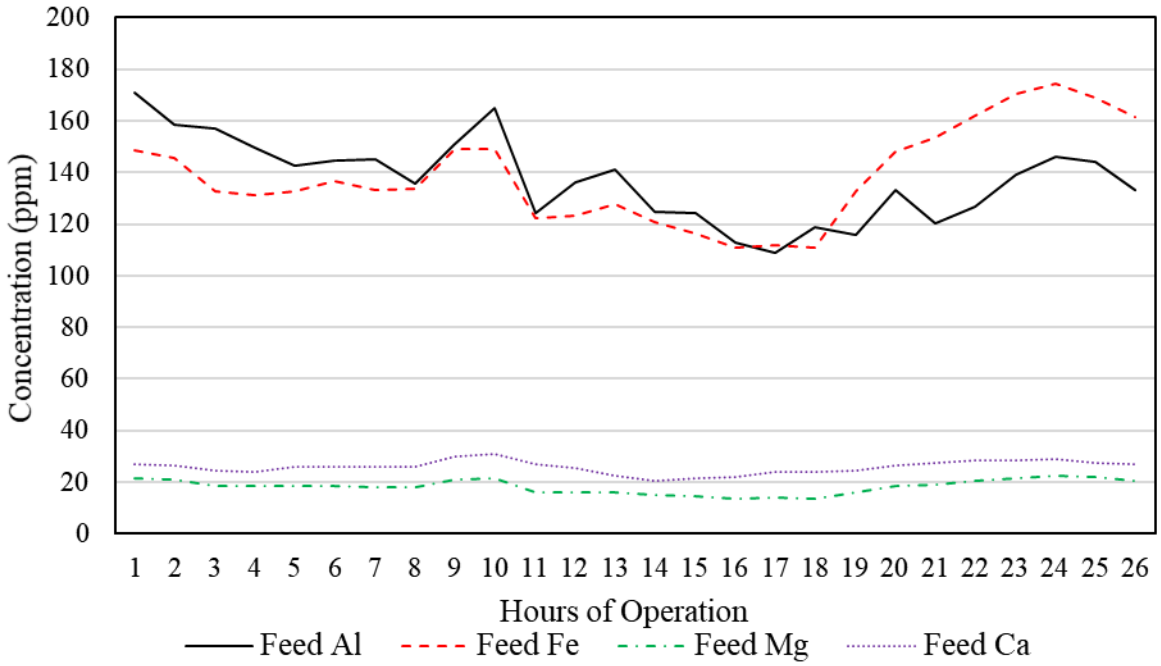

Figure 3.5.50. Contaminants Concentration in Feed (ppm).

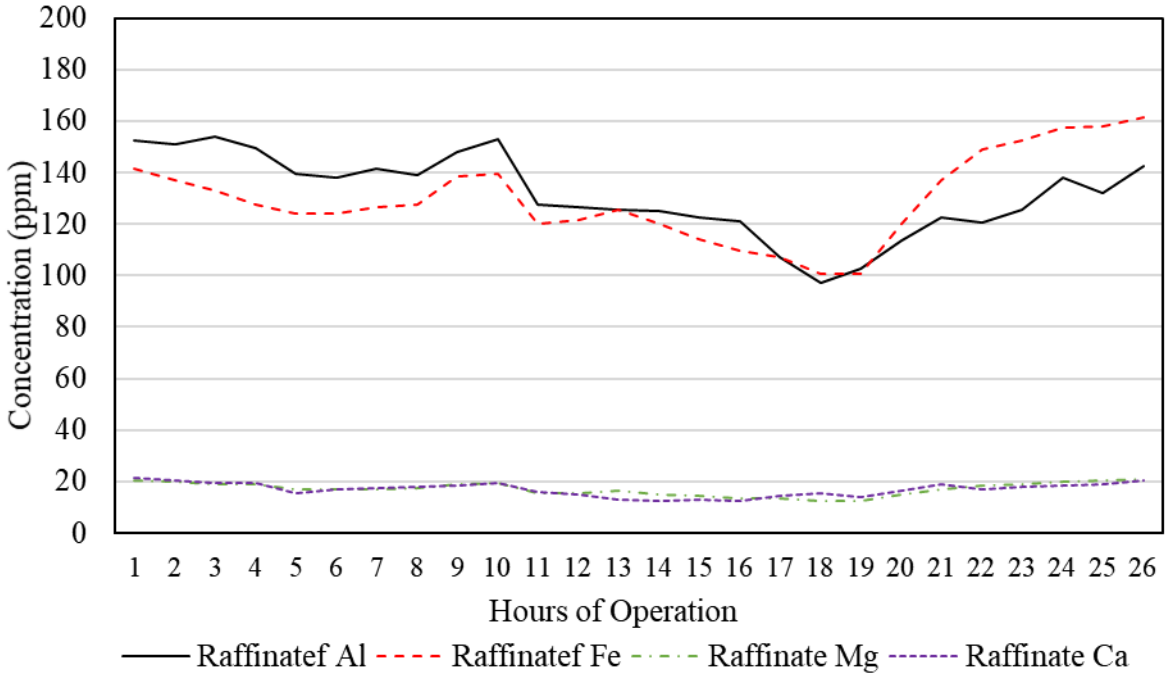

Figure 3.5.51. Contaminants Concentration in Raffinate (ppm).

Summary of Solvent Extraction Trial Test Findings:

1. The extracting efficiency increased with the increase in pH and extractant dosage.
2. Scoping study indicated the maximum percent extraction that can be achieved was 65.93 percent at pH 2.5 and 25 % v/v DEHPA. Increasing pH or extractant dosage any further could cause operational problem such as localized precipitation and viscosity of the organic hence was not pursued at this stage.
3. More study on creating the distribution isotherm is required to identify the number of stages required for loading so that percent extraction of more than 90 percent could be achieved.
4. It took 27 hours of operation to build up the rare earth concentration greater than 600 ppm in the stripping solution at 25 % v/v DEHPA dosage. Hence, detailed process modeling is required to understand the time behavior of the circuit at different feed and extractant condition to aid in the operation in future.
5. Parametric study of the SE system at different aqueous, organic and stripping agent flowrate is required to optimize the circuit for maximum extraction.
6. The recovery of contaminants was very low particularly Fe and Al which was expected as the ascorbic acid was added to suppress their extraction.

3.5.7 Selective precipitation

3.5.7.1 Laboratory Precipitation Tests

A leachate was generated in the plant by leaching the calcination product of the West Kentucky No. 13 coarse refuse. The solid material of 25 kg was put into 250 liters of water which has an initial pH of 2.0. Temperature of the system was maintained at 75℃ and the reaction was continued for 2 hours. Finally, a leachate was obtained by filtering the slurry. Sequential precipitation tests were performed in lab using a simple apparatus consisting of a pH meter, a magnetic stirrer, and a 1-liter glass beaker (see Figure 3.5.52).

Sodium hydroxide of 1M concentration was added into the solution to gradually increase the solution pH. For each addition, solely 0.1 ml of the base was added to ensure sufficient dispersion was achieved. When the solution pH reached a certain value, two suspension samples of 15 ml and 9.5 ml were collected into two 15ml centrifuge tubes respectively. Concentrated nitric acid of 0.5 ml was added into the tube which contained the 9.5 ml suspension. The 15 ml suspension was centrifuged at 3,000 rpm for 10 min and 9.5 ml supernatant was collected into another tube together with 0.5 ml nitric acid. The purpose of adding nitric acid is to acidify the suspension and re-dissolve the precipitate. Elemental concentration of the acidified solution was analyzed using ICP-OES. Recovery (R) of an element i in the leachate to precipitate was calculate using the following equation:

$$R_i\% = \frac{C_{9.5,i} - C_{15,i}}{C_{9.5,i}} \times 100$$

where $C_{9.5,i}$ and $C_{15,i}$ means elemental concentration of i in the non-centrifuged and centrifuged samples, respectively. By collecting representative samples at different pH, recovery of both the REEs and major elements was plotted as a function of pH and/or molar concentration of the 1M NaOH added.

Figure 3.5.52. Experimental apparatus used for the precipitation tests.

Elemental composition of the leachate obtained using an initial pH of 2.0 and without control of the pH during the leaching process is shown in Table 3.5.16. The leachate contained 2.35 ppm of total REEs and the major contaminant is Fe (181 ppm) and Ca (307 ppm). Al concentration in the leachate is solely 2.89 ppm, which is much lower than the leachate obtained by maintaining the slurry pH at 2.0 or smaller values (e.g., 0). As such, to obtain a high-grade rare earth product, the major task is to separate the REEs from Fe and Ca in the filtrate. Furthermore, the REE concentration in the leachate is too low to economically remove the containments and obtain a concentrated REE solution. The total operational and capital costs of using the existing solvent extraction system to produce 1 kilogram of a rare earth product were plotted as a function of REE concentration in the leachate. The results are shown in Figure 3.5.53. The cost is extremely high (more than 300 $/kg) to treat the filtrate which solely contained 2.89 ppm of REEs even without using reduction. The economic analysis also indicated that if the cost needs to be reduced to an acceptable level such as 50 $/kg, REE concentration in the solution fed to the solvent extraction circuit should be higher than 700 ppm without using the reduction step.

The staged precipitation process developed at University of Kentucky (Zhang and Honaker, 2018) is able to generate a rare earth pre-concentrate which contained several thousand ppm of REEs. In the staged precipitation process, the majority of iron and aluminum are precipitated out when the leachate pH is elevated to around 5, under which condition most of the rare earth cations stay in the solution. When the pH is further increased to 8, more than 90% of REEs are precipitated, which enables the collection of a REE pre-concentrate. Most of the other contaminants such as calcium and magnesium are left in the solution. Several advantages of the staged precipitation process have been proposed including: (1) most of the elements such as iron which are difficult to be handled in the downstreaming purification processes have been removed; and (2) the acidic leachate has to be neutralized for discharging, which means the cost associating with the pH elevation step can be consider as zero.

Table 3.5.16. REE and major elements concentrations in the leachate generated using an initial pH of 2.0.

Element	***TREE***	***HREE***	***LREE***	***Sc***	***Y***	***La***	***Ce***	***Pr***	***Nd***	***Sm***
Conc.	2.35	0.30	2.05	0.005	0.12	0.53	0.97	0.13	0.37	0.05
Element	***Eu***	***Gd***	***Tb***	***Dy***	***Ho***	***Er***	***Tm***	***Yb***	***Lu***	***Al***
Conc.	0.01	0.1	0.01	0.04	0.002	0.005	bld	0.008	bld	2.89
Element	***Fe***	***K***	***Ca***	***Mn***	***Li***	***Mg***	***Na***	***Ni***	***Sr***	
Conc.	181	82	307	14.3	2.96	0.26	0.36	0.13	9.31	

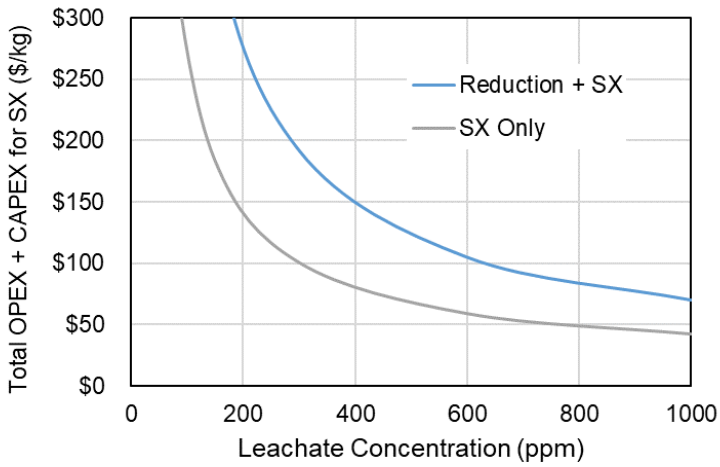

Figure 3.5.53. Sum of operational and capital costs of using the current solvent extraction system to produce a rare earth product as a function of total REE concentration in the leachate.

Recoveries of total REEs, Fe, Al, and some individual REEs as a function of pH are shown in Figure 3.5.54. When the solution pH was gradually increased, Al was firstly precipitated with more than 80% being removed when the pH was elevated to 5.5. However, for this leachate, the Al precipitate was not separated from the solution prior to the REE precipitation since its concentration is very low. When the solution pH was further increased to about 7, 90% of REEs were precipitated together with 42% of iron. Previous studies showed that iron cations existing in acid mine drainage e were completely removed when pH was increased to 4. The reason for the difference is that most of the iron cations in the filtrate exist as ferrous ions (Fe^{2+}) which has a higher precipitation point than ferric ions (Fe^{3+}). The valence states of iron cations in solution can be discerned from the color of the solutions. As shown in Figure 3.5.55, when hydrogen peroxide was added into the filtrate, its color was changed from transparent to reddish, which indicates the transformation of ferrous to ferric ions (Fe^{2+} to Fe^{3+}). Figure 3.5.54 shows that HREEs such as Y and Nd were more readily precipitated relative to LREEs such as Ce. For example, about 64% of Ce was precipitated at pH 6.45, while more than 75% of Y was precipitated under the same pH.

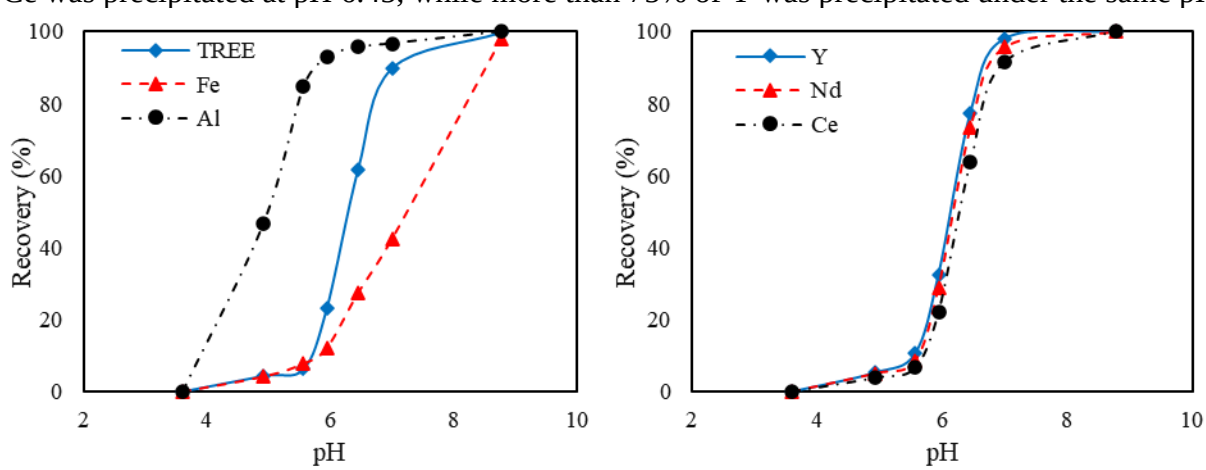

Figure 3.5.54. Recovery of total REEs, Fe, Al and some individual REEs to the precipitate as a function of solution pH.

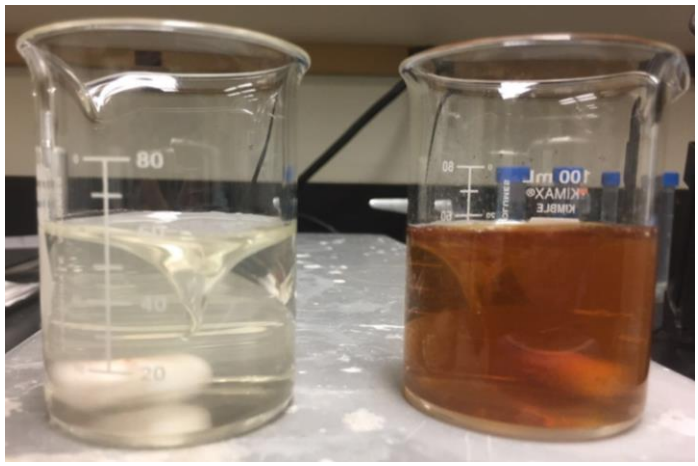

Figure 3.5.55. Pictures of the original filtrate (left) and the filtrate with some hydrogen peroxide added (right).

Preliminary economic analysis was performed on the filtrate which contained 2.35 ppm of REEs. As shown in Figure 3.5.56, NaOH cost to produce a certain amount of precipitate which contains 1 kg of REO gradually reduces with the increase in solution pH. The most economical pH locates in the range of 6-8, which agrees with the fact that most of the REEs are precipitate in this range. For the filtrate containing 2.35 ppm of REEs, the minimum alkaline cost is about 45 $/kg of REO, which occurred at pH around 7. A filtrate containing relatively high REEs (4.57 ppm) was obtained by leaching another roasted sample under the same conditions. As shown in Figure 3.5.56, the minimum alkaline cost occurred in the range of 6-7, which is similar to the former liquid. However, due to the higher REE concentration, the minimum cost value is solely about 18 $/kg of REO. This indicated that the chemical cost for recovering REEs from coal coarse refuse can be reduced using a mild leaching condition, under which the contaminants are less likely leached relative to the REEs.

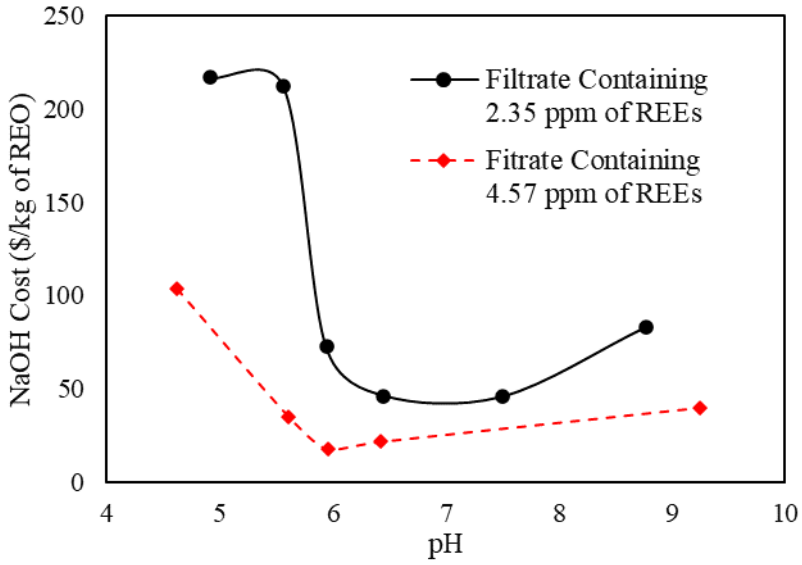

Figure 3.5.56. Sodium hydroxide costs to produce 1 kilogram of rare earth oxide by increasing the solution pH to different values.

3.5.7.2 Scaling-up of the Precipitation Tests

The laboratory precipitation test results showed that REE pre-concentrates are able to be obtained using the staged precipitation process. The chemical cost is in an acceptable level. As such, larger scale precipitation tests were performed in the plant using a 100-gallon tank. A mixer is mounted on the top of the tank and its rotation speed is controlled using a VFD (variable-frequency drive). Several baffles are installed on the inside wall of the tank to create enough mixing.

A comparison was made between the laboratory test results and the results obtained using the 100-gallon tank with a mixing speed of 37 Hz. In the tank precipitation test, 250 liters of the same filtrate as the laboratory test were added into the tank. It is difficult to get a stable reading of the solution pH, and thus the recovery was plotted as a function of the amount of sodium hydroxide that added into the system. As shown in Figure 3.5.57, the recovery of REEs is lower than the laboratory test. For example, when the dosage of NaOH reached 4.6 mM, solely 54% of REEs were precipitated which is much lower than the laboratory test (about 95%). The recovery of iron was also reduced compared with the laboratory test results.

Ferrous hydroxide ($Fe(OH)_2$) has a dark green color which is different from ferric hydroxide ($Fe(OH)_3$). During the tank precipitation test, it was observed that the suspension had a light brown color which is different from the laboratory test. This phenomenon indicated that ferric hydroxide was generated during the tank leaching process. One ferric cation combines with three hydroxyl groups which is more than ferrous ions. As such, when same amount of alkaline was added into the leachate, less REEs and iron were precipitated from the tank test relative to the laboratory test. The different states of iron in the 100-gallon tank and 1-liter beaker were caused by difference strengths of mixing. Due to the fact that the 100-gallon tank was designed to achieve sufficient mixing of leaching slurries, as indicated by the baffles that installed on the inner wall, a significant amount of air was entrapped into the solution. Many bubbles of various sizes were observed in the solution. Oxygen in the air accelerated the following reactions:

$$Fe^{2+} \rightarrow Fe^{3+}$$
$$4Fe(OH)_{2s} + O_2 + 2H_2O \rightarrow 4Fe(OH)_{3s}$$

Valence of iron was changed from 2+ to 3+ in both reactions.

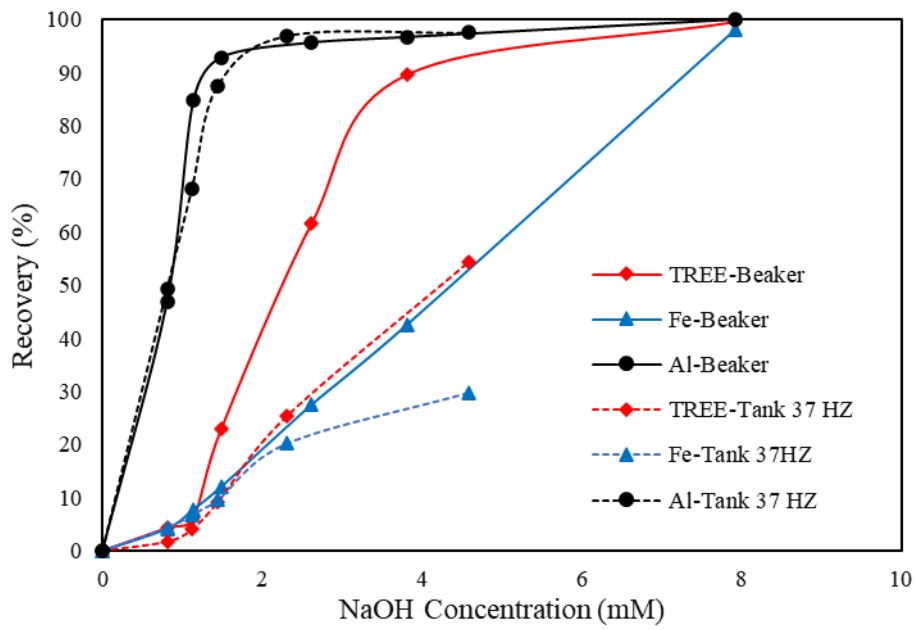

Figure 3.5.57. A comparison of the laboratory test results and the results obtained using a 100-gallon tank with a mixing speed of 37 Hz.

Based on the above discussion, it is critical to reduce the amount of oxygen that interacts with the solution when precipitation test is performed in the 100-gallon tank. As such, another test was performed using a lower mixing speed (10 Hz). The same amount of alkaline was also added within a shorter period of time relative to the laboratory test. A comparison of the laboratory test results and the results obtained using the 100-gallon tank with a mixing speed of 10 Hz is shown in Figure 3.5.58. By adding the same amount of sodium hydroxide, the recoveries of Al, REEs, and Fe in the tank precipitation test were similar to the laboratory scale test. Since the mixing speed is low (10 Hz), no air bubbles were observed in the solution indicating that the dissolution of oxygen solely occurred on the surface of the solution. As such, mixing is critical for pilot scale testing of the staged precipitation process.

Another evidence which shows the importance of mixing is presented in Figure 3.5.59. The tank precipitation test was performed using a mixing speed of 20 Hz and 3.49 mM alkaline were added all at once instead of in several batches. Recoveries of Al, REEs, and Fe were similar to the laboratory test results. When the precipitate was allowed to settle for 30 min, the REE recovery was increased while Fe recovery was decreased slightly. This is due to that the alkaline was not dispersed thoroughly since it was added all at once. The localized precipitates of iron were re-dissolved during the settlement, which resulted in the precipitation of REEs.

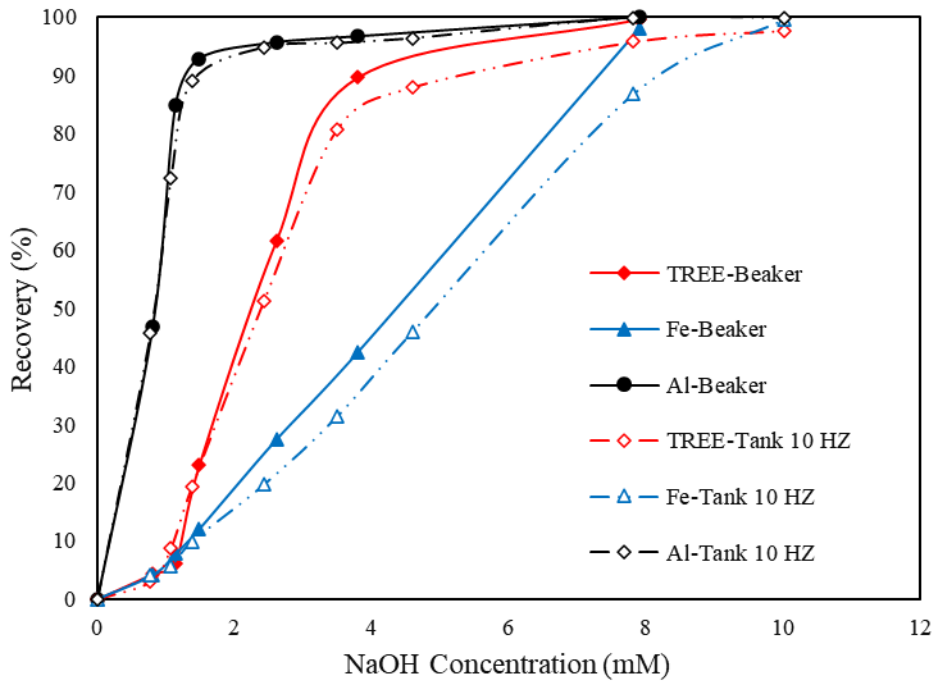

Figure 3.5.58. A comparison of the laboratory test results and the results obtained using a 100-gallon tank with a mixing speed of 10 Hz.

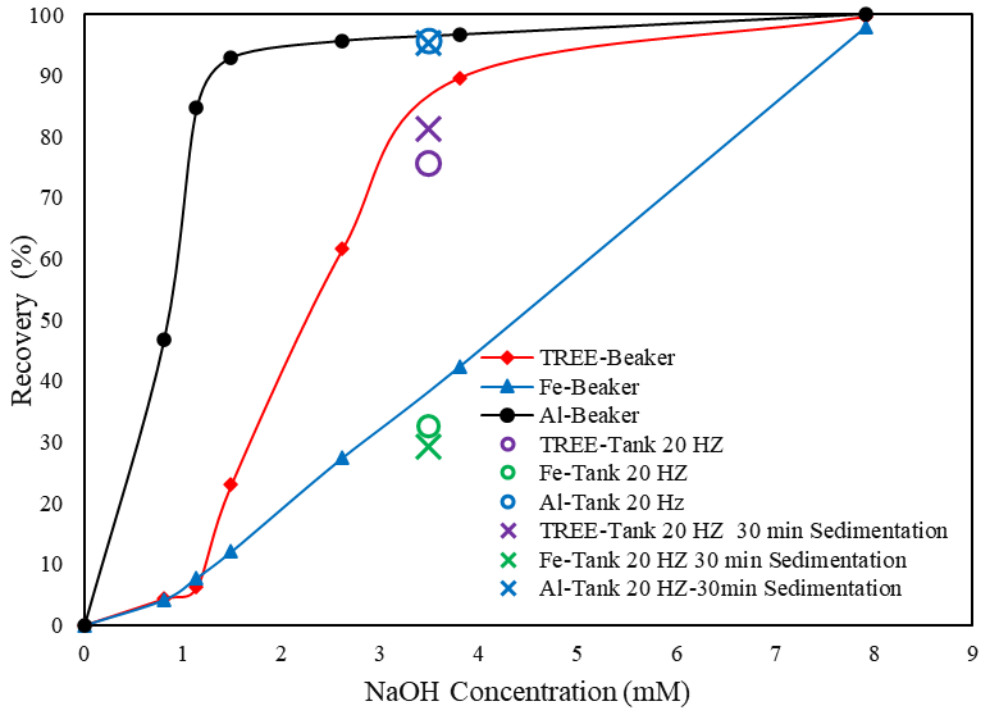

Figure 3.5.59. A comparison of the laboratory test results and the results obtained using a 100-gallon tank with a mixing speed of 20 Hz.

3.5.7.3 Re-dissolution of the REE Precipitate

A rare earth pre-concentrate was generated by using the staged precipitation process. Despite that most of the contaminants stayed in the solution, the REE content in the precipitate is still much lower than commercial products (e.g., REO>90%). This is due to that the containment concentration in the solution is much higher than the REEs. In the pilot-scale process, the pre-concentrate will be filtered using a plate and frame filter. The filter cake will be dissolved by adding hydrochloric or nitric acid. To predict the REE concentration in the re-dissolved solution, lab scale filtration and re-dissolution tests were performed using a vacuum filter and a digestion tube. Specifically, a rare earth precipitate was obtained by adding 1M sodium hydroxide solution into 250 liters of filtrate, after which the precipitate was settled for 30 min and a pre-condensed slurry of the REE precipitate was collected into a 5 gallon bucket. The slurry was settled for 2 hours and the supernatant was decanted. Finally, a condensed slurry of about 7 liters was obtained and used for the following experimental tests.

The REE concentrated slurry of 1 liter was filtered using a vacuum filter and a filter paper of 0.45μm pore size. The vacuum filtration was stopped when no continuous flow of water was observed at the bottom of the filtration funnel. Precipitate of 5 grams were representatively collected from the filter cake and transferred into a 50 ml digestion tubes, which are shown in Figure 3.5.60. A total number of four tests were performed and the detailed parameters are as shown in Table 3.5.17.

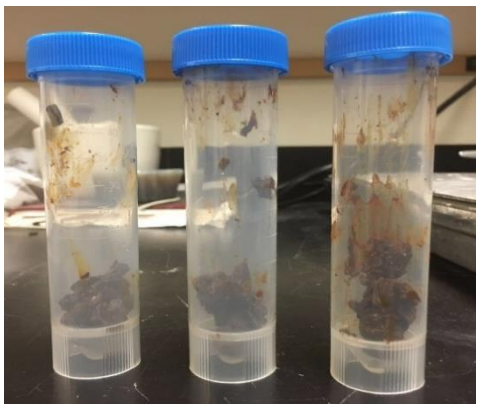

Figure 3.5.60. Re-dissolution of the precipitate in 50 ml digestion tubes.

Table 3.5.17. Experimental parameters for the re-dissolution tests.

Test Code	Precipitate (g)	HCl (ml)	H_2O (ml)	Reaction Time(min)	Final pH
RD-1	5	1	0	300	0.63
RD-2	5	0.75	0.25	300	1.42
RD-3	5	0.5	0.5	300	1.60
RD-4	5	0.25	0.75	300	1.83

REE concentration in the re-dissolved solution is shown in Table 3.5.18. The highest TREE concentration of 675 ppm was obtained by dissolving 5 gram of the precipitation using 0.5 ml HCl and 0.5 ml deionized water (RE-3). REE concentrate in the filtrate that used to produce the precipitate is solely 2.35 ppm. When a filtration containing more REEs (e.g., 5 ppm) is used for the test, a re-dissolved solution containing more than 1,000 ppm will be obtained. Based on the economic viability analysis, cost of the subsequent solvent extraction process will be less than 50 $/kg of REO. The overall cost of the flowsheet will be in an acceptable level. The dominant contaminant is iron which had a concentration over 30,000 ppm. Solvent extraction will be able to remove the contaminants and generate a relatively pure REE concentrated solution.

Table 3.5.18. Major element concentration in the solution obtained by re-dissolving the precipitate.

Tests	TREE	HREE	LREE	Al	Ca	Fe	K	Mg	Mn	Zn
RD-1	588	83	506	1,505	386	34,504	102	25	47	25
RD-2	627	88	539	1,605	395	36,194	98	26	49	26
RD-3	675	95	580	1,661	403	37,000	104	27	50	28
RD-4	641	90	550	1,534	400	34,648	102	26	48	26

3.5.7.4 Dissolution Characteristics of Perlite

As mentioned previously, REE precipitate needs to be filtered to obtain a filter cake. However, perlite needs to be added for filtration using a plate and frame filter, which forms a penetrative layer around the filter membranes and prevents them from being blocked. As such, the filter cake of REE precipitate will mingle with some perlite. The perlite will also be placed in an acidic environment together with the precipitate for the redissolution purpose. As such, leaching characteristics of perlite under acidic conditions were characterized to check whether significant amounts of contaminants were dissolved. Perlite of 1 gram was dispersed in 50 ml of deionized water and the slurry pH was reduced to a predetermined value using hydrochloric acid. Three leaching pH values were selected, i.e., 1.0, 1.5 and 2.0. As shown in Figure 3.5.61, major elements in the leachate were Al and Ca which has very low concentrations relative to the re-dissolved solution of the REE pre-concentrate. As such, dissolution of perlite will be negligible.

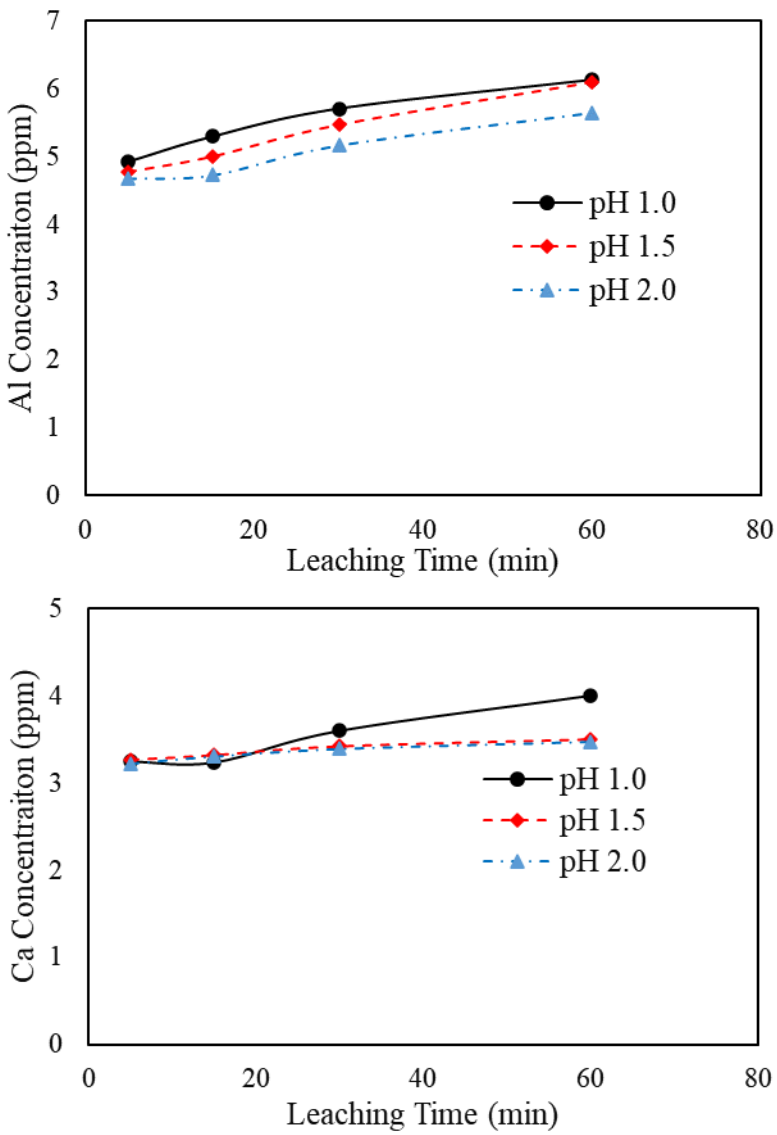

Figure 3.5.61. Concentrations of major elements (Al and Ca) in leachate obtained by leaching perlite under different solution pH values.

3.5.8 Pilot Scale Leaching and Multi-stage Precipitation Circuit Testing

Based on the information collected from the pilot plant trial run, a modified hydrometallurgical circuit was proposed and redesigned to replace solvent extraction circuit with multiple stage selective precipitation. A pilot scale continuous test run was carried out using the modified flowsheet.

The test was conducted using the west Kentucky No. 13 coarse refuse material. The material was processed through the X-ray sorter to achieve the light density fraction (S.G. 2.0 float) which contains elevated total REE concentration. The sorted material was crushed using a jaw crusher and passed through a hammer mill to achieve a top particle size of 1 mm. It was then

screened at 1 mm using a Sweco vibrating screen to eliminate oversize bypass. The material was roasted and feed into the hydrometallurgical circuit to produce a refined rare earths oxide product.

3.5.8.1 Acid leaching

The benefit provided by roasting the material was to allow REEs extraction at lower acidity during acid leaching reaction. A previous study showed that, within 2 hours, the TREE leaching recovery achieved by using 0.001M, 0.01M, 0.1M, and 1M sulfuric acid were 5%, 26%, 38%, and 60%, respectively. As shown in Figure 3.5.62, the optimal condition occurs between 0.01M and 0.1M sulfuric acid leaching. Therefore, 0.05M of sulfuric acid concentration was selected to conduct a continuous leaching test on the roasted material. The leaching recovery of individual REEs under this condition is shown in Figure 3.5.63. The recovery values represent an average of 10 sample analyses from samples collected over 20 hours of operation time and the error bars represent the standard deviation.

.

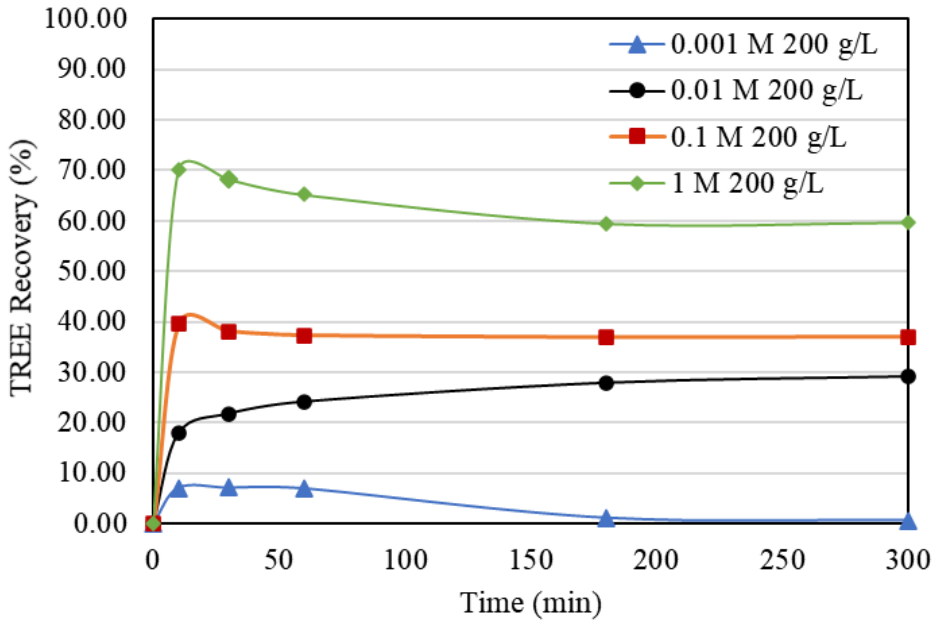

Figure 3.5.62. Effect of acid concentration on TREE leaching recovery at 75°C (bench scale).

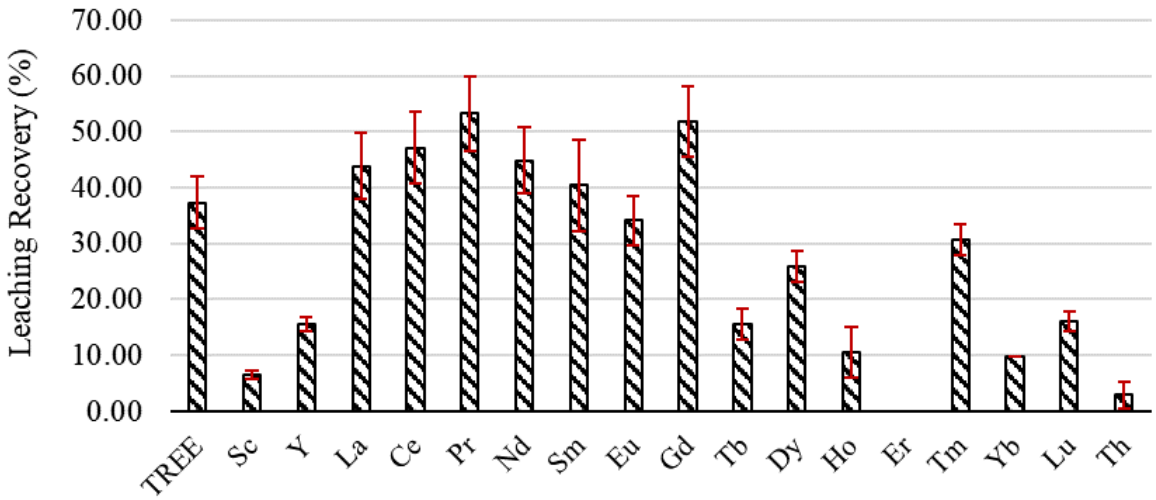

Figure 3.5.63. Leaching recovery of TREE and individual elements in leaching stage using 0.05M sulfuric acid at 75 °C with solid/liquid ratio of 1/10 (w/v) (pilot scale). (Retention time 2 hours)

3.5.8.2 REEs Precipitation

The TREE content in the pregnant leachate solution (PLS) generated from leaching West Kentucky No. 13 coarse refuse averaged 12 ppm and the contaminant ion concentrations were 348 ppm Al, 485 ppm Ca, and 717 ppm Fe. To efficiently selectively concentrate the REEs and produce high purity mixed REE product, the ratio of contaminants to REE concentration in the PLS was reduced by multistage precipitation and selective redissolution. A beaker level test was conducted using a representative leachate solution of 1 L to determine the pH for REE precipitation. As shown in Figure 3.5.64, over 99% of the REEs precipitated at pH 6.5 as well as the Al and Fe while nearly 100% of the calcium remained in solution.

The pH value of the fresh PLS filtered from the slurry produced by the acid leaching circuit averaged 2.54±0.18. The leachate was then pumped into a neutralization tank (Tank 4) at a flow rate of 1 gpm. An online pH control system in the tank was automatically regulated to a value of 6.5. The slurry carrying the precipitates overflowed into a surge tank was subsequently pumped into another plate and frame filter (Filter B). A sample of the leachate feed to Tank 4 and the filtrate from Filter B were collected every two hours to evaluate the precipitation efficiency and stability of the continuous process. The average precipitation efficiency of the individual REEs is plotted as shown in Figure 3.5.65 with error bars that represent the variation among the 10 samples collected over a 20 hour operating period.

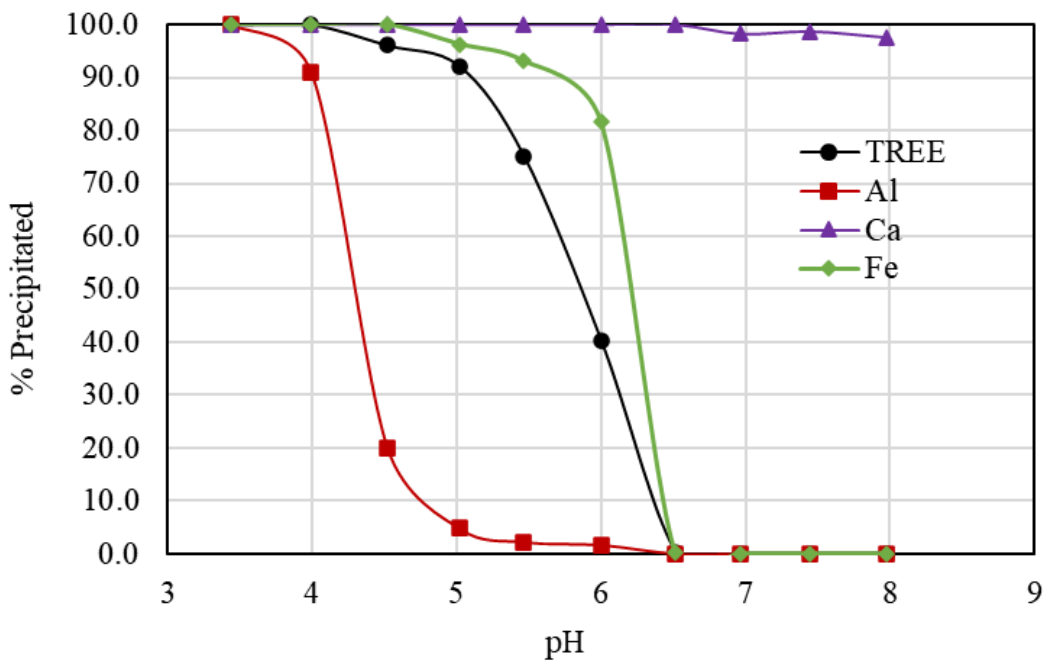

Figure 3.5.64. Precipitation efficiency of TREEs and major contaminants in the leachate solution using 1M NaOH (bench scale).

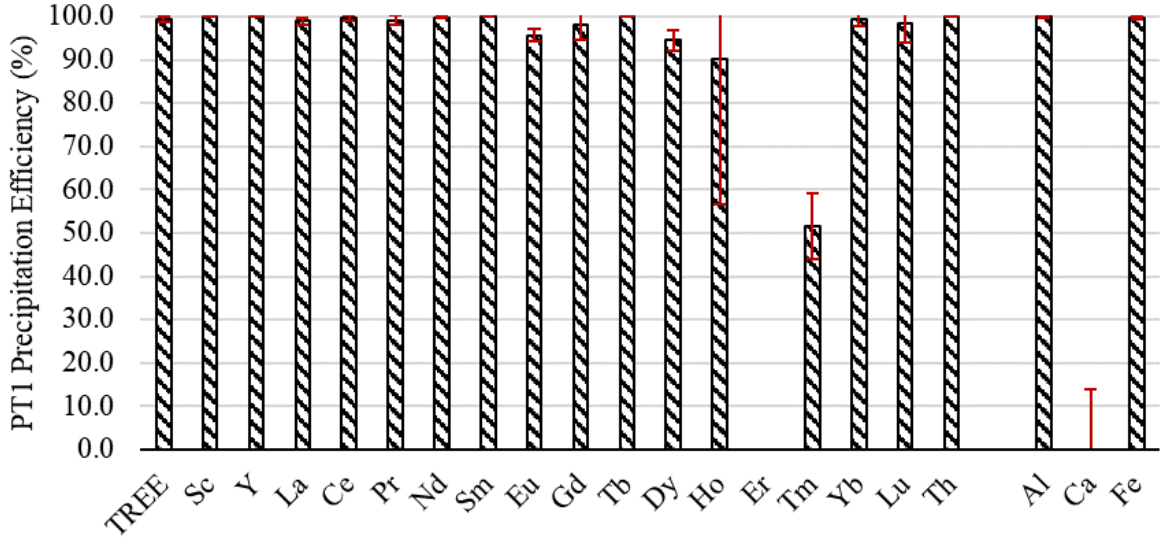

Figure 3.5.65. REEs and major contaminant precipitation efficiency values at pH 6.5. The values represent average values obtained for samples collected every two hours of a 20 hour operating period in the pilot plant.

3.5.8.3 REEs Redissolution

i. <u>Redissolution using pure HCl</u>

A sequential bench top precipitation test was performed on the leachate generated by acid leaching of the West Kentucky No. 13 roasted coarse refuse. Rare earth elements in the leachate were concentrated into the precipitate which was re-dissolved by adding hydrochloric acid with the final solution pH stabilized at 2.5. The rare earth element and major contaminant concentrations in the solution are shown in Table 3.5.19. The total concentration of REEs in the solution was around 245 ppm while the iron content was 44.2 ppm. The REE content was an order of magnitude higher than the raw leachate while the iron content was an order of magnitude lower. Therefore, chemical consumption and overall cost of REE recovery from the re-dissolved solution will be significantly reduced relative to treating the raw leachate. The aluminum content of 3360 ppm was the major focus of the subsequent purification steps.

Table 3.5.19. Rare earth element and major contaminant concentrations in the re-dissolved solution of the rare earth preconcentrate.

Elements	***TREE***	***Sc***	***Y***	***La***	***Ce***	***Pr***	***Nd***	***Sm***	***Eu***	***Gd***
Conc. (ppm)	245.2	0.3	8.8	51.7	106.4	12.9	46.5	8.0	1.4	5.0
Elements	***Tb***	***Dy***	***Ho***	***Er***	***Tm***	***Yb***	***Lu***	***Al***	***Fe***	
Conc. (ppm)	0.0	2.2	0.3	1.0	0.2	0.5	0.1	3360.2	44.2	

The leachate containing the re-dissolved precipitate was subsequently precipitated by adding sodium hydroxide to analyze the precipitation characteristics of the elements. As shown in Figure 3.5.66, the solution pH has to be increased from 2 to 5 to completely remove Al and Fe, whereas nearly 40% of the REEs were also lost to the precipitate. As the pH was further increased to around 6, nearly 100% of the REEs were precipitated. Based on the test results, the findings suggest that iron and aluminum cannot be separated from REEs in the concentrated solution effectively without losing REEs. Some other approaches were needed for removing the contaminants.

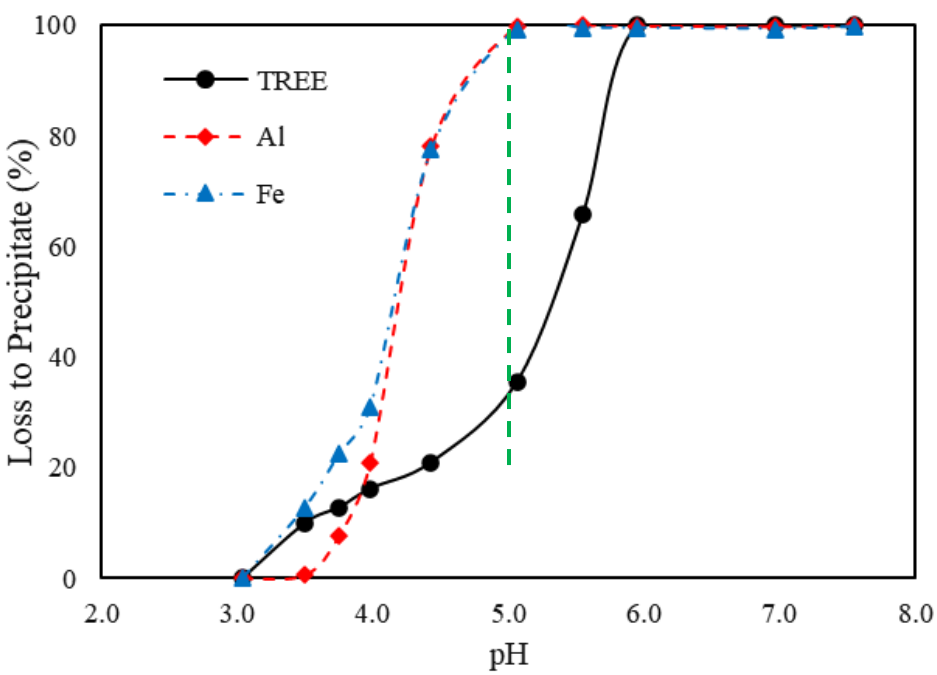

Figure 3.5.66 Sequential precipitation characteristics of REEs, Al, and Fe in the re-dissolved solution.

In addition to base, phosphates may also be utilized initiate the precipitation of REEs in solution due to the relatively low solubility products of rare earth phosphates. Therefore, precipitation characteristics of REEs and the major contaminants in the presence of sodium phosphate were assessed. A re-dissolved solution of 500 ml was put into a beaker and the initial solution pH was measured to be 3. Sodium phosphate of 0.5M was prepared by dissolving a certain amount of sodium phosphate in deionized water. During each incremental addition, 1.0 ml of the precipitant solution was added followed by 1 min of conditioning. Sodium hydroxide solution of 5M was added simultaneously to maintain the solution pH at 3. However, it was found that, even with a high dosage of the precipitant, no precipitates were observed. Therefore, another precipitation test was performed with the solution pH evaluated to 3.5 prior to adding the sodium phosphate solution. As shown in Figure 3.5.67, the selectivity between REEs and the contaminants was poor when using sodium phosphate as the precipitant. REEs were gradually precipitated out from the solutions, whereas Al and Fe followed a similar precipitation trend as the REEs. Therefore, efficient separation of REEs and the contaminants in the re-dissolved solution cannot be achieved using the phosphate precipitation approach.

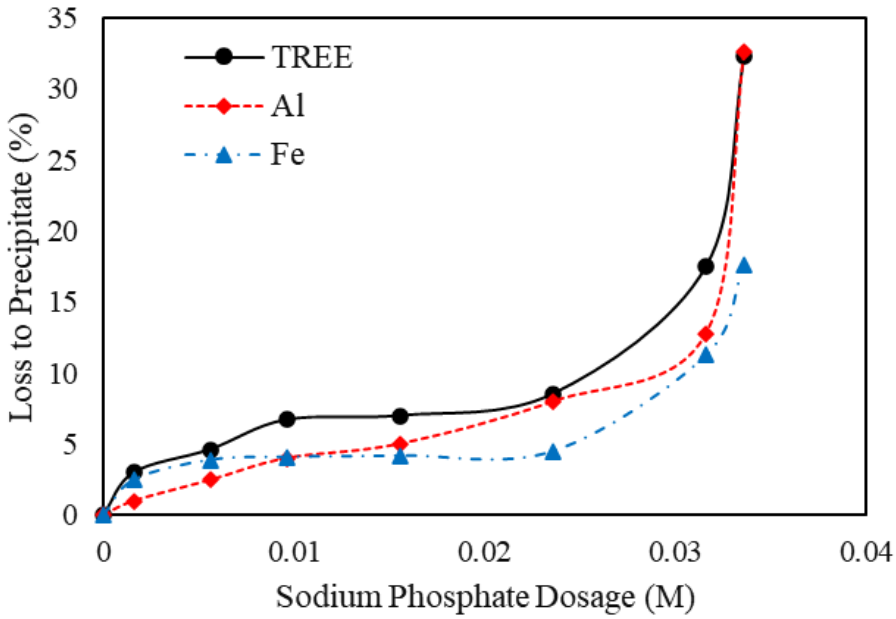

Figure 3.5.67. Precipitation characteristics of REEs, Al, and Fe from the re-dissolved solution when using sodium phosphate as the precipitant.

ii. *<u>REE Redissolution using a diluted system</u>*

In the previous approach, redissolution of the original REE precipitate cake provided a high concentration of REEs in solution (~245 ppm). However, due to the high solid content in the sludge, a large portion of REEs was lost in the filtration process. The filter cake obtained from the plate and frame filter typically contained 70-75% of moisture. As such, high REE concentrations in the redissolved solution results in greater REE losses to the filter cake. To minimize the loss of REEs, the system was diluted 10 times before redissolution and the selectivity of REEs, Al, Ca and Fe during redissolution was studied at various levels of pH values.

The filter cake obtained from the REE precipitation stage was 238 lbs with a solid content of 22.7% by weight. The cake material contained 413 ppm TREEs on a whole basis, 8729 ppm Al, 1593 ppm of Ca and 2.9% (29000 ppm) Fe. Fresh water was added to the filter cake to achieve a total volume of 200 gallons and the slurry was mixed under agitation for 24 hours. A bench-scale test was performed to identify the optimized redissolution pH to recover most of the REEs from the filter cake while discarding most of the contaminants. A 500-ml sample of the well-blended slurry was obtained and mixed in a beaker into which pure HCl was gradually added to the slurry to reduce the pH to different levels. At each pH value, a slurry sample was collected after stabilization of the pH value. The supernatant was analyzed for REEs and other elemental concentrations. The maximum concentration of TREEs, Al, Ca, and Fe achieved by completely redissolving the cake into solution was 94 ppm, 1981 ppm, 361 ppm, and 6669 ppm, respectively. The redissolution efficiency of each element is shown in Figure 3.5.68. The results suggested that a pH value of 2.5 was the optimal condition for redissolution which recovers about 90% of REEs while leaving about 90% of the Fe in the undissolved cake. About 15.5 liters of 37% HCl solution was added to the 200 gallons of slurry to reduce the pH to 2.5. The redissolution efficiency of individual elements at this stage is shown in Figure 3.5.69.

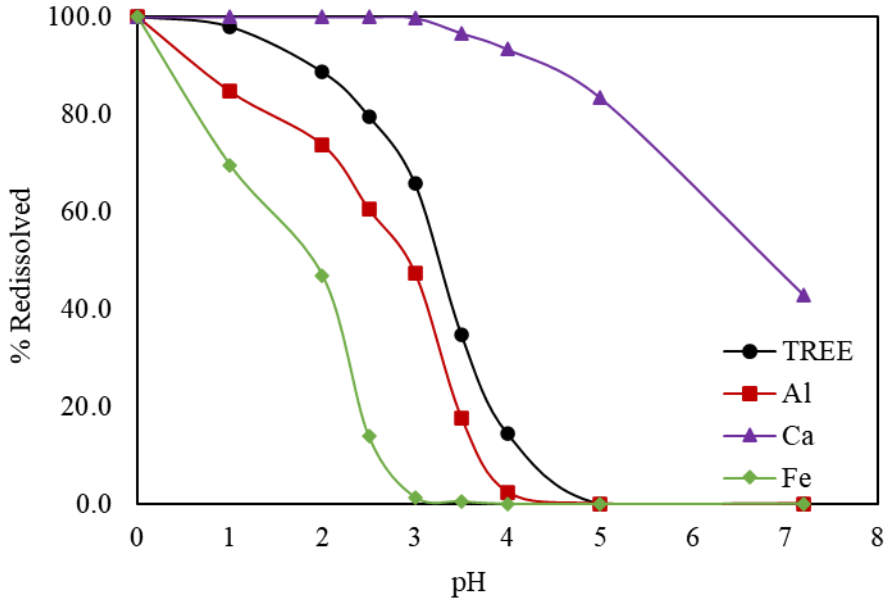

Figure 3.5.68. Redissolution efficiency of REEs, Al, Ca and Fe at various pH (bench scale test).

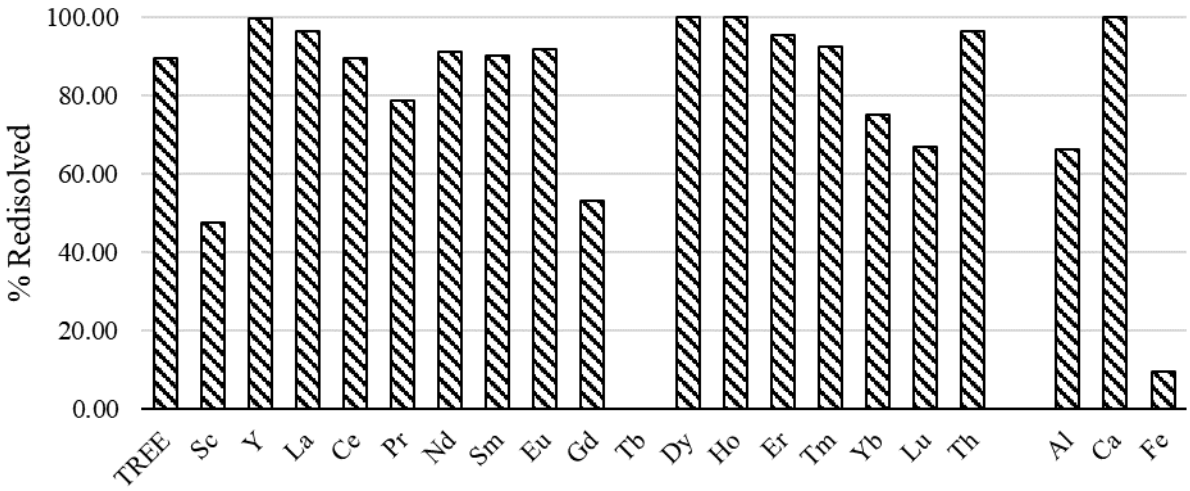

Figure 3.5.69. Redissolution efficiency of rare earth elements and major contaminants from the pilot-plant circuit using a solution pH value of 2.5

3.5.8.4 REEs Oxalate Precipitation

The re-dissolved slurry was filtered in a plate and frame filter to eliminate the iron and aluminum waste. The filtrate contained 76 ppm of TREEs, 1669 ppm of Al, 392 ppm of Ca, and only 94 ppm of Fe. The composition of the solution was suitable for oxalate precipitation of REEs. A series of preliminary selective precipitation tests was conducted on the concentrated rare earth bearing solution over a range of oxalic acid dosages and pH values as shown in Table 3.5.20. The results suggested that oxalic acid dosage is a critical parameter. At a dosage of 12.8 gms/L, over 85% of the TREEs was precipitated with about 11-12% of the Al, Ca, and Fe at a pH value of 2.5. At the same dosage but lower pH values, the REE precipitation efficiency reduced by about 10%, whereas higher pH values resulted in 20% more Fe to be precipitated into final product. At lower oxalic acid dosages, the REE precipitation efficiency was significantly lower regardless of the solution pH.

A set of systematic experiments were carried out based on the preliminary results to further study the effect of pH and the oxalic acid dosage on REE oxalate precipitation efficiency and final product purity (contamination ion precipitation efficiency). At a pH of 2.5, the REE oxalate precipitation barely occurred when the dosage of oxalic acid was lower than 8 g/L. With 12.8 g/L oxalic acid, the REE oxalate precipitation efficiency was approaching 100% at pH value of 2.5 as shown in Figure 3.5.70. At oxalic acid dosage of 12.8 g/L, the reaction pH has significant impact on the grade of REE oxalate purity. At pH of 1, less than 10% of contamination ions was picked up in precipitation, however, with compromising the REE precipitation recovery of 83%. With increasing the pH from 1.0 to 2.5, the precipitation efficiency of both REEs and contamination ions increased by about 10 percentage points, as shown in Figure 3.5.71.

Table 3.5.20. Preliminary test results on REEs precipitation using oxalic acid.

Test	Dosage (g/L PLS)		Precipitation	% Precipitated			
	Oxalic Acid	NaOH	pH	TREE	Al	Ca	Fe
DTK-C2-B1	6.4	0	1.1	31.59	14.46	17.37	38.02
DTK-C2-B2	12.8	0.04	0.9	75.05	6.96	8.38	0.00
DTK-C2-B3	1.6	0	1.6	3.23	4.01	1.89	8.11
DTK-C2-B4	6.4	0.04	1.1	10.09	1.27	2.00	2.79
DTK-C2-B5	12.8	1.6	1.0	74.75	15.10	14.41	0.00
DTK-C2-B6	12.8	6.4	2.5	85.20	12.09	11.33	11.53
DTK-C2-B7	12.8	6.08	3.6	79.90	5.17	9.91	28.59
DTK-C2-B8	6.4	4.8	4.1	16.01	7.81	9.02	35.08
DTK-C2-B9	12.8	3.2	1.1	82.50	7.36	9.04	10.21

In the current process, a pH value of 2.5 was selected for the pilot scale operation with an oxalic acid dosage of 12.8g/L to achieve the optimal REE recovery. About 600 Liters (158 Gallons) of concentrated REE bearing solution was obtained by filtering the re-dissolved slurry. The filtrate was fed into a 10-Liter tank at flow rate of 300 ml/min. Oxalic acid solution was prepared in a separate reagent tank at a concentration of 40 g/L and was pumped into the reaction tank at flow rate of 96 ml/min. The pH of the reaction tank was adjusted using 4M NaOH solution that was pumped automatically through a PID programmed peristaltic pump to achieve a constant pH of 2.5. The total base solution consumed during the oxalate precipitation process was recorded. Mixing in the reaction tank was provided by a mechanical mixer at agitation speed of 370 rpm. The overall precipitation efficiency achieved in the oxalate precipitation circuit for the individual elements is shown in Figure 3.5.72. The mixed solution carrying REE precipitates was overflowing to a bench top vacuum filter. The filter cake collected on the filter paper was dried in the oven and roasted at 750°C for 2 hours to be converted to RE oxide product. Total 77 grams of REO was produced from the current operation. The purity of the REO product was 71.83% with 1% Al_2O_3, 15.4% CaO, and 3.5% of Fe_2O_3. The grade of individual RE in the REO mix is listed in Table 3.5.21.

.

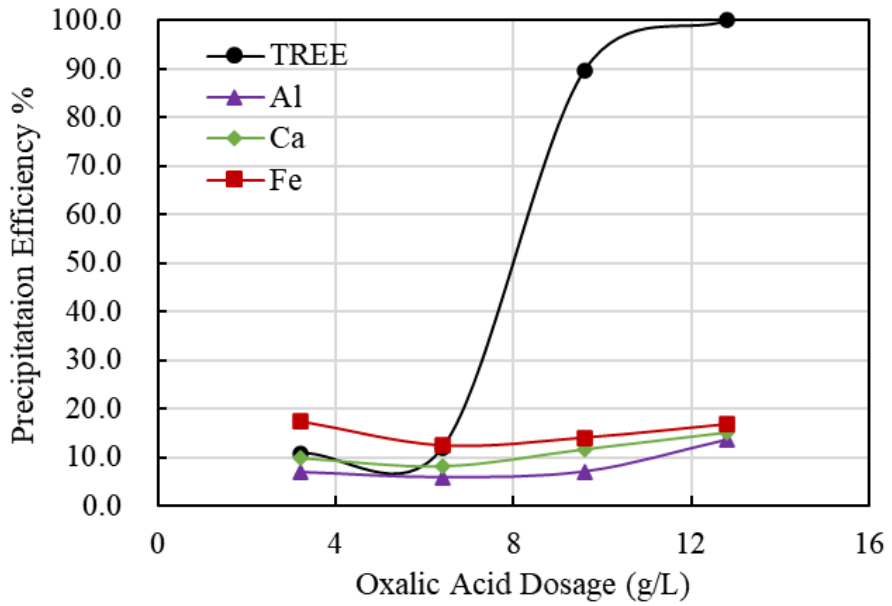

Figure 3.5.70. Effect of oxalic acid dosage in rare earth oxalate precipitation. (Retention time = 20minutes, Reaction pH =2.5)

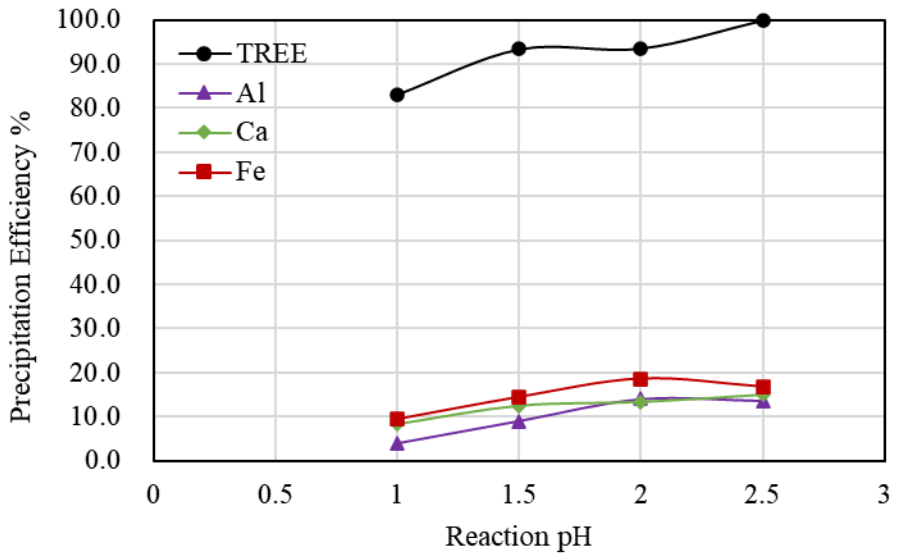

Figure 3.5.71. Effect of pH on rare earth and contaminate ion oxalate precipitation (Retention time = 20minutes, oxalic acid dosage = 12.8 g/L).

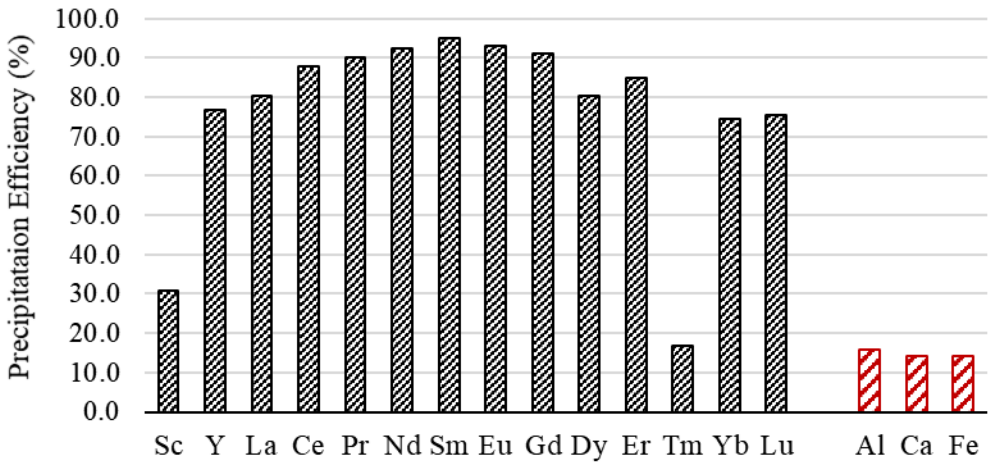

Figure 3.5.72. Oxalic precipitation efficiency of individual rare earth elements and contaminant ions (Oxalic acid dosage 12.8g/L at pH 2.5 regulated using 4M NaOH, pilot scale).

Table 3.5.21. REO product purity produced from Dotiki coarse refuse material in pilot plant.

Elements	REE Content		Molecular Wt.	RE Oxides	REO Content
	ppm	% dry weight	g/mol		% dry weight
Sc	299	0.0	45	Sc_2O_3	0.05
Y	17862	1.8	89	Y_2O_3	2.27
La	104216	10.4	139	La_2O_3	12.22
Ce	258333	25.8	140	CeO_2	31.73
Pr	35086	3.5	141	Pr_6O_{11}	4.24
Nd	132481	13.2	144	Nd_2O_3	15.45
Sm	23962	2.4	150	Sm_2O_3	2.78
Eu	3810	0.4	152	Eu_2O_3	0.44
Gd	13417	1.3	157	Gd_2O_3	1.55
Tb	0	0.0	159	Tb_4O_7	0.00
Dy	5018	0.5	163	Dy_2O_3	0.58
Ho	851	0.1	165	Ho_2O_3	0.10
Er	2404	0.2	167	Er_2O_3	0.27
Tm	0	0.0	169	Tm_2O_3	0.00
Yb	1206	0.1	173	Yb_2O_3	0.14
Lu	156	0.0	175	Lu_2O_3	0.02
TREE	599103	59.9			71.83
Th	7390	0.739	90.00	ThO_2	1.00
Al	3993	0.399	13.00	Al_2O_3	1.14
Ca	110321	11.032	40.00	CaO	15.44
Fe	24812	2.481	56.00	Fe_2O_3	3.54
Total					92.96

3.5.8.5 Flowsheet and economic analysis

Continuous operation of the pilot plant over a 20-hour period (Code: C2) successfully produced 77 grams of over 71% grade of REO from the Dotiki coarse refuse material. The flowsheet was developed and optimized during the process with the goal of process simplification the operation process, maximizing the unit-by-unit rare earth recovery, and reducing the chemical costs. A schematic on the flowsheet with material balance over the circuit and the dosage of chemicals applied in each unit is shown in Figure 3.5.73. The chemical costs were calculated based on the dosage of each chemical at each stream as shown in Table 3.5.22.

Table 3.5.22. Chemical cost per kg of REO produced from Dotiki coarse refuse material.

Chemicals	Dosage (kg/kg REE)			
	Leaching	REE Precipitation	REE Redissolution	Oxalic Precipitation
H_2SO_4	418.1	--	--	--
NaOH	--	40.3	--	45.3
HCl	--	--	171.2	--
Oxalic Acid	--	--	--	90.6
Total				

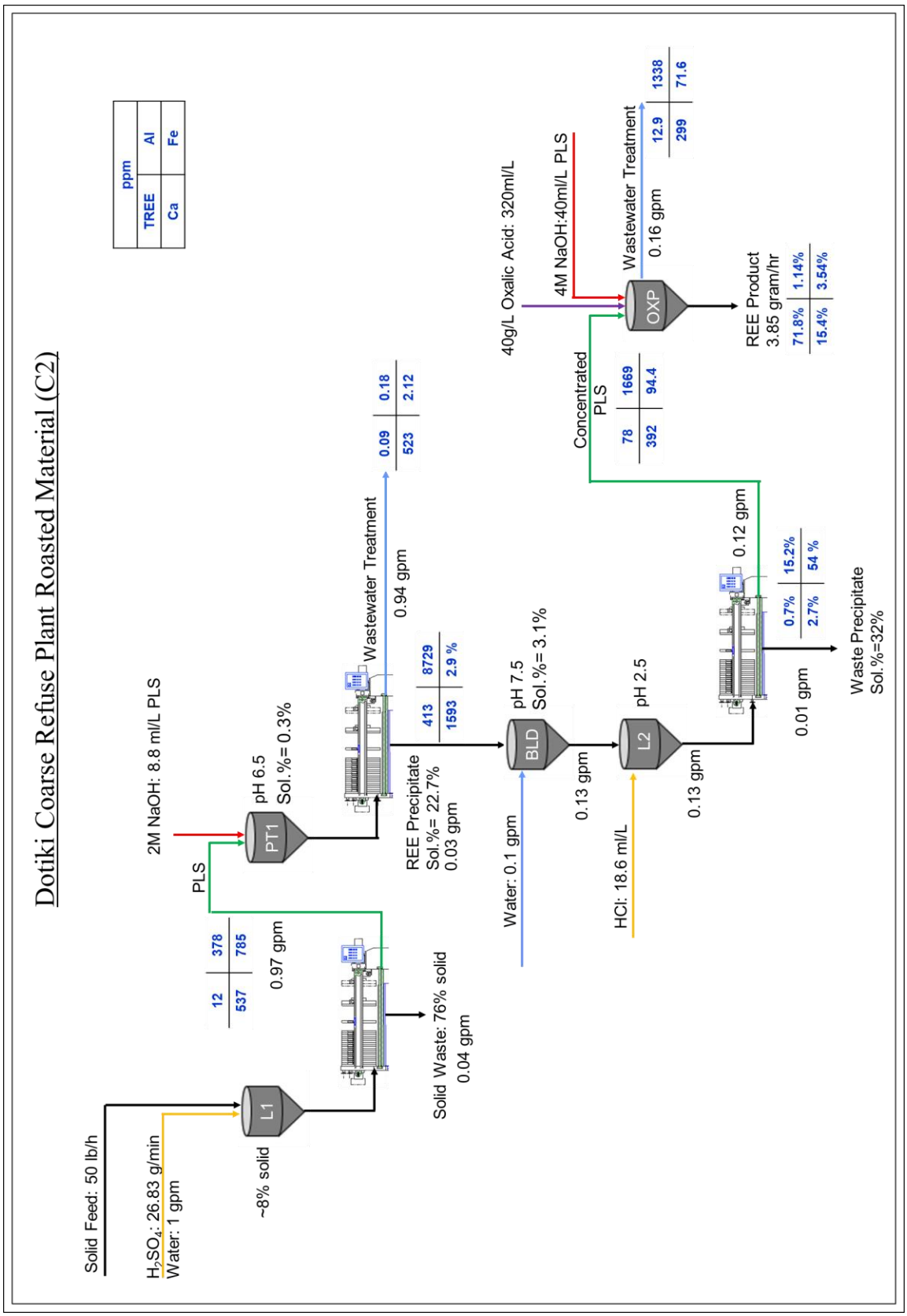

Figure 3.5.73. Flowsheet of REO production from the Dotiki coarse refuse material (Test C2).

3.5.8.6 RE Oxalate Upgrading

During the leaching process of the coal coarse refuse, a large portion of the ions released in the solution is non-REE metallic species, primarily Al^{3+} Fe^{3+}, and Ca^{2+}. A majority of Ca^{2+} (~95% of the total quantity) is rejected by selective hydrolytic precipitation of the leachate at a pH value of 6.5 followed by selective redissolution of the REEs in the precipitate in hydrochloric acid. The redissolved solution is then treated with the oxalic acid for selective precipitation of the REE as insoluble precipitates. The non-RE metallic species in the solution either complex with the oxalate or form an insoluble precipitate with the oxalate. Of the major non-RE species, Al^{3+} forms soluble complexes and do not precipitate with REEs. However, Ca^{2+} and Fe^{3+} forms precipitate with oxalic acid and reduced the purity of the final product in the form of RE oxalate. The concentrate, therefore, contains a significant amount of contaminants, mainly in the form of calcium oxalates. In this study, acid washing as the method to improve the grade of the concentrate is explored. The solubility product (K_{sp}) of Ca oxalate and Fe oxalates are in the order of 10^{-8} while the RE oxalates are in the order 10^{-27} indicating that the impurities are much more soluble than the RE oxalate. Therefore, the concentrate can be washed by a dilute solution of hydrochloric acid to selectively remove the non-RE oxalates while retaining the RE oxalates in the solid phase owing to the lower solubility of oxalate salts of REEs.

The objective of the study was to identify the optimal concentration of the acid solution and % solids for washing for which maximum rejection of the contaminants (calcium, iron, and aluminum) can be achieved for minimum loss of REEs. A full factorial experimental test program was carried out for 2 factors (acid concentration and % solids). The ratio of the concentration of contaminants to the concentration of TREE (relative concentration of contaminants) in the wash-liquid after processing was the response variable for the experimental program.

$$\text{Relative concentration} = \frac{[\text{Contaminants}]}{[\text{TREE}]}$$

Factor	Unit	Levels	Response
Acid concentration in wash solution (F1)	molar	0.1, 0.25, 0.5	Relative concentration
Solid concentration in the wash step (F2)	g/L	5, 10, 20	

50 mL of the acid solution was used to wash 0.25, 0.5 and 1 g of the RE oxalate produced from the continuous test on coal coarse refuse from WK-13 coal source (DTK-C2) in a 250 mL Erlenmeyer flask. The agitation to the solution was provided by the VWR orbital shaker at 400 RPM for 15 minutes. The solids were separated using a centrifuge and the elemental composition of the solution was determined by ICP-OES.

The relative concentration of the contaminants directly corresponds to the selectivity of the washing process, i.e. a higher value of the relative concentration indicates a better selectivity. It can be seen from the results (Figure 3.5.74) that the selectivity reduces significantly as the acid concentration was increased (40 for 0.1 M HCl to 5 for 0.5 M HCl). The selectivity also depends

on the solid concentration as higher selectivity was achieved at a higher solid concentration (40 for 20 g/L to 13 for 5 g/L)

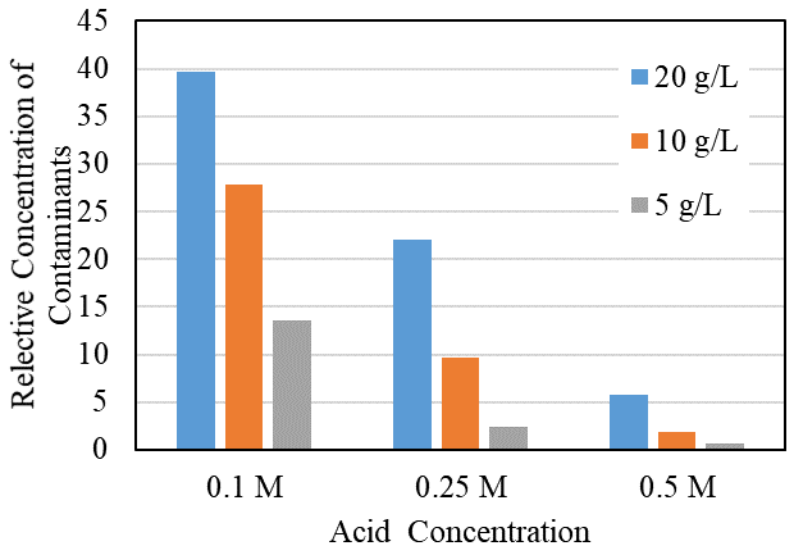

Figure 3.5.74 The relative concentration of the contaminants in the wash solution at different acid and solid concentrations.

However, the objective of the wash step is to upgrade the purity of the product by removing the majority of the contaminants. The low acid with high solids concentrations wash condition, though having a high selectivity, rejects a relatively lower amount of contaminants (close to 50% calcium, iron, and aluminum). A higher absolute quantity of contaminants can be rejected at lower solids concentration and high acid strength resulting in a relatively higher corresponding loss of REE (Figure 3.5.75).

The % rejection of metal can be used as a quantity to evaluate the process, as calculated by

$$\% \text{ Rejection} = \frac{\text{Amount of metal rejected in the wash liquid}}{\text{Amount of the metal present in the feed solids}}$$

Almost 100% of calcium and close to 70% and 75% of iron and aluminum respectively from the concentrate if the solids are washed with 0.5 M HCl at 20 g/L solid concentration. Though the selectivity in this condition is not the highest, which results in significant losses of REEs in the wash solution, the washed solids have a very high purity of REE.

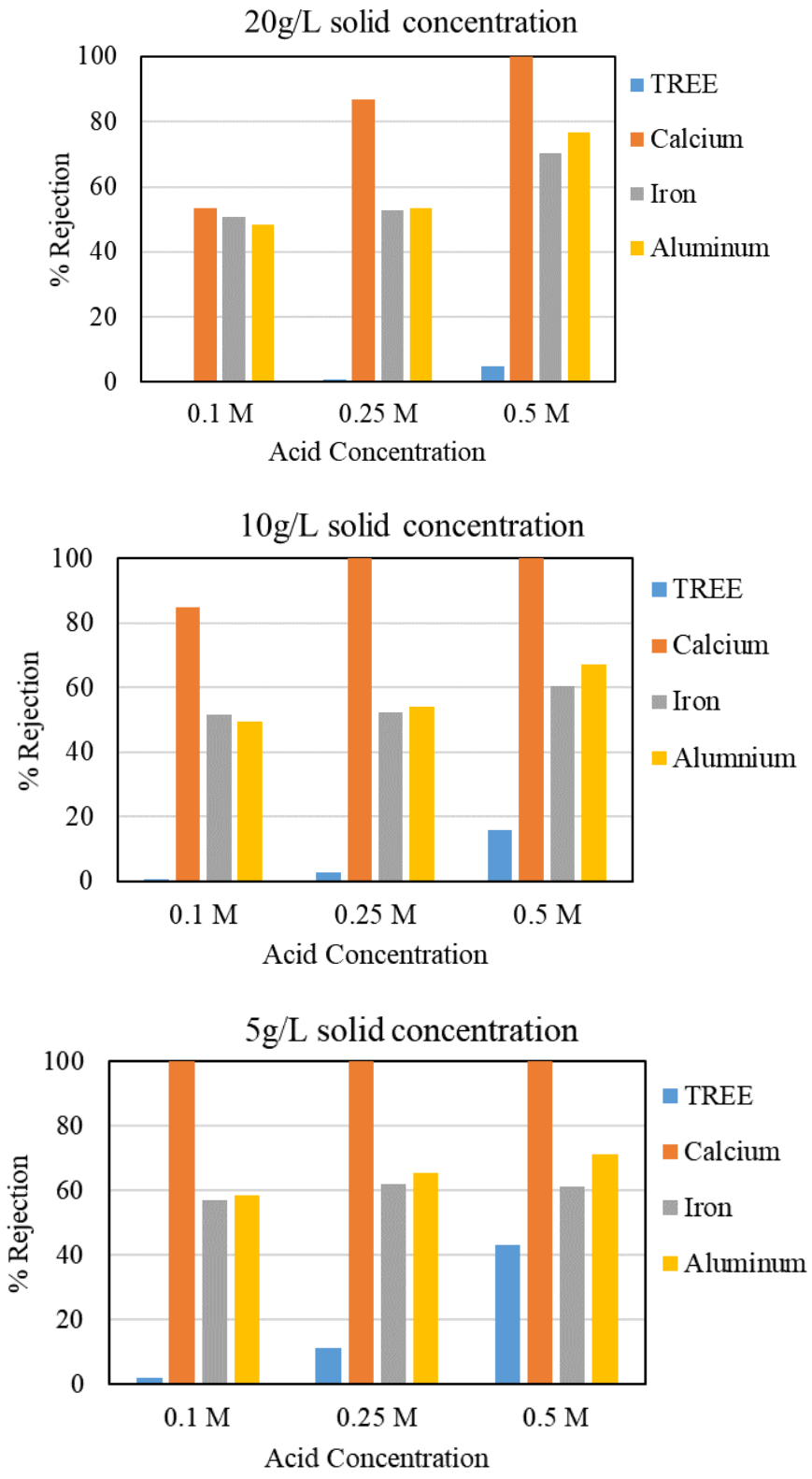

Figure 3.5.75 Rejection of different metals for different solids concentration using a range of acid concentrations.

Due to low selectivity, the wash liquid at 0.5 M HCl, 20 g/L condition contains a significant concentration of REEs (Figure 3.5.76). To prevent the loss of REEs, the wash stream can be recycled to the oxalate precipitation feed stream. The acid wash stream will be volumetrically significantly smaller than the feed stream of oxalic precipitation (smaller by a factor of 250) and would not adversely impact the performance of the oxalic precipitation circuit. The washed oxalate using the above conditions was roasted, and elemental composition was analyzed by digestion followed by ICP -OES. The TREE content of the oxide from the washed oxalate was 78.4 % by weight and the converted REO content was 94.0%, as shown in the Table 3.5.23 below.

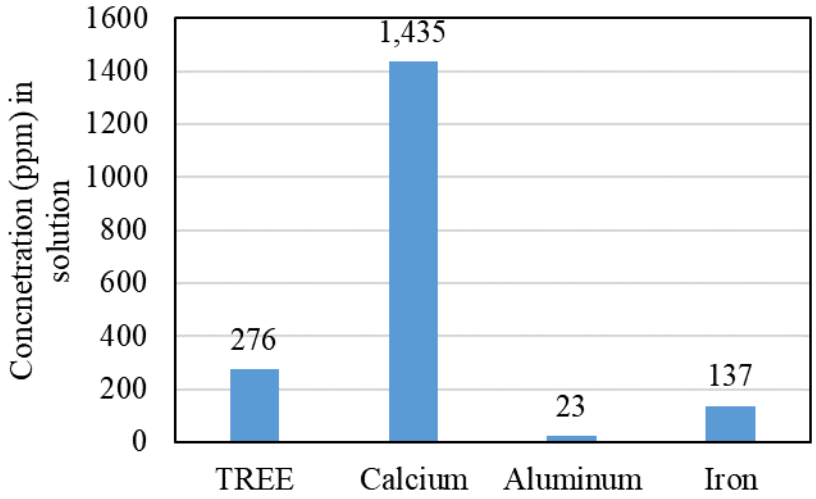

Figure 3.5.76 Elemental composition of the wash liquid at 20 g/L solids concentration using 0.5 M HCl solution

Table 3.5.23 Elemental composition of the washed product in terms of REEs and REOs by weight

Element	%REO by wt	%REE by wt
Sc	0.1	0.05
Y	3.1	2.41
La	14.8	12.67
Ce	41.6	33.89
Pr	5.6	4.68
Nd	20.6	17.69
Sm	3.7	3.23
Eu	0.6	0.54
Gd	2.2	1.90
Tb	0.0	0.00
Dy	0.8	0.70
Ho	0.1	0.13
Er	0.4	0.33
Tm	0.0	0.00
Yb	0.2	0.16
Lu	0.0	0.02
TREE	94.0	78.4

For the coal sources, the feed solution for oxalic precipitation has a significantly higher concentration of contaminants. Consequently, the oxalate precipitate contains a substantial amount of the contaminants which results in an inferior product. As the solubility of the calcium oxalate is much higher than that of rare earth oxalates, it can be washed off from the oxalate solid by using a dilute solution of hydrochloric acid. High selectivity can be achieved by using low acid concentration and high solids concentration in the wash step. However, to remove most of the calcium from the oxalate solids, a higher acid concentration is more amenable, despite having lower selectivity. The REEs lost in the wash acid stream can be recovered by recycling the stream back to the oxalic precipitation feed stream.

3.5.9 Rare earth mineral concentration (HHS)

3.5.9.1 HHS mobile unit

After the initial design and construction period, exploratory testing of the mobile HHS rig continued to evaluate potential operational and mechanical challenges. Brief descriptions of these problems and the subsequent corrective actions are given in the following paragraphs.

Figure 3.5.77. Large agglomerates

Large agglomerate formation: As explained in prior progress reports, in the first step of the HHS process, coal agglomerates are formed by agitating the coal slurry with a hydrocarbon oil in both high-shear and low-shear mixing units. Next, these agglomerates are separated from the slurry that contains mineral matter using mechanical flotation machines. Then, coal agglomerates are sent to a phase inversion tank and subsequently to a Morganizer, where they are dispersed in an oil phase and are separated from any residual water. In most of the previous test runs, this circuit performed well for the first 20-30 minutes of a test run. In this initial period, the feed to the primary flotation machine contained properly formed agglomerates. However, after this initial period, the amount of well-formed agglomerates in the primary flotation machine started decreasing. This

reduction in mass in turn affected the performance of the Morganizer, because poorly formed agglomerates would not break up and disperse in the oil phase. As a result, some of the residual water was not efficiently removed in this step. Consequently, the final product contained higher than desired moistures.

A close inspection of the low shear mixing tank after a poor test run revealed that the tank was full of large agglomerates with sizes up to an inch (Figure 3.5.77). Ideally, the agglomerate size is desired to be only a few millimeters. These agglomerates were too heavy to float. Thus, many of them sank and were not transferred downstream to the flotation cells. Only the poorly formed agglomerates were able to go to the flotation step. This explained the overall deterioration of the process performance during test runs.

The low shear mixing tank originally did not have any baffles to help with mixing. This design was thought to be the reason for the agglomerates to become so large. Once they formed, the agglomerates would roll on the sides of the tank and would keep growing almost indefinitely. Based on this theory, four baffles were added to the inside of the tank. Further testing showed that baffles really did not help with decreasing the size of agglomerates. At the end, it was determined that the overall mixing time or retention time in the tank was too long, thus causing agglomerates to grow uncontrollably. Trials performed with bypassing the low shear tank and feeding the primary flotation machine directly from the high shear tank helped in reducing agglomerate sizes. While this approach helped with reducing the size of agglomerates, a low shear tank is still a necessity when processing coals that are more difficult to agglomerate. The current low shear tank has several different discharge ports at different heights for adjusting the retention time. However, even when using the lowest port, the retention time is too high at over six minutes. Whereas, no more than 2-3 minutes of retention time is needed for low shear mixing. As a result, a new low shear tank was designed and ordered to be built by a local fabricator. This new tank will allow for varying retention times between 1 and 3 minutes. The mobile HHS rig is expected to be retrofitted with the new low shear tank and to be tested in the early parts of the next reporting period.

<u>Primary flotation launder plugging</u>: The problem with the dry agglomerate transfer was thought to be mitigated by using a bigger pump and overflowing more water with agglomerates. While this solution helped with the transfer of agglomerates, it did not completely resolve the issue. It was determined that the design of the flotation launder was not favorable for dry agglomerate transfer. The launder (Figure 3.5.78(a)) was too deep and too steep. Thus, even with the increased amount of water discharge, the agglomerates still stuck to the sides of the launder while letting most of the water pass through them. As a quick solution to this problem, a new bottom plate was added into the launder as shown in Figure 3.5.78(b). The plate greatly reduced the slope of the launder, which in turn let water carry solids over to the discharge port. Moreover, since more water is normally pushed out of the second cell, the modified launder is sloped from this cell towards the first cell. This way, the dry agglomerates overflowing from the first cell are carried to the discharge port with the help of water overflowing from the second cell. Lastly, a plexiglass window was installed on the launder to easily observe any plugging issues in the launder (Figure 3.5.78(c)).

Figure 3.5.78. New flotation launder design

Pumping air through the Morganizer: The Morganizer design relies on having consistent upward solvent flow to carry coal particles to an overflow port. The water and tailing particles that are too heavy to travel upwards would sink in the Morganizer and would be discarded as tailings. The upward velocity of the solvent has to be adjusted carefully based on the settling velocity difference between coal particles and water. If the solvent velocity is too high, then water would start traveling upwards instead of downwards. As a result, the Morganizer overflow stream would have a more than desired moisture content.

The diaphragm pump installed on the primary flotation launder is operated continually to keep the launder empty of any material. This action is done due to the tendency of agglomerates floating on water. On several occasions, it was observed that when any liquid level is kept in the launder, agglomerates would float and build up while all the new liquid overflowing from the flotation cell would go through these agglomerates and would be pumped away. Over time, the launder would become plugged up with solids. The one problem with running the launder pump in a continuous manner is that when the launder is empty, rather than liquid and solids, gas would be pumped into the Morganizer. This result effectively decreases the liquid volume in the column, which causes the overall upward solvent velocity to increase. As such, high moisture carryover is observed as explained above.

In order to fix the issue, several different solutions including adding a new deaeration tank, using the phase inversion tank as a deaeration tank, etc. were considered. In the end, a simpler route was chosen; a tee connection was added at an elevated height to the Morganizer feed line. One side of the tee is connected to the common vent system. This configuration allows the tee to be a small deaeration device and to discard all the air pumped from the primary flotation launder before it reaches the Morganizer. Preliminary tests conducted with using just water showed that the tee was very effective with deaerating the feed to the Morganizer. Therefore, the Morganizer performance is expected to perform adequately in future tests.

Vacuum pump oil in the system: The vacuum pump for the drum filter that was originally installed on the HHS trailer required a type of mineral vacuum oil to operate. Due to how the pump is designed, the vacuum oil was in continuous contact with solvent vapors coming from the drum filter during operation. This configuration caused the oil to be stripped away by the solvent, thus requiring the pump to be filled up with oil at least once during every process run. However, the vacuum oil continued accumulating in the overall HHS system over time. The Morganizer has a structured packing that is hydrophilic and would capture water while in operation. This is where

the coal agglomerates are separated from the residual water. However, the vacuum oil accumulated on the packing, as well, and made the packing surface hydrophobic. Therefore, the residual water in the coal agglomerates did not have a chance to coalesce on the packing. This action, in turn, caused product moisture to increase. In order to resolve this issue, a new vacuum pump with a liquid ring seal was ordered and installed on the trailer. Initial tests indicated that this pump performed far better than the original vacuum pump.

Figure 3.5.79. HHS Trailer was set up in the storage shed at Virginia Tech facilities (b)

Relocation of HHS Trailer: The mobile rig was originally set up outside at Virginia Tech facilities. This placement was mainly done because of safety issues related with using an organic solvent in the process. Having the rig outside provided the best ventilation possible. However, to get prepared for the coming cold winter months, the HHS testing rig was moved into the storage shed located near the Mining and Minerals Engineering Department's testing facility with permission from the Virginia Tech Health and Safety Office and the University Building Official (Figure 3.5.79). This shed is far enough from the main facility and any other residential buildings that it was deemed safe to store and run the mobile HHS rig. To prepare for the move, the shed was emptied and cleaned out. The 480 V electrical connection required by the mobile rig was moved with the rig into the shed by a certified electrician. Since the shed did not have any lighting, new explosion proof light fixtures were installed on the mobile rig.

The Proof-of-Concept (POC) HHS pilot plant (mentioned in earlier progress reports) was originally operated in this shed during warm months due to the lack of good heaters and heat insulation. Also, one side of the building was open to the outside air. In order to be able to operate the mobile HHS rig during winter months, this space needed to be heated and at least partially insulated. There were existing explosion-proof electrical heaters in the shed that were left over from the old POC plant. However, these heaters did not have enough capacity to provide the required heating for the mobile HHS rig operation. Fortunately, there is a large gas heater in the main facility that can easily heat the main building as well as the storage shed given the shed is

insulated enough. So, the open side of the shed was covered with a heavy-duty tarp to minimize heat loss. Also, new ductwork was installed between the main building and the shed to provide heating (Figure 3.5.81). The ductwork was connected to one of the exhaust ports of the large gas heater. An exhaust fan was also installed on an opening on the tarp (Figure 3.5.80) to provide good air circulation and to prevent any buildup of solvent vapors in the shed over time. Temperature measurements taken inside the shed revealed that this setup allowed for inside of the shed to be 20-30°F warmer than the outside temperature. As a result, the mobile rig could be operated in the shed even during the coldest days of the year.

Figure 3.5.80. Exhaust fan installed on the side of the shed.

Figure 3.5.81. Heating ductwork was installed from the main building into the shed. The open side of the shed was covered with a clear plastic tarp for heat insulation.

3.5.9.2 Decarbonization

Detailed testing of the mobile HHS platform was initiated using approximately 2400 gallons of slurry obtained from the Leatherwood coal preparation plant. The test samples were obtained from the thickener underflow stream produced when the Leatherwood plant was treating primarily run-of-mine coal from the Fireclay seam. Samples were collected on two different occasions. The thickener underflow sample collected during the first sampling campaign contained

a very high ash content of approximately 80% ash, while those collected during the second sampling campaign contained only about 66% ash. Five complete sets of test runs were conducted. Test runs 1 through 3 were run with the higher ash (80%) feed and test runs 4 and 5 were run with the lower ash (66%) feed.

The results obtained from the detailed tests are summarized in Table 3.5.24. The data is also plotted in Figure 3.5.82 and Figure 3.5.83 for ease of comparison. The test data indicate that the HHS technology consistently produced a clean coal product with a marketable ash content regardless of which feed was treated by the HHS platform. For the higher ash feed, clean coal products containing 7.5-10% ash were generated in test runs 1 to 3, respectively. Unfortunately, the clean coal yield in the first test was very low (i.e., 0.8%), which resulted in a recovery of combustible matter of only 10.3%. The low yield was attributed to an operating issue that was resolved prior to conducting additional tests with the high ash feed. The two additional tests (runs 2 and 3) performed with the high ash feed achieved exceptional combustible recovery values of 99.9% and 98.8%, respectively, and generated marketable clean coal products containing 8.4% to 10.0% ash. Due to the large amount of ash-bearing material in the feed, the clean coal yields from these two test runs were still relatively low (i.e., 14.7% and 14.8%). As should be expected, the next two tests (runs 4 and 5) that were conducted using the lower ash (67%) feed provided substantially higher clean coal yields of 27.4% and 29.7% and provided good combustible recoveries of 90-95%. The higher yields obtained in test runs 4 and 5 did not appear to diminish the quality of the clean coal product, which ranged from 7.4% to 9.3% ash when treating the lower ash feedstock. The only performance indicator that did not meet expectations during the detailed testing program was the product moisture content. The test data showed that the mobile HHS platform produced higher than desirable final moisture values ranging from a low of 16.6% in test run 3 to 23.3% moisture in test run 4. The root cause(s) of the higher moisture contents, which appear to be related to issues with agglomerate formation/dispersion, are currently being addressed by the project team.

While the focus of the work conducted with the HHS test rig was primarily to evaluate the capabilities of this technology for feedstock decarbonization, the data obtained from this portion of the test plan also indicated that the decarbonization step significantly increased the concentrations of rare earth elements (REEs) in the remaining ash-rich product streams. The separation data for the REEs are summarized in Table 3.5.25. Some of the key performance data is also plotted in Figures 10 and 11 to make it easier to compare each test run. Note that the REE assay values are reported on both an “ash-basis” parts-per-million (ppm_a) and on a “whole-basis” parts-per-million (ppm_w). The results show that the overwhelming vast majority of REEs contained in this particular feedstock reported to the ash-rich REE product stream and very little reported to the clean coal stream (Figure 3.5.82). For example, test run 2 recovered 93.9% of the REEs in the ash-rich stream, while allowing only 6.1% of the REEs to be lost with the carbon-rich clean coal product. The resulting REE enrichment appears to be largely due to the removal of organic/carbonaceous matter that serves to dilute the REE concentration. This suggestion is supported by the data plotted in Figure 3.5.84 to Figure 3.5.86, which shows that the whole-sample REE concentrations are linearly related to the dry ash contents of the product samples. Since the intercept of this linear plot is non-zero, the ash-based REE content increases sharply as the ash content approaches zero.

Table 3.5.24. Decarbonization data from five series of detailed HHS test runs.

Test Run	Mass (%, dry)	Ash (%, dry)	Mineral (%, dry)	Moisture (%, ar)	Distribution (%)	
					Ash	Comb.
Run 1 (Higher Ash Feed)*						
ROM Feed	100.0	85.8	92.7	-	100.0	100.0
Coal Product	0.8	7.5	8.1	24.7	0.1	10.3
REE Product	99.2	86.5	93.4	-	99.9	89.7
Run 2 (Higher Ash Feed)						
ROM Feed	100.0	80.2	86.6	-	100.0	100.0
Coal Product	14.7	8.4	9.1	18.6	1.5	99.9
REE Product	85.3	92.6	100.0	-	98.5	0.1
Run 3 (Higher Ash Feed)						
ROM Feed	100.0	80.2	86.6	-	100.0	100.0
Coal Product	14.8	10.0	10.8	16.6	1.9	98.8
REE Product	85.2	92.4	99.8	-	98.1	1.2
Run 4 (Lower Ash Feed)						
ROM Feed	100.0	66.6	71.9	-	100.0	100.0
Coal Product	27.4	7.4	8.0	23.3	3.1	89.7
REE Product	72.6	88.9	96.0	-	96.9	10.3
Run 5 (Lower Ash Feed)						
ROM Feed	100.0	66.6	71.9	-	100.0	100.0
Coal Product	29.7	9.3	10.0	21.6	4.1	95.0
REE Product	70.3	90.7	98.0	-	95.9	5.0

**Note: Process experienced operational issues*

Table 3.5.25. REE concentration data from five series of detailed HHS test runs.

Test Run	Mass (%, dry)	Ash (%, dry)	TREE (ppm_a)	TREE (ppm_w)	Distribution TREE
Run 1 (Higher Ash Feed)*					
ROM Feed	100.0	85.8	379.5	305.7	100.0
Coal Product	0.8	7.5	1442.4	108.2	2.3
REE Product	99.2	86.5	371.1	320.9	97.7
Run 2 (Higher Ash Feed)					
ROM Feed	100.0	80.2	376.8	302.2	100.0
Coal Product	14.7	8.4	1389.8	117.0	6.1
REE Product	85.3	92.6	359.4	332.7	93.9
Run 3 (Higher Ash Feed)					
ROM Feed	100.0	80.2	376.8	302.2	100.0
Coal Product	14.8	10.0	1220.3	122.5	68.4
REE Product	85.2	92.4	351.9	325.2	91.6
Run 4 (Lower Ash Feed)					
ROM Feed	100.0	66.6	412.2	274.4	100.0
Coal Product	27.4	7.4	1488.3	110.7	13.9
REE Product	72.6	88.9	366.0	325.4	86.1
Run 5 (Lower Ash Feed)					
ROM Feed	100.0	66.6	412.2	274.4	100.0
Coal Product	29.7	9.3	1239.6	115.3	13.1
REE Product	70.3	90.7	371.0	336.6	86.3

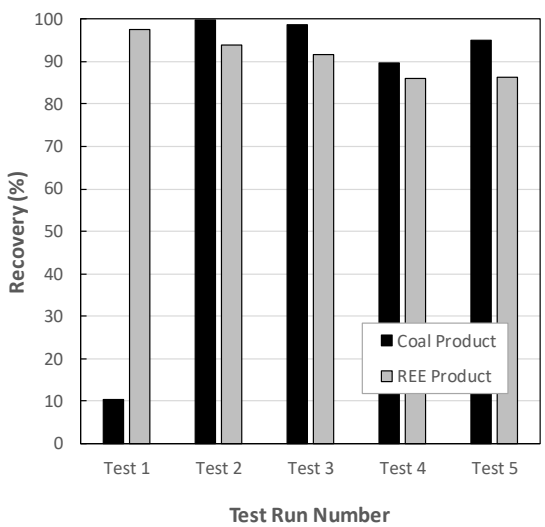

Figure 3.5.82 Recovery of combustible matter to the clean product and REEs to the REE product (high-ash tails).

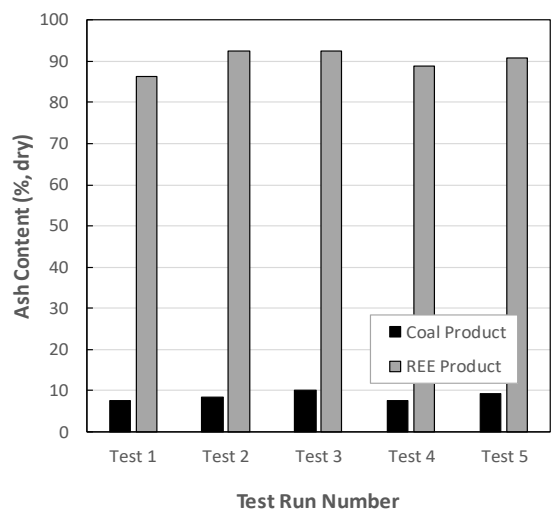

Figure 3.5.83 Ash contents of the clean product and REE product (high-ash tails).

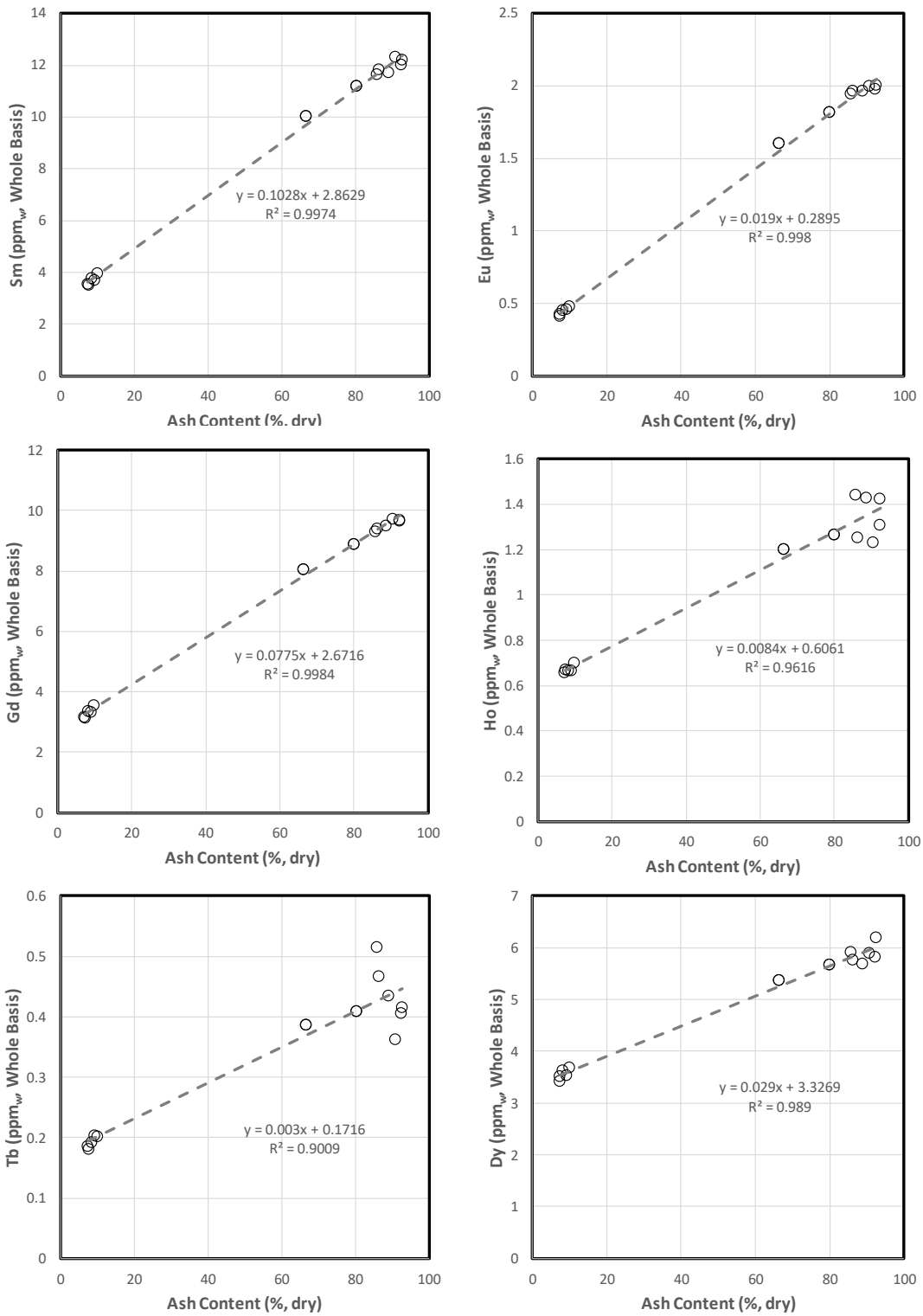

Figure 3.5.84 Element concentration versus ash content for selected elements.

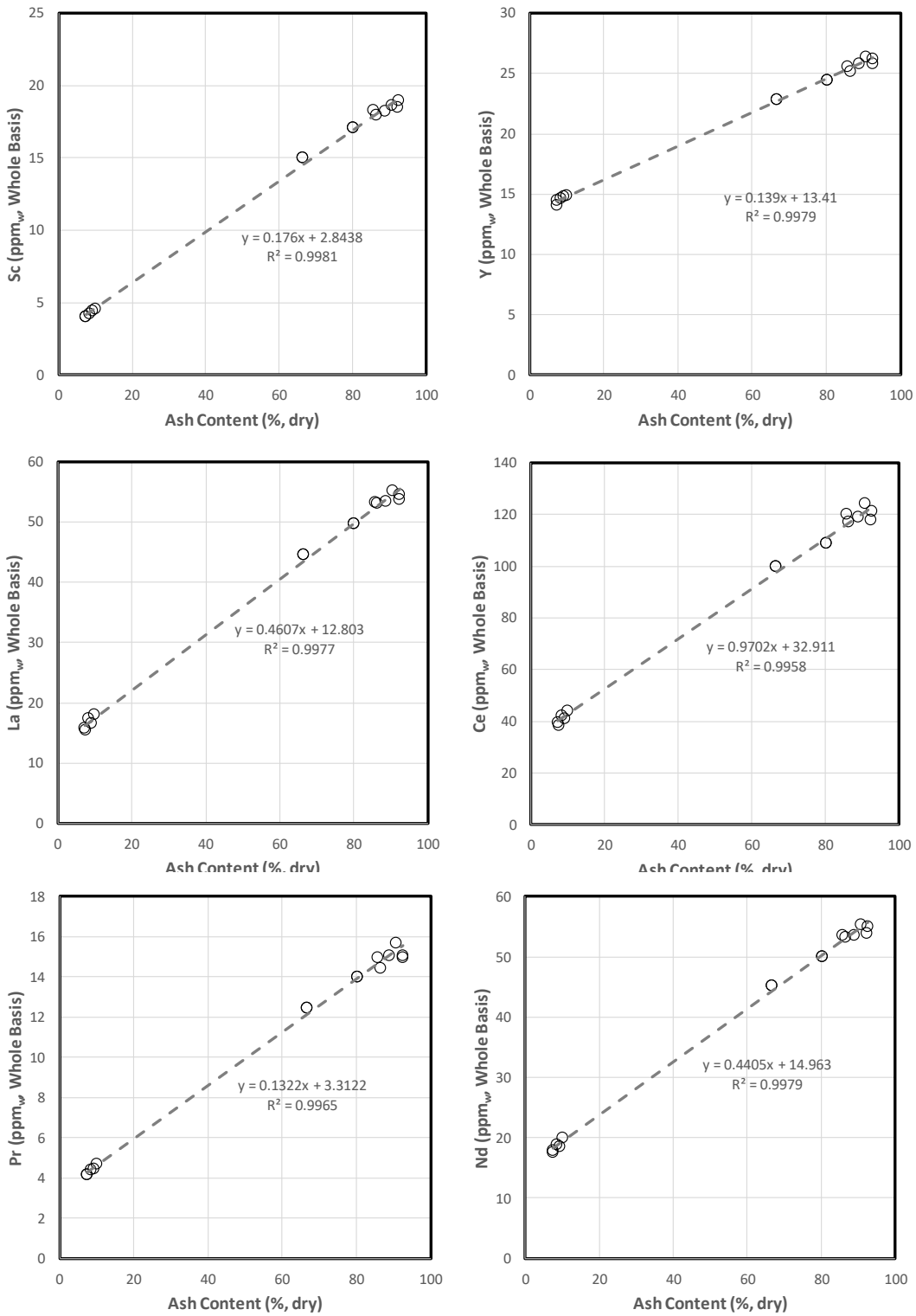

Figure 3.5.85. Element concentration versus ash content for selected elements.

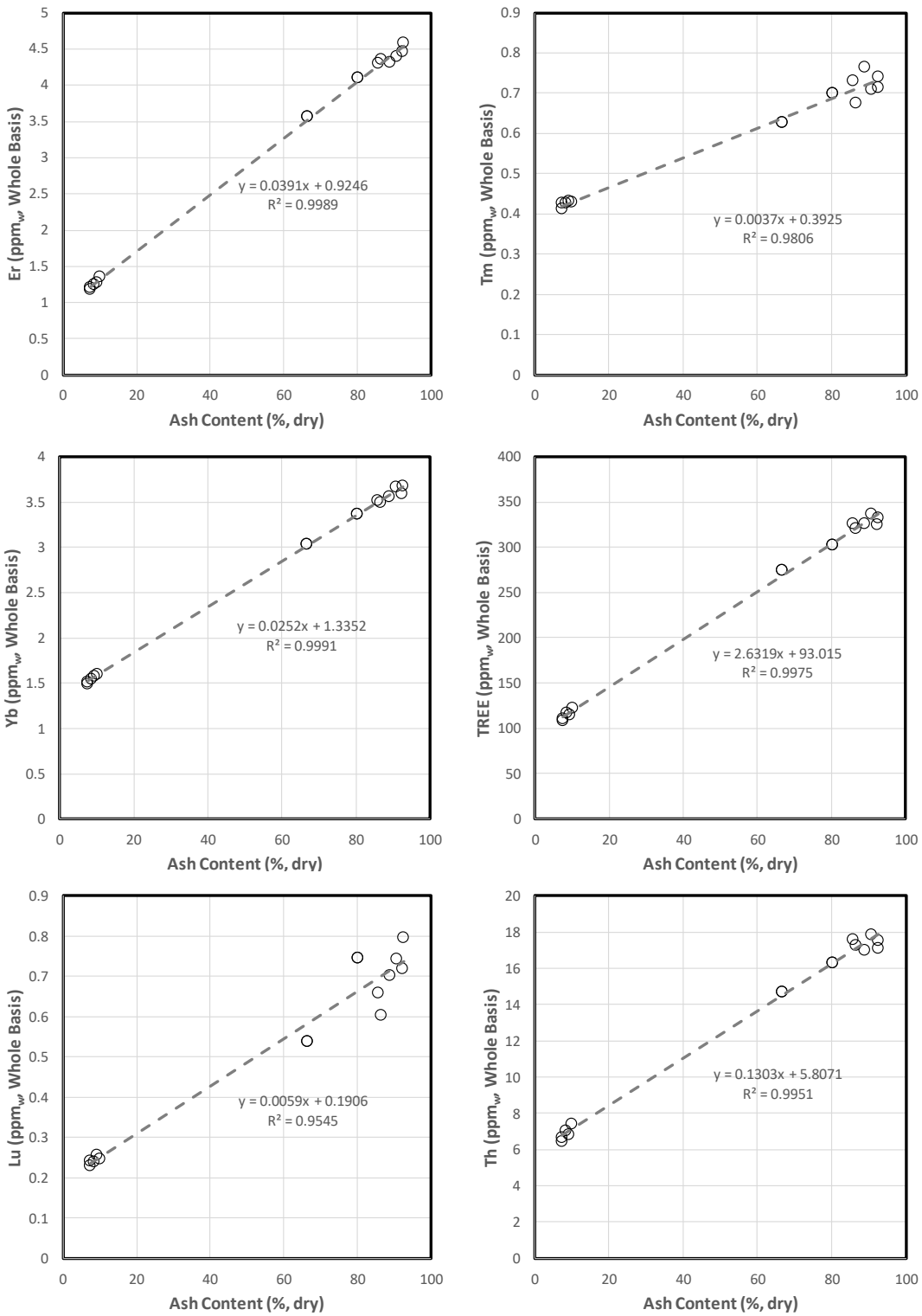

Figure 3.5.86. Element concentration versus ash content for selected elements.

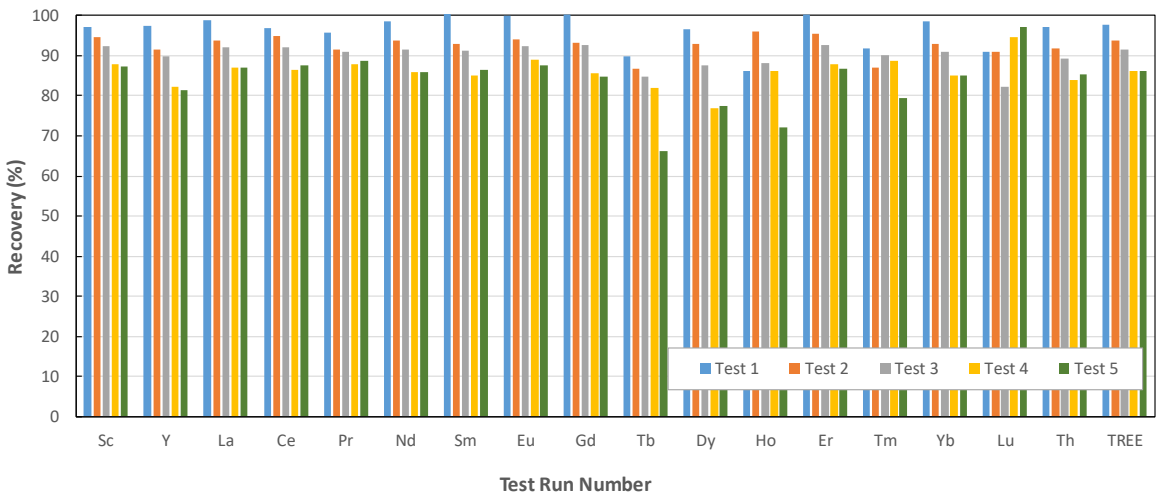

Figure 3.5.87. Element-by-element recoveries achieved during decarbonization testing.

A final noteworthy observation from the data collected from the detailed testing of the HHS process is that the recoveries of individual REEs to the ash-rich product stream remained very high in all test runs. Element-by-element recoveries, which are plotted in Figure 3.5.87 for each of the five test runs, show that >85-90% recoveries of REEs were achieved for every element during the decarbonization step. As a result, the total concentration of REEs were all well above 300 ppm_w (whole-basis) after HHS processing.

3.5.9.3 Batch HHS REM Recovery Testing

Coincident with the pilot-scale construction and testing, batch laboratory-scale HHS tests were conducted to determine the optimal reagent dosages, grind sizes, and other experimental parameters needed to optimize the REM recovery process. Figure 3.5.88 shows the various experimental apparatuses used in these tests, while Figure 3.5.89 shows the flowsheet utilized for the majority of the tests. Depending on the test procedure, samples were first ground in a laboratory attrition mill to reach a target particle size for the test. Grinding times varied from 30 minutes to several hours, while the resultant particle sizes typically varied from 35 to <5 microns. After grinding, the fine goal conditioned with the appropriate reagent mixture and then mixed with the hydrocarbon with high agitation in a commercial kitchen blender. This high shear mixing induces agglomerate formation, which is then followed by a lower speed mixing with an overhead blender. Lastly, the contents of the blender are transferred to separatory funnel where they hydrocarbon and water phases are separated creating a concentrate and tailings product.

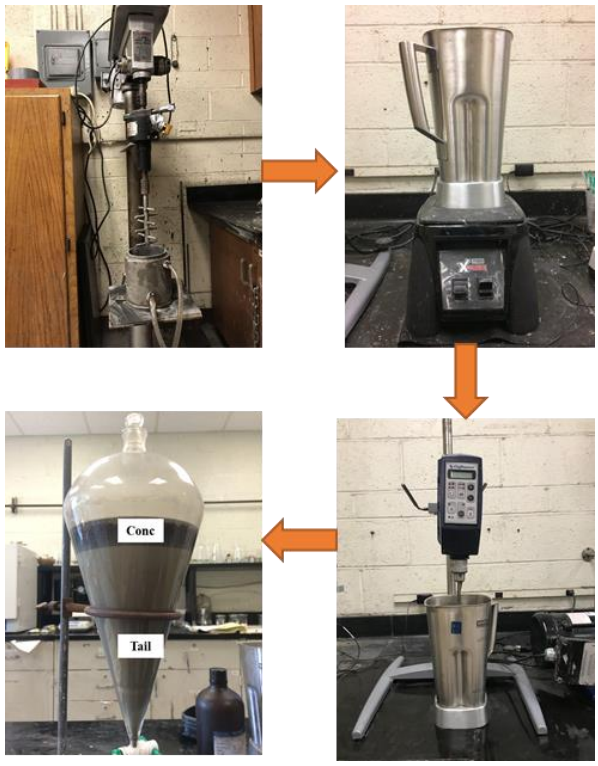

Figure 3.5.88. Experimental Apparatus used in laboratory-scale HHS testing.

The flowsheet utilizes for the tests included several stages of scavenging and cleaning as depicted in Figure 3.5.89. Additional hydrophobizing and dispersing agents were also added at various locations in the circuit. In all tests, the Fire Clay thickener underflow material was utilized.

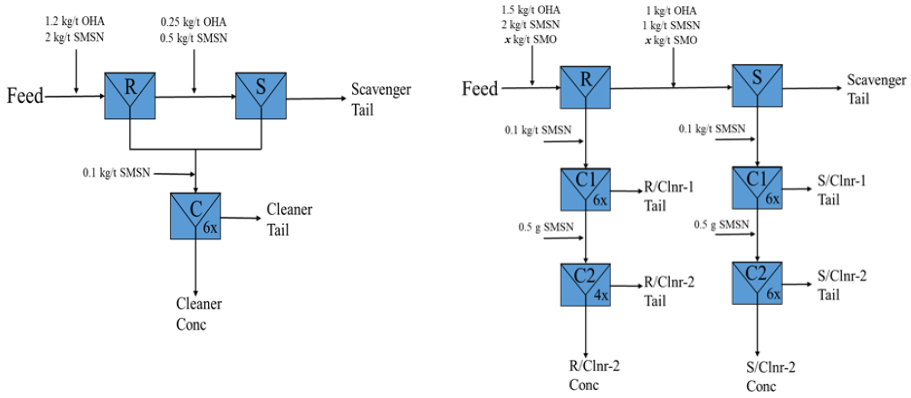

Figure 3.5.89. HHS flowsheet used for laboratory-scale testing.

Figure 3.5.90 through Figure 3.5.93 show the influence of several operating parameters on flotation performance, i.e. the effect of particle size (Figure 3.5.90), the effect of a polyelectrolyte dispersant (Figure 3.5.91), the effect of a hydrophobicity enhancing agent (Figure 3.5.92), and the effect of sample aging (Figure 3.5.93). In all cases, the results show an inverse relationship between sample grade and recovery, as the highest grade products were usually produced lower

recovery values. Nevertheless, the process intensifications and additions were typically successful at increasing recovery and grade. For example, grind size was shown to have a significant impact on recovery and grade, as decreasing the particle size from 35 microns to 3.9 microns produced an increase in recovery from approximately 5% to 40%, while increasing the grade from 3500 ppm to nearly 9000 ppm (Figure 3.5.90). Modest dosages of sodium silicate (5 kg/t) and SME (0.9 kg/t) were also shown to produce similar improvements (Figure 3.5.91 and Figure 3.5.92, respectively).

Interestingly, Figure 3.5.93 also suggest that sample age may influence the grade and recovery of REM products. By testing the same sample under the same conditions after various degrees of aging, the research team observed deteriorating performance over time. After 5 months of storage, the REE recovery values were found to be extremely low, <5% for all data points. Following this result, the team made an intentional effort to only test fresh samples with aging times less than one month. New samples were thus periodically requested from our industrial partners over time.

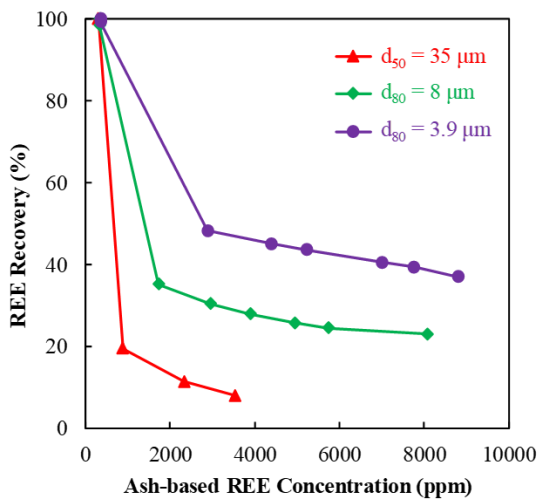

Figure 3.5.90. Effect of grind size on REE recovery and grade in laboratory-scale HHS process.

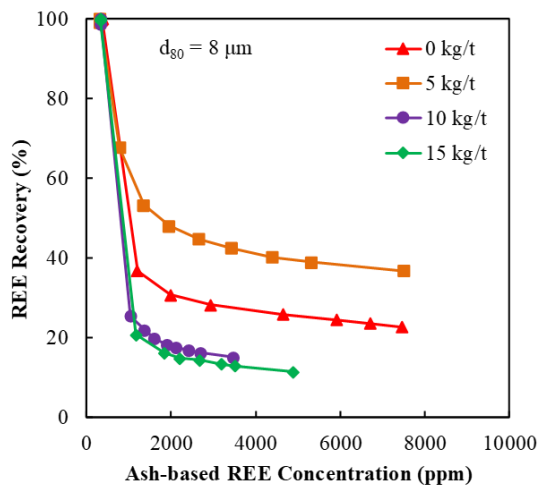

Figure 3.5.91. Effective of sodium metallicate dosage on REE recovery and grade in laboratory-scale HHS process.

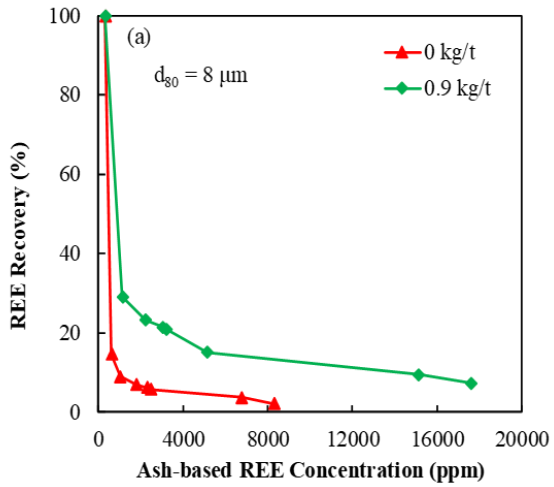

Figure 3.5.92. Effect of sorbitan monooleate (SMO) dosage on recovery and grade in laboratory-scale HHS process.

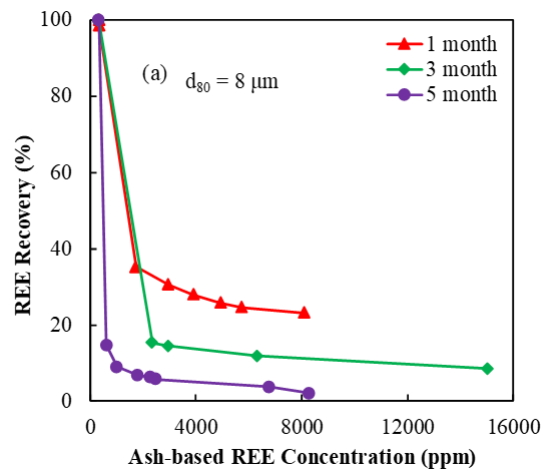

Figure 3.5.93. Effect of sample aging on recovery and grade of laboratory-scale HHS process.

The optimal results from the HHS tests were compared to that of column and conventional flotation, all conducted in the laboratory-scale. Figure 3.5.94 shows these comparisons both has recovery versus grade and as HREE/LREE ratio versus grade. The data clearly shows that HHS is superior to flotation for fine particle separation. Not only was the HHS process able to produce a maximum product grade nearly 3-4x that of flotation, but it also consistently showed higher recovery.

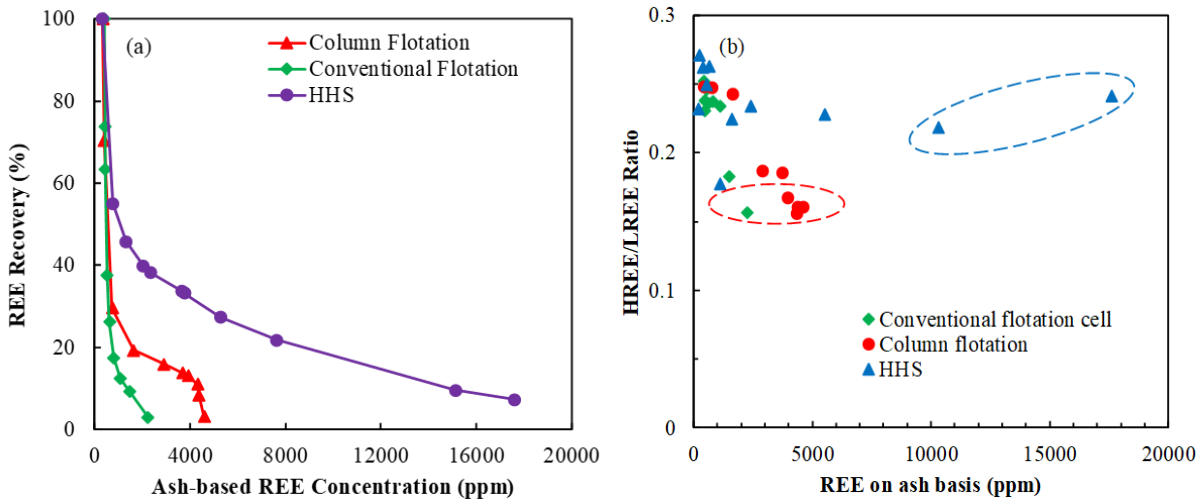

Figure 3.5.94. Comparison between column flotation, conventional flotation, and the HHS process on REE recovery.

The cumulative results from all laboratory-scale HHS REM recovery tests conducted in this project are shown Figure 3.5.95. This data includes tests conducted at a variety of chemical conditions and grind sizes, including those with and without hydrophobicity enhances, activators, depressants, and other modifiers. As such, there is a large variation in the results with recoveries varying from <5% to >40% across all cases. Likewise, the product grade varied from around 4,000 ppm to nearly 18,000 ppm on an ash basis. This represents a significant increase from the feed content, which typically varied from 250 to 300 ppm on an ash basis.

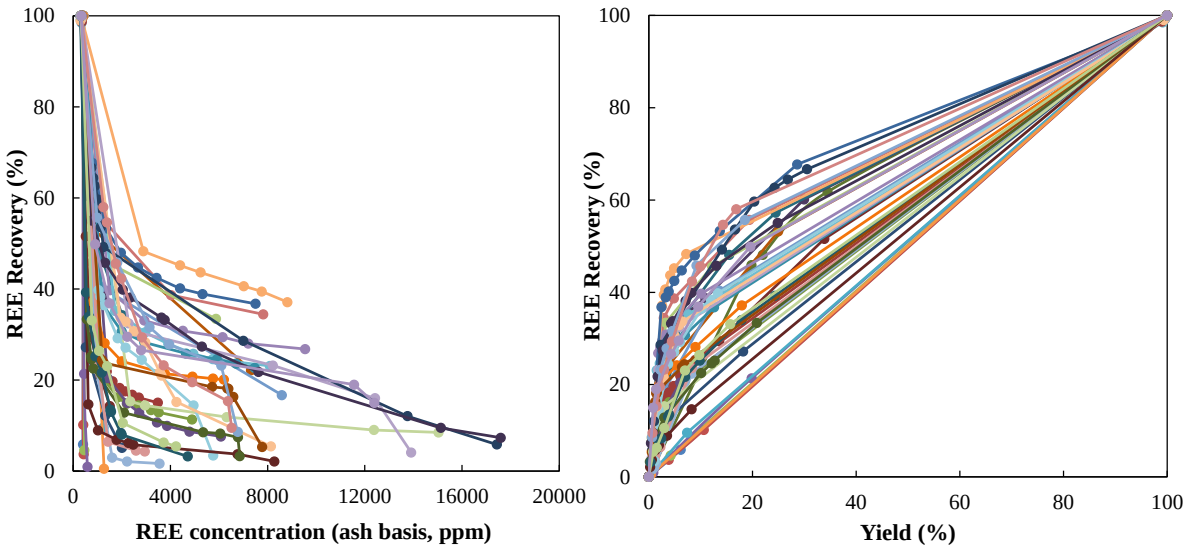

Figure 3.5.95. Summary of all laboratory-scale HHS trials

For the highest grade samples assaying nearly 18,000 ppm, a microscopic study was conducted to evaluate the morphology and composition of the HHS concentrate product. SEM backscatter images as well EDX spectra collected from this study are shown in Figure 3.5.96 and Figure 3.5.97. The SEM image shows a high prevalence of fine (<10 micron) well-liberated particles. The concentrate contained a high number of REM particles, with a broad surface scan showing approximately 1% of the area fraction being occupied by REE particles. EDX analysis of individual particles showed that Ce, La, Nd, and in some instances, Th were all strongly associated with P. While this finding suggests that the REM particles are monazite, the mineralogy cannot be confirmed by SEM-EDX alone.

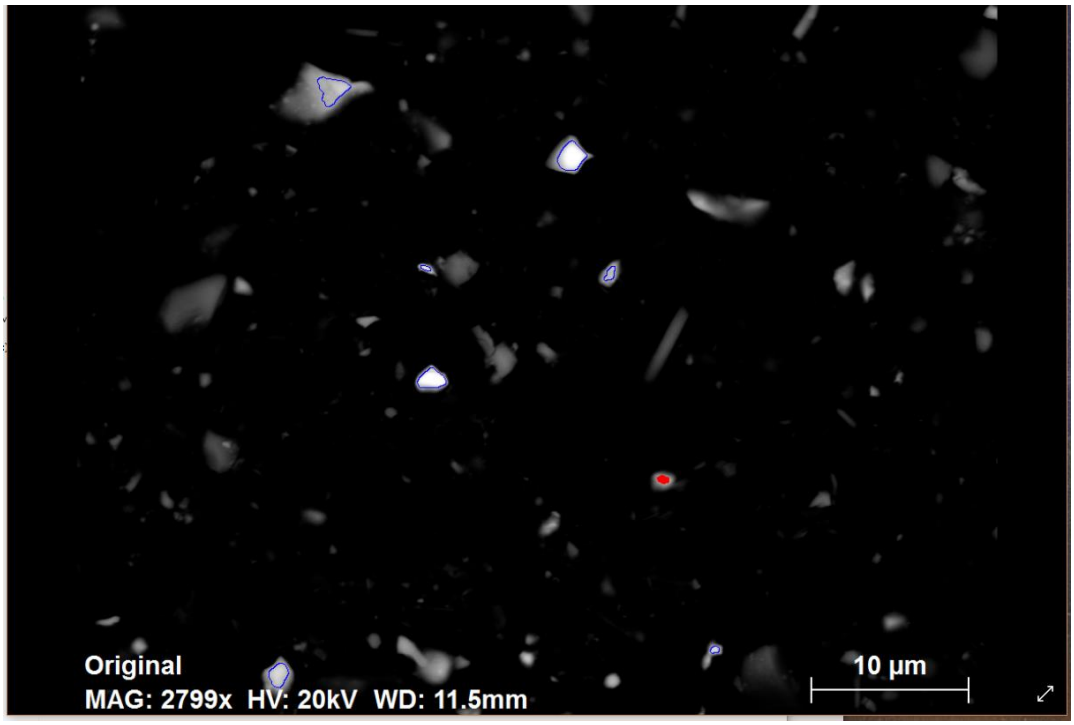

Figure 3.5.96. SEM micrograph of high grade REM product from HHS concentration tests. Lighter areas are indicative of higher atomic numbers.

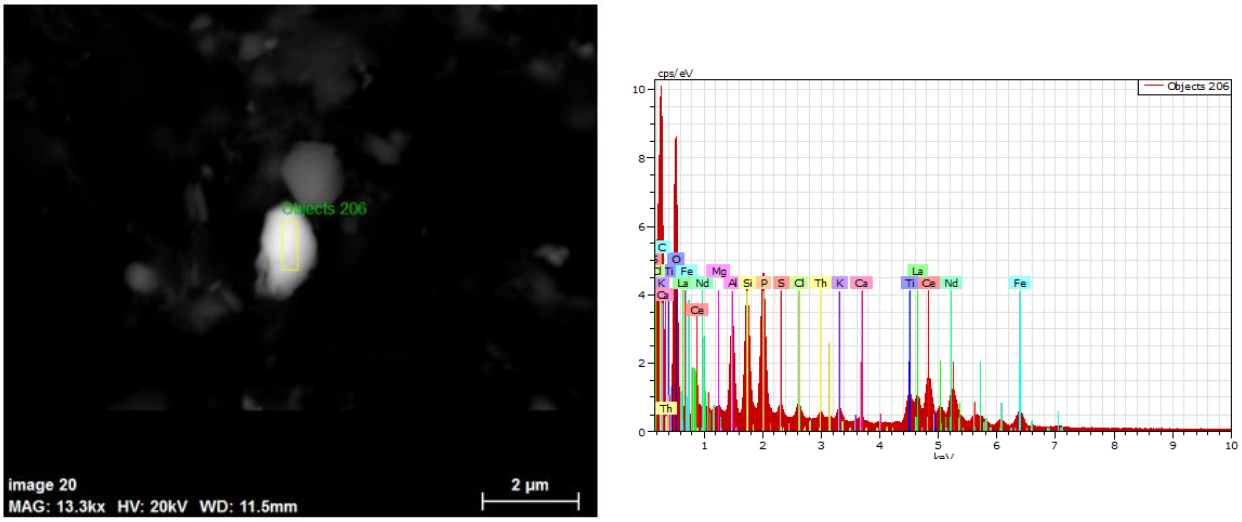

Figure 3.5.97. SEM micrograph and corresponding EDX spectra for high grade REM product from HHS concentration tests.

In a follow on study, one of the REM particles was further analyzed by TEM and diffraction (Figure 3.5.98). EDX spectra from the REE bearing phosphate show the presence of a significant fraction of Al which is usually not present in monazite or apatite. Sr is also present. The lattice spacings measured from diffraction patterns were not found to be a good match for monazite or apatite and the difference is too large to simply be attributed to measurement error. However, from

EDS spectrum and diffraction pattern the best match is svanbergite/florenciate, an aluminum phosphate mineral that replaces apatite in acidic, sulfur rich environments. While this finding only applies to a single REM particle and is not necessarily indicative of the bulk, it does suggest that some uncommon REM species may be present in the coal measures.

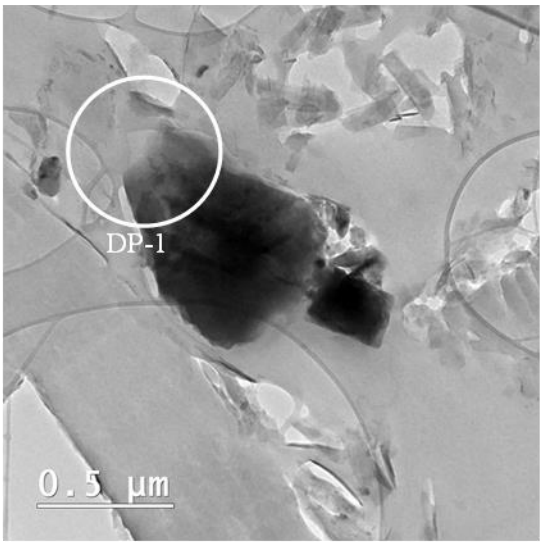

TEM micrograph, phosphate with REE. The diffraction pattern DP-1 was acquired from the area marked by the white circle.

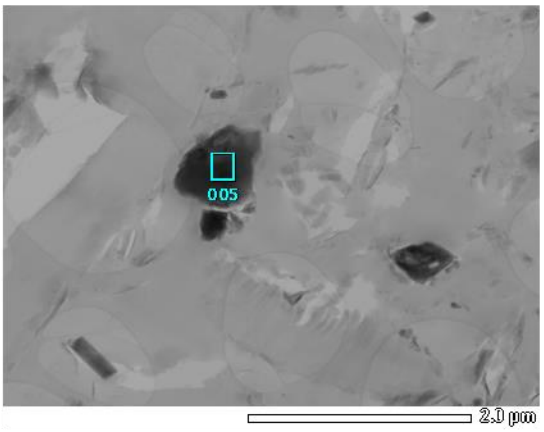

STEM image of the same grains. Note 90 degree rotation. Square shows location of EDS

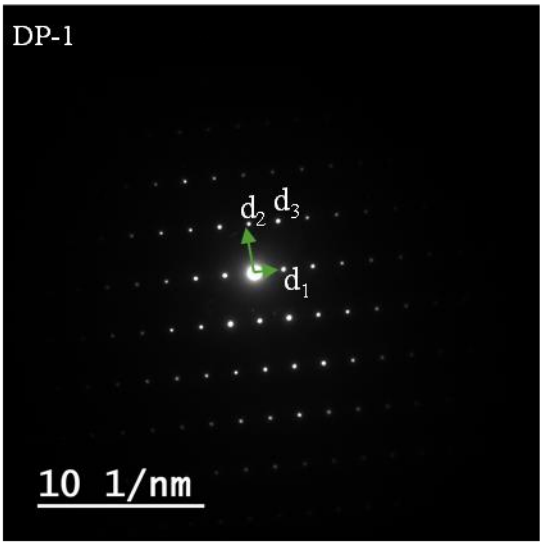

Lattice spacing measured: d1=0.56 nm; d2=0.342 nm; angled1 d2=90; d3=0.292 nm

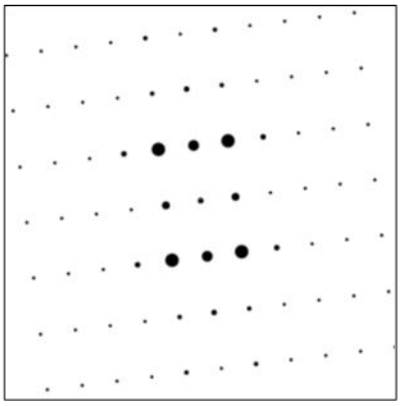

Simulation of the diffraction pattern of svanbergite along [-110]

Figure 3.5.98. TEM and diffraction analysis for high grade REM product from HHS concentration tests.

3.5.9.4 Semi-Continuous HHS REM Recovery Testing

Pursuant to the original project objectives, the mobile HHS process was designed to operate in two steps. In the first step, the discarded coal feed obtained from one of the participating sites was decarbonized. The product from this step is a low-ash, low-moisture saleable coal. Next, the tailings would be conditioned with appropriate chemicals to render the rare earth minerals (REMs) hydrophobic. This material would then be processed through the HHS trailer again to concentrate the REMs for further processing through leaching/solvent extraction to obtain a final REM product. The aim of this task was to produce a bulk REM concentrate using the HHS process.

The test samples were obtained from the thickener underflow stream produced when the Leatherwood plant was primarily treating run-of-mine coal from the Fireclay seam. This sample contained about 66% ash and a significant amount of coarse material (>150 microns) similar to the previous samples. Since the current HHS mobile unit is designed to handle particle sizes smaller than 150 microns, the fresh sample was screened using a fine wire sieve screen to a top size of 150 microns to prevent plugging and other operational issues. The sample was also diluted to 8% solids (by weight) before the test run. The results of the test run are given in Table 3.5.26. As can be seen, the coal product contained only about 5% ash and 9% moisture, while the recovery of organics was high at about 97%. These results are in line with the ones obtained in previous reporting periods using the packed extraction column Morganizer. Although the oscillating column used in this run was not fully optimized, it was still able to produce a high-quality coal product. This result is very encouraging, because the oscillating column is highly unlikely to plug in any condition compared to the easier plugging nature of the extraction column.

Table 3.5.26. Decarbonization data from the HHS test run using Leatherwood thickener underflow samples

	Mass	**Ash**	**Mineral**	**Moisture**	**Distribution (%)**	
	(%, dry)	**(%, dry)**	**(%, dry)**	**(%)**	**Ash**	**Organic**
ROM Feed	100.0	66.0	71.3	-	100.0	100.0
Coal Product	29.6	5.1	5.5	8.8	2.3	97.4
REE Product	70.4	91.6	98.9	-	97.7	2.6

The next task after the decarbonization run was to perform a second run through the HHS process for obtaining a bulk REM concentrate. Because the REMs are finely disseminated within the ash bearing minerals, grinding to a fine size is essential to liberate the REMs for further processing. So, the tailing material from the decarbonization step was ground using an attrition mill to obtain a material containing about 80% passing 9 microns. This material was then placed in a mixing tank and was conditioned with the hydroxamate reagent for about 45 minutes to ensure all REM material was hydrophobized. Next, the conditioned sample was processed through the low shear and high shear mixing stages of the mobile HHS process to form REM agglomerates. Normally, this material would be sent to the primary flotation machine for phase separation, where agglomerates are separated from the rest of the material. However, the amount of REM agglomerates formed at this stage was so low compared to the coal agglomerates that are normally formed, it wasn't possible to process this material through the rest of the mobile unit. Therefore, it was decided to finish the process in the lab using a previously constructed lab scale continuous HHS testing rig. Since the phase separation could not be completed using the flotation machine on

the mobile pilot plant, the material was transferred to a small tank where the water that contained unwanted minerals was simply drained from the bottom of this tank. The leftover material containing REM agglomerates was then stored in sealed 5-gallon buckets for further processing in the lab.

To assess the leachability and REE mode of occurrence before and after REM concentration, a seven step sequential extraction process was conducted on the decarbonized thickener underflow after the first stage of HHS processing. Test results from sequential extraction showed that a large portion (>50%) of the extractable REEs were bound with carbonates and leachable with 0.11 M acetic acid. Unfortunately, the overall leachability of the REEs was quite low, perhaps indicating deficiencies in the specific sequential extraction methodology that was utilized.

Given REEs content in the feed is only ~300 ppm on an ash basis, it would be very difficult to produce a REMs product in the HHS pilot plant without the supply of a very large quantity of feed. Therefore, the original strategy of using the HHS pilot plant to recover REMs was modified to use the pilot plant to produce a high-grade REMs pre-concentrates that could be further processed in a lab-scale HHS testing unit. Figure 3.5.99 represents the flowsheet of the semi-continuous pilot-scale HHS test for pre-concentrating REMs. In the test, 25 gallons of the ground feed containing approximately 5% solids was conditioned in a barrel using a portable agitator for 30 min at pH = 9.5 in the presence of 2 kg/t sodium silicate and 1.5 kg/t octyl hydroxamic acid as a dispersant and a collector, respectively. The hydrophobized slurry was then fed to the high-shear centrifugal pump (¾ HP) at a flow rate of 0.25 GPM, in which the slurry was mixed with the injected iso-hexane (400 ml/min) at 3600 RPM to allow for the hydrophobized REMs particles were collected by the small droplets of oil in the form of an oil-in-water Pickering emulsions. The pump discharge pressure was regulated at 20 psi using a ball valve and the high-shear retention time was set at 12 mins by maintaining the active volume of the slurry sump at 3 gallons. Thereafter, the oil-slurry mixture produced in the high-shear loop was further conditioned in a low-shear tank at 900 RPM for 24 mins. After allowing the mixture to stand for phase separation, the aqueous phase at the bottom of the low-shear tank was removed, while the o/w emulsions left in the tank was agitated along with a suitable amount of fresh water for 10 mins to remove gangue minerals entrained in the oil phase.

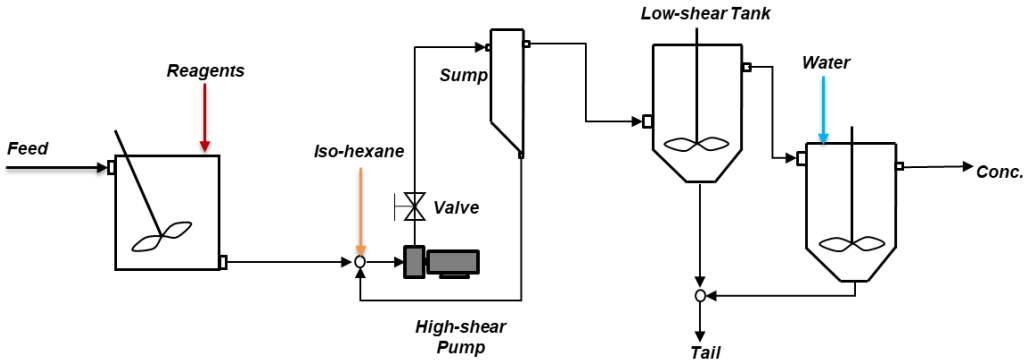

Figure 3.5.99. HHS flowsheet for the recovery of REMs

Parametric testing of the HHS process to produce high-grade rare-earth mineral (REM) concentrates continued throughout the reporting period. Fresh feed samples for these tests were collected from the thickener underflow from the Leatherwood coal preparation plant in Kentucky, USA. The samples were first decarbonized in the HHS pilot plant at Virginia Tech. The decarbonized material was determined to be 90.4% ash with a total REE concentration of 603 ppm on dry, ash basis. For the REM concentration tests, octanohydroxamic acid (OHA) of >95% purity was used as a primary collector and reagent grade sodium metasilicate nonahydrate (SMSN) was used as a depressant for clay material. Sorbitan monooleate was used as a mixture with kerosene to enhance the hydrophobicity of the REM. Heptane was used as the organic solvent to generate agglomerates. The pH during reagent conditioning was controlled using hydrochloric acid and sodium hydroxide solutions. Tap water was used for dilution and during washing stages.

Prior to REM recovery with the HHS, the decarbonized material was ground in a laboratory attrition mill to ensure adequate liberation of the REMs from the host matrix. To achieve optimal performance in the attrition mill, the percent solids of the mill feed was set to 20-25% by weight. While this higher percent solids is necessary for grinding, the decarbonized product from the HHS was often much more dilute, in the range of 8 to 10% solids. To address this discrepancy, two methods were used to increase the solids density of the slurry. First, flocculant was used to increase the settling rate of the solids and secondly, samples was allowed to air dry for 4 days. These 2 slurry samples were then evaluated independently using the batch HHS process.

As has been reported earlier, the grain size of monazite in coal refuse of often below 5 microns. To promote adequate liberation, the decarbonized samples (~150g) were ground in a laboratory attrition mill (Union Process) for 1 hour to reduce the particle size. Grinding media in the mill included ¼ inch diameter stainless steel balls, and as mentioned above, the pulp density was maintained between 20-25%. The 80% passing size of the mill products after 1 hour for the two samples were 8.07 μm (flocculated feed sample) and 9.92 μm (air dried sample). HHS tests were then conducted on these samples.

In the HHS tests, approximately 1L of milled sample at (10-15% solids) was agitated at 600 rpm with 2 kg/t of SMSN for 5 minutes to disperse/depress gangue or clay minerals present. Next, 1.5 kg/t of OHA was added at a pH of 9.5, and the material was then conditioned for 5 minutes using a high shear blender. After the initial conditioning, 1.5 kg/t of SMO was added to the mixer and agitated for 10 minutes. SMO is intended to increase the hydrophobicity of REE bearing particles and promote rapid agglomeration. After completing the reagent addition steps, 400 mL of heptane was then added and subjected to a low-shear mixing for 5 minutes for the formation of oil-in-water (o/w) emulsions where oil was preferentially attached to the hydrophobized REMs. For reporting purposes, this stage of conditioning was referred to as the rougher stage. After these steps, the mixture was transferred to a 3L separatory funnel and allowed to stand for approximately 5-10 minutes for phase separation. The aqueous phase was removed as tails and was subjected to the similar conditioning process to recover additional REE-bearing particles.

In the oil phase, the oil drops coalesce and produce oil-water-oil emulsion, which can be subjected to wash water to remove the entrained hydrophilic gangue particles. In this cleaner stage, fresh water was added with SMSN to the o/w/o emulsions and shaken. The water was then drained

by gravity after the phase separation was achieved. The wash water in this stage collected gangue particles and cleaned the concentrate. This process was repeated until the drained water became clear indicating the removal of all entrained gangue particles. The final concentrate was denoted as rougher-cleaner concentrate. The tailings generated in each wash stage were combined and denoted as rougher-cleaner tails.

The aqueous phase collected from the rougher stage was subjected to additional processing stage, herein denoted as the scavenger. The aqueous reject was first conditioned in a manner similar to that of the rougher stage, albeit with a reduced dosage of reagents. Here, 1 kg/T of SMSN, OHA and SMO were used in this conditioning step. After the phase separation in the separatory funnel was achieved, the aqueous phase was removed as scavenger tails and the oil phase was subjected to the cleaning stage. In order to enhance the oil-water-oil emulsion, a small amount of SMO ($8x10^{-4}$ M) was added to the oil phase. Washing was conducted in a manner similar to that of the rougher-cleaner stage, and the product was denoted as scavenger cleaner concentrate. As in the prior cycle, the tailings generated in each wash stage were combined and named as scavenger cleaner tails. Figure 3.5.100 shows the flowsheet of the HHS tests conducted.

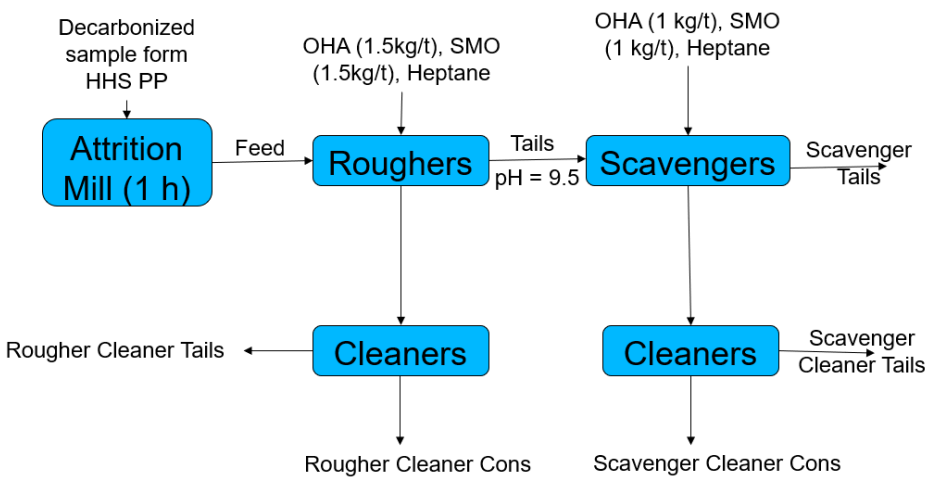

Figure 3.5.100. Flowsheet of the HHS batch scale process

Table 3.5.27 shows the results of the HHS tests done with the first sample (with Floc Feed) and second sample (with air drying). The maximum amount of REM concentrate grade attained was in scavenger cleaner concentrate from the second test and it was 0.94%. This shows a concentration increase of approximately 15 times (0.06% in the feed) in the final concentrates. The overall recoveries were calculated by combining rougher-cleaner concentrates and scavenger cleaner concentrates.

Table 3.5.27. Batch HHS REM Concentration Test Results

Sample ID	REE Concentration ash basis, ppm	
	Test #1 (Flocculant)	**Test #2 (Air-Dried)**
Feed	603.0	603.0
Rougher Cleaner Concentrate	2,333.4	3,563.3
Scavenger Cleaner Concentrate	2,860.3	9,405.2
TREE Recovery	0.64%	3.03%

3.6 Test Plan Revision (PB3-Task5)

3.6.1 Hydrometallurgical circuit

A revised test plan was developed to reflect new knowledge gained during process shakedown, startup, and exploratory testing. Two key factors required modification of the test plan for the leach circuit testing and downstream purification studies. The first factor was the integration of roasting into the process circuit to pretreat the leach feed. The impact was the ability to reduce acid concentrations. The second significant impact on the test program was the removal of the solvent extraction circuit in place of the selective precipitation circuit which significantly reduced chemical cost and reduced the potential of negative environmental impacts. The revised test program for the leach circuit included changing the acid concentration range to 0.025M to 0.075M which represents an order of magnitude decrease in acid cost. These acid dosages were evaluated over a range in solid concentration in the leach tank from 10% to 20% by weight. Under each condition, the pregnant leach solution (PLS) will be processed to produce a high purity mixed rare earth oxide (REO) concentrate. Chemical consumption throughout the process circuit will be recorded from each test and used to identify the conditions that provide an optimum techno-economic outcome.

The most significant update dealt with the battery of parameters requiring evaluation in the acid leaching and multistage precipitation circuits. The key input parameters for these circuits were identified as:

- Solids Feed Rate (50, 75, 100 lb/hr)
- Volumetric Flow Rate (1 gpm)
- Acid concentration (0.025M to 0.5M)
- Leaching Temperature (25, 50, 75°C)
- Multistage precipitation pH (3.0, 4.5, 7.0)
- Redissolution pH (2.0, 2.5, 3.0)
- Oxalate precipitation pH (2.0-2.5)
- Oxalate dosage (3.2g/L-12.8g/L)

For the acid leaching circuit, the primary process response variables include:

- Acid Consumption (lb/ton)
- Power Consumption (kW/ton)
- REE Recovery (%)

- Contaminant Recovery (%)
- Elemental concentration in PLS (ppm)

For the multi-stage and selective precipitation circuits, the primary process response variables include:

- NaOH Base Consumption (lb/ton)
- HCl Acid Consumption (lb/ton)
- Power Consumption (kW/ton)
- Oxalic Acid Consumption (lb/ton)
- REE Recovery (%)
- Contaminant Recovery (%)
- TREO and Elemental Grade (%)

3.6.2 Mobile HSS Unit

The work with the HHS module involves the testing of various slurry slipstreams were produced by alternative technologies within the circuitry installed at the Dotiki pilot plant site. Test plans that involved the HHS process redirected to use the technology as an alternative pathway for (i) decarbonizing/dewatering the coal-laden feed slurry from the grinding and micronizing operations, (ii) further upgrading and dewatering of the coal-rich froth product from the decarbonization flotation column, and (iii) directly recovering and concentrating rare earth minerals such as monazite as part of the de-alkalinization step. Also, the HHS module was not designed as a fully linked component inside the pilot-plant area due to safety concerns associated with flammable liquids and explosive gases within the building structure.

3.7 Detailed Parametric Testing (PB3-Task6)

3.7.1 West Kentucky No. 13 Source

3.7.1.1 Detailed parametric study

Detailed parametric test was carried out to investigate the effect of acid leaching conditions on rare earth extraction, downstream processing efficiency and chemical dosages. Each continuous run followed the flowsheet as shown in Figure 3.7.1. The acid leaching was conducted in a 100-Gallon tank at 75 Celsius degree with various solid and acid concentrations.

i. *<u>Leaching</u>*

The parameters and leaching conditions are listed in Table 3.7.1 including the responding leaching pH which is a response of leaching solid concentration and acid concentration. Based on the previous report, the leaching circuit requires 2-4 hours to reach steady state, therefore, the leaching tests were conducted for at least 16 hours. The average TREE leaching recovery and leachate concentration at steady state are as shown in Table 3.7.2, including the downstream chemical consumption. Results show that with increasing acid dosage in terms of kg acid per ton of feed solid, the recovery increased, however, Figure 3.7.1 showed that not every gram of acid was used to extract RE from solids. Figure 3.7.2 and Figure 3.7.3 indicate that with increasing acid

dosage, the required dosage of NaOH and HCl for precipitation and redissolution increased. However, the elbow points in the figures indicate that 0.4 kg acid per gram of RE is the optimal dosage. Beyond 0.4 kg acid per gram of RE, every incremental gram of RE extracted result in exponentially increased amount of chemicals in the downstream process.

Table 3.7.1. Leaching conditions in parametric study with responding leaching pH.

Test Code	**Solid Feed (lb/hr)**	**Water (GPM)**	**H_2SO_4 (M)**	**Retention (h)**	**Duration (h)**	**Leaching Reactor**	**Leaching pH**
DTK-C1	50	1	0.05	2	26	1 Tank	2.64
DTK-C2	50	1	0.05	2	20	1 Tank	2.54
DTK-C3	50	1	0.05	4	16	2 Tank	2.2 / 3.0
DTK-C4	50	1	0.025	2	16	1 Tank	2.86
DTK-C5	50	1	0.075	2	19	1 Tank	2.45
DTK-C6	75	1	0.05	2	16	1 Tank	2.84
DTK-C7	100	1	0.05	2	16	1 Tank	3.01
DTK-C8	75	1	0.075	2	16	1 Tank	2.58

Table 3.7.2. Chemical consumption per gram of RE recovered under various leaching conditions.

Test Code	H_2SO_4 (kg/hr)	kg Acid/ ton of feed	TREE in Leachate (ppm)	TREE Recovery (%)	Chemical Consumption		
					kg Acid/g TREE	kg NaOH/g TREE	Liter HCl/g TREE
DTK-C1	1.1	45.42	11.86	36.05	0.42	0.12	0.101
DTK-C2	1.1	45.42	12.24	37.20	0.41	0.12	0.189
DTK-C3	1.1	45.42	8.75	26.60	0.57	0.24	0.428
DTK-C4	0.6	22.71	9.34	28.38	0.27	0.11	0.133
DTK-C5	1.7	68.13	14.38	43.71	0.52	0.17	0.226
DTK-C6	1.1	30.28	15.75	31.91	0.32	0.11	0.114
DTK-C7	1.1	22.71	14.76	22.43	0.34	0.10	0.113
DTK-C8	1.7	45.42	15.88	32.18	0.47	0.13	0.184

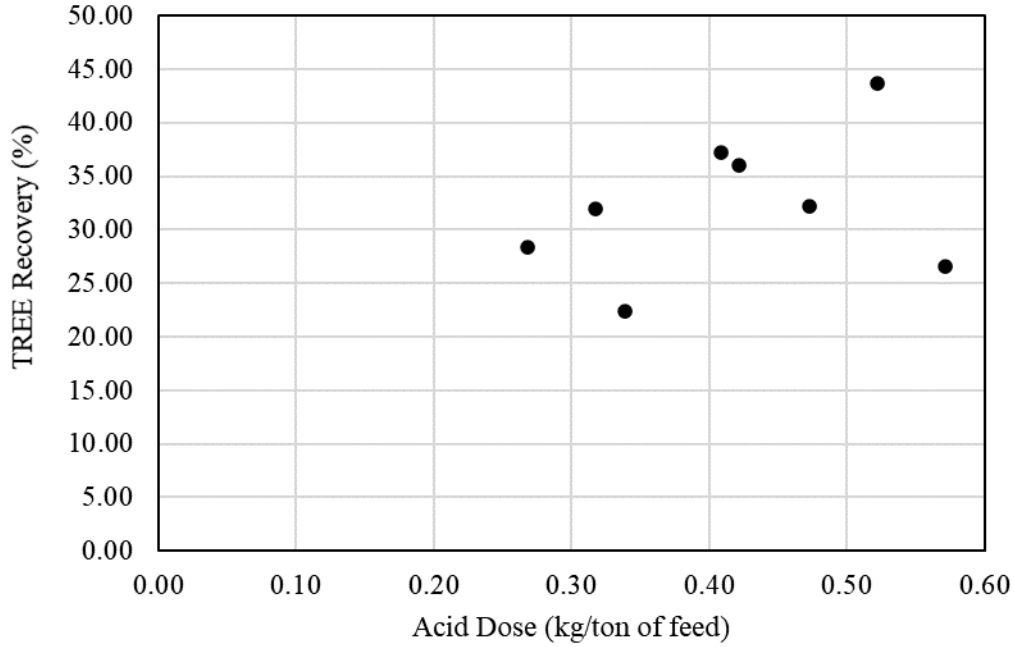

Figure 3.7.1. Effect of acid dosage on TREE recovery.

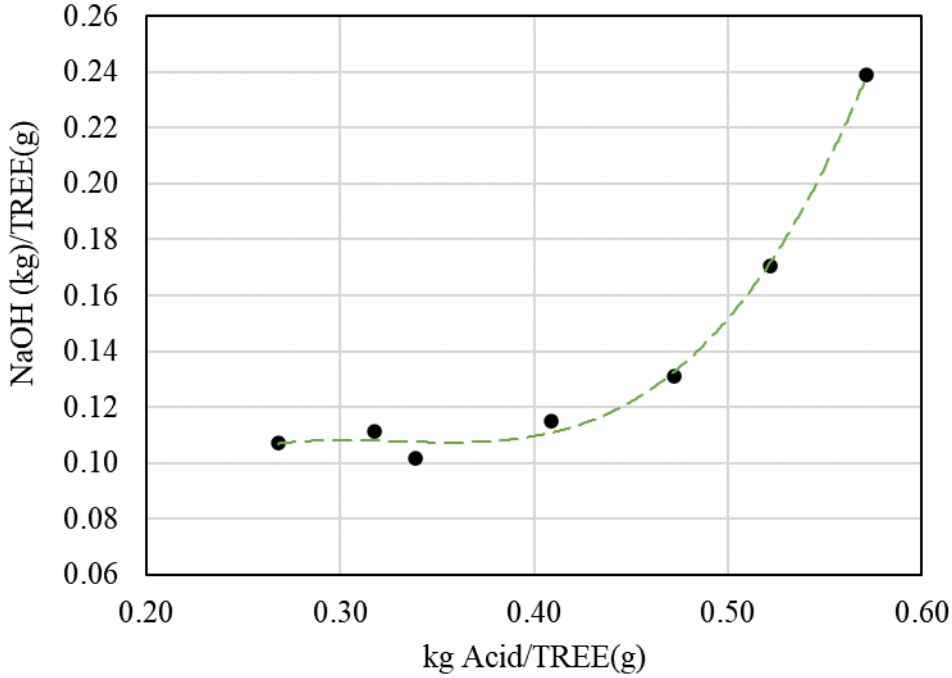

Figure 3.7.2. Effect of leaching acid dosages on NaOH consumption during RE precipitation.

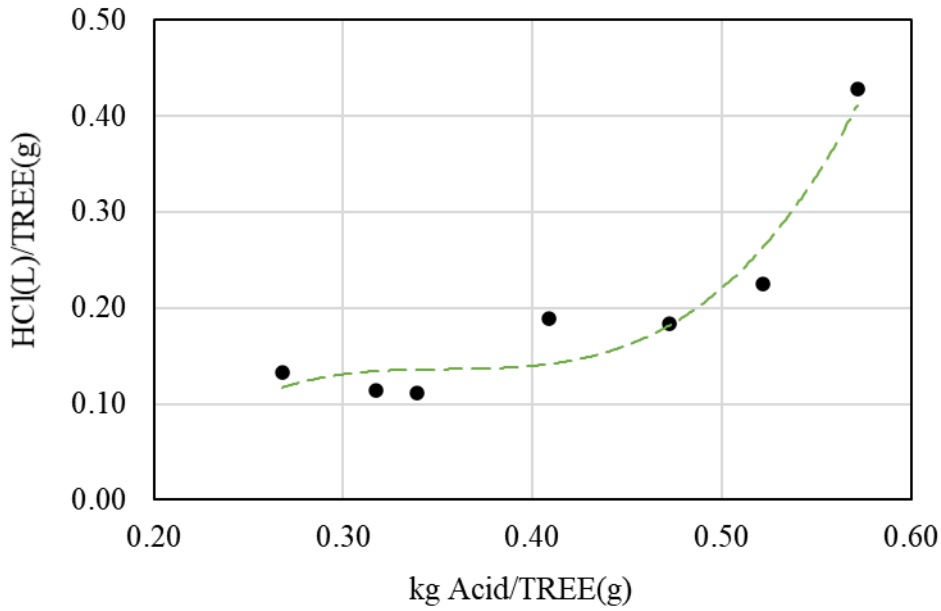

Figure 3.7.3. Effect of leaching acid dosages on HCl consumption during RE redissolution.

The effect of acid concentration and solid concentration is plotted as shown in Figure 3.7.4 and Figure 3.7.5. At solid-to-liquid ratio of 1/10 (w/v), the RE recovery achieved using 0.025M, 0.05M, and 0.075M acid were 29%, 38%, and 44%, respectively. The recovery of REEs did not increase proportionally with increasing acid concentration. However, the recovery of Al, Ca, and Fe increased stoichiometrically with increasing the acid concentration. Using acid concentration of 0.05M, the leaching recovery decreased with increasing solid concentration. The TREE recovery achieved using 0.05M acid at solid/liquid ratio of 1/10, 1.5/10, and 2/10 were 37.9%, 32.1%, and 22.6%, respectively.

The inefficiency is due to the reduced acid-to-solid ratio; therefore, the effect of acid dosage was analyzed by comparing leaching recovery under same acid-to-solid ratio. As shown in Figure 3.7.6, leaching using 45.4 kg acid per ton of solid, the TREE recovery achieved at S/L ratio of 1/10 and 1.5/10 were 37.9% and 32.4%, respectively; whereas using 22.71 kg acid per ton of feed solid, the TREE recovery at 1/0 and 2/10 solid-liquid ratio were 28.6% and 22.6%, respectively. Higher solid concentration resulted in higher ionic strength in solution, thus suppressed the hydrogen ion activity. It should be noted that the solid concentration has a significant impact on Ca recovery, which was observed in the laboratory tests as well. It indicates the formation of calcium sulfate during leaching process.

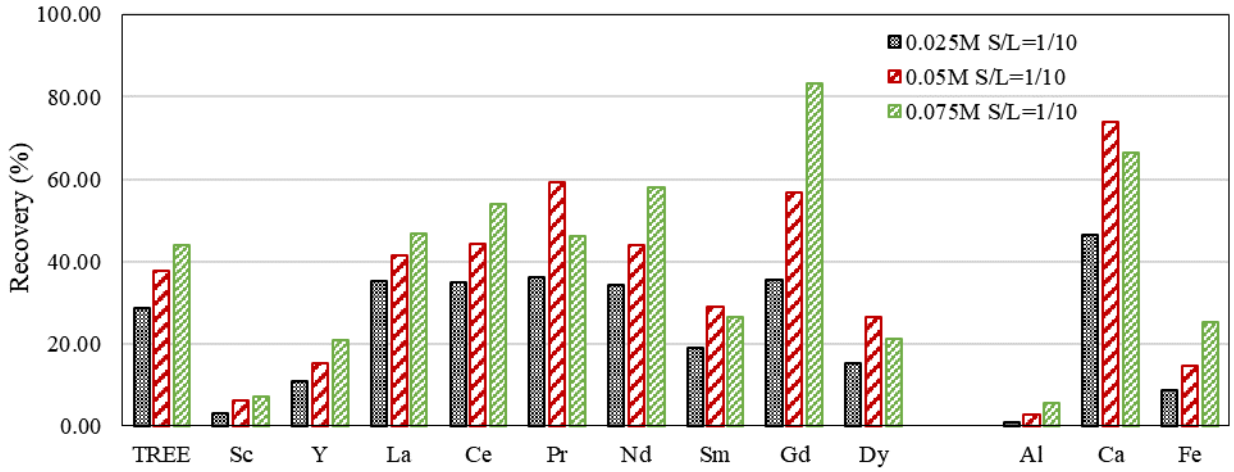

Figure 3.7.4. Effect of acid concentration on major REE and contaminants leaching recovery.

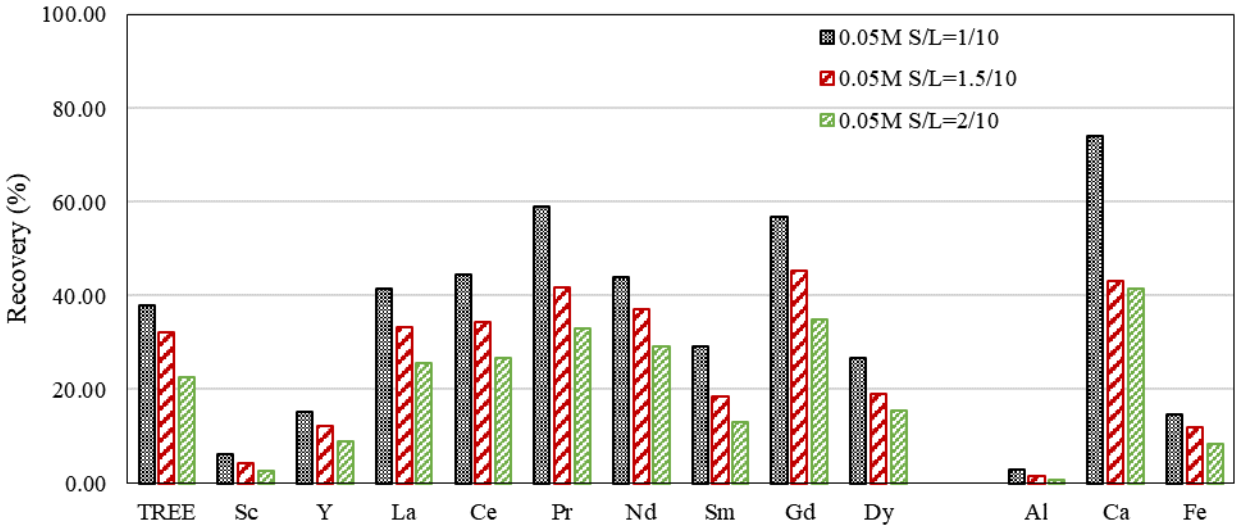

Figure 3.7.5. Effect of solid concentration on major REE and contaminants leaching recovery.

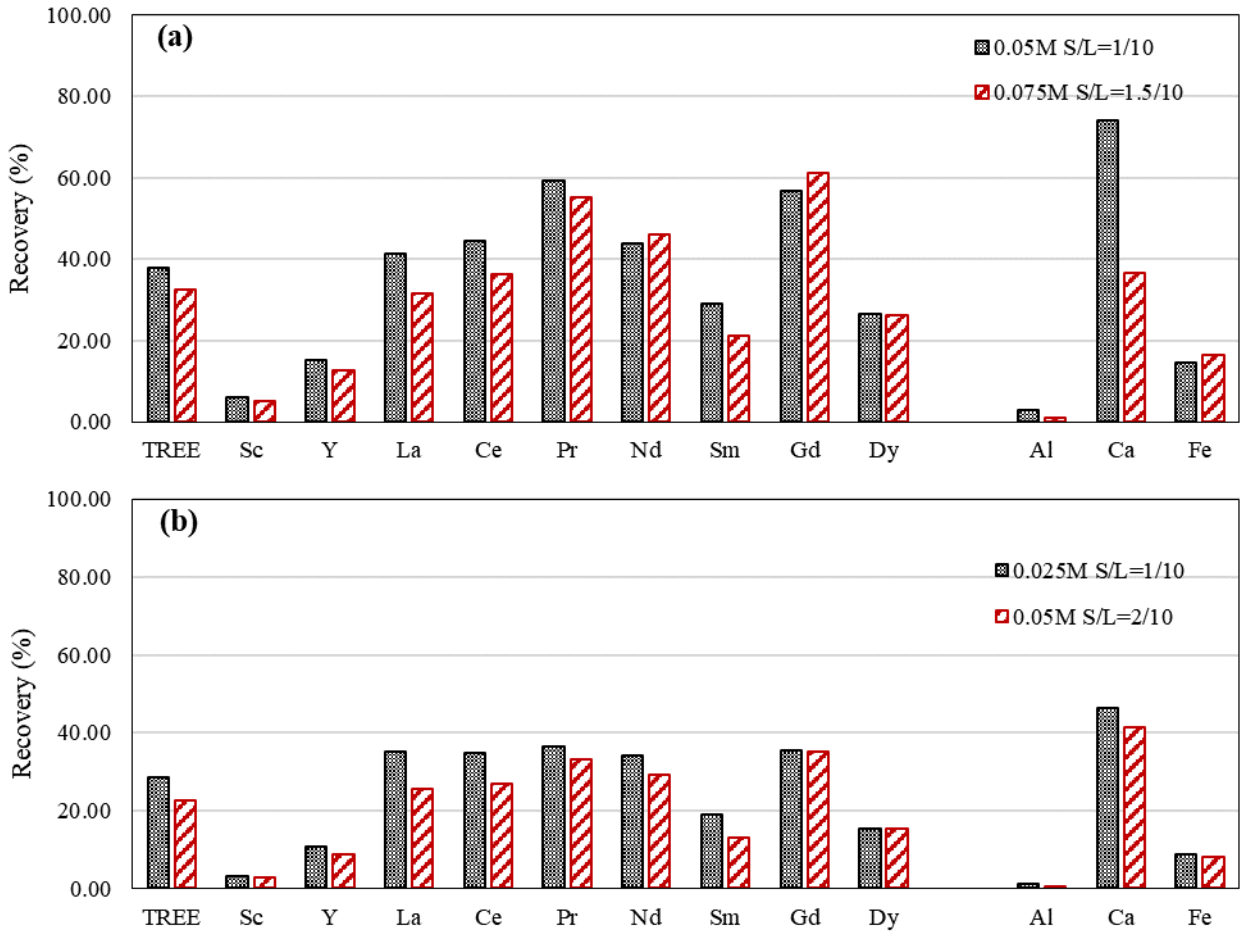

Figure 3.7.6. Effect of acid dosage in terms of kg acid/ton feed a) 45.42 kg acid/ton of feed; b) 22.71 kg acid/ton of feed.

ii. RE Precipitation

The precipitation process was operating simultaneously with acid leaching process in the pilot plant operation. The slurry was then filtered using a plate and frame pressure filter immediately to separate solid residue from REE pregnant leachate solution (PLS). The PLS was then transferred to a pH adjustment tank to precipitate REEs at pH 6.5, along with some other precious metal and contaminants. The average precipitation efficiency is as shown in Figure 3.7.7. Above 97% of TREE, 99% of Al, and 96% of Fe were precipitated regardless of the leaching condition. Small amount of Ca reported to the precipitate due to entrainment and co-precipitation. Precipitation efficiency of other critical elements of interest is also plotted. The results show that the precipitation pH of 6.5 is suitable for recovering over 90% of Co and Ni from PLS, whereas, for Li and Mn, the optimal precipitation pH required is higher.

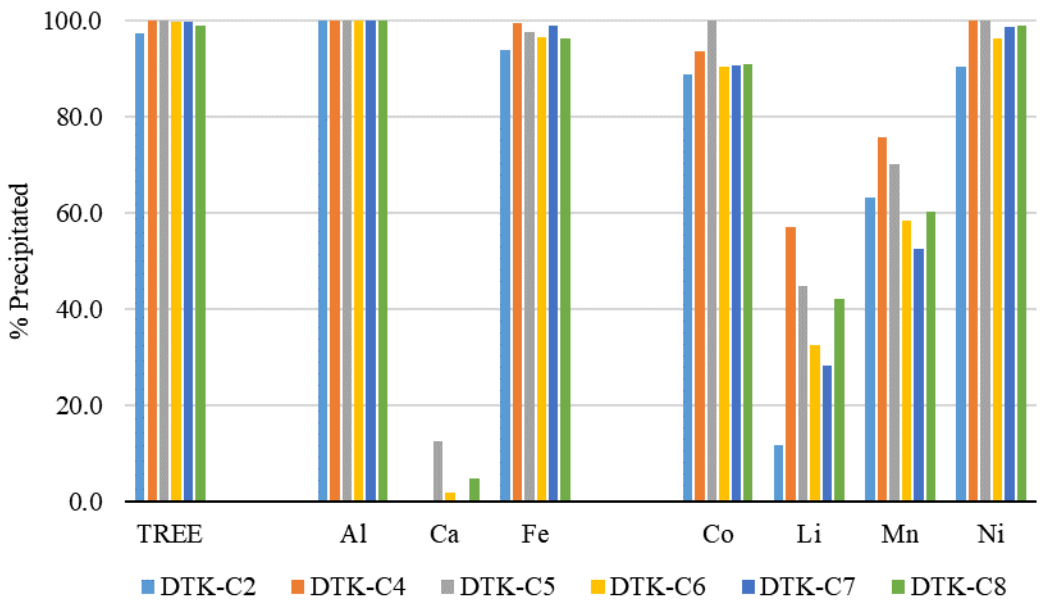

Figure 3.7.7. Precipitation efficiency of RE, major contaminants, and some critical elements at pH 6.5 using NaOH.

iii. <u>RE Redissolution</u>

The precipitate was filtered using a plate and frame pressure filter and then blended with water to homogenized. The precipitate filter cake was transferred into a 250 gallon tank and blend with 100 gallon water for 24 hours. After blending, the precipitate slurry volume was finalized at 200-gallon with additional water. Bench scale experiments were conducted to determine the dosage of HCl needed to bring down the pH value to 2.5. The calculated amount of HCl was then added into the blended precipitate slurry to dissolve REEs. The redissolution efficiency of RE, Al, Ca, Fe, and selected critical elements of interest is as shown in Figure 3.7.8. The result shows that the TREE redissolution efficiency is greatly associated with Al. Over 80% of TREEs were recovered from the precipitate cake produced from low solid concentration leaching, whereas the high solid concentration in initial leaching process has a significant impact on RE redissolution efficiency. Figure 3.7.9 shows the redissolution efficiency of individual RE under the impact of various solid concentration in leaching process. The results indicated that the leachate generated from high solid concentration leaching contained more ions that need to be redissolved in a more diluted system.

The application of multi-stage selective precipitation and redissolution was developed to gradually eliminate contaminant elements from the PLS. The efficiency of contaminant removal can be evaluated by tracking the contamination-to-RE ratio at each stage. Table 3.7.3 summarize the ratio of Al/RE, Ca/RE, and Fe/RE in each stage of the process. The results indicated that majority of Ca was eliminated in the RE precipitation stage, and most of the Fe was eliminated in the RE redissolution stage. Whereas RE migrates together with Al in the current two stages and can only be separated at the oxalic acid precipitation process.

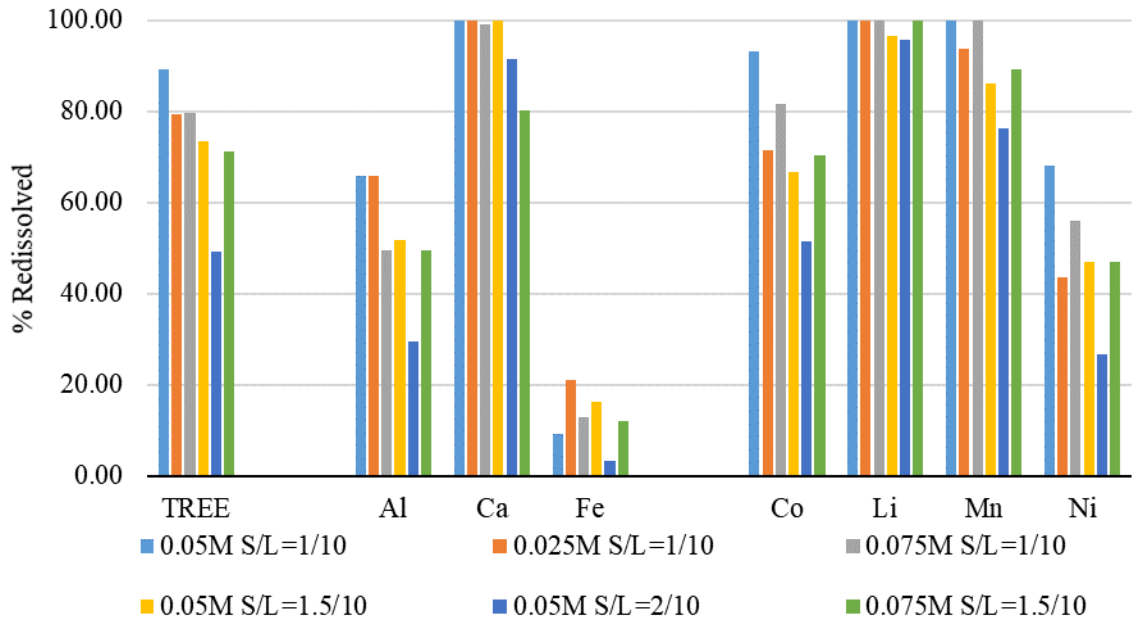

Figure 3.7.8. Redissolution efficiency of RE, major contaminants, and some critical elements at pH 2.5 using HCl.

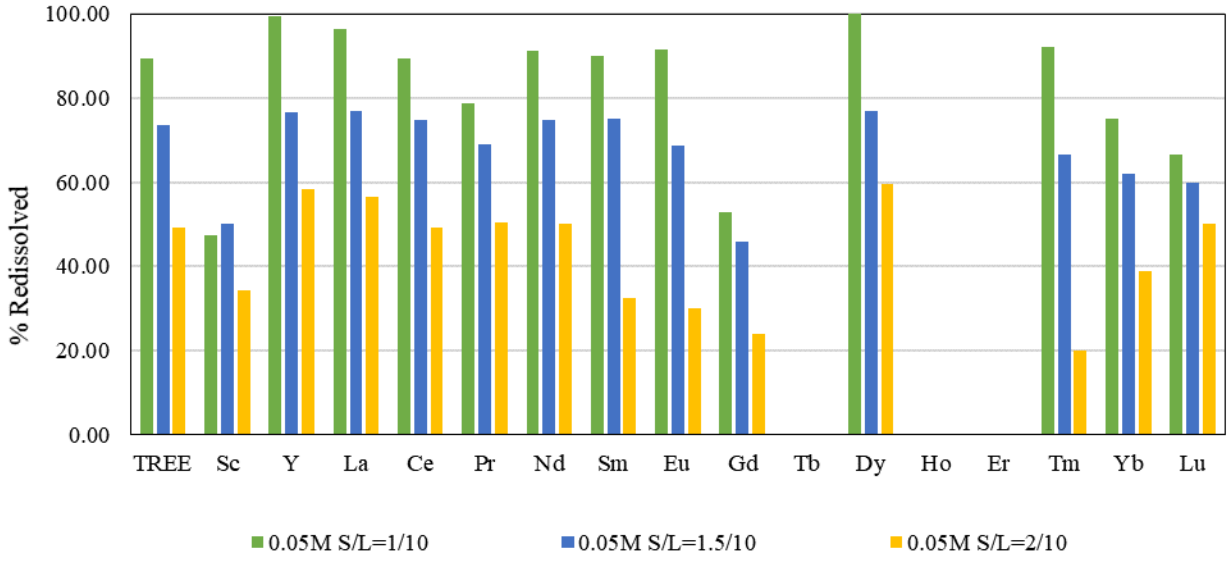

Figure 3.7.9. Effect of solid concentration in initial leaching process on RE redissolution efficiency.

Table 3.7.3. The ratio of contaminants to RE in leaching, precipitation and redissolution stage showing the elements association and migration in the flowsheet.

Leaching Condition	PLS Leachate			Precipitate Cake			Redissolved Solution		
	Al/RE	Ca/RE	Fe/RE	Al/RE	Ca/RE	Fe/RE	Al/RE	Ca/RE	Fe/RE
0.05M S/L=1/10	30.6	43.4	63.5	21.6	3.6	67.9	23.8	5.3	1.0
0.025M S/L=1/10	14.6	35.1	51.1	12.2	2.8	48.9	13.1	3.3	3.7
0.075M S/L=1/10	49.1	32.6	94.6	52.6	4.4	93.8	32.1	6.3	1.4
0.05M S/L=1.5/10	18.5	29.1	60.9	17.8	4.3	62.0	17.0	6.8	1.7
0.05M S/L=2/10	10.3	39.6	60.0	7.4	2.9	69.2	14.7	6.6	1.1
0.075M S/L=1.5/10	12.0	24.3	83.6	13.8	2.2	82.2	25.8	4.1	1.8

iv. *Oxalic Precipitation*

The redissolved precipitate from the leaching circuit was used as feed in the oxalic precipitation circuit. The purpose of the oxalic precipitation was to selectively precipitate the rare earths from the solution as rare earth oxalates while discarding the major impurities such as calcium and aluminum. In order to achieve the precipitation process on the pilot scale a two-tank system along with a pressure filter was set up. The intent was to perform the chemical reaction in the tanks and separate the solid precipitate from filtrate using the pressure filter. The first tank served as the mixing tank where the incoming feed was mixed with the oxalic acid and NaOH. While the second tank was used as the holding tank. The pH of the solution in the mixing tank was monitored and controlled by using pH probe and proportional relay controller respectively. The set point for pH and oxalic acid dosage for each test program were determined experimentally. Figure 3.7.10 shows a schematic of the precipitation circuit implemented on the pilot scale. The volume of the mixing tank was 5 gallons. The feed flowrate to the tank was adjusted to 0.25 gpm to provide a residence time of 20 minutes required for precipitation process. The residence requirement was determined earlier from laboratory tests the details of which can be found in the previous reports. The pressure filter shown in the circuit was operated on a batch scale which processed 0.8 gallons of supernatant liquid per batch at a pressure of 60 psi. The filtration time for every batch was approximately 25 minutes. However, the filtration time was influenced by other factors such as cake resistance and supernatant liquid chemistry which would slow down the filtration rate in some cases.

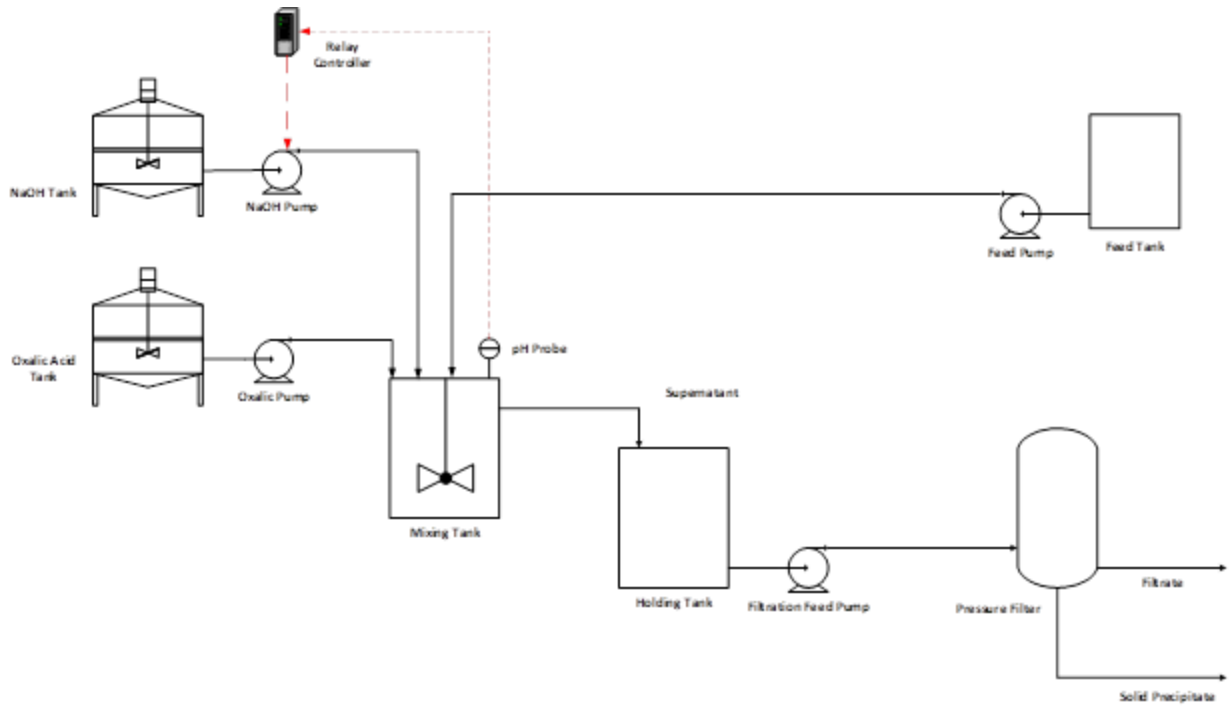

Figure 3.7.10: Schematic of Oxalic precipitation circuit

After the set-up was established two sets of feed stock generated from the leaching circuit was processed. The feed stocks were named as C4 and C5. Figure 3.7.11 and Figure 3.7.12 shows the concentration of individual rare earths and major contaminants (aluminum, calcium and iron) in the feed.

The material was processed under different operating condition listed in Table 3.7.4. Samples of feed, filtrate and supernatant were collected during the operation to access the performance of the circuit. From the analysis it was found that the TREE recovery was greater than 90 percent and the recovery of calcium and aluminum was less than 20 percent for both the cases (Figure 3.7.13 and Figure 3.7.14). The recovery of iron for both the case was almost negligible. The result indicated the success of the precipitation process in selectively recovering the rare earths.

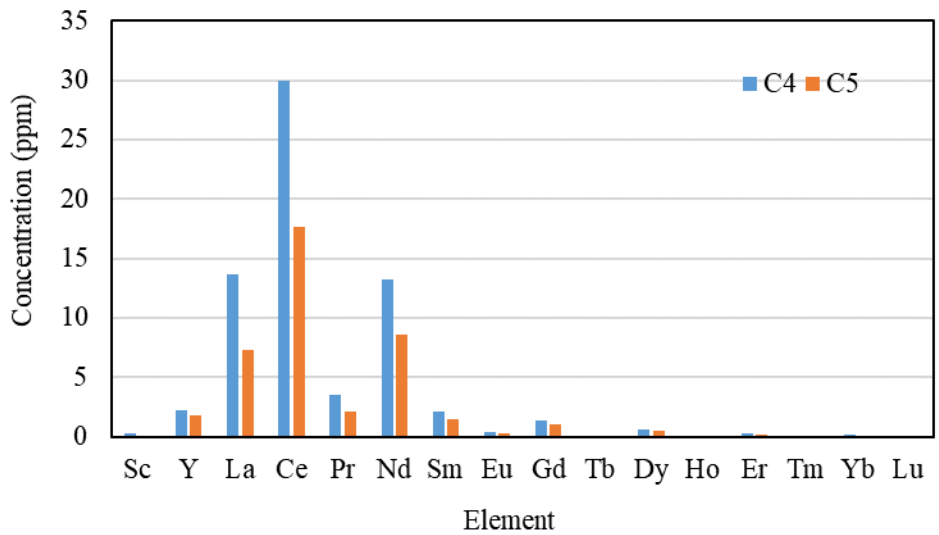

Figure 3.7.11: Concentration of individual REE in C4 and C5

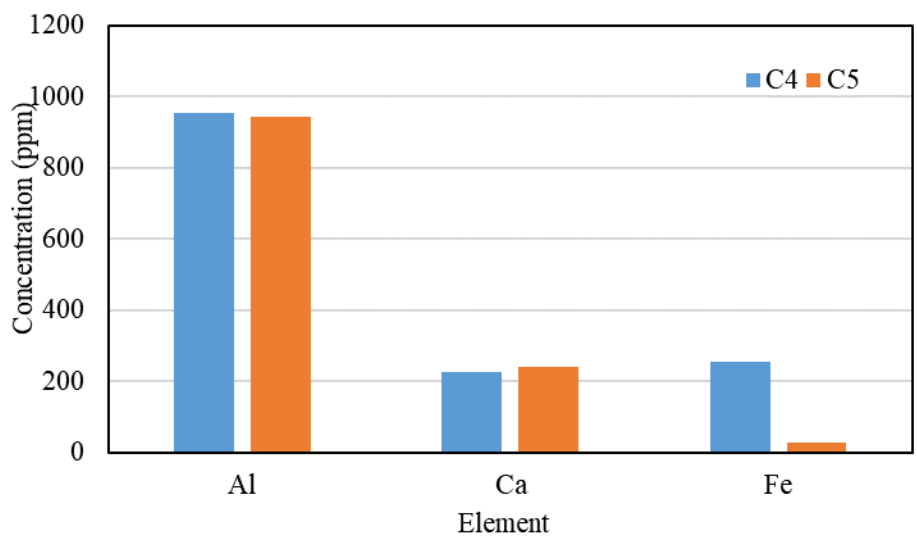

Figure 3.7.12: Concentration of major contaminants

Table 3.7.4: Operating condition for C4 and C5

Feed Stock	Oxalic Dosage (gm/L)	Operating pH
C4	9.6	1.00
C5	12.8	1.50

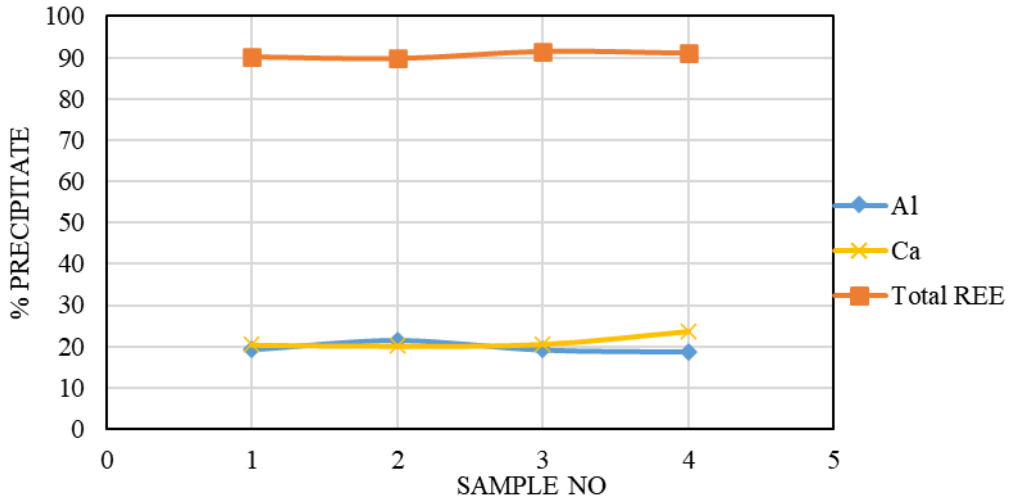

Figure 3.7.13: Recovery of REE and Contaminants from C4

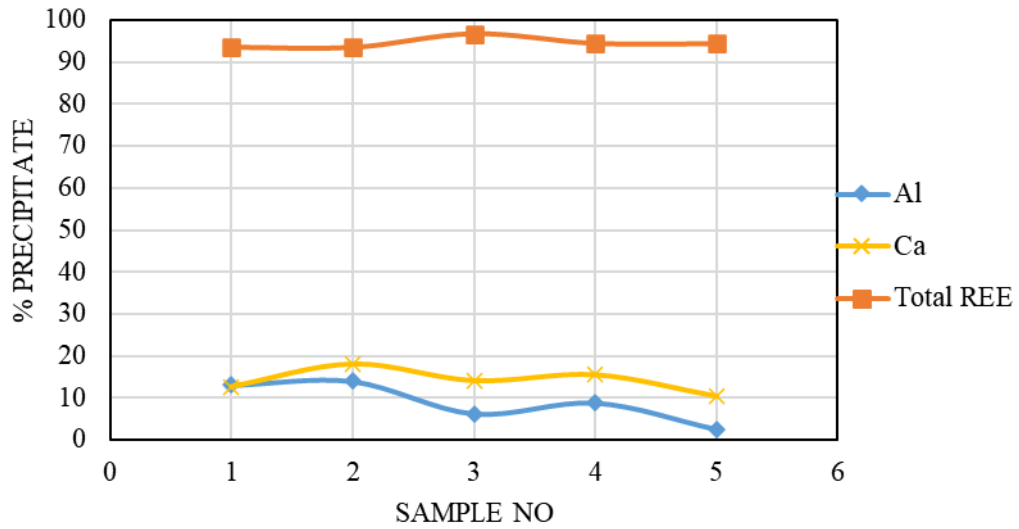

Figure 3.7.14: Recovery of REE and Contaminants from C5

However, during operation using this set-up, the major performance bottleneck was the filtration rate in the circuit. Slow filtration rate and batch nature of pressure filter was causing inconsistency in the operation making it discontinuous. Hence to mitigate this challenge the pressure filter was replaced by a high-pressure press and frame filter (Figure 3.7.15). The advantage of press and frame filter was its high capacity and ability to operate to a pressure of 100 psi which increased the filtration rate significantly. However, because of the high capacity of the press and frame the existing mixing and holding tanks were required to be up scaled to match its capacity. Hence the oxalic precipitation set-up was reconfigured with a new 50-gallon mixing tank and holding tank. The flowsheet of the reconfigured circuit was similar to shown in Figure 1 but with large capacity tanks and new filter. Three batch of feed stock named C6, C7 and C8 were then processed using the new system. Table 3.7.5 and Table 3.7.6 shows the operating condition and concentration of individual rare earths and contaminant for the three-feed stock.

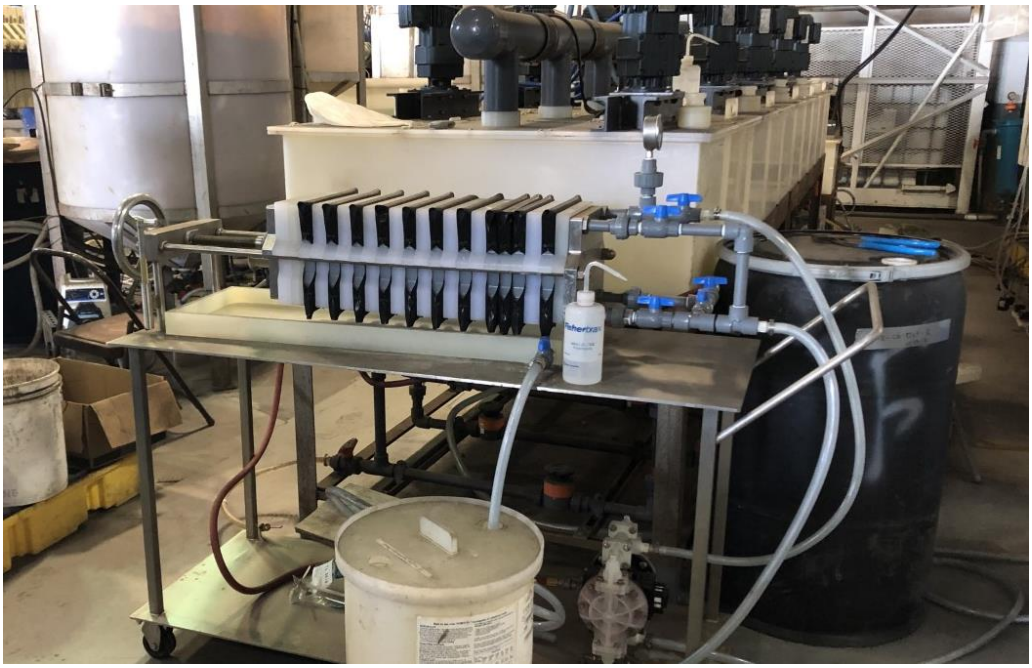

Figure 3.7.15: Press and frame filter

Table 3.7.5: Operating Condition for C4, C5 and C6

Feed Stock	Oxalic Dosage (gm/L)	Operating pH
C6	9.6	1.50
C7	6.40	1.50
C8	12.8	1.50

Table 3.7.6: Concentration of individual REE and Contaminants in feed

Element	C6	C7	C8
Sc	0.09	0.14	0.36
Y	1.53	1.42	2.44
La	8.22	7.59	10.50
Ce	18.80	15.40	26.40
Pr	2.29	2.02	3.28
Nd	9.47	7.83	13.30
Sm	1.50	1.31	2.31
Eu	0.25	0.22	0.39
Gd	0.96	0.84	1.46
Tb	0.10	0.08	0.11
Dy	0.44	0.41	0.66
Ho	0.05	0.05	0.09
Er	0.17	0.16	0.29
Tm	0.04	0.04	0.03
Yb	0.12	0.11	0.16
Lu	0.02	0.01	0.02
TREE	44.051	37.636	61.801
Al	544.80	597.00	1672.00
Ca	305.50	263.60	251.00
Fe	43.30	46.80	116.50
Contaminants	893.6	907.4	2039.5

From the analysis of the operation data of C6 batch it was found that the recovery of TREE was more than 90 percent but calcium recovery was also high in the precipitate (Figure 3.7.16). The possible reason for such high calcium recovery attributed was pH adjustment rate which was significantly low. This resulted in large residence time during the precipitation operation causing calcium to precipitate. In order to resolve the challenge two steps were taken. The first step was the base addition pump was replaced by large flowrate pump which could adjust the pH within few minutes so that the conditioning time (residence time) including based addition is within 20 to 30 minutes. Secondly, the holding tank was bypassed to prevent unnecessary aging because of the holdup time. After applying the solutions to the process, the C7 feedstock was then processed. The C7 stock was split into two halves named as C7-Split-1 and C7-Split-2 and processed separately. The operating condition for both halves was same. The purpose of processing material separately was to test the acid washing capability of the precipitate in wet condition to remove calcium. It is sought that washing precipitate with mild acid could remove calcium and improve the purity of product. However, the process is still under investigation and method to implement this on the pilot scale is being explored. Nevertheless, the recovery of calcium was around 30 percent for C7-Split-1 and around 22 percent for C7-Split-2. The recovery of rare earths was above

90 percent for both the case (Figure 3.7.17 and Figure 3.7.18). The C-8 stock showed results similar to C7 with almost no recovery of aluminum in the precipitate (Figure 3.7.19).

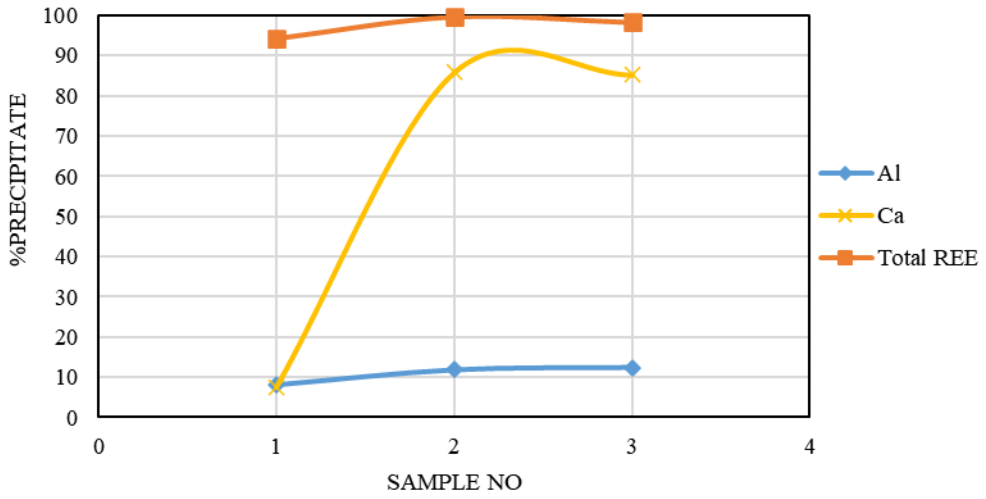

Figure 3.7.16: Recovery of TREE and Contaminants from C6

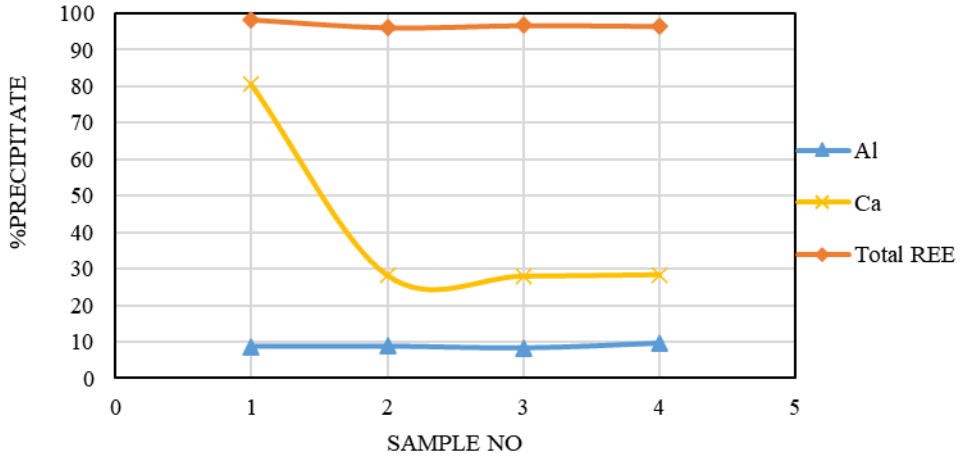

Figure 3.7.17: Recovery of TREE and Contaminants from C7-Split-1

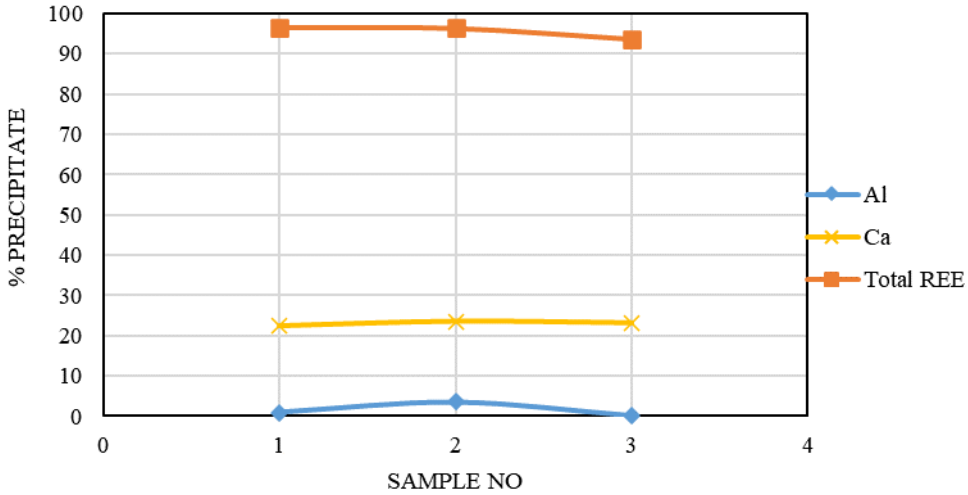

Figure 3.7.18: Recovery of TREE and Contaminants from C7-Split-2

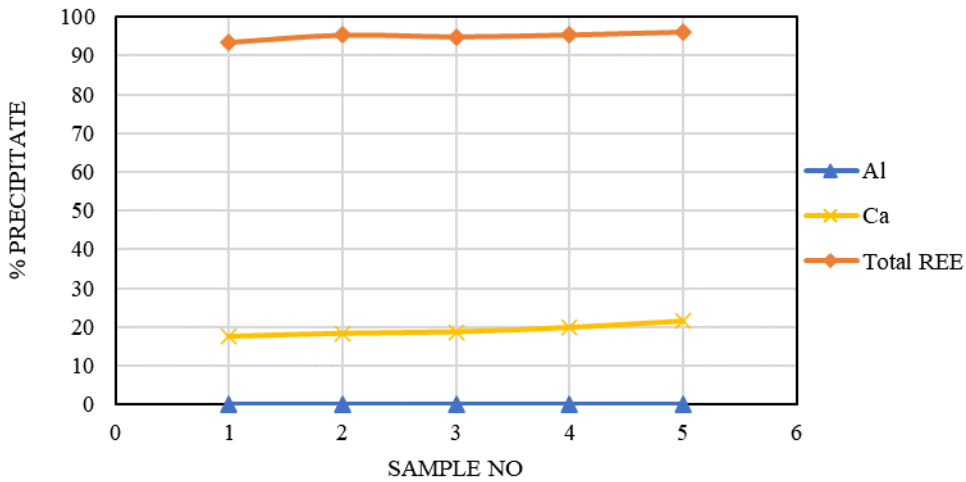

Figure 3.7.19: Recovery of TREE and Contaminants from C8

v. *<u>Oxalic acid precipitation speciation study</u>*

To further understand the rare earth precipitation behavior in the oxalate system, studies were carried out to examine the speciation distribution in solution at equilibrium. Visual MINTEQ 3.1 software was utilized to conduct the equilibrium calculations. Since rare earth elements possess similar chemical properties, lanthanum (La) was selected to perform the calculations for the LA-Oxalate precipitation system. The equilibrium reactions and the corresponding constants for La-oxalate precipitation at 25 °C are expressed as:

$$2La^{3+} + 3C_2O_4^{2-} \rightleftarrows La_2(C_2O_4)_{3\,(s)},\ \log Ks = 28.22^{a}$$
$$La^{3+} + C_2O_4^{2-} \rightleftarrows La(C_2O_4)^{+},\ \log K = 5.99^{a}$$
$$La^{3+} + 2C_2O_4^{2-} \rightleftarrows La(C_2O_4)_2^{-},\ \log K = 9.55^{a}$$

[a]Cited from Visual MINTEQ software.

The absolute concentration of rare earth elements significantly contributes to the precipitation efficiency of RE-oxalate in solution at equilibrium. With 0.01M oxalate concentration in the system, the stoichiometric concentration of La needed for the formation of $La_2(C_2O_4)_3$ was calculated to be 1000 ppm (~$7.2x10^{-3}$M). Results in Figure 3.7.20 show that in a La-oxalate system, with 1000 ppm of La^{3+} and 0.01M of $C_2O_4^{2-}$, the precipitation of $La_2(C_2O_4)_3$ starts to occur from pH 0.2 and the degree of reaction reaches >90% at pH >1.5. When the concentration of La was reduced to 100 ppm, the excessive amount of oxalate ions prompted the reaction to where >99% of La precipitated as pH 1.5. However, with reducing the La concentration to 10 ppm, the precipitation curve shifted to a higher pH range due to the promoted formation of $La(C_2O_4)^+$ under the excessive concentration of $C_2O_4^{2-}$. With one ppm of La, the peak precipitation of 86% occurs at pH 2.8 and start to show a trend of decreasing due to the elevated concentration of $La(C_2O_4)_2^-$. Consequently, in the mixed rare earth leachate solution generated from mine waste material, some of the rare earth elements with low concentration resulted in low efficiency of precipitation even with an excessive amount of oxalate. Comparing within the four-scenario presented in Figure 3.7.20, scenario c) is the optimal scenario where the precipitation completes at lower pH and improves the selectivity, whereas scenario a and b are more expected in the rare earth leachate obtained from mine waste (as shown in the experiments) due to the low grade of rare earth and high concentration of impurities in the feed material. Results indicated that increasing the concentration of REEs in feed would improve the oxalate precipitation efficiency and improve the selectivity by lowering the reaction pH.

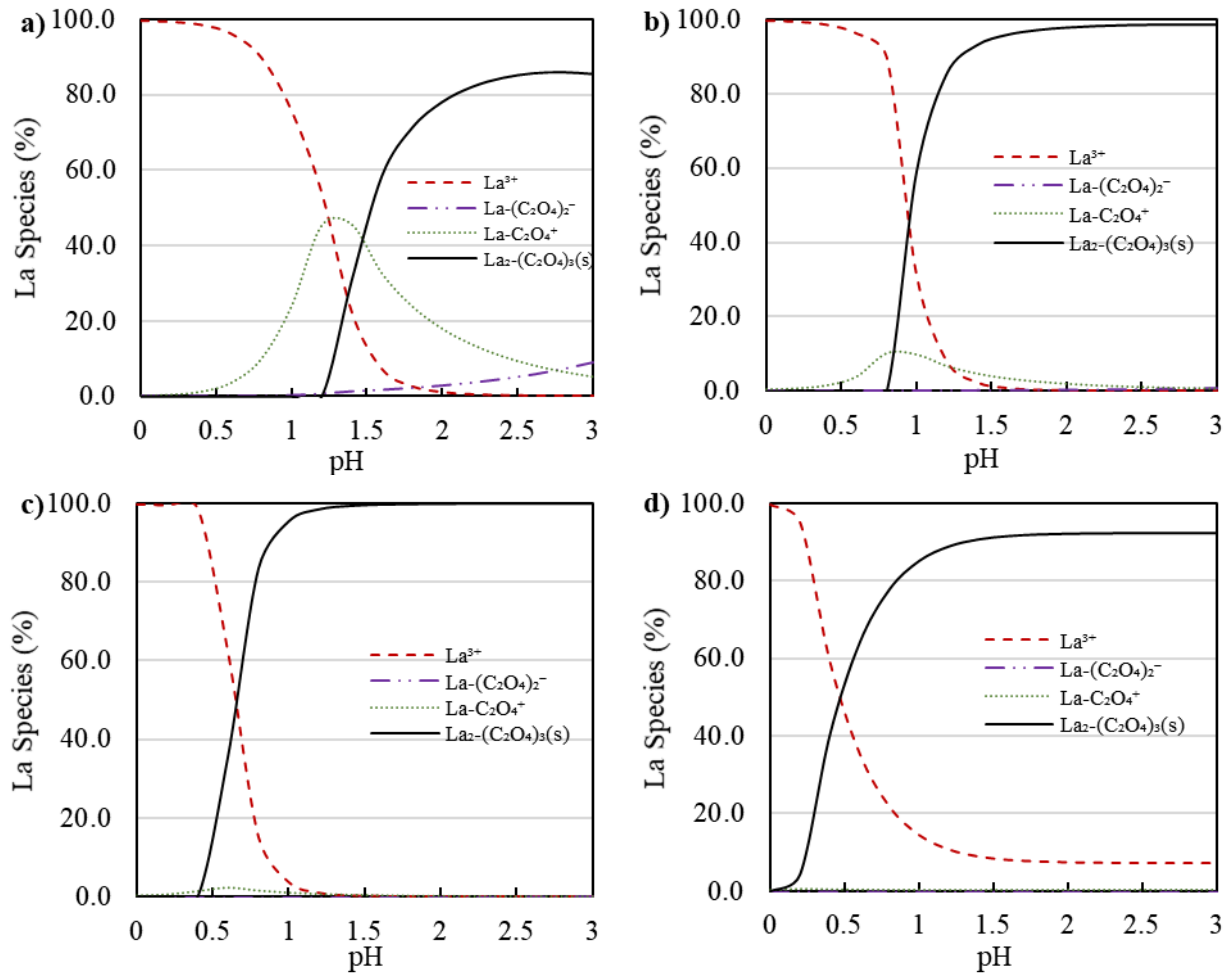

Figure 3.7.20. La species distribution in solution at equilibrium and La oxalate precipitation efficiency at a) 1 ppm La; b) 10 ppm La; c) 100 ppm La; d) 1000 ppm La with 0.01 M oxalate 25 °C simulated using Visual MINTEQ software. (The $La(C_2O_4)_3^{3-}$ and $LaOH^{2+}$ species are calculated to be less than 0.1% in these four systems, therefore not included in the plots.)

The concentration of Fe in both ferric or ferrous forms directly influences the RE precipitation efficiency. The iron present in the solution can react with oxalate anions to form various species depending upon the pH of the system. Visual MINTEQ 3.1 software was used to simulate the speciation behavior of Fe at equilibrium. The developed speciation distribution shown in Figure 3.7.21 indicates that $Fe\text{-}(C_2O_4)_3^{3-}$, $Fe\text{-}(C_2O_4)^{2-}$, and $Fe\text{-}(C_2O_4)^{+}$ are a dominant specie between 0-3 pH range. The dominant species seems to change drastically with even a small change in the pH. Furthermore, there is only a minimal concentration of $FeCl^{2+}$, $FeOH^{2+}$, Fe^{2+}, and Fe^{3+} present in the same pH range.

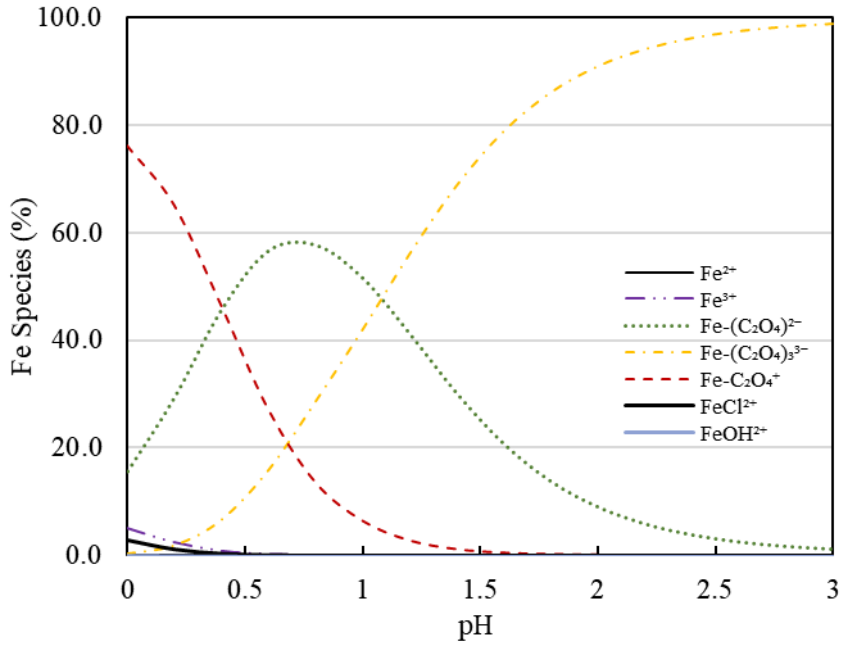

Figure 3.7.21. Fe species distribution in the precipitation system at equilibrium with 0.035M $C_2O_4^{2-}$, 0.1M Cl^-, 150 ppm Fe^{3+}, 60 ppm Al^{3+}, 130 ppm Ca^{2+}, and 35 La^{3+} at 25 °C simulated using Visual MINTEQ software. (Species less than 0.01% were included in the calculation but not plotted)

It has been established in the previous studies that iron oxalate precipitates in the ferrous form (Panias et al. 1996; Sun and Qiu 2012; Zeng, Li, and Shen 2015). As oxalic acid is a mild reducing agent, the excessive quantity of the oxalic acid can reduce iron from ferric to ferrous and precipitate it as ferrous oxalates by undergoing reactions (1)-(3) (Bard, Parsons, and Jordan 1985). Therefore, it can be inferred that the excessive concentration of oxalic acid at lower concentrations of Fe(III) will not only reduce more iron to ferrous it will also decrease the purity of rare earth precipitates.

$$C_2O_4^{2-} \leftrightarrow 2CO_2 + 2e^- \quad (1)$$

$$2Fe^{+3} + 2e^- \rightarrow 2Fe^{+2} \quad (2)$$

$$Fe^{+2} + 3C_2O_4{}^{2-} \leftrightarrow Fe\ C_2O_4.2H_2O(s) + 2C_2O_4{}^{2-} \quad (3)$$

Contrarily, the higher concentration of Fe(III) is also not desirable as it drastically reduces the RE precipitation efficiency. To thoroughly study its effect, various iron concentrations were analyzed in the MINTEQ by varying the Fe^{+3} concentration between 150-950 ppm. The impact of the increase in Fe concentration at other species present in the system showed a significant increment in the concentration of various iron-oxalate species in the solution. Furthermore, the free oxalate anion content drops from 0.149% to 0% when the Fe^{3+} concentration increases from 150 to 950 ppm. It can be deduced that the additional iron introduced in the system is decreasing the oxalate anions available for the reaction with REEs and other contaminants too. Therefore, the lanthanum precipitation, shown in Figure 3.7.22, also showed a significant drop while raising the iron concentration present in the solution. The maximum lanthanum precipitation of approximately 97% was achieved when the iron contamination was minimum, i.e., 150 ppm. The precipitation decreases with the further increase in the iron content. However, the impact on the precipitation is insignificant up to 550 ppm, indicating that there are oxalate anions still available to react with lanthanum. Increasing the concentration above 550 ppm starts significantly influencing the

lanthanum precipitation, signifying a non-availability of oxalate anions. This can be also be seen in the oxalate species distribution shown in Table 3.7.7, where the oxalate anion content drops from 0.039% at 550 ppm of iron to 0% at 950 ppm. The simulation data corroborate the experimental data, which also showed a significant decrease in RE precipitation efficiency beyond 500 ppm iron concentrations.

Interestingly, an increase in iron contamination also influences the precipitation of other impurities, resulting in a relatively pure product. This behavior was observed while modeling the calcium-oxalate monohydrate, the primary precipitant, at various iron concentrations. The results shown in Figure 3.7.23 show a substantial decrease in the calcium precipitation from approximately 92% to 32% at pH 1.5 when the iron contamination increases from 150 ppm to 950 ppm. This adverse impact on calcium precipitation is because of the reduced availability of oxalate anions at higher iron concentrations. The equilibrium constants (Ks) of various oxalate species shown in Table 3.7.8 can help elucidate the consumption of oxalate anions by iron (III) cations. It is evident that the equilibrium constants for REEs ranging from 10^{-29} to 10^{-32} are significantly smaller in contrast to the Ks values for Fe and other contaminants. As per the definition of the equilibrium constant, it is a ratio of activities of the products to the activity of reactants. Therefore, smaller Ks values indicate a higher concentration of the reactants in the solution, and a larger Ks value implies a higher concentration of products in the solution. The higher equilibrium constants for the contaminants than REEs indicate a higher concentration of products as compared to the reactants. It can be deduced that the decrease in efficacy is owing to the preferential reaction of oxalate anions with Fe^{+3} cations instead of REEs present in the solution. It should be noted here that even though a preferential reaction takes place between the Fe and oxalate anions, the majority of the metal oxalates do not precipitate, resulting in a higher oxalic acid precipitation selectivity as compared to other precipitating agents.

Table 3.7.7. The percentage distribution of oxalate species in solution with various amounts of Fe.

Oxalate Species	% of total concentration				
	150 ppm Fe^{3+}	350 ppm Fe^{3+}	550 ppm Fe^{3+}	750 ppm Fe^{3+}	950 ppm Fe^{3+}
$C_2O_4^{2-}$	0.149	0.085	0.039	0.017	0
$Fe\text{-}C_2O_4^{+}$	0.059	0.345	1.651	5.657	14.115
$H_2\text{-}C_2O_4$	18.329	10.28	4.721	2.087	0.969
$H\text{-}C_2O_4^{-}$	42.33	23.884	10.978	4.847	2.246
$La\text{-}C_2O_4^{+}$	0	0	0.014	0.019	0.027
$AlH\text{-}C_2O_4^{2+}$	0.017	0.032	0.065	0.105	0.134
$Al\text{-}(C_2O_4)_3^{3-}$	7.281	4.652	2.061	0.695	0.202
$Al\text{-}(C_2O_4)_2^{-}$	8.201	8.927	8.407	6.219	3.823
$Al\text{-}C_2O_4^{+}$	0.474	0.913	1.837	2.956	3.809
$Fe\text{-}(C_2O_4)_3^{3-}$	18.897	36.779	38.711	27.78	15.602
$Fe\text{-}(C_2O_4)_2^{-}$	4.246	14.083	31.508	49.61	59.059

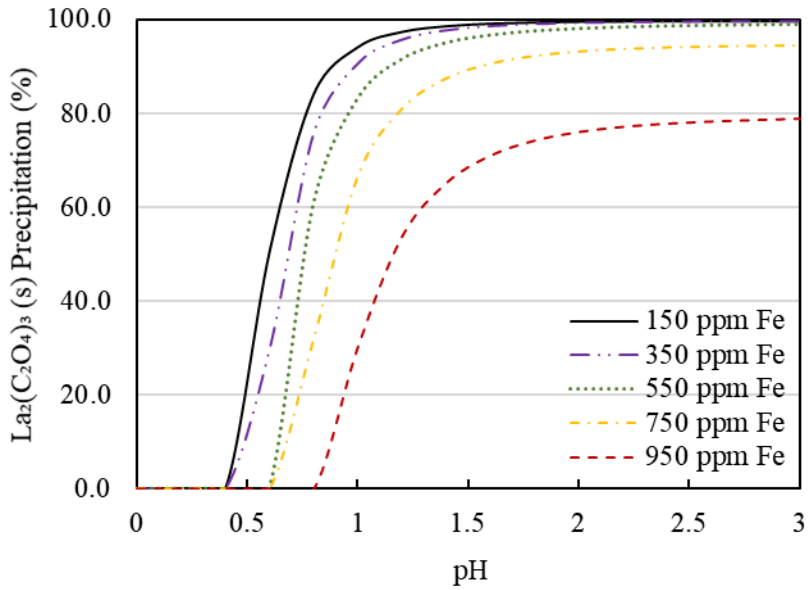

Figure 3.7.22. Effect of Fe concentration on La oxalate precipitation pH and efficiency. (0.035M $C_2O_4^{2-}$, 0.1M Cl^-, 60 ppm Al^{3+}, 130 ppm Ca^{2+}, and 35 La^{3+} at 25 °C calculated using Visual MINTEQ software).

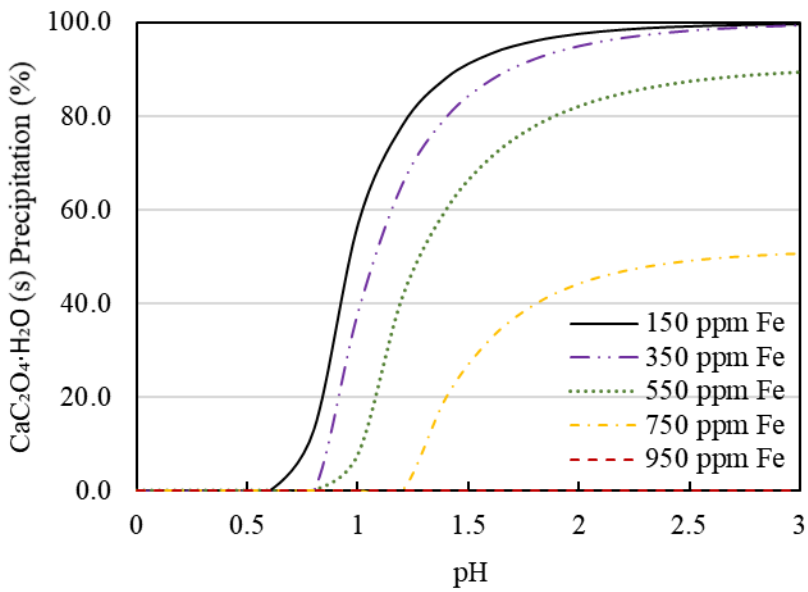

Figure 3.7.23. Effect of Fe concentration on La oxalate precipitation pH and efficiency. (0.035M $C_2O_4^{2-}$, 0.1M Cl^-, 150 ppm Fe^{3+}, 60 ppm Al^{3+}, 130 ppm Ca^{2+}, and 35 La^{3+} at 25 °C simulated using Visual MINTEQ software.)

Table 3.7.8 The equilibrium constants of REEs and other contaminants obtained from (Zhang et al. 2020) and (Watts and Leong 2020)

Specie	K	Specie	K
$Ce_2(C_2O_4)_{3\ (s)}$	6.61 x 10^-31	$Al(C_2O_4)_2^-$	3.89 x 10^-14

$Y_2(C_2O_4)_{3\ (s)}$	5.37 x 10^$^{-29}$	$Al(C_2O_4)_2^{-3}$	8.13 x 10^$^{-18}$
$Nd_2(C_2O_4)_{3\ (s)}$	7.76 x 10^$^{-32}$	$Al(HC_2O_4)^{+2}$	6.46 x 10^$^{-4}$
$La_2(C_2O_4)_{3\ (s)}$	6.00 x 10^$^{-30}$	$Fe(C_2O_4)_2^{-}$	3.55 x 10^$^{-16}$
$Sm_2(C_2O_4)_{3\ (s)}$	4.50 x 10^$^{-32}$	$Fe(C_2O_4)_2^{-2}$	1.26 x 10^$^{-6}$
$Eu_2(C_2O_4)_{3\ (s)}$	4.20 x 10^$^{-32}$	$Fe(C_2O_4)_3^{-3}$	1.48 x 10^$^{-20}$
$Gd_2(C_2O_4)_{3\ (s)}$	4.25 x 10^$^{-32}$	$Ca\ (C_2O_4)_{(aq)}$	6.46 x 10^$^{-4}$
$Dy_2(C_2O_4)_{3\ (s)}$	2.0 x 10^$^{-31}$	$Er_2(C_2O_4)_{3\ (s)}$	9.00 x 10^$^{-31}$

Reference

Bard, AllenJ., R Parsons, and J Jordan. 1985. "Standard Potentials in Aqueous Solution."

Panias, D., M. Taxiarchou, I. Paspaliaris, and A. Kontopoulos. 1996. "Mechanisms of Dissolution of Iron Oxides in Aqueous Oxalic Acid Solutions." *Hydrometallurgy* 42 (2): 257–65. https://doi.org/10.1016/0304-386X(95)00104-O.

Sun, Liang, and Keqiang Qiu. 2012. "Organic Oxalate as Leachant and Precipitant for the Recovery of Valuable Metals from Spent Lithium-Ion Batteries." *Waste Management* 32 (8): 1575–82. https://doi.org/10.1016/j.wasman.2012.03.027.

Watts, Harry, and Yee-Kwong Leong. 2020. "Predicting the Logarithmic Distribution Factors for Coprecipitation into an Organic Salt: Selection of Rare Earths into a Mixed Oxalate." *Minerals* 10 (8): 712. https://doi.org/10.3390/min10080712.

Zeng, Xianlai, Jinhui Li, and Bingyu Shen. 2015. "Novel Approach to Recover Cobalt and Lithium from Spent Lithium-Ion Battery Using Oxalic Acid." *Journal of Hazardous Materials* 295 (September): 112–18. https://doi.org/10.1016/j.jhazmat.2015.02.064.

Zhang, Wencai, Aaron Noble, Bin Ji, and Qi Li. 2020. "Effects of Contaminant Metal Ions on Precipitation Recovery of Rare Earth Elements Using Oxalic Acid." *Journal of Rare Earths*, November. https://doi.org/10.1016/j.jre.2020.11.008.

3.7.1.2 Circuit optimization

Based on the parametric study results, several additional pilot scale continuous tests were carried out to 1) examine the pre-wash effect prior to leaching circuit with a goal of reducing calcium content in fresh leachate solution that is carried over to the downstream process; 2) implement leachate recirculation around the first stage leaching unit to reuse the un-consumed acid; and 3) evaluate the benefit on downstream chemical consumption reduction by removal of Al before rare earth precipitation. The test condition and corresponding subjects are listed in Table 3.7.9. All the five additional tests applied changes to the acid leaching circuit (unit L1) on and/or before RE precipitation (unit PT1), the downstream circuit remained the same, including RE redissolution (unit L2) and RE oxalate precipitation (OXP) to produce the final RE product. Due to the modification applied on leaching condition, the solution composition in the downstream process changed, therefore, operation condition for redissolution and oxalate precipitation for each of the five tests were determined and optimized individually through parametric tests.

Table 3.7.9. Circuit optimization test conditions and subjects.

Test Code	Solid Feed (lb/hr)	Water (GPM)	H2SO4 (M)	Retention (h)	Duration (h)	Subject
DTK-C9	50	1	0.05	2	18	Solid Feed Prewash
DTK-C10	50	1	0.05	1	16	PLS Recirculate
DTK-C11	50	1	0.025	2	16	Al Removal
DTK-C12	50	0.5	0.025	2	16	PLS Recirculation+ Al Removal
DTK-C13	50	0.5	0.075	2	16	PLS Recirculation+ Al Removal

i. *Solid Feed Prewash*

The goal of prewash the roasted solid feed using water before acid leaching was to wash off part of the Ca from the feed before it reports to acid leaching and consume hydrogen ions. Calcite was found out to be one of the major modes of occurrence of calcium existed in coal refuse system in the previous characterization studies. Most of the calcite decomposes in the roasting process and converts to calcium oxide. Calcium oxide can react with water and produce calcium hydroxide which has low solubility. However, the preliminary lab test shows that the roasted solid feed also released acid generating material to naturally bring down the water pH to about 6.4 under 75 ˚C. The acid generating material was likely formed during decomposition of sulfide minerals (i.e. pyrite) during roasting process and a portion of the SO_2 adheres on the particle surface formed sulfate compounds that generates acid in contact with water.

Table 3.7.10. Solid feed and solid residue analysis before and after water wash.

Sample ID	Description	Ash (%)	Element Concentration on dry ash basis (ppm)			
			TREE	Al	Ca	Fe
DTK-C9-PW-F	Before Water Wash	95.1	324.1	138438	5643	46724
DTK-C9-PW-SR	After Water Wash	94.5	323.9	137468	3764	47887
DTK-C9-L1-SR	After Acid Leach	93.1	217.4	134365	1185	45073

The wash water contains average of 202 +/-79 ppm of Ca over the 18 hours operation, which corresponds to in average of 38% of the Ca removal from the feed solid. The Ca content in solid feed reduced from 5643 ppm to 3764 ppm as shown in Table 3.7.10. There was no RE loss observed during water wash process. However, the prewash process also served as a thermal activating pretreatment process that resulted in elevated the leaching efficiency of contamination ions, such as Al and Fe. In comparison, under the same acid leaching condition (0.05M H_2SO_4, 10% solid concentration, 75°C, 2 hours retention time), the level of Al and Fe concentration in the RE pregnant leachate solution (PLS) increased drastically. The ratio of contamination ions to TREE in the PLS are compared in Figure 3.7.24. Based on the previous findings, 94% of the Ca is removed in the RE precipitation stage at pH 6.5, which left with 6% Ca carried over to the downstream RE refining process. Whereas the increased Al and Fe level would result in higher chemical consumption in the RE redissolution and oxalate precipitation stage. The application of Ca prewash is not a benefit on the circuit.

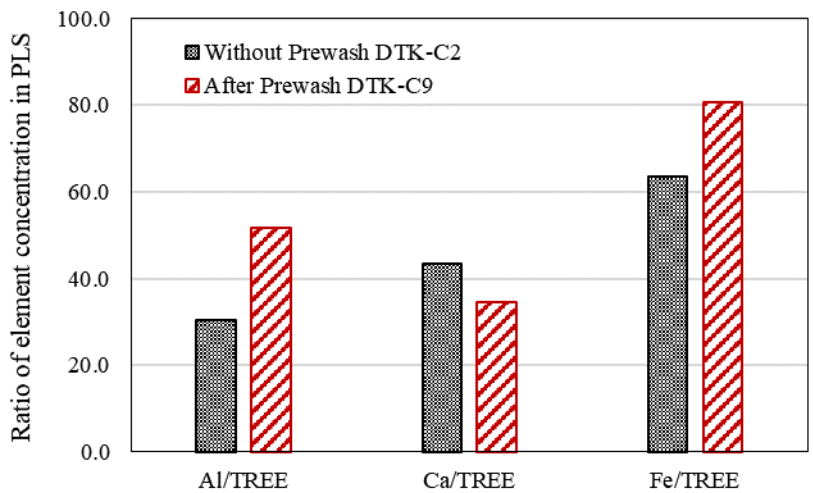

Figure 3.7.24. Comparison of Al, Ca and Fe to TREE ratio in the acid leaching RE pregnant leachate solution with and without prewash.

ii. *Aluminum Removal*

Based on the previous test runs, 94% of the Ca contamination is removed in the RE precipitation stage, over 90% of Fe is removed in the RE redissolution stage, however, the Al is carried over to the concentrated RE solution and removed in the oxalic precipitation stage. Al is a major consumer of the oxalic acid due to its ability to form $Al(C_2O_4)_2^-$ and $Al(C_2O_4)_3^{3-}$ complexes with oxalate and report to the wastewater stream. Efforts were directed to evaluate a location which Al can be removed before reporting to the oxalate precipitation process. The Al can be removed from the fresh leachate before RE precipitation by adjusting the pH between 4 to 5 as shown in Figure 3.7.25. To identify an optimal condition for Al removal, the precipitation behavior of Al and rare earths was examined in a narrower range of pH as shown in Figure 3.7.26. The results show that 86% of Al can be removed from the leachate by precipitation with about 10% RE loss at pH 4.5.Figure 3.7.25

To examine the Al removal effect on the downstream process, a continuous test was carried out in the pilot plant (DTK-C11) for 16 hours exploiting the same leaching condition as DTK-C4 (0.05M H_2SO_4, 10% solid concentration, 75°C, 2 hours retention time). The operation information is shown in Table 3.7.11, where the L1 denotes the acid leaching operation unit, PT0 denotes the Al precipitation operation unit, and PT1 denotes the RE precipitation unit. The average solid concentration after leaching is about 9% and the pH was in average of 3.2 +/-0.2 during 16 hours leaching. The roasted solid feed material contains 324±26 ppm of total REEs on a dry whole mass basis, and the solid residue collected after leaching contains 174+/-15 ppm of total REEs on a dry whole mass basis.

The precipitation behavior of individual elements in the Al precipitation stage is shown in Figure 3.7.27. The results indicated that majority of the scandium and vanadium were also precipitated with Al. It was observed that about 27% of Fe was removed together with Al, which was higher than the expectation from the lab test results. This is due to the conversion of ferrous

hydroxide to ferric hydroxide during precipitation which shifted the Fe precipitation curve closer to the Al precipitation.

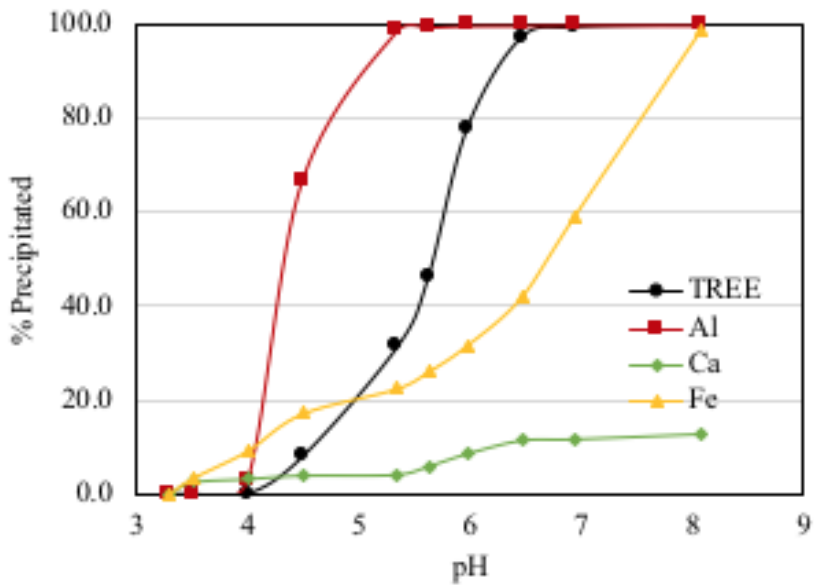

Figure 3.7.25. Precipitation behavior of RE and major contaminants in PLS solution by increasing pH. (DTK-C4)

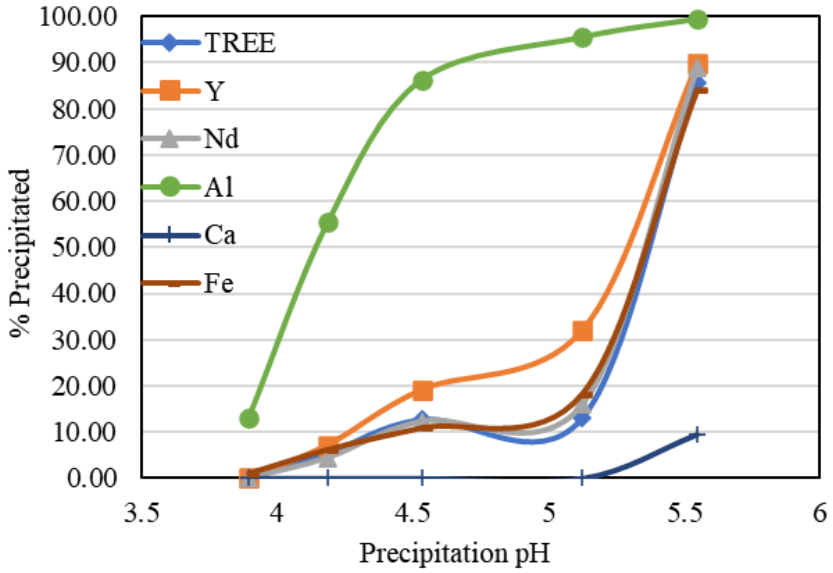

Figure 3.7.26 Precipitation behavior of RE and major contaminants in PLS solution by increasing pH. (DTK-C11)

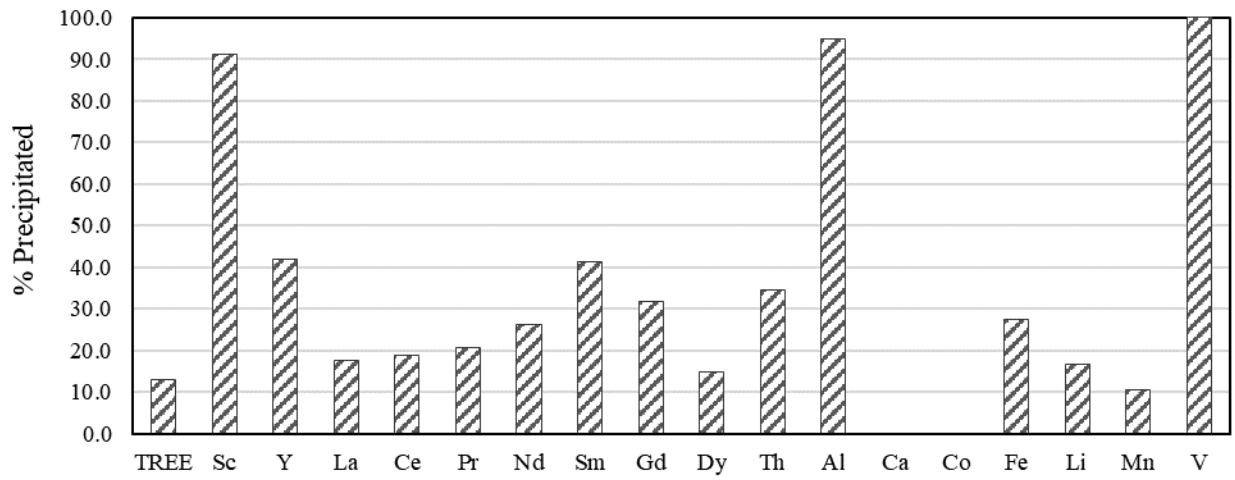

Figure 3.7.27. Precipitation behavior of element of interest at pH 4.5 in the continuous pilot plant operation.

iii. <u>Leachate recirculation</u>

In the previous circuit, the fresh leachate containning REs produced from unit L1 was directly transported to unit PT1 to increase the pH to 6.5 for RE precipitation. The fresh leachate can be recirculated in the L1 leaching unit to recover the free hydrogen ions remained in the leachate instead of neutrulized with base solution. An example of 100% leachte recirculation flowsheet is shown in Figure 3.7.28. Other than recovering unconsumed acid, a recirculation stream has an effect on leaching retention times by varying the recirculation load. Based on previous studies, the leaching kinetic of RE is faster than that of the contamiation ions, such as Al and Fe. Thus, shortening the retention time can reduce the ratio of impurities-to-REs in the leachate solution.

The recirculation around the leaching unit was tested under different leaching acid concentrations. At low acid concentration leaching (0.025M sulfuric acid leaching, DTK-C12 test), the impact of leachate recirculation had minimal effect on improving RE leaching recovery due its lack of active hydrogen ions in the leachate solution. However, at high acid concentration leaching (test DTK-C13, 0.075M H_2SO_4), the impact of leachate recirculation with 100% loading rate improved the RE leaching recovery by 7% absolute percentage points. The steady state leaching pH with 100% recirculation was 2.2 whereas the leaching pH without recirculation was 2.9. The Sc leaching recovery was nearly doubled due to its sensitivity to leaching acidity.

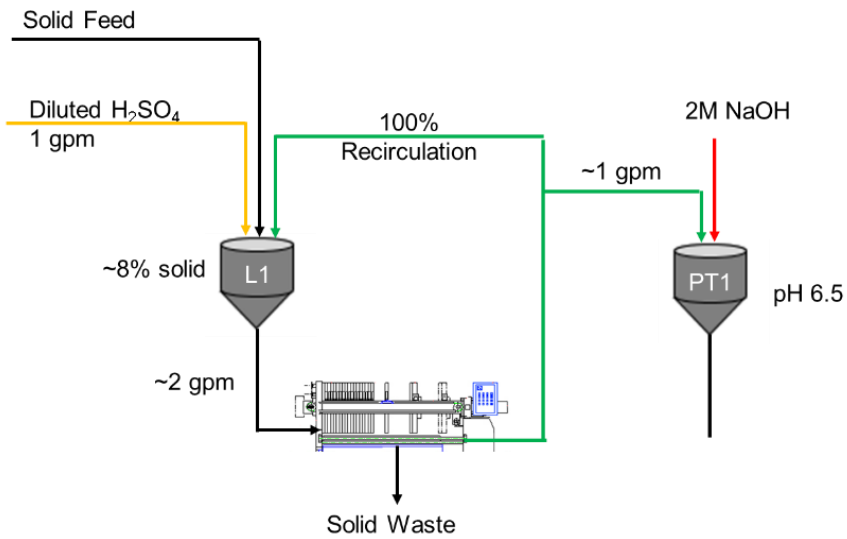

Figure 3.7.28. Schematic flowsheet of leachate recirculation to optimize leaching circuit.

The roasted solid feed material feed into C13 test contains 338 +/-14 ppm of TREEs on a dry whole mass basis. The solid was fed into leaching tank (unit L1) at a rate of 50 lb/hr. At the beginning of the test, the leaching tank (L1) and acid preparation tank (AP1) was fed with 1 GPM of 0.075M H_2SO_4, which is equivalent to 68 kg sulfuric acid per metric ton of solid feed. With the operation going forward, the leachate solution was reported to a surge tank (also referred to recirculation tank, RC1) where 0.5 GPM of leachate was pumped back into the acid preparation tank. To maintain a steady flowrate, the flowrate of fresh water feed into the acid preparation tank was reduced to 0.5 GPM, and the sulfuric acid flow rate remained the same to provide acid dosage of 68 kg/ton of feed.

The test was in continuous operation for 16 hours (2 shifts was employed). Sample were collected every 2 hours from the leaching tank (L1), acid preparation tank (AP1) and recirculation tank (RC1) to monitor the pH and RE concentration change. Each tank has a total volume of 100 gallon resulting in a 2 hours retention time with the current flowrate. The pH recorded for sample collected around the cricuit is shown in the operation log in Table 3.7.11. The recirculation started at 4 hours of operation time. The results show that the pH of the RC1 tank was 2.7 at 6 hours of operation, and stablized at pH value of 2.4 after reaching steady state.

As a result of leachate recirculation, the TREE concentration in PLS leachate solution kept building up and reached plateau after about 12 hours of operation. As shown in Figure 3.7.29, the TREE concentration in the acid leaching tank reached 14 ppm after 4 hours of leaching without recirculation, and increased to about 28 ppm at 12 hours of operation, which was 6 hours after recirculation, and stabilized. The steady state of recirculation tank is 2 hours behind the leaching tank, and the acid preparation tank is 2 hours behind the recirculation tank. That explain the increasing concentraion of TREEs in the AP1 and RC1 solution. Figure 3.7.30 shows the concentration of Al, Ca and Fe in the leaching tank (L1) together with TREEs. The Al concentration started from 730 ppm at the beginning of the test and leveled out at about 120 ppm. The Ca concentration did not increase significantly due to the recirculation, and reached about 480

ppm all along the test. However, though the TREEs reached plateau after 12 hours, the Fe concentration in leaching solution kept increasing through out the test.

Table 3.7.11. DTK-C13 operation log on leaching and leachate recirculation.

ID	#	Date	Tank	Time	Hours in Run	Temp (C)	% Solids	pH
DTK-C13-L1	P1	2020/3/17	T14	11:40	2:00	75	9.371	3.16
DTK-C13-L1	P2	2020/3/17	T14	13:40	4:00	75	9.255	2.332
DTK-C13-L1	P3	2020/3/17	T14	15:40	6:00	75	8.279	2.189
DTK-C13-L1	P4	2020/3/17	T14	17:40	8:00	75	9.277	2.353
DTK-C13-L1	P5	2020/3/17	T14	19:40	10:00	75	9.757	2.341
DTK-C13-L1	P6	2020/3/17	T14	21:40	12:00	75	9.561	2.251
DTK-C13-L1	P7	2020/3/17	T14	23:40	14:00	75	9.036	2.261
DTK-C13-L1	P8	2020/3/18	T14	2:00	16:00	75	9.500	
ID	#	Date	Tank	Time	Hours in Run	Temp (C)	% Solids	pH
DTK-C13-AP1	1	2020/3/17	T6	14:00	6:00	-	-	1.179
DTK-C13-AP1	2	2020/3/17	T6	16:00	8:00	-	-	1.236
DTK-C13-AP1	3	2020/3/17	T6	18:00	10:00	-	-	1.243
DTK-C13-AP1	4	2020/3/17	T6	20:00	12:00	-	-	1.234
DTK-C13-AP1	5	2020/3/17	T6	22:00	14:00	-	-	1.258
DTK-C13-AP1	6	2020/3/18	T6	0:00	16:00	-	-	1.209
ID	#	Date	Tank	Time	Hours in Run	Temp (C)	% Solids	pH
DTK-C13-RC1	1	2020/3/17	T8	14:00	6:00	-	-	2.71
DTK-C13-RC1	2	2020/3/17	T8	16:00	8:00	-	-	2.614
DTK-C13-RC1	3	2020/3/17	T8	18:00	10:00	-	-	2.536
DTK-C13-RC1	4	2020/3/17	T8	20:00	12:00	-	-	2.455
DTK-C13-RC1	5	2020/3/17	T8	22:00	14:00	-	-	2.495
DTK-C13-RC1	6	2020/3/18	T8	0:00	16:00	-	-	2.404

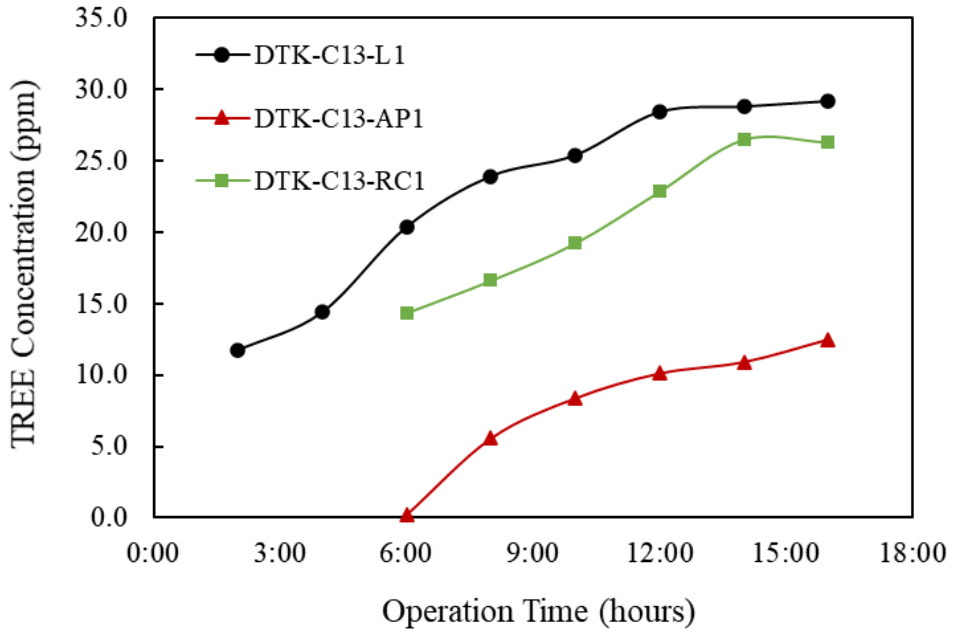

Figure 3.7.29. Concentration of TREE in leaching (L1), acid preparation (AP1), and recirculation tank (RC1).

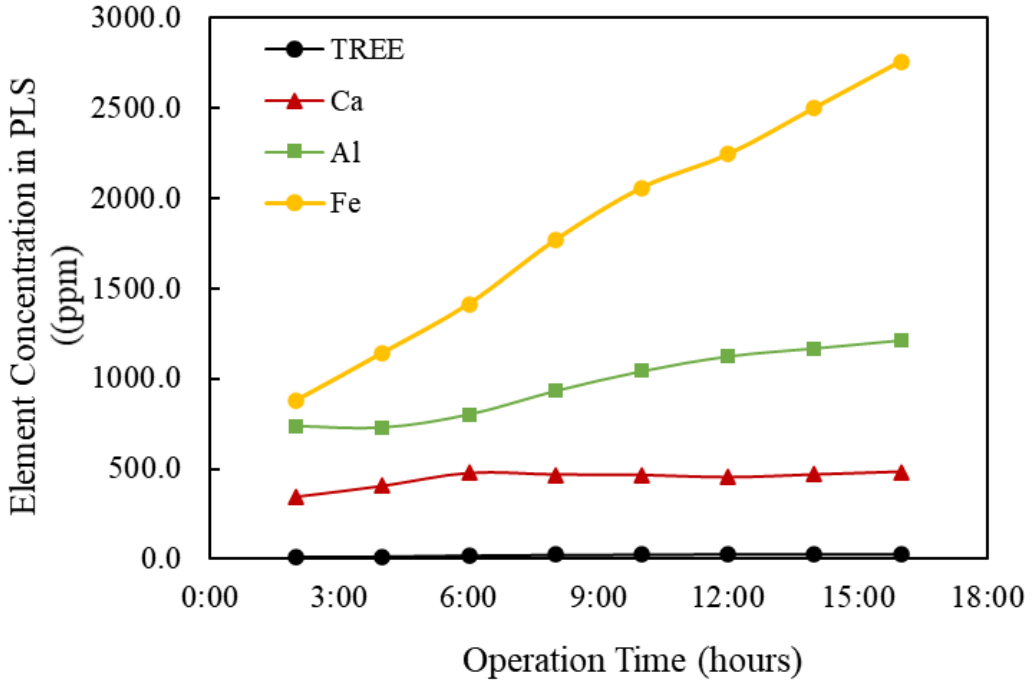

Figure 3.7.30. Concentration of TREE and major impurities in the leaching tank (L1).

To compare the leaching recovery increase gained from the recirculation, the leaching recovery at 4 hours represents the leaching performance before recirculation, and the leaching

recoery at 16 hours represents the performance under the influence of recirculation. The absolute RE gain in the leaching process at time *t (hours)* is calculated as:

$$c_{TREE\ gain,\ t} = c_{TREE\ in\ L1,\ t} - c_{TREE\ in\ AP1,\ t\text{-}2}$$

where $c_{TREE\ in\ L1,\ t}$ is the TREE concentration in leaching tank L1 at time *t*; $c_{TREE\ in\ AP1,\ t\text{-}2}$ is the concentration of TREE in acid preparation tank AP1 at 2 hours before time *t*.

The roasted solid feed material feed into C13 test contains 338 +/-14 ppm of TREEs on a dry whole mass basis. The solid residue collected after 4 hours leaching and 16 hours leaching contains 237 ppm and 212 ppm of TREEs on a dry whole mass basis. The leaching recovery was calculated based on both leachate and solid residue. The comparison of leaching recovery for individual RE element and other elements of interest is shown in Figure 3.7.31. The TREE recovery increased from 39.5% to 46% after recirculation. Due to the pH decrease, the recovery of Sc increase from 7.4% to 13.2%.

The leachate was then subject to Al removal as discussed in the previous section. The lab precipitation scoping test results (Figure 3.7.32) shows the similar precipitation performance of RE and Al as preciously discussed. At pH 4.5, 87% of Al can be removed with losing 9.2% TREE. The leachate solution in the pilot plant continuous test was transported to a pH adjustment tank where 2M NaOH solution was automatically pumped through a PID control system. The precipitation efficiency of Al and other elements of interested is as shown in Figure 3.7.33. Above 95% of Al was removed from the solution with 8.9% RE loss. Majority of the REs loss was contributed by scandium due to its similar precipitation performance to Al. Future investigation is recommended to 1) discover alternative precipitation reagent instead of NaOH to separate Al and Sc precipitation curve; and 2) develop effective method to recover Sc from Al precipitate.

The leachate solution after Al removal was then subject to RE precipitation at pH 6.5 following with the downstream process developed in the previous studies. The RE precipitation efficiency is shown in Figure 3.7.34, where 89% of TREE was precipitated with 73% of Co, 26% of Mn, and 79% of Ni. 97% of Ca was rejected to the effluent stream and 74% of Mn was reported to the effluent as well. Therefore, the PT1 effluent is the potential feed to concentrate Mn as a byproduct.

The PT1 precipitate was filtered in a filter press and the filter cake was concentrated in RE and Fe. The RE filter cake was then conditioned in water and blend for 2 hours to homogenize. A centrifugal pump was aiding the homogenization process and also to expedite the oxidation process of ferrous hydroxide to ferric hydroxide. This oxidation process consumed OH^- which resulted in slurry pH to drop from 7.5 to 5.8 naturally. After blending, 6.8 L of 36% HCl solution was added to the slurry to re-leach/re-dissolve the RE in solution at pH 2.5. As shown in Figure 3.7.35, 78% of TREE was re-leached into solution together with almost 100% of Co. 94% of Fe was remained in the undissolved solid cake.

The concentrated RE solution was subject to selective precipitation using oxalic acid to produce high purity RE oxalate. The oxalate precipitation operation was conducted in 3 overflow fed co-current reaction tank to provide a total 20 minutes retention time to form RE oxalate

precipitate. A smaller press and frame filter was programed to filter the precipitate slurry at a constant rate of 2 gallons per minute to ensure the continuity of the RE oxalate precipitation in the reaction tanks. The precipitation efficiency is shown in Figure 3.7.36, where 92% of TREE was precipitated with small amount of Al and Ca. The Co was observed to mostly stay together with the RE through leaching, precipitation, and redissolution, does not precipitate with oxalic acid. Therefore, the effluent in the OXP process is a feasible stream to recover and concentrate Co in the future studies. A schematic of the most optimized flowsheet with material balance over the circuit and the dosage of chemicals applied in each unit is shown in Figure 3.7.37.

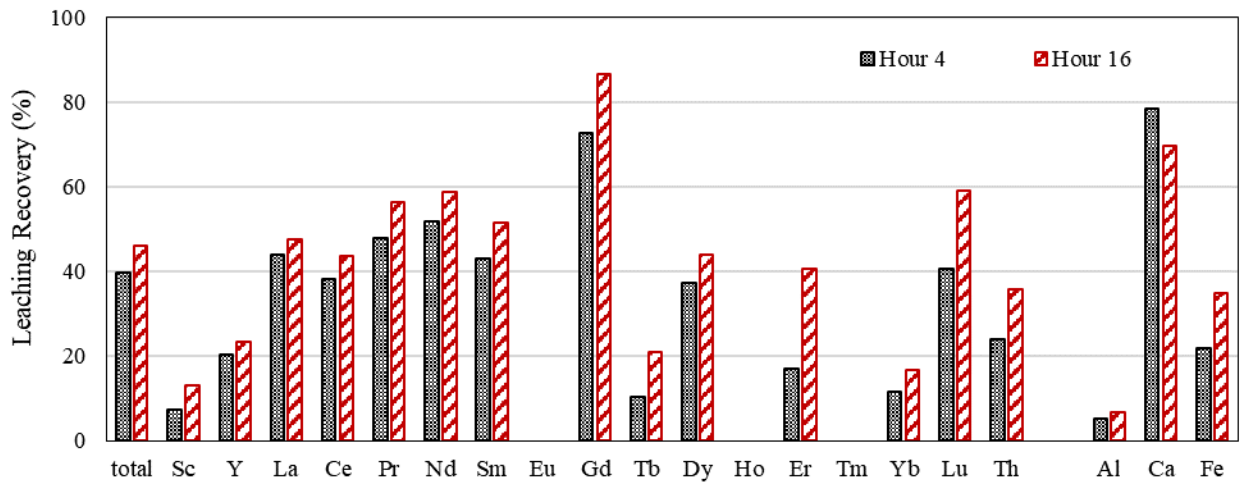

Figure 3.7.31 Comparison of leaching performance before (hour 4) and after (hour 16) leachate recirculation.

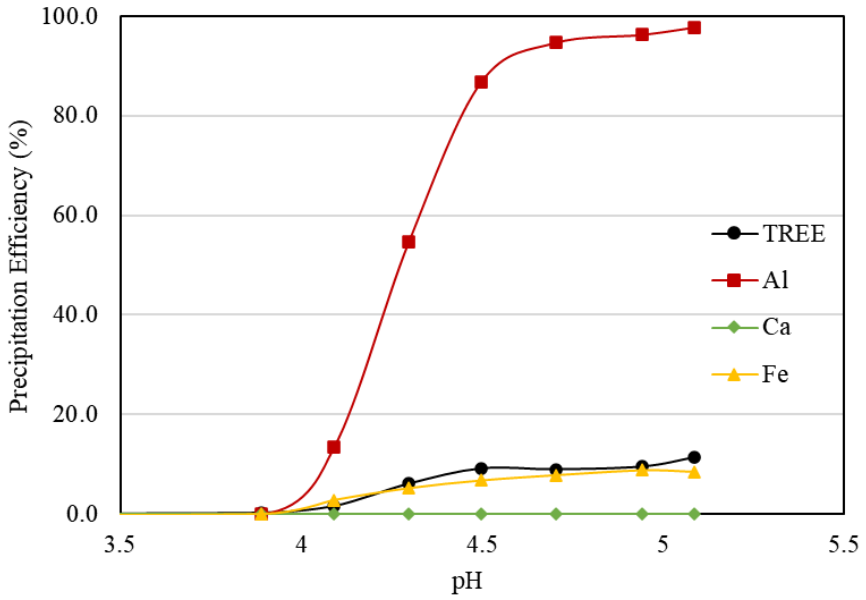

Figure 3.7.32. Precipitation efficiency of RE and major contaminants in PLS solution with increasing pH (DTK-C13).

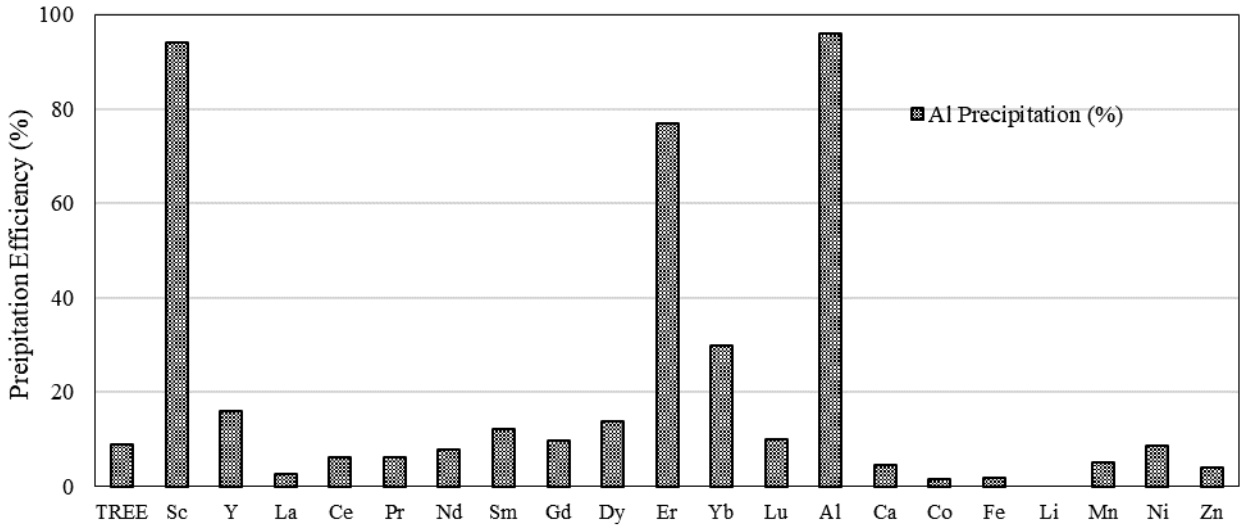

Figure 3.7.33 Al precipitation (PT0) efficiency of major RE and elements of interest (pilot scale, feed rate 1 GPM, pH 4.5 automatically adjusted using 2M NaOH).

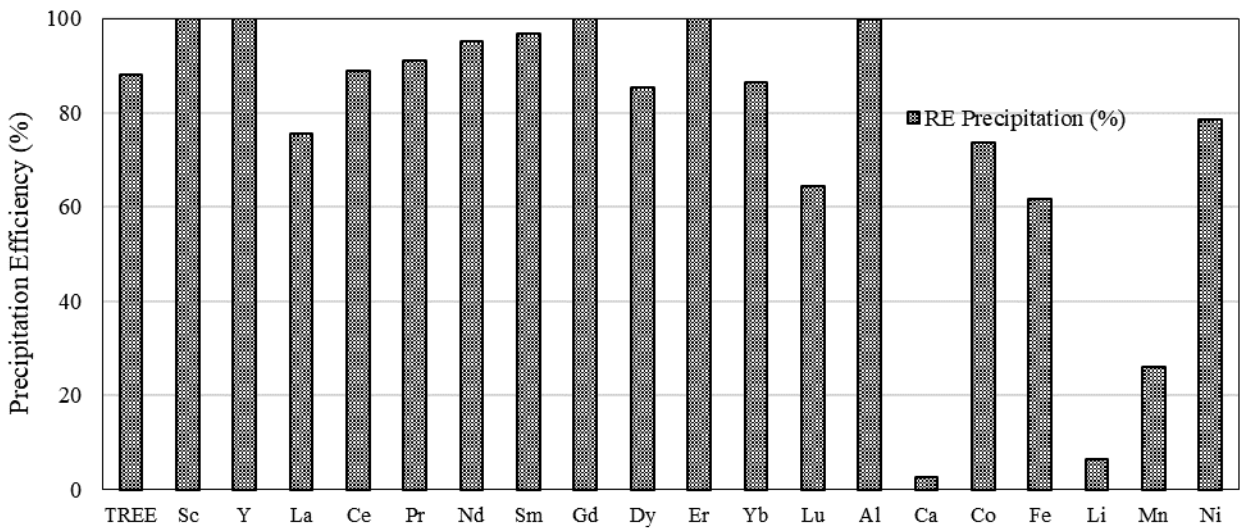

Figure 3.7.34. RE precipitation (PT1) efficiency of major RE and elements of interest (pilot scale, feed rate 1 GPM, pH 6.5 automatically adjusted using 2M NaOH).

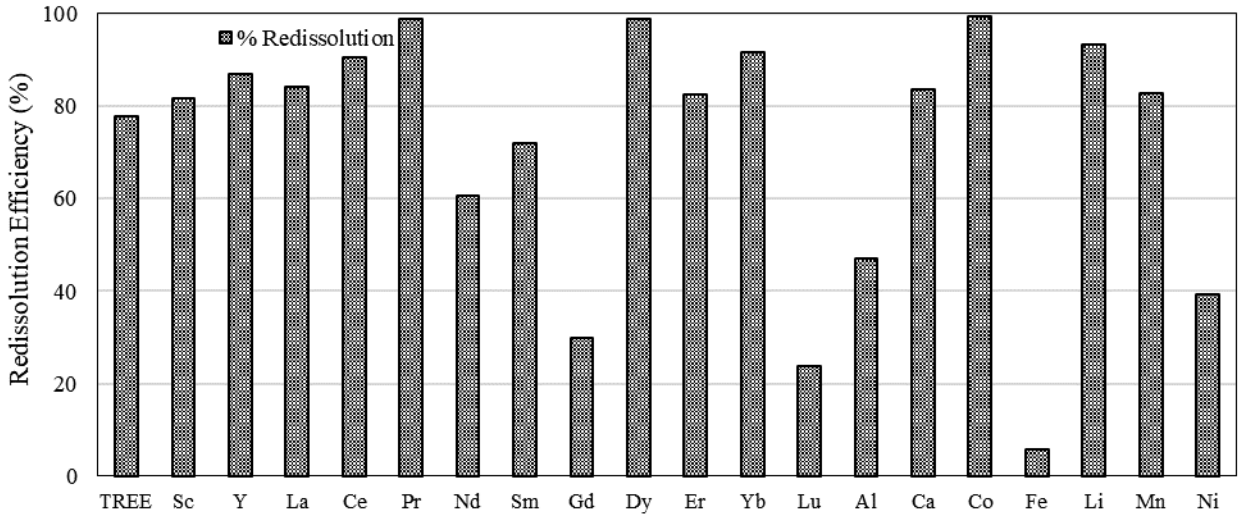

Figure 3.7.35. Redissolution (L2) efficiency of major RE and elements of interest (pilot scale, 200 Gallons, HCl 9ml/L, pH 2.5).

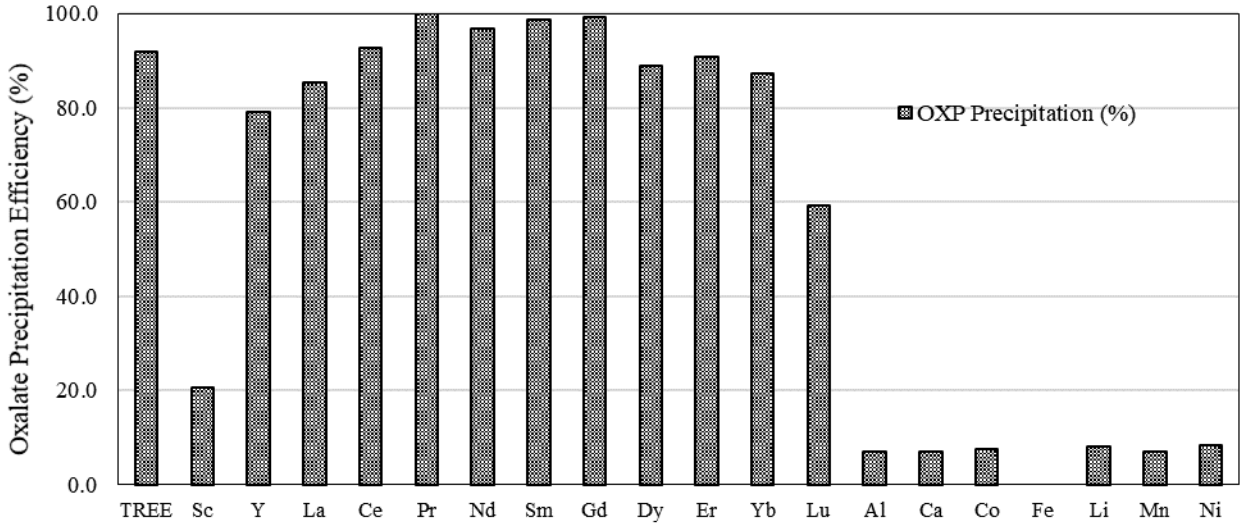

Figure 3.7.36. Oxalate precipitation (OXP) efficiency of major RE and elements of interest (pilot scale, feed rate 2 GPM, oxalic acid 6.4 g/L, pH 1.5, 20 min retention time).

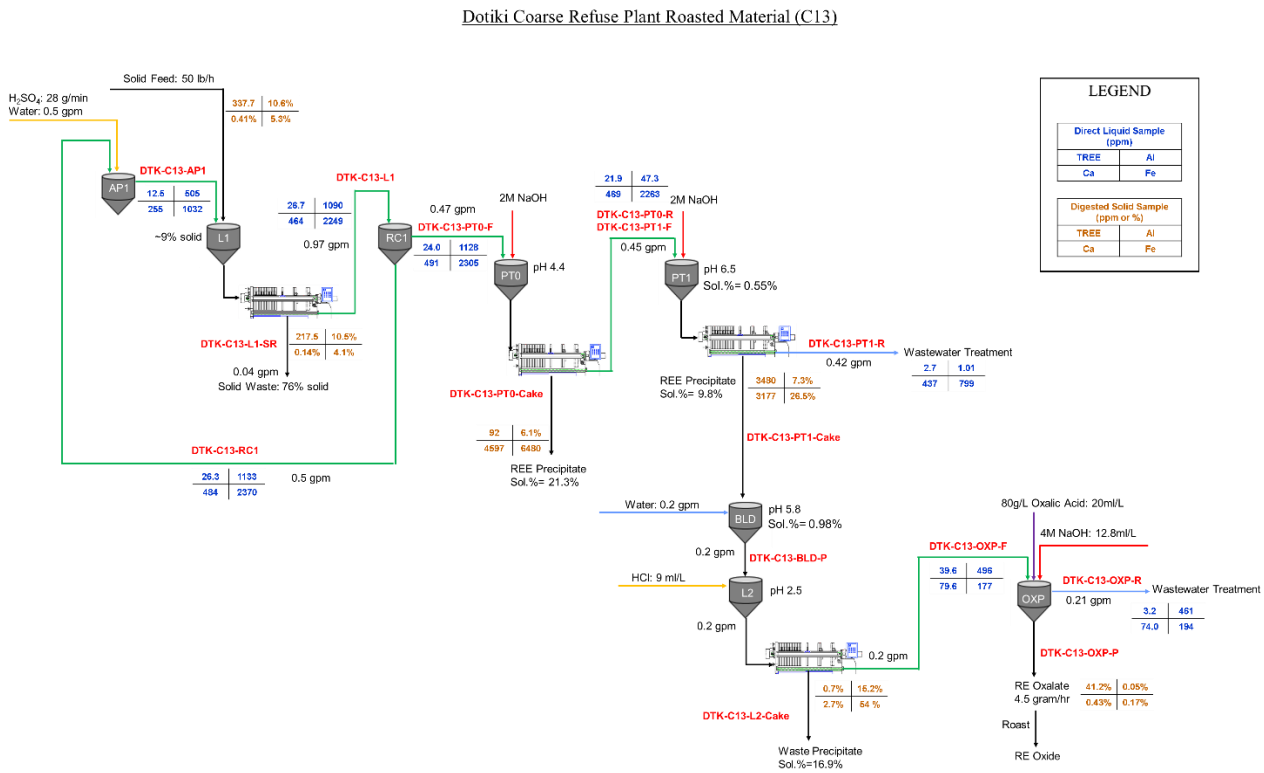

Figure 3.7.37. DTK-C13 RE production flowsheet.

3.7.1.3 Modified circuit testing

DTK-C14 Test

Test DTK-C14 continuous pilot test was conducted on 2-shift operation. It is to repeat DTK-C12 test conditions with more systematically controlled reaction times and cut-points. The test was carried out using the plant roasted west KY 13 coarse refuse material with a solid feed rate of 50 lb/hr feed rate. Leachate recirculation was applied in this test. At the beginning of the test, 0.025M (2.5 gram concentrated sulfuric acid in 1 Liter of water) of sulfuric acid solution was prepared in the 100-gallon acid preparation tank (AP) then overflowed to the 100-gallon leach tank (L1). The tanks with acid solution were preheat to 75 °C then solid feed was fed into the leach tank at feed rate of 50 lb/hr. The solid feed was fed for 2 hours without feeding the acid solution. After 2 hours, the acid solution feed resume at a rate of 1 gpm. The solid to liquid ratio in the leaching tank is 1:10, which made the solid concentration of 9.07%. The slurry in the leach tank was pumped out at 1 gpm rate to the filter feed tank, additional volume in the leach tank was free flowed to the filter feed tank through an overflow weir. The filtration was stored in the leachate recirculation tank till the hour 6 in the run. At hour 6, 0.5 gpm of leachate was pumped back into acid preparation tank to make up acid. The flowrate of concentrated sulfuric acid remains 1.1 kg/h, whereas the freshwater flow rate reduced to be 0.5 gpm.

The absolute RE gain in the leaching process at time *t (hours)* is calculated as:

$$C_{TREE\ gain,\ t} = C_{TREE\ in\ L1,\ t} - C_{TREE\ in\ AP1,\ t-2}$$

where $c_{TREE\ in\ L1,\ t}$ is the TREE concentration in leaching tank L1 at time *t*; $c_{TREE\ in\ AP1,\ t-2}$ is the concentration of TREE in acid preparation tank AP1 at 2 hours before time *t*.

The leaching recovery is calculated using the mass of element leached out into pregnant solution and the mass of the elements left in the solid residual.

$$\text{Recovery \%} = \frac{c_L * V_L}{c_L * V_L + c_{SR} * m_{SR}}$$

where, c_L is the element concentration in leachate (mg/L), V_L is the volume of leachate (L), c_{SR} is the element concentration in solid residual (mg/kg), m_{SR} is the weight of solid residual (kg).

The leaching recovery of total REEs increased from 22% at the beginning of the operation to about 26% at the end of the run. The Ca concentration in pregnant leachate solution (PLS) was 285 ppm at the beginning of the operation and increased to 440 ppm at the end. Even though the absolute concentration increased, the leaching recovery decreased over time, which likely due to the precipitation of gypsum caused by sulfate ion accumulation in solution. Similar to Ca, Co and Dy also showed a decreasing trend over time. The pH of the leach tank is in a range of 3.0 to 3.3 over 16 hour time period as shown in Figure 3.7.39. At this mild leaching condition, the Sc leaching recovery is only 3-4 percentage. The leachate recirculation methodology does not improve recovery of mild acid concentration leaching as significant as the recovery of high acid concentration leaching, because the remaining H+ ions in the PLS is very low in concentration (i.e. 0.001M H+ at pH 3).

The precipitation curve was generated for the PLS solution as shown in Figure 3.7.40. The precipitation behavior of Al and Sc aligned well with the test DTK-C12 results. In the DTK-C12 test, pH 4.5 was selected for Al precipitation. The Al removal was 95%, however, there was a 91% Sc loss with Al. In this test, an adjustment was made to move the pH cut point slightly lower so that the Sc loss can be reduced with a lower Al removal efficiency. Since Sc holds the highest economic value, the cost of carrying Al to the downstream maybe compensated.

There is a very narrow window between pH 4 and 4.2 to realize a slight separation of Sc and Al. Therefore, pH 4.2 was selected for the pilot plant continuous run for Al precipitation (Unit PT0). Since the curve between 4.0 to 4.2 is very sharp, the Al precipitation within that range is not very stable. Some post precipitation was observed in filtrate after filtering the Al precipitate cake. The post-precipitates usually contain some amount of co-precipitated REEs which was captured in the RE precipitation stage (Unit PT1).

After Al precipitation, the RE precipitation was carried out at pH 6.5. The TREE precipitation pH is slightly lower than that has been seen in the previous tests. At pH 6, almost all the TREEs were precipitated together with Fe. The efficiency of Al precipitation and RE precipitation are as shown in Figure 3.7.42 and Figure 3.7.43. In PT0 unit, only 46% Al was removed, however the loss of Sc reduced to 32% together with about 7% of TREEs and 10% of Fe. In the RE precipitation step, about 98% of TREEs are captured in the precipitate with 99% of the rest of Al and 94% Fe. About 32% Gd and 35% Dy was lost to the effluent but can be captured

in a subcircuit. 66% of Co precipitated with REEs in this test, whereas only 21% of Mn reports to the RE precipitate.

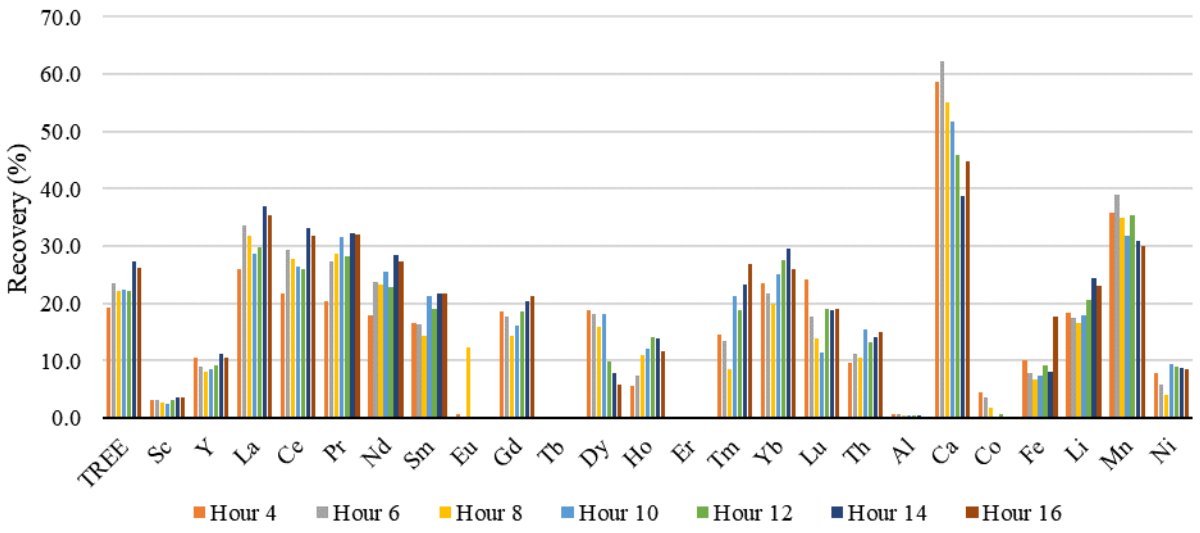

Figure 3.7.38. The bi-hourly leaching recovery of REEs, CMs and major elements of interest. (pilot scale continuous operation, 50lb/hr feed, 50kg/ton sulfuric acid, 50% leachate recirculation.)

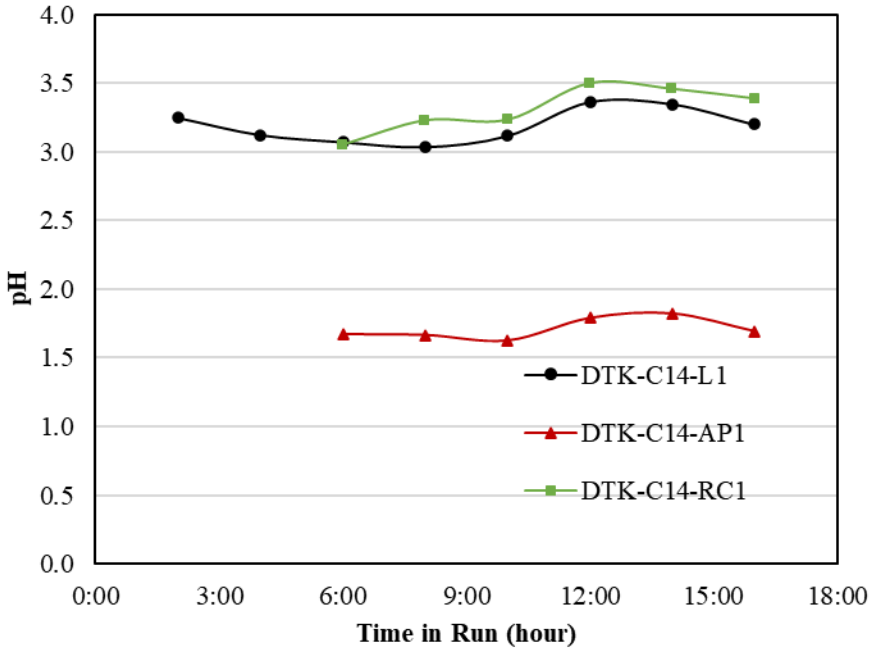

Figure 3.7.39. Recorded pH of three PLS streams in leaching circuit.

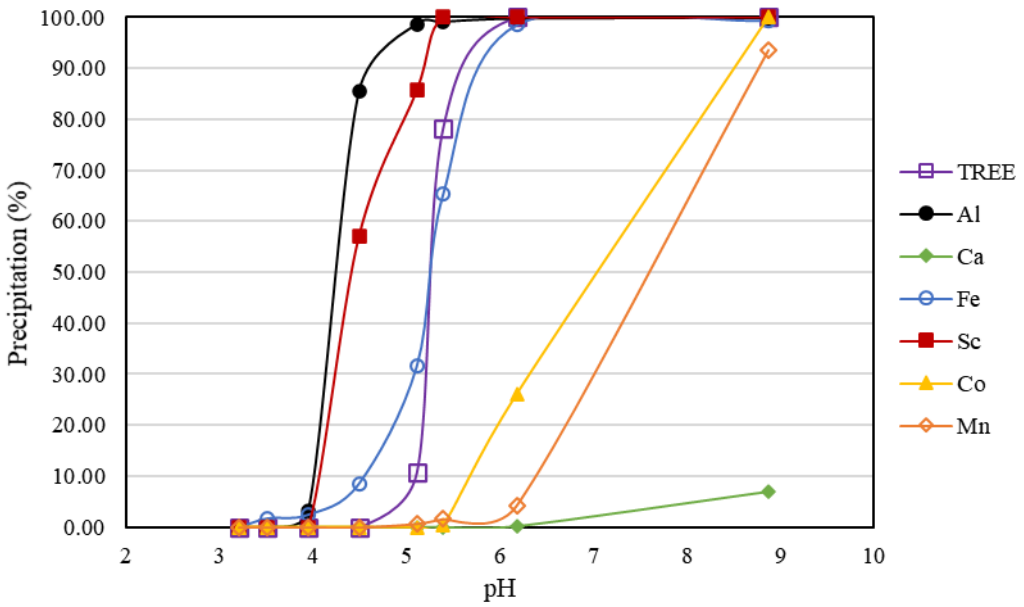

Figure 3.7.40 . Precipitation efficiency curve of the DTK-C14 PLS.

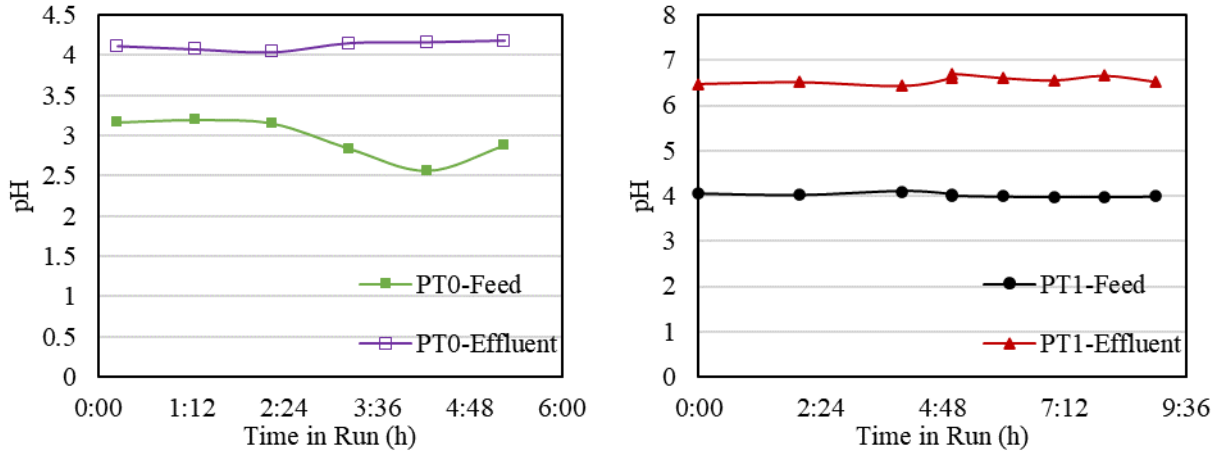

Figure 3.7.41. Recorded pH of Al precipitation and RE precipitation operation.

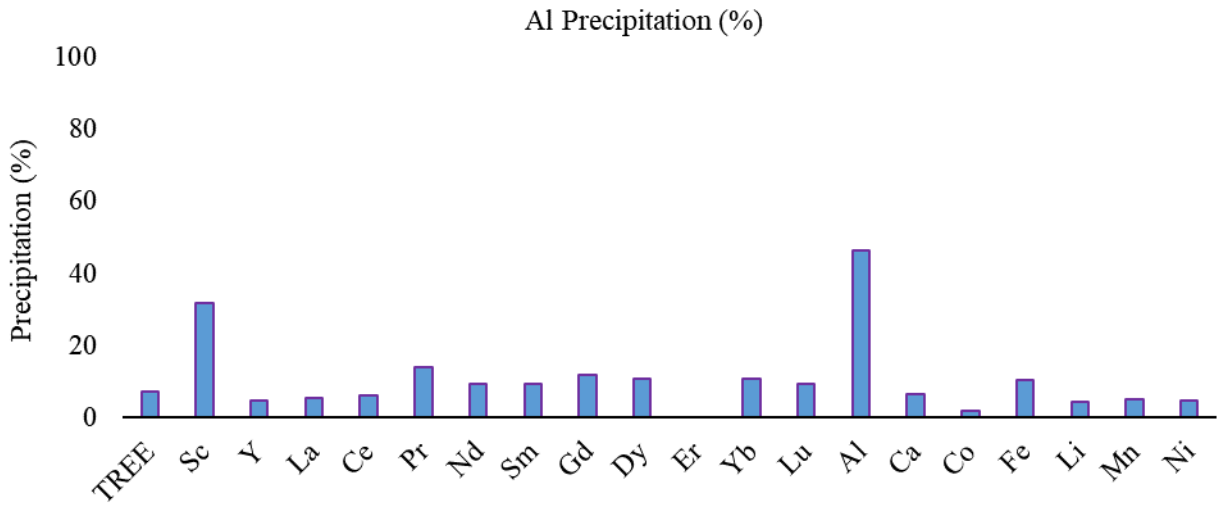

Figure 3.7.42. Precipitation efficiency of REEs and elements of interest. (DTK-C14-PT0 Al precipitation at pH 4.2, residence time 1 hour.))

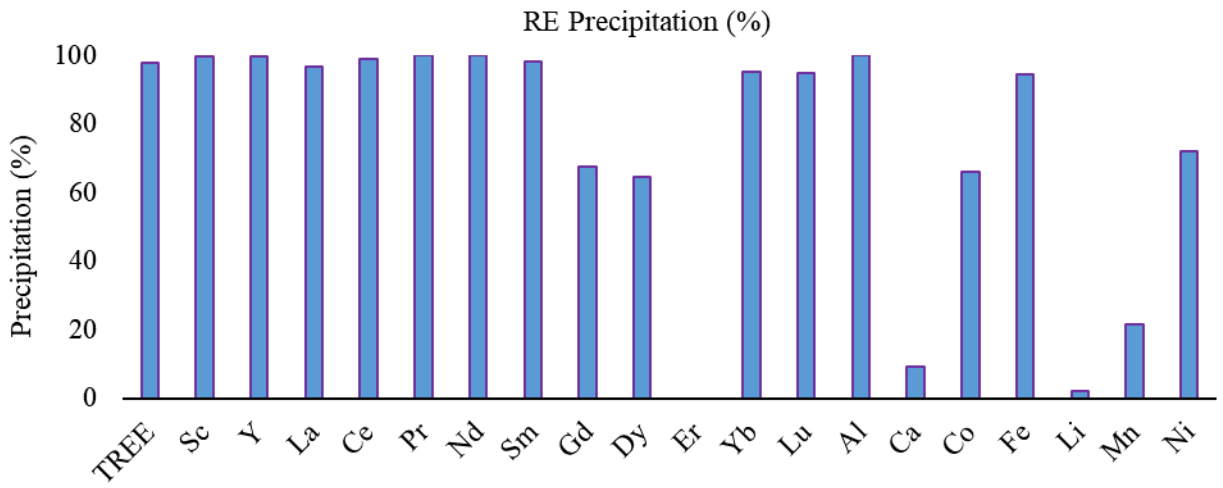

Figure 3.7.43. Precipitation efficiency of REEs and elements of interest. (DTK-C14-PT1 RE precipitation at pH 6.5, residence time 2 hour.)

The PT1 RE sludge cake was 92.5 lbs (without perlite) collected in a barrel. The solid concentration of the cake is about 11.8% by weight. The TREE concentration in the RE preconcentrate sludge cake is about 4464 ppm on a dried whole mass basis, with 3.5% Al, 0.6% Ca, and 20% Fe. The sludge cake was transferred into a mixing tank and add water to a total volume of 100 gallon. A tank recirculation centrifugal pump was installed to expedite the cake blending. The mixture was blended for 3 hours until the pH was stabilized. A 500-ml slurry sample was collected from the centrifugal pump recirculation line, then the re-dissolution test was carried out using concentrated HCl (36% by weight, trace metal grade). The maximum concentration of TREEs can be redissolved from the cake to solution is about 54 ppm, with 368 ppm Al, 132 ppm Ca, and 4432 ppm Fe. This is measured by digesting the sludge cake completely in pure HCl and analyze in ICP-OES. The redissolution curve is shown in Figure 3.7.44. At pH 2.5, the TREE

recovery was 62% with 45% Al, 90% Ca and 11% Fe, whereas at pH 2.0, the TREE recovery is about 80% with 68% Al, 99% Ca, and 28% Fe. Usually, pH 2.5 is the pH cut point for RE redissolution since the main goal was to remove 90% of Fe from the preconcentrated cake, however, the RE production is the major economic factor, not to mention the unsatisfactory Sc recovery at pH 2.5. However, at pH 2.0, the resulting concentration of contaminates will hurt the downstream oxalate precipitation by higher dosage requirement and contamination in product. A model was developed to estimate the resulting downstream process change and the gain on the RE value by reducing the redissolution pH, which will be explained in detail in Task 11. The model was carried out to compare the economics between two scenarios of pH cut point 2.0 and 2.5, and pH 2.0 was selected for the current run.

Based on the redissolution test, 6.9 ml/L of HCl was added in the blending tank and mixed for 30 minutes. The slurry was then filtered using the plate and frame filter to collect the concentrated and upgraded PLS solution. The redissolution efficiency was calculated using the element concentration in filtrate divided by the maximum concentration of this element that can be redissolved from the cake into solution, as shown in Figure 3.7.45. The filtrate contains about 40 ppm of TREEs, 192 ppm Al, 102 ppm Ca, and 677 ppm of Fe, and was fed into oxalate precipitation in the next step.

The dosage of oxalic acid needed to precipitation RE from a crude solution is highly related to the concentration of contaminants presence in the solution, especially Al and Fe in this case. Study has found that a large amount of oxalate in the solution is consumed by Al oxalate and Fe oxalate. A series of tests were carried out using different dosage of oxalic acid under different pH to determine the oxalate dosage and condition. The continuous test was carried out using 0.3 LPM of oxalic acid solution (80g/L oxalic acid in solution) added into 1 gpm feed PLS at pH 1.5 (pH adjusted using 4M NaOH, automatic controlled pump). The oxalate precipitation efficiency is shown in Figure 3.7.46.

Since the pH cut point in the redissolution step was 2.0, the Fe concentration in the oxalate feed solution was considerably higher (667 ppm). Study shows that the Fe concentration in oxalate feed will require higher dosage of oxalic acid, which would cause higher percentage of Ca precipitate as Ca oxalate. The final REO product contains 65% total rare earth oxides by weight, with 6.8% Al oxide, 3% of Fe oxide, and 22.7% Ca oxide. The Ca oxide can be washed off using mild HCl acid so that the product can be upgraded to 84%. The TREE grade in test DTK-C12 was 94% with 1.1% Al oxide, 0.5% of Fe oxide, and 2.6% Ca oxide.

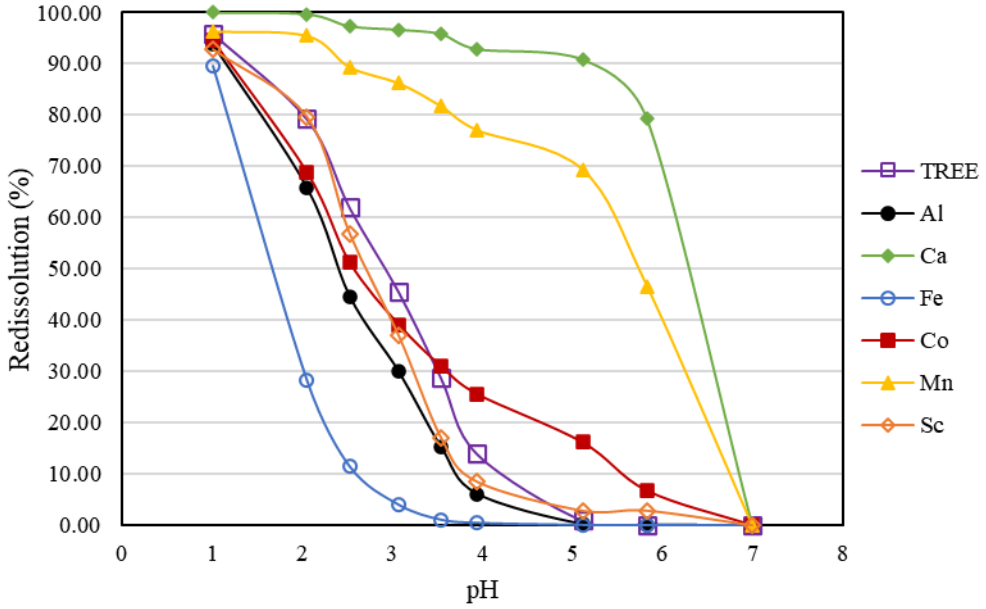

Figure 3.7.44. Redissolution curve of TREE and element of interests. (DTK-C14)

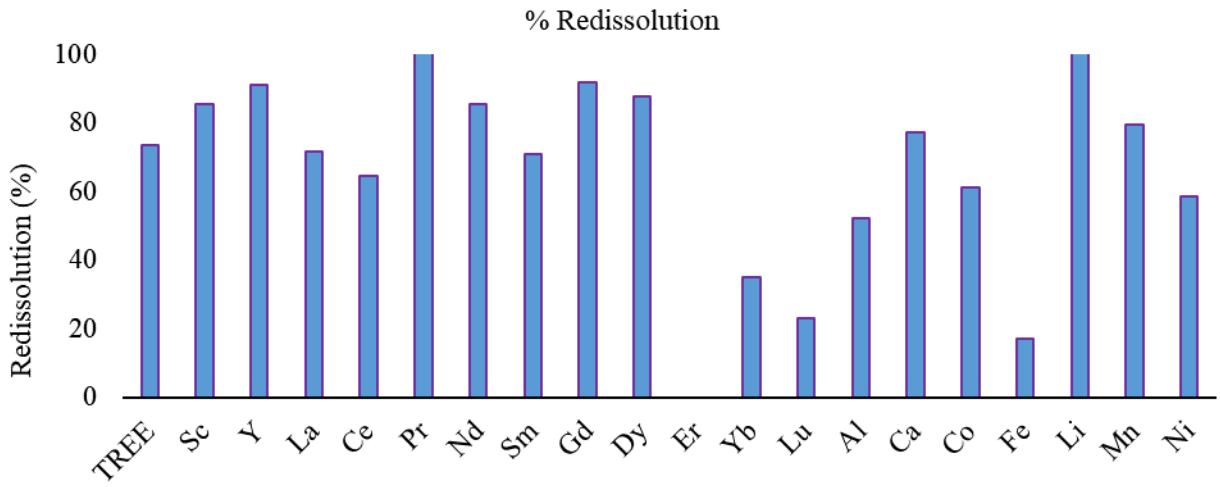

Figure 3.7.45. Redissolution efficiency of REEs and elements of interest. (DTK-C14-L2, pH2.0, HCl dosage 6.9 ml of 36% pure HCl per Liter of blended slurry.)

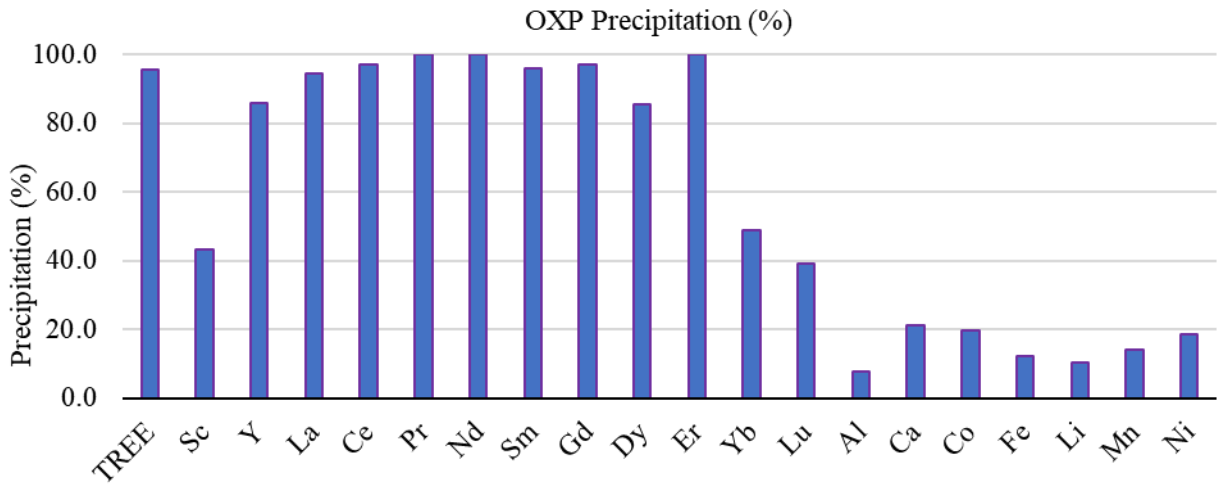

Figure 3.7.46. Oxalate precipitation recovery of REEs and elements of interest. (DTK-C14-OXP, pH 1.5 automatic control, oxalic acid dosage = 6.4 g/L of feed, oxalic acid fed in as 80g/L concentration solution.)

Even though the grade of TREE product in this test is not as high as the DTK-C12, the total recovery of TREE was improved significantly. From the roasted feed solid, to the REO product, the total recovery of TREE is 11.80% for the DTK-C14 and 7.45% for the DTK-C12 test. The major condition that was modified in the DTK-C14 test compare to C12 is 1) Al precipitation pH cut point at pH 4.2 for C14 instead of pH 4.5 for C12, and 2) RE redissolution pH cut point at pH 2.0 for C14 instead of pH 2.5 for C14.

The chemical cost was 1.14 times more for test run C14 than that of test run C12, however, with the extra REO produced by achieving a higher recovery, the $chemical per kg of RE produced for test run C14 is only 72% of the test C12. Table 3.7.12 shows a cost break down of each stage. Notice that the leaching condition for C12 and C12 are identical, only the downstream processes cut points are different. The results show that recovery is the key to the economics given the same condition of leaching.

Table 3.7.12. Comparison of cost break down in percentage for DTK-C12 and DTK-C14 in terms of $ per kg of RE produced in final product REO mix.

Run	Leaching	Precipitation	Redissolution	Oxalate Precipitation	
	H_2SO_4$/kg RE	$NaOH/kg RE	$HCl/kg RE	$Oxalic/kg RE	$NaOH/kg RE
DTK-C12	43%	27%	8%	21%	0%
DTK-C14	38%	19%	9%	30%	4%

3.7.2 Fire Clay Source Parametric Testing

In section 3.5.2, the optimal roasting condition was determined for Fire Clay material. The Fire Clay coarse refuse material contains majority of rare earth elements exist in mineral form which is difficult to decompose. Seven barrels of fire clay coarse refuse material were produced

in the pilot plant roaster at product rate of 5 lb/h and inner tube roasting temperature of 600 ºC. The roasted material contains in average of 377 ppm ±29 ppm of total rare earth content on a dry ash basis, which is 358 ± 27 ppm of TREE on a while mass basis. The ash content is in average of 95% ± 0.9%. The individual rare earth concentration is shown in Figure 3.7.47.

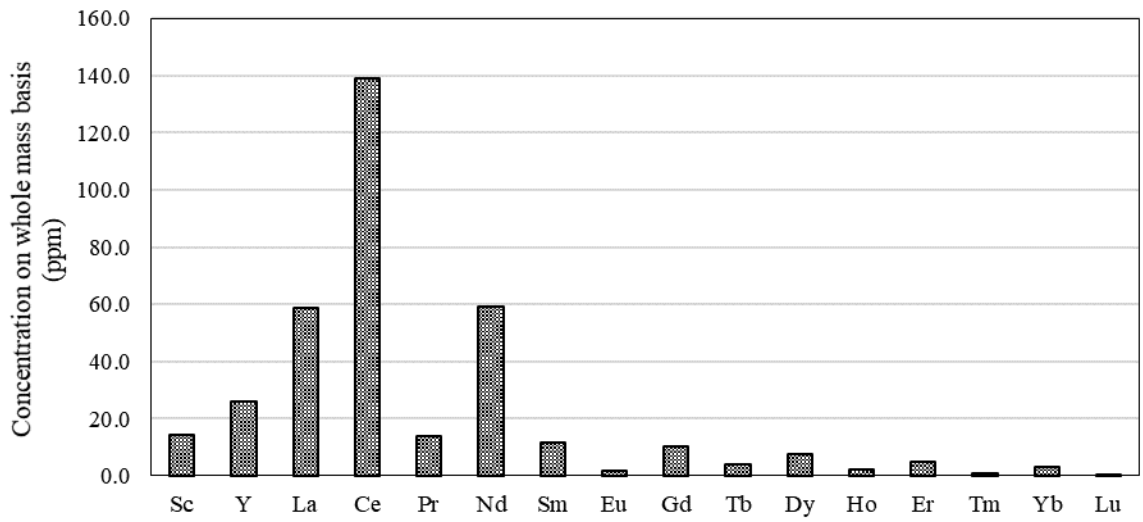

Figure 3.7.47. RE concentration on whole mass basis in the roasted fire clay material that feed into the hydrometallurgical circuit.

Three pilot scale continuous tests were carried out for fireclay material with test conditions listed in Table 3.7.13. Two shifts operation were employed during these tests run. The operation scheduled for each shift is as detailed in Table 3.7.14. In addition to the pilot plant operation, lab tests were carried out on Day 2 Night shift to determine the Al and RE precipitation condition for PT0 and PT1 operation, Day 4 Day shift to determine the RE redissolution conditions for L2 operation, and Day 4 Night shift to determine the condition for RE oxalate precipitation condition for OXP operation. The ICP-OES analytical lab is also operating at a 2-shift schedule to support the timely sensitive sample analysis and provide quality-controlled analysis report to support the pilot plant operation.

Table 3.7.13. Test conditions for fireclay continuous run (pilot scale).

Test Code	Solid Feed (lb/hr)	Water (gpm)	H_2SO_4 (M)	Retention (h)	Duration (h)	Leachate Recirculation
FC-C4	50	1	0.1	2	16	0.5 gpm
FC-C5	50	1	0.5	2	14	0.5 gpm
FC-C6	50	1	0.05	2	16	0.5 gpm

Table 3.7.14. Two-shift operation schedule on each continuous run.

Run	Day Shift	Night Shift
Day 1	Prepare for leaching	
Day 2	Leaching (L1)	Leaching (L1)
Day 3	Al Precipitation (PT0)	RE Precipitation (PT1)
Day 4	RE Precipitate Blending (BLD)	RE Redissolution (L2)
Day 5	RE Oxalate Precipitation (OXP)	

The flowsheet used to run the 3 tests on fireclay material is as shown in Figure 3.7.48. The leachate recirculation was employed to maximize the leaching efficiency and improve the leaching recovery. Leachate samples were collected from the leaching tank (L1), acid preparation tank (AP1) and recirculation tank (RC1) to track the leaching performance. Solid feed sample and leaching residual samples were collected every two hours and the sample were sent to KGS for digestion and ICP analysis. The absolute RE gain in the leaching process at time *t (hours)* is calculated as:

$$c_{TREE\ gain,\ t} = c_{TREE\ in\ L1,\ t} - c_{TREE\ in\ AP1,\ t\text{-}2}$$

where $c_{TREE\ in\ L1,\ t}$ is the TREE concentration in leaching tank L1 at time *t*; $c_{TREE\ in\ AP1,\ t\text{-}2}$ is the concentration of TREE in acid preparation tank AP1 at 2 hours before time *t*.

The leaching recovery is calculated using the mass of element leached out into pregnant solution and the mass of the elements left in the solid residual. The

$$\text{Recovery \%} = \frac{c_L * V_L}{c_L * V_L + c_{SR} * m_{SR}}$$

where, c_L is the element concentration in leachate (mg/L), V_L is the volume of leachate (L), c_{SR} is the element concentration in solid residual (mg/kg), m_{SR} is the weight of solid residual (kg).

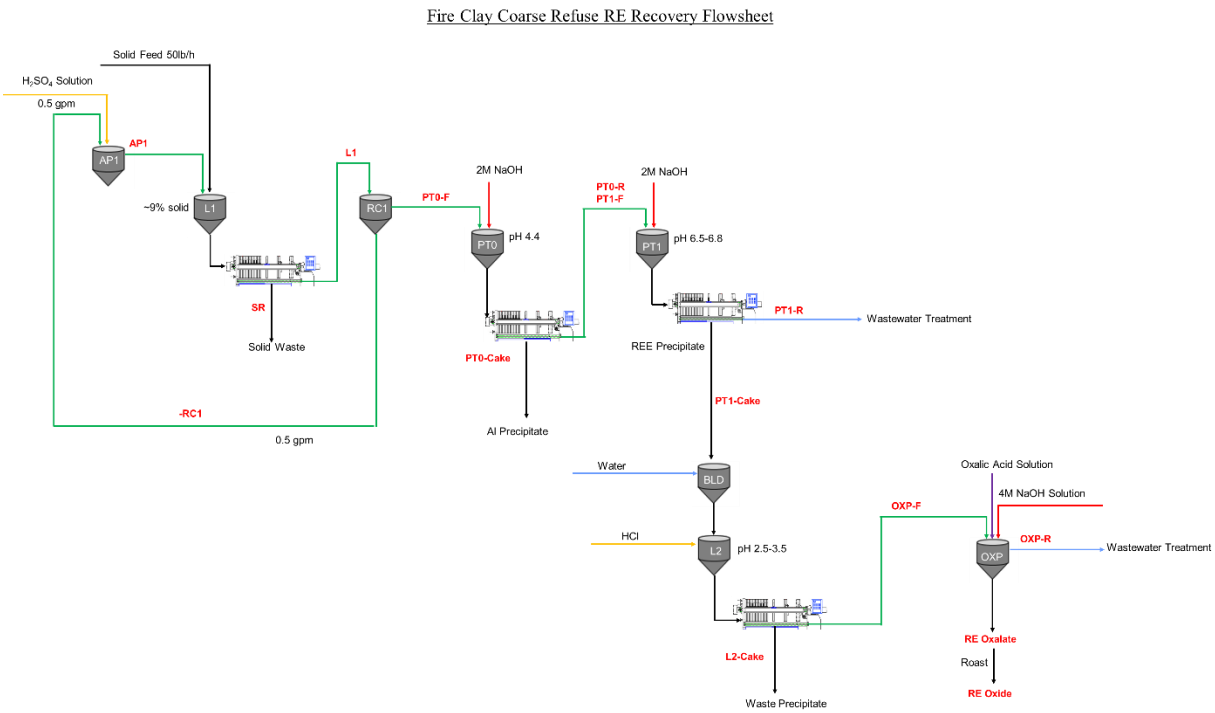

Figure 3.7.48**.** Schematic of flowsheet used in Fire Clay parametric testing.

3.7.2.1 Leaching

As reported in the previous section, the leachate recirculation scheme provides benefit on leaching recovery when leaching at a higher acid dosage. The 3 test results verified the conclusion. The results in Figure 3.7.49 show that with 0.1M sulfuric acid leaching at 75ºC, the concentration of TREE reached 10 ppm in the first two hours leaching, the concentration of REE fluctuates over the time of leaching and stabilized at around 10 ppm after 14 hours. Similar trend was observed in test FC-C6 with 0.05M sulfuric acid leaching. However, in test FC-C5 with 0.5M acid leaching, the concentration of REEs continuously increased over the 16 hours of leaching time and reached nearly 14 ppm of TREE at the end of the test run. The leaching test log sheet as shown in Table 3.7.15, Table 3.7.16, and Table 3.7.17 for test FC-C4, C5, and C6. The ending pH for C4, C5, C6 is 1.6, 0.7, and 2.1, respectively. For test C4, the pH in leaching tank (L1) stabilized after one retention time after the recirculation started. For test C6, the pH in leaching slightly increased over the period of leaching time. It may be due to slightly accumulation of the solid as shown in the solid concentration column.

With decreasing the pH in the leaching tank, the recovery of contamination material increased as well. The Al concentration in the leachate solution in C5 test reached 3000 ppm at the end of the test run. It resulted in an elevated Al/RE in the downstream process which caused difficulties for RE purification. The leaching recovery of Fe and Ca reached steady state within one retention time after recirculating started for test C4 and C6. It indicated that the Fe containing

material reached equilibrium at the value of pH. For test C5, the Fe recovery increased after the recirculation started since the pH of the leaching tank (L1) reduced significantly.

The leaching recovery of REE and other major elements are plotted in Figure 3.7.52. The recovery of TREE for test C4, C5, and C6 was 14%, 19%, and 26%, respectively. The recovery of Al, Ca, and Fe increased significantly with increase the acid concentration to 0.5M.

Table 3.7.15. Operation log of FC-C4 test leaching and recirculation circuit.

ID	#	Date	Tank	Time	Hours in Run	Temp (C)	% Solids	pH
FC-C4-L1	P1	5/5/2020	T14	9:15	2	75	6.29	2.51
FC-C4-L1	P2	5/5/2020	T14	11:15	4	75	8.02	1.82
FC-C4-L1	P3	5/5/2020	T14	13:15	6	75	6.95	1.68
FC-C4-L1	P4	5/5/2020	T14	15:15	8	75	7.15	1.69
FC-C4-L1	P5	5/5/2020	T14	17:15	10	75	8.01	1.70
FC-C4-L1	P6	5/5/2020	T14	19:15	12	75	6.21	1.57
FC-C4-L1	P7	5/5/2020	T14	21:15	14	75	7.56	1.66
FC-C4-L1	P8	5/5/2020	T14	23:15	16	75	7.67	1.59
Average							7.23	1.77
ID	**#**	**Date**	**Tank**	**Time**	**Hours in Run**	**Temp (C)**	**% Solids**	**pH**
FC-C4-AP1	1	5/5/2020	T6	13:15	6	-	-	1.13
FC-C4-AP1	2	5/5/2020	T6	15:15	8	-	-	1.10
FC-C4-AP1	3	5/5/2020	T6	17:15	10	-	-	1.13
FC-C4-AP1	4	5/5/2020	T6	19:15	12	-	-	1.13
FC-C4-AP1	5	5/5/2020	T6	21:15	14	-	-	1.09
FC-C4-AP1	6	5/5/2020	T6	23:15	16	-	-	1.15
ID	**#**	**Date**	**Tank**	**Time**	**Hours in Run**	**Temp (C)**	**% Solids**	**pH**
FC-C4-RC1	1	5/5/2020	T8	13:15	6	-	-	1.81
FC-C4-RC1	2	5/5/2020	T8	15:15	8	-	-	1.78
FC-C4-RC1	3	5/5/2020	T8	17:15	10	-	-	1.66
FC-C4-RC1	4	5/5/2020	T8	19:15	12	-	-	1.67
FC-C4-RC1	5	5/5/2020	T8	21:15	14	-	-	1.59
FC-C4-RC1	6	5/5/2020	T8	23:15	16	-	-	1.56

Table 3.7.16. Operation log of FC-C5 test leaching and recirculation circuit.

ID	#	Date	Tank	Time	Hours in Run	Temp (C)	% Solids	pH
FC-C5-L1	P1	5/12/2020	T4	9:00	2:00	75	4.277	0.86
FC-C5-L1	P2	5/12/2020	T4	11:00	4:00	75	6.922	1.07
FC-C5-L1	P3	5/12/2020	T4	13:00	6:00	75	7.079	1.91
FC-C5-L1	P4	5/12/2020	T4	15:00	8:00	75	7.430	0.851
FC-C5-L1	P5	5/12/2020	T4	18:00	11:00	75	8.248	0.838
FC-C5-L1	P6	5/12/2020	T4	20:00	13:00	75	6.788	0.764
FC-C5-L1	P7	5/12/2020	T4	22:00	15:00	75	-	0.712
Average							6.791	1.001
ID	**#**	**Date**	**Tank**	**Time**	**Hours in Run**	**Temp (C)**	**% Solids**	**pH**
FC-C5-AP1	1	5/12/2020	T6	13:00	6:00	-	-	1.56
FC-C5-AP1	2	5/12/2020	T6	15:00	8:00	-	-	0.534
FC-C5-AP1	3	5/12/2020	T6	18:00	10:00	-	-	0.561
FC-C5-AP1	4	5/12/2020	T6	20:00	12:00	-	-	0.543
FC-C5-AP1	5	5/12/2020	T6	22:00	14:00	-	-	0.555
ID	**#**	**Date**	**Tank**	**Time**	**Hours in Run**	**Temp (C)**	**% Solids**	**pH**
FC-C5-RC1	1	5/12/2020	T8	13:00	6:00	-	-	0.856
FC-C5-RC1	2	5/12/2020	T8	15:00	8:00	-	-	1.082
FC-C5-RC1	3	5/12/2020	T8	18:00	10:00	-	-	1.031
FC-C5-RC1	4	5/12/2020	T8	20:00	12:00	-	-	0.856
FC-C5-RC1	5	5/12/2020	T8	22:00	14:00	-	-	-

Table 3.7.17. Operation log of FC-C6 test leaching and recirculation circuit.

ID	#	Date	Tank	Time	Hours in Run	Temp (C)	% Solids	pH
FC-C6-L1	P1	5/19/2020	T4	8:20	2.00	75	3.187	1.451
FC-C6-L1	P2	5/19/2020	T4	10:20	4.00	75	6.846	1.906
FC-C6-L1	P3	5/19/2020	T4	12:20	6.00	75	7.205	1.916
FC-C6-L1	P4	5/19/2020	T4	14:20	8.00	75	7.381	1.938
FC-C6-L1	P5	5/19/2020	T4	16:20	10.00	75	7.800	1.945
FC-C6-L1	P6	5/19/2020	T4	18:20	12.00	75	8.611	2.117
FC-C6-L1	P7	5/19/2020	T4	20:20	14.00	75	8.698	2.119
FC-C6-L1	P8	5/19/2020	T4	22:20	16.00	75	8.560	2.156
Average							7.286	1.944
ID	**#**	**Date**	**Tank**	**Time**	**Hours in Run**	**Temp (C)**	**% Solids**	**pH**
FC-C6-AP1	1	5/19/2020		12:20	6.00			1.32
FC-C6-AP1	2	5/19/2020		14:20	8.00			1.395
FC-C6-AP1	3	5/19/2020		16:20	10.00			1.27
FC-C6-AP1	4	5/19/2020		18:20	12.00			1.355
FC-C6-AP1	5	5/19/2020		20:20	14.00			1.363
FC-C6-AP1	6	5/19/2020		22:20	16.00			-
ID	**#**	**Date**	**Tank**	**Time**	**Hours in Run**	**Temp (C)**	**% Solids**	**pH**
FC-C6-RC1	1	5/19/2020		12:20	6.00			1.828
FC-C6-RC1	2	5/19/2020		14:20	8.00			1.988
FC-C6-RC1	3	5/19/2020		16:20	10.00			1.995
FC-C6-RC1	4	5/19/2020		18:20	12.00			2.085
FC-C6-RC1	5	5/19/2020		20:20	14.00			2.169
FC-C6-RC1	6	5/19/2020		22:20	16.00			2.21

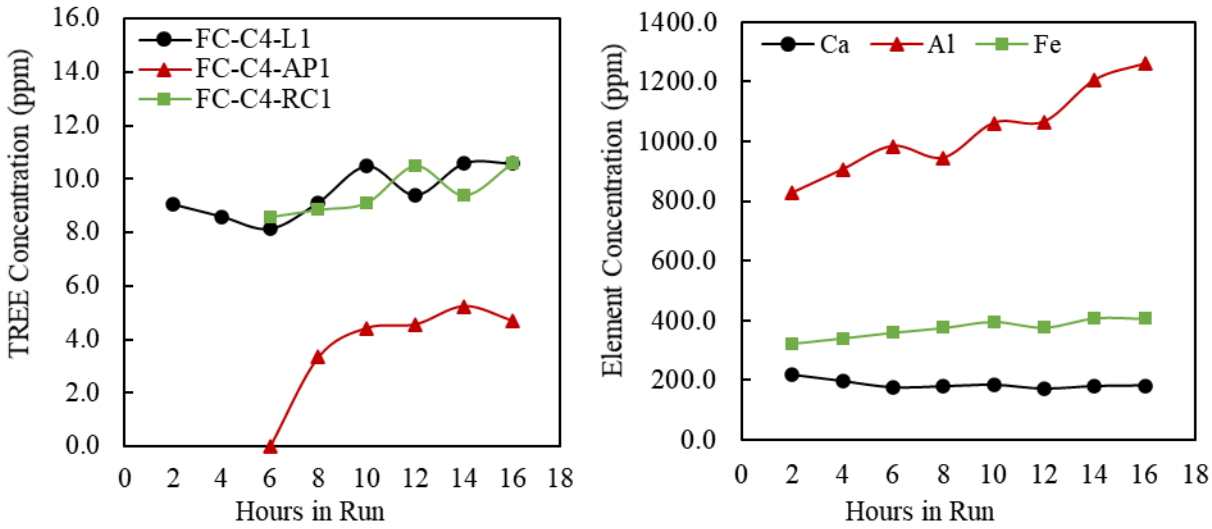

Figure 3.7.49. PLS Concentration at 0.1M acid leaching. Left: Concentration of TREE in leaching (L1), acid preparation (AP1), and recirculation tank (RC1). Right: Concentration of major impurities in the leaching tank (L1).

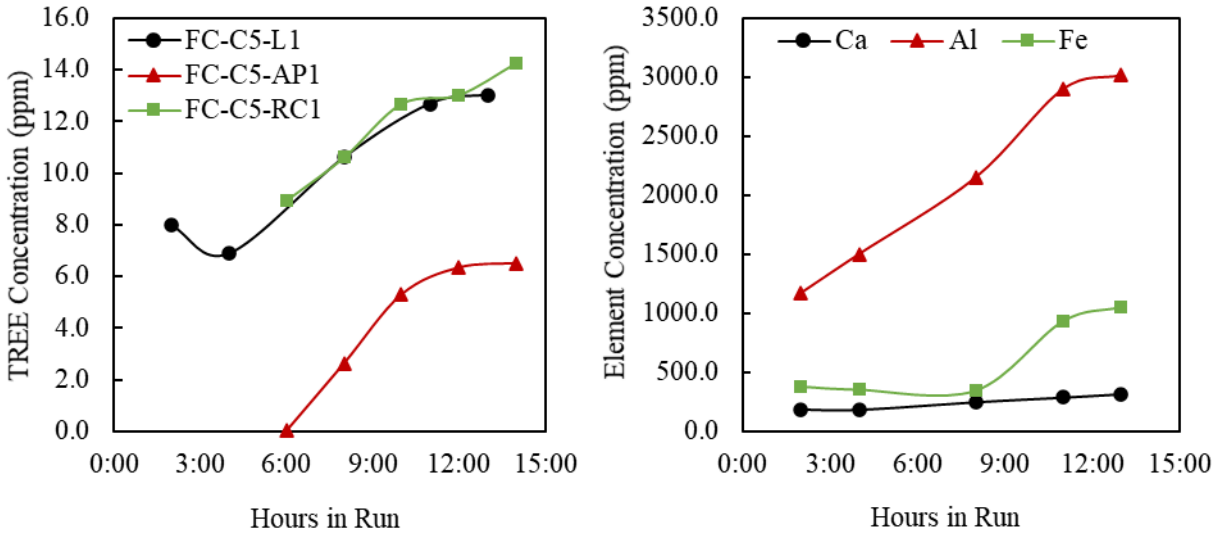

Figure 3.7.50**.** PLS Concentration at 0.5M acid leaching. Leaching Left: Concentration of TREE in leaching (L1), acid preparation (AP1), and recirculation tank (RC1). Right: Concentration of major impurities in the leaching tank (L1).

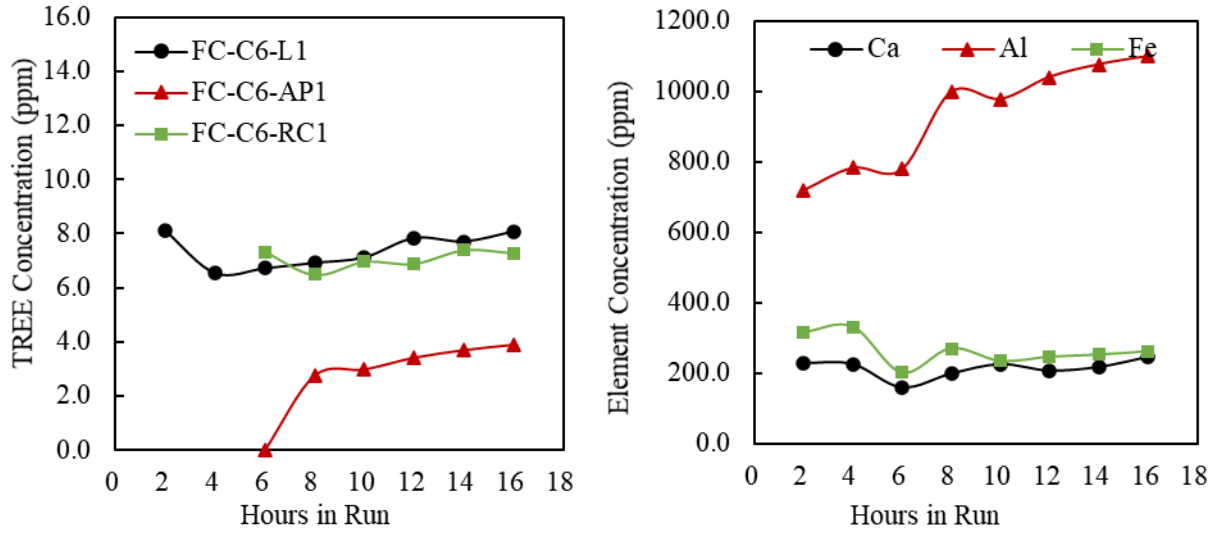

Figure 3.7.51. PLS Concentration at 0.05M acid leaching. Left: Concentration of TREE in leaching (L1), acid preparation (AP1), and recirculation tank (RC1). Right: Concentration of major impurities in the leaching tank (L1).

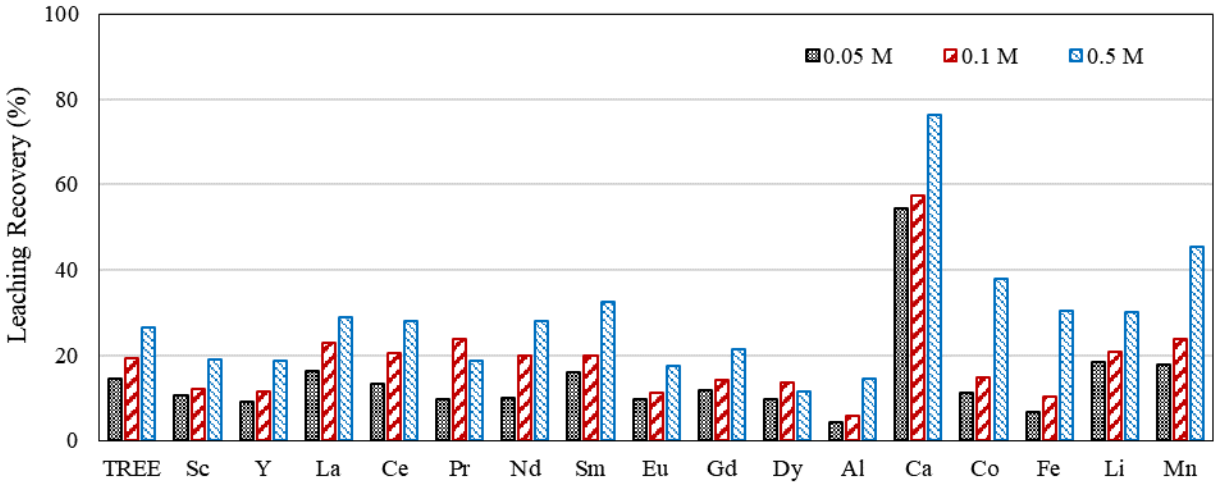

Figure 3.7.52. Leaching recovery of RE and other elements of interest at the end of continuous run in pilot scale operation (FC-C4: 0.1M, FC-C5: 0.5M, FC-C6: 0.05M Sulfuric acid, 75 ºC).

3.7.2.2 Al Precipitation

As observed in the past study, the precipitation curve of rare earth elements shifts with various ionic concentration of the solution. This set of tests created a ideal set of solution to examine the shift of curves with various ionic concentration of the solution. Figure 3.7.53, Figure 3.7.54, and Figure 3.7.55 show the precipitation curve of major elements of interest generated in lab scale swiping test. The curves show that most of the elements started precipitating from pH 4 in the leachate solution obtained from C4 and C5 test run, whereas in test C6, elements started to precipitate at pH 3.5. The ending pH of Al precipitation appear to be similar among three solutions. The Al precipitation efficiency at pH at for test C4, C5, and C6 is 86%, 92%, and 95%, respectively. The RE loss in Al precipitation stage vary significantly with different solution ionic concentration. The RE precipitation recovery at pH 4.5 for test C4, C5, C6 is 11%, 28%, and 11%, respectively, as shown in the lab test.

The pilot plant operation showed slightly misalignment with the lab test results due to the change of solution oxidation state. As shown in Figure 3.7.56, the RE loss in the Al precipitation stage for the C4, C5, and C6 tests at pH of 4.5 is 21%, 28% and 10%. The iron precipitation efficiency of the three tests is 39%, 45%, and 40%, respectively. The majority of the Fe exist in the fresh pregnant leachate solution is in ferrous state, as the pH increases, Fe2+ precipitated in the solution as a iron hydroxide compound and it may complex with other anions in the solution as well. The ferrous hydroxide compound oxidation rate is very sensitive to the mixing condition of the tank, precipitation temperature and the retention time of the precipitation. The Fe speciation curve shows that ferrous hydroxide precipitates after pH 6.5 whereas the ferric hydroxide precipitates at pH 3. The current Fe precipitation curve is a combination of both states of iron. A detailed study will be carried out with monitoring the redox potential (Eh) variation during precipitation.

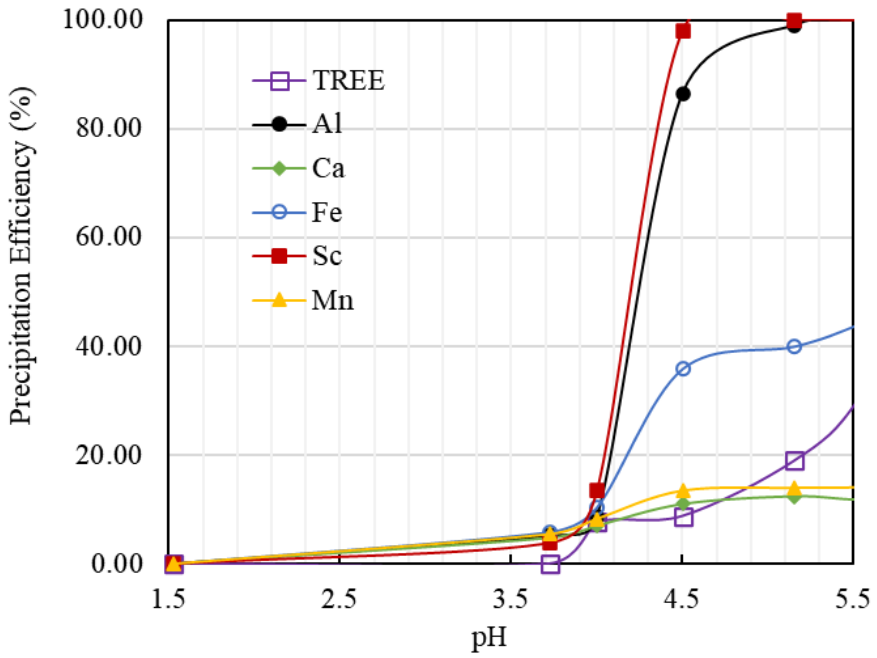

Figure 3.7.53. Precipitation efficiency of RE and major contaminants in PLS solution with increasing pH (FC-C4).

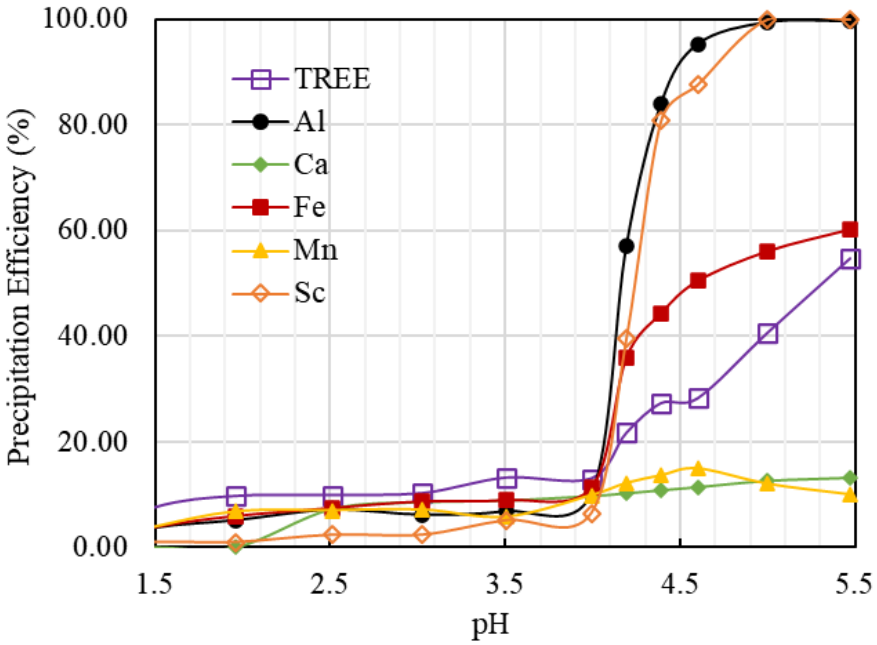

Figure 3.7.54. Precipitation efficiency of RE and major contaminants in PLS solution with increasing pH (FC-C5).

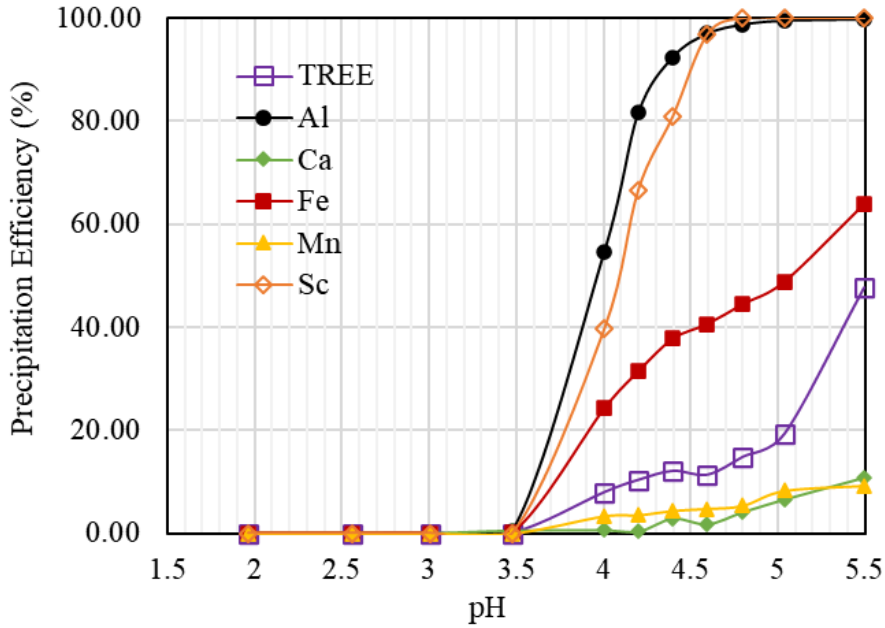

Figure 3.7.55. Precipitation efficiency of RE and major contaminants in PLS solution with increasing pH (FC-C6).

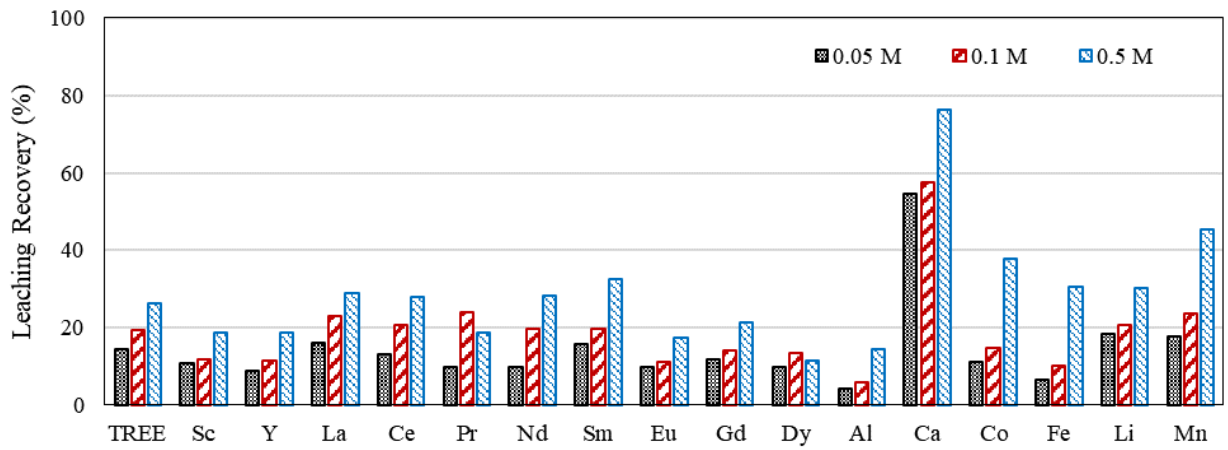

Figure 3.7.56. Al precipitation (PT0) efficiency of major RE and elements of interest (pilot scale, feed rate 2 GPM, 1 h retention time, pH 4.5 automatically adjusted using 2M NaOH).

3.7.2.3 Redissolution

After Al removal, the RE precipitation is a straightforward process by further elevating the pH to 6.8-7.0. The RE precipitate cake is blended in water and recirculated using a centrifugal pump to aid oxidation of the ferrous hydroxide compounds to ferric hydroxide. Since the fresh leachate contains mainly ferrous state iron, this is an essential step for the Fe removal in RE redissolution stage. The redissolution curve shows that Fe redissolution starts to occur from pH 3.5, and at pH 3, the %Fe dissolved into solution is 16%, 12%, and 17% for test C4, C5, and C6, respectively.

The C5 curve appears to be more biased due to the high ionic concentration. All three curves indicate a clear separation of TREE and Fe redissolution efficiency. The pH selected for RE redissolution is 3.5, 2.8, and 3.0 for FC-C4, C5, and C6 pilot scale test. The acid used in the current test is industrial grade hydrochloric acid. The acid dosage required to adjust the pH is plotted in Figure 3.7.60. The acid dosage in the redissolution stage is highly correlated to the amount of total dissolved solids (TDS) presents in the dissolved solution. The dissolution efficiency of REEs and other elements of interest is as shown in Figure 3.7.61.

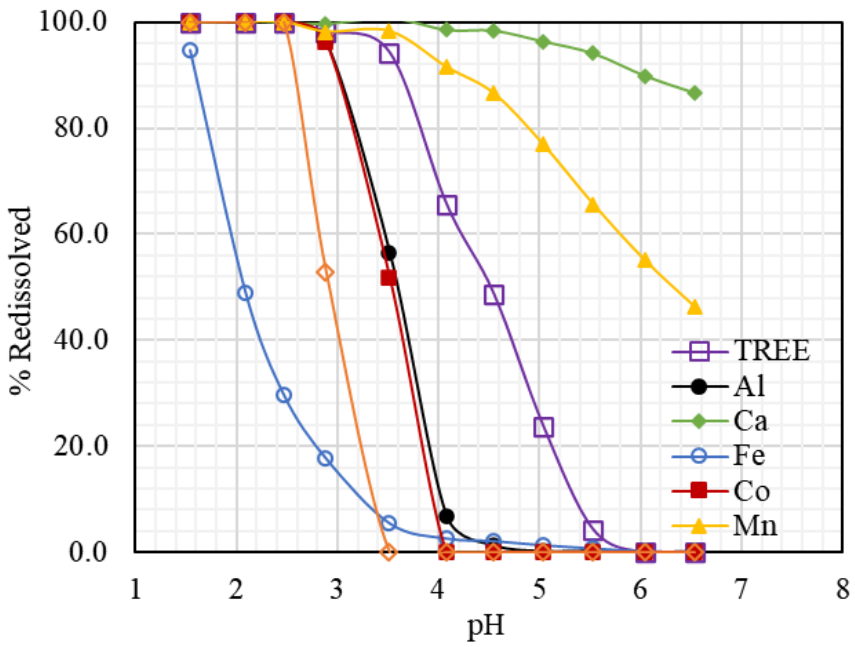

Figure 3.7.57. Redissolution efficiency of RE and major contaminants from PT1 cake using 36% HCl (FC-C4).

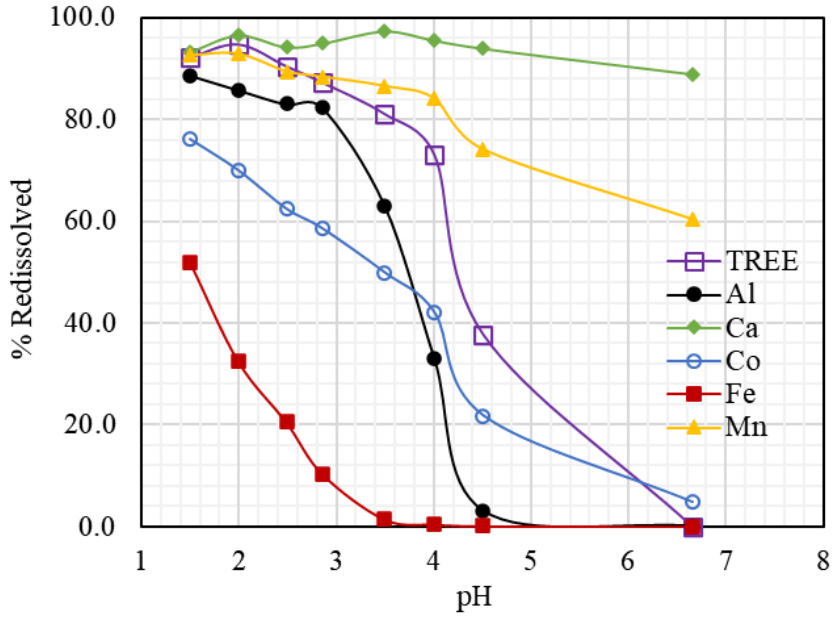

Figure 3.7.58. Redissolution efficiency of RE and major contaminants from PT1 cake using 36% HCl (FC-C5).

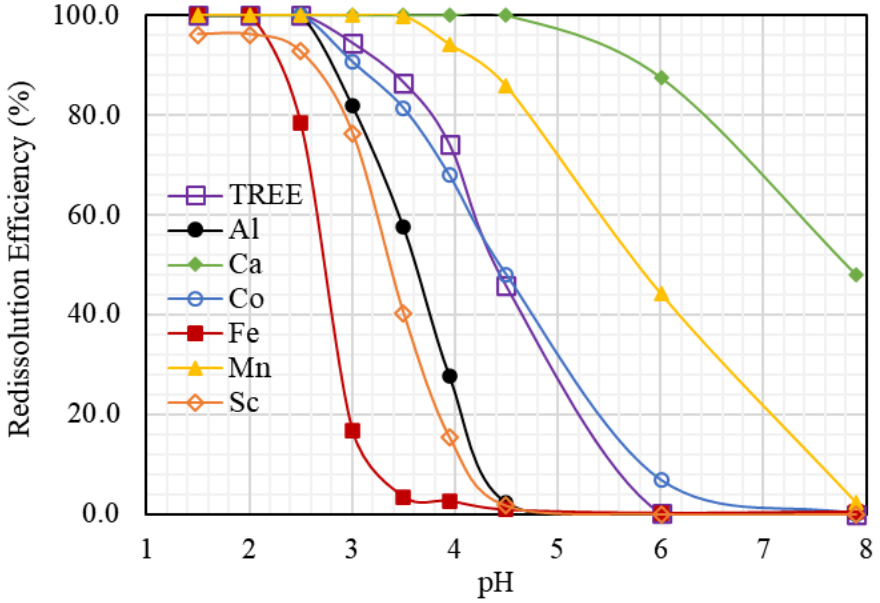

Figure 3.7.59. Redissolution efficiency of RE and major contaminants from PT1 cake using 36% HCl (FC-C6).

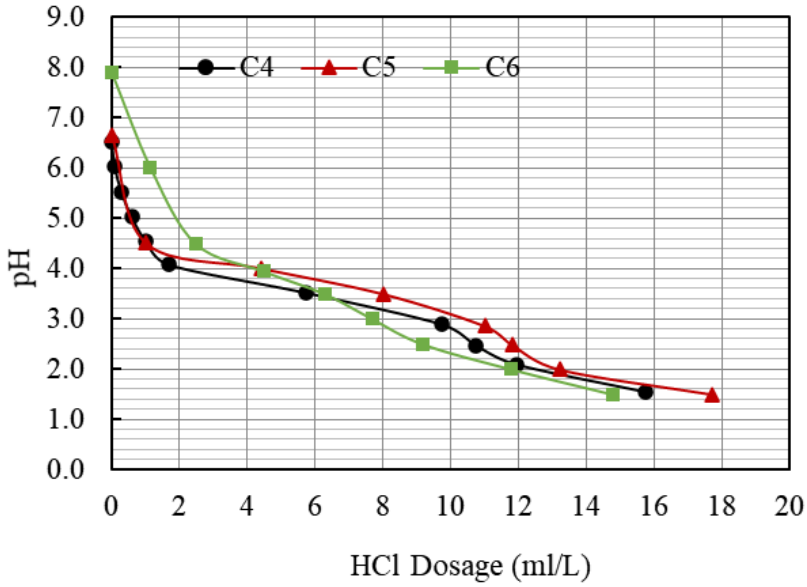

Figure 3.7.60. Dosage of HCl used to adjust the pH in RE redissolution stage.

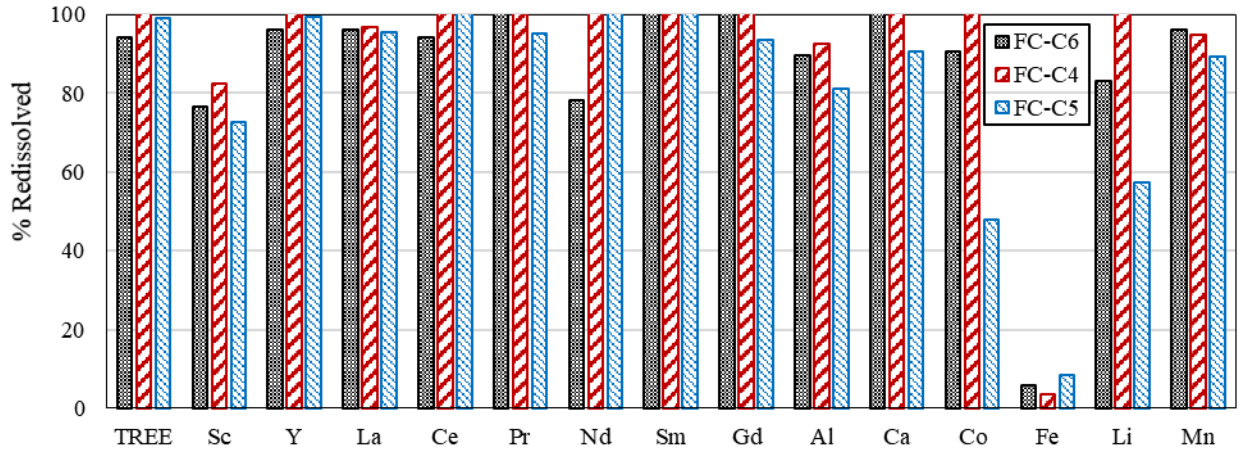

Figure 3.7.61. RE redissolution (L2) efficiency of major RE and elements of interest (pilot scale, pH adjusted using HCl, C4-200 gallon, C5-200 gallon, C6-100 gallon).

3.7.2.4 Oxalate precipitation

The concentrated RE solution achieved from redissolution stage contains less than 100 ppm of Ca and Fe using the current circuit. The Al concentration in the solution is highly dependent on the leaching condition of the test. Due to the intensive acidity required for fire clay material leaching, the concentration of Al in leachate solution is much higher than that of the west Kentucky 13 material. However, this circuit is universal to manage different characteristic of the feed stock. In the current 3 tests, above 80% of Al was removed during Al precipitation, nearly 100% of Ca removed in RE precipitation, and over 90% Fe removed in redissolution stage. The major contamination in the concentrated solution feeds into selective RE oxalate precipitation is shown

in Table 3.7.18. In this case, Al is the major consumer of the oxalic acid in the RE selective precipitation.

A series lab tests were carried out using various dosage of oxalic acid at pH 1.5 and pH 2.0. Based on the precipitation efficiency and the selectivity of the lab analysis, the oxalate precipitation conditions selected for test C4, C5, and C6 are 6.4g/L, 12.8g/L, and 6.4g/L of oxalic acid, respectively, in the concentrated RE pregnant solution. The precipitation efficiency of major elements in the oxalate precipitation stage is shown in Figure 3.7.62.

The RE oxalate product was then dried and roasted in a muffle furnace at 750ºC for 2 hours to convert to RE oxides. The REO product was submitted to KGS for digestion and ICP analysis. The grade in terms of % REO of the three products is listed in Table 3.7.19. The results show that the product grade achieved from the three tests are almost identical from one source. The cost analysis on chemical consumption was carried out for all three tests as shown in

Table 3.7.20. The table indicates that the highest cost of the circuit is the sulfuric acid consumption. The total chemical cost is almost linear to the acid concentration used in the leaching process.

Table 3.7.18. RE and major composition of the solution achieved from RE redissolution.

OXP-Feed	TREE (mg/L)	Al (mg/L)	Ca (mg/L)	Fe (mg/L)
FC-C4	24.1	891.8	77.0	23.2
FC-C5	23.9	994.3	51.4	82.7
FC-C6	29.4	490.0	90.1	40.5

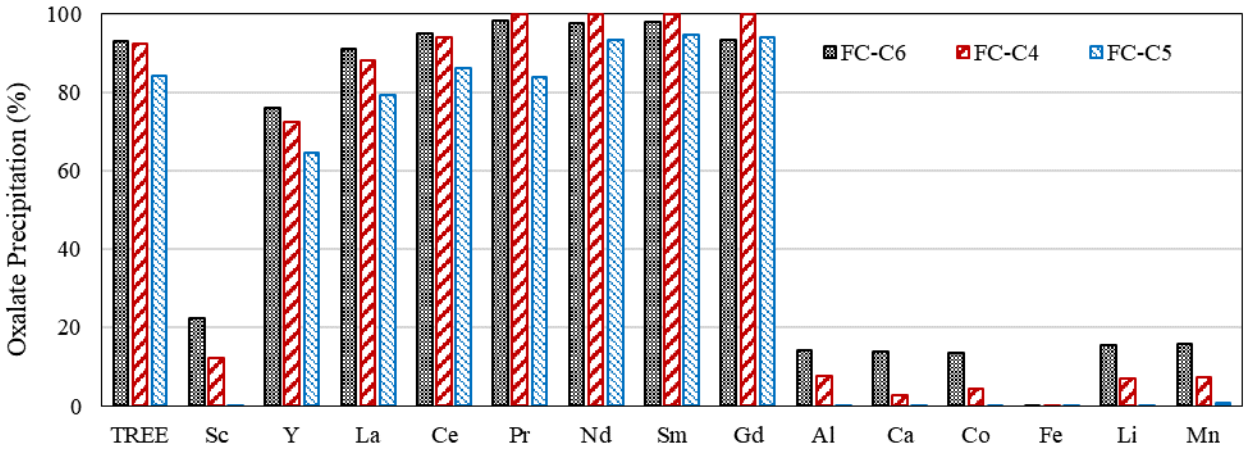

Figure 3.7.62. Oxalic precipitation efficiency (OXP) of major RE and elements of interest (pilot scale, feed rate 1 gpm, pH 1.5, Oxalic Dosage: 6.4g/L for FC-C6 and FC-C4, 12.8 g/L for FC-C5).

Table 3.7.19. RE grade in terms of %REO produced from Fireclay coarse refuse material.

RE Elements	RE Oxides	FC-C4 REO %	FC-C5 REO %	FC-C6 REO %
Sc	Sc_2O_3	0.0	0.0	0.0
Y	Y_2O_3	4.0	3.7	3.3
La	La_2O_3	15.0	11.9	15.6
Ce	CeO_2	45.0	43.5	43.3
Pr	Pr_6O_{11}	4.9	4.5	4.4
Nd	Nd_2O_3	16.9	16.2	15.4
Sm	Sm_2O_3	3.8	3.4	2.6
Eu	Eu_2O_3	0.5	0.5	0.4
Gd	Gd_2O_3	2.3	2.4	1.9
Tb	Tb_4O_7	0.0	0.0	0.0
Dy	Dy_2O_3	1.5	1.4	1.3
Ho	Ho_2O_3	0.2	0.4	0.5
Er	Er_2O_3	0.3	0.3	0.3
Tm	Tm_2O_3	0.0	0.0	0.0
Yb	Yb_2O_3	0.2	0.2	0.2
Lu	Lu_2O_3	0.1	0.1	0.1
TREE		94.7	88.5	89.3
Al	Al_2O_3	0.0	0.1	0.0
Ca	CaO	2.0	2.0	2.0
Fe	Fe_2O_3	2.7	1.7	1.3
Total		99.4	92.3	92.6

Table 3.7.20. Cost comparison of 3 Fireclay continuous run under various condition.

Test Code	H_2SO_4 (M)	$H_2SO_4	$NaOH	$HCl	$Oxalic Acid	$NaOH	$Chem/Run
FC-C4	0.1	$8.02	$6.09	$1.55	$3.20	$0.71	$19.58
FC-C5	0.5	$35.09	$16.24	$2.97	$6.41	$1.02	$61.72
FC-C6	0.05	$4.01	$1.33	$1.04	$1.60	$0.15	$8.13

**Bulk price used in the table: H_2SO_4 - $200/ton, NaOH - $380/ton, HCl - $270/ton, Oxalic acid - $600/ton.*

3.8 Optimization & Validation (PB3-Task7)

Based on the test results collected from the detailed parametric tests performed in Task 6.0, a comprehensive model of the entire circuit using empirical or semi-empirical models were developed to optimize the entire circuit by employing different approach for model development. Three criteria were considered in the optimization process: 1) recovery efficiency; 2) product grade and composition; 3) chemical consumption/cost (economic analysis). The recovery is the key factor for economic viability as mentioned in Task 6.0. To increase the recovery efficiency of each process in the circuit, often time the change of pH cut point will increase the contamination recovery, which will result in lower grade product and higher chemical cost on removal of the

contaminants. Therefore, the optimization was addressed on determination of the upstream process cut point to maximize the recovery and optimize the downstream. Efforts were made to develop empirical equation to model the performance of leaching, precipitation, redissolution and oxalate precipitation processes.

3.8.1 Modelling and optimization

The performance of each stage (leaching, precipitation, and redissolution) of the circuit can be predicted with the correlation of the separation efficiency versus the pH cut point. The chemical consumption of each stage in the circuit can be estimated based on the projected efficiency curve.

3.8.1.1 Leaching

The leaching process is the most critical step in the current circuit for recovery of REEs and CMs entering the downstream. Leaching efficiency can be predicted by varying the acid dose in terms of kg of acid per ton of solid feed. The concentration of major contaminants (Al, Ca, and Fe) leached in the PLS is a function of acid dose, which has an adverse impact on the downstream process efficiency and chemical consumption. An empirical model was established for leaching recovery and contamination level projections in leachate to estimate the downstream separation performance.

The leaching process is the most critical step in the current circuit for recovery of REEs and CMs entering the downstream. Higher acid concentration and lower solid-to-liquid ratio in leaching process will enhance the leaching recovery. Based on previous study, high leaching concentration increase the amount of contamination entering the downstream as shown in Figure 3.8.1. To achieve a leaching recovery of 38%, 50 kg/ton of acid dose is needed. However, to improve the leaching recovery from 40% to 60%, the acid dosage required in terms of kg acid per ton of feed increase exponentially, which also resulted in exponentially increased chemical cost. The contamination level dramatically increased while increasing the acid dosage. Therefore, the optimal performance of leaching occurs in the “elbow” area (acid dose 50 kg/ton feed). A series of tests were carried out in pilot scale operation using sulfuric acid concentration of 0.025M, 0.05M, and 0.075M, with solid concentration of 10%, 15%, and 20%, which provides an acid dose in a range of 22 to 68 kg acid/ton feed (Figure 3.8.2). The lower points on recovery at the same level of acid dose represent lower leaching efficiency when higher solid-to-liquid ratio was applied. Using one stage leaching, the improvement of leaching recovery with increasing the acid dose is almost linear from 22 to 50 kg/ton feed, whereas beyond 50kg/ton, the acid dose required to achieve marginal recovery increased. The recovery improved using leachate recirculation is insignificant at lower acid dosage leaching since very limited free acid presence in the spent leachate solution. However, at higher acid dose, the recirculation improved the leach recovery significantly. Since Al and Fe are the major consumers in the downstream chemical consumption, the correlation of Al and Fe recovery to acid dose is shown in Figure 3.8.3. The data were used to generate an empirical model for contamination level projection in leachate to estimate the downstream chemical consumption.

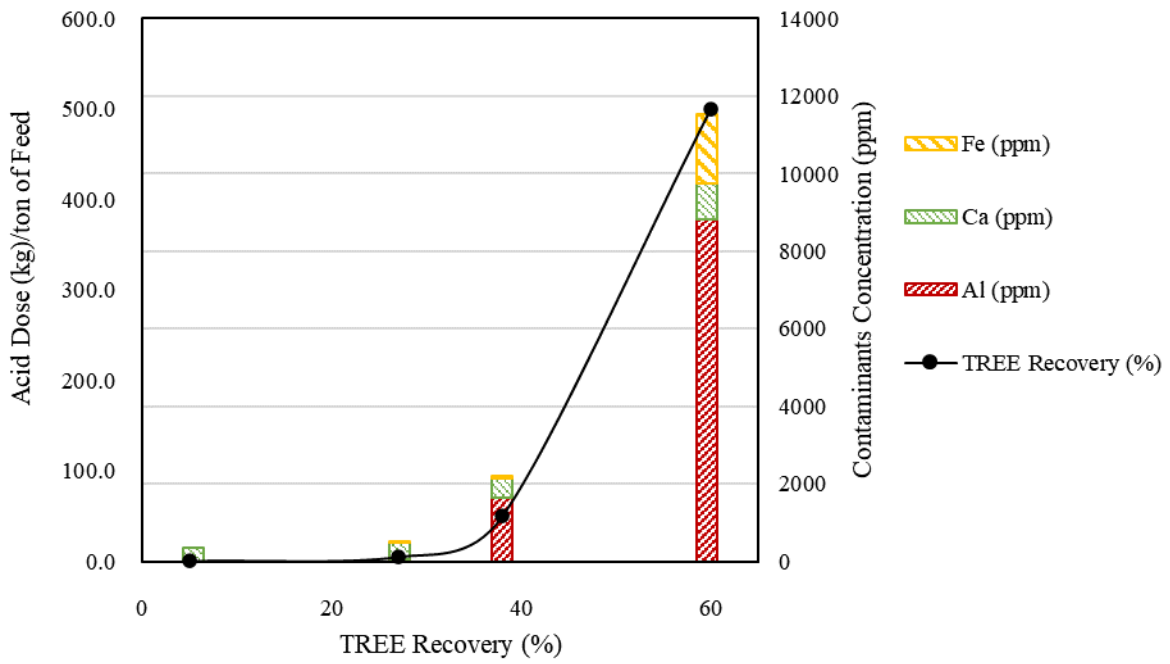

Figure 3.8.1. Leaching recovery and contamination level as function of acid dose. (West Kentucky 13 coarse refuse material, roasted, leaching with 0.001M, 0.01M, 0.1M, and 1M sulfuric acid, S/L 200g/L at 75°C.)

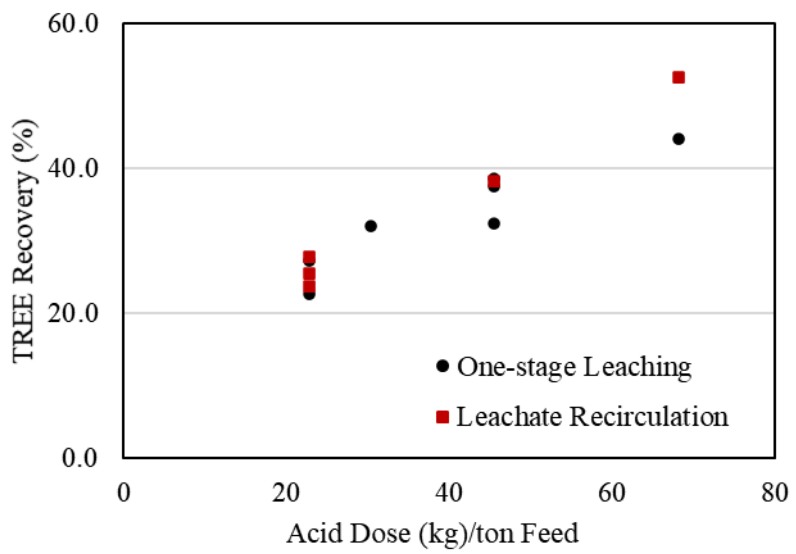

Figure 3.8.2. Correlation of TREE leaching recovery to acid dose (kg/ton feed).

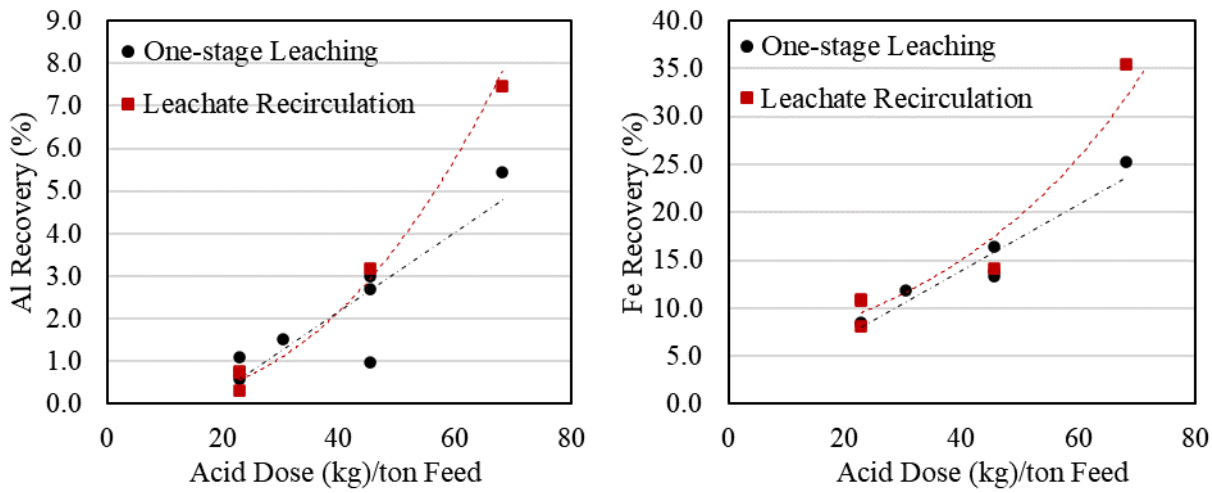

Figure 3.8.3. Correlation of leaching recovery of Al and Fe to acid dose (kg/ton feed).

3.8.1.2 Precipitation

As discussed in the previous section, Al in solution starts precipitated around pH 4.0 and end at pH 4.5 despite of the solution composition. However, Fe precipitation curve is highly related to the state of iron presence in the solution. Ferric ion precipitation completed at around pH 3.0-3.2, whereas ferrous ion precipitate can start from pH 4 and ends at pH 7. Figure 3.8.4 shows Al and Fe precipitation curve in three different solutions. Al precipitation curve are almost identical in the three systems despites of the concentration of the elements. The projection of Al precipitation efficiency can be achieved by using MINTEQ. However, Fe precipitation curve is highly depending on the solution chemistry. In the AMD solution, majority of Fe exists in Fe^{3+} state that can be completely precipitated at pH 3.2. Whereas in WKY 13 and Fire Clay pregnant leaching solution, iron mostly exists in ferrous form.

Once the precipitation pH cut point is selected for a specific unit, the prediction of base solution is needed to estimate cost of chemical consumption. Theoretically, the amount of base needed to precipitate major metal ions in solution can be calculated using the concentration of the metal ion within a pH range. As shown in Figure 3.8.5, the NaOH dosage increased significantly from pH 2.6 to 3.2 and 4.0 to 4.5 for Fe and Al precipitation, respectively. The Fe concentration in the AMD solution is 720 ppm which is 0.0128 mol/L. The stoichiometric ratio of Fe^{3+} to OH^- is 3:1 (assuming all the Fe in AMD is ferric ion and $Fe(OH)_3$ is the form of the precipitate), the NaOH needed is 0.0128 mol/L*3*40g/mol=1.54 g/L. From Figure 3.8.5, the amount of base consumed in pH range of 2.6 to 3.2 is 1.9 g/L. Similarly, for Al precipitation, the NaOH needed to precipitate 330 ppm of Al is 1.464 g/L, while the experimental dosage is 1.7 g/L from pH 4.0 to 4.5. Although there are some other elements that consumes OH^- during pH increase and some other factors need to be considered, the methodology can be used to predict chemical consumption at any pH cut point if the precipitation efficiency can be successfully projected.

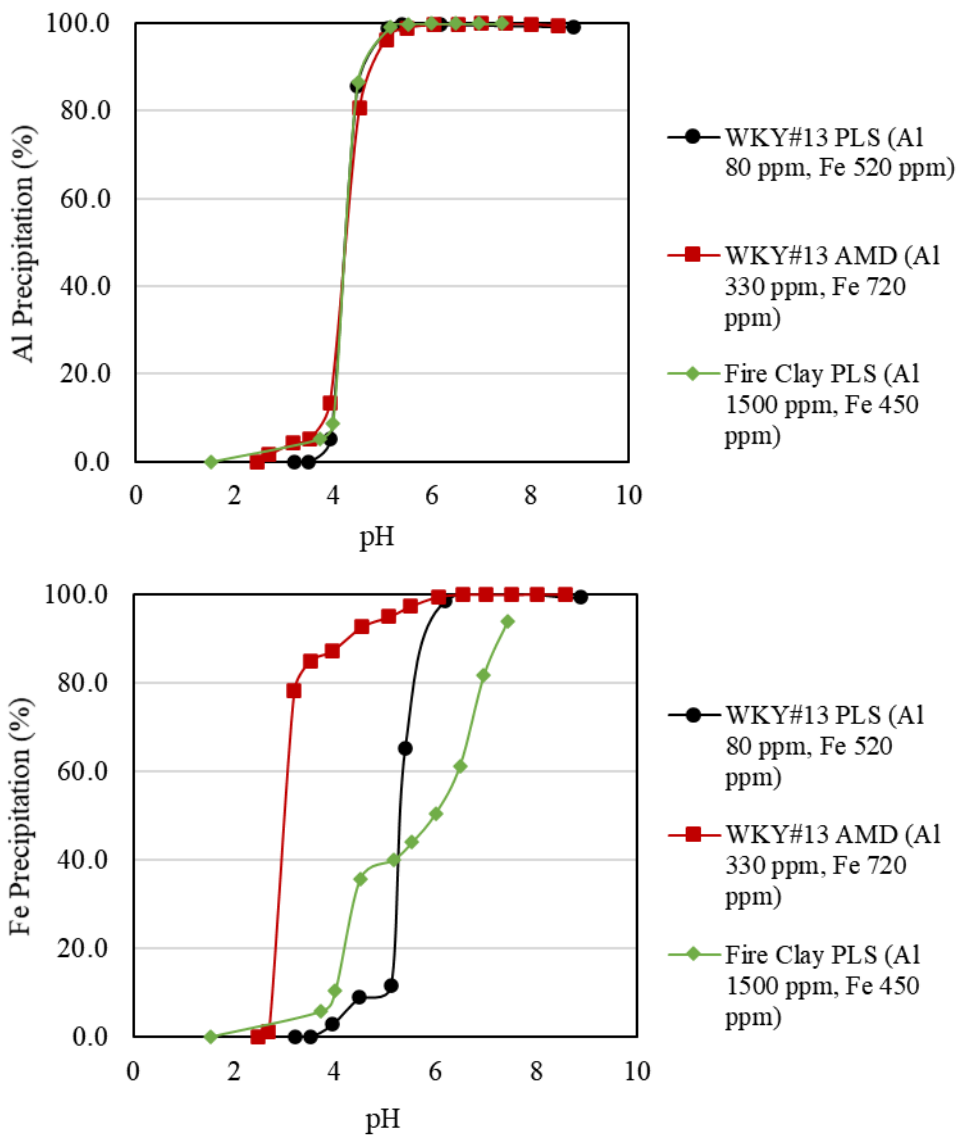

Figure 3.8.4. Precipitation curve of Al and Fe in three different solution with different solution chemistry.

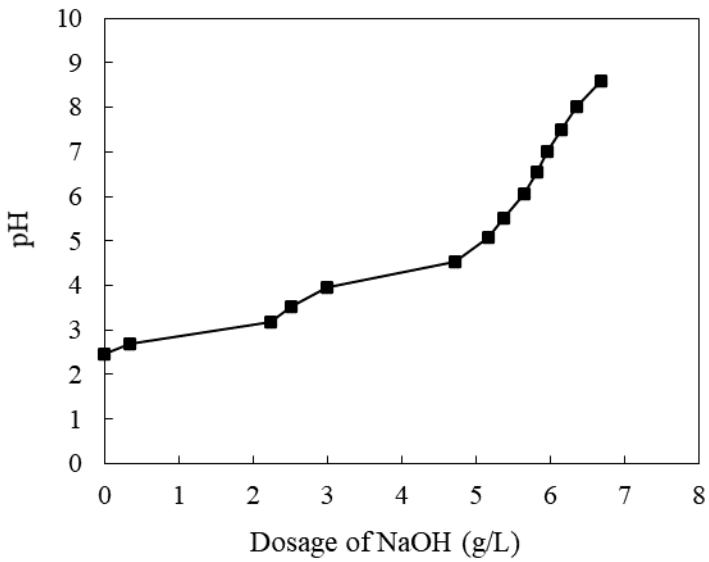

Figure 3.8.5. Correlation of NaOH dosage to precipitation pH in WKY13 AMD (Al 330 ppm, Fe 720ppm).

3.8.1.3 Redissolution

To model the redissolution efficiency and acid dosage needed to redissolve the TREE into a concentrated solution, the amount of Al, Ca, and Fe concentration expected in the redissolved concentrated RE solution was projected. The projected mass of contaminants (i.e. Al, Ca, and Fe) that dissolved in the solution were used to calculate the dosage of HCl needed in the redissolution unit based on the stoichiometric ratio of H^+ needed to extract the Al^{3+}, Ca^{2+}, and Fe^{3+} into solution.

To model the redissolution efficiency and acid dosage needed to redissolve the TREE into a concentrated solution, the amount of Al, Ca, and Fe concentration expected in the redissolved concentrated RE solution needs to be projected. Figure 3.8.6 shows redissolution of a same RE cake under different dilution ratio. The results show that despite the solid concentration used to redissolve the cake, the projected mass of contaminants (i.e. Al, Ca, and Fe) that will be dissolved in the solution will determine the acid consumption. The dosage of HCl needed in the redissolution unit can be calculated using the stoichiometric ratio of H^+ needed to replace the Al^{3+}, Ca^{2+}, and Fe^{3+} in the cake solid.

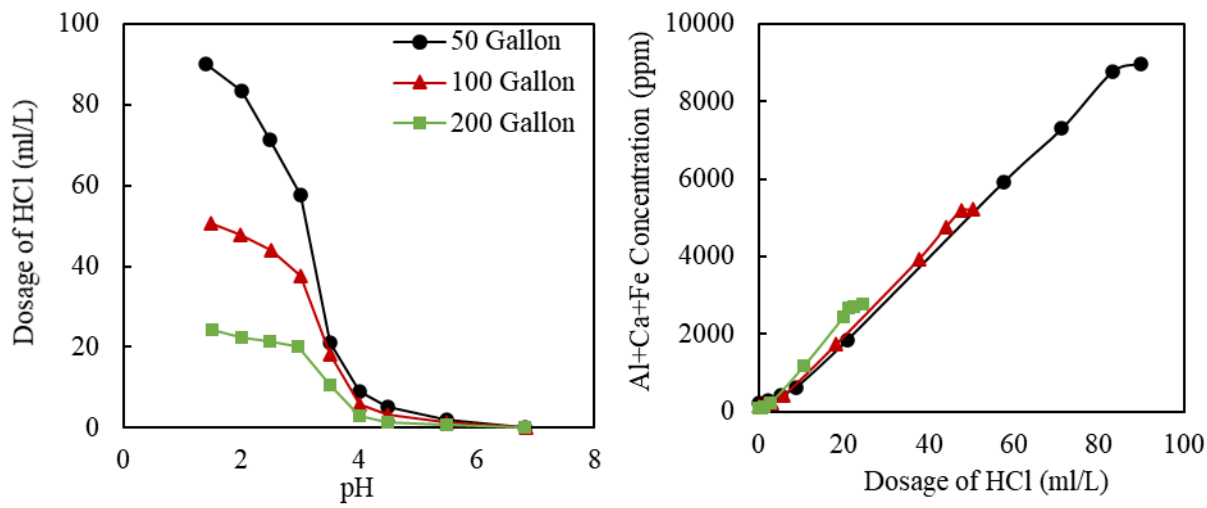

Figure 3.8.6. Acid dosage needed to achieve targeted pH of the liquified RE precipitate cake under different dilution ratio (left). And the ending concentration of Al, Ca, and Fe in the redissolved RE solution as a function of the acid dosage used (right).

3.8.1.4 Oxalate precipitation

The oxalate precipitation efficiency was established based on the experimental data collected in each run with various concentration of Al and Fe at pH 1.5. The correlation of the Al and Fe concentration in oxalate precipitation feed to the oxalic acid dosage was established for pH 1.5 precipitation system.

3.8.1.5 Modelling

The performance of the hydrometallurgy circuit was modeled based on the information gathered from the parametric study. The chemical dosage was projected using the abovementioned methodology. The case analyses for the west Kentucky No. 13 coarse refuse and Fire Clay coarse refuse material are presented in the Table 3.8.1 and Table 3.8.2. The leaching condition selected for this run is using 0.075M sulfuric acid with 50% leachate recirculation and 75 lb/hr solid feed rate on a total operation time of 16 hours at 75°C. The projected leaching pH under the leachate recirculation condition is between 2-2.5, the TREE, Al, Ca, and Fe concentration in the leachate that reports to the Al removal unit is estimated to be 16 ppm, 500 ppm, 400 ppm, and 1500 ppm, respectively. For the Fire Clay material, the leaching condition for the validation test was selected to be 0.1M sulfuric acid with 50% leachate recirculation and 50 lb/hr solid feed rate on a total operation time of 16 hours at 75°C. The projected leaching pH under the leachate recirculation condition is around 1.5, and the TREE, Al, Ca, and Fe concentration in the leachate is estimated to be 12 ppm, 1600 ppm, 200 ppm, and 400 ppm, respectively. The Fire Clay material contains more clay material in the coarse refuse compare to the west Kentucky No. 13, which decomposes during roasting process and result in higher Al content in the leachate. Whereas the west Kentucky No. 13 material contains more pyrite which provides the source of Fe in the leachate.

Due to the difference of Al concentration in the leachate solution in two different materials, the Al precipitation pH was selected to be 4.4 for the west Kentucky No. 13 material and 4.2 for the Fire Clay material to remove 90% of Al with about 15% of TREE loss. The base consumption projected for the PT0 stage is based on the amount of Al and Fe precipitated. Subsequently, in the RE precipitation stage, the RE recovery was projected to be 100%, with 100% Al, 5% Ca, and 90% Fe carry over to the RE precipitate. In the redissolution stage, the recovery of TREE, Al, Ca, and Fe used in the case analysis model is predicted to be 80%, 100%, 100%, and 5%, respectively. The resulting concentration of Al and Fe was used to predict the dosage of oxalic acid in the RE oxalate process. Based on the bulk price of the abovementioned chemicals, the chemical cost for the continuous run is predicted with a break down.

Table 3.8.1. Circuit performance prediction and case analysis for west Kentucky No. 13 coarse refuse material.

Case Analysis DTK-C16

Stream	pH	PLS Solution					Leaching	Precipitation	Redisolution	Oxalate Precipitation	Total
		Vol (Gallon)	TREE (ppm)	Al (ppm)	Ca (ppm)	Fe (ppm)	H_2SO_4 (kg)	NaOH (kg)	HCl (L)	Oxalic Acid (kg)	$Chemical
Leachate	2-2.5	630	16	500	400	1500	30.0				6.00
Al Precipitation	4.4	630	13	50	400	1350		5.54			2.10
RE Precipitation	6.8	630	0	0	380	135		6.74			2.56
RE Redisolution	2.3	100	68	315	126	383			2.28		0.51
RE OXP	1.5	100	65							2.24	1.35
Total											12.52

Table 3.8.2. Circuit performance prediction and case analysis for Fire Clay coarse refuse material.

Case Analysis FC-C8

Stream	pH	PLS Solution					Leaching	Precipitation	Redisolution	Oxalate Precipitation	Total
		Vol (Gallon)	TREE (ppm)	Al (ppm)	Ca (ppm)	Fe (ppm)	H_2SO_4 (kg)	NaOH (kg)	HCl (L)	Oxalic Acid (kg)	$Chemical
Leachate	1.5	630	12	1600	200	400	40.0				8.00
Al Precipitation	4.2	630	10	160	200	360		15.47			5.88
RE Precipitation	6.8	630	0	0	190	36		3.35			1.27
RE Redisolution	2.3	100	51	1008	63	102			4.38		0.99
RE OXP	1.5	100	49							3.64	2.18
Total											18.32

3.8.2 Validation Tests

3.8.2.1 West Kentucky No. 13 Source

Based on the optimized condition, validation test was carried out for the West Kentucky No. 13 coarse refuse material in the pilot plant. The feed material was roasted at 600°C with a retention time of 5 minutes. The material was feed into the leaching tank at a solid feed rate of 75 lb/hr. The industrial grade (>93%) sulfuric acid was feeding into the acid preparation tank at ratio of 50kg acid per ton of feed. At the beginning of the continuous run, 1 gpm of water was injected into the acid preparation tank to make the initial concentration of 0.075M, after 6 hours of leaching, the pregnant leachate solution (PLS) was started to be recirculated back to the leaching tank at a flow rate of 0.5 gpm and the freshwater feed rate to the acid preparation tank was reduced to 0.5 gpm to maintain a consistent total solid concentration of 150 g/L in the leaching tank. The

converted feed solid content in the leach tank is 13.01% by weight. As shown in Table 3.8.3, the average solid content after leaching is 12.34% by weight, which indicated that the solid dissolution during leaching is ~5%. The pH in the leaching tank over the 16 hour varied between 2.1 and 2.5 and stabilized at 2.375. The Eh of the leaching process was ~500 RmV indicating the majority of the Fe presented in the leachate solution is in ferrous state.

The leaching recovery of individual element was calculated based on the elemental concentration leached out in leachate and solid residue. The recovery of TREE in the leaching process is 24.72% ±6.37% over the 16 hour continuous run. The average leaching recovery of Al, Ca and Fe was 1.99%, 63.14%, and 10.95%, respectively, as shown in Figure 3.8.7.

The leachate solution was transferred to the Al precipitation tank at a flow rate of 2 gpm. The residence time for the Al removal was 1 hour, and the pH setpoint was 4.4 automatically adjusted by a base pump. The base solution consumed in this stage is 6.5 gallon of 4M NaOH. The Eh value after the precipitation is in average of 400 RmV, which indicated that the Fe precipitation is not significant in this stage (Table 3.8.4). The precipitation efficiency of the individual elements are shown in Figure 3.8.8. The removal of Al and Fe was 93.5% and 26.3%, respectively, with 15% loss of TREEs. Majority of the radioactive material was also removed in the Al precipitation stage, i.e. 92% Th and 53% of U removal. The Sc can be recovered priory to the Al precipitation using solvent extraction as discussed in the previous reports. The % solid by weight in the precipitation tank is ~0.4% and was filtered in a plate and frame filter. The Al precipitate filter cake collected in this run was 174 lb (with moisture and chemically bonded water). The solid content of the dry cake was determined to be 11% by weight, and the dry cake contains 15% Al, 9% Fe and 386 ppm of TREE.

Table 3.8.3. Operation log of Dotiki validation test leaching circuit.

ID	#	Tank	Time	Hours in Run	Temp (C)	% Solids	pH	Eh	H_2SO_4 (Gal)
DTK-C16-L1	P1	14	9:00	2:00	75	9.231	3.096	493.8	20.5
DTK-C16-L1	P2	14	10:00	3:00	75	10.531	2.174	519.2	20.2
DTK-C16-L1	P3	14	11:00	4:00	75	11.058	2.187	499.2	20
DTK-C16-L1	P4	14	12:00	5:00	75	10.500	2.226	493.4	19.8
DTK-C16-L1	P5	14	13:00	6:00	75	11.260	2.351	485.5	19.5
DTK-C16-L1	P6	14	14:00	7:00	73	11.699	2.46	496.7	19.2
DTK-C16-L1	P7	14	15:00	8:00	75	12.482	2.479	501.2	19
DTK-C16-L1	P8	14	16:00	9:00	74	12.775	2.486	497.9	18.8
DTK-C16-L1	P9	14	17:00	10:00	73	13.162	2.485	480.5	18.6
DTK-C16-L1	P10	14	18:00	11:00	75	14.144	2.55	492.7	18.4
DTK-C16-L1	P11	14	19:30	12:00	76	14.316	2.556	495.1	18.2
DTK-C16-L1	P12	14	20:30	13:00	75	13.390	2.282	501.2	18
DTK-C16-L1	P13	14	21:30	14:00	75	13.531	2.359	493	17.8
DTK-C16-L1	P14	14	22:30	15:00	73	13.597	2.32	495.1	17.6
DTK-C16-L1	P15	14	23:30	16:00	75	13.424	2.337	492.1	17.4
Average						12.340	2.375	495.9	

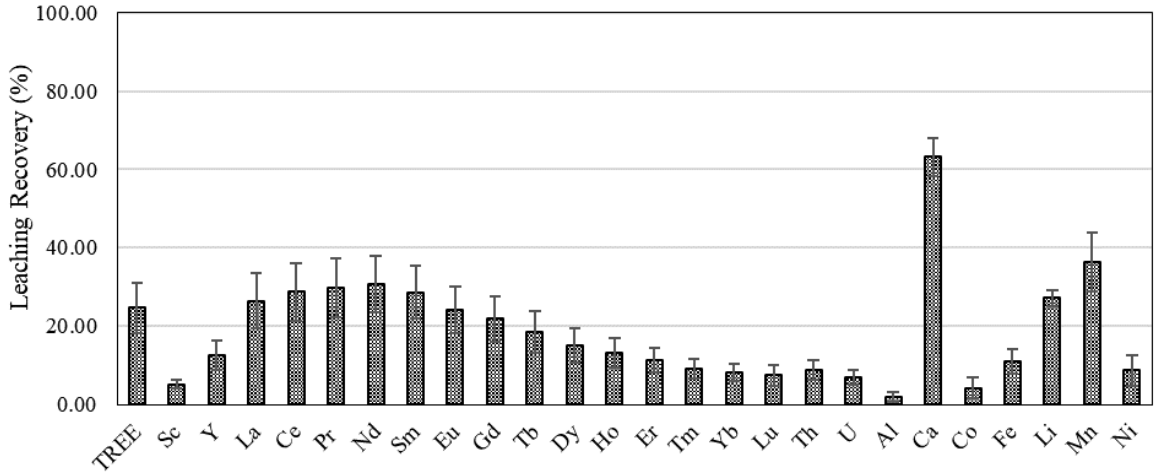

Figure 3.8.7. Leaching recovery of RE and other elements of interest over the continuous run in pilot scale operation (Test code DTK-C16:50kg H_2SO_4 per ton of feed, 75lb/hour feed solid, 75 ºC, with 50% recirculation).

Table 3.8.4. Operation log of Dotiki validation test Al precipitation circuit.

ID	#	Tank	Time	Hours in Run	Temp (C)	% Solids	pH	Eh (RmV)	4M NaOH Base (Gal)
DTK-C16-PT0	F1	4	10:00	0:00			2.515	539.9	
DTK-C16-PT0	F2	4	11:00	1:00			2.564	529.9	
DTK-C16-PT0	F3	4	12:00	2:00			2.469	538.8	
DTK-C16-PT0	F4	4	13:00	3:00			2.483	539.1	
DTK-C16-PT0	F5	4	14:00	4:00			2.487	537.4	
DTK-C16-PT0	F6	4	15:00	5:00			2.541	536.5	
DTK-C16-PT0	R1	4	10:00	0:00		0.367	4.522	403.1	36
DTK-C16-PT0	R2	4	11:00	1:00		0.399	4.652	374.4	35
DTK-C16-PT0	R3	4	12:00	2:00		0.420	4.449	400.4	34
DTK-C16-PT0	R4	4	13:00	3:00		0.442	4.473	393.6	32.5
DTK-C16-PT0	R5	4	14:00	4:00		0.449	4.495	386.7	31
DTK-C16-PT0	R6	4	15:00	5:00		0.466	4.428	394	29.5

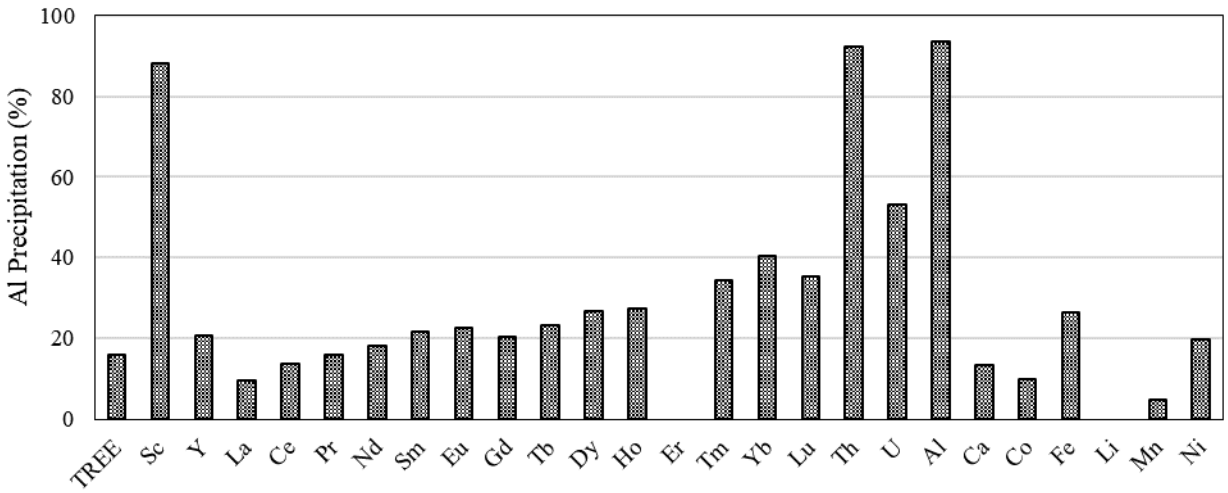

Figure 3.8.8. Precipitation efficiency of REEs and elements of interest. (DTK-C16-PT0 Al precipitation at pH 4.5, residence time 1 hour.)

The PLS after Al removal was then transferred to a 100 gallon reaction tank for RE precipitation at pH 6.8 using 4M NaOH solution as the pH modifier Table 3.8.5. The solid content in the RE precipitation tank is about 0.3% in average, which resulted in about 96.5 lb of filter cake as received. The water (physically bond and chemically bond) content in the filter cake was determined to be 67% by weight. The dry cake contains 4456 ppm of TREE, 5% of Al, and 32% of Fe. The precipitation efficiency of REs and other elements of interests are shown in Figure 3.8.9.

Table 3.8.5. Operation log of Dotiki validation test RE precipitation circuit.

ID	#	Tank	Time	Hours in Run	Temp (C)	% Solids	pH	Eh (RmV)	4M NaOH Base (Gal)
DTK-C16-PT1	F1	4	20:00	0:00			4.398	295.2	
DTK-C16-PT1	F2	4	22:00	2:00			4.393	275.1	
DTK-C16-PT1	F3	4	0:00	4:00			4.341	269.4	
DTK-C16-PT1	F4	4	9:00	5:00			4.199	437	
DTK-C16-PT1	F5	4	11:00	7:00			4.102	444.4	
DTK-C16-PT1	F6	4	13:00	9:00			4.399	408.5	
DTK-C16-PT1	R1	4	20:00	0:00		0.204	6.861	34.7	27.5
DTK-C16-PT1	R2	4	22:00	2:00		0.227	6.7	98	27
DTK-C16-PT1	R3	4	0:00	4:00		0.245	6.738	93.4	26
DTK-C16-PT1	R4	4	9:00	5:00		0.387	6.889	175.5	25
DTK-C16-PT1	R5	4	11:00	7:00		0.289	6.826	333.2	24.5
DTK-C16-PT1	R6	4	13:00	9:00		0.345	6.928	336.2	24

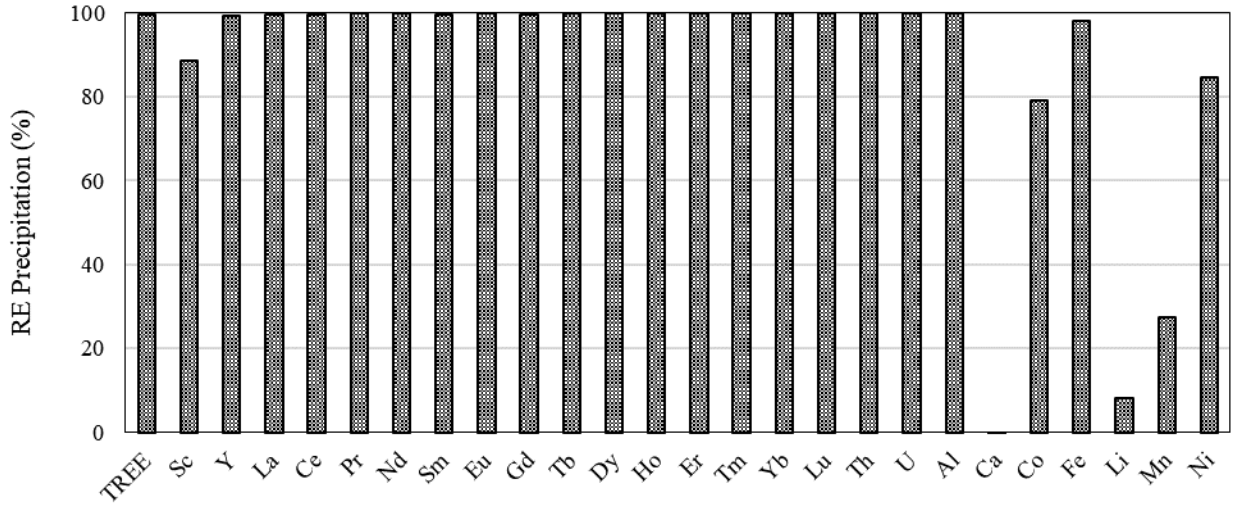

Figure 3.8.9. Precipitation efficiency of REEs and elements of interest. (DTK-C16-PT1 RE precipitation at pH 6.8, residence time 2 hour.)

The filter cake collected from RE precipitation stage was transferred into a 200 gallon mixing reaction tank with water added into a total slurry volume of 100 gallon. The cake was completely dispersed through high speed mixing and recirculation through a centrifugal pump for 2 hours, then 2.2 liters of industrial grade HCl was added into the reaction tank for RE redissolution. The target pH of the redissolution was 2.5, whereas the ending pH of the leachate solution was 2.4. The residue solid after RE redissolution was filtered using a plate and frame filter, and 86 lbs of filter cake was collected in a drum. The major content of the residue cake was 27.4% of Fe and 4.1% of Al. The redissolution efficiency was determined by digesting the RE precipitate cake before redissolution and obtaining a maximum concentration of each elements under the circumstances that all the solid was redissolved. The recovery of REs and other elements in the redissolution stage is as plotted in Figure 3.8.10. The results show that nearly 96.7% of Fe was further removed in this stage.

The concentrated RE solution after redissolution contains 68.6 ppm of TREEs, 537 ppm of Al, 185 ppm of Ca, and 196 ppm of Fe. Compare to the prediction, the concentration of Al was about 40% underestimated and the Fe concentration was nearly 2 times overestimated, however, the prediction of TREEs is considerably reliable to be 68 ppm.

The concentrated RE solution was successively reported to the oxalate precipitation (OXP) circuit. The pH of 1.5 was selected for the OXP circuit and controlled by an automated base pump with 4M NaOH solution. The reaction time was 20 minutes and 4 sets of feed and reject sample were collected (Table 3.8.6). The Eh was decreased from an average of 760 RmV in feed to 495 RmV in reject, which indicated the reducing potential of oxalic acid to ferric ion in solution. The precipitation efficiency of TREEs achieved was 94.5% with other elements plotted as shown in Figure 3.8.11. The total RE oxalate cake produced in this test run was 60.4 grams as dry. After roasting at 750°C for 2 hours, the RE oxides obtained was 30 grams with a REO grade of 92.8%.

Table 3.8.6. Operation log of Dotiki validation test RE oxalate precipitation circuit.

ID	#	Tank	Time	Hours in Run	pH	Eh (RmV)
DTK-C16-OXP	F1	12	4:10	0:00	2.353	776.6
DTK-C16-OXP	F2	12	4:25	0:15	2.371	782.2
DTK-C16-OXP	F3	12	4:40	0:30	2.372	783.4
DTK-C16-OXP	F4	12	4:55	0:45	2.476	699.2
DTK-C16-OXP	R1	Waste	4:10	0:00	1.505	491.1
DTK-C16-OXP	R2	Waste	4:25	0:15	1.511	494.7
DTK-C16-OXP	R3	Waste	4:40	0:30	1.502	497.3
DTK-C16-OXP	R4	Waste	4:55	0:45	1.525	498.9

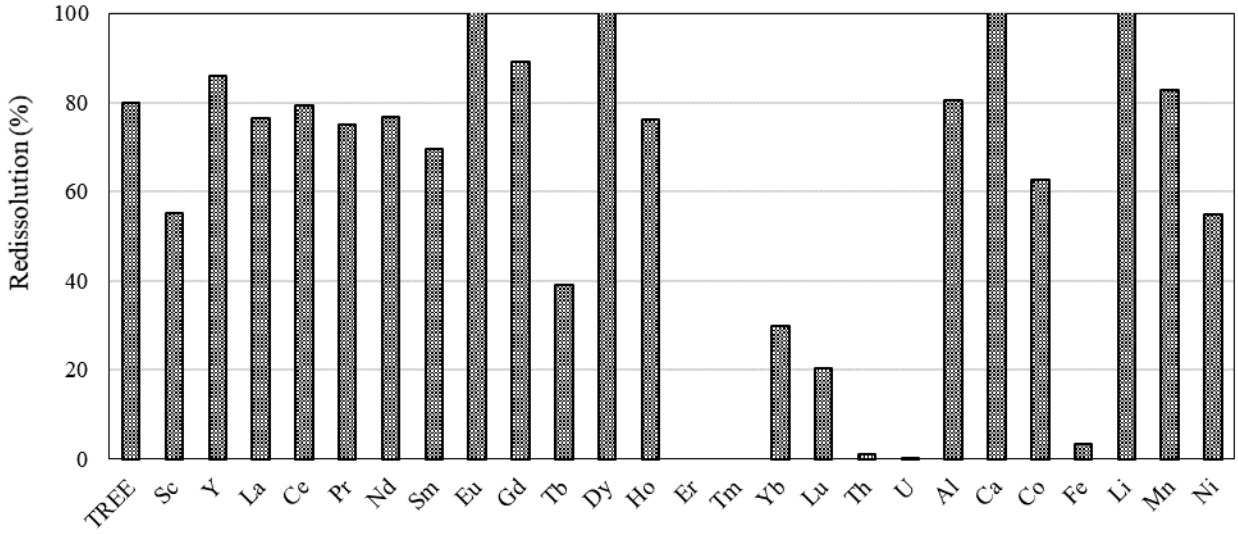

Figure 3.8.10. Redissolution efficiency of REEs and elements of interest. (DTK-C16-L2, pH2.3, HCl dosage 6.5 ml of 36% pure HCl per Liter of blended slurry, residence time 30 min)

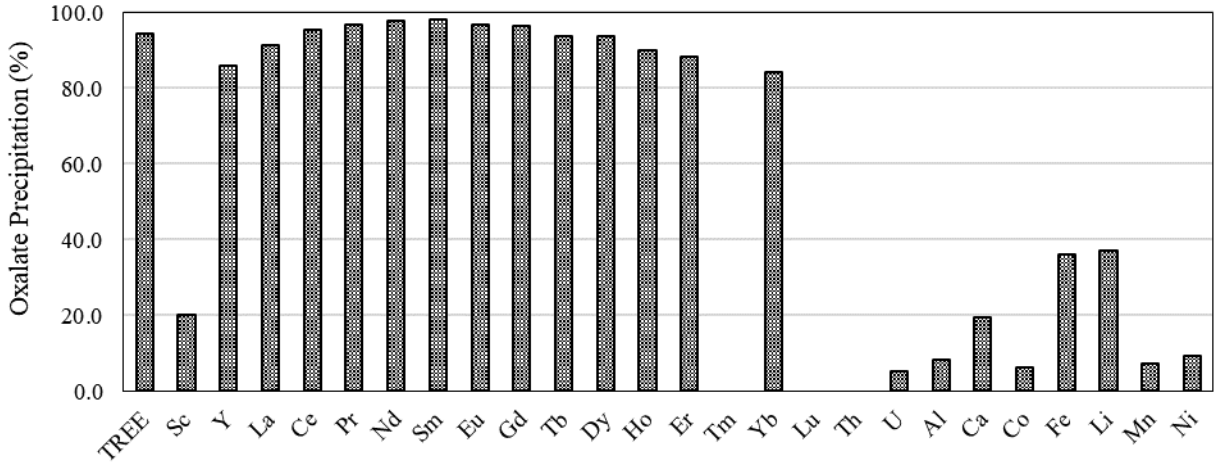

Figure 3.8.11. Oxalate precipitation efficiency of REs and other elements of interest. (pH 1.5, oxalic acid dosage 6.21 g/L of concentrated PLS, residence time 20 min)

3.8.2.2 Fire Clay coarse refuse

The validation test for the Fire Clay coarse refuse material was carried out using the light density fraction of the coarse refuse material. The leaching condition was selected based on the leaching characteristic of the Fire Clay material, whereas the downstream process condition was determined based on the parametric study results achieved from the West Kentucky No. 13 coarse refuse material in the pilot plant. The feed material was roasted at 600°C with a retention time of 20 minutes. The material was feed into the leaching tank at a solid feed rate of 50 lb/hr. The industrial grade (>93%) sulfuric acid was feeding into the acid preparation tank at ratio of 100kg acid per ton of feed. At the beginning of the continuous run, 1 gpm of water was injected into the acid preparation tank to make the initial concentration of 0.1M, after 6 hours of leaching, the pregnant leachate solution (PLS) was recirculated back to the leaching tank at a flow rate of 0.5 gpm and the freshwater feed rate to the acid preparation tank was reduced to 0.5 gpm to maintain a consistent total solid concentration of 100 g/L in the leaching tank. The converted feed solid content in the leach tank is 9.07 % by weight. As shown in Table 3.8.7, the average solid content after leaching is 7.0% by weight, which indicated that the solid dissolution during leaching is ~22.8%. The higher solid lose was due to the higher acid concentration, which resulted in an elevated concentration of contaminants in solution. The pH in the leaching tank over the 16 hours varied between 1.5 and 1.9 and stabilized at 1.655 at the end of the leaching period. The Eh of the leaching process was 619.6 RmV which is slightly higher than that of the west KY No. 13 material. Total 5 gallons of sulfuric acid was consumed during the 16 hours leaching process.

The leaching recovery of individual element was calculated based on the elemental concentration leached out in leachate and solid residue. The recovery of TREE in the leaching process is 22.23% ±5.74% over the 16 hour continuous run. The average leaching recovery of Al, Ca and Fe was 6.13%, 73.8%, and 11.66%, respectively, as shown in Figure 3.8.12.

Table 3.8.7. Operation log of Fire Clay validation test leaching circuit.

ID	#	Tank	Time	Hours in Run	Temp (C)	% Solids	pH	Eh	H_2SO_4 (Gal)
FC-C8-L1	P1	14	9:30	2:00	74	5.732	1.985	561.9	16.8
FC-C8-L1	P2	14	10:30	3:00	75	5.968	1.718	590	16.5
FC-C8-L1	P3	14	11:30	4:00	75	7.220	1.611	604.2	16.1
FC-C8-L1	P4	14	12:30	5:00	75	7.379	1.618	614.3	15.8
FC-C8-L1	P5	14	13:30	6:00	75	6.815	1.756	616.3	15.5
FC-C8-L1	P6	14	14:30	7:00	75	7.349	1.696	621.4	15
FC-C8-L1	P7	14	15:30	8:00	74	7.568	1.657	629.8	14.8
FC-C8-L1	P8	14	16:30	9:00	74	5.453	1.591	632.1	14.5
FC-C8-L1	P9	14	17:30	10:00	75	8.374	1.637	642.8	14
FC-C8-L1	P10	14	18:30	11:00	74	7.306	1.583	632.5	13.5
FC-C8-L1	P11	14	19:30	12:00	74	6.890	1.571	635.5	13
FC-C8-L1	P12	14	20:30	13:00	74	5.569	1.699	557	12.6
FC-C8-L1	P13	14	21:30	14:00	74	8.377	1.562	648.5	12.4
FC-C8-L1	P14	14	22:30	15:00	74	6.066	1.532	649.1	12
FC-C8-L1	P15	14	23:30	16:00	74	9.110	1.605	659.3	11.8
Average						7.012	1.655	619.6	

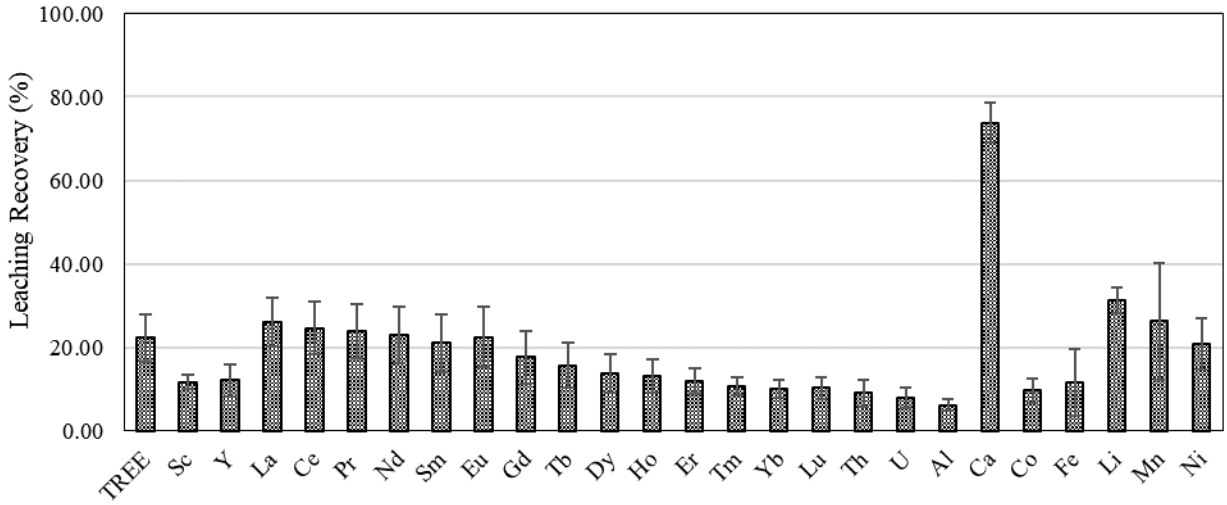

Figure 3.8.12. Leaching recovery of RE and other elements of interest over the continuous run in pilot scale operation (Test code FC-C8: 0.1M H_2SO_4, 50lb/hour feed solid, 75 ºC, with recirculation).

The leachate solution was transferred to the Al precipitation tank at a flow rate of 2 gpm. The residence time for the Al removal was 1 hour, and the pH setpoint was 4.2 automatically adjusted by a base pump. The base solution consumed in this stage is 13.5 gallon of 4M NaOH. The Eh value after the precipitation is in average of 445 RmV, which indicated that the Fe precipitation is not significant in this stage (Table 3.8.8). The precipitation efficiency of the individual elements is shown in Figure 3.8.13. The removal of Al and Fe was 95.8% and 46.0%, respectively, with 15% loss of TREEs. Majority of the radioactive material was also removed in the Al precipitation stage, i.e. 98.5% Th and 31.4% of U removal. The Sc can be recovered priory to the Al precipitation using solvent extraction as discussed in the previous reports. The % solid by weight in the precipitation tank is 5.3% and was filtered in a plate and frame filter. The high concentration of Al contributed to the high solid content in the precipitation reaction tank. The Al precipitate filter cake collected in this run was 182.5 lb (with moisture and chemically bonded water). The solid content of the dry cake was determined to be 20% by weight, and the dry cake contains 17.5% Al, 2% Fe and 125 ppm of TREE.

The PLS after Al removal was then transferred to a 100 gallon reaction tank for RE precipitation at pH 6.8 using 4M NaOH solution as the pH modifier Table 3.8.9. The solid content in the RE precipitation tank is about 0.28% in average, which resulted in about 92 lbs of filter cake as received. The water (physically bond and chemically bond) content in the filter cake was determined to be 84.5% by weight. The dry cake contains 3881 ppm of TREE, 9.8% of Al, and 9.0% of Fe. The precipitation efficiency of REs and other elements of interests are shown in Figure 3.8.14.

Table 3.8.8. Operation log of Fire Clay validation test Al precipitation circuit.

ID	#	Tank	Time	Hours in Run	Temp (C)	% Solids	pH	eH	4M NaOH Base (Gal)
FC-C8-PT0	F1	4	7:00	0:00			1.483	628.1	
FC-C8-PT0	F2	4	8:00	1:00			1.458	632.7	
FC-C8-PT0	F3	4	9:00	2:00			1.525	627.8	
FC-C8-PT0	F4	4	10:00	3:00			1.527	628.7	
FC-C8-PT0	R1	4	7:00	0:00		3.471	4.146	449.5	61.5
FC-C8-PT0	R2	4	8:00	1:00		6.307	4.266	431.6	57
FC-C8-PT0	R3	4	9:00	2:00		5.736	4.258	436.3	51
FC-C8-PT0	R4	4	10:00	3:00		5.681	4.188	464.3	48

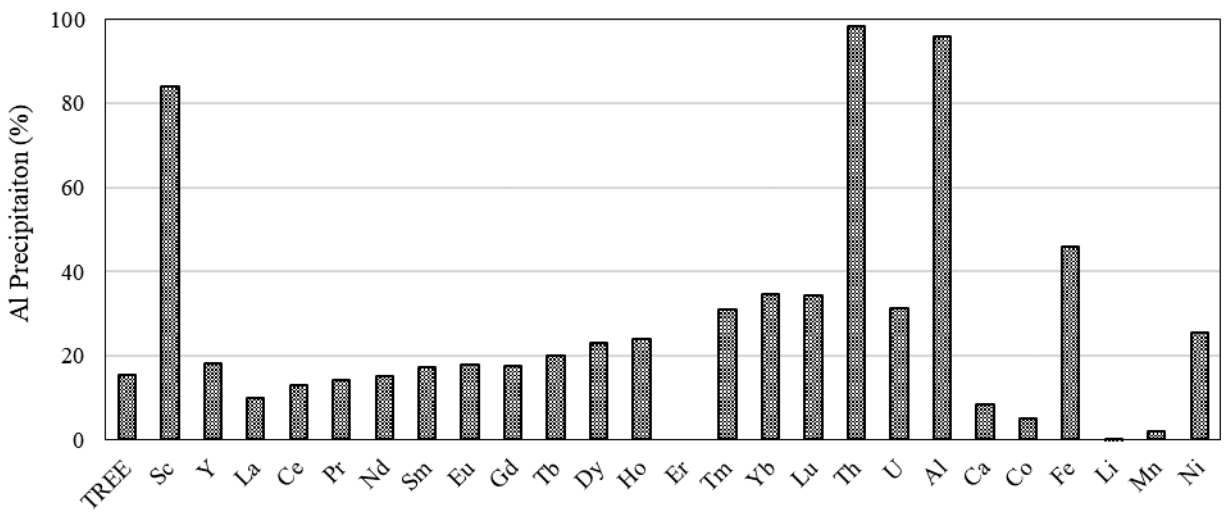

Figure 3.8.13. Precipitation efficiency of REEs and elements of interest. (FC-C8-PT0 Al precipitation at pH 4.2, residence time 1 hour.)

Table 3.8.9. Operation log of Fire Clay validation test RE precipitation circuit.

ID	#	Tank	Time	Hours in Run	Temp (C)	% Solids	pH	Eh	4M NaOH Base (Gal)
FC-C8-PT1	F1	4	13:30	0:00			4.198	461.9	
FC-C8-PT1	F2	4	15:30	2:00			4.218	472.5	
FC-C8-PT1	F3	4	17:30	4:00			4.097	484.4	
FC-C8-PT1	F4	4	19:30	6:00			4.089	479.7	
FC-C8-PT1	R1	4	13:30	0:00		0.358	6.815	346.6	45
FC-C8-PT1	R2	4	15:30	2:00		0.184	6.834	335.7	44
FC-C8-PT1	R3	4	17:30	4:00		0.290	6.681	272.8	44
FC-C8-PT1	R4	4	19:30	6:00		0.307	6.834	250.1	43.5

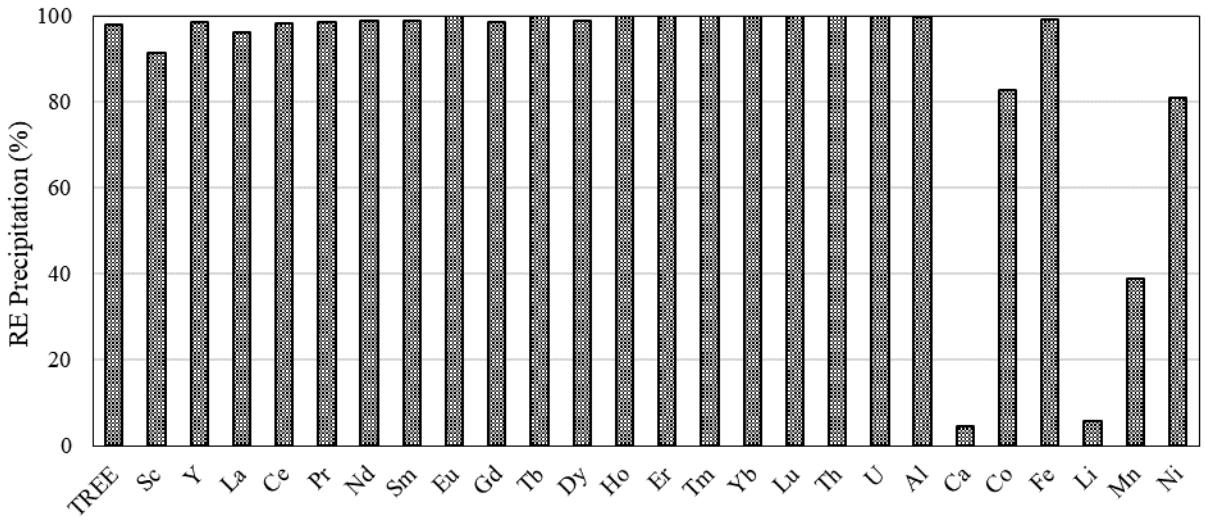

Figure 3.8.14. Precipitation efficiency of REEs and elements of interest. (FC-C8-PT1 RE precipitation at pH 6.8, residence time 2 hour.)

The filter cake collected from RE precipitation stage was transferred into a 200 gallon mixing reaction tank with water added into a total slurry volume of 100 gallon. The cake was completely dispersed through high speed mixing and recirculation through a centrifugal pump for 2 hours, then 4.4 liters of industrial grade HCl was added into the reaction tank for RE redissolution. The target pH of the redissolution was 2.5, whereas the ending pH of the leachate solution was 2.2. The residue solid after RE redissolution was filtered using a plate and frame filter, and 110 lbs of filter cake (as received, with water) was collected in a drum. The major content of the residue cake was 3.4% of Fe and 7.6% of Al. The redissolution efficiency was determined by digesting the RE precipitate cake before redissolution and obtaining a maximum concentration of each elements under the circumstances that all the solid was redissolved. The recovery of REs and other elements in the redissolution stage is as plotted in Figure 3.8.15. The results show that 76.3% of Fe was further removed in this stage.

The concentrated RE solution after redissolution contains 53.7 ppm of TREEs, 595 ppm of Al, 86 ppm of Ca, and 298 ppm of Fe. Compare to the prediction, the concentration of Al was overestimated, and the Fe concentration was underestimated due to the preference and selectivity of the redissolution process. However, the prediction of TREEs is considerably reliable to be 51 ppm. The total chemical consumption is in the confidence range.

The concentrated RE solution was subsequently reported to the oxalate precipitation (OXP) circuit. The pH of 1.5 was selected for the OXP circuit and controlled by an automated base pump with 4M NaOH solution. The reaction time was 20 minutes and 4 sets of feed and reject sample were collected (Table 3.8.10). The Eh was decreased from an average of 807 RmV in feed to 474 RmV in reject, which indicated the reducing potential of oxalic acid to ferric ion in solution. The precipitation efficiency of TREEs achieved was 92.3% with other elements plotted as shown in Figure 3.8.16. The total RE oxalate cake produced in this test run was 44.6 grams as dry. After roasting at 750°C for 2 hours, the RE oxides obtained was 24 grams with a REO grade of 79.52%.

Table 3.8.10. Operation log of Fire Clay validation test RE oxalate precipitation circuit.

ID	#	Date	Tank	Time	Hours in Run	pH	eH
FC-C8-OXP	F1	2020/8/28	12	10:10	0:20	2.217	794.6
FC-C8-OXP	F2	2020/8/28	12	10:30	0:40	2.206	813.4
FC-C8-OXP	F3	2020/8/28	12	10:50	1:00	2.209	812.3
FC-C8-OXP	F4	2020/8/28	12	11:10	1:20	2.182	808.9
FC-C8-OXP	R1	2020/8/28	Waste	10:10	0:20	1.397	519.2
FC-C8-OXP	R2	2020/8/28	Waste	10:30	0:40	1.419	481.2
FC-C8-OXP	R3	2020/8/28	Waste	10:50	1:00	1.413	451.1
FC-C8-OXP	R4	2020/8/28	Waste	11:10	1:20	1.415	445.9

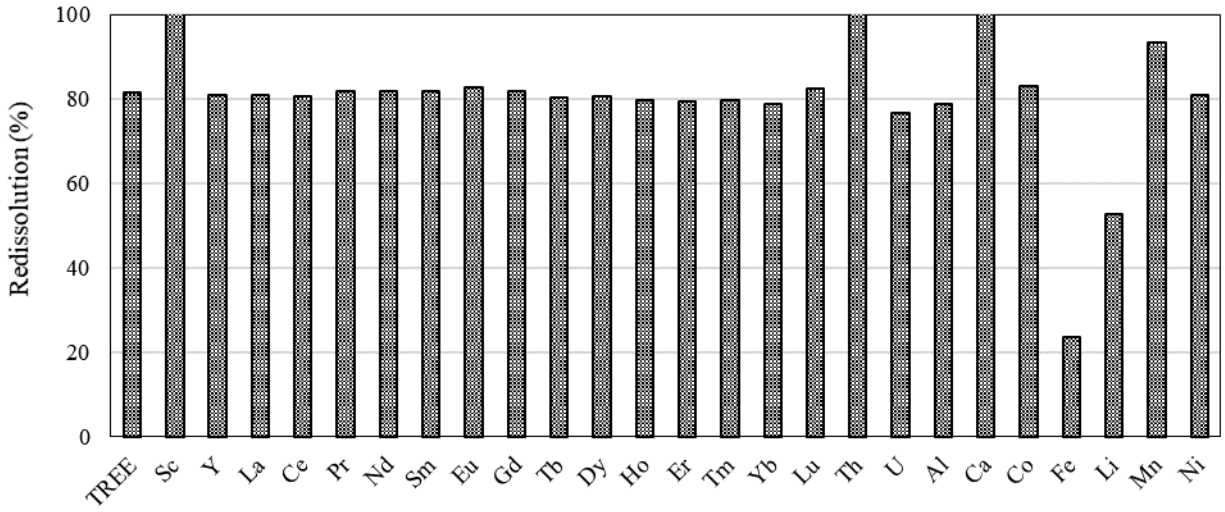

Figure 3.8.15. Redissolution efficiency of REEs and elements of interest. (FC-C8-L2, pH2.2, HCl dosage 12 ml of 36% pure HCl per Liter of blended slurry, residence time 30 min)

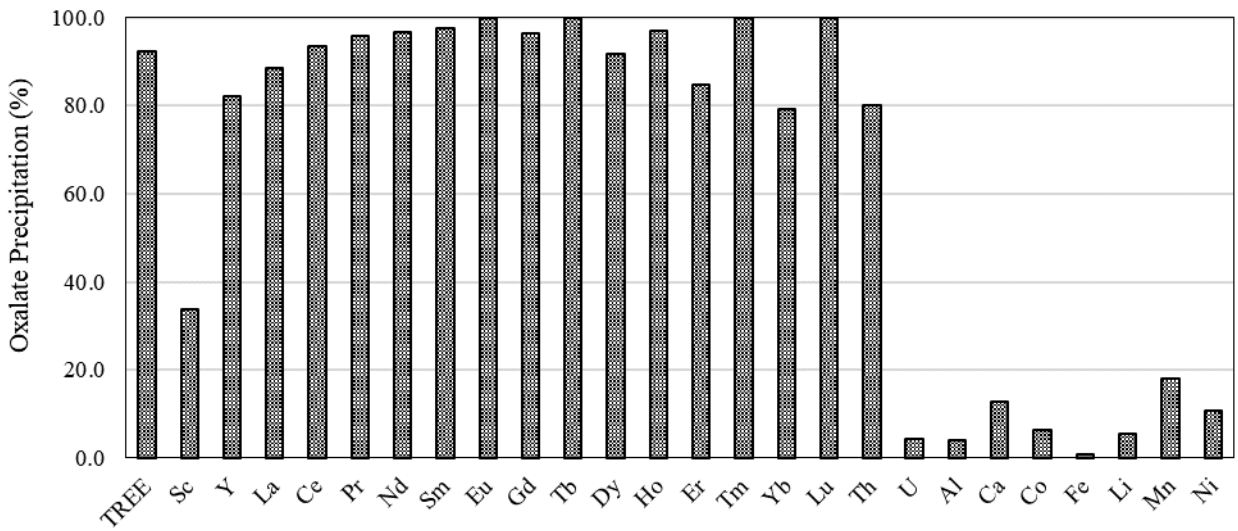

Figure 3.8.16. Oxalate precipitation efficiency of REs and other elements of interest. (pH 1.5, oxalic acid dosage 9.85 g/L of concentrated PLS, residence time 20 min)

3.8.3 Chemical cost analysis and validation

The chemical cost of both test runs was calculated based on the chemical dosage recorded using the industrial bulk chemical prices listed in Table 3.8.13. A breakdown of the chemical cost per each operation stage is shown in Table 3.8.12, which indicated that the acid cost in leaching was the most significant source for further improvement and optimization. The projected chemical cost for DTK and FC validation tests was $12.52 and $18.32, respectively, whereas the actual chemical cost in the validation tests was $11.44 and $15.26, respectively. The grade of REO produced from the west KY No. 13 material and Fire Clay material was 92.7% and 79.5%, respectively. This is due to the differences of leachate composition in the two materials leaching system consequently causing a slight difference in the downstream processes modelling results.

Table 3.8.11. RE recovery and REO grade of each pilot scale test run performed on west Kentucky No. 13 coarse refuse material.

Test Code	H_2SO_4 (M)	Solid Feed (lb/hr)	Feed Solid (lbs)	Estimate RE in Feed (gram)	RE Element Produced (g)	Total Recovery (%)	REO Grade (%)	REO Produced (gram)
DTK-C16	0.075	75	1200	174.0	30.0	17.25	92.7	32.4
FC-C8	0.1	50	800	137.7	19.1	13.86	79.52	24

Table 3.8.12. Break down of chemical cost per run on individual stage of the circuit.

Test Code	Times in Run	Leaching	Precipitation	Redissolution	Oxalate Precipitation		$ChemTotal/Run
		H_2SO_4	$NaOH	$HCl	$Oxalic	$NaOH	
DTK-C16	16	$6.02	$2.54	$1.25	$1.44	$0.20	$11.44
FC-C8	16	$8.02	$3.81	$1.54	$1.64	$0.25	$15.26

Table 3.8.13. Chemical prices used to evaluate the chemical cost of each run.

Bulk Price	$/lb	$/ton
H_2SO_4	0.1	200
NaOH	0.19	380
HCl	0.135	270
Oxalic Acid	0.3	600

3.9 Provide Split Samples (PB3-Task8)

Three REOs mix sample produced from the pilot plant were submitted to NETL according to the original statement of work. The three samples submitted were produced from West Kentucky No. 13 coarse refuse validation test run, Fire Clay coarse refuse validation test run, and West Kentucky No. 13 acid mine drainage. The sample REO grade and the individual elemental concentration are listed in Table 3.9.1, Table 3.9.2, and Table 3.9.3, respectively.

Table 3.9.1. Grade of REOs produced from West Kentucky No. 13 coarse refuse. (analyzed using ICP-OES at UK and ICP-MS at VT)

Marketable RE Oxides	**RE Oxides Concentration (% dry weight)**	
	ICP-OES	ICP-MS
Sc_2O_3	0.01	0.04
Y_2O_3	3.90	3.98
La_2O_3	17.00	17.04
CeO_2	44.41	41.99
Pr_6O_{11}	4.20	4.85
Nd_2O_3	16.18	17.16
Sm_2O_3	2.39	3.07
Eu_2O_3	0.49	0.54
Gd_2O_3	2.06	2.15
Tb_4O_7	0.00	0.21
Dy_2O_3	1.05	0.88
Ho_2O_3	0.43	0.14
Er_2O_3	0.27	0.32
Tm_2O_3	0.04	0.04
Yb_2O_3	0.20	0.19
Lu_2O_3	0.08	0.03
Total	92.70	92.62

Table 3.9.2. Grade of REOs produced from Fire Clay coarse refuse. (analyzed using ICP-OES at UK and ICP-MS at VT)

Marketable RE Oxides	**RE Oxides Concentration (% dry weight)**	
	ICP-OES	ICP-MS
Sc_2O_3	0.02	0.07
Y_2O_3	3.05	3.03
La_2O_3	15.34	14.70
CeO_2	38.78	34.56
Pr_6O_{11}	3.57	4.01
Nd_2O_3	13.20	13.21
Sm_2O_3	1.76	2.30
Eu_2O_3	0.35	0.37
Gd_2O_3	1.63	1.57
Tb_4O_7	0.00	0.16
Dy_2O_3	0.88	0.72
Ho_2O_3	0.38	0.12
Er_2O_3	0.24	0.28
Tm_2O_3	0.04	0.03
Yb_2O_3	0.20	0.18
Lu_2O_3	0.07	0.03
Total	79.52	75.34

Table 3.9.3. Grade of REOs produced from West Kentucky No. 13 Acid Mine Drainage. (analyzed using ICP-OES at UK)

Marketable RE Oxides	**RE Oxides Concentration (% dry weight)**
	ICP-OES
Sc_2O_3	0.16
Y_2O_3	20.45
La_2O_3	6.88
CeO_2	23.31
Pr_6O_{11}	3.33
Nd_2O_3	14.72
Sm_2O_3	5.02
Eu_2O_3	1.12
Gd_2O_3	5.95
Tb_4O_7	0.62
Dy_2O_3	5.56
Ho_2O_3	0.78
Er_2O_3	1.48
Tm_2O_3	0.21
Yb_2O_3	1.11
Lu_2O_3	0.17
Total	90.86

3.10 Secondary Feedstock Testing (PB3-Task9)

3.10.1 Heap leach REE extraction

At the end of fiscal year 2018, the operation and testing of an integrated pilot plant for rare earth element (REE) recovery and concentration was initiated with specific concentration on the solvent extraction and selective precipitation processes. The circuit utilizes a pretreatment circuit, rougher circuit, cleaner circuit, wastewater treatment system and selective precipitation circuit. All components of the circuits were operated simultaneously. The circuit utilized an acid water source from Alliance Coal's Dotiki preparation plant as feed and produced a final REO concentrate of grade >90% REO by weight, recovering >97% of the REEs present in the feed.

3.10.1.1 Materials

In an effort to isolate the initial testing of the solvent extraction (SX) circuit, pregnant solution was obtained from a simple 'heap leach' system constructed using the coarse refuse material generated from the cleaning of West Kentucky No. 13 seam coal. An assay of the pregnant solution shown in Table 3.10.1 shows that the total REE content was 14.45 ppm. The heavy REE content was relatively high as indicative by yttrium accounting for 27% of the total REEs and dysprosium representing another 7%. The H:L ratio was 0.65. The primary contaminants were iron, aluminum, calcium and magnesium.

A trace element analysis of the leachate found that the primary contaminants were iron, aluminum, magnesium and calcium as indicated in Table 3.10.2. The high levels of iron required the addition of a significant amount of ascorbic acid to reduce the Fe^{3+} to Fe^{2+}. Regarding the radionuclides, the thorium level was around a part per billion while uranium content was significant at 1.53 ppm. The total SX process system including the rougher and cleaner circuit along with selective precipitation using oxalic acid was designed to handle these quantities of contaminants.

Table 3.10.1. Rare earth element analysis results obtained for a pregnant solution produced from the oxidation and acid generation of West Kentucky No. 13 coal coarse refuse using ICP-OES.

Element	Sc	Y	La	Ce	Pr	Nd	Sm	Eu	Gd	Tb
Content (ppm)	0.776	3.897	0.309	2.248	0.878	1.093	0.619	0.194	2.648	0.294
Element	Eu	Gd	Tb	Dy	Ho	Er	Tm	Yb	Lu	Total
Content (ppm)	0.194	2.648	0.294	0.949	< 0.003	0.014	0.087	0.312	0.136	14.45

Table 3.10.2. Trace element analysis results obtained for a pregnant solution produced from the oxidation and acid generation of West Kentucky No. 13 coal coarse refuse using ICP-OES.

Element	Th	U	Al	Fe	Mg	Mn	Ca	K	P	As
Content (ppm)	<0.003	1.53	1467	5453	572	77.6	459	<0.044	57.6	3.7
Element	Ni	V	Co	Li	Zn	Cu	Na	Cr	Pb	Cd
Content (ppm)	22.2	1.4	8.7	4.1	36.7	14.9	1.1	1.1	0.8	0.32

3.10.1.2 Process Flowsheet

The continuous SX rougher plant was comprised of seven mixer settlers as shown in the Figure 3.10.1. The setup consisted of 2 stages of loading and stripping, and 1 stage of scrubbing, saponification and reprotonation. The mixer-settlers for scrubbing, stripping, saponification and reprotonation were plumbed to internally recirculate the aqueous stream while the loading stage was plumbed to not have any internal recirculation. For the startup, the scrubbing stage mixer settler was filled with 0.1M HCl, saponification stage was filled with 2M NaOH and stripping and reprotonation stages were filled with 6M HCl solution.

The recirculation of the aqueous stream from settler back to mixer allowed the concentration of metals in the solution to build up so to operate the process at equilibrium conditions. The flowsheet of the SX circuit was modified slightly in light of new data generated during the operation of the pilot plant. There were two changes made in the flowsheet: 1) the scrubbing solution bleed stream was redirected from the waste water stream where it was previously going to the SX feed tank and 2) the reprotonation bleed stream was redirected from raffinate stream where it was previously going to the SX feed tank. Both changes were made to improve the overall recovery of the system. Performance data indicated that the changes reduced the amount of REEs which were leaving the system.

3.10.1.3 Circuit Performance

The two key operating parameters of the rougher circuit were feed pH of the solution and the flowrate of the fresh stripping solution introduced in the system. These parameters were closely related and were varied based on the concentration of metals in the stripped solution and the overall recovery of the REEs in the circuit. As shown in the Figure 3.10.2, the recovery of the REEs remained around 90% for the 1st 120 hours of operation. It then starts to drop as the stripped solution started to get saturated and the organic phase started to get poisoned, reducing the extraction efficiency. The stripped solution pump rate rate was gradually increased from 6 to 20 RPM over the next 60 hours of operation. As the REE concentration in the stripped started to diminish (as shown in Figure 3.10.3), it was ascertained that to increase the recovery of the REEs the feed pH will have to be increased. As shown in the Figure 3.10.2, as the feed pH was increased to 2.1 the recovery increased to over 97%. The stripped solution consequently reduced from 20 RPM to 18 RPM and the REE concentrations in the stripped solution stablized at around 250 ppm.

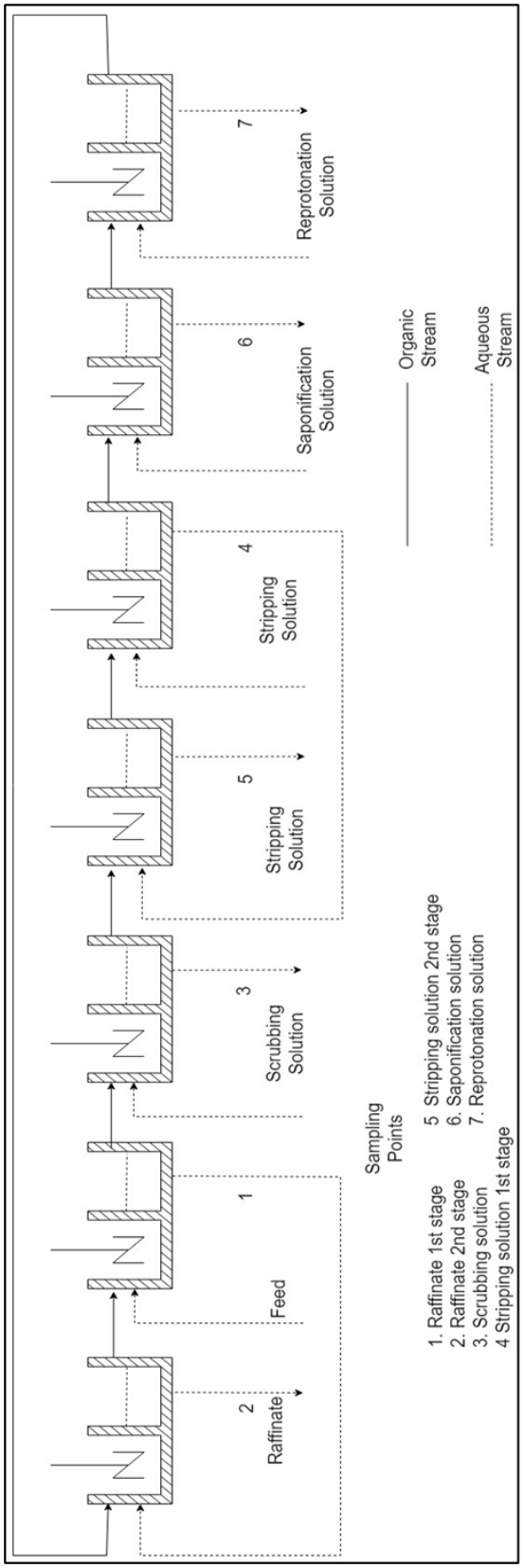

Figure 3.10.1. SX Flowsheet for REE Recovery in the Pilot Plant

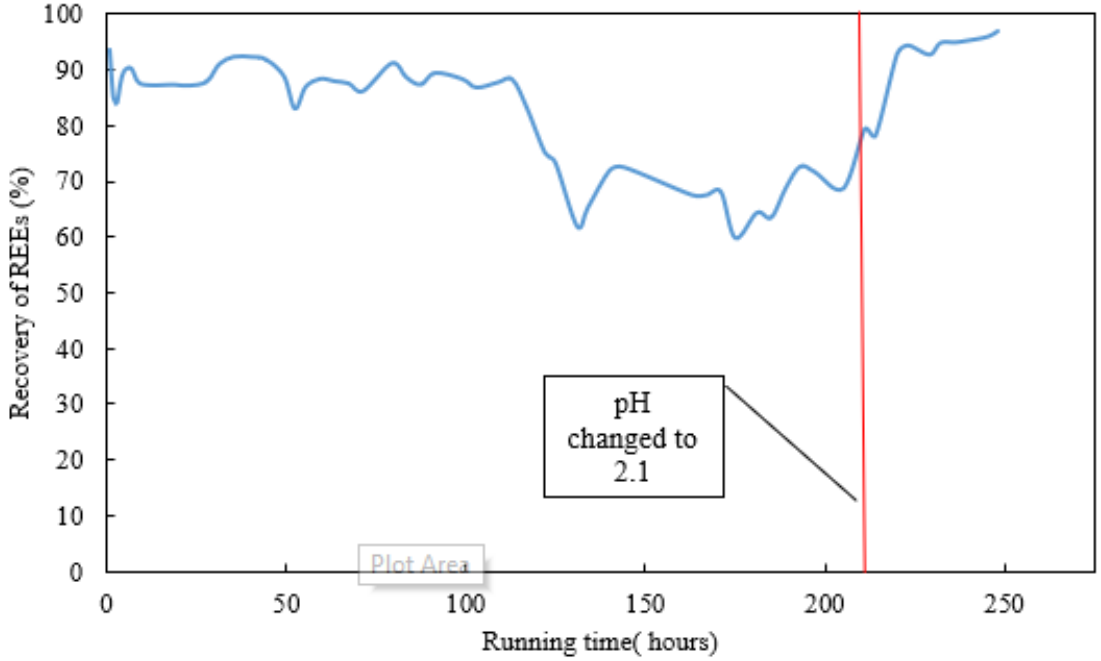

Figure 3.10.2. Recovery of REEs present in the feed in the rougher circuit of with respect to running time

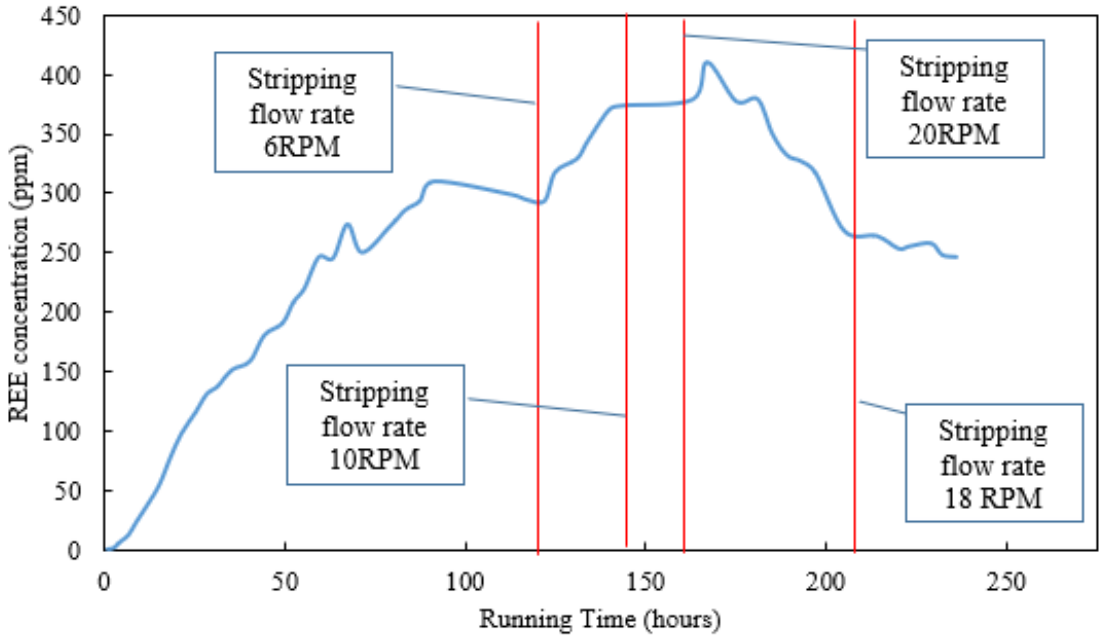

Figure 3.10.3. Concentration buildup of REEs in the stripping solution with running time and different stripping flow rates

Additionally, two important parameters for the operation of the rougher circuit were the level of contaminants in the final stripped solution. For the given feed, the biggest contaminants

were iron and calcium. As shown in the Figure 3.10.4, the calcium concentration stayed constantly high until 180 hours of operation after which its concentration decreased substantially. This was primarily due to the bleeding of the scrubbing solution from the scrubbing circuit. As more and more calcium was rejected in the scrubbing circuit, the contamination level in the stripping circuit reduced as well. The effect of scrubbing bleed is discussed in the later section as well.

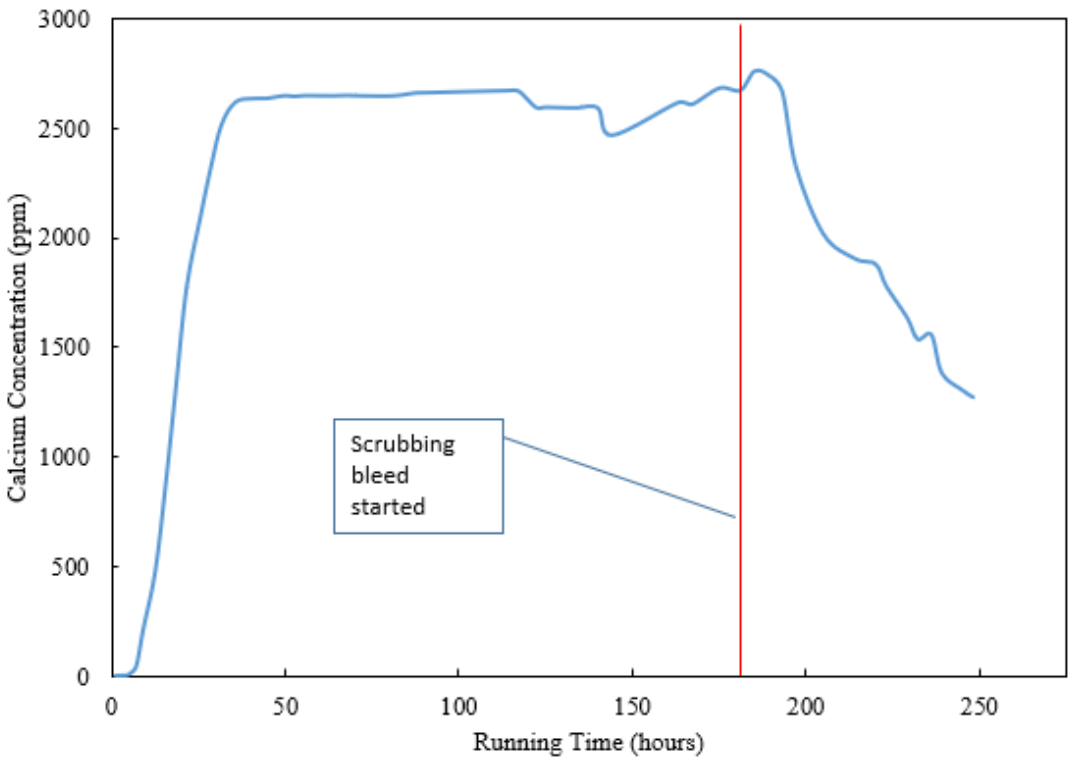

Figure 3.10.4. Concentration buildup of calcium in the stripped solution with running time and the effect of bleed of scrubbing solution

The other big contaminant in the stripped solution was iron. Unlike calcium, the most significant factor for coextraction of iron was the dosage of ascorbic acid. As shown in the Figure 3.10.5, the contamination level of iron in the stripped solution was elevated two times during the entire operation. Both the times, the reason was insufficient dosage of ascorbic acid resulting in ferric ions present in the feed. As the ferric ion has a high distribution coefficient, it results in the elevated contamination. As the ascorbic acid dosage was increased, the iron concentration in the stripped solution also dropped substantially.

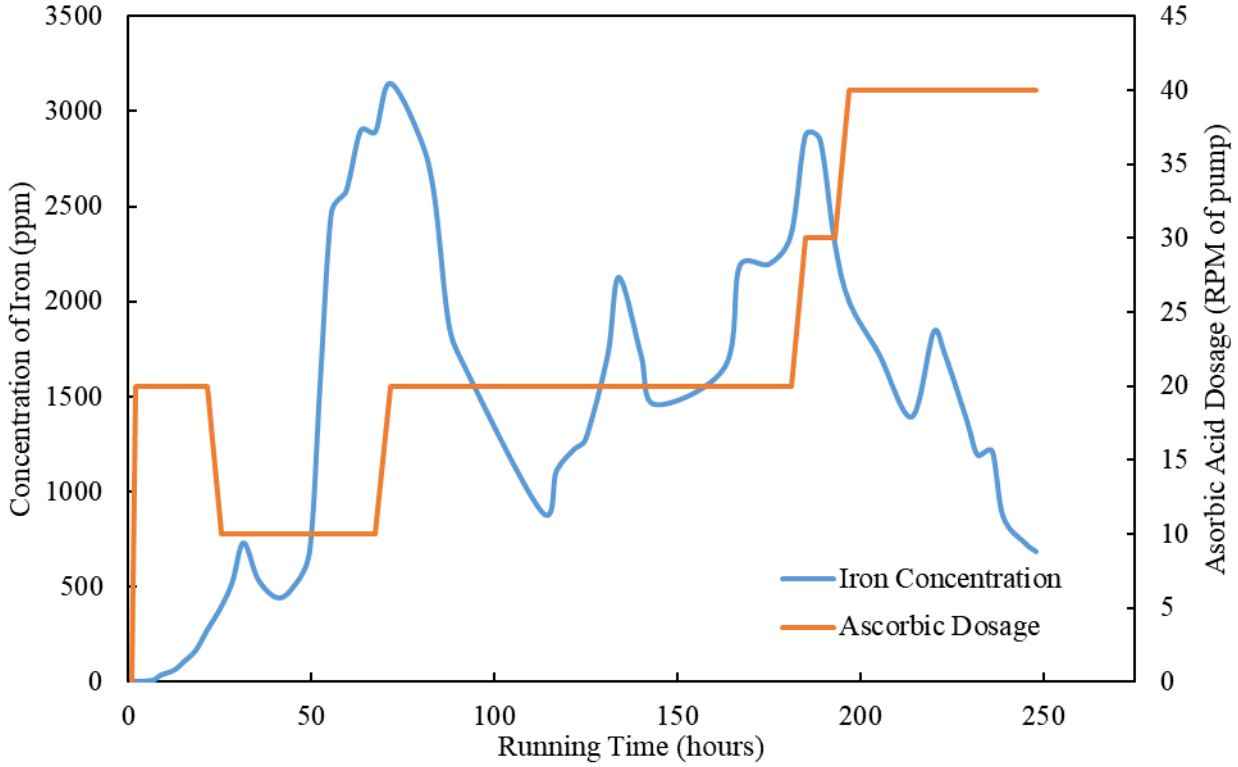

Figure 3.10.5. Concentration buildup of iron in the stripped solution with running time and the effect of corresponding ascorbic acid dosage

Scrubbing circuit: The purpose of scrubbing circuit was to reject the co-extracted calcium in the organic phase to reduce the contamination in the final stripped solution. For this purpose, a mild acid of 0.1M HCl was used in the scrubbing section. The 0.1 M acid was recirculated in the mixer until the concentration of calcium sufficiently built up. Following that, fresh 0.1M solution of HCl was added in the mixer and equal volume was bled off to the neutralization tank of waste water. Following the change in the flowsheet, the bleed off of scrubbing stream was recirculated back to the feed tank to preserve the REE in the system.

As shown in Figure 3.10.6, the scrubbing bleed was started after circuit reconfiguration at the 170th hour of operation. The scrubbing solution pump rate was fixed at 20 RPM. The calcium concentration decreased continuously for the rest of the test which would resulted in improved extraction efficiency of REE with a reduced contamination level.

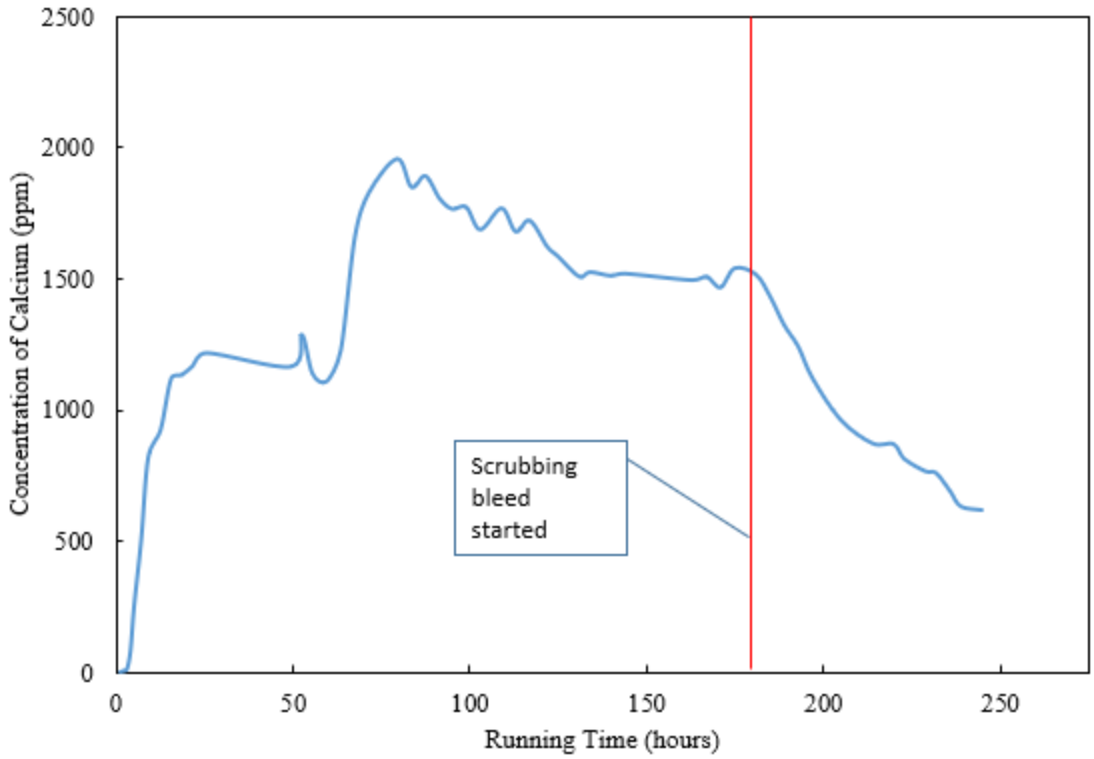

Figure 3.10.6. Concentration buildup of calcium in the scrubbing solution with running time and the effect of bleed of scrubbing solution

The Cleaner Unit**,** shown in Figure 3.10.7, is comprised of six mixer settlers of which three were used for loading and three for stripping. The stripping stages, like the rougher stage, were plumbed to internally recirculate the aqueous stream from the settler to mixer to allow for the concentrations of REE to build up to the equilibrium level. Since the concentration of REEs in the feed of the cleaner was an order of magnitude higher than that of the rougher feed, organic extractant composition of the cleaner was 20% DEHPA in Orfom v/v% to load REEs into the organic phase.

Figure 3.10.7. Setup for cleaner stage for SX circuit in the continuous plant.

To estimate the optimum operating pH for the cleaner circuit with the chosen organic extractant, an exploratory shakeout test was conducted with the stripped solution bleed stream. 50 mL of stripped solution was contacted with 50 mL of the organic extractant at different pH values. As shown in the Figure 3.10.8, the recovery of the REEs increased from 35% to 70% when the pH of the solution was increased from 0.1 to 1.0. Iron as a contaminant interfered with the oxalate precipitation of REEs as it tended to precipitate with the REEs. Therefore, it was critical for the production of high grade REE concentrate to reject a maximum amount of iron in the cleaner stage. The co-extraction of the contaminants in the cleaner also increased from 0.7% to 10% for iron over the range of pH values evaluated.

It was also observed from the data in the Figure 3.10.8 that the heavy REEs have a higher tendency to be extracted at lower pH values than the light REEs. The HREE/LREE ratio decreases from 3.1 to 0.65 as the pH increased from 0.1 to 1.0 as more and more light REEs were extracted into the organic phase.

The purpose of employing the cleaner unit was not to achieve maximum recovery but to reject maximum amount of iron. The reject stream of the cleaner i.e. raffinate was recirculated back to the feed of the rougher circuit to allow an opportunity for the fraction of REEs lost in the raffinate to be recovered in the rougher circuit.

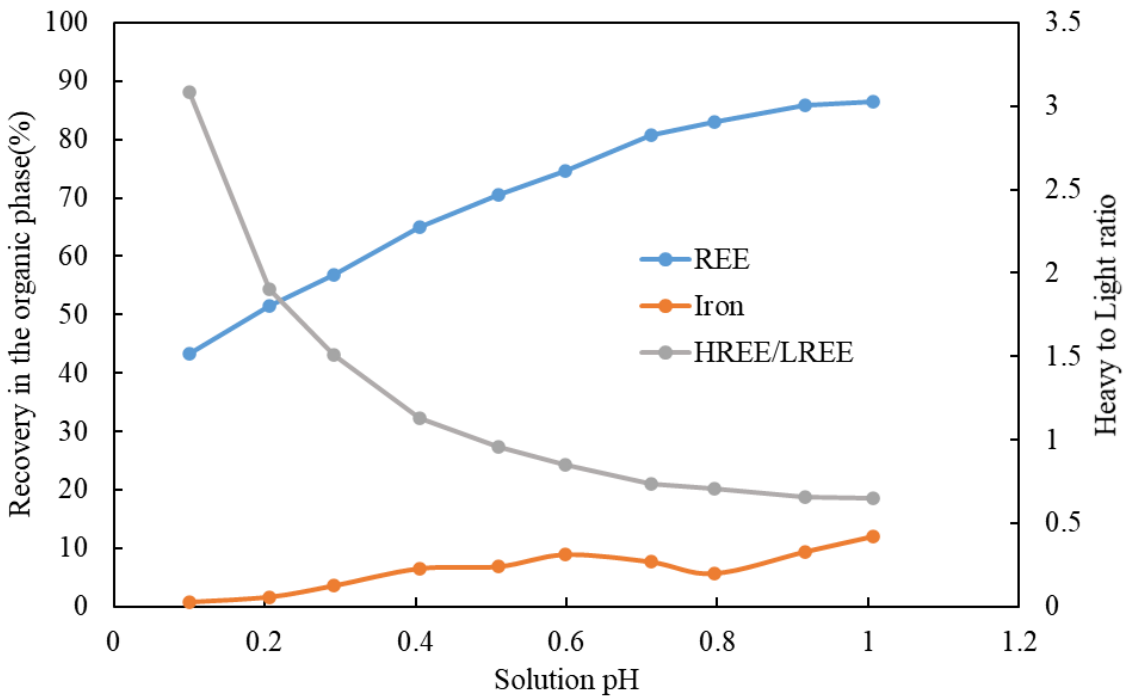

Figure 3.10.8. Extraction curves of REEs and Iron with pH of the feed solution for cleaner circuit and HREE/LREE ratio for different pH solutions.

During operation, periodic samples were collected at three points in the cleaner circuit, i.e., the circuit feed solution, the raffinate generated by the cleaner circuit and the stripped solution produced in the process. The raffinate and feed samples were required to compute the recovery of the REEs in the circuit while the stripped solution was the feed for selective precipitation circuit and required a high concentration of REEs for better precipitation efficiency.

The feed pump rate of the cleaner circuit was fixed at 25 rpm as the feed was dependent on the flow rate of the stripped solution in the rougher circuit. The stripped solution pump rate was varied based on the concentration of REEs in the stripped solution and recovery of REEs in the circuit. As shown in the Figure 3.10.9, the stripped solution rate was initially maintained at 6 RPM. At the 220th hour of operation, a rise in the concentration of both calcium and REE was observed. Additionally, the recovery of REE in the stripped solution was low as shown in Figure 3.10.10. Following these observations, the flow rate of stripping solution was increased to 10 RPM. The effect was observed as the concentration of both REE and calcium started declined. Consequently, the recovery of REE increased to values above 99%. At the 240th hour of operation, the stripped solution flowrate was decreased to 8 RPM to increase the concentration of REE in the stripped solution. Consequently, the REE concentration stabilized with recovery remaining above 99% in the cleaner circuit. It was concluded that, for the given feed rate of 25 RPM, a stripped solution pump rate of 8 RPM resulted in high recovery as well as high REE concentration for selective precipitation.

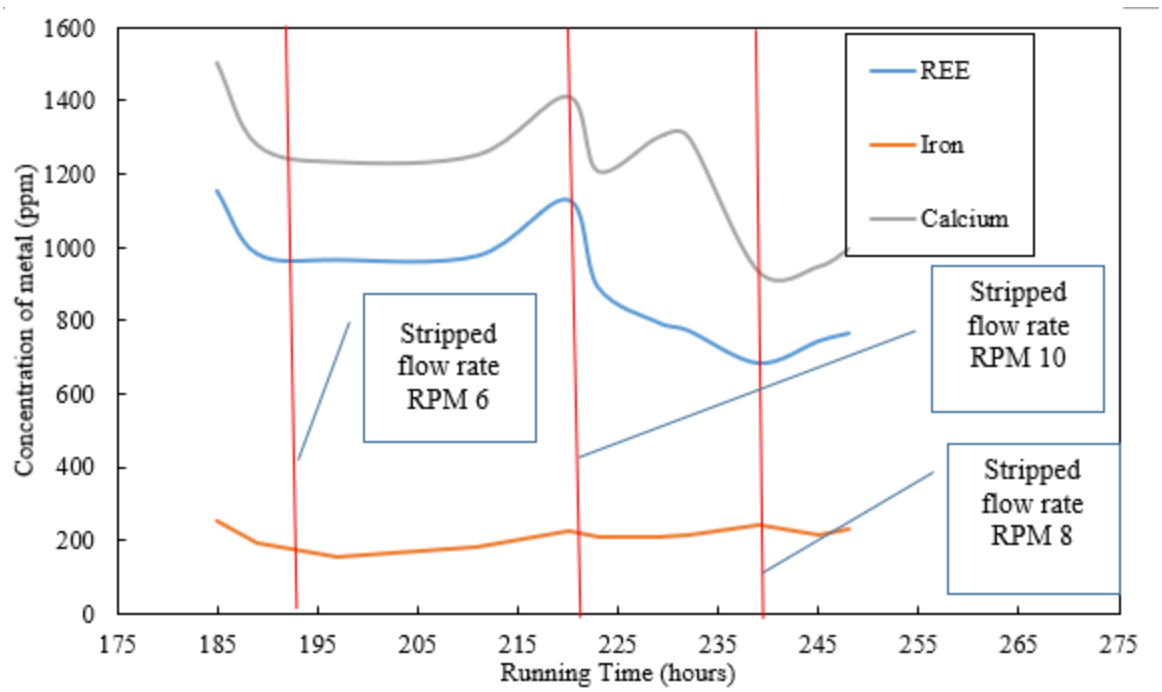

Figure 3.10.9. Concentration buildup of REEs and contaminants in the stripped solution of cleaner circuit with running time and the effect of flow rates of stripped solutions.

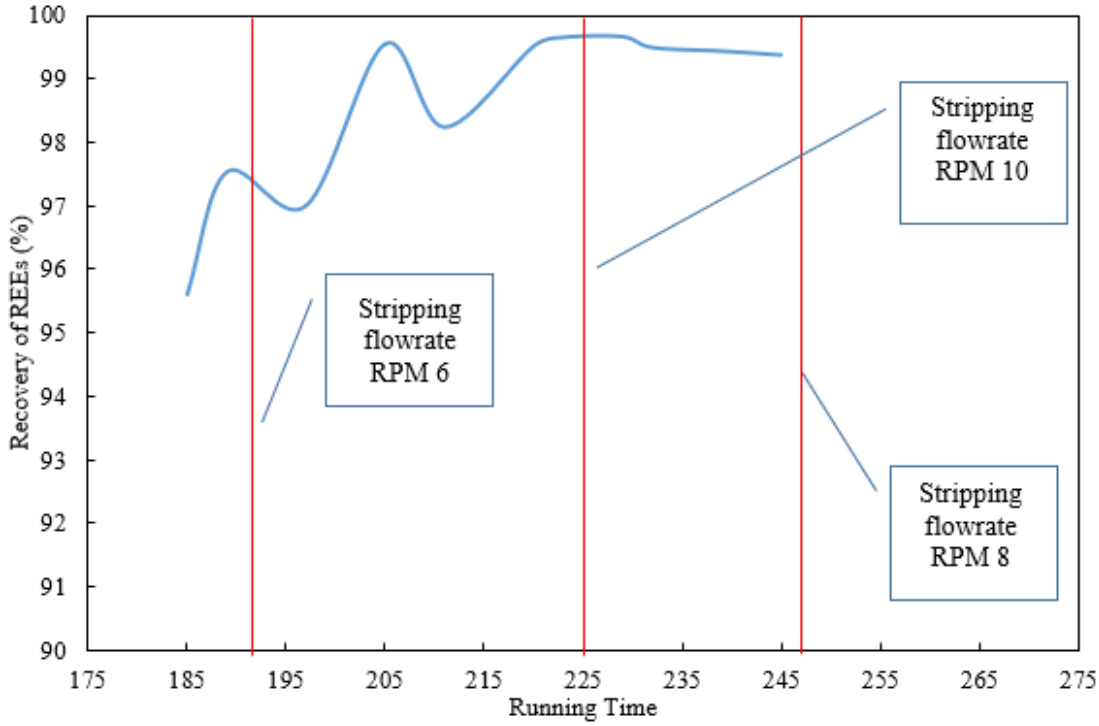

Figure 3.10.10. Recovery of REEs in the cleaner circuit and the effect of stripped solution flowrates.

3.10.2 Will Scarlet Acid Mine Drainage

Approximately 5000 gallons of acid mine drainage (AMD) water shipped from the Will Scarlet mine site (Williamson County, Illinois) was treated using the selective precipitation circuit. The water was stored in polypropylene tank coated with lightproof material. The water contains about 1 ppm of total rare earth (TREE) in which the heavy rare earth element (HREE) content was 0.5 ppm and the light rare earth element (LREE) was 0.52 ppm. The major rare earth elements present in the mine water were Y, Ce, and Nd as shown in Table 3.10.3. The major contaminations in the mine water are 100 ppm of Al, 350 ppm of Ca, and 76 ppm of Fe. Since the TREE concentration in the mine water is significantly lower than the contaminations, pre-concentration of TREEs was required to generate a more concentrated solution to feed into the downstream REE refining process.

Table 3.10.3. Will Scarlet mine water composition and concentration.

Rare Earth Elements	Concentration (mg/L)	Other Elements	Concentration (mg/L)
Sc	0.00	Al	109.35
Y	0.29	Ca	353.79
La	0.03	Co	0.29
Ce	0.19	Cu	0.03
Pr	0.03	Fe	76.71
Nd	0.20	K	21.19
Sm	0.05	Li	0.23
Eu	0.01	Mg	2.96
Gd	0.09	Mn	23.63
Tb	0.01	Na	248.10
Dy	0.07	Ni	0.56
Ho	0.00	P	0.10
Er	0.02	Pb	0.05
Tm	0.00	Sr	0.26
Yb	0.02	Zn	2.57
Lu	0.00		

3.10.2.1 Rare earth element precipitation

Exploratory experiments were performed to determine the precipitation pH of each individual element. A 2-L sample of the AMD was collected from the storage tank for the precipitation test. Agitation was provided using a magnetic stir at a rotation speed of 500 rpm. The initial pH of the mine water was 2.75 and was gradually increased by incrementally adding 0.1 mL of a 1 mol/L NaOH solution. A 2 ml sample was collected from the mixed slurry sample after reaching pH values of 3, 4, 5, 6, 7, and 8. The samples were centrifuged and 1 ml of the effluent diluted 10 times with 5% (v/v) nitric acid for ICP analysis.

The results showed that the majority of Fe and Al precipitated at pH values between 4 and 5, whereas the REEs precipitated in the pH range of 6 to 7 as shown in Table 3.10.4. The Ca remained in solution up to a pH value of 8. The separation curves plotted in Figure 3.10.11 indicate that, at a pH value of 4, 75% of the Fe precipitated with 7% TREE loss; however, Al removal was only 11% at pH 4. At a pH value of 4.5, 50% of the Al precipitated. As such, pH 4.5 was selected based on a target to eliminate 80% of the Fe and 40% of the Al. The condition provides a TREE loss of 17%. After the first stage contamination removal, the waste precipitate was filtered and discarded. The effluent containing REEs and reduced contaminants was subject to a second precipitation stage to concentrate the REEs in a precipitate cake. Based on the lab results, a pH value of 7.5 was selected to recover over 95% of the REEs.

The 5000 gallons of AMD was processed in the pilot plant over a period of 20 hours of continuous operation. The mine water was pumped into a 200-gallon reaction tank (Tank 6) at a flow rate of 4 gallons per minute (gpm). The pH was regulated to 4.5 using 1M NaOH solution in Tank 6. Next, the slurry carrying fine precipitate overflowed into a surge tank and then pumped to a plate and frame filter. The filtrate was sent to another 200-gallon tank (Tank 19) in which the pH was automatically adjusted to a value of 7.5. In both tanks, the pH was regulated by automatically pumping 1M NaOH base solution through a peristatic pump which was PID programmed. Figure 3.10.12 shows the consistency and stability of the pH control system for the two-stage precipitation.

Samples were collected from the feed stream and the filtrate streams from Tank 6 and Tank 19 every 2 hours during the 20 hours of operation. The filtrate after the 1st stage contamination precipitation in Tank 6 (pH 4.5) contained an average of 0.92 ppm of TREE, 32 ppm of Al, 264 ppm of Ca, and 25 ppm of Fe. This stage eliminated 64% of Al and 31% of Fe while losing only 2.4% of TREEs. In the REE precipitation tank (Tank 19), the filtrate contained only 0.03 ppm of TREEs, 1.5 ppm Al, 267 ppm Ca, and 0.4 ppm Fe. Almost all of the TREEs along with Al and Fe were precipitated in this stage except for Ca. The precipitation efficiency of REEs and major contaminants for both stages are plotted in Figure 3.10.13.

Table 3.10.4. Concentration of total REEs and major contaminants remained in solution at different pH.

Sample Code	pH	1M NaOH (ml)		Remained in solution (ppm)			
		Increment	Cumulative	TREE	Al	Ca	Fe
Feed	2.745	0	0	1.02	109.4	353.8	76.7
1	2.978	2	2	1.02	106.3	356.6	74.6
2	4.025	4.5	6.5	0.96	97.3	356.1	16.7
3	5.017	4.5	11	0.75	30.0	349.2	11.8
4	6.484	1	12	0.15	16.7	351.6	7.9
5	7.241	0.5	12.5	0.05	6.1	348.7	4.3
6	8.008	0.5	13	0.02	3.3	348.6	1.8

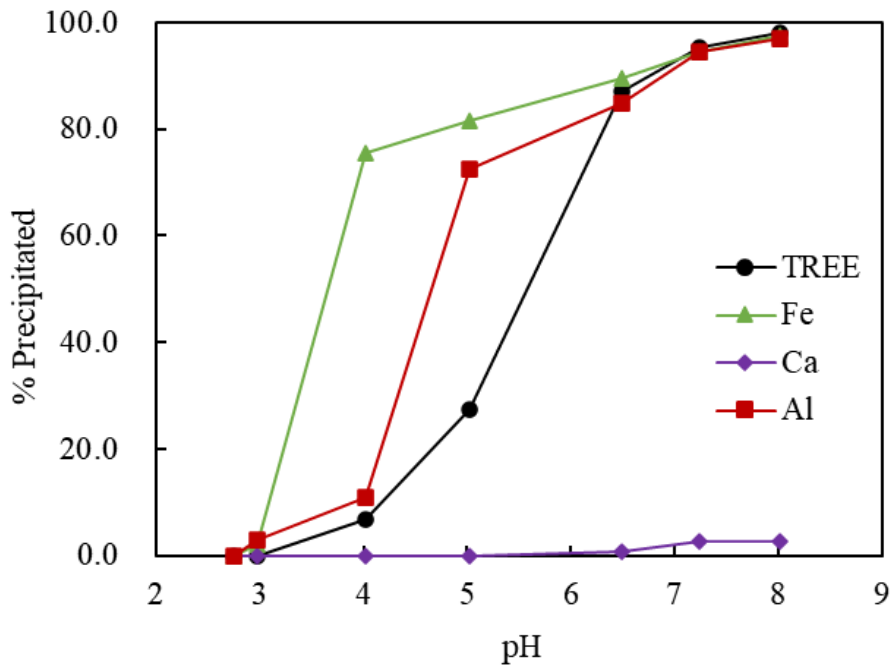

Figure 3.10.11. Separation curves of TREEs, Fe, Al, and Ca during selective precipitation over a range of pH.

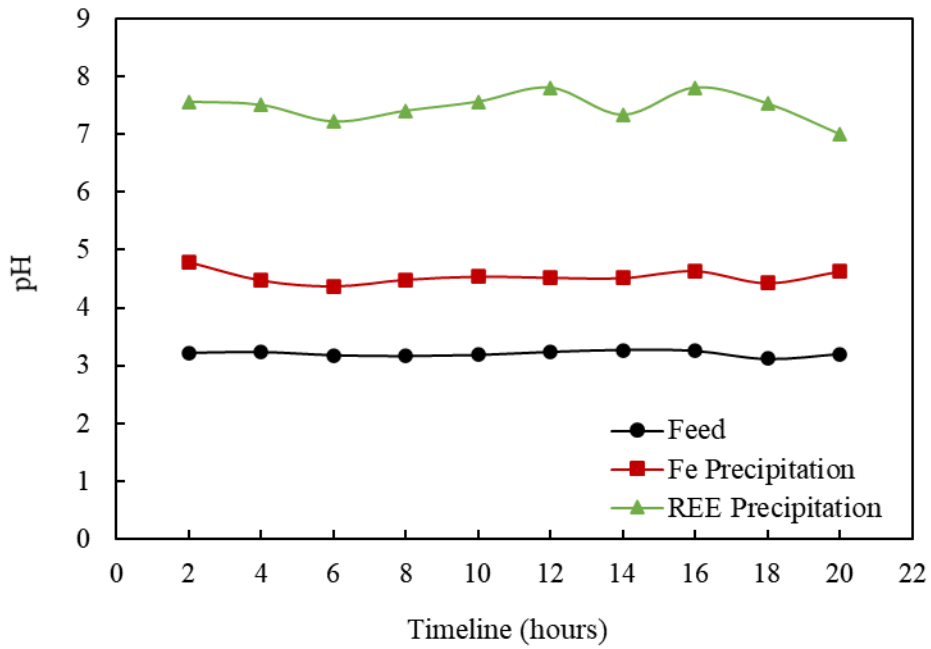

Figure 3.10.12. The recorded pH of continuous process of REEs and contamination precipitation over 20 hours of operation.

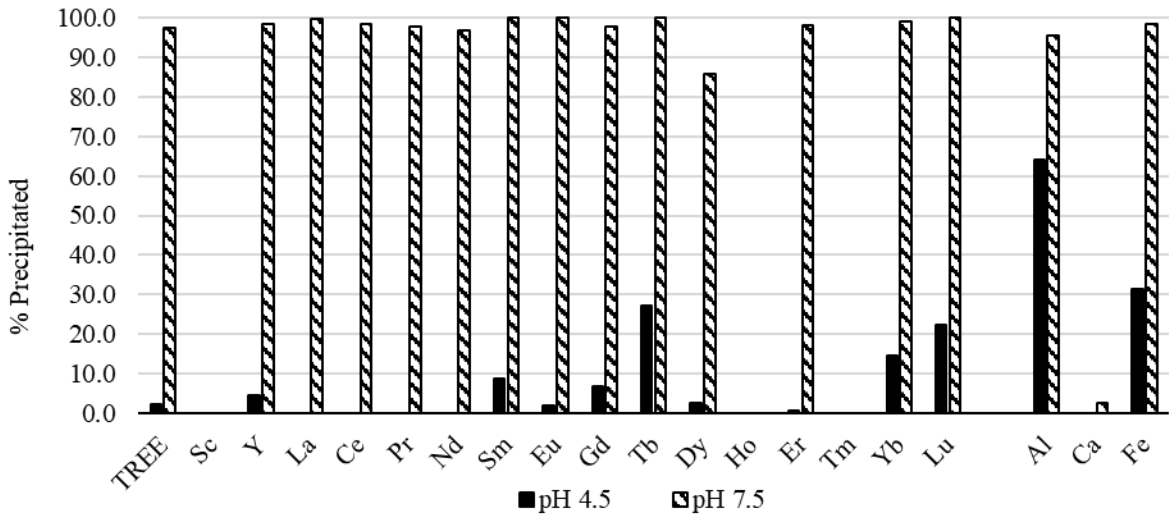

Figure 3.10.13, Precipitation efficiency of individual REEs compare to Al, Ca, and Fe in two stage precipitation at pH 4.5 and pH 7.5 during the continuous process over an operation period of 20 hours.

3.10.2.2 Rare Earth Precipitate Re-dissolution

The filter cake obtained from the REE precipitation stage contained concentrated REEs that redissolution for further refining. The cake formed in the plate-and-frame filter appeared to be a tightly packed structure. However, the solid content was only about 29% by weight including 6.5% (by weight) of perlite that was used as a filtration aid. The high water content in the sludge was due to the chemically bound water in the $Al(OH)_3$ and $Fe(OH)_3$ precipitates. The filter cake was liquified after blending using a mechanical mixer at high rotation speed for 24 hours without any additives.

A lab test was carried out to identify the optimum redissolution pH value for the REEs from the liquified slurry. A hydrochloric acid solution (37% by weight) was used by incremental additions to dissolve the precipitates as shown in Table 3.10.5. Figure 3.10.20 shows the solution color change of the supernatant obtained at different pH which indicates the change of solution composition as a function of pH during redissolution. The maximum concentration of REEs, Al, Ca, and Fe that could be achieved from completely dissolve the sludge was around 200 ppm, 3467 ppm, 2000 ppm, and 4000 ppm, respectively.

The redissolution efficiency of REEs and major contaminants (Al, Ca, and Fe) achieved as the pH value was reduced is plotted in Figure 3.10.15. The results indicate that optimum redissolution pH occurs between pH values of 2.5 to 3.5 which maximizes REE recovery and Fe rejection. At a pH of 2.5, over 97% of the REEs were dissolved with over 95% of Al, 97% of Ca, and about 45% of Fe. Whereas at a pH value of 3.5, only 5% of Fe and 40% of Al were redissolved while only 67% of the REEs were redissolved. Scandium loss was especially high with only 18% being redissolved. Therefore, from an economic standpoint, a pH value of 2.5 was selected for REE redissolution. The redissolution efficiency of individual REE and the corresponding Al, Ca, and Fe recovery at pH value of 2.5, 3.0, and 3.5 is as shown in Figure 3.10.16.

Table 3.10.5. REEs and contaminants redissolution using HCl at various pH (1-Liter of slurry).

Sample	37% HCl (ml)	pH	Concentration in Supernatant (ppm)			
			TREE	Al	Ca	Fe
WS-C2-RPRD-F	0	8.182	0.4	1.8	310	0.47
WS-C2-RPRD-1L	12	4.114	55	127	1780	2.59
WS-C2-RPRD-2L	5	3.519	133	1540	1981	185
WS-C2-RPRD-3L	13	3.025	185	3063	1963	1000
WS-C2-RPRD-4L	11.5	2.486	194	3303	2056	1671
WS-C2-RPRD-5L	4	1.926	204	3432	2054	3689
WS-C2-RPRD-6L	5.5	1.499	196	3390	1990	3723
WS-C2-RPRD-7L	5.5	0.976	199	3467	2033	4000

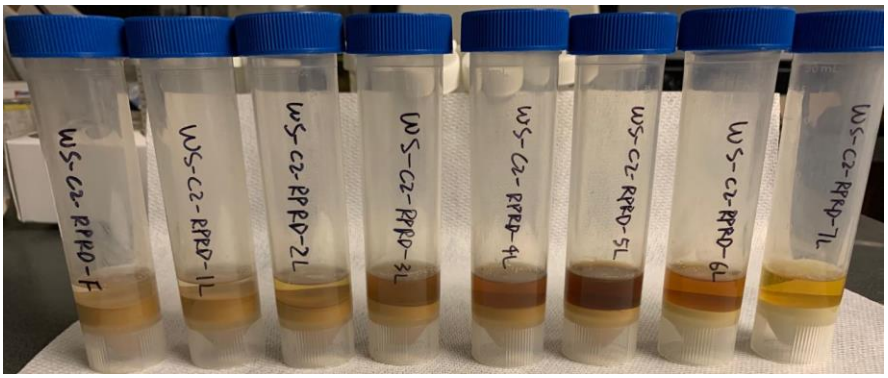

Figure 3.10.14. REE precipitate re-dissolved at various pH value after centrifuge.

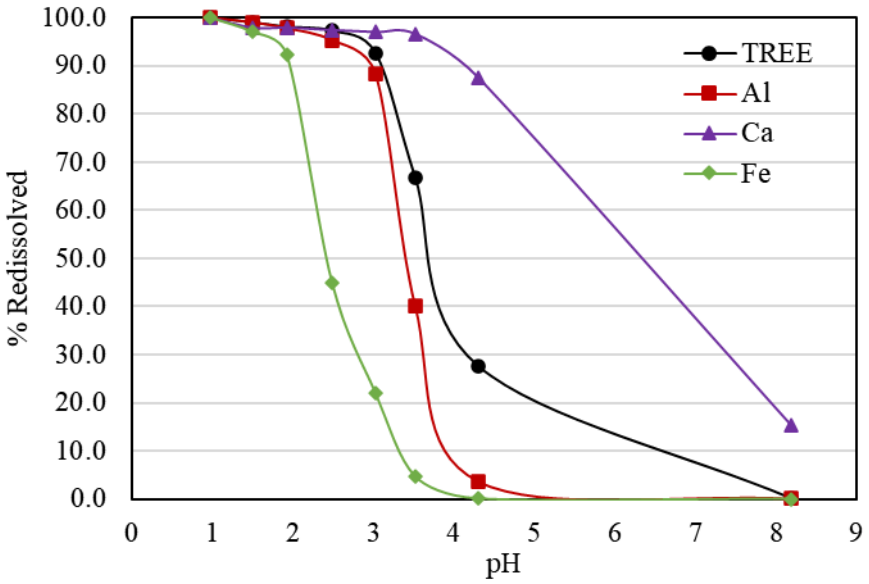

Figure 3.10.15. Rare earth redissolution efficiency as the solution pH value is reduced using hydrochloric acid.

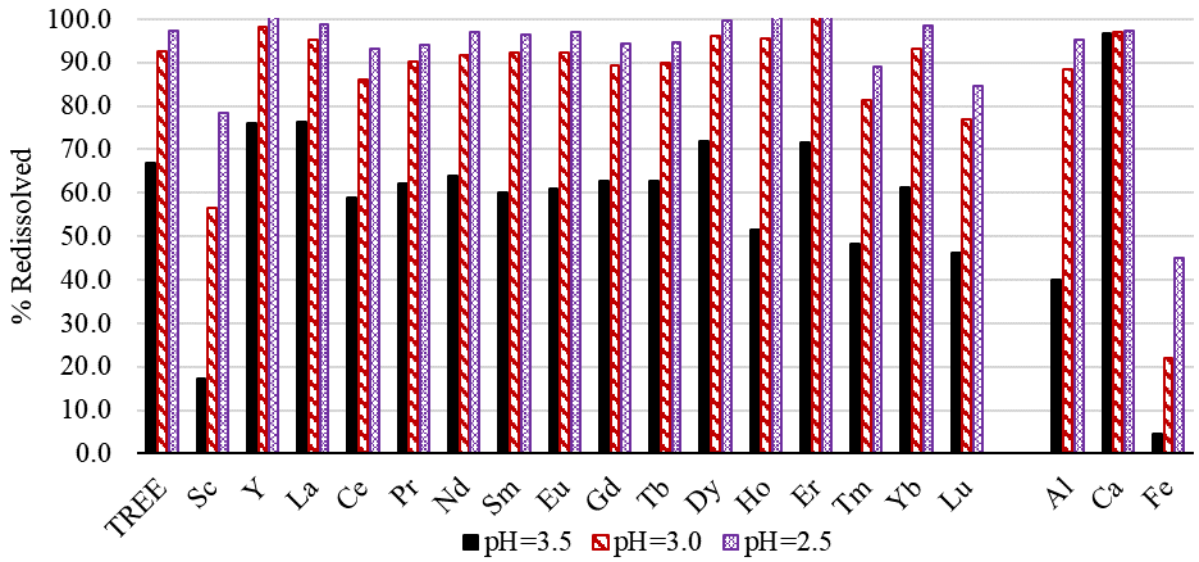

Figure 3.10.16. Redissolution efficiency of individual REE and major contaminants at pH of 3.5, 3.0, and 2.5.

3.10.2.3 Comparison of 2nd stage Fe precipitation and solvent extraction

The solution obtained from redissolution remained relatively high in Al, Ca and Fe content. In a past study, solvent extraction operation was applied to extract REEs from a pregnant solution and successfully produced high purity of rare earth oxides (>90% pure). However, the economics of solvent extraction circuit was highly dependent on the absolute concentration of REEs in the feed solution and the ratio of contaminant ion to REE content. In this section, a comparative study was performed for staged precipitation and solvent extraction (SX) for separating rare earth elements (REE) from the contaminants. The effectiveness and economics of both processes for the production of high purity REO concentrate were evaluated and compared.

3.10.2.4 Staged Precipitation

The contaminant rejection and production of high purity REO were tested using staged precipitation followed by oxalate precipitation. The pH of the redissolved pregnant solution (RPS) was raised incrementally from 2.5 to 5.35 by carefully adding 4M NaOH solution dropwise and stirring using a magnetic stirrer. The precipitate generated was filtered out at each increment. The elemental composition of filtrate at each increment was analyzed and the percentage loss to the precipitated was shown in Figure 3.10.17. At a solution pH value of 4.88, 99.95% of the iron and 99.08% of the aluminum precipitated. However, 45.7% of the REE present in the RPS also co-precipitated in the process.

The solution after iron and aluminum precipitation was subjected to oxalic precipitation to selectively precipitate REEs. A 160 g/L oxalic acid solution was prepared by dissolving 8 g of oxalic acid in 50 mL of deionized water (DI). One milliliter of oxalic acid solution was added to the solution recovering 82.9% of the REE present in the solution. The rare earth oxalates were

calcined at 750°C for 2 hours to produce a rare earth oxide mix which contained 98.49% REO by weight.

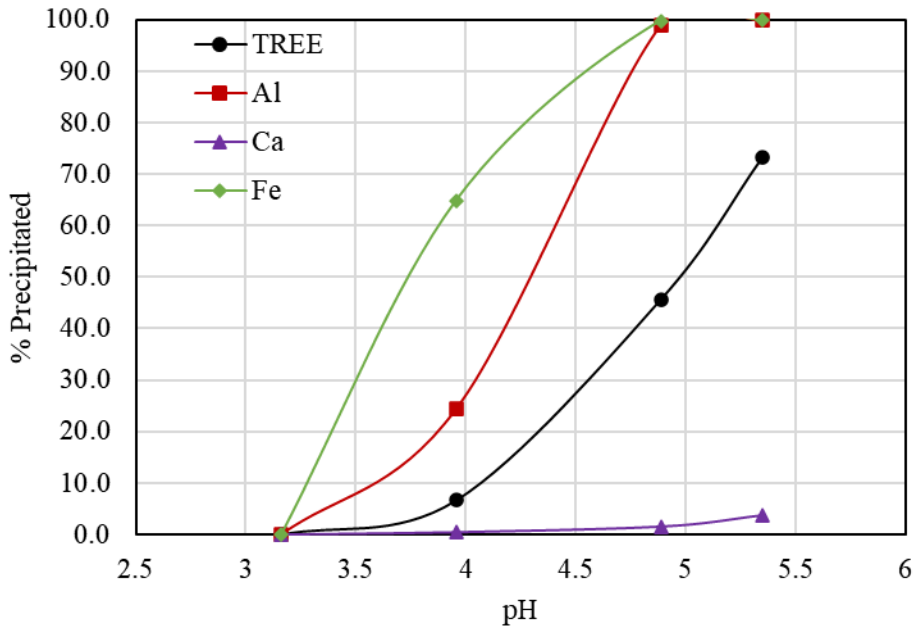

Figure 3.10.17. Precipitation efficiency of TREEs and major contaminants at various pH values using NaOH.

3.10.2.5 Solvent Extraction

The contaminant rejection and production of high purity REO was tested using SX followed by oxalate precipitation as well. As the objective of the study was to compare the costs associated with both the processes, the three aspects of the SX process which were studied in this test were the optimum dosage of ascorbic acid, the optimum volume of stripping solution (6M HCl) required to strip the organic phase and the amount of NaOH required to adjust the pH of the stripped solution to a value of 1.7.

It was necessary to reduce iron from its ferric (Fe^{3+}) state to its ferrous (Fe^{2+}) state as the distribution coefficient of ferric ions is higher than ferrous ions by orders of magnitude. For this study, ascorbic acid was used as the reducing agent. A 200g/L solution of ascorbic acid was prepared by dissolving 10g of food-grade ascorbic acid in 50 mL of DI water. Incremental volumes of the ascorbic acid solution were added to the RPS and mixed with an organic solution of 5% v/v. It was observed that the extraction efficiency of iron dropped from 59% to 18% with 20 ml of ascorbic acid solution dosed per liter of RPS as shown in Figure 3.10.18.

As a part of the study, the optimal volume of stripping solution (6 M HCl solution) required to recover the REEs into the aqueous phase was also determined. A 5% v/v solution of DEHPA was contacted with the RPS solution at an initial pH of 2.0 with an aqueous-to-organic ratio of 1:1. 100 mL of the loaded organic solutions were contacted with different volumes of 6M HCl and were mixed for 5 minutes using a magnetic stirrer. The two phases were separated and disengaged

in a separatory funnel and the stripping solution was analyzed using ICP-OES. The stripping efficiency of the REE was determined by the following equation:

$$\text{Stripping Efficiency} = \frac{[\text{REE}]_{\text{org}} * \text{volume}_{\text{org}}}{[\text{REE}]_{\text{aq}} * \text{volume}_{\text{aq}}}$$

in which the $[\text{REE}]_i$ is the concentration of REE in the ith phase and volume_i is the volume of the ith phase. It was observed that the stripping efficiency of the REEs increased with the increase in the volume of stripping solution per liter of the organic phase. The minimum volume of stripping solution which stripped >95% of REEs from the organic solution was determined to be 60 mL per liter of the loaded organic phase in Figure 3.10.19.

The stripped solution from the SX process was neutralized with NaOH and the pH was adjusted to 1.7. The solution was subsequently treated with oxalic precipitation followed by roasting in the same way as the staged precipitation process. It was determined that 30 mL of 50 % w/v solution of NaOH was required to raise the pH of the stripped solution to 1.7.

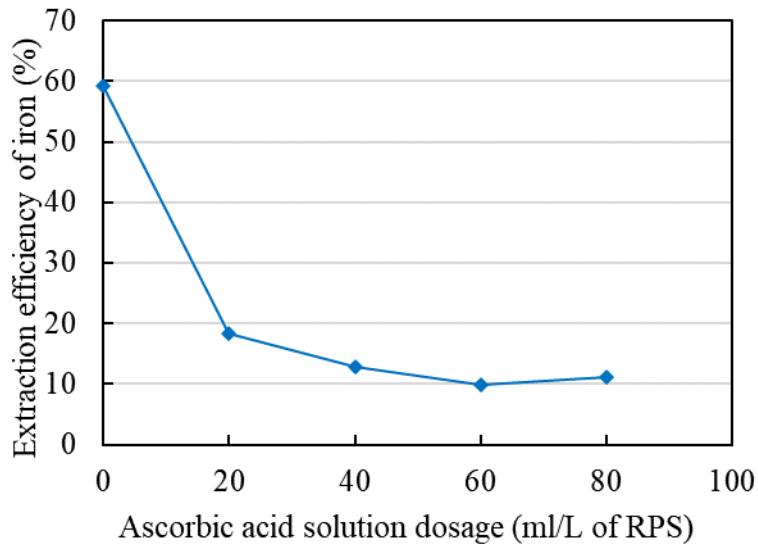

Figure 3.10.18. Extraction efficiency of iron from the re-dissolved precipitate solution using 5% DEHPA solution at different dosages of 200 g/L solution of ascorbic acid.

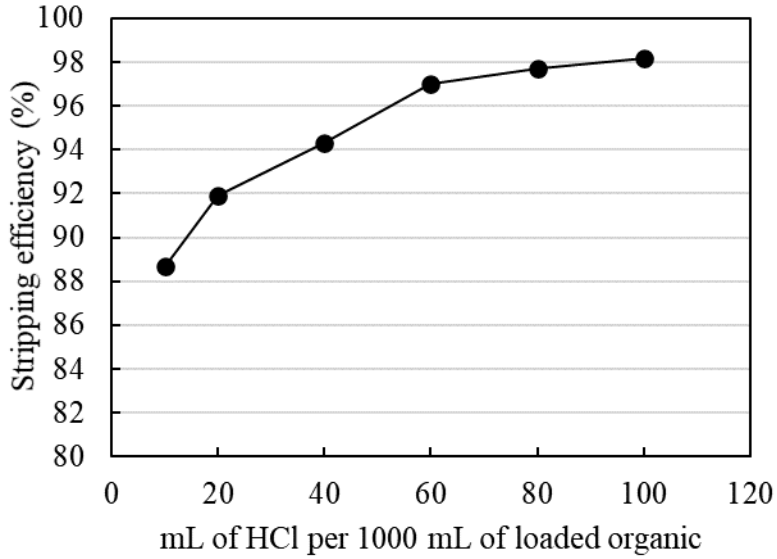

Figure 3.10.19. Stripping efficiency of REE with different volumes of 6M HCl on a 5% DEHPA solution loaded with the re-dissolved precipitate solution at pH 2.0.

3.10.2.6 Cost Comparison

For the two alternate processes, the cost of reagents associated with the pretreatment as well as the oxalic precipitation was the same. The difference in the cost of the contaminant removal stage between staged precipitation and the SX process was analyzed. It was calculated that the reagent costs associated with staged precipitation were $0.02581 per liter of RPS treated (Table 3.10.6). The only reagent which was consumed in the staged precipitation was the NaOH solution which was used for raising the pH of the RPS solution. The NaOH used for increasing pH was 4 M in concentration; however, as the NaOH is procured as a 50% w/v solution, the consumption was converted to appropriate concentration prior to calculating costs.

For the SX option, the reagent costs were $0.06316 per liter of RPS treated (Table 3.10.7). The reagents used for the REE separation were ascorbic acid (used for iron reduction), HCl (used for stripping REE) and NaOH (neutralizing the stripping solution before the oxalic precipitation step). The consumption of the chemicals was converted to the concentration in which they were procured before calculating costs. It was concluded that the staged precipitation was 2.44 times cheaper than the SX process for the production of high purity REO concentrates. It is noted that the exact cost of the reagent consumption will vary significantly for leachates from different sources. This is primarily due to substantial differences in the solution chemistry of the leach solutions.

Table 3.10.6. Cost of reagents used for the contaminant removal using the staged precipitation method. The cost is calculated per liter of the re-dissolved precipitate solution treated.

Reagent	Dosage (per liter of RPS)	Cost (per unit)	Cost (per liter of RPS treated)
NaOH (50%w/v)	26.66 mg	0.000968	$0.02581
TOTAL		$0.02581	

Table 3.10.7.Cost of reagents used for contaminant removal for the SX process method. The cost is collected per liter of the re-dissolved precipitate solution treated.

Reagent	Dosage (per liter of RPS)	Cost (per unit)	Cost (per liter of RPS treated)
NaOH (50%w/v)	20 mg	0.000968	$0.01936
HCl (12 M)	30 mL	0.00066	$0.0198
Ascorbic Acid (99%)	4 g	0.006	$0.024
TOTAL		$0.06316	

3.10.2.7 Conclusion

Mine water collected from Will Scarlet reject pile was processed using multistage precipitation and selective redissolution to produce mixed REO product. The REEs in mine water was precipitated at pH 7.5 and redissolved at pH 2.5 to be concentrated in solution by 2 orders of magnitude with less contamination ion concentration. Compare to solvent extraction process, multi-stage precipitation technique is more economical to process a REE bearing solution that contains 2-3 orders of magnitude higher of contamination ions than REEs.

3.10.3 West Kentucky No. 13 Acid mine drainage

Acid mine drainage collected from West Kentucky No.13 mine was processed as a secondary resource using the newly modified flowsheet, and a >90% weight grade REO was produced. 5000-gallon of acid mine water was hauled from west Kentucky No. 13 mine in early June and stored in lighttight polyethylene tanks. The AMD contains in average 5.57 ±0.24 ppm of total rare earth, 796 ±98 ppm of Fe, 348.5 ±15 ppm of Al, 504.5 ±42 ppm of Ca. The other valuable elements concentration is as shown in Table 3.10.8. The pH value of the AMD is average of 2.5 ±0.025. During loading at the mine site and transportation, the AMD contacted with industrial oil that formed a thin layer of black oil on top of the tank. The top layer of the AMD was drained into a pipe slightly immersed under the surface of the liquid and pumped through a coalescer to remove the oil from aqueous.

Table 3.10.8. Composition of RE and other major elements in the WKY No. 13 AMD.

Rare Earth Elements	Concentration (mg/L)	Other Major Elements	Concentration (mg/L)
Sc	0.2 ±0.01	Al	348.5 ±15
Y	1.3 ±0.04	As	0.0 ±0.0
La	0.4 ±0.05	Ca	504.5 ±42
Ce	1.0 ±0.11	Co	1.7 ±0.1
Pr	0.1 ±0.01	Cr	0.3 ±0.14
Nd	0.6 ±0.06	Cu	2.8 ±0.1
Sm	0.3 ±0.02	Fe	796 ±98
Eu	0.0 ±0.00	K	3.7 ±1.5
Gd	0.3 ±0.10	Li	1.2 ±0.05
Tb	0.0 ±0.01	Mg	342 ±17.8
Dy	0.5 ±0.03	Mn	65.9 ±4.6
Ho	0.1 ±0.01	Na	918.4 ±33.1
Er	0.1 ±0.02	Ni	4.8 ±0.19
Tm	0.0 ±0.01	V	0.25 ±0.03
Yb	0.2 ±0.01	Zn	8.6 ±0.26
Lu	0.0 ±0.00		
Total REE	5.6 ±0.24		

3.10.3.1 Fe, Al, and REE Precipitation

The precipitation efficiency curve was first generated to determine the pH cut point for Fe removal, Al removal and RE precipitation (Figure 3.10.20). The test was carried out with 500 ml of AMD gradually dose in using 4 M NaOH solution. The results show that at pH of 3.2, about 78% of iron can be removed with 5.8% of TREE and 5.3% of Sc. The Co and Mn loss in the iron precipitation is only 1.7% and 1.8%, respectively. Therefore, pH 3.2 was selected as the operation pH cut point for Fe precipitation (PT0). The pH was recorded over 48 hours' period for both feed and effluent stream as shown in Figure 3.10.21. The 2M NaOH base solution consumption was 31 gallons for the entire 4020 gallons of AMD processed over 48 hours of run time, which is equivalent to dosage of 0.62 g/L of NaOH. After Fe removal, the filtrate solution contains about 5.5±0.47 ppm of TREEs, with 336±34 ppm of Al, 483±29 ppm of Ca, and 144±63 ppm of Fe. The precipitation efficiency of other REEs and CMs are as shown in Figure 3.10.22.

The Fe concentration varies significantly during the 48 hours of operation due to its aging process which converts ferrous iron to ferric ion. There is a slightly post-precipitation of Fe occurred after Fe removal and before feeding into Al precipitation circuit, therefore, the Fe concentration in the feed solution to Al precipitation dropped to about 44 ppm. The Al precipitation process was carried out at pH 4.5 as shown in Figure 3.10.23. The 2M NaOH solution consumption over the 33 hour run time was 39 gallons for 3960 gallons of AMD, which equivalent to 0.79 g/L of NaOH. The precipitation efficiency for REEs and other elements are shown in Figure 3.10.24. About 85% of Al was removed together with the remaining 99% of Fe from the AMD. The loss of TREEs to Al cake is about 5%, whereas the loss of Sc is 66%. Therefore, the recovery of Sc from the Al precipitation cake is evaluated. The Al cake was first blended without any additional water under high shear mixing. Then 500 ml of the slurry was collected and redissolved using 35%

HCl at different pH as shown in Figure 3.10.25. At pH 2.5, the Sc recovery is 100%, with 94% of Al and 81% of Fe redissolved into solution as well. The HCl dosage used to achieve pH 2.5 is about 76g/L of the 36% pure HCl. The Sc concentration in the solution is 3.2 ppm, however, the Al concentration is about 8900ppm. Therefore, a more economically feasible process to recover the Sc from AMD is to add a solvent extraction process before the Al removal and after the Fe removal, as discussed in the previous report.

After Al removal, the filtrate contains 5.3 ppm of TREEs with 48 ppm of Al, 458 ppm of Ca and only 0.3 ppm of Fe. Till this process, the REEs to Al+Ca+Fe concentration ratio changed from 1:300 in the feed AMD to 1:100 after Fe and Al removal. This solution was then subject to RE precipitation at pH 6.5. The recorded pH and the 2M NaOH base solution consumption are as shown in Figure 3.10.26. 9-gallon of 2M NaOH solution was consumed treating 3840 gallon of solution over 32 hours of operation. The dosage of NaOH in this process is 0.19 g/L. The precipitation efficiency of REEs and other element of interests is as shown in Figure 3.10.27. About 89% of TREEs are precipitated in the cake with capturing 98% of Sc. Since Ca does not precipitated at this pH, the Ca was removed, which further upgraded the TREEs to Al+Ca+Fe ratio to be 1:20.

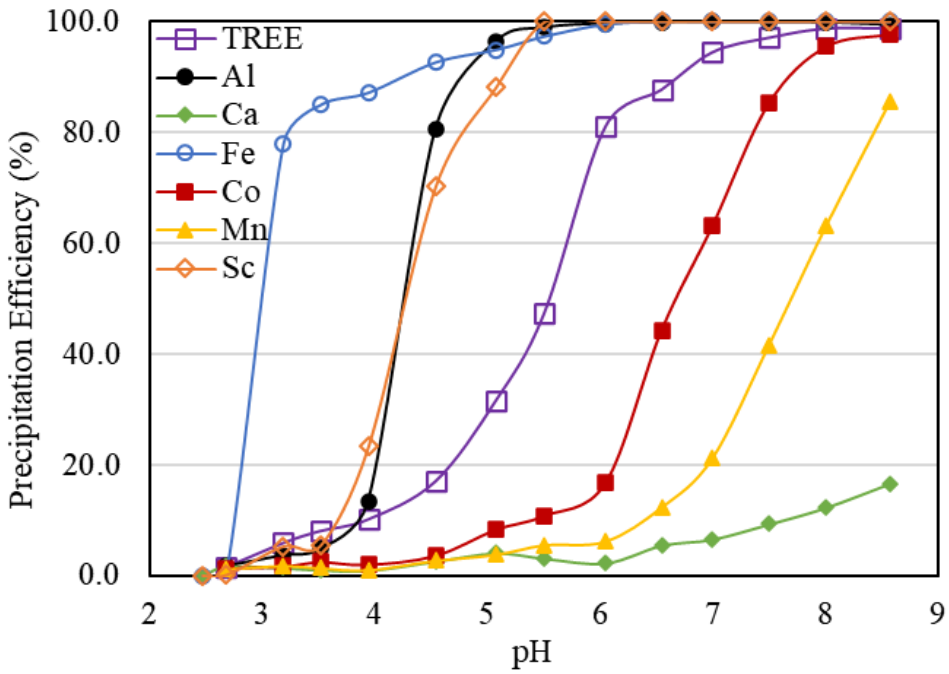

Figure 3.10.20. Precipitation efficiency curve of the DTK-AMD2020.

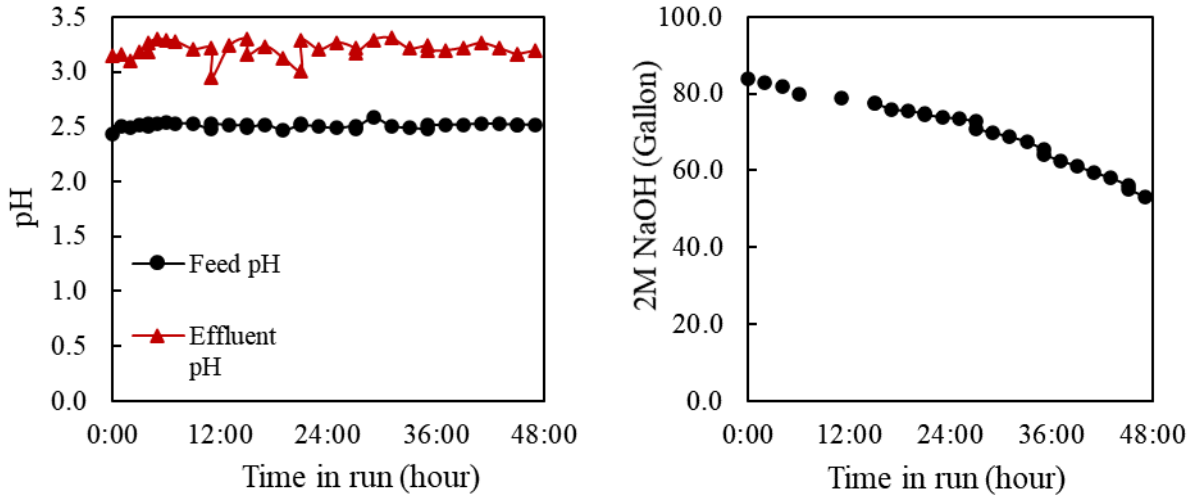

Figure 3.10.21. Recorded pH of feed and effluent solution in the Fe precipitation operation over time period of 48 hours (left). Recorded 2M NaOH solution consumption to fulfill the targeted pH in the Fe precipitation operation over 48 hours (right).

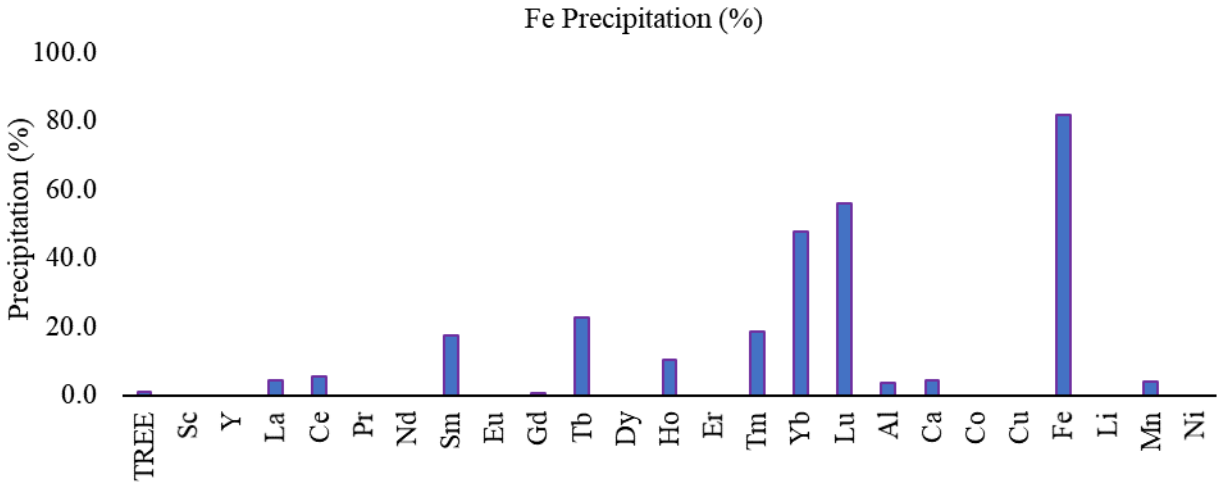

Figure 3.10.22. Precipitation efficiency of REEs and other element of interest at Fe precipitation. (DTK-AMD-PT0, pH 3.2, NaOH dosage 0.62g/L AMD solution, pump automatic controlled, residence time 1 hour.)

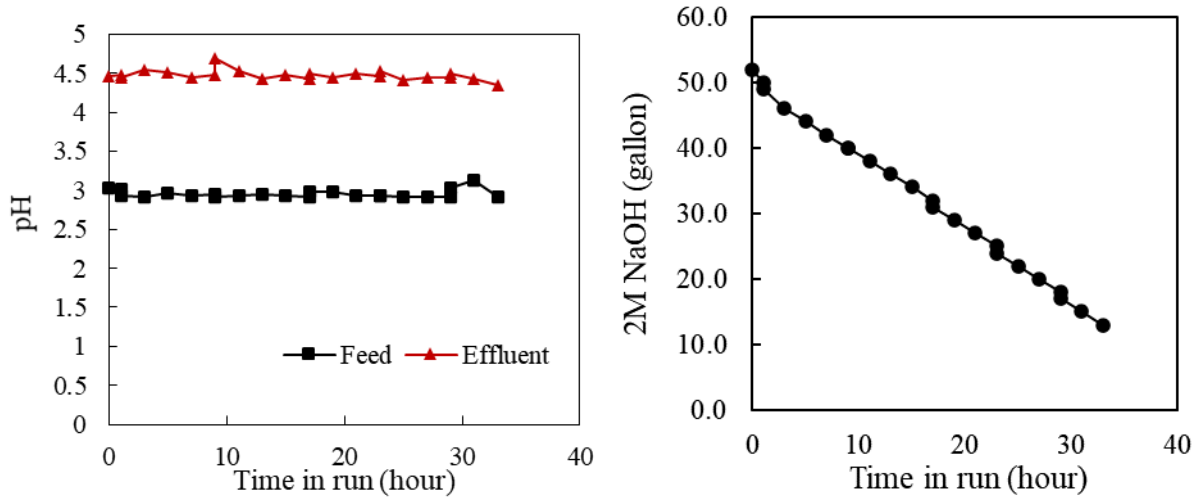

Figure 3.10.23. Recorded pH of feed and effluent solution in the Al precipitation operation over time period of 33 hours (left). Recorded 2M NaOH solution consumption to fulfill the targeted pH in the Al precipitation operation over 33 hours (right).

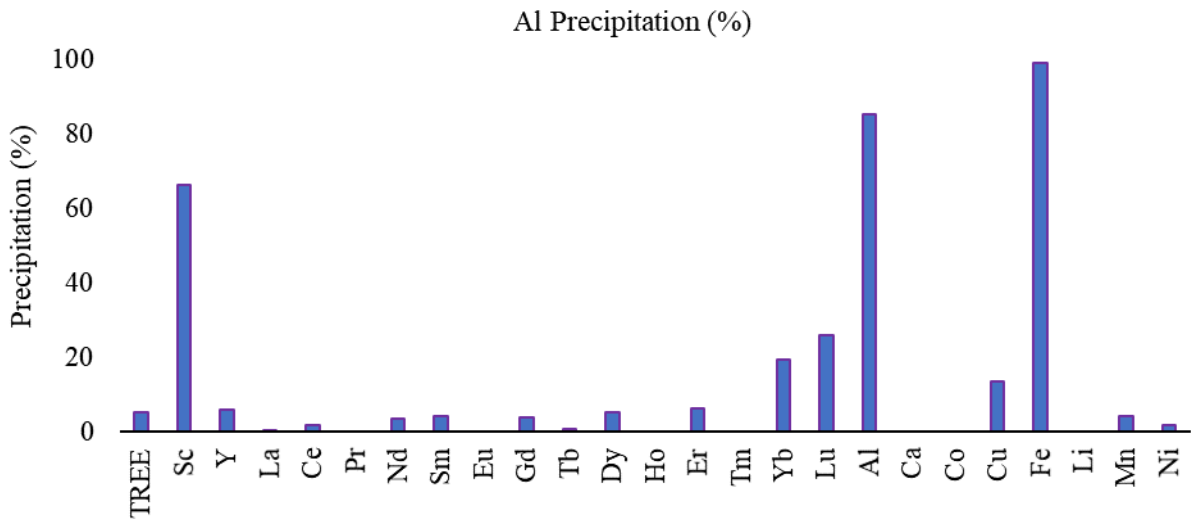

Figure 3.10.24. Precipitation efficiency of REEs and other element of interest at Al precipitation step. (DTK-AMD-PTAl, pH 4.5, NaOH dosage 0.79 g/L of AMD, automatic controlled, residence time 1 hour).

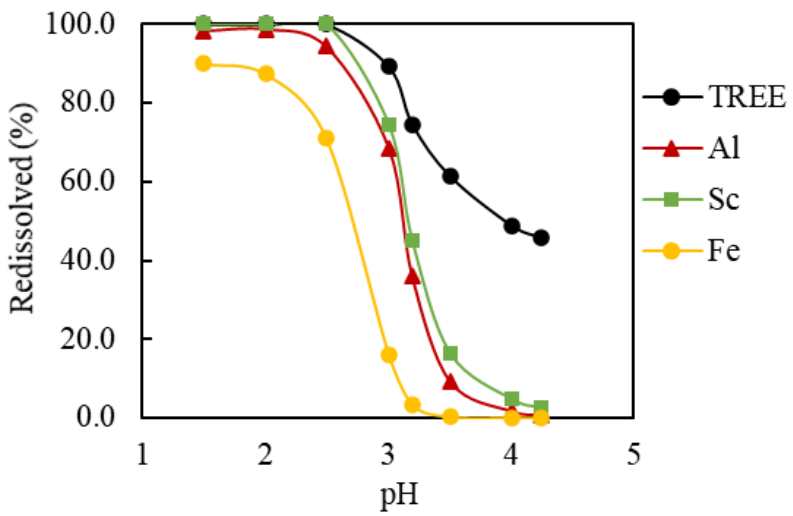

Figure 3.10.25. Redissolution curve of Sc from the Al precipitation cake using HCl.

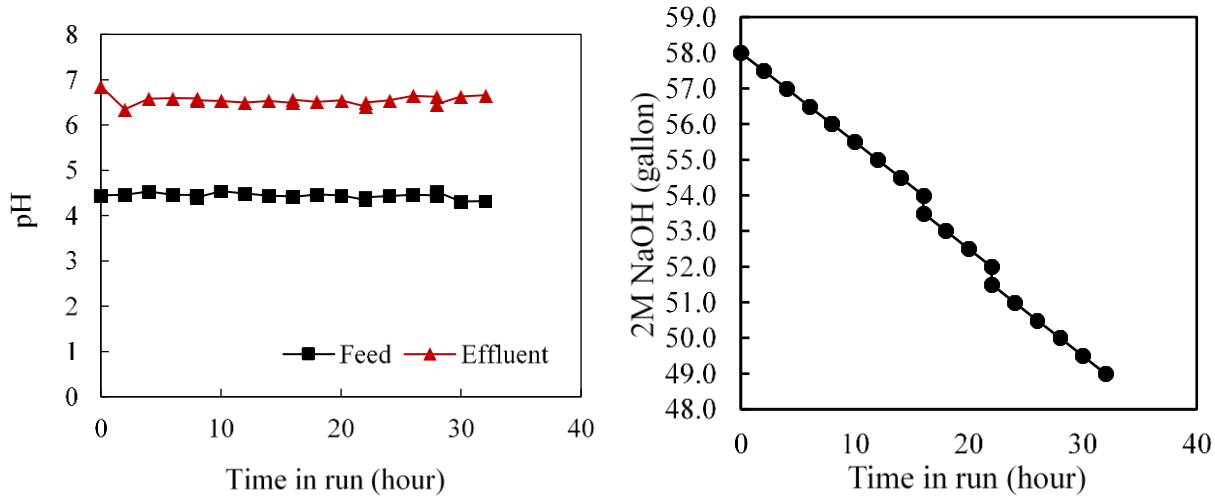

Figure 3.10.26. Recorded pH of feed and effluent solution in the Al precipitation operation over time period of 32 hours (left). Recorded 2M NaOH solution consumption to fulfill the targeted pH in the Al precipitation operation over 32 hours (right).

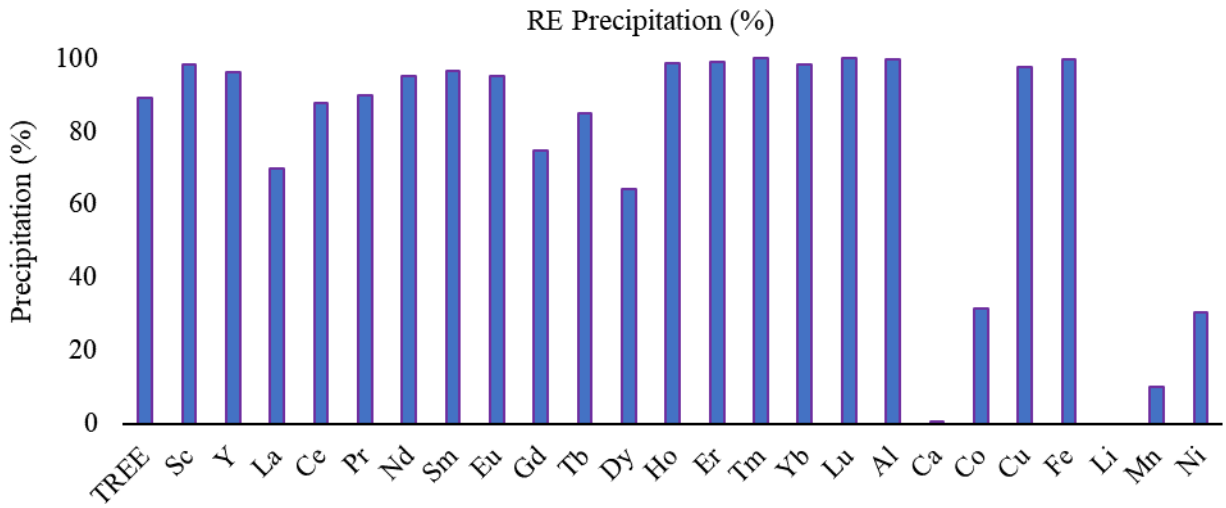

Figure 3.10.27. Precipitation efficiency of REEs and other element of interest at RE precipitation step. (DTK-AMD-PT1, pH6.5, NaOH dosage 0.19 g/L AMD, automatic controlled, residence time 1 hour).

3.10.3.2 Redissolution

The cake produced in the RE precipitation process is about 203 lbs with about 15.4% pf solid concentration, which indicated that there is some liquid reported to the RE cake as either physical or chemical bond water. The TREEs concentration in the dried RE precipitation cake is about 5722 ppm on a dried whole mass basis. The cake also contains about 3794 ppm of Cu on a dried mass basis, with about 12% Al, 0.7% Ca, and 0.5% Fe. The cake was blended in a 66-gallon barrel under high shear mixing for 3 hours until the cake was liquified. The dilution factor effect on the redissolution process efficiency was investigated.

A 50 mL sample of the slurry was taken, and the density was determined to be 1.14 g/ml. From the total mass of cake and calculated density, the total slurry volume was estimated to be 34.1 gal. To mimic the conditions of diluting the slurry volume to 50 gallons, 100 gallons, and 200 gallons, three 550 mL sample volumes were blended using the slurry to water volume ratios of 34.1:15.9, 34.1:65.9, and 34.1:165.9, respectively. After thorough mixing, 50 mL samples were taken from each of the three dilutions, centrifuged, and dried to calculate total solid percentage in the slurry. From there, the remaining 500 mL of each dilution were incrementally treated with 36 wt% hydrochloric acid (Sigma-Aldrich, trace-metal grade) and sampled at target pH values to assess redissolution of rare earth elements and contaminants through inductively coupled plasma – optical emission spectroscopic techniques (ICP-OES). Prior to introduction of hydrochloric acid to induce redissolution, two 2 mL samples of the feed were taken, with one being analyzed directly with ICP-OES, and the other being fully dissolved in 2 mL of hydrochloric acid and 16 mL of 5 vol% nitric acid to obtain a maximum redissolution concentration for each of the selected elements to be analyzed (LMAX).

i. *<u>50-Gallon Slurry Dilution</u>*

For the representative sample of a 50-gallon slurry volume, the diluted slurry had a 7.75% solid content, as compared to the 15.4% solid content of the non-diluted slurry, indicating the

workup of the sample prior to the lab-scale experimentation was closer to a 65 gallon dilution than 50 gallon. It is plausible that due to the thickness of the slurry solution, and the presence of air pockets in the mixture when sampling, slight errors in density calculations could have skewed the total approximated volume of slurry prior to dilutions being made, leading to incorrect slurry: water ratios when being mixed. Too, improper drying of the cake sample, or a non-representative cake sample, being used when calculating total solids in the non-diluted mixture would have skewed the preceding calculations.

Regardless of this, elemental redissolution percentages were still able to be calculated in conjunction with the maximum redissolved elemental concentrations obtained from the analysis of LMAX for each target pH sample. In Figure 3.10.28 below, it was seen that the total rare earth element concentration (TREE) redissolved into solution began to plateau at a pH of between 3 and 3.5, going from 80% redissolution to nearly 99% redissolution over that pH range. From this, due to the expense of aliquoting additional acid to the slurry, it appears a target redissolution pH of 3 is optimal for ensuring a near-complete uptake of rare earths into solution. Adding to this, a pH of 3 only redissolves 15% of the total iron content in the dispersion, which is a primary contaminant that will result in additional oxalic acid consumption in the rare earth oxalate precipitation circuit in downstream processing.

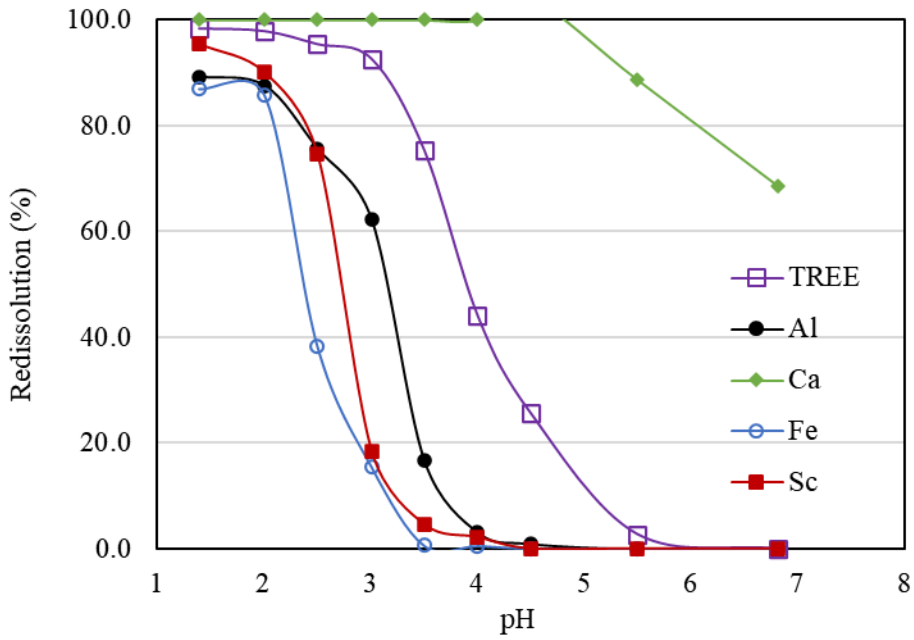

Figure 3.10.28. Redissolution curves of select elements in the DTK-AMD20 rare earth hydroxide cake at a 50-gallon dilution. Hydrochloric acid aliquots were added to the slurry to induce redissolution, and samples were taken and analyzed at 0.5 pH intervals.

However, the downside of targeting a pH of 3 in the redissolution process is that only 80% of the scandium is redissolved. Due to the close proximity of the aluminum (also a primary contaminant that results in similar issues in the oxalic circuit as iron) and scandium redissolution curves, it becomes necessary to balance aluminum uptake with scandium uptake based on the cost-benefit analysis of the additional oxalic acid expense aluminum will incur on the process. Here, it seems that while only 80% of the scandium will be redissolved, only 66% of the aluminum will

be, as well. Since a large portion of the scandium is lost during the PTA1 aluminum precipitation stage, the extra 15% of scandium obtained at a pH of 2.5 is not enough to offset the additional 15% of aluminum, let alone the additional 22% of iron uptake.

ii. 100- and 200-Gallon Slurry Dilutions

When analyzing the sample created to mimic the 100-gallon slurry dilution characteristics, it was found that total solid content in the dilution was 4.10%, being nearly half of the solids content as the 50 gallon dilution, indicating consistency within the makeup of the dilutions. As noted, before with the 50 gallon dilution, however, the percent solids in the cake prior to diluting would indicate the 100-gallon dilution would be closer to a 130-gallon dilution. When analyzing the 200-gallon dilution, the total solids content was again cut in half when going from the 100- to 200-gallon makeups, having 2.1% total solids content in the slurry, further verifying the dilution procedure and calculations performed.

In Figure 3.10.29 as shown below, the striking similarity in the precipitation curves as to those obtained from the 50-gallon dilution sample is to be noted. The 100-gallon dilution corroborates setting the target redissolution pH to roughly 3, as it was found here that, again, 99% of rare earths were redissolved, nearly 86% of the total scandium content was redissolved, and only 24% of iron and 76% of aluminum. When comparing this to a pH of 3.5, only 88% of the TREE redissolved, while a drastic decrease in aluminum uptake, being 32%, and iron uptake, being less than 2%, occurred. The initial aluminum content remaining in the PT1 cake that managed to pass through the PTA1 processing stage will be the greatest determinant here as to whether the target redissolution pH should be closer to 3 or to 3.5, for if the aluminum precipitation stage is effective, 76% aluminum redissolution, or even slightly higher, may still be a negligible amount, and the additional uptake of rare earths into solution may be warranted. The aluminum and scandium redissolution curves also overlay each other more closely for the 100-gallon dilution, as compared to the 50-gallon dilution.

In regard to the 200-gallon dilution, at a pH of 3, 99% of TREE content redissolved, 96% of scandium content was redissolved, and 24% of iron and 90% of aluminum contaminants were redissolved, as compared to 87%, 46%, 3.6%, and 45%, respectively, at a pH of 3.5. The trend continues here, as well, as noted previously, in that as dilution factor increases, the aluminum and scandium redissolution curves begin to overlay each more closely, as the two curves are almost indistinguishable from each other at a 200-gallon dilution.

In comparison among three dilution factors in redissolution process, large deviations occur between the trials for all elements in the 2.5 to 3.5 pH range. Time allowed for the reaction to reach equilibrium before sampling is the primary variable across the data sets, and slight variations in final pH at sampling can result in vastly different elemental redissolution percentages, due to the steep nature of the precipitation curves in this range. Overall, the pH range of 3 to 3.5 is still found to be optimal across all three trials.

Final aluminum content in the rare earth hydroxide cake will be the primary determinant in deciding the most effective target pH for redissolution. Based on the results of the dilution trials, a range of 3-3.5 is going to be the most effective for ensuring near-complete redissolution of TREE content, while also limiting contaminant reuptake. However the efficiency of the PTA1

stage in removing the greatest portion of the aluminum prior to rare earth precipitation is crucial in determining whether it will be cost effective to target a pH closer to 3, or if a pH of 3.5 will have to suffice.

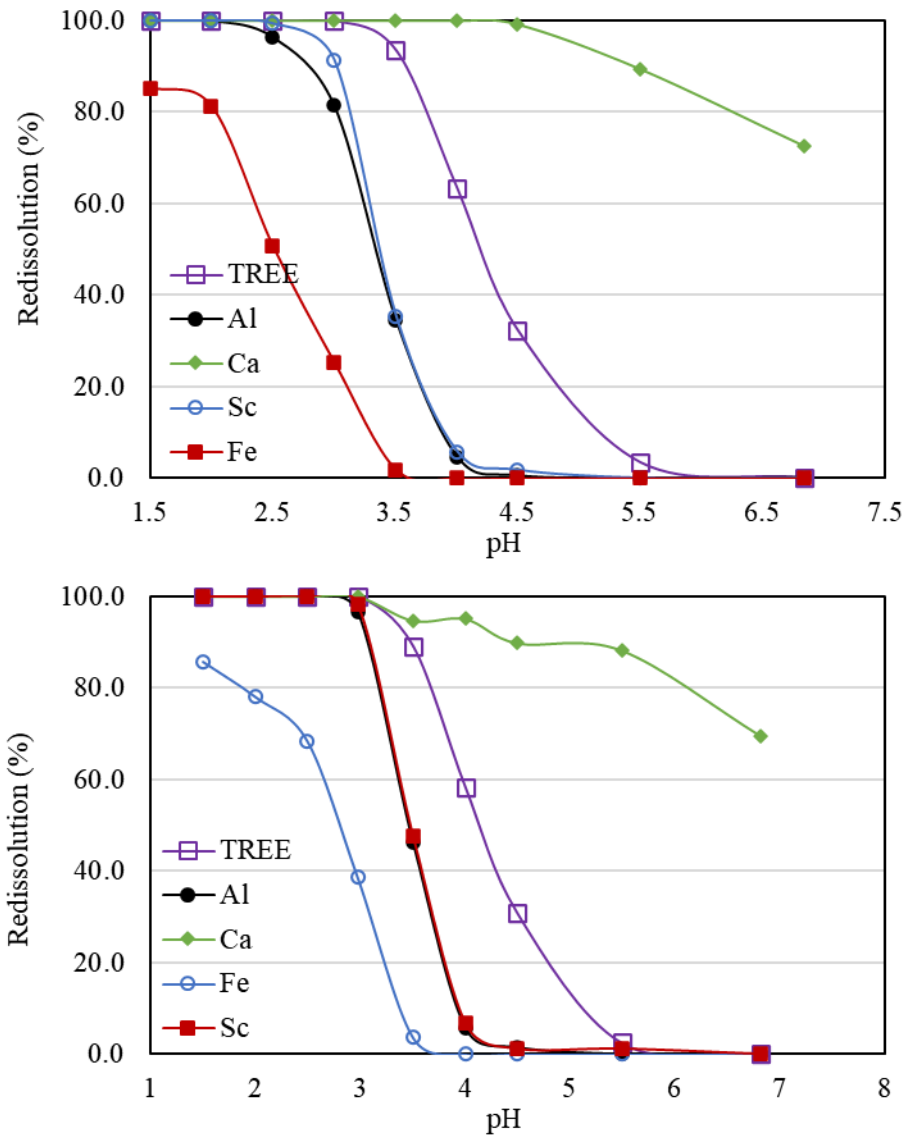

Figure 3.10.29. Redissolution curves of select elements in DTK-AMD20 rare earth hydroxide cake at 100-gallon (top) and 200-gallon dilutions (bottom) dilutions. Samples were analyzed at 0.5 pH intervals.

Therefore, the 100-gallon dilution scenario was selected for the pilot scale test. The cake was mixed in a 400 gallon mixing tank and fresh water was added into achieve a total volume of 100 gallon. Centrifugal pump was used to recirculate the slurry to expedite the mixing. Then 14.7 L of 36% HCl (industrial grade) was added into the mixture and pH was stabilized at pH 3.0. The slurry was then filtered using a plate frame filter to collect the filtrate for feeding into the oxalate precipitation. The concentrated pregnant solution contains 144 ppm of TREEs (upgraded 26 times from the received AMD solution), 2368 ppm of Al, 181ppm of Ca, and 59 ppm of Fe. By this

selective redissolution step, the RE to Al+Ca+Fe ratio improved to be 1:18. The redissolution process efficiency is shown in Figure 3.10.30, where 81.6% of TREEs are recovered in the filtrate stream with nearly 100% of Sc, Al and Ca. The Fe rejection is 88% as expected from the redissolution efficiency curve.

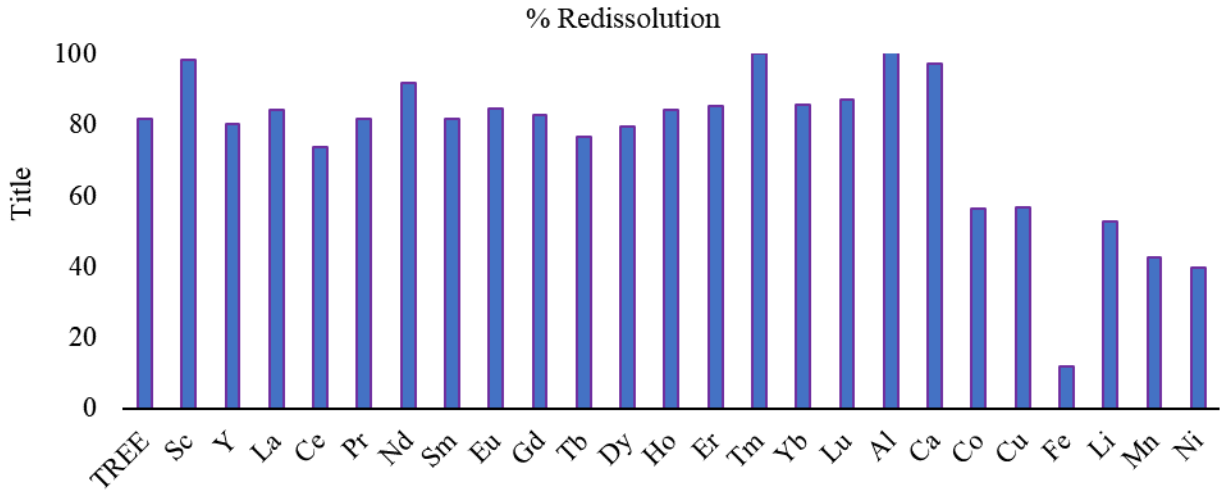

Figure 3.10.30. Redissolution efficiency of REEs and other elements of interest at pH 3.0, HCl dosage 39 ml/L of blended slurry.

3.10.3.3 Oxalate precipitation

The oxalate precipitation was carried out using 250 ml oxalic acid solution per liter of the concentrated PLS feed solution. The oxalic acid in the oxalic acid solution used in the process is 80g/L, which is equivalent to 20 g/L of powder form oxalic acid in concentrated PLS feed solution. The precipitation pH was at 1.5 and the residence time for reaction is 20 minutes. To maintain the reaction pH at 1.5, 4M NaOH solution was pumped automatically into the first reaction tank. The 4M NaOH used was 65ml/L of the feed solution, which is equivalent to 10.4g of NaOH per liter. The precipitation efficiency of TREEs was 89% in average (Figure 3.10.31). 16% of Cu was recovered during this process, which resulted in about 8% CuO in the final REO product. Sc precipitation efficiency was about 20% with leaving 1.3 ppm of Sc in the effluent. The oxalate precipitate cake was washed with water in the plate and frame filter, then dried in an oven overnight at 75°C. The dried solid was then roasted in a muffle furnace at 75°C for 2 hours to convert the oxalate to oxide. The final grade of the mix RE oxide produced from AMD was 90.84% as shown in Table 3.10.9.

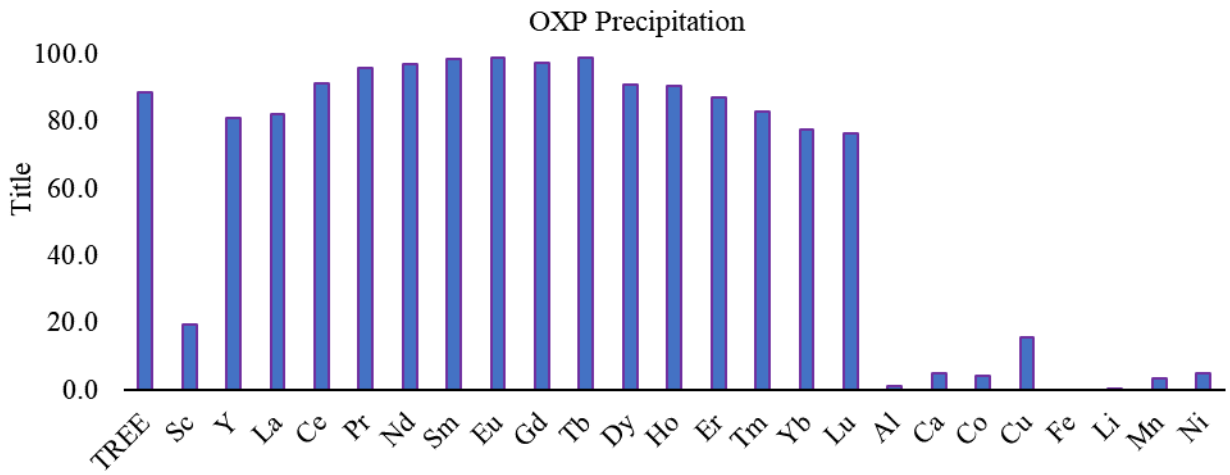

Figure 3.10.31. Oxalate precipitation efficiency of REs and other elements of interest. (pH 1.5, oxalic acid dosage 20 g/L of concentrated PLS, NaOH dosage 10.4 g/L of concentrated PLS)

Table 3.10.9. Product grade and composition of the REO mix produced from the Dotiki AMD solution.

RE Elements	Rare earth elemental concentration		Elemental Molecular Wt.	Marketable RE Oxides *	RE Oxides Concentration
	mg/kg	% dry weight	g/mol		% dry weight
Sc	1011.9	0.1	45	Sc2O3	0.16
Y	161039.0	16.1	89	Y2O3	20.45
La	58627.1	5.9	139	La2O3	6.88
Ce	189795.9	19.0	140	CeO2	23.31
Pr	27580.7	2.8	141	Pr6O11	3.33
Nd	126159.6	12.6	144	Nd2O3	14.72
Sm	43265.3	4.3	150	Sm2O3	5.02
Eu	9658.6	1.0	152	Eu2O3	1.12
Gd	51651.2	5.2	157	Gd2O3	5.95
Tb	5309.8	0.5	159	Tb4O7	0.62
Dy	48423.0	4.8	163	Dy2O3	5.56
Ho	6816.3	0.7	165	Ho2O3	0.78
Er	12912.8	1.3	167	Er2O3	1.48
Tm	1833.8	0.2	169	Tm2O3	0.21
Yb	9781.1	1.0	173	Yb2O3	1.11
Lu	1469.0	0.1	175	Lu2O3	0.17
TREE	755335.1	75.5			90.86

3.11 Analytical Lab Construction & Operation (PB3-Task10)

To enable the team to receive relatively quick turnaround on rare earth element analyses, a lab was constructed onsite and equipped with an ICP-OES and fume hood. A construction company completed the installation of a ventilation system during the reporting period to support both the ICP and fume hood. A photograph of the completed laboratory is shown in Figure 3.11.1. Intake air into the laboratory is filtered using a medical-grade air filter to remove contaminants. A two-stage deionized water system was purchased and installed at the plant and supplied to the laboratory through a stainless steel faucet and sink. The ICP unit is equipped with an autosampler which allows automatic analysis of over 50 samples over a two-hour period. Standard calibration samples for a wide range of elements including the REEs were purchased and used to establish the elemental spectrum library for the ICP unit. A standard solution with known elemental contents is used to enure accuracy of the analytical results when performing an elemental analysis on samples collected from the REE pilot plant.

The analytical lab has been operating since September 2018 and has proven to be a very valuable addition to the project. In addition to being able to analyze the elemental contents of the process streams in our pilot plant on a near real time basis, the lab is also used to conduct bench top experiments as needed to determine optimum chemical dosages for various process steps for solution conditions that vary due to the testing of various feed sources and leach conditions. The ICP-OES unit has been serviced by a qualified technician as routine maintenance since the start of the pilot plant operation. Semi-annual maintenance of the de-ionized water system has been provided twice. Water quality is checked daily using the ICP-OES. The lab also includes drying ovens, a muffle furnace for roasting, fume hood, magnetic stirrers, four-digit balances, filters, centrifuge, etc.

Figure 3.11.1. Photograph of the onsite laboratory equipped with an ICP-OES, fume hoop and sink that is supplied with high quality deionized water.

3.12 Modeling & Simulation (PB3-Task11)

A circuit simulation package was developed for REE extraction and concentration. The simulation routines were compiled using a spreadsheet-based platform (Microsoft Excel). This open-source programming platform was selected (i) to avoid licensing fees commonly required by other software alternatives, (ii) to provide a user-friendly interface that can customized without formal training in advanced programming languages, and (iii) to take advantage of open-source built-in features such as an iteration engine, form controls, and VBA (Visual Basic for Applications) coding. The simulation routine, which has been designated as "REESim" by the programming team, utilizes as separate worksheet "tab" for each unit operation included within a process flowsheet. The interconnection of streams between the various unit operations (spreadsheet tabs) is handled using built-in dropdown menus that specify which streams within a process circuit are fed to a particular unit operation. To facilitate transfer of process stream data, a standard input/output matrix was incorporated into each unit operation/worksheet. The input/output matrix provides an interface for entering and reporting values for dry solids mass rate, volumetric slurry flow rate, chemical/reagent addition rates and species/component assay values.

The REESim circuit simulation package is configured to track the mass and volume flows of components passing through a series of unit operations specified and configured by the user. Examples of tracked components include the mass flow rates of organic matter, ash, rare earth elements and other elemental impurities (e.g., Si, Al, Ca, etc.). These components are either (i) manually input using a "Feed" worksheet that contains feedstock characterization data entered by the user or (ii) automatically transferred to a computational worksheet (unit operation) as a process stream from one of the unit operations included in the process circuit workbook. The mass rates can then be utilized by the user to determine important performance indicators such as product mass yields, concentrate purity levels, element-by-element recoveries, and so forth. Each computational worksheet also keeps track of water entering and leaving each unit operation. The "fresh" or "external" water entering each unit operation can also be manually adjusted by the user to attain target values for slurry compositions (e.g., percent solids) entering or leaving each unit operation.

It is important to note that the mass rates entering and leaving a unit operation must also be tracked in several categories of "species" to accurately represent the liberation, extraction and recovery processes used in a process circuit. For example, coal feedstocks will typically contain some portion of insoluble solids containing rare earth elements that will not go into aqueous solution. This limiting constraint will vary from one feedstock to another and with changes to either (i) physical conditions such as the degree of liberation as a result of size reduction or (ii) chemical conditions such as increasing the aggressiveness of the leaching solution by lowering pH. Pyrometallurgical operations, such as roasting, can also increase the solubility of species as a result of surface oxidation/reduction, dehydration and/or surface exposure/expression. Species that are soluble can be converted back and forth between solid and aqueous forms depending on the solution conditions. Moreover, soluble species can be transferred between aqueous solution and organic solvent by hydrometallurgical processes such as solvent extraction. Therefore, to work effectively, the REESim routines track the following forms of mass species moving through the process circuitry:

- TIS(s) = Total Insoluble Solids in Solid Form
- TDS(s) = Total Dissolvable Solids in Solid Form
- TDS(a) = Total Dissolved Solid as Aqueous Solution
- TDS(o) = Total Dissolved Solid in Organic Solution

Based on these "rudimentary" species, several "derived" groupings of species are also tracked by the worksheet routines. These include:

- TS(s) = TIS(s) + TDS(s) = Total Solids in Solid Form
- TS = TIS(s) + TDS(s) + TDS(a) = Total Solids (Solid and Dissolved Forms)
- Sol'n = Water + Reagents + TDS(a) = Total Solution
- Total = TS(s) + Sol'n = Total Solids and Solution
- %Solids = 100 TS(s)/Total = Percent Solids for Solid Forms

This information can be utilized by the user to determine important performance indicators such as product yield, purity, recovery, separation efficiency, and so forth.

The latest version of the REESim spreadsheet package includes the following standard worksheet tabs: (1) Overview, (2) Flowsheet, (3) Nodes, (4) Reagents and (5) Blank. It is recommended that these five worksheets, which are color-coded as white tabs, be included in every simulation workbook. As the name suggests, the "Overview" tab provides a summary of the various types of unit operations that are currently available for flowsheet simulations (see Figure 3.12.1). At present, nine categories of unit operations are available:

- Feed (Black)
- Size Control (Blue)
- Separator (Brown)
- Junction/Splitter (Grey)
- Pyromet Units (Red)
- Hydromet Units (Orange)
- Thickener (Purple)
- Filter (Yellow)
- Solvent Extraction (Green)

The worksheet tabs used to represent the various categories of unit operations are color-coded for ease of identification.

The next tab, which is labeled as "Flowsheet", is simply an open worksheet/workspace that has been provided to paste in a graphical illustration of the REE processing circuit being simulated (see Figure 3.12.3). Currently there is no linkage between the graphical illustration and the process simulation modules used within the spreadsheet workbook. Thus, the illustration must be manually drawn and pasted into this worksheet or excluded from the workbook to avoid confusion. The addition of a graphical interconnection module is being considered by the project team provided that time and funds permit.

			Sheet Inputs				Sheet Outputs				Species Impact		
Unit Operation	Tab	Type	A	B	C	D	A	B	C	D	TIS(s)	TDS(s)	TDS(a)
Feed		--	Input 1	Input 2	Input 3	--	Feed 1	Feed 2	Feed 3	Total Feed	--	--	--
Size Control		Crusher	Input 1	Input 2	Input 3	Total	Feed	Product	--	--	↓	↑	--
		Ball Mill	Input 1	Input 2	Input 3	Total	Feed	Product	--	--	↓	↑	--
		Screen	Input 1	Input 2	Input 3	Total	Feed	Oversize	Undersize	--	--	--	--
		Classifier	Input 1	Input 2	Input 3	Total	Feed	Oversize	Undersize	--	--	--	--
Separator		Generic	Input 1	Input 2	Input 3	Total	Feed	Product	Middling	Reject	--	--	--
		Flotation	Input 1	Input 2	Input 3	Total	Feed	Froth	Middling	Tails	--	--	--
		Sorter	Input 1	Input 2	Input 3	Total	Feed	Retain	Middling	Eject	--	--	--
		HHS	Input 1	Input 2	Input 3	Total	Feed	Product	--	Tails	--	--	--
		Density	Input 1	Input 2	Input 3	Total	Feed	Heavies	Middling	Lights	--	--	--
Junction/Splitter		Mix Tank	Input 1	Input 2	Input 3	Total	Feed	Split 1	Split 2	Split 3	--	--	--
		Tee	Input 1	Input 2	Input 3	Total	Feed	Split 1	Split 2	Split 3	--	--	--
Pyromet Units		Roaster	Input 1	Input 2	Input 3	Total	Feed	Feed (Roasted)	Product	Volatiles	↓	↑	--
		Cracker	Input 1	Input 2	Input 3	Total	Feed	Feed (Cracked)	--	--	↓	↓	↑
Hydromet Units		Precip	Input 1	Input 2	Input 3	Total	Feed	Feed (Precip)	--	--	--	↑	↓
		Leach	Input 1	Input 2	Input 3	Total	Feed	Feed (Leached)	--	--	--	↓	↑
Thickener		--	Input 1	Input 2	Input 3	Total	Feed	--	Overflow	Underflow	--	--	--
		Precip	Input 1	Input 2	Input 3	Total	Feed	Feed (Precip)	Overflow	Underflow	--	↑	↓
		Leach	Input 1	Input 2	Input 3	Total	Feed	Feed (Leached)	Overflow	Underflow	--	↓	↑
Filter		--	Input 1	Input 2	Input 3	Total	Feed	--	Effluent	Cake	--	--	--
		Precip	Input 1	Input 2	Input 3	Total	Feed	Feed (Precip)	Effluent	Cake	--	↑	↓
		Leach	Input 1	Input 2	Input 3	Total	Feed	Feed (Leached)	Effluent	Cake	--	↓	↑
Solvent Extraction		Load	Input 1	Input 2	Input 3	Total	Aqueous In	Aqueous Out	Organic In	Organic Out	--	--	--
		Strip	Input 1	Input 2	Input 3	Total	Aqueous In	Aqueous Out	Organic In	Organic Out	--	--	--

Figure 3.12.1. Overview worksheet that lists the types of calculation worksheets for different unit operations that are current available in the REESim simulation tool.

The "Nodes" worksheet is a list of all tabs (units) that have been included in the spreadsheet workbook (Figure 3.12.4). To avoid errors created by misspellings or missed tabs, this list of nodes can be automatically generated by clicking on the "Update Nodes" button at the top of the Nodes page. Since this feature was created with a Macro routine, it can only be used when "Enable Macros" has been selected when the spreadsheet is opened. In addition, the spreadsheet must be saved as a macro-enabled workbook. This action can be performed during a "Save As" step by selecting "Excel Macro-Enabled Workbook" under the "Save as type:" option just below the entered file name for the spreadsheet.

The "Reagents" tab/worksheet is simply a listing of chemical additives that are to be used in the process flowsheet (Figure 3.12.2). For each reagent, a correlation table listing solution concentration (percent by weight) and density (kg/L) is required. This relationship is a simple linear correlation for most reagents and, as such, the user only needs to enter a slope and intercept to complete the reagent table. Unfortunately, the density of some reagents, such as sulfuric acid, versus density information must be entered manually by the user.

Finally, a "Blank" tab has been included simply as a placeholder to divide the five standard tabs from the remaining worksheets that represent actual unit operations with a process circuit. It

is also recommended that the “Blank” tab be selected as a “dummy” input sheet for fields that are not used in placeholder cells.

The REESim circuit simulation tool utilizes as separate computational worksheet “tab” for each unit operation included within a process flowsheet. The interconnection of streams between the various unit operations (spreadsheet tabs) is handled using Excel’s built-in dropdown menus that specify which streams within a process circuit are fed/recirculated to a particular unit operation. To facilitate transfer of process stream data, a standard input/output matrix was incorporated into each unit computational worksheet describing the various unit operations. The input/output matrix provides an interface for entering and reporting values for dry solids mass rate, volumetric slurry flow rate, chemical/reagent addition rates and species/component assay values.

All circuit require that a “Feed” worksheet be included. Characterization data for up to three different coal-based feedstock sources can be entered on this page. It should be noted that this particular computational worksheet is unique in no information is automatically transferred to this page. Instead, all of the pertinent feedstock characterization data must be manually entered into this worksheet by the user based on experimental data or other sources of user knowledge. To facilitate the entry of the feed data, the format of this computational worksheet is slightly different than the standard format used for all other computational worksheets (unit operations). Figure 3.12.5 shows the general layout of the “Feed” worksheet. As shown, the worksheet consists of four sections that are individual self-contained pages when printed as a hardcopy. The feed worksheet is color-coded with a black tab for quick identification.

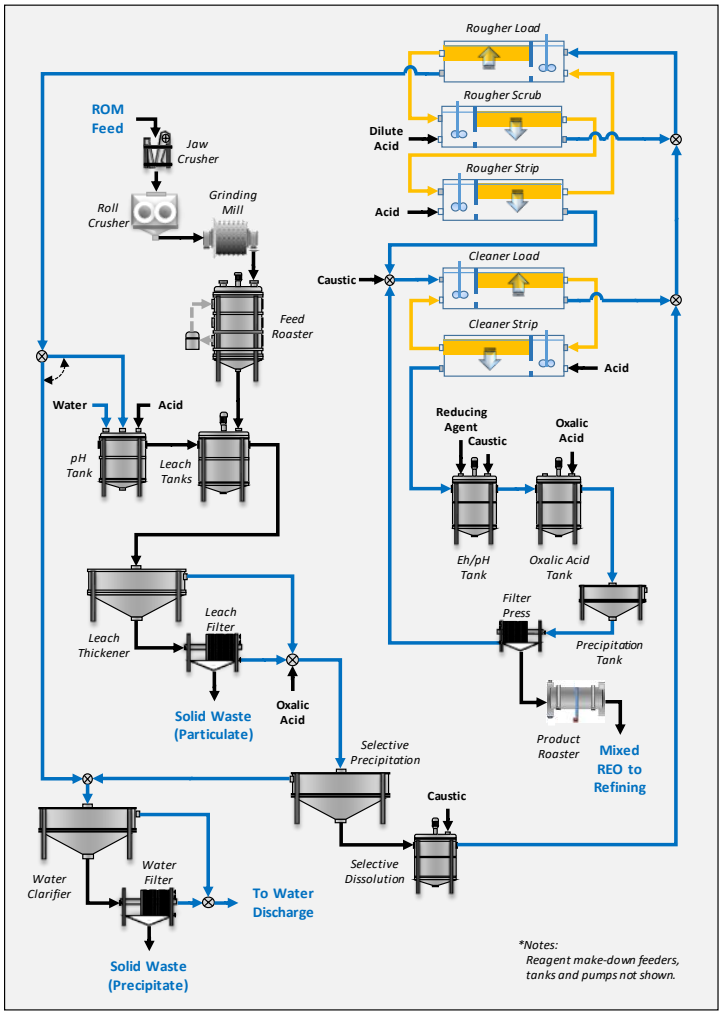

Figure 3.12.3. Sample flowsheet pasted into REESim.

	UNIT OPERATIONS
	Update Nodes
	Sheet Name
1	Overview
2	Flowsheet
3	Nodes
4	Reagents
5	Blank
6	Feed
7	Sorter
8	Crusher
9	Mill
10	Feed_Roaster
11	Leach_Tanks
12	Leach_Thickener
13	Leach_Filter
14	Splitter
15	pH_Tank
16	PLS_Precipitation
17	PLS_Dissolution
18	Water_Clarifier
19	Water_Filter
20	SXR_Feed
21	SXR_Load
22	SXR_Scrub
23	SXR_Strip
24	SXC_Load
25	SXC_Strip
26	EhpH_Tank
27	OA_Tank
28	Product_Thickener
29	Product_Filter
30	Product_Roaster

Figure 3.12.4. "Nodes" worksheet example.

Type	Water	H2SO4	HCl	NaOH	C6H8O6	C2H2O4	ChemX								
SG	1.000	1.840	1.763	2.130	1.650	1.900	1.200	0.000	0.000	0.000	0.000	0.000	0.000	0.000	0.000
Slope	0.0000	--	0.0050	0.0106	0.0042	0.0047	0.0020	0.0000	0.0000	0.0000	0.0000	0.0000	0.0000	0.0000	0.0000
Inter.	1.0000	--	0.9980	1.0028	0.9966	0.9984	1.0000	0.0000	0.0000	0.0000	0.0000	0.0000	0.0000	0.0000	0.0000
Conc'n	Density	Density	Density	Density	Density	Density	Density	Density	Density	Density	Density	Density	Density	Density	Density
(%, Wt)	(kg/L)	(kg/L)	(kg/L)	(kg/L)	(kg/L)	(kg/L)	(kg/L)	(kg/L)	(kg/L)	(kg/L)	(kg/L)	(kg/L)	(kg/L)	(kg/L)	(kg/L)
0	1.000	1.000	0.998	1.003	0.997	0.998	1.000	0.000	0.000	0.000	0.000	0.000	0.000	0.000	0.000
1	1.000	1.005	1.003	1.013	1.001	1.003	1.002	0.000	0.000	0.000	0.000	0.000	0.000	0.000	0.000
2	1.000	1.012	1.008	1.024	1.005	1.008	1.004	0.000	0.000	0.000	0.000	0.000	0.000	0.000	0.000
3	1.000	1.018	1.013	1.035	1.009	1.012	1.006	0.000	0.000	0.000	0.000	0.000	0.000	0.000	0.000
4	1.000	1.025	1.018	1.045	1.014	1.017	1.008	0.000	0.000	0.000	0.000	0.000	0.000	0.000	0.000
5	1.000	1.032	1.023	1.056	1.018	1.022	1.010	0.000	0.000	0.000	0.000	0.000	0.000	0.000	0.000
6	1.000	1.039	1.028	1.067	1.022	1.026	1.012	0.000	0.000	0.000	0.000	0.000	0.000	0.000	0.000
7	1.000	1.045	1.033	1.077	1.026	1.031	1.014	0.000	0.000	0.000	0.000	0.000	0.000	0.000	0.000
8	1.000	1.052	1.038	1.088	1.030	1.036	1.016	0.000	0.000	0.000	0.000	0.000	0.000	0.000	0.000
9	1.000	1.059	1.043	1.098	1.035	1.041	1.018	0.000	0.000	0.000	0.000	0.000	0.000	0.000	0.000
10	1.000	1.066	1.048	1.109	1.039	1.045	1.020	0.000	0.000	0.000	0.000	0.000	0.000	0.000	0.000
11	1.000	1.073	1.053	1.120	1.043	1.050	1.022	0.000	0.000	0.000	0.000	0.000	0.000	0.000	0.000
12	1.000	1.080	1.058	1.130	1.047	1.055	1.024	0.000	0.000	0.000	0.000	0.000	0.000	0.000	0.000
13	1.000	1.087	1.063	1.141	1.051	1.059	1.026	0.000	0.000	0.000	0.000	0.000	0.000	0.000	0.000
14	1.000	1.095	1.068	1.152	1.056	1.064	1.028	0.000	0.000	0.000	0.000	0.000	0.000	0.000	0.000
15	1.000	0.110	1.073	1.162	1.060	1.069	1.030	0.000	0.000	0.000	0.000	0.000	0.000	0.000	0.000
16	1.000	1.109	1.078	1.173	1.064	1.073	1.032	0.000	0.000	0.000	0.000	0.000	0.000	0.000	0.000
17	1.000	1.117	1.083	1.183	1.068	1.078	1.034	0.000	0.000	0.000	0.000	0.000	0.000	0.000	0.000

Figure 3.12.2. "Reagents" worksheet listing reagents type, concentration and density.

The first section (Page 1) of the "Feed" worksheet provides an area for entering the compositions of various components entering the processing circuit (see Figure 3.12.6). These include (i) ash content, (ii) primary ash constituents, and (iii) trace ash constituents. The ash content is entered as a mass percentage of the whole feedstock on a dry basis. The total content of combustible matter and estimated content of organic matter is back-calculated from the ash content. The primary ash constituents are entered as a mass percentage of ash on a dry ash basis. Typically, this category would include elements such as Al, Ca, Fe and Si, which are frequently contaminates to the final REE product. Space is reserved in this data entry area for up to 10 primary elements. A category of "unknown" elements is also back-calculated in this section to ensure that the total mass of ash is tracked thought the simulation routines. Finally, the trace ash constituents are entered as a mass parts-per-million of ash on a dry ash basis. Typically, this category would include elements of interest such as REEs or other critical elements of potential market value. The part-per-million concentrations of some undesirable trace contaminants, such as Th or U, can also be entered under this category so that impurity levels can be calculated. Space is reserved in the data entry sheet for up to 24 total trace elements. To achieve the most realistic simulations, the characterization data must include a percentage breakdown of the current form of each component in terms of TIS(s), TDS(s) and TDS(a). For solid feedstocks, only TIS(s) and TDS(s) would typically be present. Likewise, for aqueous feedstocks, only TDS(a) may be present. In any case, the total percentage of all three forms of TIS(s), TDS(s) and TDS(a) must sum to 100%.

The second section (Page 2) of the "Feed" worksheet includes space that has been reserved for the creation of user tools (see Figure 3.12.7). For example, one such tool is a calculator for estimating primary element concentrations from a standard laboratory ash analysis. Typically, commercial ash analyses report the concentrations of CaO, Al_2O_3, Fe_2O_3, MgO, SO_3, P_2O_5, K_2O, TiO_2 and Na_2O as equal to 100% of the ash mass. The current version of the software provides a conversion tool that allows ash analysis to be directly entered and the elemental concentrations of Al, Ca, Fe, etc., needed by the software to be calculated. Other such tools can be created in this area as needed to obtain characterization data in the proper format required by the worksheet.

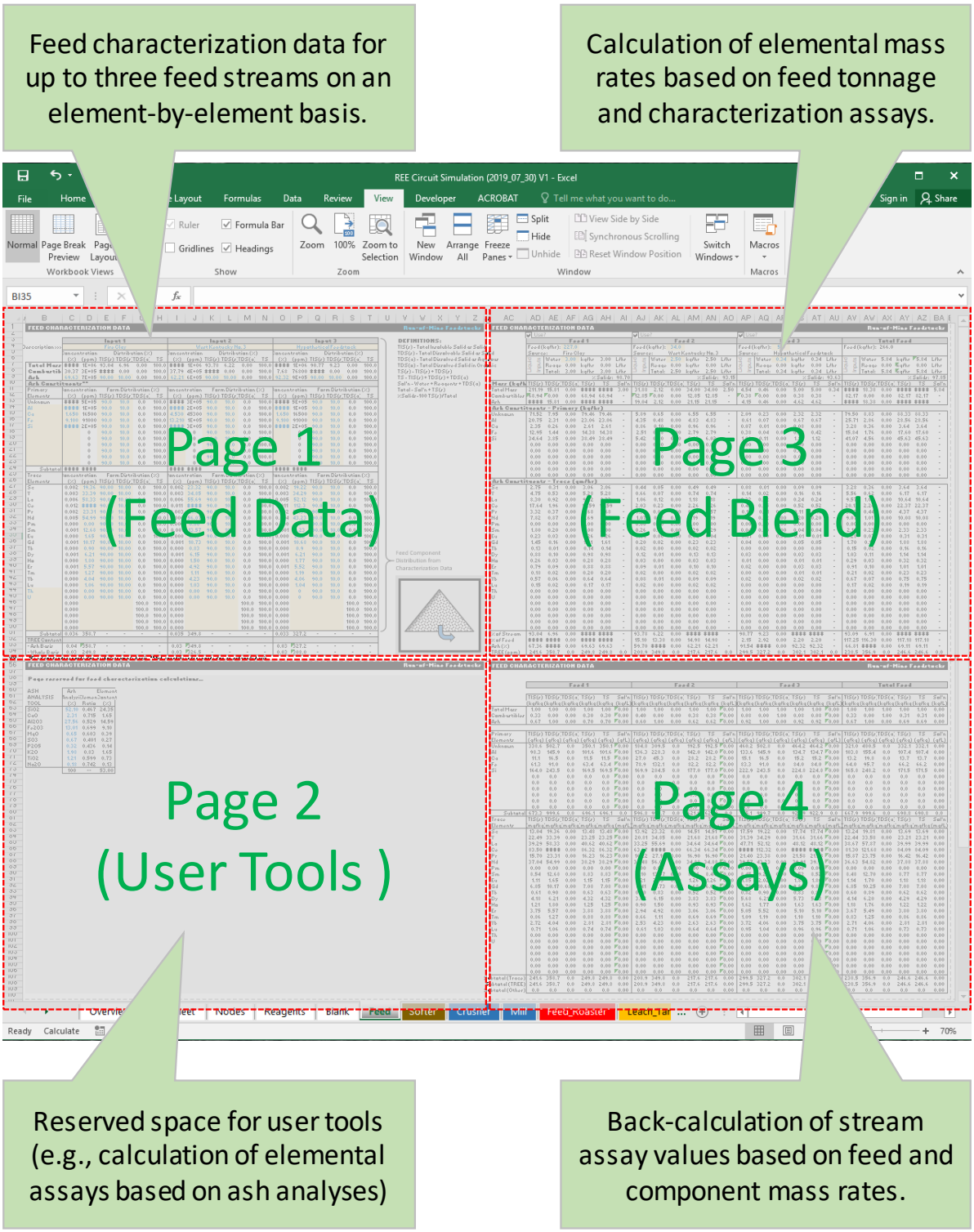

Figure 3.12.5. Illustration of the pages utilized by the "Feed" computational worksheet.

FEED CHARACTERIZATION DATA — Run-of-Mine Feedstocks

Description >>>	Input 1: Fire Clay						Input 2: West Kentucky No. 3						Input 3: Hypothetical Feedstock					
	Concentration*		Distribution (%)				Concentration*		Distribution (%)				Concentration*		Distribution (%)			
	(%)	(ppm)	TS(s)	TDS(s)	TDS(e)	TS	(%)	(ppm)	TS(s)	TDS(s)	TDS(e)	TS	(%)	(ppm)	TS(s)	TDS(s)	TDS(e)	TS
Total Mass	100.00	1E+06	93.04	6.96	0.00	100.0	100.00	1E+06	93.78	6.22	0.00	100.0	100.00	1E+06	90.77	9.23	0.00	100.0
Combustibles	30.37	3E+05	100.00	0.00	0.00	100.0	37.79	4E+05	100.00	0.00	0.00	100.0	7.68	76800	100.00	0.00	0.00	100.0
Ash	69.63	7E+05	90.00	10.00	0.00	100.0	62.21	6E+05	90.00	10.00	0.00	100.0	92.32	9E+05	90.00	10.00	0.00	100.0
Ash Constituents**																		
Primary Elements	Concentration**		Form Distribution (%)				Concentration**		Form Distribution (%)				Concentration**		Form Distribution (%)			
	(%)	(ppm)	TS(s)	TDS(s)	TDS(e)	TS	(%)	(ppm)	TS(s)	TDS(s)	TDS(e)	TS	(%)	(ppm)	TS(s)	TDS(s)	TDS(e)	TS
Unknown	50.274	5E+05	90.0	10.0	0.0	100.0	30.945	3E+05	90.0	10.0	0.0	100.0	50.277	5E+05	90.0	10.0	0.0	100.0
Al	14.590	1E+05	90.0	10.0	0.0	100.0	22.630	2E+05	90.0	10.0	0.0	100.0	14.590	1E+05	90.0	10.0	0.0	100.0
Ca	1.650	16500	90.0	10.0	0.0	100.0	4.530	45300	90.0	10.0	0.0	100.0	1.650	16500	90.0	10.0	0.0	100.0
Fe	9.100	91000	90.0	10.0	0.0	100.0	13.210	1E+05	90.0	10.0	0.0	100.0	9.100	91000	90.0	10.0	0.0	100.0
Si	24.350	2E+05	90.0	10.0	0.0	100.0	28.450	3E+05	90.0	10.0	0.0	100.0	24.350	2E+05	90.0	10.0	0.0	100.0
		0	90.0	10.0	0.0	100.0		0	90.0	10.0	0.0	100.0		0	90.0	10.0	0.0	100.0
		0	90.0	10.0	0.0	100.0		0	90.0	10.0	0.0	100.0		0	90.0	10.0	0.0	100.0
		0	90.0	10.0	0.0	100.0		0	90.0	10.0	0.0	100.0		0	90.0	10.0	0.0	100.0
		0	90.0	10.0	0.0	100.0		0	90.0	10.0	0.0	100.0		0	90.0	10.0	0.0	100.0
		0	90.0	10.0	0.0	100.0		0	90.0	10.0	0.0	100.0		0	90.0	10.0	0.0	100.0
		0	90.0	10.0	0.0	100.0		0	90.0	10.0	0.0	100.0		0	90.0	10.0	0.0	100.0
Subtotal	99.964	######					99.965	######					99.967	######				
Trace Elements	Concentration**		Form Distribution (%)				Concentration**		Form Distribution (%)				Concentration**		Form Distribution (%)			
	(%)	(ppm)	TS(s)	TDS(s)	TDS(e)	TS	(%)	(ppm)	TS(s)	TDS(s)	TDS(e)	TS	(%)	(ppm)	TS(s)	TDS(s)	TDS(e)	TS
Sc	0.002	19.36	90.00	10.00	0.0	100.0	0.002	23.32	90.0	10.0	0.0	100.0	0.002	19.22	90.0	10.0	0.0	100.0
Y	0.003	33.39	90.00	10.00	0.0	100.0	0.003	34.85	90.0	10.0	0.0	100.0	0.003	34.29	90.0	10.0	0.0	100.0
La	0.006	58.33	90.00	10.00	0.0	100.0	0.006	55.69	90.0	10.0	0.0	100.0	0.005	52.12	90.0	10.0	0.0	100.0
Ce	0.012	123.97	90.00	10.00	0.0	100.0	0.011	106.54	90.0	10.0	0.0	100.0	0.011	112.3	90.0	10.0	0.0	100.0
Pr	0.002	23.31	90.00	10.00	0.0	100.0	0.003	27.16	90.0	10.0	0.0	100.0	0.002	23.38	90.0	10.0	0.0	100.0
Nd	0.005	54.99	90.00	10.00	0.0	100.0	0.006	56.07	90.0	10.0	0.0	100.0	0.004	43.23	90.0	10.0	0.0	100.0
Pm	0.000	0.00	90.00	10.00	0.0	100.0	0.000	0.00	90.0	10.0	0.0	100.0	0.000	0	90.0	10.0	0.0	100.0
Sm	0.001	12.68	90.00	10.00	0.0	100.0	0.001	13.57	90.0	10.0	0.0	100.0	0.001	9.23	90.0	10.0	0.0	100.0
Eu	0.000	1.65	90.00	10.00	0.0	100.0	0.000	2.03	90.0	10.0	0.0	100.0	0.000	2.02	90.0	10.0	0.0	100.0
Gd	0.001	10.17	90.00	10.00	0.0	100.0	0.001	10.73	90.0	10.0	0.0	100.0	0.001	10.68	90.0	10.0	0.0	100.0
Tb	0.000	0.90	90.00	10.00	0.0	100.0	0.000	0.83	90.0	10.0	0.0	100.0	0.000	0.9	90.0	10.0	0.0	100.0
Dy	0.001	6.21	90.00	10.00	0.0	100.0	0.001	6.15	90.0	10.0	0.0	100.0	0.001	6.21	90.0	10.0	0.0	100.0
Ho	0.000	1.80	90.00	10.00	0.0	100.0	0.000	1.50	90.0	10.0	0.0	100.0	0.000	1.77	90.0	10.0	0.0	100.0
Er	0.001	5.57	90.00	10.00	0.0	100.0	0.000	4.92	90.0	10.0	0.0	100.0	0.001	5.52	90.0	10.0	0.0	100.0
Tm	0.000	1.27	90.00	10.00	0.0	100.0	0.000	1.11	90.0	10.0	0.0	100.0	0.000	1.19	90.0	10.0	0.0	100.0
Yb	0.000	4.04	90.00	10.00	0.0	100.0	0.000	4.23	90.0	10.0	0.0	100.0	0.000	4.05	90.0	10.0	0.0	100.0
Lu	0.000	1.05	90.00	10.00	0.0	100.0	0.000	1.03	90.0	10.0	0.0	100.0	0.000	1.04	90.0	10.0	0.0	100.0
Th	0.000	0.00	90.00	10.00	0.0	100.0	0.000	0.00	90.0	10.0	0.0	100.0	0.000	0	90.0	10.0	0.0	100.0
U	0.000	0.00	90.00	10.00	0.0	100.0	0.000	0.00	90.0	10.0	0.0	100.0	0.000	0	90.0	10.0	0.0	100.0
	0.000				100.0	100.0	0.000				100.0	100.0	0.000				100.0	100.0
	0.000				100.0	100.0	0.000				100.0	100.0	0.000				100.0	100.0
	0.000				100.0	100.0	0.000				100.0	100.0	0.000				100.0	100.0
	0.000				100.0	100.0	0.000				100.0	100.0	0.000				100.0	100.0
	0.000				100.0	100.0	0.000				100.0	100.0	0.000				100.0	100.0
Subtotal	0.036	358.7	-	-	-	-	0.035	349.8	-	-	-	-	0.033	327.2	-	-	-	-
TRRE Content																		
- Ash Basis	0.04	358.7	-	-	-	-	0.03	349.8	-	-	-	-	0.03	327.2	-	-	-	-
- Whole Basis	0.03	249.8	-	-	-	-	0.03	326.5	-	-	-	-	0.03	308.0	-	-	-	-

*Feed contents reported on a whole-sample basis. **Ash constituents reported on an ash-only basis.

DEFINITIONS:
TS(s) = Total Insoluble Solid as Solid
TDS(s) = Total Dissolvable Solid as Solid
TDS(e) = Total Dissolved Solid as Aqueo
TDS(o) = Total Dissolved Solid in Organi
TS(s) = TS(s) + TDS(s)
TS = TS(s) + TDS(s) + TDS(e)
Soln = Water + Reagents + TDS(e)
Total = Soln + TS(s)
%Solids=100 TS(s)/Total

Feed Component Distribution from Characterization Data

Figure 3.12.6. Page 1 (Feed Data) contained within the "Feed" computational worksheet.

FEED CHARACTERIZATION DATA — Run-of-Mine Feedstocks

Page reserved for feed characterization calculations...

ASH ANALYSIS TOOL	Ash Analysis (%)	Element Ratio	Element Content (%)
SiO2	52.10	0.467	24.35
CaO	2.31	0.715	1.65
Al2O3	27.56	0.529	14.59
Fe2O3	13.01	0.699	9.10
MgO	0.65	0.603	0.39
SO3	0.67	0.401	0.27
P2O5	0.32	0.436	0.14
K2O	1.96	0.83	1.65
TiO2	1.21	0.599	0.73
Na2O	0.18	0.742	0.13
	100	--	53.00

Figure 3.12.7. Page 2 (User Tools) contained within the "Feed" computational worksheet

The third section (Page 3) of the "Feed" worksheet performs three functions (see Figure 3.12.8). First, the page converts the percentage and part-per-million characterization data input by the user on page 1 into dry mass rates based on feed rates of dry total solids entered by the user for each feedstock. The mass rate unit for the total feed and all primary ash constituents is kilograms per hour (kg/hr), while trace ash constituents are tracked in mass rate units of grams per hour (gm/hr). Second, the page performs upfront blending calculations for up to three feedstocks labeled as "Feed 1", "Feed 2" and "Feed 3". The blending can be achieved by simply selecting (or deselecting) a particular feed by checking (or unchecking) the "Use?" checkbox above each feed source. When all three checkboxes are checked, the "Total Feed" is the sum of the mass rates for all three feedstocks. When two are checked, the "Total Feed" includes mass rates for only the two checked feedstocks, and so forth. The third function of the page allows the user to enter process water into the circuit. This is achieved by entering mass flow rates of water in kilograms per hour (kg/hr) in the "Liquid Inputs" section of the page. A different amount of water can be added to each feedstock. A listing for "Reagents" is also included in the "Liquid Input" table to maintain formatting consistency with the other computational worksheets describing unit operations that require chemical additions. However, no reagent additions should be entered as part of the "Feed" worksheet.

The fourth and final section (Page 4) of the "Feed" worksheet is a summary of assay values that have been back-calculated from the total and component mass rates (see Figure 3.12.9). This page is consistent in format with all other computational worksheets representing unit operations included in the user configured circuitry. For total mass, the assays are reported as kilograms of ash or kilograms of combustibles per unit of feed (kg/kg). The assays are reported as grams of component (e.g., Al, Ca, Fe, etc.) per unit of feed for primary elements and as milligrams of component (e.g., Sc, Y, La, etc.) per unit of feed for trace elements. In addition, concentrations are calculated to show the amounts of each type of constituent contained in the total aqueous solution. These assay values are reported as kilogram per liter of solution (kg/L), gram per liter of solution (g/L) or milligram per liter of solution (mg/L) for the total mass, primary elements and trace elements, respectively.

Most of the worksheets (tabs) included in a typical REESim simulation will consist of computational worksheets that describe individual unit operations that are incorporated into the process circuit. For all of these units, the input feed stream data will be automatically transferred into the computational worksheet from (i) the feed worksheet or (ii) one or more of the product streams generated by the unit operations within the circuit. To facilitate this unit interconnection and data transfer, the computational worksheets used to describe the various unit operations have a slightly different format layout than the "Feed" worksheet, as illustrated in Figure 3.12.10.

The first section (Page 1) of all computational worksheets used to represent different processes within a circuit contain built-in pull-down menus for selecting the unit operation (worksheet tab name) and product stream (available from that particular unit operation tab) that will feed the process. For example, Figure 3.12.11 shows the drop-down menu that appears for feed selection to an acid leaching

tank. In this case, the worksheet used to model a roaster has been selected as the “Input Sheet” for the acid leaching tank. Likewise,

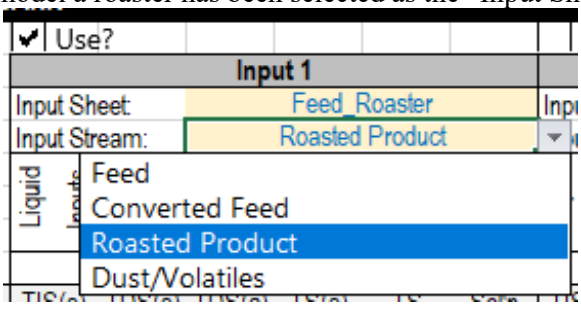

Figure 3.12.12 shows that the “Roasted Product” has been selected as the stream to be passed to the worksheet for calculation purposes.

FEED CHARACTERIZATION DATA — Run-of-Mine Feedstocks

	Feed 1						Feed 2						Feed 3						Total Feed					
	✔ Use?						✔ Use?						✔ Use?											
	Feed (kg/hr): 227.0						Feed (kg/hr): 34.0						Feed (kg/hr): 5.0						Feed (kg/hr): 265.0					
	Source: Fire Clay						Source: West Kentucky No. 3						Source: Hypothetical Feedstock											
	Liquid Inputs	Water: 3.00 kg/hr 3.00 L/hr					Liquid Inputs	Water: 2.50 kg/hr 2.50 L/hr					Liquid Inputs	Water: 0.34 kg/hr 0.34 L/hr					Liquid Inputs	Water: 5.84 kg/hr 5.84 L/hr				
		Reagent: 0.00 kg/hr 0.00 L/hr						Reagent: 0.00 kg/hr 0.00 L/hr						Reagent: 0.00 kg/hr 0.00 L/hr						Reagent: 0.00 kg/hr 0.00 L/hr				
		Total: 3.00 kg/hr 3.00 L/hr						Total: 2.50 kg/hr 2.50 L/hr						Total: 0.34 kg/hr 0.34 L/hr						Total: 5.84 kg/hr 5.84 L/hr				
		%Solids: 98.70						%Solids: 93.15						%Solids: 93.63						%Solids: 97.85				
Mass (kg/hr)	TS(s)	TDS(s)	TDS(el)	TS(s)	TS	Sol'n	TS(s)	TDS(s)	TDS(el)	TS(s)	TS	Sol'n	TS(s)	TDS(s)	TDS(el)	TS(s)	TS	Sol'n	TS(s)	TDS(s)	TDS(el)	TS(s)	TS	Sol'n
Total Mass	211.19	15.81	0.00	227.00	227.00	3.00	31.88	2.12	0.00	34.00	34.00	2.50	4.54	0.46	0.00	5.00	5.00	0.34	247.62	18.38	0.00	266.00	266.00	5.84
Combustibles	68.94	0.00	0.00	68.94	68.94	-	12.85	0.00	0.00	12.85	12.85	-	0.38	0.00	0.00	0.38	0.38	-	82.17	0.00	0.00	82.17	82.17	-
Ash	142.25	15.81	0.00	158.06	158.06	-	19.04	2.12	0.00	21.15	21.15	-	4.15	0.46	0.00	4.62	4.62	-	165.44	18.38	0.00	183.83	183.83	-
Ash Constituents - Primary (kg/hr)																								
Unknown	71.52	7.95	0.00	79.46	79.46	-	5.89	0.65	0.00	6.55	6.55	-	2.09	0.23	0.00	2.32	2.32	-	79.50	8.83	0.00	88.33	88.33	-
Al	20.75	2.31	0.00	23.06	23.06	-	4.35	0.48	0.00	4.83	4.83	-	0.61	0.07	0.00	0.67	0.67	-	25.71	2.86	0.00	28.56	28.56	-
Ca	2.35	0.25	0.00	2.61	2.61	-	0.86	0.10	0.00	0.96	0.96	-	0.07	0.01	0.00	0.08	0.08	-	3.28	0.36	0.00	3.64	3.64	-
Fe	12.95	1.44	0.00	14.38	14.38	-	2.51	0.28	0.00	2.79	2.79	-	0.38	0.04	0.00	0.42	0.42	-	15.84	1.76	0.00	17.60	17.60	-
Si	34.64	3.85	0.00	38.49	38.49	-	5.42	0.60	0.00	6.02	6.02	-	1.01	0.11	0.00	1.12	1.12	-	41.07	4.56	0.00	45.63	45.63	-
	0.00	0.00	0.00	0.00	0.00	-	0.00	0.00	0.00	0.00	0.00	-	0.00	0.00	0.00	0.00	0.00	-	0.00	0.00	0.00	0.00	0.00	-
	0.00	0.00	0.00	0.00	0.00	-	0.00	0.00	0.00	0.00	0.00	-	0.00	0.00	0.00	0.00	0.00	-	0.00	0.00	0.00	0.00	0.00	-
	0.00	0.00	0.00	0.00	0.00	-	0.00	0.00	0.00	0.00	0.00	-	0.00	0.00	0.00	0.00	0.00	-	0.00	0.00	0.00	0.00	0.00	-
	0.00	0.00	0.00	0.00	0.00	-	0.00	0.00	0.00	0.00	0.00	-	0.00	0.00	0.00	0.00	0.00	-	0.00	0.00	0.00	0.00	0.00	-
	0.00	0.00	0.00	0.00	0.00	-	0.00	0.00	0.00	0.00	0.00	-	0.00	0.00	0.00	0.00	0.00	-	0.00	0.00	0.00	0.00	0.00	-
	0.00	0.00	0.00	0.00	0.00	-	0.00	0.00	0.00	0.00	0.00	-	0.00	0.00	0.00	0.00	0.00	-	0.00	0.00	0.00	0.00	0.00	-
Ash Constituents - Trace (gm/hr)																								
Sc	2.75	0.31	0.00	3.06	3.06	-	0.44	0.05	0.00	0.49	0.49	-	0.08	0.01	0.00	0.09	0.09	-	3.28	0.36	0.00	3.64	3.64	-
Y	4.75	0.53	0.00	5.28	5.28	-	0.66	0.07	0.00	0.74	0.74	-	0.14	0.02	0.00	0.16	0.16	-	5.55	0.62	0.00	6.17	6.17	-
La	8.30	0.92	0.00	9.22	9.22	-	1.06	0.12	0.00	1.18	1.18	-	0.22	0.02	0.00	0.24	0.24	-	9.57	1.06	0.00	10.64	10.64	-
Ce	17.64	1.96	0.00	19.59	19.59	-	2.03	0.23	0.00	2.26	2.26	-	0.47	0.05	0.00	0.52	0.52	-	20.13	2.24	0.00	22.37	22.37	-
Pr	3.32	0.37	0.00	3.68	3.68	-	0.52	0.06	0.00	0.57	0.57	-	0.10	0.01	0.00	0.11	0.11	-	3.93	0.44	0.00	4.37	4.37	-
Nd	7.82	0.87	0.00	8.69	8.69	-	1.07	0.12	0.00	1.19	1.19	-	0.18	0.02	0.00	0.20	0.20	-	9.07	1.01	0.00	10.08	10.08	-
Pm	0.00	0.00	0.00	0.00	0.00	-	0.00	0.00	0.00	0.00	0.00	-	0.00	0.00	0.00	0.00	0.00	-	0.00	0.00	0.00	0.00	0.00	-
Sm	1.80	0.20	0.00	2.00	2.00	-	0.26	0.03	0.00	0.29	0.29	-	0.04	0.00	0.00	0.04	0.04	-	2.10	0.23	0.00	2.33	2.33	-
Eu	0.23	0.03	0.00	0.26	0.26	-	0.04	0.00	0.00	0.04	0.04	-	0.01	0.00	0.00	0.01	0.01	-	0.28	0.03	0.00	0.31	0.31	-
Gd	1.45	0.16	0.00	1.61	1.61	-	0.20	0.02	0.00	0.23	0.23	-	0.04	0.00	0.00	0.05	0.05	-	1.70	0.19	0.00	1.88	1.88	-
Tb	0.13	0.01	0.00	0.14	0.14	-	0.02	0.00	0.00	0.02	0.02	-	0.00	0.00	0.00	0.00	0.00	-	0.15	0.02	0.00	0.16	0.16	-
Dy	0.88	0.10	0.00	0.98	0.98	-	0.12	0.01	0.00	0.13	0.13	-	0.03	0.00	0.00	0.03	0.03	-	1.03	0.11	0.00	1.14	1.14	-
Ho	0.25	0.03	0.00	0.28	0.28	-	0.03	0.00	0.00	0.03	0.03	-	0.01	0.00	0.00	0.01	0.01	-	0.29	0.03	0.00	0.32	0.32	-
Er	0.79	0.09	0.00	0.88	0.88	-	0.09	0.01	0.00	0.10	0.10	-	0.02	0.00	0.00	0.03	0.03	-	0.91	0.10	0.00	1.01	1.01	-
Tm	0.18	0.02	0.00	0.20	0.20	-	0.02	0.00	0.00	0.02	0.02	-	0.00	0.00	0.00	0.01	0.01	-	0.21	0.02	0.00	0.23	0.23	-
Yb	0.57	0.06	0.00	0.64	0.64	-	0.08	0.01	0.00	0.09	0.09	-	0.02	0.00	0.00	0.02	0.02	-	0.67	0.07	0.00	0.75	0.75	-
Lu	0.15	0.02	0.00	0.17	0.17	-	0.02	0.00	0.00	0.02	0.02	-	0.00	0.00	0.00	0.00	0.00	-	0.17	0.02	0.00	0.19	0.19	-
Th	0.00	0.00	0.00	0.00	0.00	-	0.00	0.00	0.00	0.00	0.00	-	0.00	0.00	0.00	0.00	0.00	-	0.00	0.00	0.00	0.00	0.00	-
U	0.00	0.00	0.00	0.00	0.00	-	0.00	0.00	0.00	0.00	0.00	-	0.00	0.00	0.00	0.00	0.00	-	0.00	0.00	0.00	0.00	0.00	-
	0.00	0.00	0.00	0.00	0.00	-	0.00	0.00	0.00	0.00	0.00	-	0.00	0.00	0.00	0.00	0.00	-	0.00	0.00	0.00	0.00	0.00	-
	0.00	0.00	0.00	0.00	0.00	-	0.00	0.00	0.00	0.00	0.00	-	0.00	0.00	0.00	0.00	0.00	-	0.00	0.00	0.00	0.00	0.00	-
	0.00	0.00	0.00	0.00	0.00	-	0.00	0.00	0.00	0.00	0.00	-	0.00	0.00	0.00	0.00	0.00	-	0.00	0.00	0.00	0.00	0.00	-
	0.00	0.00	0.00	0.00	0.00	-	0.00	0.00	0.00	0.00	0.00	-	0.00	0.00	0.00	0.00	0.00	-	0.00	0.00	0.00	0.00	0.00	-
	0.00	0.00	0.00	0.00	0.00	-	0.00	0.00	0.00	0.00	0.00	-	0.00	0.00	0.00	0.00	0.00	-	0.00	0.00	0.00	0.00	0.00	-
%of Stream	93.04	6.96	0.00	100.00	100.00	-	93.78	6.22	0.00	100.00	100.00	-	90.77	9.23	0.00	100.00	100.00	-	93.09	6.91	0.00	100.00	100.00	-
%of Feed	100.00	100.00	0.00	100.00	100.00	-	15.10	13.38	0.00	14.98	14.98	-	2.15	2.92	0.00	2.20	2.20	-	117.25	116.30	0.00	117.18	117.18	-
Ash (%)	67.36	100.00	0.00	69.63	69.63	-	59.70	100.00	0.00	62.21	62.21	-	91.54	100.00	0.00	92.32	92.32	-	66.81	100.00	0.00	69.11	69.11	-
TREE (ppm)	241.6	358.7	0.0	249.8	249.8	0.0	208.9	349.8	0.0	217.6	217.6	0.0	299.5	327.2	0.0	302.1	302.1	0.0	238.5	356.9	0.0	246.6	246.6	0.0

Figure 3.12.8. Page 3 (Feed Blend) contained within the "Feed" computational worksheet.

FEED CHARACTERIZATION DATA — Run-of-Mine Feedstocks

	Feed 1						Feed 2						Feed 3						Total Feed					
	TS(s) (kg/kg)	TDS(s) (kg/kg)	TDS(el) (kg/kg)	TS(s) (kg/kg)	TS (kg/kg)	Sol'n (kg/L)	TS(s) (kg/kg)	TDS(s) (kg/kg)	TDS(el) (kg/kg)	TS(s) (kg/kg)	TS (kg/kg)	Sol'n (kg/L)	TS(s) (kg/kg)	TDS(s) (kg/kg)	TDS(el) (kg/kg)	TS(s) (kg/kg)	TS (kg/kg)	Sol'n (kg/L)	TS(s) (kg/kg)	TDS(s) (kg/kg)	TDS(el) (kg/kg)	TS(s) (kg/kg)	TS (kg/kg)	Sol'n (kg/L)
Total Mass	1.00	1.00	0.00	1.00	1.00	0.00	1.00	1.00	0.00	1.00	1.00	0.00	1.00	1.00	1.00	1.00	1.00	0.00	1.00	1.00	1.00	1.00	1.00	0.00
Combustibles	0.33	0.00	0.00	0.30	0.30	0.00	0.40	0.00	0.00	0.38	0.38	0.00	0.08	0.00	1.00	0.08	0.08	0.00	0.33	0.00	1.00	0.31	0.31	0.00
Ash	0.67	1.00	0.00	0.70	0.70	0.00	0.60	1.00	0.00	0.62	0.62	0.00	0.92	1.00	0.00	0.92	0.92	0.00	0.67	1.00	0.00	0.69	0.69	0.00
Primary Elements	TS(s) (g/kg)	TDS(s) (g/kg)	TDS(el) (g/kg)	TS(s) (g/kg)	TS (g/kg)	Sol'n (g/L)	TS(s) (g/kg)	TDS(s) (g/kg)	TDS(el) (g/kg)	TS(s) (g/kg)	TS (g/kg)	Sol'n (g/L)	TS(s) (g/kg)	TDS(s) (g/kg)	TDS(el) (g/kg)	TS(s) (g/kg)	TS (g/kg)	Sol'n (g/L)	TS(s) (g/kg)	TDS(s) (g/kg)	TDS(el) (g/kg)	TS(s) (g/kg)	TS (g/kg)	Sol'n (g/L)
Unknown	338.6	502.7	0.0	350.1	350.1	0.00	184.8	309.5	0.0	192.5	192.5	0.00	460.2	502.8	0.0	464.2	464.2	0.00	321.0	480.5	0.0	332.1	332.1	0.00
Al	98.3	145.9	0.0	101.6	101.6	0.00	136.3	228.3	0.0	142.0	142.0	0.00	133.6	145.9	0.0	134.7	134.7	0.00	103.8	155.4	0.0	107.4	107.4	0.00
Ca	11.1	16.5	0.0	11.5	11.5	0.00	27.0	45.3	0.0	28.2	28.2	0.00	15.1	16.5	0.0	15.2	15.2	0.00	13.2	19.8	0.0	13.7	13.7	0.00
Fe	61.3	91.0	0.0	63.4	63.4	0.00	78.9	132.1	0.0	82.2	82.2	0.00	83.3	91.0	0.0	84.0	84.0	0.00	64.0	95.7	0.0	66.2	66.2	0.00
Si	164.0	243.5	0.0	169.5	169.5	0.00	169.9	284.5	0.0	177.0	177.0	0.00	222.9	243.5	0.0	224.8	224.8	0.00	165.8	248.2	0.0	171.5	171.5	0.00
	0.0	0.0	0.0	0.0	0.0	0.00	0.0	0.0	0.0	0.0	0.0	0.00	0.0	0.0	0.0	0.0	0.0	0.00	0.0	0.0	0.0	0.0	0.0	0.00
	0.0	0.0	0.0	0.0	0.0	0.00	0.0	0.0	0.0	0.0	0.0	0.00	0.0	0.0	0.0	0.0	0.0	0.00	0.0	0.0	0.0	0.0	0.0	0.00
	0.0	0.0	0.0	0.0	0.0	0.00	0.0	0.0	0.0	0.0	0.0	0.00	0.0	0.0	0.0	0.0	0.0	0.00	0.0	0.0	0.0	0.0	0.0	0.00
	0.0	0.0	0.0	0.0	0.0	0.00	0.0	0.0	0.0	0.0	0.0	0.00	0.0	0.0	0.0	0.0	0.0	0.00	0.0	0.0	0.0	0.0	0.0	0.00
	0.0	0.0	0.0	0.0	0.0	0.00	0.0	0.0	0.0	0.0	0.0	0.00	0.0	0.0	0.0	0.0	0.0	0.00	0.0	0.0	0.0	0.0	0.0	0.00
	0.0	0.0	0.0	0.0	0.0	0.00	0.0	0.0	0.0	0.0	0.0	0.00	0.0	0.0	0.0	0.0	0.0	0.00	0.0	0.0	0.0	0.0	0.0	0.00
Subtotal	573.3	999.6	0.0	696.1	696.1	0.0	596.8	999.7	0.0	621.9	621.9	0.0	915.1	999.7	0.0	922.9	922.9	0.0	667.9	999.6	0.0	690.8	690.8	0.0
Trace Elements	TS(s) (mg/kg)	TDS(s) (mg/kg)	TDS(el) (mg/kg)	TS(s) (mg/kg)	TS (mg/kg)	Sol'n (mg/L)	TS(s) (mg/kg)	TDS(s) (mg/kg)	TDS(el) (mg/kg)	TS(s) (mg/kg)	TS (mg/kg)	Sol'n (mg/L)	TS(s) (mg/kg)	TDS(s) (mg/kg)	TDS(el) (mg/kg)	TS(s) (mg/kg)	TS (mg/kg)	Sol'n (mg/L)	TS(s) (mg/kg)	TDS(s) (mg/kg)	TDS(el) (mg/kg)	TS(s) (mg/kg)	TS (mg/kg)	Sol'n (mg/L)
Sc	13.04	19.36	0.00	13.48	13.48	0.00	13.92	23.32	0.00	14.51	14.51	0.00	17.59	19.22	0.00	17.74	17.74	0.00	13.24	19.81	0.00	13.69	13.69	0.00
Y	22.49	33.39	0.00	23.25	23.25	0.00	20.81	34.85	0.00	21.68	21.68	0.00	31.39	34.29	0.00	31.66	31.66	0.00	22.44	33.58	0.00	23.21	23.21	0.00
La	39.29	58.33	0.00	40.62	40.62	0.00	33.25	55.69	0.00	34.64	34.64	0.00	47.71	52.12	0.00	48.12	48.12	0.00	38.67	57.87	0.00	39.99	39.99	0.00
Ce	83.50	123.97	0.00	86.32	86.32	0.00	63.67	106.64	0.00	66.34	66.34	0.00	102.82	112.32	0.00	103.69	103.69	0.00	81.30	121.68	0.00	84.09	84.09	0.00
Pr	15.70	23.31	0.00	16.23	16.23	0.00	16.22	27.16	0.00	16.90	16.90	0.00	21.40	23.38	0.00	21.58	21.58	0.00	15.87	23.75	0.00	16.42	16.42	0.00
Nd	37.04	54.99	0.00	38.29	38.29	0.00	33.48	56.07	0.00	34.88	34.88	0.00	39.57	43.23	0.00	39.91	39.91	0.00	36.63	54.82	0.00	37.88	37.88	0.00
Pm	0.00	0.00	0.00	0.00	0.00	0.00	0.00	0.00	0.00	0.00	0.00	0.00	0.00	0.00	0.00	0.00	0.00	0.00	0.00	0.00	0.00	0.00	0.00	0.00
Sm	8.54	12.88	0.00	8.83	8.83	0.00	8.10	13.57	0.00	8.44	8.44	0.00	8.45	9.23	0.00	8.52	8.52	0.00	8.48	12.70	0.00	8.77	8.77	0.00
Eu	1.11	1.65	0.00	1.15	1.15	0.00	1.21	2.03	0.00	1.26	1.26	0.00	1.85	2.02	0.00	1.86	1.86	0.00	1.14	1.70	0.00	1.18	1.18	0.00
Gd	6.85	10.17	0.00	7.08	7.08	0.00	6.41	10.73	0.00	6.68	6.68	0.00	9.78	10.68	0.00	9.86	9.86	0.00	6.85	10.25	0.00	7.08	7.08	0.00
Tb	0.61	0.90	0.00	0.63	0.63	0.00	0.50	0.83	0.00	0.52	0.52	0.00	0.82	0.90	0.00	0.83	0.83	0.00	0.60	0.89	0.00	0.62	0.62	0.00
Dy	4.18	6.21	0.00	4.32	4.32	0.00	3.67	6.15	0.00	3.83	3.83	0.00	5.68	6.21	0.00	5.73	5.73	0.00	4.14	6.20	0.00	4.29	4.29	0.00
Ho	1.21	1.80	0.00	1.25	1.25	0.00	0.90	1.50	0.00	0.93	0.93	0.00	1.62	1.77	0.00	1.63	1.63	0.00	1.18	1.76	0.00	1.22	1.22	0.00
Er	3.75	5.57	0.00	3.88	3.88	0.00	2.94	4.92	0.00	3.05	3.05	0.00	5.05	5.52	0.00	5.10	5.10	0.00	3.67	5.49	0.00	3.80	3.80	0.00
Tm	0.86	1.27	0.00	0.88	0.88	0.00	0.66	1.11	0.00	0.69	0.69	0.00	1.09	1.19	0.00	1.10	1.10	0.00	0.83	1.25	0.00	0.86	0.86	0.00
Yb	2.72	4.04	0.00	2.81	2.81	0.00	2.53	4.23	0.00	2.63	2.63	0.00	3.72	4.06	0.00	3.75	3.75	0.00	2.71	4.06	0.00	2.81	2.81	0.00
Lu	0.71	1.06	0.00	0.74	0.74	0.00	0.61	1.03	0.00	0.64	0.64	0.00	0.95	1.04	0.00	0.96	0.96	0.00	0.71	1.06	0.00	0.73	0.73	0.00
Th	0.00	0.00	0.00	0.00	0.00	0.00	0.00	0.00	0.00	0.00	0.00	0.00	0.00	0.00	0.00	0.00	0.00	0.00	0.00	0.00	0.00	0.00	0.00	0.00
U	0.00	0.00	0.00	0.00	0.00	0.00	0.00	0.00	0.00	0.00	0.00	0.00	0.00	0.00	0.00	0.00	0.00	0.00	0.00	0.00	0.00	0.00	0.00	0.00
	0.00	0.00	0.00	0.00	0.00	0.00	0.00	0.00	0.00	0.00	0.00	0.00	0.00	0.00	0.00	0.00	0.00	0.00	0.00	0.00	0.00	0.00	0.00	0.00
	0.00	0.00	0.00	0.00	0.00	0.00	0.00	0.00	0.00	0.00	0.00	0.00	0.00	0.00	0.00	0.00	0.00	0.00	0.00	0.00	0.00	0.00	0.00	0.00
	0.00	0.00	0.00	0.00	0.00	0.00	0.00	0.00	0.00	0.00	0.00	0.00	0.00	0.00	0.00	0.00	0.00	0.00	0.00	0.00	0.00	0.00	0.00	0.00
	0.00	0.00	0.00	0.00	0.00	0.00	0.00	0.00	0.00	0.00	0.00	0.00	0.00	0.00	0.00	0.00	0.00	0.00	0.00	0.00	0.00	0.00	0.00	0.00
Subtotal (Trace)	241.6	358.7	0.0	249.8	249.8	0.00	208.9	349.8	0.0	217.6	217.6	0.00	299.5	327.2	0.0	302.1	302.1	0.00	238.5	356.9	0.0	246.6	246.6	0.00
Subtotal (TREE)	241.6	358.7	0.0	249.8	249.8	0.00	208.9	349.8	0.0	217.6	217.6	0.00	299.5	327.2	0.0	302.1	302.1	0.00	238.5	356.9	0.0	246.6	246.6	0.00
Subtotal (Other)	0.0	0.0	0.0	0.0	0.0	0.00	0.0	0.0	0.0	0.0	0.0	0.00	0.0	0.0	0.0	0.0	0.0	0.00	0.0	0.0	0.0	0.0	0.0	0.00

Figure 3.12.9. Page 4 (Assays) contained within the "Feed" computational worksheet.

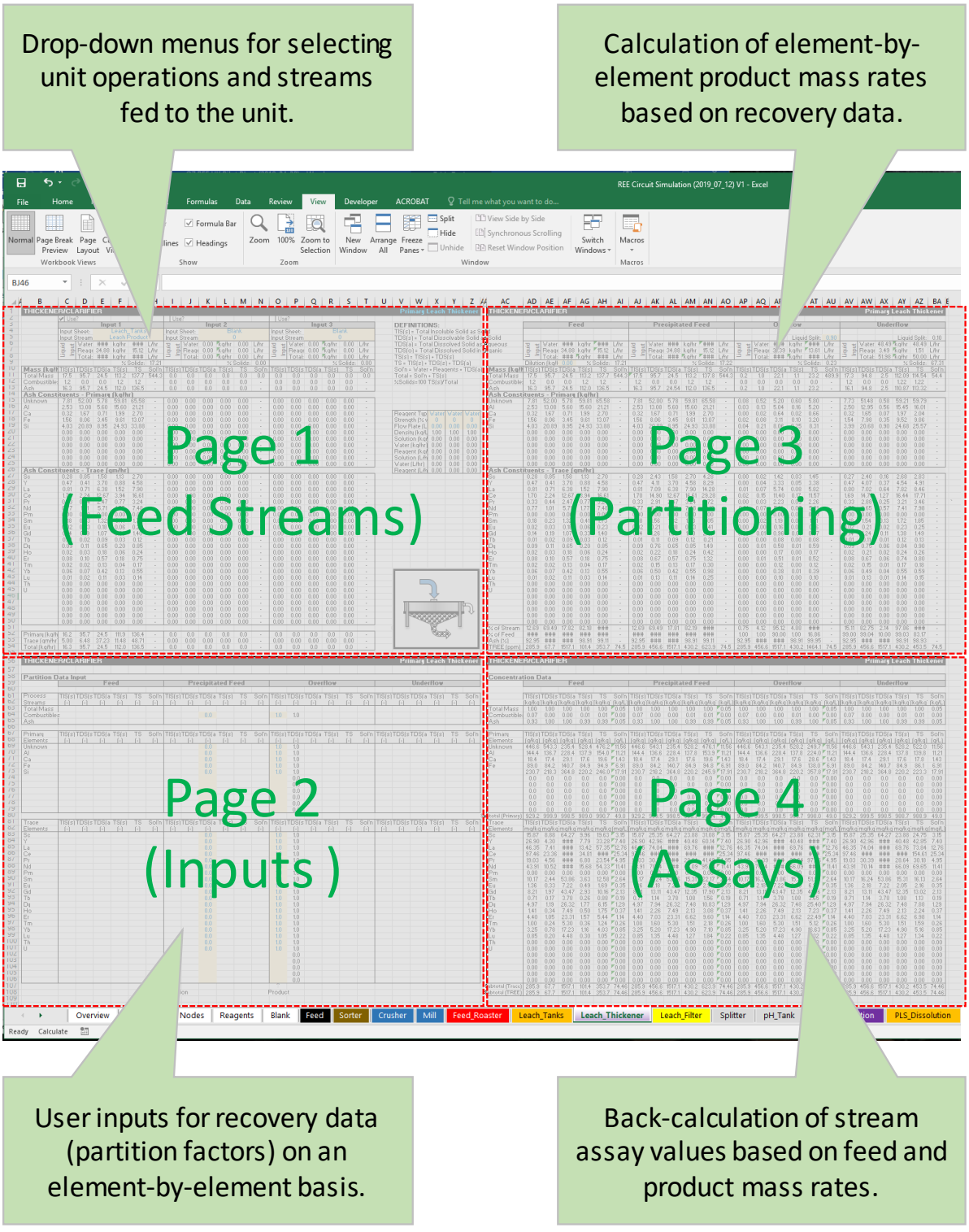

Figure 3.12.10. Illustration of typical pages for "Unit Operation" computational worksheets.

The three remaining pages in the computational worksheet include the following:

Page 2 – This portion of the worksheet is used to input recovery data for each element to be tracked by the software. The recovery data is entered as a partition factor, which is simply a fractional multiplier on the mass rate of given species.

Page 3 – This portion of the worksheet lists the resultant product mass rates of all species passing through the circuit after the fractional recovery calculations have been applied.

Page 4 – This portion of the worksheet is used to back-calculate the stream assay values for each species based on the feed and product mass rates. Values are reported on either a parts-per-million (ppm) or percentage (%) concentration, depending on which is most appropriate.

Appendix I provides the printout from an example of an REESim simulation run.

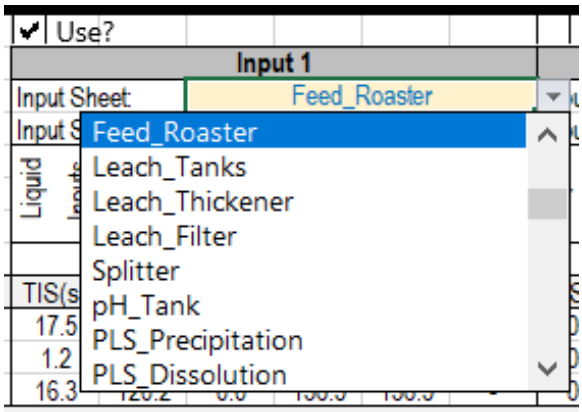

Figure 3.12.11. Drop-down menu for selecting unit operation worksheets.

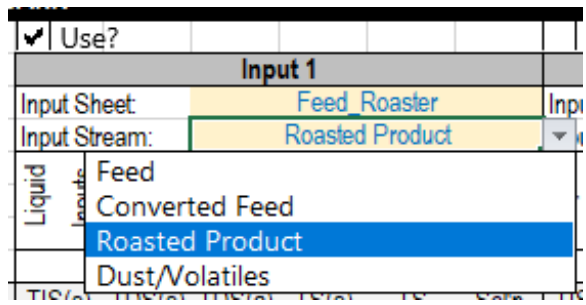

Figure 3.12.12. Drop-down menu for selecting process stream for a chosen unit operation.

3.13 Sample Analyses (PB3-Task12)

All the solid and liquid samples collected in the hydrometallurgy circuit (i.e., leaching, solvent extraction and selective precipitation units) were analyzed for rare earth content as well as other elements of interest using an in-house inductively coupled plasma-optical emission spectrometer (ICO-OES). The ICP-OES was located at the pilot plant facility to allow relatively quick turnaround of the analytical results. The unit was well maintained by following routinely scheduled technical maintenance visits from the vendor. An analytical quality control plan was developed and executed throughout the project.

Selected representative samples were also sent out to other research labs and commercial analytical labs for analysis, quality control and validation. The analytical instrumentation and independent labs included:

ICP-OES/ICP-MS/GDMS - EAG Laboratories (Eurofins) located in San Diego, CA.
ICP-OES - Environmental Research Training Laboratories (ERTL), University of Kentucky.
ICP-OES - Kentucky Geological Survey (KGS) laboratory.
ICP-MS - West Virginia University Energy Institute Analytical Lab.
ICP-MS – Virginia Tech Analytical Lab.

3.13.1 Solid sample analysis

Elemental content of a solid material requires complete digestion using an acid mix and analysis of the resultant solution using an analytical instrument, i.e., ICP. The sample preparation procedure used follows the ASTM D6357 method for ashing and digestion of coal and refuse samples with modifications made for digestion using a digestion block apparatus. Two standard samples with known elemental compositions as supplied by NIST were included in one out of every 20 samples to assess the quality of both the digestion process and the ICP-OES analysis. In addition, a duplicate from a given solid sample will be included every 40 samples. The criteria for the REE recovery of these check standards are +/- 10% RSD before the results from the analyses of a batch of samples are accepted. Lastly, to isolate the analytical results provided by the ICP-OES unit, two liquid standards having known rare earth element contents were analyzed every 50 samples. The same recovery criteria (i.e., +/- 10% RSD) were used to accept or reject a set of data obtained from a given batch of samples.

3.13.2 Liquid sample analysis

The analytical instrument used in the pilot plant is a Spectro Arcos II Inductively Coupled Plasma-Optical Emission Spectrophotometer (ICP-OES). This instrument utilizes the inductively coupled plasma flame to excite atoms and ions contained within the nebulized feed stream. Once the atoms and ions reach their excited energy states, they begin to decompose while emitting electromagnetic radiation at characteristic emission wavelengths associated with the respective element. An analytical quality control plan was developed and followed.

i. *Calibration*

The ICP-OES unit is operated in a 5% (w/w) nitric acid matrix. The argon plasma is ignited and stabilized for a minimum of 30 minutes prior to calibrating or analyzing samples. Daily calibration is performed by using a multielement certified reference material (CRM) standard of the following concentrations: 0 µg/mL, 0.05 µg/mL, 0.5 µg/mL, 1 µg/mL, 5 µg/mL, and 10 µg/mL. To account for any signal drift, the Spectro software is used to adjust the peak position if needed after calibration. A linear model is applied to the calibration curve points for each elemental peak with a minimum correlation coefficient of 0.996 criteria.

The ICP-OES unit was calibrated using four standards made at the following concentrations: 0 ppm, 0.2 ppm, 1.0 ppm and 10.0 ppm. The calibration was verified by two independent sourced check standards at the frequency of not less than every 20 samples:

Check 1 @ 2.5 ppm (from individual 1000ppm stds - CPI);

Check 2 @ 1.0 ppm (from multi element 100 ppm std – VHG Labs).

The recovery of these check standards was +/- 10% RSD.

One duplicate sample was chosen at random and ran through the entire process to verify repeatability at the frequency of not less than one every 40 samples. A total of 54 duplicates were analyzed during the program. The average difference in the total REEs + Y content between the duplicate samples was 15 ppm with a standard deviation of 16 ppm.

One or more standard reference materials was digested and analyzed alongside unknown samples and compared against best known values in each batch of samples. These included SRMs from the USGS, NIST, SARM and other round robin proficiency testing programs.

ii. Peak Selection

For most of the elements included in this analytical matrix, there are multiple emission wavelengths tracked for verification purposes. The wavelengths selected for this method have been chosen based on their ability to differentiate and quantify the analyte throughout the detectable range, the minimization of relative standard deviation (RSD) of the readings, and the minimization of interference effects due to the composition of the varying sample assays. The complete list of emission wavelengths tracked in the method can be found in the Supporting Information.

iii. Detection Range

The detection range is defined as the range at which a concentration can be determined within 10% of the true value with 95% statistical confidence. In order to establish the bounds of the detection range, a series of tests were performed to determine what these bounds were for each element. The detection range for each element is tabulated and can be found in the Supporting Information.

iv. CCV, CCB

The calibration is verified by multielement CRM solutions of concentrations 1 µg/mL and 0 µg/mL known as the CCV and CCB, respectively, after every 10-sample interval. If the CCV measurement for any element is not within 1 ± 0.2 µg/mL at this point, the values for the preceding interval of samples are not accepted and the samples are reanalyzed. If the CCB measurement shows a non-zero measurement for any element, the value is subtracted from the preceding interval of samples to account for the effects of contamination.

3.13.3 Process mass balancing

A "Megasheet" was developed for the modified flowsheet to balance the mass and volumetric flow for the solid and liquid stream, and the mass of each element in all the streams in the circuit. The mass of solid and volume of liquid stream will be entered with the elemental analysis of each stream to mass balance each unit based on the rule of mass in equals to mass out. The balanced data can be used to calculate the step-by-step recovery of each unit. The constraints need to be fulfilled in different unit are:

For leaching unit:

Mass balance: $m_{FD} + m_{Lx} = m_{SR} + m_{PLS}$

Elemental balance: $m_{FD} * c_{FD} + V_{Lx} * c_{LX} = m_{SR} * c_{SR} + V_{PLS} * c_{PLS}$

For precipitation unit:

Mass balance: $m_{PLS} = m_{SR} + m_{EFF}$

Elemental balance:$V_{PLS} * c_{PLS} = m_{cake} * c_{cake} + V_{EFF} * c_{EFF}$

Where, c_{LX}, c_{PLS} and c_{EFF} are the concentration of element in lixiviant, leachate and effluent (in mg/L); c_{FD}, c_{SR}, and c_{cake} are the concentration of element in feed solid, solid residue and precipitate cake (in mg/kg).

V_{Lx}, V_{PLS}, and V_{EFF} stands for the volume of lixiviant, leachate, and effluent (in Liter), c_{BA} is the concentration of element in bioleach acid, V_{BA} is the volume of bioleach acid.

The constraints need to be fulfilled in each unit, with adjusting the mass and assays by minimizing the weighted sum of square (WSSQ) of the acceptable relative error for all the assays:

$$\text{WSSQ} = \sum_{i=1} \sum_{k=1} \frac{(A_i{}^* c_{i,k}{}^* - A_i c_{i,k})^2}{(e\% * A_i c_{i,k})^2}$$

Where, $c_{i,k}$ is the mass or volume of the stream *i*; $c_{i,k}$ is the concentration of element in stream *i* for element *k*, either in mg/L for liquid or mg/kg for solid. * represents the mass and concentration of element in stream *i* for element *k* after adjustment. The acceptable relative error *e%* used in this calculation is 0.01% for feed stream and 5% for other streams.

A front page was created for the Megasheet with linkage to the corresponding mass and volumetric flow rates, concentration and recovery of selected element. A dropdown list was created to select the element of interest to show on the flowsheet (Figure 3.13.1). The second sheet of the Megasheet includes the input of the mass and volumetric flow information, raw data, acceptable error, percentage change after mass balancing, and the calculation for mass balancing constraints and WSSQ. (Figure 3.13.2). The third page displays the output of the unit recoveries of rare earth elements and major elements of interests based on the mass balanced data presented in second sheet. (Figure 3.13.3)

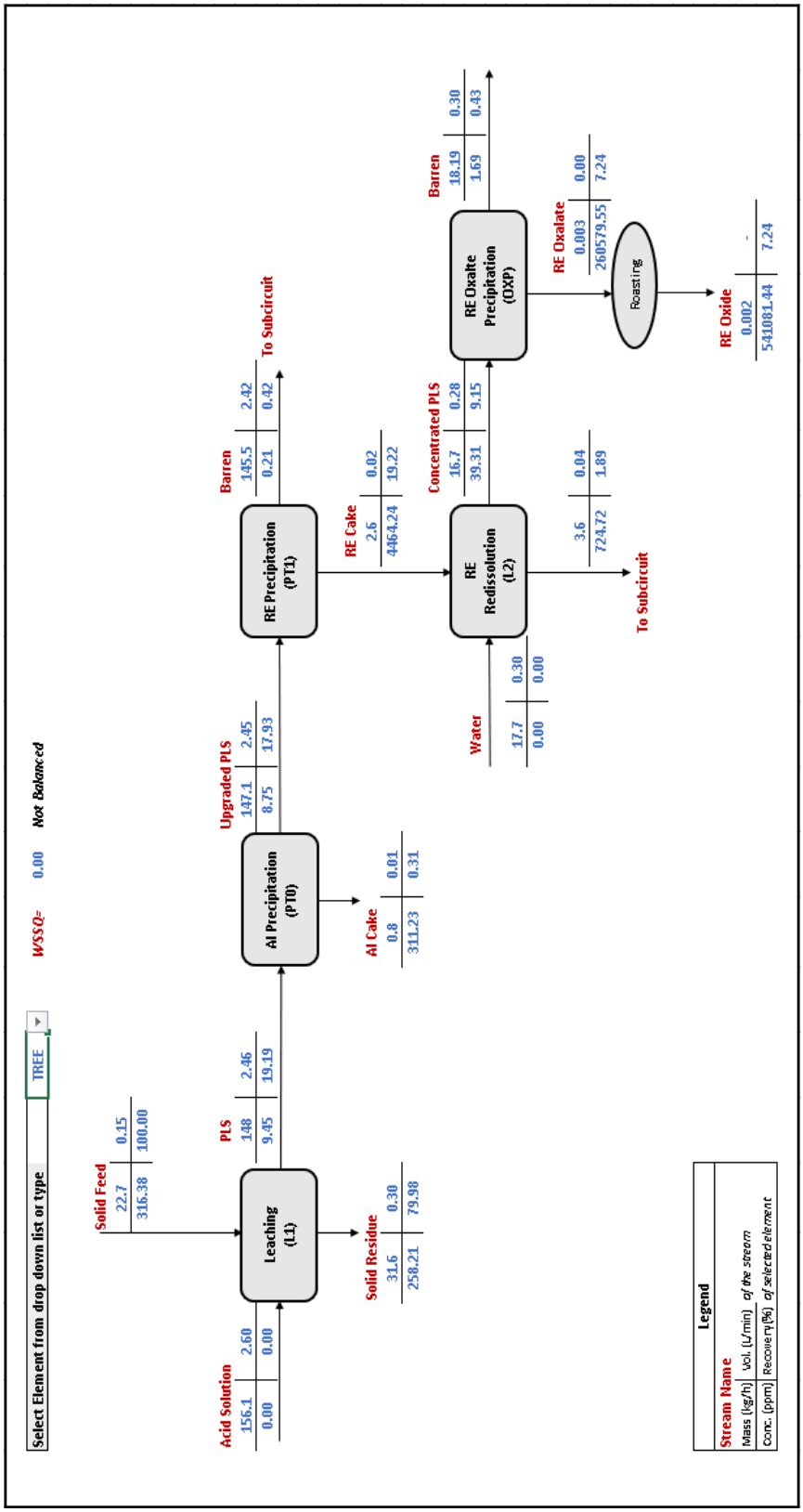

Figure 3.13.1. Mass balance Megasheet output. (First sheet)

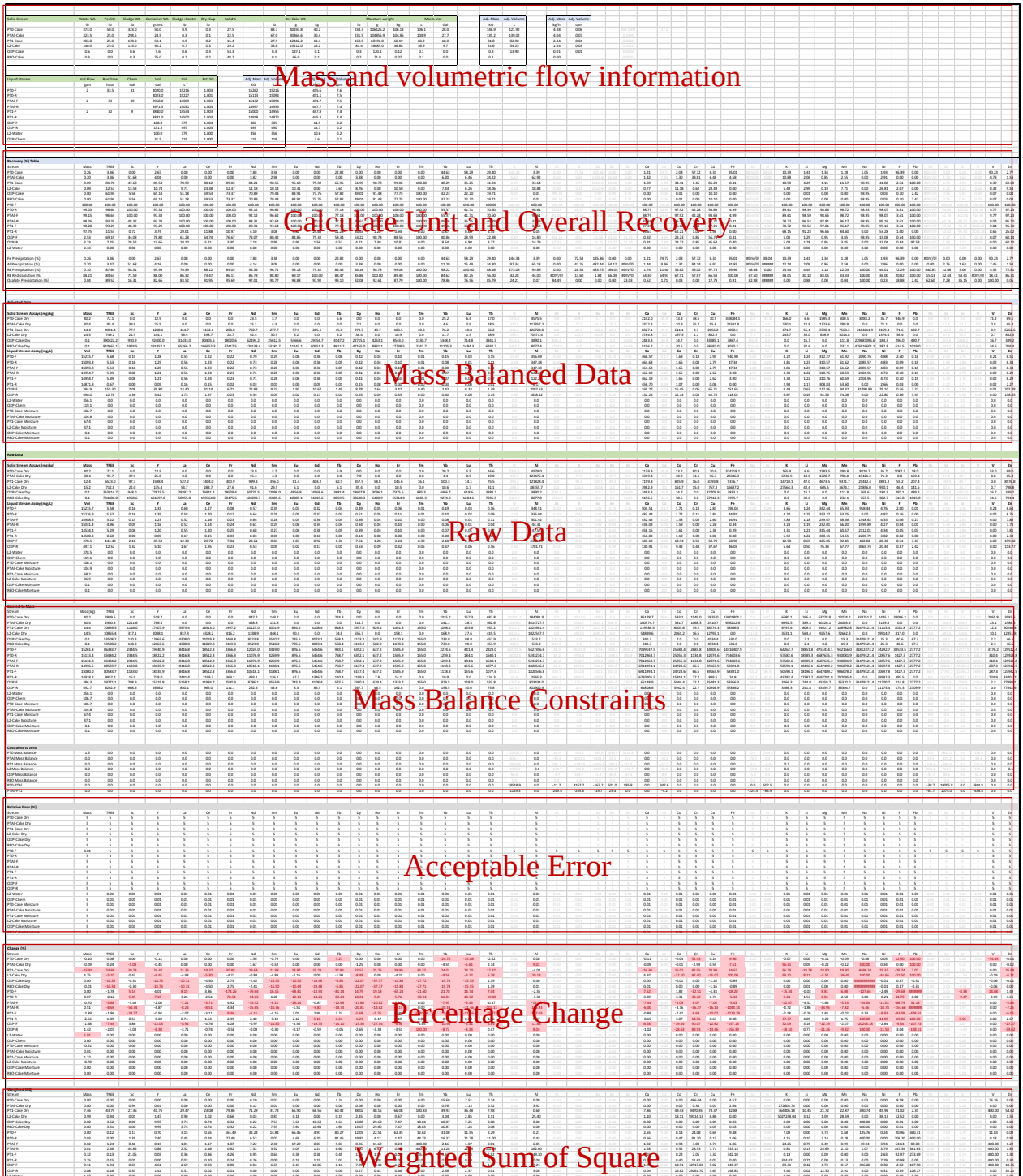

Figure 3.13.2. Megasheet mass balance calculation sheet. (Second sheet)

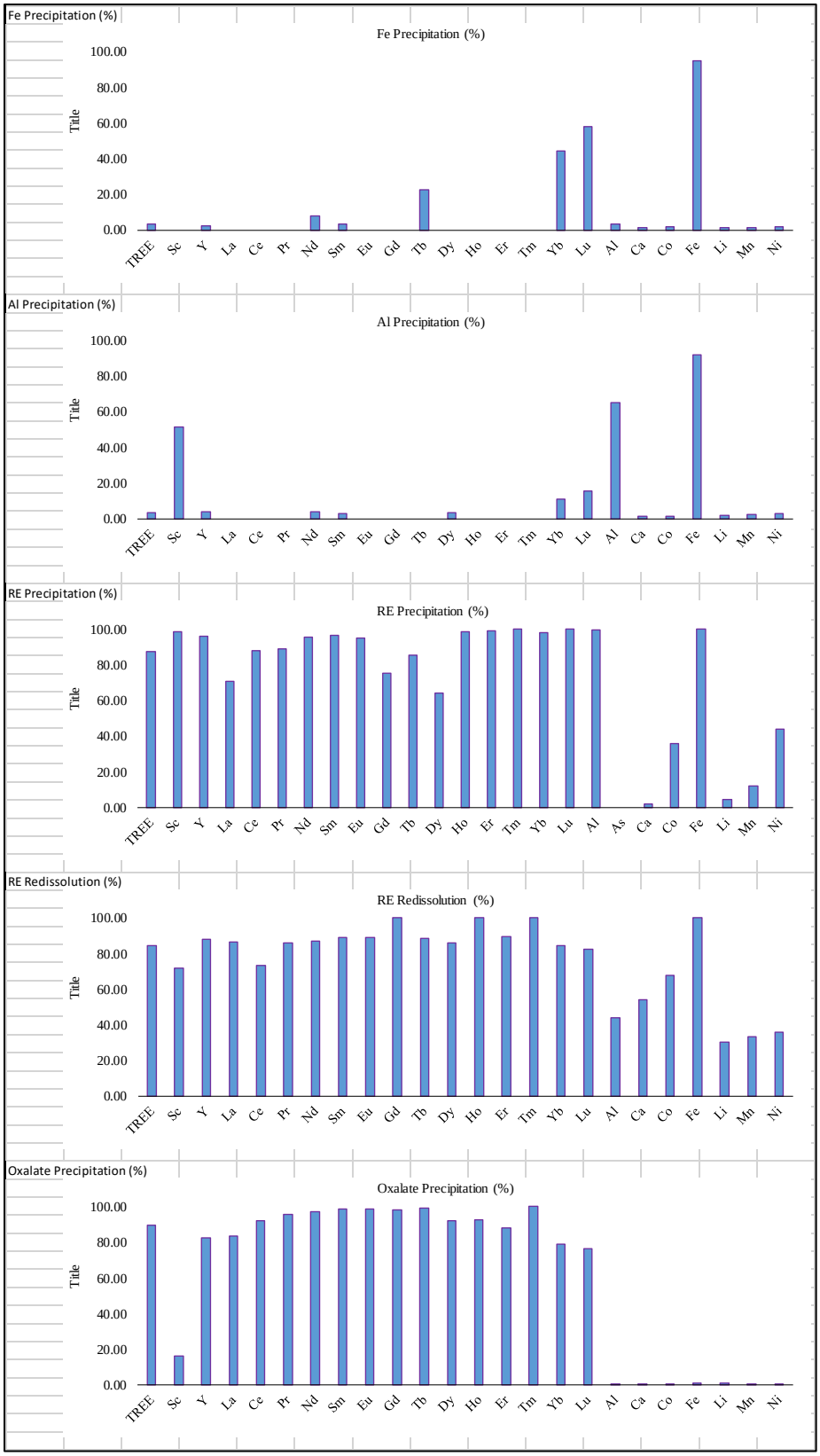

Figure 3.13.3. Megasheet results output page. (Third sheet)

3.14 Technical & Economic Analyses (PB3-Task13)

3.14.1 Approach and Task Objectives

To assess the economic feasibility and future commercial viability of the process technologies developed in this project, a detailed techno-economic evaluation was conducted. The primary input data for this analysis consisted of experimental testing conducted at both the bench-scale and pilot-scale as well as cost models for capital, labor, consumables, and power. Key output metrics included project capital costs, REE production cost ($/kg), 20-year project NPV, rate of return, and payback period. Numerous scenarios were evaluated in the model to assess multiple pathways to commercialization.

To facilitate this techno-economic assessment, a spreadsheet-based economic modeling tool was developed and utilized. This spreadsheet tool, herein denoted *REE-Econ* (ver 5.1) was originally developed as part of the current project, but it has also been adapted, upgraded, and used in other similar DOE projects including DE-FE0029956, DE-FE0031525, and DE-FE0031827. Since the software, and by proxy, the same methodology, was used in each project, portions of this report, namely the guiding assumptions and cost estimation methodology, duplicate those prior investigations. Specific work completed under the current project included the initial tool develop, the application of the software to the specific flowsheets evaluated in this study, and the subsequent analysis and interpretation of the results.

This *REE-Econ* software integrates both technical factors (e.g., process feed rates, unit recovery values, reagent consumption rates, scale-up criteria, etc.) and economic factors (e.g., process capital costs, reagent costs, finance and tax structure, etc.), while outputting key economic indicators, such as line-item operating cost estimates, equipment and installed capital cost projections, a pro forma cash flow, net present value *(NPV)*, internal rate of return *(IRR*), and capital payback period. Overall, this assessment represents an AACE Class 4 estimate (-30% to +50%), as it relies on equipment scaling factors and parametric models for the determination of unit costs.

The software workflow is driven by various worksheet "tabs." For typical use, the flow is left to right across the worksheets and top to bottom within the worksheets. A listing and description of each worksheet tab is shown in Table 3.14.1. Within each worksheet, the spreadsheet cells are delineated between a printable area, highlighted with a white background, and a nonprintable area denoted by a grey background. The printable area contains key process information and economic indicators, while the nonprintable area contains secondary calculations, explanatory text, and other information. The workbook also includes integrated instructions for use.

Table 3.14.1. Worksheet Descriptions for REE-Econ Software

Worksheet Name	Brief Description
Cover Page	Contains model run metadata.
Economic	Specifies global economic assumptions.
Technical	Specifies process recovery and feed rates.
CAPEX	Compiles total capital costs for process modules.
OPEX	Compiles total operating costs for process modules.
Revenue	Estimates revenue from various product streams.
Cash Flow	Shows pro forma cash flow based on revenue and costs.
PMx	Contains design and costing data for each process module.
Global Constant	Contains important model parameters.

3.14.2 Global Economic Assumptions

Several technical and economic assumptions were required to complete the techno-economic analysis. Regarding technical inputs, the experimental input data used to create each material balance was obtained directly from various project participants and represents a combination of both laboratory and pilot-scale test results. In addition, many of the economic assumptions, including those regarding the financing structure, escalation rates, tax calculations, and operating period have been supplied by National Energy Technology Laboratory (NETL) in the *Guidance for Development of Techno-Economic Analyses* document. Key economic assumptions utilized in this study include:

- All amounts are in US dollars.
- The total operational period for the plant is 20 years.
- The plant feed rate to the roasting operation is fixed as an input that varies between scenarios. This value varied from 100 to 500 st/hr for the scenarios considered in this study.
- The feedstock grade for each case reflects laboratory analyses from material sampled during this study.
- Inflation has been applied to sales revenue and operating costs using a fixed rate of 3 percent.
- Capital costs are spread over a period not to exceed three years, and the allocation between those three years is 10 percent, 60 percent, and 30 percent for years one through three, respectively. Thus, the total analysis period (capital purchase plus operating) is not to exceed 23 years.
- During the capital expenditure period, capital costs escalate at a constant rate of 3.6 percent.
- The project is debt financed for 50 percent of the total overnight capital requirement. The remaining 50 percent is financed by equity.
- The debt repayment terms include: 6 percent interest rate, 10-year loan period, and no grace period on debt repayment. The repayment uses a standard amortization schedule with constant payments throughout the payoff period.

- Working capital is not included in this estimate and will instead be borne by the operating entity at no cost to the project.
- The combined federal and local tax rate is fixed at 26 percent. This value is lower than the one required in the NETL guidance document; however, it reflects a recent reduction in corporate tax rates.
- All capital is depreciable, using a 150 percent declining balance depreciation schedule over 20 years. The depreciation method was NOT changed to straight line when conditions favored the switch.
- The mineral depletion rate for REEs is 14 percent. Depletion is charged at the appropriate rate times the net sales revenue after deducting royalties and any severance tax, provided that the total amount calculated by depletion rates does not exceed 50 percent of the taxable income before depletion.
- The plant is part of a larger commercial entity with sufficient revenue to offset negative taxable income. Thus, losses are not carried forward and are instead calculated as a "negative tax" that indicates the reduction in tax burden required for overall entity.
- The land and mineral rights are leased, and royalties will be paid to the landowner.
- Royalties are charged at standard rate of 6.5 percent of total sales revenue.
- All process modules are located at the same facility with no significant transportation cost between modules.
- The plant operation schedule is fixed at eight (8) hours per shift, three (3) shifts per day, 336 operational days per year.
- Equipment costs were determined by scale-factor analysis. Installation costs were determined by an overall Lang factor.
- Reagents, consumables, power, and labor were determined by itemized cost analysis.
- Other operating costs, including maintenance and supply, QA/QC, sales, admin, property tax, insurance, and plant overhead were all calculated using proportional factors.

3.14.3 Scale-Up and Cost Estimation Procedures

A detailed bottom-up assessment was performed to determine the total expected capital expenditures for a hypothetical commercial-scale facility. After completing a mass and energy balance for the process scenario under consideration, the unit capacity (and subsequently the size and number) of each unit operation was determined by a fundamental assessment of the processing needs. Not all unit operation costs scale by simple feed throughput, so a detailed unit-by-unit appraisal was required. For example, the capital cost of roasting operations tends to scale exponentially with respect to heat input in terms of million BTUs/hour (MBtu/hr.), while the capital cost of grinding mills scale is related to power (expressed as horsepower (HP) draw). The engineering team consulted several standard cost engineering reference guides, including the Mine and Mill Estimator's Guide, Matches.com, Gentry and O'Neil (1986), and Garett (1989), to determine the relevant scaling criteria for each equipment type. These scaling parameters were then used to calculate the unit capacity required at the commercial feed rate. Once the capacity

was determined, an exponential capital cost model was used to determine the final cost. Details on the scale-up criteria and unit capacity measures are shown in Table 3.14.2.

Table 3.14.2. Scale-up criteria used in techno-economic analysis

Process Operation	Cost Model Input	Scale-Up Criteria
Loaders	Bucket Capacity	Constant TPH per unit (unit size fixed)
Crushers	Power Draw [HP]	Constant HP per TPH
Screens	Screen area [ft^2]	Constant TPH/ft^2 screen area for a given screen opening size
Conveyors	Throughput [TPH]	Simple throughput
Storage Bins	Storage capacity [tons]	Percent of Hourly production surge capacity
Mills	Power Draw [HP]	Constant Bond Work Index
Storage Tanks	Storage capacity [gallons]	Constant Storage time/retention time
Mixers	Power Draw [HP]	Constant Power Intensity (HP/1000 gal.)
Pumps	Feed rate [gpm]	Simple throughput
Cyclones	Feed rate [gpm]	Simple throughput
Thickeners	Thickener area [ft^2]	Constant unit capacity (ft^2/t/day)
Filter Presses	Filter volume [ft^3]	Constant cycle time
Belt Filter	Throughput [TPH]	Simple throughput
Dryers	Water evaporation rate [lb/hr H_2O]	Constant moisture reduction
Roasters	Heat Input [MBtu/hr]	Constant heat requirement per unit feed
Scrubbers	Gas rate [cfm]	Constant airflow per TPH
Spray Quenchers	Gas rate [cfm]	Constant airflow per TPH
Chillers	Heat Input [MBtu/hr]	Constant heat requirement
Leach Tanks	Volume [gal]	Constant Retention Time
Solution Heaters	Heat Input [MBtu/hr]	Constant heat requirement
Mixer Settlers	Volume [gal]	Constant Retention Time

For estimation and analysis purposes, all capital costs were determined assuming new equipment, free-on-board *(FOB)* shipping point. All costs were initially estimated using a 2016 index year, which was then escalated to 2021 construction year using the Chemical Engineering Plant Cost Index *(CEPCI)*. Using the scale-up factors and design capacities, commercial-scale equipment requirements were determined based on a nominal plant feed rate of 100 to 500 st/hr depending on the scenario. Capital cost estimates for individual units were then determined using scale factor estimates dictated by a standard exponential cost model:

$$CAPEX = \left[\frac{CI_C}{CI_H}\right][K][aX^b]$$

where CI_C and CI_H are the current and historic cost indices, K is the equipment cost ratio (or Lang) factor, X is the unit capacity, and "a" and "b" are fitting constants unique to each equipment item (Gentry and O'Neil, 1986). Table 3.14.3 shows the capital cost model fitting parameters (a and b) for the major equipment categories used in the cost model. The data used to generate these models were gathered from multiple standard equipment costing resources (MAMEC, Gentry and O'Neil, Garett, 1989).

Table 3.14.3. Capital cost model parameters used in techno-economic analysis.

Process Operation	Coefficient, a	Exponent, b	Capacity Unit, X	Reference
Front End Loader (2yd)	Constant Cost = $147,400 / unit			MAMEC, 2016
Front End Loader (10yd)	Constant Cost = $945,700 / unit			MAMEC, 2016
VSI Crusher	3,247	0.68	HP	MAMEC, 2016
Roll Crusher	1,120	0.8484	HP	MAMEC, 2016
Vibrating Screen	1,002	0.9093	ft^2	MAMEC, 2016
Conveyor	2,092	0.5491	TPH	MAMEC, 2016
Storage Bins	4,441	0.6185	Tons	MAMEC, 2016
Roaster	390,000	0.48	MBTU/hr	Garrett, 1989
Gas Scrubber	7	0.9414	cfm	MAMEC, 2016
Chiller	97,585	0.6	MBTU/hr	Matches
Polyethylene Tank	1	0.9492	gal	MAMEC, 2016
Steel Tanks	179	0.5624	gal	MAMEC, 2016
Tank Mixer	10,640	0.564	HP	MAMEC, 2016
Process Pump	2,152	0.3814	gpm	MAMEC, 2016
Thickener	280	0.8023	ft^2	MAMEC, 2016
Filter Press	6,068	0.72	ft^3	MAMEC, 2016
Solution Heater	25,929	0.953	MBTU/hr	MAMEC, 2016
Belt Filter	207,819	0.249152	TPH	MAMEC, 2016

After the base equipment prices were established, installed capital costs were determined by applying Lang factors to the direct equipment costs. Typical ranges for Lang factors are specified by Gentry and O'Neil (1986) and are shown in Table 3.14.4. The Lang factors used in the current analysis reflect "brownfield" conditions, where existing infrastructure, including buildings, utilities, and plant services, are already in place. Each individual Lang Factor is categorized as an ancillary cost; a buildings/infrastructure cost; or an engineering, procurement, construction, and management *(EPCM)* cost. An overall 15% capital contingency was also applied to the final base equipment price.

Table 3.14.4. Lang factor estimation for commercial-scale installation.

Module	Type	% of Base	Typical
Piping, Materials and Labor	Ancillary	20%	7 to 25%
Electrical, Materials and Labor	Ancillary	20%	13 to 25%
Instrumentation	Ancillary	8%	3 to 12%
Plant Services	Ancillary	10%	7 to 15%
Process Buildings	Buildings	40%	33 to 50%
Auxiliary Buildings	Buildings	15%	7 to 15%
Site Improvements	Buildings	10%	3 to 18%
Equipment Installation	EPCM	17%	17 to 25%
Field Expenses	EPCM	12%	10 to 12%
Project Management and Construction	EPCM	30%	30 to 33%
Contingency	Contingency	15%	10 to 15%
Total Lang Factor (=1+sum % Base): 297.00%			
Alternatively, a multiplier of: 2.97			

The operating expense estimate for the proposed facility was categorized according to both process module as well as a functional accounting code. Accounting codes used in this study include: (i) operating labor, (ii) technical labor, (iii) power/utilities, (iv) lease/toll agreements, (v) consumables/reagents, (vi) waste disposal, (vii) plant overhead, and (viii) general sales and administration. Like the capital cost estimate, a bottom-up approach was used to determine the expected operating costs from first principles. Direct operating costs were specified using designed labor requirements along with publicly available wage and burden rates (Table 3.14.5).

Table 3.14.5. Labor Cateogry Descriptions.

Labor Category	Code	Labor Rate ($/hr.)	Fringe Benefits	Source/Notes
Skilled Operator	OL	$ 24.98	25%	May 2018 KY BLS, Occupation Code: 51-9011
Operator	OL	$ 19.08	25%	May 2018 KY BLS, Occupation Code: 51-9012
Foreman/System Operator	OL	$ 30.39	25%	May 2018 KY BLS, Occupation Code: 47-1011
Maintenance	OL	$ 22.73	25%	May 2018 KY BLS, Occupation Code: 49-9043
Lab Technician	TL	$ 21.97	25%	May 2018 KY BLS, Occupation Code: 19-4031
Metallurgist/Chemical Engineer	TL	$ 45.85	25%	May 2018 KY BLS, Occupation Code: 17-2041

Power costs were determined via itemized listing of the horsepower requirements for every major unit operation, assuming an industrial electricity cost of $0.0683 /kw-hr and an overall electrical efficiency of 85%. Other direct operating costs included reagent dosing requirements, waste disposal costs, and expected maintenance requirements, which were all itemized and calculated directly. General sales and administrative *(GSA)* costs were specified using standard overhead charge rates. For accounting and analysis purposes, costs were allocated based on cost type (fixed, variable or overhead), and each line item cost was also allocated to a process unit. Details on the specific factors and unit costs used in the analysis can be found in *REE-Econ* printouts included in the *Appendix* to this report.

Revenue for the commercial-scale facility was estimated using market REE prices and the expected REE production for various products. A standard price deck, which has been provided by NETL is shown in Table 3.14.6. All standard prices were then subjected to a fixed reduction/discount. For the mixed REEs in a combined REO product, a 25% discount was used to account for the downstream separation. The selection of a 25% discount was based on the discussion given by Dahlberg et al (2014).

Table 3.14.6. REE Price deck used for commercial-scale economic analysis

Element	REE Oxide Price ($/kg)	REE Price (Elemental Basis) ($/kg)	Price Source
Scandium	$ 4,200	$ 6,442	[1]
Yttrium	$ 6	$ 8	[1]
Lanthanum	$ 2	$ 2	[1]
Cerium	$ 2	$ 2	[1]
Praseodymium	$ 52	$ 63	[1]
Neodymium	$ 42	$ 49	[1]
Samarium	$ 2	$ 2	[2]
Europium	$ 34	$ 39	[1]
Gadolinium	$ 32	$ 37	[1]
Terbium	$ 400	$ 470	[1]
Dysprosium	$ 230	$ 264	[1]
Holmium	$ 53	$ 61	[2]
Erbium	$ 34	$ 39	[1]
Thulium	$ -	$ -	[2]
Ytterbium	$ 29	$ 33	[2]
Lutetium	$ 797	$ 906	[2]

[1] NETL Dec 2016 Price Deck
[2] Asian Metal

3.14.4 Process Descriptions

To aggregate costs across functional unit operations, the research team identified and defined a series of process modules. In this regard, a process module is defined as a group of similar unit operations that perform a single process function and can be described by a common feed rate. Each process module has a unique worksheet tab in the spreadsheet TEA model (denoted as PM1, PM2, PM3, etc.), which contains all of the pertinent design and costing data. This approach allows capital and operating costs to be compared between process modules to assess cost drivers and identify opportunities for improvement. A complete listing of the process modules used for this project is shown in Table 3.14.7. Further detail on each individual process module is provided below.

Table 3.14.7. Listing of process modules used in economic analysis.

Module ID	Process	Feed Type
PM1	Feed Preparation	Solid, Dilute
PM2	Roasting	Solid, Dilute
PM3	Leaching	Solid, Dilute
PM4	Leachate Precipitation	Aqueous
PM5	RE-Redissolution	Solid, Dilute
PM6	REE Oxalate Precipitation	Aqueous
PM7	Sc Recovery (optional)	Aqueous

3.14.4.1 PM1: Feed Preparation

Raw plant feed consisting of either coarse preparation plant refuse, existing refuse pile material, preparation plant middlings, or similar solid materials are first processed through the feed preparation circuit. This circuit crushes, sizes, and partially enriches the feedstock to generate a material suitable for the downstream roasting and leaching operations.

Based on the business case assumptions, the REE plant is assumed to be co-located at a coal preparation or waste disposal site, and as such, no significant haulage costs are incurred. Rather, the bounds of the overall process start with a 10-yd^3 front end loader feeding the plant from the preparation plant refuse pile. For some feedstocks, the material is first passed through a double deck screen to isolate the 2 inch by 0.5 inch material before being processed by an x-ray sorter. Not all feedstocks are amenable to x-ray sorting, and in these cases the screening and sorting steps are bypassed.

X-ray sorting is a nascent technology in the coal industry that is used to separate coarse rock from coarse coal using a dry separation technique. Several manufacturers currently offer sorting models optimized for coal separations, and these models often allow the operator to designate a desired SG cut point for separation. In this process, material will enter the ore sorter via a designated feed system. The sorter itself contains a conveyor belt that feeds the material into the x-ray sensor. Once in the sensor zone, the sorter compares the x-ray transmission of each particle to that of a preset calibration curve to determine if the particle is to be accepted or ejected. If selected for ejection, the sorter controller actuates an air nozzle at the end of the conveyor belt in such a manner as to alter the trajectory of the particle. This trajectory path thus distinguishes the particles into two separate lots representing the two products around the SG cut point. The system is typically set up so that the minority species is ejected while the majority species is retained.

For this process, the x-ray sorter is configured to eject extremely high-density waste material, which contains low overall rare earth content. By ejecting the high-density material and retaining the lower density coarse refuse stream, the sorter is able to generate a nominal middlings feedstock suitable for REE recovery. The high-density reject is discarded as a final circuit product. For costing purposes, the sorter is assumed to be operated under a simple $/ton processed lease agreement with the equipment manufacturer, as these arrangements are common in the industry.

Following the sorter, the material will be processed through a vertical shaft impactor (VSI) crusher and a roll crusher, each followed by a vibratory sizing screen, to stage crush the material to a nominal 1 to 2 mm product suitable for roasting. The module also includes five conveyor belts for materials handling of the various intermediate and final product streams.

3.14.4.2 PM2: Roasting

Following feed preparation, the crushed solids are directed to a high temperature oxidation/roasting process prior to leaching. In this process module, solid material is conveyed into a rotary kiln where the material is heated to an optimal temperature (nominally 650° C). This thermal-oxidation process dramatically improves the leachability of the REEs and CMs contained in the refuse material. The roasting is fueled by an external natural gas source; however, a significant portion of the required fuel is anticipated to be supplied by the residual carbonaceous material in the coal refuse. This practice is common in the roasting of gold ores, which can contain as little as 3% carbon (Mular et al., 2002).

The roasting operation includes several downstream ancillary/environmental control units to capture any dust or off gasses produced during the roasting process. The roasted product is then directed to a chiller and finally to a product surge bin. This bin provides a consistent feed to the leaching circuit.

3.14.4.3 PM3: Leaching

Following roasting, the feed material is conveyed to a series of cascading rubber lined tanks where leaching is used to extract the REEs from the refuse feedstock. In these tanks, the solid material is mixed with sulfuric acid and or other leaching lixiviants at a moderate solids concentration of 10% to 25% by weight. The retention time in this stage is uniquely calibrated for each feedstock and lixiviant to promote the optimal tradeoff between the recovery of REEs and major metal contaminants such as Al and Fe. A natural gas-powered solution heater is used to maintain an elevated temperature suitable for effective leaching.

After leaching, the material is passed to a thickener, where the pregnant leach solution is separated from the residual solids. The loaded leach solution is passed to a storage tank upstream of the concentration and recovery operations, while the residue reports to a belt filter for further dewatering. The primary effluent of the belt filter is combined with the thickener overflow in the leach solution storage tank, while the purge cycle effluent can be recycled to the leaching feed tank or directed to the wastewater treatment. The dewatered residual solids are discharged from the belt filter and conveyed back to the coarse refuse disposal area at the host site.

3.14.4.4 PM4: Leachate Precipitation

In one embodiment of the process, the PLS after leaching may be initially subjected to Sc recovery (see PM7); however, this step is optional, as scandium recovery may not be warranted for all feedstocks. Moreover, the remaining PLS (or SX raffinate if PM7 is employed) is too dilute for processing with direct oxalic acid precipitation. As a result, an intermediate stage of

concentration is needed to increase the concentration of REEs while rejecting gangue metals to the largest extent possible.

In the current flowsheet iteration, this preliminary upgrading is achieved by precipitation and re-dissolution. During the precipitation stage, a caustic solution is used to raise the pH of the leachate to the point where nearly all of the REEs are recovered into a solid precipitate. As a result, the overflow from this vessel is barren of REEs and sent to final waste water disposal. Alternatively, the REE-enriched precipitate from the thickener underflow is further dewatered in a filter press and then passed to the re-dissolution stage (PM5). The reactions in this step are conducted in rubber lined tanks and/or thickeners with a retention time long enough to facilitate full settling of the precipitated solids.

3.14.4.5 PM5: Re-Dissolution

In this module, the enriched REE solid is re-dissolved into solution using HCl. The reaction is conducted in a series of cascading polyethylene tanks in a manner similar to that of the leaching circuit (PM3). Following re-dissolution, a thickener is used to separate the concentrated REE solution from the minor amount of residual solids. These solids are then dewatered in a filter press and conveyed to the final waste pile, while the enriched solution is pumped to final REO recovery.

3.14.4.6 PM6: REE Oxalate Precipitation

After selective precipitation and re-dissolution, the enriched REE leach solution is ready for final processing and recovery. In this process module, the REEs are precipitated from the leach solution using oxalic acid and a mild base solution. This process step incorporates an oxalic/caustic mix tank, a leaching tank/thickener, a filter press, and a small product roaster. Overall, this process generates a concentrated REE-oxalate product, which is then roasted to generate a final mixed REE oxide with a nominal grade of 90% to 99% REO. These oxides are then suitable for toll refining or final sales, depending on the purchase order requirements and the final product purity. Any residual solution generated in this module is directed to the waste water treatment process prior to final discharge.

3.14.4.7 PM7: Sc SX Separation

This process module, which is currently being developed under DE-FE0031827, utilizes solvent extraction to directly recover scandium from the initial PLS, while leaving the other REEs in the raffinate. The raw leachate is first pumped to a two-stage loading circuit where the scandium is selectively recovered into the organic phase. To optimize for selective scandium recovery, an Orfom diluent and Cyanex 272 extractant are used in the organic phase. In the loading stage, an O:A ratio of 1:1 is maintained within the mixer; however, the organic is internally recycled in the loading stage to establish an O:A advance ratio of 1:50. The raffinate from the loading stage is directed to the downstream REE recovery operations, while the loaded organic is pumped to the stripping stage. In stripping, 2 molar sulfuric acid is used as a stripping reagent. Here, an O:A ratio of 1:1 is maintained in the mixer; however, the acidic strip solution is internally recycled in

the stripping stage to maintain an O:A advance ratio of 10:1. The resulting solution is then precipitated with 2 molar NaOH and filtered to produce a high grade Sc_2O_3 product.

3.14.5 Scenario Matrix and Descriptions

3.14.5.1 Scenario Matrix

To evaluate several potential pathways to commercialization, the project team identified 10 unique scenarios that were then evaluated using the *REE-Econ* TEA model. These scenarios build upon the pilot-scale data collected during the project but also incorporate other notable findings and accomplishments identified by the research team during the current project. Table 3.14.8 shows the list of scenarios and the feedstock description for each. Further details and descriptions of each scenario are provided below.

Table 3.14.8. List of Scenarios Evaluated in Techno-Economic Analysis

ID	Scenario Name	Feedstock
1	Raw Pilot Plant Data	West KY No. 13 Coarse Refuse
2	Pilot Plant Data w/ Process Optimization	West KY No. 13 Coarse Refuse
3	Pilot Plant Data w/ Optimization and Sc Recovery	West KY No. 13 Coarse Refuse
4	Pilot Plant Data w/ Optimization, Sc Recovery, and Sorting	West KY No. 13 Coarse Refuse
5	AS Leaching	West KY No. 13, 1.4 Float
6	AS Leaching w/ Sc Recovery	West KY No. 13, 1.4 Float
7	Roasted Middlings	Pocahontas No. 3 Middlings
8	Roasted Middlings w/ Sc Recovery	Pocahontas No. 3 Middlings
9	FBC w/ Acid Recovery	FBC Ash (Roasted Middlings)
10	FBC Ash w/ Sc Recovery	FBC Ash (Roasted Middlings)

3.14.5.2 Scenario Specific Assumptions

In addition to the global technical and economic assumptions described in Section 3.14.2 above, each scenario also includes specific technical and economic assumptions unique to the individual case. The lists below include these assumptions as well as a brief description of the approach or objective of each scenario.

ID1: Raw Plant Data

Scenario ID1 was developed based upon direct measurements of the process performance and chemical consumption rates as determined in pilot-scale testing. All pilot plant data was utilized directly, with appropriate scaling functions added to translate the dosing rates to a commercial scale operation. No further adjustments were made optimize the process or leverage other information for laboratory tests or process models. As such, this data reflects the most conservative outlook for the commercial scale implementation.

- All chemical consumption values are based on Pilot Test DTK-C16. Dose values (e.g. kg acid/ton feed) are held constant from pilot data.

- The commercial process feed rate is fixed at 500 tph to the roaster, 460 tph to the leaching vessels.
- Process recovery values and the full process material balance are based on Pilot Test DTK-C16. Overall REE recovery for this case is 17%.
- The leach % solids is fixed at 8%, as tested in Pilot Test DTK-C16.
- The feed assay based is based on actual measurements of West KY No. 13 coarse refuse (see Q2-2019 RPRP, Table 14).
- No other adjustments or intensifications.

ID2: Pilot Plant Data with Process Optimization

Scenario ID2 uses similar chemical consumption rates as that of ID1; however, the unit-by-unit recovery values have been increased to reflect the best results obtained from sequential laboratory testing of each unit operation at similar chemical conditions. Moreover, recognizing the importance of feed percent solids in reducing production and capital costs (see Section 3.14.6), the percent solids in leaching was increased from the pilot scale test value of 8% to a more aggressive value of 20%. Due to the improved recovery and solids loading, this scenario produces superior outcomes relative to that of ID1 and thus reflects the potential of the current flowsheet and feedstock combination after further process optimization. This case was used as the "baseline" upon which subsequent cases were compared.

- All assumptions and inputs are identical to ID1, except as noted.
- All chemical consumption values are based on Pilot Test DTK-C16. Dose values (e.g. kg acid/ton feed) are held constant from pilot data.
- Process recovery values are based on optimal unit-by-unit values, using data from Q2-2019 RPPR, i.e. 30.5% overall.
- This leach % solids is fixed at 20%.
- No other adjustments or intensifications.

ID3: Pilot Plant Data with Optimization and Sc Recovery

Scenario ID3 makes an incremental change on ID2 by adding dedicated Scandium recovery circuit and intensified recovery of scandium in the leaching circuit. This scenario was developed after an initial assessment of ID1 and ID2 showed extremely low recovery of Scandium, <1% for the overall process. While a dedicated Scandium recovery circuit was not specifically addressed in this pilot project, data collected by the project team in DE-FE0031827 shows that the approach is technically feasible and potentially cost effective. While the Scandium recovery circuit will incur capital and operating costs, the addition is easily justified given the relatively high market value of Scandium.

- All assumptions and inputs are identical to ID2, except as noted.
- All chemical consumption values are based on Pilot Test DTK-C16. Dose values (e.g. kg acid/ton feed) are held constant from pilot data.
- A Scandium recovery module (PM7) is added. The cost model is based on ongoing work conducted in DE-FE0031827.

- The Scandium leaching recovery is intensified to 30%; the downstream recovery of scandium is intensified to 80%.
- No other adjustments or intensifications.

ID4: Pilot Plant Data with Optimization, Sc Recovery, and Sorting

Scenario ID4 was evaluated to assess the economic impact of pre-concentration sorting on overall project viability. Other than the increased feed grade and the additional sorter leasing costs, all other inputs are identical to ID3.

- All assumptions and inputs are identical to ID3, except as noted.
- The feed grade to leaching was increased to15%. Sorter Yield = 70%. Sorter c/f = 1.15.
- No other adjustments or intensifications.

ID5: Ammonium Sulfate Leaching

Scenario ID5 was developed to assess an alternative feedstock and leaching approach. Earlier laboratory data showed that the 1.4 SG float material from the West KY No. 13 seam (after roasting) could be effectively leached using modest doses of ammonium sulfate rather than acid. This scenario evaluates that approach and also includes provisions for reduced downstream processing costs due to reduced leachate contamination.

- All assumptions and inputs are identical to ID1, except as noted.
- The chemical consumption values were adjusted to reflect AS leaching of 1.4 Float material (see Zhang and Honaker, 2019a)
- Acid dose = 0.09 kg/t (ph = 4); AS = 120 kg/t (0.1 mol/L); NaOH dose = 20% of baseline.
- The leach % solids is fixed at 10%. The dissolved solids in leaching was reduced to 5%.
- The volatile loss in roasting was increased to 93.3%. The feed rate entering the roaster increased to 6866 tph to maintain feed rate to leaching similar to that of ID1.
- The feed assay and distribution based are on (Zhang and Honaker, 2019a), 30.82 ppm whole sample basis, 460 ppm on an ash basis.
- The leaching time was evaluated from 5 to 300 minutes based on laboratory data. The techno-economic optimum was determined to be 60 minutes.
- No other adjustments or intensifications.

ID6: AS Leaching with Sc Recovery

Similar to Scenario ID3, this scenario makes an incremental change to Scenario ID5 by including a dedicated Scandium recovery circuit.

- All assumptions and inputs are identical to ID5, except as noted.
- A Scandium recovery module (PM7) was added. The cost model is based on ongoing work conducted in DE-FE0031827.
- The Scandium leaching recovery is equal to that of ID5; the downstream recovery is intensified to 80% overall.
- No other adjustments or intensifications.

ID7: Roasted Middlings

When compared to the baseline case, Scenario ID7 assess a different feedstock with a higher REE concentration and a higher leaching recovery in similar chemical conditions. Given the higher carbon content relative to the baseline case, a larger loss of volatiles is expected in the roasting operation, and as a result, a higher roaster feed rate was selected to maintain a consistent feed rate to the leaching vessels.

- All assumptions and inputs are identical to ID1, except as noted.
- All chemical consumption values are based on Pilot Test DTK-C16. Dose values (e.g. kg acid/ton feed) are held constant from pilot data.
- The feed assay and distribution values are based on (Zhang and Honaker, 2019b), 719 ppm on ash basis.
- The leaching recovery is based on (Zhang and Honaker, 2019b), Table 7 data: Middling sample, 0.06 M acid. (Note: data show little variation between HCl and H2SO4 at low doses).
- The leach % solids is fixed at 20%. The dissolved solids in leaching is fixed at 15%.
- The volatile loss in roasting was increased to 70%. The Feed rate entering roaster increased to 1533 tph to maintain leach feed rate similar to ID1.
- The leaching time was evaluated from 5 to 300 minutes based on laboratory data. The techno-economic optimum was determined to be 45 minutes.
- No other adjustments or intensifications.

ID8: Roasted Middlings with Sc Recovery

Similar to Scenario ID3 and ID6, this scenario makes an incremental change to Scenario ID8 by including a dedicated Scandium recovery circuit.

- All assumptions and inputs are identical to ID7, except as noted.
- A Scandium recovery module (PM7) was added. The cost model is based on ongoing work conducted in DE-FE0031827.
- The Scandium leaching recovery is equal to that of ID7; the downstream recovery is intensified to 80% overall.
- No other adjustments or intensifications.

ID9: FBC with Acid Recovery

Scenario ID9 evaluates a novel implementation approach whereby the REE recovery operation is co-located at a waste-to-energy facility. This scenario seeks to leverage both the REE value and the energy value contained in middling or waste coals. If operated in a low temperature range (600 to 800 °C), a fluidized bed combustor (FBC) can increase the REE leachability of the resultant combustion ash in a manner similar to the roasting operation while also co-producing electricity. Prior testing by the project team has shown that the REE leaching characteristics of FBC ash closely resembles that of roasted middlings, usually with deviations in recovery less than 10% (Honaker et al, 2019). Moreover, by reducing the lime addition into the combustion chamber, the off gas from the FBC unit can be captured and used to generate the

sulfuric acid needed for REE leaching. This addition will result in a lower effective acid cost relative to that of bulk acid purchased from a chemical supplier.

For this scenario, an independent techno-economic evaluation was conducted on both the energy production system and the REE recovery plant to determine if both have independent economic benefit. The FBC system was assumed to be a 500 MW unit that burns 30% ash 8,000 BTU/lb. coal with an overall thermal efficiency of 33%. Under these conditions, the unit produces 100 TPH of ash, which is collected and directed to the REE recovery system.

- All assumptions and inputs are identical to ID7, except as noted.
- The economics of the FBC unit are modeled separately. The REE recovery begins with ash feedstock.
- Costs for PM2 (roasting) were removed. Likewise, the crushing and screening components of PM1 were removed, leaving only the cost of the loader in this unit.
- To model the potential acid recovery from the FBC gas, the price of the leaching acid was assumed to 50% of standard bulk price.
- The REE leaching recovery was reduced to 90% of ID7 values to reflect slight differences between roasted middlings and FBC ash.
- The feed stream mass flow was reduced to a value more representative of FBC ash: 100 st/hr, 719 ppm REE, 0% volatile loss.
- No other adjustments or intensifications.

ID10: FBC Ash with Sc Recovery

Similar to aforementioned cases, this scenario makes an incremental change to Scenario ID9 by including a dedicated Scandium recovery circuit.

- All assumptions and inputs are identical to ID9, except as noted.
- A Scandium recovery module (PM7) was added. The cost model is based on ongoing work conducted in DE-FE0031827.
- The Scandium leaching recovery is equal to that of ID9; the downstream recovery is intensified to 80% overall.
- No other adjustments or intensifications.

3.14.6 Results and Discussion

3.14.6.1 Scenario Summary Results

Table 3.14.9 and Table 3.14.10 show the summarized technical and economic results from the 10 scenarios. Further details on these scenarios can be found in the Appendix, which contains detailed reports from the REE-Econ software. In addition, several scenarios are discussed in further detail in individual sections below.

Other than the FBC ash scenarios (IDs 9 and 10), which were assumed to be limited by the ash production, all scenarios utilized a standard feed rate of 460 st/hr. to the leaching unit operation. As described above, the feed rate to the roasting unit (and to the sorter, if applicable) was then varied depending on the carbon content and subsequent volatile loss in the roasting step.

Alternatively, the feed grades (336 to 719 ppm), REE recovery (16.6% to 40.1%), and REE production (188 to 946 t/yr) varied considerably between the scenarios depending on the assumptions and business case.

Of the 10 scenarios, three were found to be economically favorable with a positive NPV (ID6, ID8, and ID10). Each of these three included the dedicated scandium recovery circuit, which in turn lead to an elevated product basket price sufficient to overcome operating and capital costs. Of these three, the ammonium sulfate leaching scenario (ID6) was shown to have the greatest NPV, predominantly due to the relatively high scandium leaching recovery (>30%) and extremely high scandium feed content (>12% of total REEs) associated with the 1.4 float feedstock. However, the scenarios using 1.4 float material both had relatively high capital costs due to the large roasting operation needed to prepare a sufficient amount of feed for the REE production process. In addition, it may also be difficult to procure a sufficient volume of 1.4 float feed material, as this fraction largely constitutes coal with an existing product market To this end, either the roasted middlings scenario (ID8) or FBC scenario (ID10) may be more commercially viable.

Table 3.14.9. Summarized Technical Results from 10 TEA Scenarios

ID	Scenario Name	Feedstock	Leach Feed (tph)	Feed Grade (ppm)	Recovery (%)	REE Prod. (tpy)	TREO Grade (%)
1	Raw Pilot Plant Data	West KY No. 13 Coarse Refuse	460	336	16.6%	188	92.7%
2	Pilot Plant Data w/ Process Optimization	West KY No. 13 Coarse Refuse	460	336	30.5%	345	92.7%
3	Pilot Plant Data w/ Optimization and Sc Recovery	West KY No. 13 Coarse Refuse	460	336	31.7%	359	91.5%
4	Pilot Plant Data w/ Optimization, Sc Recovery, and Sorting	West KY No. 13 Coarse Refuse	460	386	31.7%	413	91.4%
5	AS Leaching	West KY No. 13, 1.4 Float	460	460	23.5%	364	92.0%
6	AS Leaching w/ Sc Recovery	West KY No. 13, 1.4 Float	460	460	25.9%	401	92.9%
7	Roasted Middlings	Pocahontas No. 3 Middlings	460	719	39.1%	946	92.3%
8	Roasted Middlings w/ Sc Recovery	Pocahontas No. 3 Middlings	460	719	40.1%	971	92.4%
9	FBC w/ Acid Recovery	FBC Ash (Roasted Middlings)	100	719	35.0%	184	92.3%
10	FBC Ash w/ Sc Recovery	FBC Ash (Roasted Middlings)	100	719	35.9%	189	92.4%

Table 3.14.10. Summarized Economic Results from 10 TEA Scenarios

ID	Scenario Name	Revenue (Mil $/yr)	OPEX (Mil $/yr)	OPEX ($/kg REE)	CAPEX (Mil $)	CAPEX Intensity $/(kg REE/yr)	NPV (Mil $)	Payback (years)	Product Basket Price ($/kg REE)
1	Raw Pilot Plant Data	$ 3.94	$ 106.96	$ 570.22	$ 111.31	$ 593.44	$ (846.71)	NA	$ 20.99
2	Pilot Plant Data w/ Process Optimization	$ 7.52	$ 96.99	$ 281.44	$ 91.23	$ 264.73	$ (731.08)	NA	$ 21.82
3	Pilot Plant Data w/ Optimization and Sc Recovery	$ 75.90	$ 101.40	$ 282.64	$ 102.09	$ 284.56	$ (327.64)	NA	$ 211.55
4	Pilot Plant Data w/ Optimization, Sc Recovery, and Sorting	$ 87.28	$ 101.99	$ 247.19	$ 102.33	$ 248.02	$ (257.66)	NA	$ 211.55
5	AS Leaching	$ 50.73	$ 113.42	$ 311.54	$ 235.29	$ 646.30	$ (726.05)	NA	$ 139.35
6	AS Leaching w/ Sc Recovery	$ 231.32	$ 123.34	$ 307.25	$ 252.96	$ 630.14	$ 438.25	3.50	$ 576.22
7	Roasted Middlings	$ 40.65	$ 102.39	$ 108.18	$ 121.33	$ 128.20	$ (586.38)	NA	$ 42.95
8	Roasted Middlings w/ Sc Recovery	$ 157.56	$ 107.08	$ 110.32	$ 132.19	$ 136.19	$ 174.88	4.50	$ 162.33
9	FBC w/ Acid Recovery	$ 7.75	$ 18.48	$ 100.42	$ 23.78	$ 129.19	$ (105.27)	NA	$ 42.11
10	FBC Ash w/ Sc Recovery	$ 30.38	$ 19.53	$ 103.49	$ 28.12	$ 149.02	$ 39.42	4.50	$ 160.96

To explore the natural correlations and trends in the overall economic results, additional analyses were conducted comparing the various technical and economic output parameters. Figure 3.14.1, for example, shows the capital intensity (herein defined as dollar of capital of investment per kg/yr of REE production) as a function of REE process recovery. The data, which includes several very distinct models runs, shows a clear exponential trend with an asymptote developing above 40% REE recovery. This result suggests that increased recovery beyond 50% may only provide diminishing returns with respect to capital utilization.

Figure 3.14.2 shows a similar plot; however, in this case, the y axis is operating cost expressed $/kg REE produced. This plot shows a similar asymptote and suggests that very high recoveries may be needed to reduce operating costs below target values of $20 to $50/kg. Both figures indicate that the FBC ash/roasted middlings have the lowest capital intensity and unit operating cost for the scenarios evaluated in this study. Much of this result may be prompted by the higher feed grade for this material.

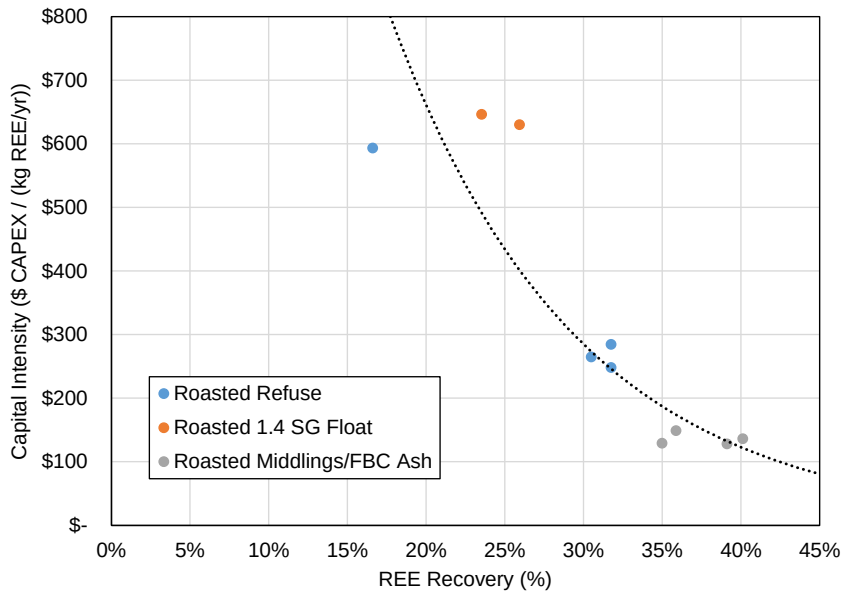

Figure 3.14.1. Relationship between REE recovery and capital intensity (defined as $ of capital cost per kg per year of REE production capacity) for 10 scenarios evaluated in this study.

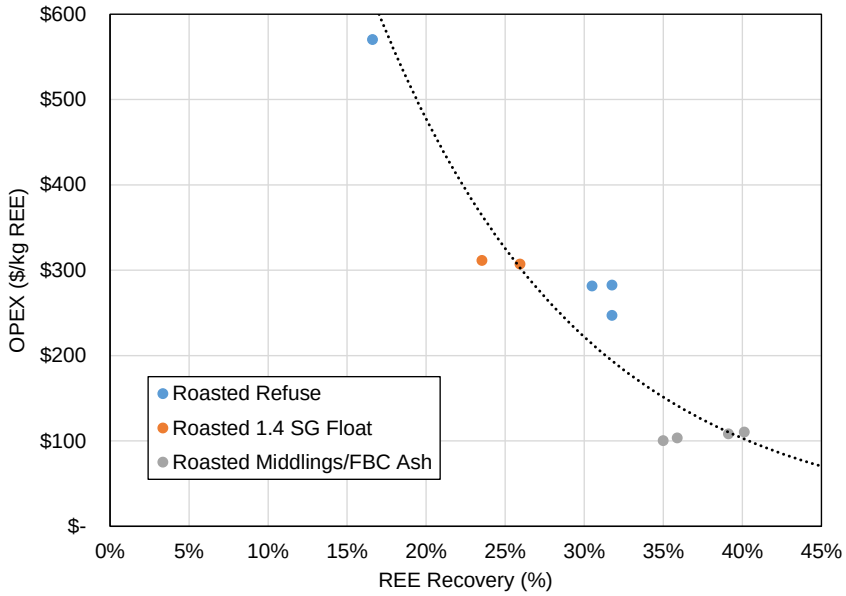

Figure 3.14.2. Relationship between REE recovery and total operating cost ($/kg REE) for 10 scenarios evaluated in this study.

Figure 3.14.3 shows the relationship between project NPV and product basket price. Overall, this trend indicates that across all feedstocks and process options, the basket price must minimally be $150/kg to $200/kg for the project to be economically viable. For the current scenarios, elevated basket price was typically prompted by increased Sc content in the product; however, product basket price could also be promoted by more favorable REE prices or other high value heavy REEs, such Tb and Dy.

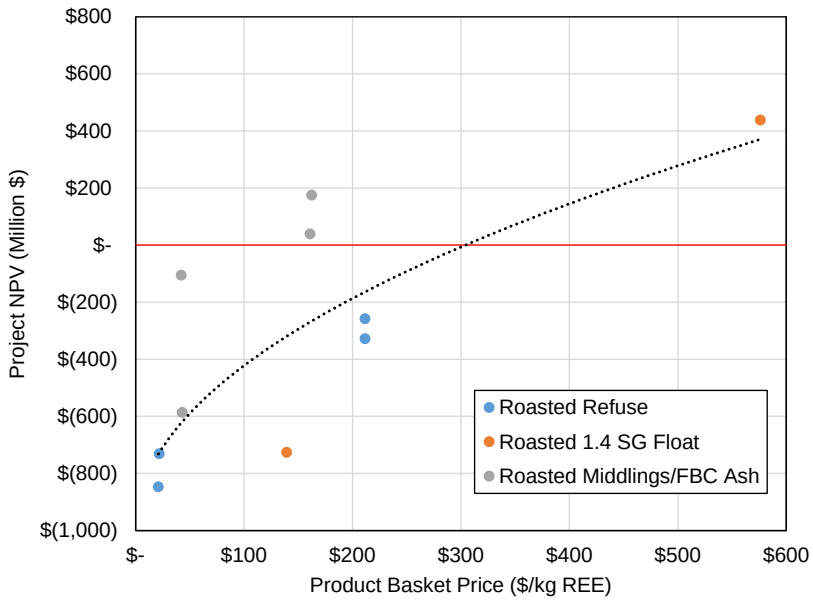

Figure 3.14.3. Relationship between project NPV and product basket price ($/kg REE) for 10 scenarios evaluated in this study.

In addition to these summarized findings, detailed findings from some select scenarios are provided below.

3.14.6.2 Pilot Plant Chemical Cost Data

Throughout pilot-scale testing, 18 independent and unique multi-day pilot runs were conducted to evaluate different chemical conditions and a host of other operational settings. Throughout each test, chemical consumption was monitored, and the final data were normalized to show the chemical cost per mass of REE produced. Throughout the trials, chemical consumption varied from $381 to $2,200 / kg REE, with six of the best runs occurring in the final seven trials. A detailed assessment of the data shows that the first five runs averaged over $1,000 / kg REE, while the last five runs averaged on $460 /kg. This trajectory of reduced processing costs is typical for pilot-scale operations as operators become more familiar with the process and identify opportunities for optimization. It is reasonable to expect that even further optimization may be tenable, and as a result, Scenario ID2 was developed to show the potential for further cost reductions through process optimization. For this reason, Scenario ID2, rather than Scenario ID1, was selected as the base case upon which other scenarios were built.

The data used to build Scenario ID1 was based on the optimal pilot run, DTK-C16, which was conducted over a period of 16 hours and produced 30 grams of MREO product. The total

chemical cost for this run was measured to be $381 /kg REE, which was translated directly to the commercial scale simulation using constant normalized dosing rates (e.g. kg of acid per ton of feed). While this single data point was used for the simulation, analysis of the full set of pilot data reveals some interesting correlations with respect to reagent utilization. Figure 3.14.4 shows three correlation plots for reagents utilized in various unit operations within the process. The top figure shows the correlation between the acid in the leaching operation and the base in the subsequent neutralization operation. The strong positive correlation is expected, as the higher acid concentration will require a proportional increase in base to effectively neutralize the solution to a target endpoint pH. The large variance of base doses at a single leaching dose may be due to either variations in leachate contamination (which will consume base) or variations in the neutralization endpoint during operation.

The next two plots in Figure 3.14.4 show the correlation between oxalic acid and HCl re-dissolution acid as well as NaOH in oxalic acid precipitation and HCl re-dissolution acid. Once again, both of these relationships are anticipated from a fundamental standpoint, and the data here helps to quantify the relationship.

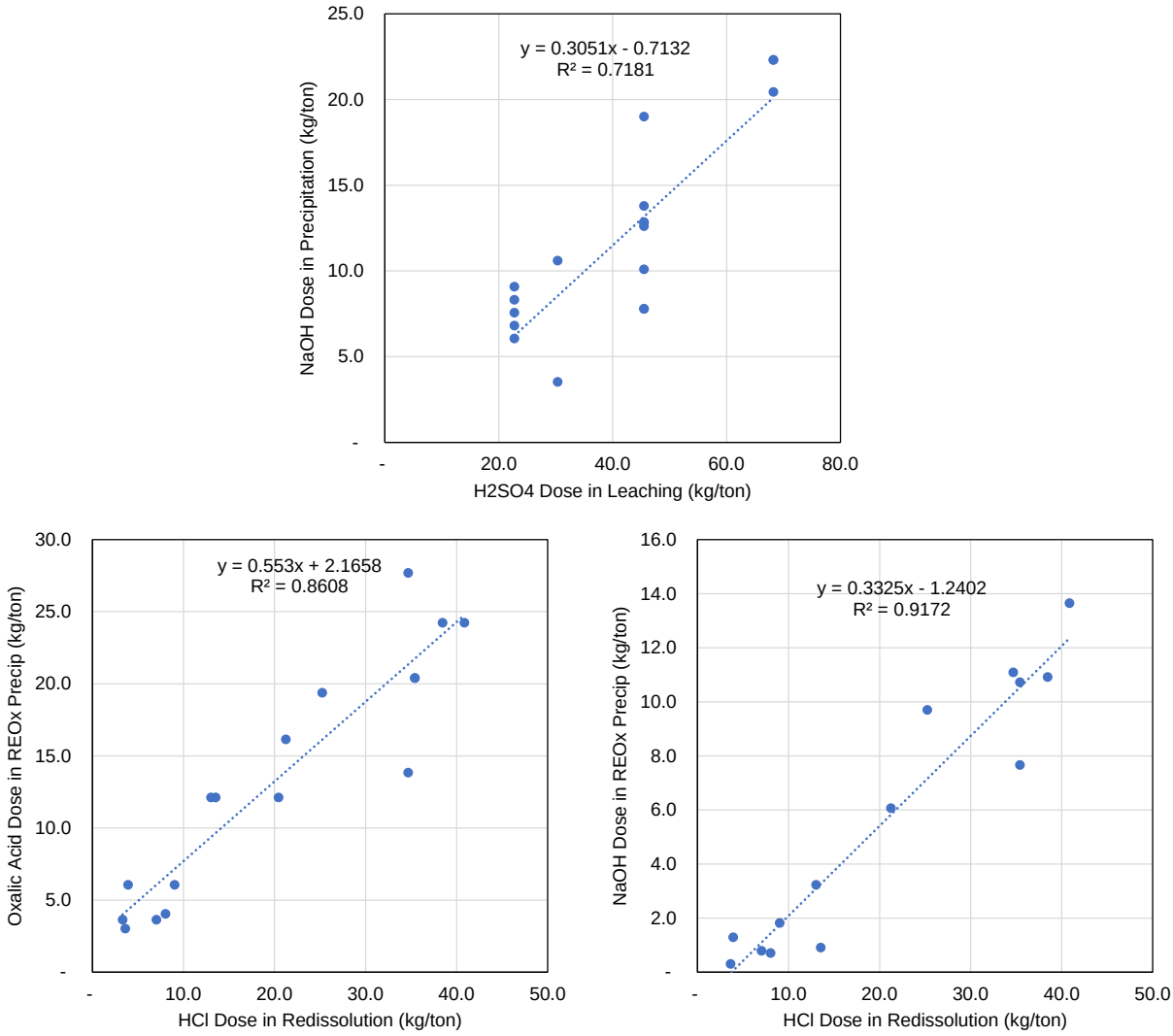

Figure 3.14.4. Reagent utilization correlations determined from multiple pilot-scale trials. All data is shown as mass of reagent normalized to overall plant feed mass.

3.14.6.3 Detailed Analysis of ID2 Data

To demonstrate the relationship between the mass balance and economic assessment, a detailed assessment of the ID2 Scenario is presented herein. Similar data for the other scenarios are included in the *Appendix* to this report. While ID2 did not prompt an economically favorable outcome, it was selected for this detailed analysis, as these findings and the subsequent sensitivity analyses were what prompted the team to look at specific alternative scenarios. Moreover, the material balance and chemical consumption values in ID2 have been largely validated through laboratory and pilot-scale testing.

For the ID2 Scenario, coarse refuse from the West Kentucky No. 13 seam in western Kentucky, was identified as the designated feedstock for the REE recovery process. This feedstock is readily available and was used for laboratory and pilot studies. For this scenario, the nominal feed rate was fixed at 500 st/hr., with the REE grade and distribution shown in Table 3.14.11. Given these feed rate and grade values, the total mass flow of REEs into the process from the feed solids is calculated to be 140 kg/hr.

Table 3.14.11. REE Grade for West Kentucky No. 13 Coarse Refuse material considered in techno-economic analysis.

REE	Feed Conc. (ppm)	Distribution (%)
Scandium	16.77	5.43
Yttrium	25.28	8.18
Lanthanum	50.30	16.28
Cerium	113.49	36.73
Praseodymium	12.38	4.01
Neodymium	47.46	15.36
Samarium	13.67	4.42
Europium	1.81	0.58
Gadolinium	11.09	3.59
Terbium	0.52	0.17
Dysprosium	4.64	1.50
Holmium	2.84	0.92
Erbium	4.38	1.42
Thulium	0.77	0.25
Ytterbium	3.35	1.09
Lutetium	0.26	0.08
Total REE	**309**	**100.00**

To determine the overall recovery of REEs to the product stream, element-by-element recovery values from individual unit operations were combined in a simple multiplicative manner. Table 3.14.12 shows these recovery values, itemized by individual REE and unit operation. For this "optimized" case, these recovery values were determined from sequential batch laboratory testing of the individual unit operations on a consistent feedstock. These values are commensurate with those in the pilot plant operation and are reasonable for the level of chemical intensity.

Table 3.14.12. Element-by-element recovery values by unit operation used in techno-economic analysis

REE	Recovery in Various Unit Operations				Total
	Leaching	Precipitation	Re-Dissolution	OXP Precipitation	
Scandium	6.3%	100.0%	47.6%	30.6%	0.9%
Yttrium	15.7%	100.0%	99.4%	76.7%	11.9%
Lanthanum	44.0%	99.0%	96.5%	80.6%	33.9%
Cerium	47.3%	99.4%	89.6%	88.1%	37.2%
Praseodymium	53.3%	99.0%	78.8%	90.5%	37.6%
Neodymium	45.0%	100.0%	91.3%	92.7%	38.1%
Samarium	40.5%	100.0%	90.0%	94.8%	34.6%
Europium	34.2%	95.4%	92.0%	93.1%	27.9%
Gadolinium	52.0%	98.1%	52.8%	91.2%	24.6%
Terbium	15.5%	100.0%	0.0%	0.0%	0.0%
Dysprosium	26.0%	94.4%	100.0%	80.6%	19.8%
Holmium	10.7%	90.0%	100.0%	0.0%	0.0%
Erbium	0.0%	0.0%	95.7%	79.3%	0.0%
Thulium	30.7%	51.6%	92.2%	16.8%	2.5%
Ytterbium	9.8%	100.0%	75.1%	74.4%	5.5%
Lutetium	16.2%	98.5%	66.9%	75.6%	8.1%

To support the economic analysis, these recovery values and other technical factors and reagent consumption rates were used to generate simplified material balances for each individual process module. These material balances not only show major solid mass and liquid flow, but they also show the balance of REEs throughout the circuit as well as the dosing rates for major consumables. Figure 3.14.5 through Figure 3.14.10 show these material balances for process modules PM1 through PM6 respectively.

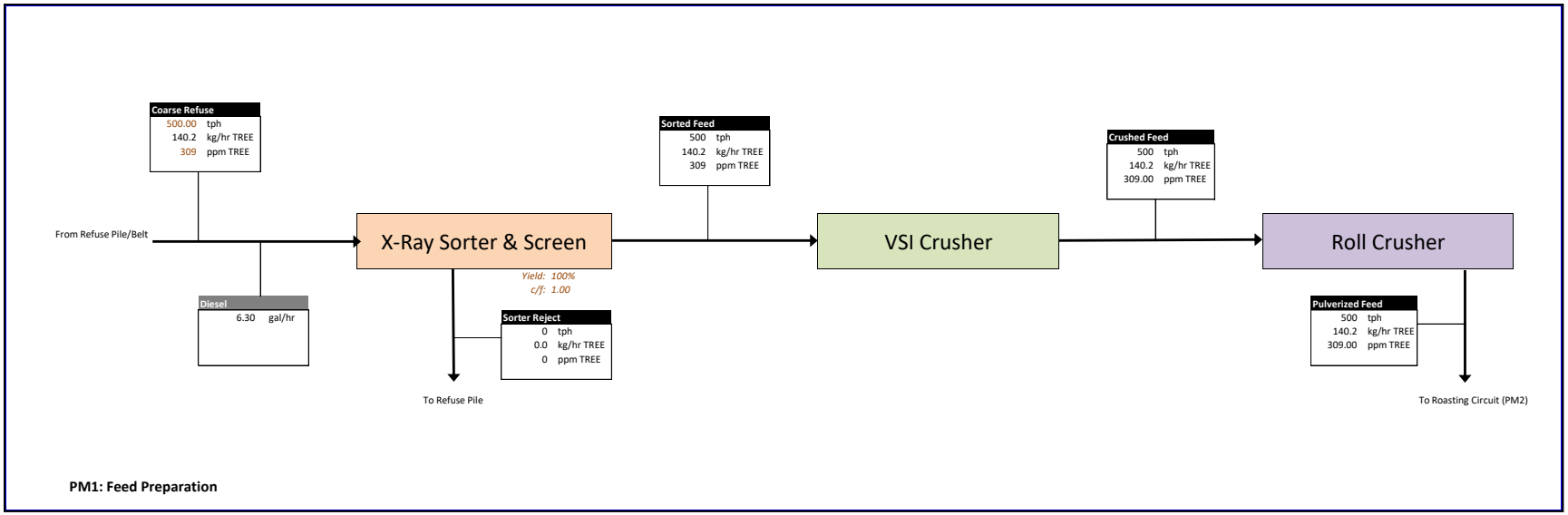

Figure 3.14.5. Mass, water, and reagent balance for PM1: Feed Preparation.

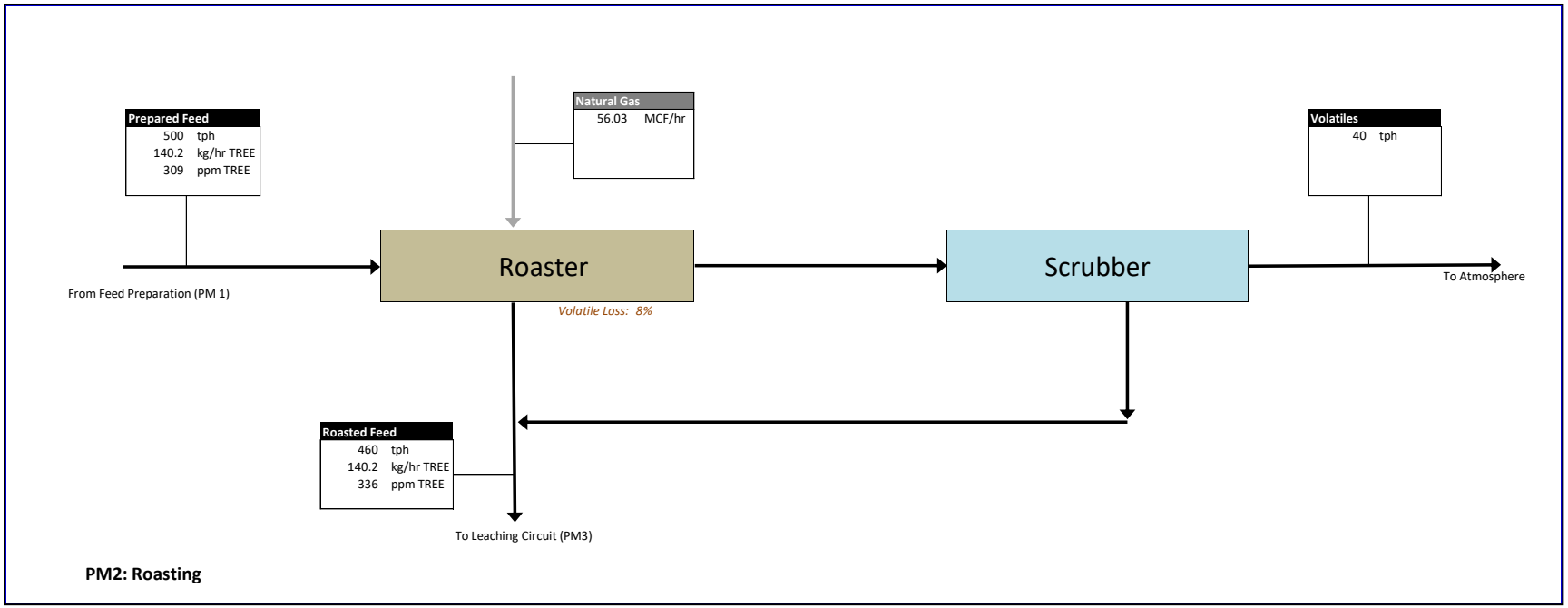

Figure 3.14.6. Mass, water, and reagent balance for PM2: Roasting.

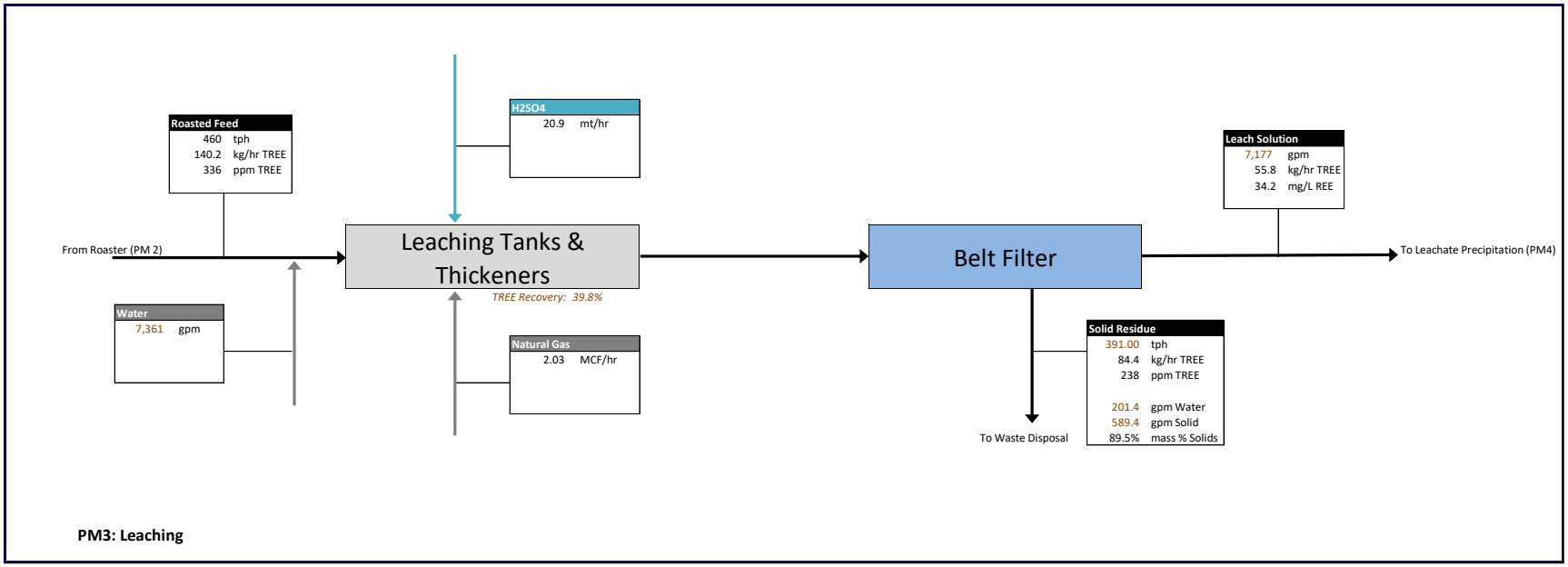

Figure 3.14.7. Mass, water, and reagent balance for PM3: Leaching.

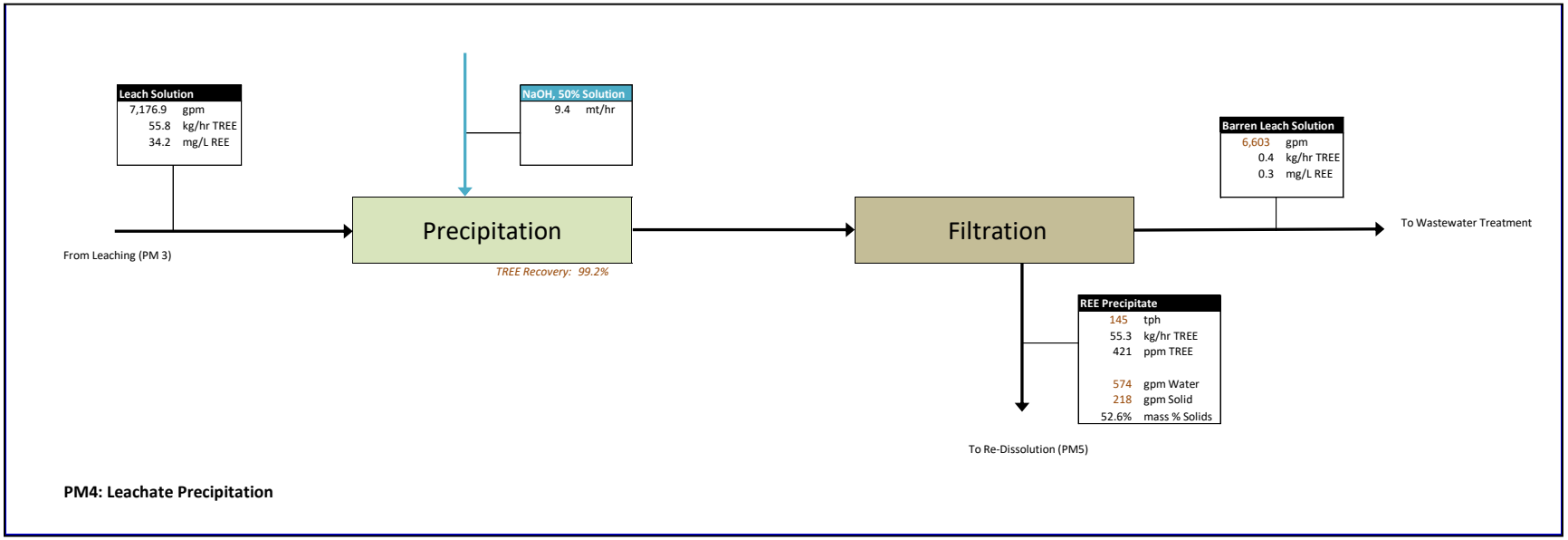

Figure 3.14.8. Mass, water, and reagent balance for PM4: Leachate Precipitation.

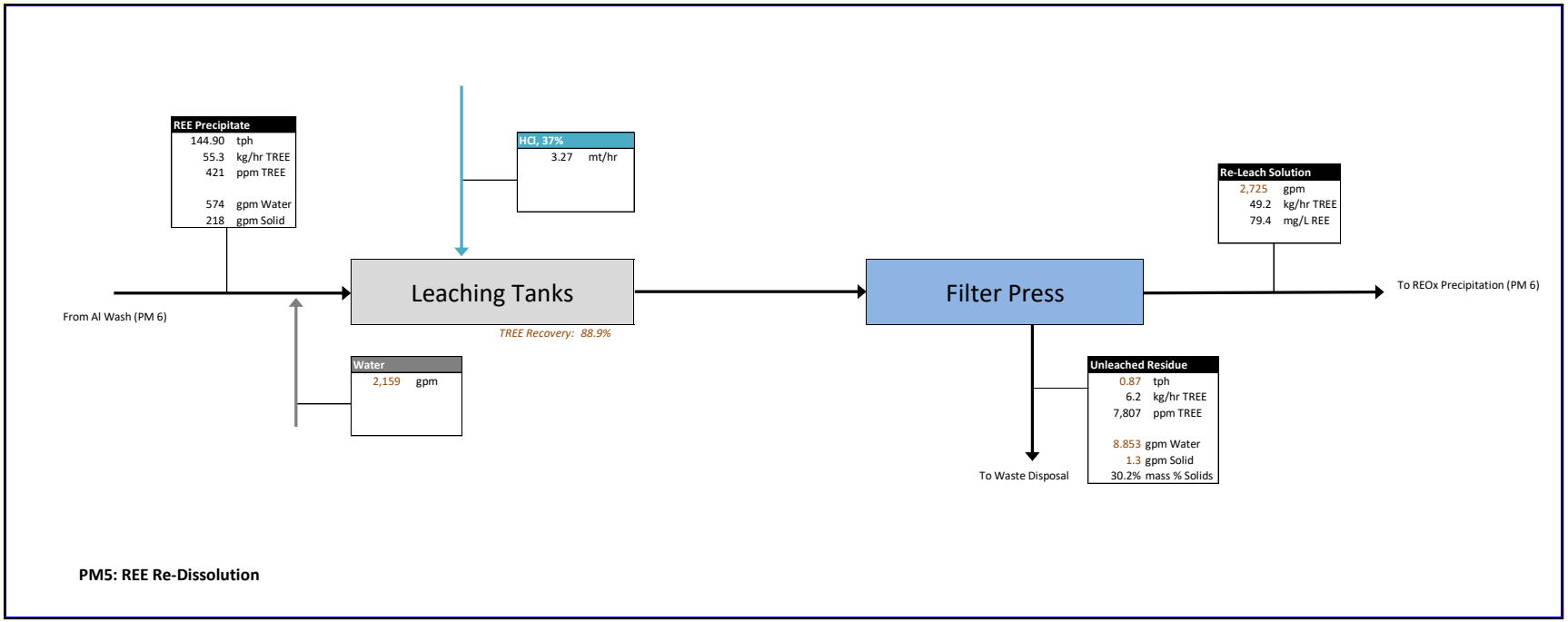

Figure 3.14.9. Mass, water, and reagent balance for PM5: REE Re-Dissolution.

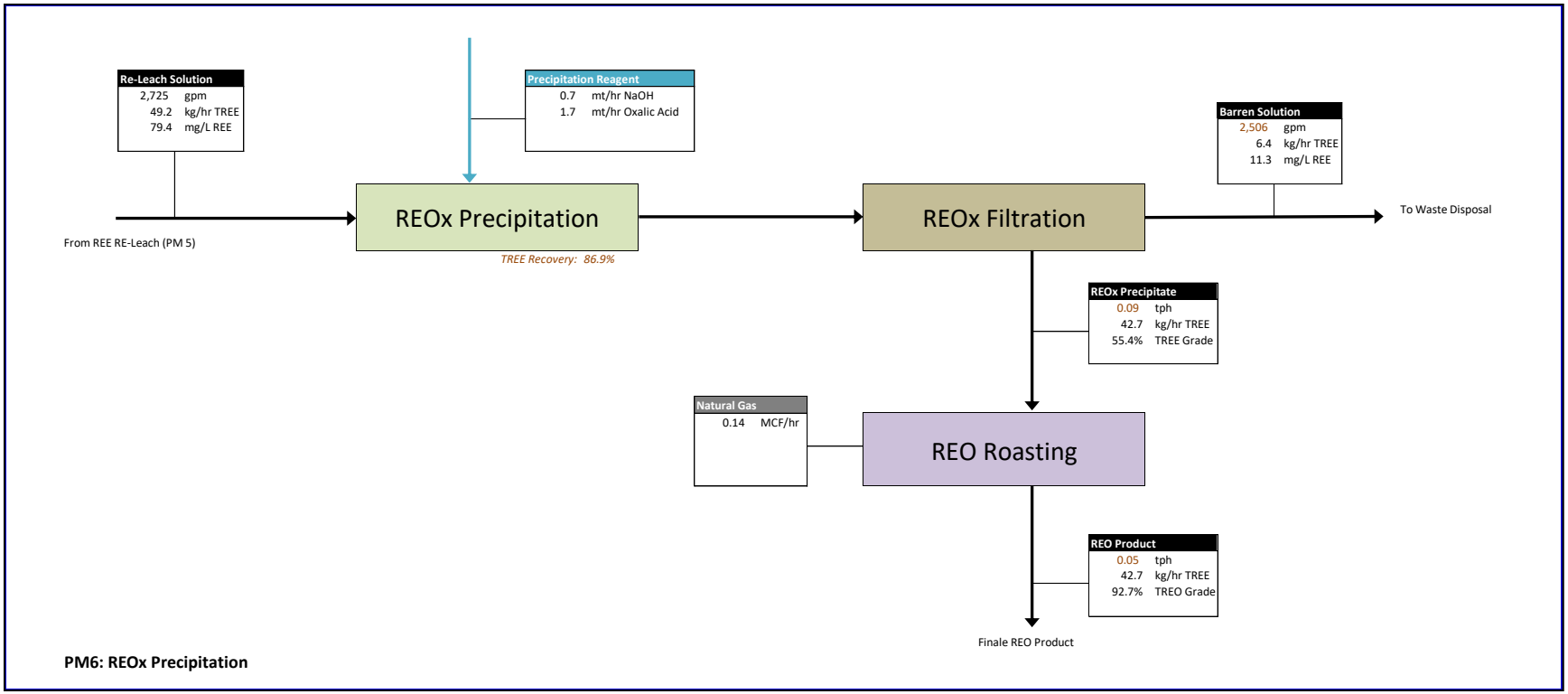

Figure 3.14.10. Mass, water, and reagent balance for PM6: REOx Precipitation.

Using these material balances as well as the cost models descripted above, the total capital cost for the 500 st/hr. plant was determined to be approximately $91 million. Table 3.14.13 shows this cost itemized by process module and capital cost category. This analysis shows that the roasting circuit and the leaching circuit are the most significant capital costs, each contributing approximately 30% of the total.

Table 3.14.13. Module-level capital cost for commercial scale plant, Scenario ID 2 (500 st./hr).

Module ID	Process Module	Equipment Cost	Ancillary	Buildings	EPCM	Contingency	TOTAL PLANT COST Index Year	TOTAL PLANT COST Constructed Year
PM1	Feed Preparation	$ 1,820,387	$ 1,055,824	$ 1,183,251	$ 1,074,028	$ 273,058	$ 5,406,548	$ 6,432,532
PM2	Roasting	$ 9,340,565	$ 5,417,527	$ 6,071,367	$ 5,510,933	$ 1,401,085	$ 27,741,477	$ 33,005,892
PM3	Leaching	$ 8,183,634	$ 4,746,508	$ 5,319,362	$ 4,828,344	$ 1,227,545	$ 24,305,394	$ 28,917,754
PM4	Leachate Precipitation	$ 4,301,024	$ 2,494,594	$ 2,795,666	$ 2,537,604	$ 645,154	$ 12,774,041	$ 15,198,132
PM5	RE-Redissolution	$ 1,180,435	$ 684,652	$ 767,283	$ 696,456	$ 177,065	$ 3,505,891	$ 4,171,193
PM6	REE Oxalate Precipitation	$ 991,967	$ 575,341	$ 644,779	$ 585,261	$ 148,795	$ 2,946,143	$ 3,505,224
	TOTAL:	**$ 25,818,011**	**$ 14,974,447**	**$ 16,781,707**	**$ 15,232,627**	**$ 3,872,702**	**$ 76,679,494**	**$ 91,230,727**

Final summaries of total operating cost by cost type and cost center are given in Table 3.14.14. As shown, the total operating cost for this process was determined to be $281 / kg REE produced, which represents a notable improvement over prior analyses conducted on similar REE recovery operations. An assessment of the cost breakdown shows that consumables are the single largest cost item, representing nearly 70% of the total costs. Nevertheless, the chemical cost for this scenario ($203 / kg REE) was superior to that of the raw plant data ($385 / kg REE) primarily through improved REE recovery (i.e. total chemical cost was similar for the two studies). General overhead costs constituted the next largest item; however, this category was a much smaller fraction, only 13% of the total.

With respect to process module, the leaching operation was the costliest, representing 40% of the total. Given the high relative significance of power and chemical costs, those expenses have been itemized separately, by process module, Table 3.14.15 and Table 3.14.16, respectively. This data shows that the total chemical cost is $203/ kg REE, with the primary contributors being leaching and to a lesser extent leachate precipitation. Likewise, power costs were much smaller in magnitude, only requiring $7.78 / kg REE. Altogether, these results indicate that leaching acid is the single highest cost item for process and likely, the item with the most potential for improvement.

Additional itemized line-by-line costing details for all process modules and all cost components can be found in the *Appendix* to this report.

Table 3.14.14. Total operating cost breakdown for commercial-scale plant, Scenario ID2 (500 st/hr.).

Summary by Cost Type

Cost Type	Shift Cost	Daily Cost	Annual Cost	Per kg Cost	Per Ton Cost	Relative Cost
Fixed	$ 4,547.14	$ 13,641.41	$ 4,583,514	$ 13	$ 1.14	II
Power	$ 2,660.44	$ 7,981.32	$ 2,681,724	$ 8	$ 0.67	I
Consumables	$ 71,766.96	$ 215,300.88	$ 72,341,094	$ 210	$ 17.94	IIIIIIIIIIIIIIIIIIIIIIIIIIIIIIIIIIII
Leasing/Tolling	$ -	$ -	$ -	$ -	$ -	
Waste Disposal	$ 4,695.66	$ 14,086.97	$ 4,733,222	$ 14	$ 1.17	II
General Overhead	$ 12,550.53	$ 37,651.59	$ 12,650,933	$ 37	$ 3.14	IIIIII
TOTAL	$ 96,221	$ 288,662	$ 96,990,488	$ 281	$ 24.06	

Summary by Process Module

Process Module	Shift Cost	Daily Cost	Annual Cost	Per kg Cost	Per Ton Cost	Relative Cost
Feed Preparation	$ 695	$ 2,084	$ 700,135	$ 2.03	$ 0.17	
Roasting	$ 1,407	$ 4,221	$ 1,418,343	$ 4.12	$ 0.35	
Leaching	$ 38,030	$ 114,091	$ 38,334,645	$ 111.24	$ 9.51	IIIIIIIIIIIIIIIIII
Leachate Precipitation	$ 16,206	$ 48,619	$ 16,336,101	$ 47.40	$ 4.05	IIIIIIII
RE-Redissolution	$ 7,770	$ 23,311	$ 7,832,359	$ 22.73	$ 1.94	III
REE Oxalate Precipitation	$ 10,319	$ 30,956	$ 10,401,235	$ 30.18	$ 2.58	IIIII
Reserved	$ -	$ -	$ -	$ -	$ -	
Reserved	$ -	$ -	$ -	$ -	$ -	
Reserved	$ -	$ -	$ -	$ -	$ -	
Reserved	$ -	$ -	$ -	$ -	$ -	
Reserved	$ -	$ -	$ -	$ -	$ -	
Unallocated	$ 21,793	$ 65,380	$ 21,967,670	$ 64	$ 5.45	IIIIIIIIII
TOTAL	$ 96,221	$ 288,662	$ 96,990,488	$ 281	$ 24.06	

Summary by Cost Center

Cost Center	Code	Shift Cost	Daily Cost	Annual Cost	Per kg Cost	Per Ton Cost	Relative Cost
Operating Labor	OL	$ 1,617.20	$ 4,851.60	$ 1,630,138	$ 5	$ 0.40	
Technical Labor	TL	$ 678.20	$ 2,034.60	$ 683,626	$ 2	$ 0.17	
Power/Utilities	PR	$ 2,660.44	$ 7,981.32	$ 2,681,724	$ 8	$ 0.67	I
Lease Agreements	LS	$ -	$ -	$ -	$ -	$ -	
Consumables/Reagents	CR	$ 71,766.96	$ 215,300.88	$ 72,341,094	$ 210	$ 17.94	IIIIIIIIIIIIIIIIIIIIIIIIIIIIIIIIIIII
Waste Disposal	WD	$ 4,695.66	$ 14,086.97	$ 4,733,222	$ 14	$ 1.17	II
Plant Overhead	OH	$ 13,617.32	$ 40,851.95	$ 13,726,254	$ 40	$ 3.40	IIIIII
General Sales, and Administration	GSA	$ 1,184.95	$ 3,554.85	$ 1,194,430	$ 3	$ 0.30	
Reserved							
Reserved							
TOTAL		$ 96,221	$ 288,662.17	$ 96,990,488	$ 281	$ 24.06	

Table 3.14.15. Power cost summary by process module for commercial-scale plant, Scenario ID2 (500 st/hr.).

Module ID	Process Module	Total HP	Shift Cost	Daily Cost	Annual Cost	Cost Per Total Product kg	Cost Per Plant Feed Short-Ton
PM1	Feed Preparation	1,239	$ 593.78	$ 1,781	$ 598,529	$ 1.74	$ 0.15
PM2	Roasting	261	$ 125.10	$ 375	$ 126,098	$ 0.37	$ 0.03
PM3	Leaching	2,393	$ 1,147.25	$ 3,442	$ 1,156,431	$ 3.36	$ 0.29
PM4	Leachate Precipitation	1,010	$ 483.96	$ 1,452	$ 487,831	$ 1.42	$ 0.12
PM5	RE-Redissolution	378	$ 181.00	$ 543	$ 182,449	$ 0.53	$ 0.05
PM6	REE Oxalate Precipitation	270	$ 129.35	$ 388	$ 130,385	$ 0.38	$ 0.03
	Total:	**5,550**	**$ 2,660.44**	**$ 7,981**	**$ 2,681,724**	**$ 7.78**	**$ 0.67**

Table 3.14.16. Chemical cost summary by process module for commercial-scale plant, Scenario ID2 (500 st/hr.).

Module ID	Process Module	Shift Cost	Daily Cost	Annual Cost	Cost Per Total Product kg	Cost Per Plant Feed Short-Ton
PM1	Feed Preparation	$ 100.80	$ 302	$ 101,606	$ 0.29	$ 0.03
PM2	Roasting	$ 1,281.99	$ 3,846	$ 1,292,244	$ 3.75	$ 0.32
PM3	Leaching	$ 36,883.15	$ 110,649	$ 37,178,214	$ 107.88	$ 9.22
PM4	Leachate Precipitation	$ 15,722.49	$ 47,167	$ 15,848,270	$ 45.99	$ 3.93
PM5	RE-Redissolution	$ 7,589.20	$ 22,768	$ 7,649,910	$ 22.20	$ 1.90
PM6	REE Oxalate Precipitation	$ 10,189.34	$ 30,568	$ 10,270,850	$ 29.80	$ 2.55
	Total:	**$ 71,766.96**	**$ 215,301**	**$ 72,341,094**	**$ 209.92**	**$ 17.94**

Using these cost values as well as the revenue from the sale of the mixed rare earth concentrate, a pro forma cash flow was developed and several economic indicators were derived. Table 3.14.17 provides the final economic summary for this scenario.

Table 3.14.17. Final Economic Summary for Scenario ID2.

Parameter	Unit	Value
Technical Results		
Plant Feed Rate	sTPH	500
Plant Feed Grade	ppm	309
Overall REE Production	kg/hr	42.7
Economic Results		
Overnight Capital Cost	$	91,230,727
Constant Dollar OPEX	$ / yr	96,990,488
(unit conversion)	$/ st feed	24.06
(unit conversion)	$ /kg REE	281.44
Constant Dollar Revenue	$ / yr	7,520,454
Net Present Value (@10% discount)	$	(731,084,271)
Internal Rate of Return	%	N/A
Payback Period	Operating Years	N/A

While this scenario was not economically favorable on its own, it did provide a platform to conduct detailed sensitivity analyses to identify cost drivers as well as a potential pathway to economic viability. The first sensitivity analysis was evaluated to determine the influence of several technical parameters on total operating costs. Figure 3.14.11 shows this analysis, presented here as a tornado graph with the extent of each bar representing a +/- 30% change on the baseline input value. This data shows that REE grade and REE recovery (and REE production by proxy) are the two most sensitive parameters in the model, showing a range nearly two times greater than the next model parameter. With respect to consumables, the leaching acid was found to the most important; however, the HCl consumption is the re-dissolution also has a significant impact on overall operating costs. Leach percent solids, feed rate, and leaching retention time were found to be much less significant in the model. Moreover, given the relatively small magnitude of power, labor, and other cost categories were not considered in this analysis due to their overall low magnitude relative to that of chemical costs.

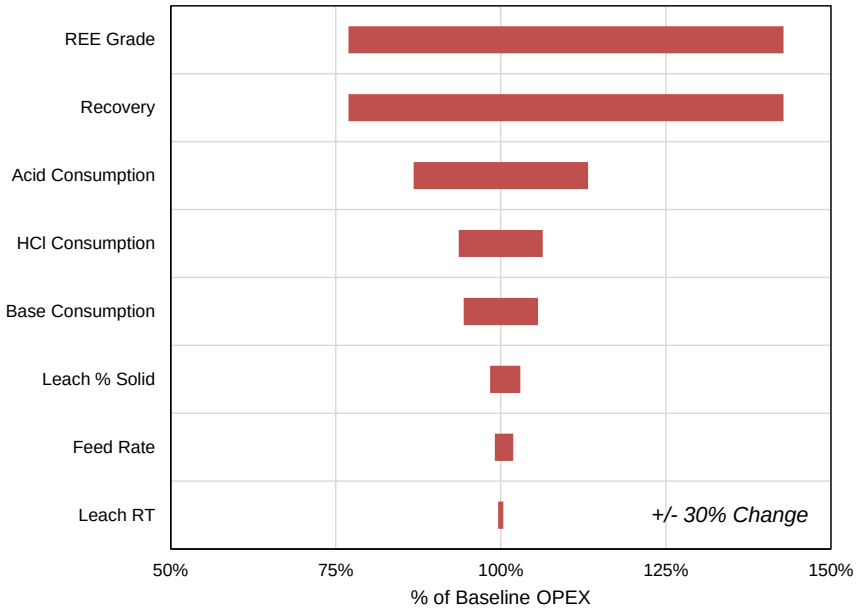

Figure 3.14.11. Sensitivity analysis showing the effect of key technical parameters on total operating cost for Scenario ID2. Limits of tornado graph indicate +/- 30% change in the input value.

Figure 3.14.12 shows the sensitivity of the overall plant capital cost as a function of plant feed. This curve follows a clear power law trend with an overall an exponent of 0.5. The power law trend is anticipated given the capital cost estimation procedures; however, the exponent is lower than typical values for chemical processes that range from 0.6 to 0.7. This result is likely due to the high prevalence of unit operation with lower exponent values, including leach tanks, pumps, mixers, and filters (see Table 3.14.3).

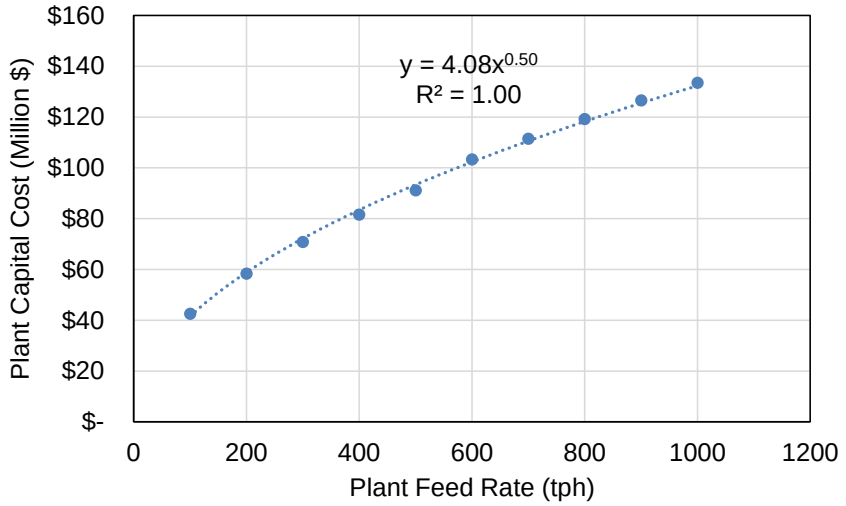

Figure 3.14.12. Sensitivity analysis showing the effect of plant feed rate on total plant capital costs for Scenario ID2.

Figure 3.14.13 shows a similar analysis, depicting the plant operating costs ($/kg REE produced) as a function of plant feed. This graph illustrates the economy of scale associated with higher feed rates. Since a large portion of the operating costs are chemical costs, which

scale linearly with feed rate, the cost savings due to economy of scale are very limited for this plant, particularly for plants greater than 200 to 250 tph.

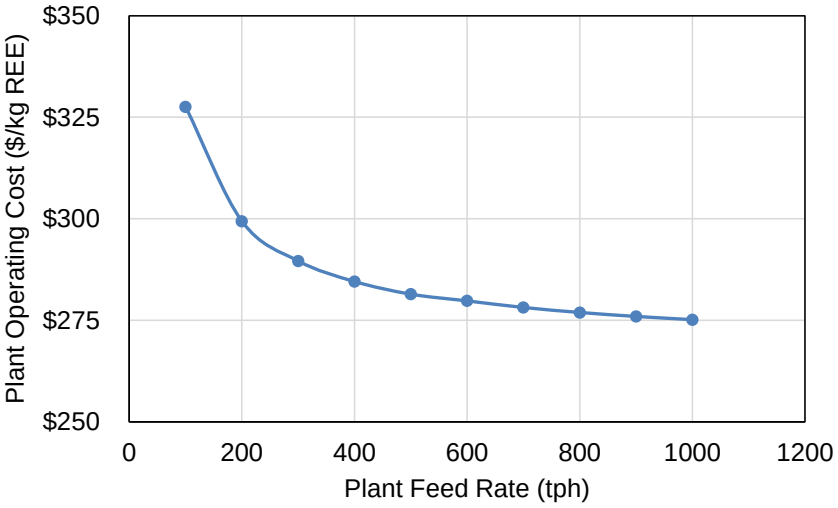

Figure 3.14.13. Sensitivity analysis showing the effect of plant feed rate on total plant operating costs for Scenario ID2

To further investigate the influence of key technical parameters on project capital costs, a two factor analysis was conducted simultaneously evaluating feed rate and leaching percent solids. Figure 3.14.14 show the results from this analysis, with the y-axis here representing capital intensity ($/(kg REE/yr)) rather than raw capital costs. For reference, the baseline case (500 tph, 20% solids is also shown on the plot). This graph indicates that capital intensity scales exponentially with respect to feed rate and even in the ranges evaluated, increases in feed rate can prompt significant reductions in capital intensity. While not directly shown on this plot, comparisons between the data series show that leaching percent solids also produces an exponential trend, as the capital intensity reduction between 20% and 30% is not as great as that between 10% and 20%. Thus percent solids values above 20% are likely only producing diminishing returns with respect to leaching percent solids. Nevertheless, higher percent solids should still be explored, as they will lead to reduced wastewater and potential higher loading of REEs in the leachate.

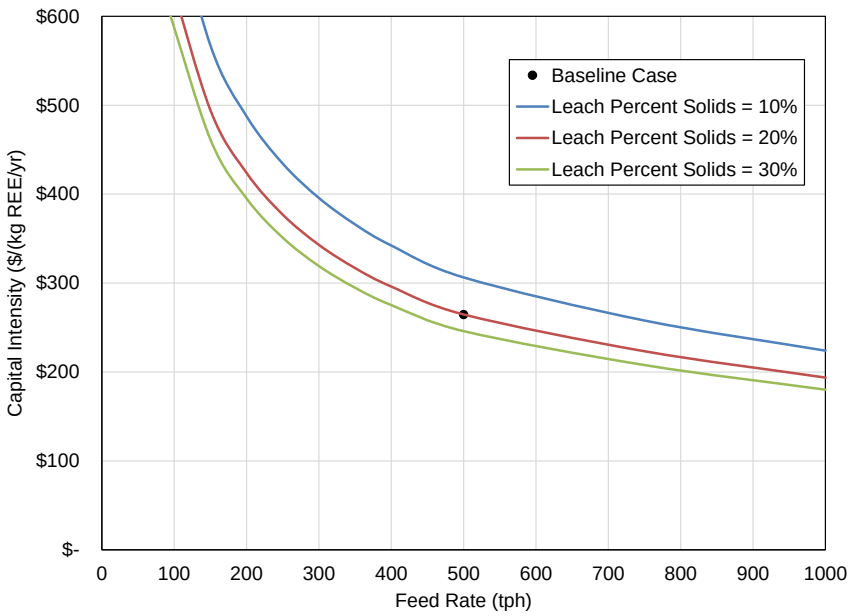

Figure 3.14.14. Sensitivity analysis showing the combined effect of plant feed rate and leach percent solids on capital intensity for Scenario ID2. Here capital intensity is defined as $ of capital cost per kg/yr of REE production.

Since the one-variable-at-a-time tornado analysis (Figure 3.14.11) showed that feed grade and acid cost were important variables with respect to processing cost, a two factor analysis was conducted to evaluate the simultaneous influence of these two parameters. Figure 3.14.15 shows the results of this analysis, with feed grade varying between 200 and 1000 ppm, while the acid cost varies from a 50% reduction to a 50% increase relative to baseline values. This result shows that operating costs follow an exponential trend with respect to feed grade, with costs below $100/kg only occurring in cases where feed grade is greater than 700 to 900 ppm. At low feed grades, the impact of acid reduction is more pronounced; however, as the feed grade increases, the absolute cost reduction from acid cost reduction is reduced. At the baseline value (approximately $281/kg), a 50% reduction in acid cost reduces overall costs to $219 /kg, a 23% reduction. This same cost reduction could also be achieved by increasing the feed grade to approximately 400 ppm (about 28% above baseline values).

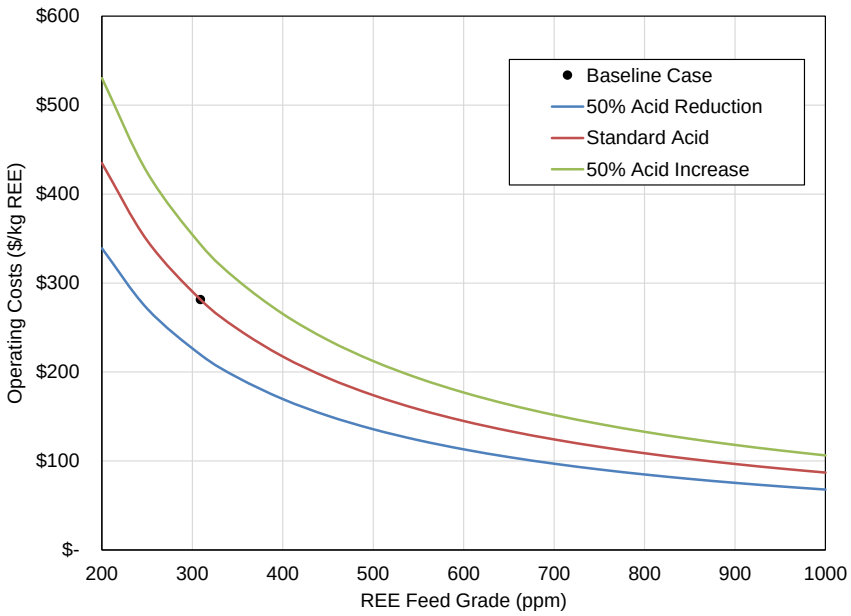

Figure 3.14.15. Sensitivity analysis showing the combined effect of plant feed grade and acid consumption/cost on capital intensity for Scenario ID2.

Altogether, this sensitivity analysis as well as the bulk data analysis shown in Figure 3.14.1 through Figure 3.14.3 suggest that the keys to better economic outcomes include: (1) increased basket price above $150 to $200 /kg; (2) reduced acid cost/consumption to 50% to 75% of baseline values; (3) increased feed grade above 700 ppm; and (4) some combination of all.

3.14.6.4 Analysis of Favorable Scenarios

Of the 10 scenarios evaluated in this study, three were found to be economically favorable. The final economic indicates from these scenarios are shown in Table 3.14.18. These three scenarios represent three distinct implementation approaches, and as such, they represent a broad range of input conditions with respect to feed rate, grade, and REE production capacity. It should be noted that the economic indicates for Scenario ID10 only include the REE recovery operation, as the energy production operation is considered an economically independent operation. Nevertheless, a high level economic summary of the energy production is given in Section 3.14.6.6 to demonstrate the standalone economic viability.

As shown in Table 3.14.18, the NPV values for the three favorable scenarios vary from $39 million for the smaller plant depicted in Scenario ID10 to $438 million for the larger plant depicted in Scenario ID6. Likewise, the rates of return vary from 27.7% to 33.1% with the larger investment (ID6) producing the highest net present value. Nevertheless, given the close range of payback periods (4 to 5 years), a similar argument for commercialization could be made for either case. To evaluate the robustness and risk factors associated with each case, additional sensitivity analyses were conducted.

Table 3.14.18. Final Economic Summary for Favorable Economic Scenarios. ID6 = ammonium sulfate leaching of 1.4 float material; ID8 = acid leaching of roasted middlings; ID10 = acid leaching of FBC ash.

Parameter	Unit	Scenario ID6	Scenario ID8	Scenario ID10
Technical Results				
Roaster Feed Rate	sTPH	6,866	1,533	NA
Roaster Feed Grade	ppm	31	216	NA
Leaching Feed Rate	sTPH	460	460	100
Leaching Feed Grade	ppm	460	719	719
Overall REE Production	kg/hr	49.8	120.4	23.4
Economic Results				
Overnight Capital Cost	$	252,964,159	132,185,069	28,122,692
Constant Dollar OPEX	$ / yr	123,342,510	107,077,702	19,530,858
(unit conversion)	$/ st feed	2.23	8.66	24.22
(unit conversion)	$ /kg REE	307.25	110.32	103.49
Constant Dollar Revenue	$ / yr	231,316,521	157,556,578	30,376,468
Net Present Value (@10% discount)	$	438,248,786	174,883,080	39,424,269
Internal Rate of Return	%	33.1%	27.7%	28.8%
Payback Period	Operating Years	4	5	5

Scenario ID6: Ammonium Sulfate Leaching with Scandium Recovery

The experimental data used to build Scenario ID6 included laboratory ammonium sulfate leaching conducted as a function of leaching retention time. During the test, samples were collected at staggered intervals varying from 5 minutes to 300 minutes. To determine the optimal leaching time in the commercial operation, a sensitivity analysis was conducted to evaluate the economic indicators at each increment of leaching time. Results from this analysis are shown in Figure 3.14.16. The upper-right plot shows the measured REE recovery values (after accounting for losses downstream from leaching), while the three other plots show various economic indicators. This data indicates that 60 minutes produced the maximum net present value; however, extended leaching times time sup to 120 minutes did not prompt an appreciable reduction in net present value. The other data series behave as anticipated: capital costs increase following a power law trend, while operating costs decrease rapidly at first followed by a period of diminishing returns. Based on this analysis, 60 minutes was selected as the optimal value and was subsequently used for the final data presented in this report.

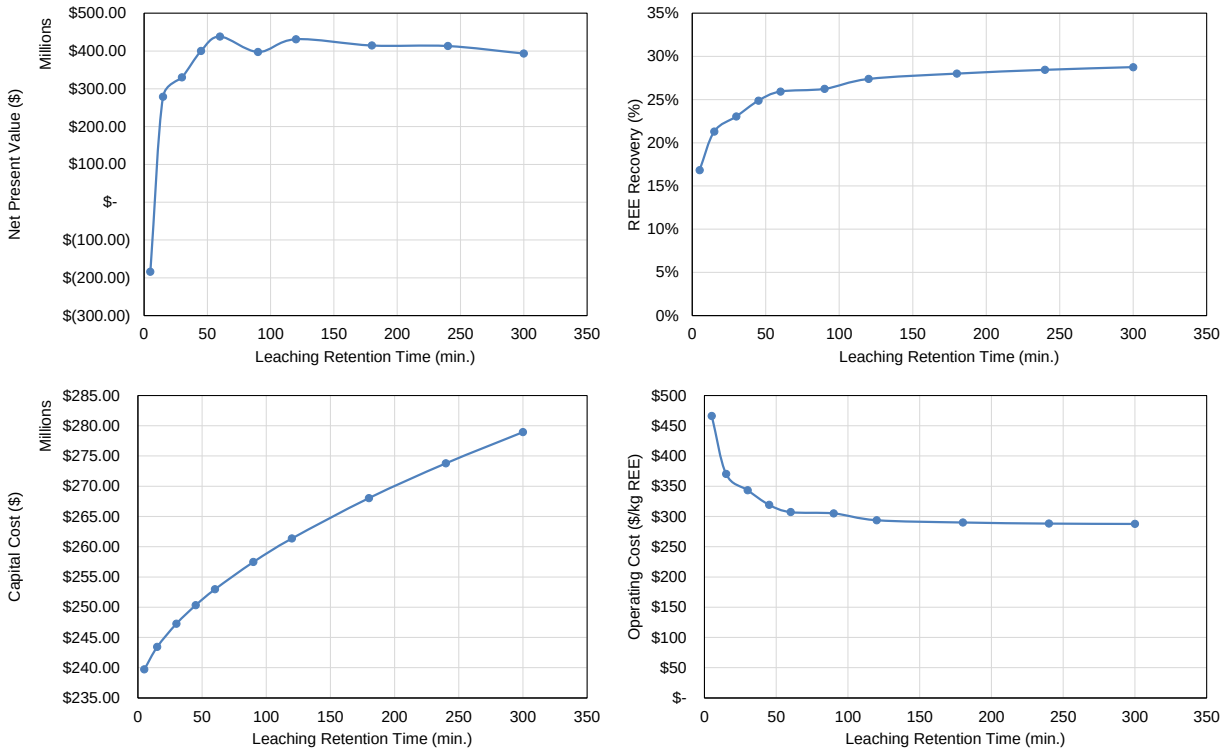

Figure 3.14.16. Sensitivity analysis showing the impact of leaching retention time on net present value, REE recovery, plant capital costs, and plant operating costs for Scenario ID 6. Leaching data based on laboratory testing at the designated leaching times.

Figure 3.14.17 shows the simultaneous impact of overall REE recovery and scandium market price on project net present value. While the economic assessment for this scenario was found to be favorable, it was also shown to be very sensitive to scandium price. The base price used in this analysis ($4,200 / kg) is extremely elevated and may not be indicative of current market prices. A lower scandium price prompts a negative NPV; however, this result can be rectified by increased REE recovery. Breakeven REE recoveries for the three scandium prices used in this analysis were determined to be approximately 20%, 31%, and 63%

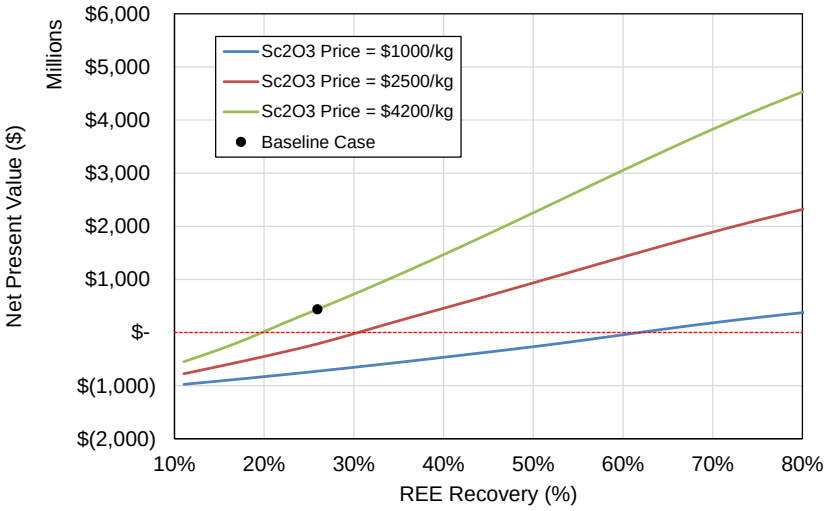

Figure 3.14.17. Sensitivity analysis showing the combined effect of scandium oxide price and overall REE recovery on project net present value for Scenario ID6.

Scenario ID8: Roasted Middlings with Scandium Recovery

As in the prior case, the experimental data used to build Scenario ID8 included laboratory-scale testing at different leaching times. A similar techno-economic optimization study was conducted and the findings are shown in Figure 3.14.18. This data shows that leaching recoveries of 45 to 90 minutes produced the maximum NPV; however, unlike the prior case, this NPV data drops off rapidly at retention times greater than 100 minutes. This result is likely due to the higher relative increase in the leaching circuit capital cost for Scenario ID8. For Scenario ID6, the roasting operation, rather than leaching constitutes the major capital item, and as such, the influence of leaching capital on overall project costs is somewhat diluted. Moreover, while the Scenario ID6 leaching data still showed some incremental improvement at higher leaching times, the Scenario ID8 levels off quite rapidly and actually decreases at the higher times. Based on this analysis, 45 minutes was selected as the optimal leaching time and for the results presented herein.

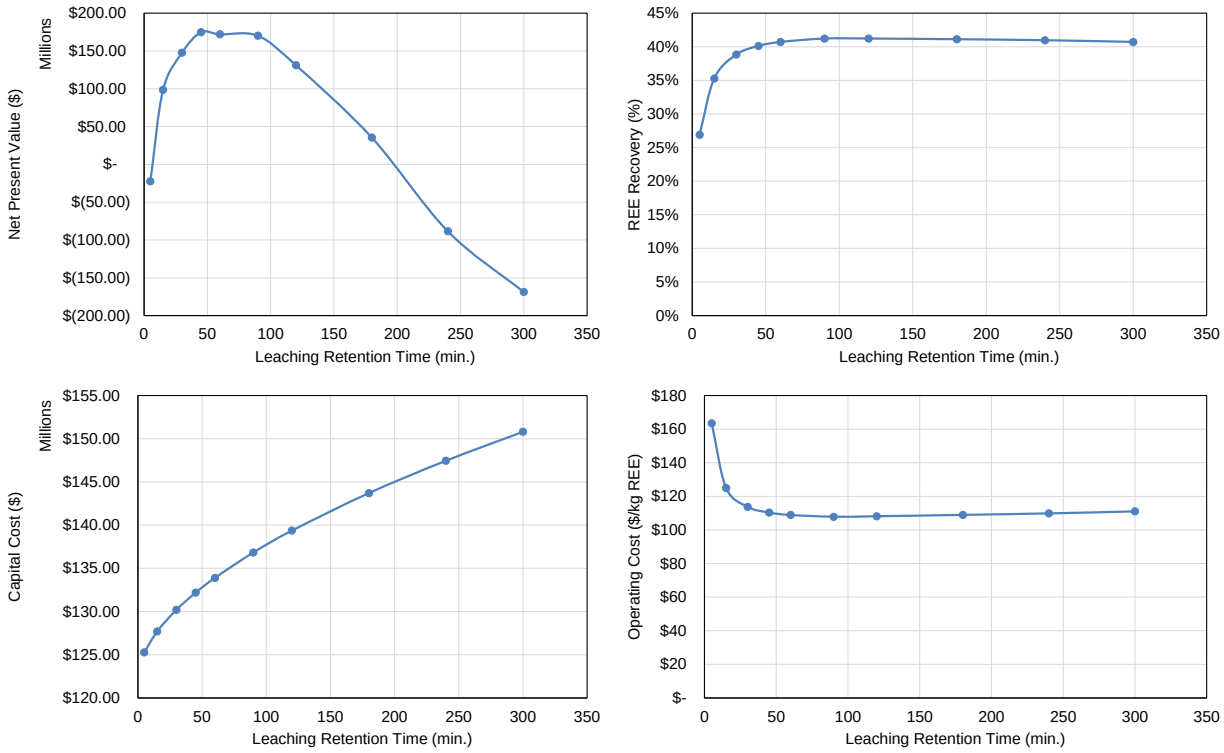

Figure 3.14.18. Sensitivity analysis showing the impact of leaching retention time on net present value, REE recovery, plant capital costs, and plant operating costs for Scenario ID 8. Leaching data based on laboratory testing at the designated leaching times.

A similar two-factor sensitivity analysis showing the combined influence of REE recovery and scandium price on NPV is shown in Figure 3.14.19 for Scenario ID8. This result follows a very similar trend to that of Scenario ID6; however, higher REE recoveries are required to breakeven. At the lowest scandium price of $1000 / kg, the breakeven REE recovery exceeds 90%, suggesting that other cost saving measures may be needed to overcome depressed market conditions.

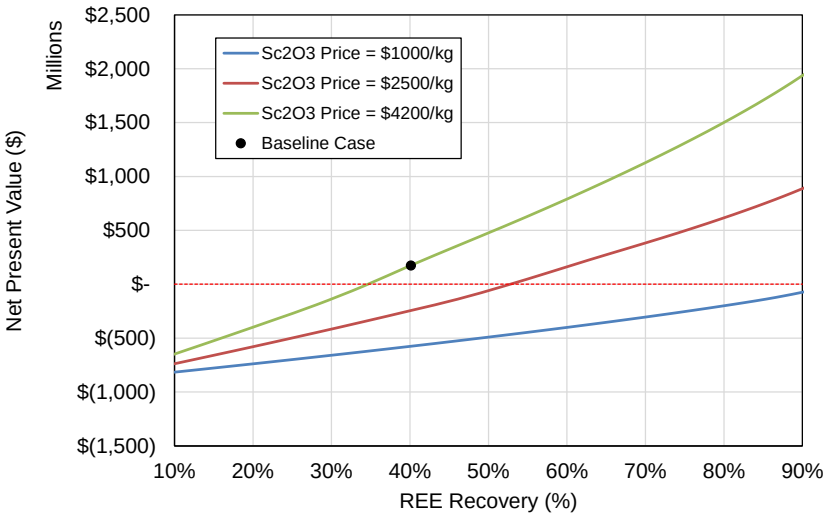

Figure 3.14.19. Sensitivity analysis showing the combined effect of scandium oxide price and overall REE recovery on project net present value for Scenario ID8.

Scenario ID10: FBC Ash with Scandium Recovery

Figure 3.14.20 shows the two-factor sensitivity for the final favorable case, Scenario ID 10. This graph follows a very similar trend to the prior two cases, with the breakeven recovery values falling between that of the earlier two. It should be noted, though, that the economic value of this venture may also be improved by the energy recovery operation.

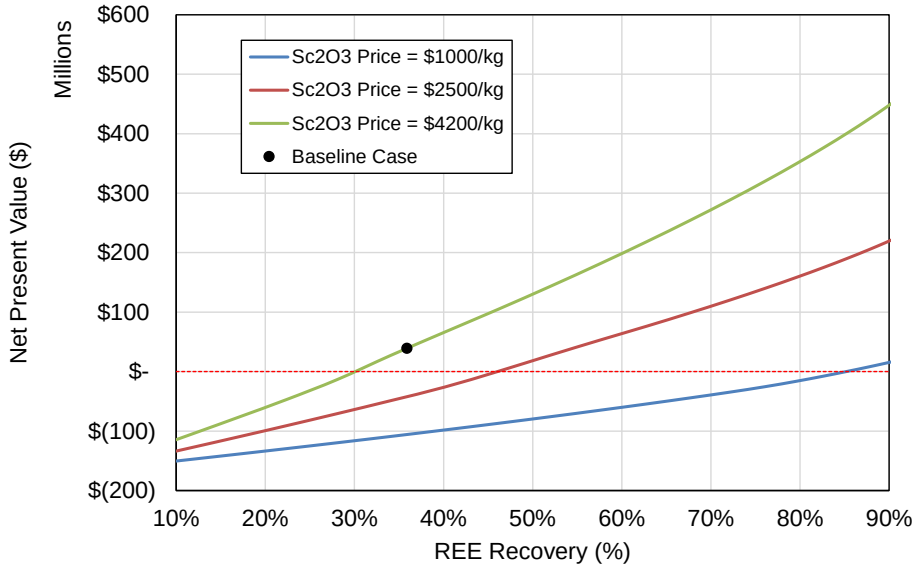

Figure 3.14.20. Sensitivity analysis showing the combined effect of scandium oxide price and overall REE recovery on project net present value for Scenario ID10.

3.14.6.5 Analysis of Roasting

Early in the project, a standalone TEA was conducted to evaluate the influence of roasting on the overall project economics. Originally, roasting was not considered in the process flowsheet; however, this TEA provided strong justification for the addition of such a unit, as the cost savings greatly exceeded the required capital expenditures. Given the importance of this TEA in guiding our final project approach, the salient finding are reproduced here.

Prior experimental data has shown that high-temperature roasting (e.g. 400° to 650° C) provides significant technical benefit to downstream acid leaching of REEs. This data has shown that roasting not only improves overall REE recovery, but it also reduces the acid dose needed to obtain that recovery. These two factors represent a significant cost savings; however, this savings must be balanced against the increased capitals costs associated with the roaster and the ancillary off-gas cleanup operations. To provide some quantitative measure of this cost-benefit tradeoff, a preliminary techno-economic model was developed and analyzed.

The techno-economic model was primarily based on scale-factor derived costs as well as the net benefits measured from laboratory testing. As shown by Garrett (1989), the capital cost of a rotary kiln-type incinerator follows a power law trend with respect to heat input (10^6 BTU/hr) with an exponent of 0.48 and an intercept of 390,000, i.e:

$$CAPEX = 39000Q^{0.48}$$

where Q is the capacity, given by total heat input (10^6 BTU/hr). After calculating this base capital expense, the total installed cost can then be estimated by applying a Lang (i.e. module) factor of 2.2 and a corrosive material factor of 1.5 [4].

Likewise, the annual operating cost can be estimated as function of the total capital cost. According to [5], the annual cost of wear parts and lubrication are approximately 5% of capital expense, while annual maintenance costs are approximately 3.5% of the capital cost. Lastly, supplemental fuel cost (e.g. natural gas) can be estimated at \$2.94 / 10^6 BTU.

For most roasting operations, the supplemental gas cleanup operations (e.g. scrubbers, dust cyclones, electrostatic precipitators, etc.) can be a costly component of the overall system. At this early stage, the extent of gas cleanup has not been evaluated, and as such, no experimental data is available to support a rigorous cost estimation. In lieu of this detail, the installed capital cost of gas cleanup operations was conservatively estimated to be equal to the installed capital cost of the actual roaster. In addition, the operating cost of these units was estimated to be 10% of the installed capital cost.

Given the structure of this cost model, the key input variable is the heat input to the roasting operation. This number can be measured experimentally using differential scanning calorimetry or estimated using thermodynamic data. The latter approach was used in this study. Thermodynamically, the required heat input to the roaster is dictated by two components: (1) the heat needed to raise the temperature of the feed material to the roasting temperature and (2) the heat consumed by the conversion reactions. The first component can be readily calculated by the material heat capacity and the temperature change. For rock material, the heat capacity was assumed to be 0.8 kJ/kg-K, and the temperature change is a design factor. The second component can be calculated by the enthalpy for the various conversion reactions occurring in the roaster operation. While the exact conversion equations are not fully known at this point, the conversion of $CaCO_3$ to CaO and CO_2 was used as a surrogate. The enthalpy of this reaction is known to be 1783 kJ/kg, and for the current study, this reaction was assumed to apply to 10% of the feed material. The current estimate is likely to be quite conservative and can be verified by thermogravimetric analysis.

During the techno-economic analysis, the sum of the heat needed to raise the temperature and the heat consumed by the conversion reactions was determined and used as the heat input value to determine overall capital costs. Moreover, this heat value was compared to the inherent heat content of the feed material to determine if any supplemental fuel is required in the roasting process. After calculating all of these costs, the overall cost savings was determined by computing the increased revenue to due improved recovery as well as cost reduction due to a reduction in acid leaching costs. All of these factors were summarized in a simple Excel spreadsheet model.

This case under evaluation considered a commercial-scale REE production facility processing 50 TPH through a hydrometallurgical circuit operating 7,550 hours/yr. The feed to the circuit was selected to model a Western Kentucky coarse coal refuse, i.e. 60% ash with 300 PPM REE and a REE basket price of \$263/kg. The moisture content of the coal was assumed to be 5%, and the dry-ash free heat content was fixed at 15,000 BTU/lb.

Prior experimental data shows that this particular coal responds very well to leaching, as the overall REE leach recovery improves by 30 percentage points when roasted at 650° C. Moreover, the acid consumption cost in the leaching operation is reduced from \$160 /kg REE

to $10/kg REE. Altogether, these values were combined to determine a net annual benefit of $23.5 million, with roughly two-thirds of the benefit ($15.4 million/yr) stemming from the acid cost savings, while the remaining benefit ($8.1) stems from the additional REE recovery.

Using these feedstock parameters as well as the aforementioned process assumptions, the total heat required by the roaster was determined to be 29.2 $x10^6$ BTU/hr, with 21.5 $x10^6$ BTU/hr being supplied to raise the temperature of the feed material and 7.7 $x10^6$ BTU/hr being consumed by the conversion reactions. The remnant coal in the feed material is adequate to meet this heat demand, as it contains nearly 500 $x10^6$ BTU/hr, and as a result, no additional fuel is required.

Using the total heat requirement of 29.2 $x10^6$ BTU/hr., the fully installed capital cost of the roaster and ancillary gas cleanup processes was estimated to be $13.0 million. Likewise, the annual operating cost for wear parts and maintenance was determined to be $1.2 million. In this scenario, the net benefit significantly exceeds the operating cost and capitalized costs. At a discount rate of 10%, the payback period for this incremental investment was determined to be 0.63 years, and the 10-year NPV was determined to be over $124 million. While many of the cost components were based on assumptions and preliminary information, the overall economic favorability is sufficient to merit further consideration.

3.14.6.6 Analysis of FBC Energy Production and REE Recovery

To supplement the techno-economic assessment of the REE production operation presented in Scenarios ID9 and ID10, a high-level economic analysis of the co-located energy production system was also conducted. Scenarios ID9 and ID10 require a fluidized bed combustion system to both produce a roasted ash product suitable for REE leaching as well as a source of acid for the leaching purpose. This analysis of the FBC energy production system serves two primary purposes. First, the results will show whether or not an independent business case can be made for the FBC boiler. If the energy production system is not economically viable by itself, the losses must be accounted for in REE production system. Second, the analysis will show the the ash produciton rate (tph) to be anticipated from an FBC unit of a specific size and fuel composition.

The techno-economic analysis presented here is only meant to assess overall feasibility and was conducted a high-level using order-of-magnitude estimates. Most of the input data are based on Koornneef et al., (2007), which includes technical and economic parameters for a range of FBC systems constructed over the last 30 years.

Table 3.14.19 shows the key technical inputs for the TEA model, while Table 3.14.20 shows the technical and economic outputs. The feed coal was selected to represent a typical middling material similar to that analyzed by Zhang and Honaker (2019b) and Honaker et al. (2019). The coal was assumed to have dry, ash free heat content of 12,500 Btu/lb. and ash yield of 30%. After adjusting for ash and moisture, the as-received coal to be combusted in the FBC unit was determined to have an energy content of 7,875 Btu/lb.

The overall size of the FBC unit was selected to optimize the amount of ash being produced for the REE recovery system. As shown in many of the earlier analysis, feed rates less than 200 tph to the REE unit typically produce inferior economic outcomes; however, as shown by Koornneef et al., (2007), the largest FBCs built to date are 500 MW_{net} output. With the assumed fuel properties an overall assume dthermal efficiency of 33%, this system was

found to only produce 100 tph of ash. As such, the Scenario ID10 feed rate was set to 100 TPH; however, higher feed rates would have prompted suprior outcomes. Options to augment this feed with alternative feed sources may produce better results by leveraging economy of scale.

The economic results shown in Table 3.14.20 indicate that the energy production system is economically favorable with a payback period of approximately 4 years. The overall system cost was found to be just over $1,100 / kw, a value commensurate for those of modern plants presented in Koornneef et al., (2007). The overall cost of electriciy was found to be $0.05 per kw-hr; however, it should be noted that both the fuel cost and the annual O&M cost were determined using relatively factors, namely the coal unit cost ($/mil BTU) and the annual O&M as a % of capital. For example, Koornneef et al., (2007) show that the annual O&M costs can range from 1.7% to 6.6% of the total capital cost and recommend a value of 2.5% as a typical average. For this study, a larger value of 5% was used. Nevertheless, these resutls are promising and suggest that the energy production system is economically viable by itself, but it alsy produces notably synergy with the REE recovery operation.

Table 3.14.19. Technical and Economic Input Parameters for Analysis of FBC Energy Production System.

Parameter	Unit	Value
Net Energy Output	MW (net)	500
Overall Thermal Efficiency	%	33%
Coal Ash Yield	%	30%
Coal Moisture	%	10%
Coal Energy Content, daf	BTU/lb	12,500
Coal Energy Content, AR	BTU/lb	7,875
Coal Unit Cost	$/mil BTU	$ 2.00
Coal Unit Cost	$/ton	$ 35.04
Retail Electricity Price	$/kW-hr	$ 0.07
Annual O&M as % of Capital	%	5%
Boiler Cost as % of Total Project Capital	%	20%

Table 3.14.20. Technical and Economic Output Data for Analysis of FBC Energy Production System.

Parameter	Unit	Value		
Material Balance				
Feed Coal Required	tph		328	
(conversion)	t/yr		2,875,455	
Total Ash Produced	tph		98	
(conversion)	t/yr		862,637	
Costs				
Boiler Cost (2002)	$	$	71,300,296	
Total Project Cost (2002)	$	$	356,501,482	
Total Project Cost (build year)		$	574,413,013	
(conversion)	$/kw	$	1,149	
Annual O&M	$/yr	$	28,720,651	(14%)
Annualized Capital Cost (20 years)	$/yr	$	76,901,713	(37%)
Annual Fuel Cost	$/yr	$	100,755,945	(49%)
Outcomes				
Electricity Revenue	$/yr	$	306,600,000	
Annual Cash Costs	$/yr	$	129,476,595	
Net profit	$/yr	$	177,123,405	
Discounted Payback Period	Years		4.35	

3.14.7 Conclusions and Recommendations

The results from the techno-economic assessment can be used to derive several key findings related to the economic performance of the proposed extraction process. These key findings include:

1. A robust techno-economic modeling software was developed and implemented during this project. The model was deployed on a Microsoft Excel platform and provides the flexibility for scenario and sensitivity analysis of various REE production approaches.
2. Data collected from the operation of the pilot plant showed that across 18 production runs, chemical consumption costs varied from $381 to $2,200 per kg of REE produced, with superior results observed in latter runs. The optimal case, $381 per kg was modeled at the commercial scale producing an overall operating cost of $570 per kg.
3. One notable contributor to the high production costs was the low REE recovery observed in the pilot scale trials. Sequential laboratory testing of each unit operation under similar chemical conditions indicated that further process improvement is possible and further reduce the operating costs to $281 per kg with no major changes to the process circuitry.
4. For the baseline case, the roasting and leaching operations were shown to be the most expensive capital items, each contributing approximately 30% to the total capital cost. Likewise, reagents were shown to be the most expensive operating cost category, representing nearly 70% of the total. Leaching acid was the single largest line item.
5. In addition to the raw plant data and the optimized plant data, eight additional scenarios were evaluated using the techno-economic model. Capital costs for these scenarios varied from $23.78 million to $252 million, while operating costs varied from $100 per kg REE to $570 per kg REE.

6. Of the ten scenarios, three were found to be economically favorable, producing internal rates of return varying from 27.7% to 33.1% and payback periods of 4 to 5 years. Likewise, the capital intensity (dollars of capital per kg/yr. of REE production) for these favorable scenarios varied from $136 to $630 /(kg/yr.).
7. The product basket price was shown to have a strong influence on the economic viability of the scenarios. All three favorable cases included a dedicated scandium recovery circuit, which prompted higher product basket prices relative to those without scandium recovery. Increased REE market prices or price guarantees for critical REEs may also prompt basket prices sufficient for economic viability.
8. Capital intensity was shown to be extremely sensitive to plant feed rate and leaching percent solids up to approximately 20%. Above 20% solids, only modest reductions in capital intensity were observed.
9. Operating cost was shown to be extremely sensitive to REE recovery, REE feed grade, and leaching acid consumption.
10. Roasting was show shown to be essential both from a technical and economic standpoint. Despite the high relative cost of this operation, the improvements to leaching efficiency and acid consumption are notable. Overall, the incremental payback period of the roasting unit was shown to be less than one year.
11. X-ray sorting, operating under a per ton lease agreement, was shown to be a cost effective approach to pre-concentration, prompting a 12% improvement to capital intensity and operating cost for the case studied.
12. Roasted middlings as well as from a fluidized bed combustion system both showed robust economic favorability, owing to their increased leachability and increased REE content.
13. One innovative scenario investigated the co-production of energy and REEs from a middling or waste coal. In this approach, the middling coal is combusted in a fluidized bed combustor (FBC) at a modest temperature. By avoiding high temperatures above 800° C, the REE leachability of the resultant ash is greatly enhanced, nearly matching that of material roasted under ideal conditions. Moreover, the off gas from the FBC unit can be collected and used to generate acid for the REE production system. Economic analyses of the energy production and REE production systems showed that both were independently viable with payback periods of 4 to 5 years.

3.15 Commercialization Analyses (PB3-Task14)

3.15.1 Market Assessment

The potential producers of REE products usually need to be in accordance with the requirements of the end users to become a qualified supplier. The process may take up to 24 months and be very costly depending on the end user requirements. In general, the potential customer would not go through the lengthy process unless the producer had shown substantial capability of producing final product from an industrial level facility over a long period of time.

Based on the conversation between the principal investigators in this project and many end users, the magnet metals such as praseodymium, neodymium, samarium, dysprosium, and terbium are of great demand. Due to the demand increase at different rates for different elements, the demand of each individual REE can vary significantly over the others over time. As predicted by Alonso et al. (2012), the demand for neodymium may be almost 40% of total demand by 2035. The demand of La and Ce are both reducing over time (Alonso et al., 2012).

The REEs produced from coal and coal byproducts has a unique product configuration as it contains higher heavy-to-light REEs ratio compare to the primary REE minerals. The production of heavy REEs is projected to be in deficit supply (Department of Energy, 2011). Scandium as a high value element with limited demand as of now. However, the market and demand for Sc has potential to increase provided that a sustainable resources and supply can be maximized and secured.

The economic feasibility of REE production from coal is highly dependent on the market value of REEs which is driven by the demand of the market. In the near future, the growing high-tech and green technologies will increase the demand for rare earth elements. The rare earth market price for high demand compounds will be significantly impacted. (DOE/NETL, 2019)

3.15.2 PESTLE analysis

A PESTLE (Political, Economic, Social, Technological, Legal and Environmental) analysis was conducted to assess the project impact. The techno-economic analysis described in section 3.14 shows that three of the 10 operational scenarios show favorable economics and will provide economic benefit to investors. In addition to these standard project economic indicators, the project has substantial social and community benefit, as quantified by tax receipts and employment payroll. For example, considering Scenario ID8 (Roasted Middlings with Scandium Recovery), the total state and federal income tax payments over the 23-year project period was determined to be $138 million. The plant will require 9 full time employees per shift for direct labor alone, and the total payroll is approximately $2.3 million per year. Using a conservative estimate of 4.8 employees per shift position (Seider et al., 2009), the total workforce is expected to include 43 direct employees in in addition to any administrative and support labor. Therefore, when at full capacity, the plant will create approximately 50 new jobs with high pay and significant benefits.

The technology developed in this project is expected to be deployed at multiple sites throughout the coal producing regions in the US. The data shown in Scenario ID8 shows that a single plant can produce just under 1000 t/yr of mixed REO concentrate, roughly 10% of the US apparent consumption (Gambogi, 2021). It is reasonable to anticipate that 5 to 10 similarly sized plants could be deployed in the region, producing a proportional increase to the tax and payroll numbers shown above.

One other positive social benefit is related to the use of waste coal as a feedstock, such as the coproduction of energy and REEs, which was analyzed in Scenario IDs 9 and 10. In addition to the economic benefit, this approach also eliminates the environmental liability of waste coal piles while creating new jobs and investment opportunities. In all cases, the commercial development of this technology should include broad stakeholder engagement (e.g., local community members, regulatory and legislative entities, suppliers, customers, and investors) from the early phases of project development.

Altogether, this analysis not only show that the recovery of rare earth elements form coal is economically viable, but it will also have provided significant net social benefit to the local communities in the coal producing regions.

3.15.3 Technology Readiness Level Assessment

Summary of core technology: The processing plant integrates physical and chemical separation processes to recover rare earth elements and other critical materials from various coal-based

sources including pre-combustion coal, refuse generated from the cleaning of coal, mine influenced water sources and precipitates produced from the treatment of mine influenced waters.

Target Commercial Application and Technology Goals: The commercial target application is a full-scale processing facility capable of treating a maximum of 500 tph of coal-based solid feedstocks. The performance targets for the plant are:

- >99% purity rare earth oxide mix product;
- Radionuclide content below acceptable levels in product and waste streams;
- Total costs below a level needed to achieve economic viability for typical coal-based feedstocks.

Test apparatus:

A ¼-tph pilot plant consisting of physical and chemical separation processes constructed into seven distinctly different bays with each serving a specific purpose. The fully continuous, automated plant has a physical separation circuit, a leaching circuit and an SX & Selective Precipitation circuit.

Key results:

- REO mix products greater than 90% purity was achieved using the technology, circuity and chemistry in this project.
- REE recovery values greater than 95% from the pregnant liquid solution (PLS) are achievable using the solvent extraction and precipitation circuit.
- Roasting the feed at around 600°C – 700°C prior to leaching provides the ability to improving leach recovery, reducing acid concentration and overall chemical costs, and limiting the release of contaminate ions including radionuclides.
- Acid concentrations in the range of 0.5M and higher are not economically feasible.
- Ion exchange leaching is a more viable option with roasted material with recovery values exceeding 50% on selected materials and elements.
- Achieving an economically acceptable solvent extraction (SX) circuit requires pre-concentration of the REEs in the pregnant solution to a level of around 500 ppm.
- Alkaline stripping is required for scandium when using DEHPA.
- Alternative extractants are effective for scandium and allow stripping using mild acid.
- Multistage precipitation and redissolution provides better economic feasibility than that of the solvent extraction circuit.
- Greater than 90% purity was achieved using both solvent extraction circuitry and multistage precipitation circuitry from varies feedstocks.

Describe Equipment/Facility Procurements/Modifications Necessary to Attain Next Stage-Gate TRL (4, 6 or 7) (or technology demonstration at TRL 9): A pilot plant that is 20 to 40 times larger than the existing plant would be needed to assess the scale-up factor and performance and to allow more testing on relevantly sized downstream REE concentration steps involving a cleaner SX circuit (if necessary), selective precipitation and roasting to a final REO product mix. Equipment required would be 1) crushing and grinding units, 2) roaster for pre-leach treatment, 3) leaching circuit or heap leach equipment, 4) solvent extraction mixer-

settlers, 5) selective precipitation tanks, 6) filters, 7) product roaster, 8) PLC systems with sensors and 9) waste treatment tanks and filters.

Estimate Cost-to-Complete to Attain Next Stage-Gate TRL (4, 6 or 7) (or technology demonstration at TRL 9), or next three years, whichever is longest: The total cost of the next stage facility would be approximately $30 million as outlined below:

Labor (6 operators/shift, 3 shifts/day, 2080 hrs/yr/operator)	4,500,000.00
Equipment:	14,000,000.00
Supplies	2,000,000.00
Subcontractors	1,200,000.00
Services	750,000.00
Other Direct Costs	1,500,000.00
Indirects:	5970000
Total	29,920,000.00

Reference

Alonso, E., Sherman, A. M., Wallington, T. J., Everson, M. P., Field, F. R., Roth, R., & Kirchain, R. E. (2012). Evaluating rare earth element availability: A case with revolutionary demand from clean technologies. Environmental science and technology, 46, 3406-3414.

Gambogi, Joseph. "Mineral Commodity Summaries – Rare Earths." United States Geological Survey. 2021.

Seider, Warren D., Junior D. Seader, and Daniel R. Lewin. Product & process design principles: synthesis, analysis and evaluation. John Wiley & Sons, 2009.

Summers, Morgan. Rare Earth Markets and Imbedded Demand. DOE/NETL 2019.

U.S. Department of Energy, (2011). Critical materials strategy (DOE/PI-0009).

3.16 Decommissioning & Disposition (PB3-Task15)

Upon receiving of award under DOE Award Numbers DE-FE0031827, the pilot plant facility is undergoing a scale up and upgrade re-construction to demonstrate scaled production of high purity rare earth oxides (REO), nominally exceeding 90% grade, from coal refuse sources using innovative technologies. Majority of the equipment are relocated in the pilot plant and rearranged to accommodate with the updated process flowsheet and floor plan. Detailed plans are stated below.

1.00 – Preconcentration (Mine Site)
2.00 – Size Reduction & Liberation
3.00 – Physical Separation
4.00 – Acid Leaching
5.00 – Solvent Extraction & Precipitation
6.00 – Chemical storage bay
7.00 – Rare Earth Mineral Concentration

Process train 1.00 – Preconcentration (Mine Site): The x-ray sorter unit remained on the mine site located at the Alliance Dotiki coal preparation plant to serve the purpose of feedstock material upgrade and preconcentration for the upscale pilot plant process. Mechanical maintenance was performed to ensure the functionality of the unit during the intermediate shutdown.

Process train 2.00 – Size Reduction & Liberation: The equipment including the jaw crusher, cone crusher, and hammer mill remained in the pilot plant facility to achieve the size reduction for preparing the feedstock material to the upscaled process. The ball mill was relocated to the coal preparation lab at the University of Kentucky to support an independent study on size reduction analysis of a graduate level course. Based on the need of the upscale plant operation, the ball mill may be reinstalled in the pilot plant in the future.

Processing train 3.00 – Physical Separation: the flotation column unit is scheduled to be returned to Virginia Tech. The thickener tanks that were originally used for flotation tailing stream dewatering are disassembled and to be used for the dewatering process in the pyrite/calcite concentration process and leaching solid/liquid separation process. The 6-inch tube furnace roaster used for feed solid pretreatment before entering the hydrometallurgical circuit remained in the pilot plant.

Process train 4.00 – Acid Leaching: The acid leaching circuit including 100-gallon leaching tanks, 200-gallon filter feed tanks, and 400-galong thickener tanks are remained and rearranged in the pilot plant to accommodate with the upscale process flowsheet and floor plan.

Process train 5.00 – Solvent Extraction & Precipitation: The 1-gpm, multistage 10-tank mixer/settler solvent extraction unit is remained in the pilot plant. It will be used to extract Sc from pregnant leachate solution followed by a SX cleaner unit with a goal of producing high purity Sc product.

Process train 6.00 – Chemical storage bay: The chemical solution storage, preparation, and leakage containment protection tanks are remained in the pilot plant and rearranged based on the upscale floorplan. The peristaltic pumps and magnetic pumps for reagent pumping, metering, and transportation are cleaned and serviced for maintenance purposes.

Process train 7.00 – Rare Earth Mineral Concentration: The use of HHS mobile unit is terminated.

4.0PRODUCTS

4.1 Journal Articles

1. Honaker, R.Q., Groppo, J., Yoon, R.H., Luttrell, G.H., Noble, A., and Herbst, J., (2017) “Process Evaluation and Flowsheet Development for the Recovery of Rare Earth Elements from Coal and Associated Waste,” Minerals and Metallurgical Processing Journal, Vol. 34, No. 3, pp. 107-115.

2. Zhang, W., Honaker, R.Q., and Groppo, J., “Concentration of Rare Earth Minerals from Coal by Froth Flotation,” Minerals and Metallurgical Processing Journal, Vol. 34 No. 3, pp. 132 – 137.

3. Zhang, W., and Honaker, R.Q., 2017, “Adsorption of Octanohydroxamic Acid on Monazite Surfaces,” International Journal of Mineral Processing, Vol. 164, pp. 26 – 36.

4. Zhang, W., and Honaker, R.Q., 2017, “Surface Charge of Monazite in Aqueous Solutions,” Powder Technology, Vol. 318, pp. 263 – 271.

5. Zhang, W., Yang, X., and Honaker, R.Q., 2017, “Association characteristic study and preliminary recovery investigation of rare earth elements from Fire Clay seam coal middlings,” Fuel, Vol. 215, pp. 551-560.

6. Huang, Q., Noble, Aaron, Herbst, John and Honaker, Rick, 2018, “Liberation and Release of Rare Earth Minerals from Middling Kittanning, Fire Clay, and West Kentucky No. 13 Coal Sources,” Powder Technology, Volume 332, pp. 242 – 252.

7. Zhang, W., and Honaker, R.Q., 2018, “Flotation of monazite in the presence of calcite part II: Enhanced separation performance using sodium silicate and EDTA,” *Minerals Engineering*, Vol. 127, P318-328.

8. Luttrell, G. H., Kiser, M., Yoon, R.-H., Noble, A., Rezaee, M., Bhagavatula, A. and Honaker, R.Q., 2019, “A Field Survey of Rare Earth Element Concentrations in Process Streams Produced by Coal Preparation Plants in the Eastern United States,” *Journal of Mining, Metallurgy and Exploration*, 36(5), 889-902.

9. Yang, X., Werner, J. and Honaker, R.Q., 2019. Leaching of rare Earth elements from an Illinois basin coal source. Journal of Rare Earths, 37(3), pp.312-321.

10. Zhang, W. and Honaker, R., 2019. Enhanced leachability of rare earth elements from calcined products of bituminous coals. Minerals Engineering, 142, p.105935.

11. Honaker, R.Q., Zhang, W., Werner, J., Noble, A., Luttrell, G.H. and Yoon, R.-H., 2020, “Enhancement of a Process Flowsheet for Recovering and Concentrating Critical Materials from Bituminous Coal Sources,” *J. Mining, Metallurgy and Exploration*, Volume 37, Issue 1, pp. 3–20.

12. Huang, Q., Noble, A., & Talan, D. (2020). Exploratory investigation on the use of low-cost alternative media for ultrafine grinding of coal. *International Journal of Coal Preparation and Utilization*, 1-18. https://doi.org/10.1080/19392699.2020.1809387

13. Talan, D., Huang, Q., (2020). Separation of Thorium, Uranium, and Rare Earths from A Strip Solution Generated from Coarse Coal Refuse. *Hydrometallurgy*. Volume 197, 105446, DOI:10.1016/j.hydromet.2020.105446.

14. Talan, D., & Huang, Q. (2020). Removal of Radionuclides to Purify Rare Earths-containing Solution Generated from Coarse Coal Refuse, under preparation.

15. Yang, X. and Honaker, R., 2020. Leaching Kinetics of Rare Earth Elements from Fire Clay Seam Coal. Minerals, 10(6), p.491.

16. Zhang, W. and Honaker, R., 2020. Process development for the recovery of rare earth elements and critical metals from an acid mine leachate. Minerals Engineering, 153, p.106382.

17. Zhang, W., & Honaker, R. (2020). Process development for the recovery of rare earth elements and critical metals from an acid mine leachate. Minerals Engineering, 153, 106382.

18. Zhang W, Noble A, Yang X, Honaker R. (2020) Lithium leaching recovery and mechanisms from density fractions of an Illinois Basin bituminous coal. Fuel. 2020 May 15;268:117319.

19. Zhang W, Honaker R. Characterization and recovery of rare earth elements and other critical metals (Co, Cr, Li, Mn, Sr, and V) from the calcination products of a coal refuse sample. Fuel. 2020 May 1;267:117236.

20. Talan, D., Huang, Q., (2021). Separation of Radionuclides from A Rare Earth-Containing Solution by Zeolite Adsorption. *Minerals*, 11 (1). doi.org/10.3390/min11010020.

21. Talan, D., Huang, Q. (2021). A Combined Experimental Approach to Remove Actinides from Rare Earth Elements. Submitted to *Fuel.* (Under review).

4.2 Peer-Reviewed Conference Articles

1. Honaker, R., Zhang, W., Werner, J., Yang, X., Chandra, A., Noble, A., Huang, Q. and Talan, D. (2020). "Pilot Plant Evaluations of Rare Earth Elements Recovery and Concentration from Pre-Combustion Bituminous Coal Sources." COM 2020, 59th Conference of Metallurgists. Toronto, Ontario, Canada, August 24 – 27, 2020. *{Conference canceled due to COVID-19}.*

4.3 Non-Reviewed Conference Articles

1. Honaker, R.Q., Groppo, J., Noble, A., Herbst, J., Luttrell, G.H., and Yoon, R.H. (2016). "Process Evaluation and Flowsheet Development for the Recovery of Rare Earth Elements from Coal and Associated Waste." 2017 SME Annual Meeting & Exhibit. Denver, CO February 21, 2017.

2. Bethell, P., Sechrist, C.M., Keles, S., Noble, A., Luttrell, G.H., and Honaker, R.Q. (2018). "Partitioning Behavior of Rare Earth Elements in a Coal Preparation Facility," Proceedings, 43nd International Technical Conference on Clean Energy, Sheraton Sand Key, Clearwater, Florida, June 3-8, 2018, 8 pp, Preprint No. 112-2018.

3. Sechrist, C.M., Keles, S., Noble, A., Luttrell, G.H., and Honaker, R.Q. (2018). "Preconcentration of Coal-Based Rare Earth Element Feedstocks Using X-Ray Sorter Technology," Proceedings, 43nd International Technical Conference on Clean Energy, Sheraton Sand Key, Clearwater, Florida, June 3-8, 2018, 8 pp, Preprint No. 113-2018.

4.4 Abstract & Conference Presentation

1. Luttrell, Gerald H., Michael Kiser, Roe-Hoan Yoon, Abhijit Bhagavatula, Mohammad Rezaee, Rick Honaker, Aaron Noble. (2016). "Rare Earth Opportunities for Coal." 41st International Technical Conference on Clean Coal and Fuel Systems 2016. The Clearwater Clean Coal Conference. Clearwater, FL. June 5, 2016.

2. Noble, Aaron, Rick Honaker, and Roe-Hoan Yoon. (2016). "Recovery of Rare Earth Minerals and Elements from Coal." West Virginia Coal Mining Institute, 2016 Spring Meeting. Daniels, WV. May 12, 2016.

3. Chandra, A., Honaker, R. Q. and Han, K., "Recovery of Rare Earth Elements from Dilute Leachates Generated from Coal," SME 2017, Denver, Colorado.

4. Honaker, R.Q., "Research in Recovering Rare Earths from Coal & Coal Byproducts," 30th Kentucky Professional Engineers in Mining Seminar, Lexington, Kentucky, September 14, 2017.

5. Honaker, R.Q., Groppo, J., Yoon, R.-H., Luttrell, G.H., Noble, A., and Herbst, J. (2017), "Process Evaluation and Flowsheet Development for the Recovery of Rare Earth Elements from Coal and Associated Waste," SME 2017, Denver, Colorado.

6. Honaker, R.Q., Groppo, J., Yoon, R.-H., Luttrell, G.H., Noble, A., and Herbst, J. (2017). "Pilot-scale Testing of an Integrated Circuit for the Extraction of Rare Earth Minerals and Elements from Coal and Coal Byproducts Using Advanced Separation Technologies." Project review meeting for crosscutting research, gasification systems, and rare earth elements research portfolios. Pittsburgh, PA. March 22, 2017.

7. Honaker, R.Q., Hower, J., Eble, C., Zhang, W., Yoon, R.-H. and Luttrell, G.H., "Coal and Coal Byproducts: A Resource for Critical Materials," SME 2017, Denver, Colorado.

8. Honaker, R.Q., Yang, X., Chandra, A., and Zhang, W., "Hydrometallurgical Extraction of Rare Earth Elements from Coal," Clearwater Clean Energy Conference, Clearwater, Florida, June 11 – 15, 2017.

9. Hower, J.C., Eble, C., Groppo, J.G., and Honaker, R.Q., "Modes of Emplacement of Rare Earth Elements in Coals: Examples from the Fire Clay Coal, Eastern Kentucky," Abstract Number 297831, GSA Annual Meeting, Seattle, Washington, USA, October 22 – 25, 2017.

10. Noble, A. "Rare Earth Elements in Coal and Coal Byproducts: Processing and Economic Considerations." Invited seminar to the National Minerals Information Center, US Geological Survey, Reston, VA. October 18, 2017.

11. Noble, A. Herbst, J**.,** Huang, Q., Luttrell, G., & Honaker, R.Q. (2017). Liberation and release of rare earth minerals from coal sources. *2017 SME Annual Conference & Expo*, Feb. 19-22, Denver, Colorado.

12. Yang, X., Honaker, R., and Han, K., "Hydrometallurgical Recovery of Rare Earth Elements from Coal Sources," SME 2017, Denver, Colorado

13. Yoon, R.-H., B. Li, S. Park, G. Luttrell, S. Suboleski, N. Gupta, J. Reyher, P. Bethell and R. Honaker, "Recovery of Rare Earth Minerals from Coal Using the HHS Process," Clearwater Clean Energy Conference, Clearwater, Florida, June 11 – 15, 2017.
14. Zhang, W., Honaker, R.Q., and Groppo, J., "Fundamental Study of the Hydroxamic Acid Adsorption on Monazite," SME 2017, Denver, Colorado.

15. Zhang, W., Honaker, R.Q., and Groppo, J., "Concentration of Rare Earth Minerals from Coal by Froth Flotation," SME 2017, Denver, Colorado.

16. Gerald H. Luttrell, Aaron Noble, Roe-Hoan Yoon, Mohammad Rezaee, A. Bhagavatula, and Rick Honaker. (2018). "Rare Earth Element Associations in the Product Streams of Coal Preparation Plants." 2018 SME Annual Meeting & Exhibit. Minneapolis, MN. February 26, 2018.

17. Honaker, R Q., Werner. J., Yoon. R., Luttrell. G.H., and Noble, A. (2018). "Production of Critical Rare Earth Element Concentrates from Coal Sources," Presentation, 43nd International Technical Conference on Clean Energy, Sheraton Sand Key, Clearwater, Florida, June 3-8, 2018, Presentation No. 153.

18. Honaker, R Q., Werner. J., Yoon. R., Luttrell. G.H., and Noble, A. (2018). "Production of Critical Rare Earth Element Concentrates from Coal Sources." 2018 SME Annual Meeting & Exhibit. Minneapolis, MN. February 26, 2018

19. Huang, Q., Herbst, J., Noble, A., & Honaker, R. (2018). The effect of grinding media characteristics on the liberation behavior of coal materials for the recovery of rare earth elements. *2018 SME Annual Conference & Expo*, February 25-28, Minneapolis, Minnesota.

20. Honaker, R Q., Werner. J., Zhang. W., Yoon. R., Luttrell. G.H., and Noble, A. (2019). "Design, Development and Testing of a Pilot-Plant for Rare Earth Recovery from Coal-Based Sources." 2019 SME Annual Meeting & Exhibit. Denver, CO. February 24-27, 2019.

21. Huang, Q., Talan, D., & Honaker, R., (2019) Evaluation Study on the Separation of Radioactive Elements from Rare Earths. *2019 WVCMI / WVCA*, March 21, Charleston, West Virginia.

22. Noble, A., Sechrist, C., Serhat, K., Luttrell, G.H., and Honaker, R. (2019). "Utilization of X-Ray Sorter Technology to Enhance the Economic Viability of Recovering Rare Earth Elements from Coal-Based Feedstocks." 2019 SME Annual Meeting & Exhibit. Denver, CO. February 24-27, 2019.

23. Keles, S., Sechrist, C., Noble. A., Luttrell, G., and Yoon, R., Reyher, J., Suboleski, S. (2019). "Design, Construction, and Testing of a Mobile Pilot-Scale Demonstration Unit for the Hydrophobic-Hydrophilic Separation Process." International Mineral Processing Conference – Eurasia. Antalya, Turkey. October 31 – November 2, 2019.

24. Talan, D., Huang, Q., & Honaker, R., (2019). Removal of Radioactive Elements from Rare Earths Using Various Separation Methods. *2019 SME Annual Conference & Expo*, February 24-27, Denver, Colorado.

25. Talan, D., Huang, Q. (2020). Separation of Thorium and Uranium from Rare Earth Elements Using Zeolite Adsorption. 2020 SME Annual Conference & Expo, Feb. 24-26, Phoenix, Arizona.

26. Talan, D., Huang, Q. (2020). A Study on Removal of Thorium and Uranium from Rare Earth Elements Using Zeolite Adsorption. *Mineral & Metallurgical Processing Division Student Poster Contest*, *2020 SME Annual Conference & Expo*, February 23-26, Phoenix, Arizona.

27. Talan, D., Huang, Q. (2021). Process Development for Separating Actinides from Rare Earth-containing Solution Generated from Coarse Coal Refuse. *2021 SME Annual Conference & Expo*, March 1-5, Virtual Event.

4.5 Other Publication Products

Separation of Radionuclides from Rare Earth-containing Solution Generated from Coarse Coal Refuse, Ph.D. Dissertation.

4.6 Patents & Patent Applications

R Honaker, W Zhang. Method for Recovering Valuable Elements from Pre-Combustion Coal-Based Materials. US Patent App. 16/832,157, 2020

Werner, J., Chandra, A. and Honaker, R.Q., Continuous Solvent Extraction Process for Generation of High-Grade Rare-Earth Oxides from Leachates Generated from Coal Sources, U.S. Utility Patent Application Serial No. 16/534,738, August 7, 2019.

5.0 PARTICIPANTS & COLLABORATING ORGANIZATIONS

The work outlined in this report has been performed as a collaboration among researchers working together as part of the Center for Advanced Separation Technologies (CAST). The team includes three academic members, i.e., University of Kentucky, Virginia Tech and West Virginia University. Industrial participants include Alliance Coal, Blackhawk Mining, Mineral Separation Technologies (MST) and Minerals Refining Company (MRC). The two coal companies are providing significant support by hosting two test sites, making modifications to facilities to ensure project success, assigning manpower to secure permits, supplying water and power, and transporting feedstock and waste materials. MST and MRC are, under lease agreements, are providing pilot-scale units to the project in addition manpower support for equipment start-up. SX Kinetics is another processing equipment company who will provide their expertise and equipment in leaching and solvent extraction to assist the efforts of the project team. A list of key team members along with their associations and contact information are provided in Table 5.1.

Table 5.1. Listing of key project personnel.

Personnel	Business Association	Primary Contact E-Mail
Rick Honaker	University of Kentucky	rick.honaker@uky.edu
John Groppo	University of Kentucky	john.groppo@uky.edu
Josh Werner	University of Kentucky	jmwe256@uky.edu
Xinbo Yang	University of Kentucky	xinbo.yang@uky.edu
Roe-Hoan Yoon	Virginia Tech	ryoon@vt.edu
Gerald Luttrell	Virginia Tech	luttrell@vt.edu
Aaron Noble	Virginia Tech	noble54@vt.edu
Wencai Zhang	Virginia Tech/University of Kentucky	wencaizhang@vt.edu
Qingqing Huang	West Virginia University	qingqing.huang@mail.wvu.edu
Hunter Davis	Alliance Coal	Hunter.Davis@arlp.com
Kevin Varney	Blackhawk Mining	kvarney@blackhawkmining.com
Stan Suboleski	Mineral Refining Company	ssuboleski@evanenergy.com
Charles Roos	Mineral Separation Technologies	charles@mineralseparationtechnologies.com

List of students, post-doctoral associates, and other researchers who contributed to the project:

- Alind Chandra, PhD Student, Post-Doctoral Associate, University of Kentucky.
- Tushar Gupta, PhD Student, University of Kentucky.
- Ahmad Nawab, PhD Student, University of Kentucky.
- Jason Backus, Laboratory Manager, Kentucky Geological Survey, University of Kentucky.
- Skyler Hornback, Undergraduate Student, University of Kentucky.
- Vincent Mounce, Undergraduate Student, University of Kentucky.
- Chad Sechrist, PhD Student, Virginia Tech.
- Biao Li, PhD Student, Post-Doctoral Associate, Virginia Tech.
- Kaiwu Huang, PhD Student, Post-Doctoral Associate, Virginia Tech.
- Wei Liu, PhD Student, Virginia Tech.
- Nikhil Gupta, Post-Doctoral Associate, Virginia Tech.
- Serhat Keles, Research Associate, Virginia Tech.
- Nathan Youmans, Undergraduate Student, Virginia Tech.
- Alexandra Russell, Undergraduate Student, Virginia Tech.
- Aly McFarland, Undergraduate Student, Virginia Tech.

6.0 CHANGES/PROBLEMS

The COVID-19 outbreak has introduced numerous challenges to the project namely: access to facilities, procurement delays, travel restrictions, and potential reductions in force. Lab access was mostly restricted during the reporting period at the three universities involved in the project. As of the date of report submission, lab access has been gained with restrictions that still limits project activities to some degree.

The COVID-19 outbreak has prompted numerous setbacks to experimental tasks at Virginia Tech, particularly those that require access to laboratory facilities. As of the time of

this report, some items have been resolved (e.g. laboratory access); however, restrictions, such as reduced authorization for travel, are anticipated to continue into the foreseeable future. Moreover, future outbreaks may prompt additional laboratory shutdowns during the project. This risk will be intensified in August 2020 when the population density on university campuses increases with the start of the fall academic semester.

The detailed timeline below shows actions taken at Virginia Tech:

- March 11th, 2020: Virginia Tech begins to scale back on campus resources as they moved all classes online and urged students to stay home.
- March 18th, 2020: Virginia Tech transitioned to scaled operations requesting those who could work from home do. Labs continued to be open but were asked to plan for a potential shutdown.
- March 30th, 2020: Virginia Governor Ralph Northam issues stay at home order for Virginia Residents.
- March 31st, 2020: Virginia Tech moved to essential staff only. Non-essential research labs were asked to close by the end of the week. All non-essential purchases (including those for research projects) were temporarily suspended.
- May 15, 2020: Virginia Governor Ralph Northam initiates Phase 1 reopening for the Commonwealth of Virginia.
- May 22, 2020: Virginia Tech Vice President for Research and Innovation Don Taylor issued guidance for a partial reopening of non-essential research.
- June 8, 2020: Virginia Tech labs for this project were authorized to reinitiate work in a reduced capacity. Work is being conducted under an approved COVID-19 mitigation

Similar challenges were faced by the research team at University of Kentucky. The timeline for actions taken at University of Kentucky is as follows:

- March 11: All the in-person classes are suspended at University of Kentucky, the classes are moved online
- March 17: University of Kentucky President Eli Capilouto communicated the need to move operations from on campus to remote as much as possible.
- March 19: Regular operation for testing at pilot plant facility halted, roaster was kept operational with essential personnel.
- April 7: Temporary freeze on any purchasing placed by the University of Kentucky

References

Abdel-Sabour, M. (2014). Uranium Fixation and Removal from Different Soil Types: Review. *Journal of Nuclear Energy Science and Power Generation Technology*.

Al-Areqi, W., Aniza, C., Bahri, C., Majid, A., & Sarmani, S. (2016). Separation and Radiological Impact Assessment of Thorium in Malaysian Monazite Processing. *Malaysian Journal of Analytical Sciences*, 770-776.

Al-Areqi, W., Majid, A., Sarmani, S., & Bahri, C. (2015). Thorium: Issues and Prospects in Malaysia. *AIP Conference Proceedings* (p. 1659). American Institute of Physics.

Alemrajabi, M., Rasmuson, A., Korkmaz, K., & Forsberg, K. (2017). Recovery of Rare Earth Elements from Nitrophosphoric Acid Solutions. *Hydrometallurgy*, 253-262.

Al-Nafai, I. (2015). *Application of Pourbaix Diagrams in the Hydrometallurgical Processing of Bastnasite.* M.S. Thesis, The Pennsylvania State University, Department of Materials Science and Engineering.

Anitha, M., Kotekar, M., Singh, D., Vijayalakshmi, R., & Singh, H. (2014). Solvent Extraction Studies on Rare Earths from Chloride Medium with Organophosphorous Extractant Dinonyl Phenyl Phosphoric Acid. *Hydrometallurgy*, 128-132.

Asselin, G., Audrieth, L., & Comings, E. (1949). The Separation of Thorium and Rare Erath Salts by Solvent Extraction. 640-648.

Balintova, M., & Petrilakova, A. (2011). Study of pH Influence on Selective Precipitation of Heavy Metals from Acid Mine Drainage. *Chemical Engineering Transactions*, 345-350.

Barkat, M., Nibou, D., Amokrane, S., Chegrouche, S., & Mellah, A. (2015). Uranium (VI) Adsorption on Synthesized 4A and P1 Zeolites: Equilibrium, Kinetic, and Thermodynamic Studies. *Comptes Rendus Chimie*, 261-269.

Belova, V., Egorova, N., Voshkin, A., & Khol'kin, A. (2015). Extraction of Rare Earth Metals, Uranium and Thorium from Nitrate Solutions by Binary Extractants. *Theoretical Foundations of Chemical Engineering*, 545-549.

Bertetti, P., Pabalan, R., Pickett, D., & Turner, D. (2011). *Radionuclide Sorption Technical Assistance Activities at the Center for Nuclear Waste Regulatory Analyses.* San Antonio, Texas.

Biswas, S., Pathak, P., Singh, D., & Roy, S. (2013). Comparative Evaluation of Tri-n-butyl Phosphate (TBP) and Tris(2-Ethylhexyl) Phosphate (TEHP) for the Recovery of Uranium from Monazite Leach Solution. *Separation Science and Technology*, 2013-2019.

Brindley, G., & Bastovanov, M. (1982). *Clay and Clay Minerals*, 135.

Brookins, D. (1983). Eh-pH Diagrams for the Rare Earth Elements at 25C and one Bar Pressure. *Geochemical Journal*, 223-229.

Brookins, D. (1988). *Eh-pH Diagrams for Geochemistry.* Albuquerque: Springer-Verlag.

Brown, C., & Sherrington, L. (1979). Solvent Extraction used in Industrial Separation of Rare Earths. *Journal of Chemical Technology and Biotechnology*, 193-209.

Camacho, L., Deng, S., & Parra, R. (2010). Uranium Removal from Groundwater by Natural Clinoptilolite Zeolite: Effects of pH and Initial Feed Concentration. *Journal of Hazardous Materials*, 393-398.

Cheira, M., Atia, B., & Kouraim, M. (2017). Uranium (VI) Recovery from Acidic Leach Liquor by Ambersep 920U SO4 Resin: Kinetic, Equilibrium and Thermodynamic Studies. *Journal of Radiation Research and Applied Sciences*, 307-319.

Chukanov, N., Blass, G., Pekov, I., Belakovskiy, D., Van, K., Rastsvetaeva, R., & Aksenov, S. (2012). Perrierite-(La), (La, Ce, Ca)4(Fe2+, Mn)(Ti, Fe3+, Al)4(Si2O7)2O8, A New Species from the Eifel Volcanic District, Germany. *Geology of Ore Deposits*, 647-655.

Couper, J., Fair, J., Penney, W., & Walas, S. (2009). *Chemical Process Equipment: Selection and Design.* Elsevier Science and Technology.

Dyer, A., & Jozefowicz, L. (1992). The Removal of Thorium from Aqueous Solutions using Zeolites. *Journal of Radioanalytical and Nuclear Chemistry*, 47-62.

Erden, K., & Donat, R. (2016). Removal of Thorium(IV) from Aqueous Solutions by Natural Sepiolite. *Radioachimica Acta*, 187-196.

Faghihian, H., Maragheh, M., Amini, M., & Nezamzadeh, A. (2004). Thorium Ion Uptake by Zeolite A Synthesized from Natural Clinoptilolite Tuffs. *Adsorption Science and Technology*. 707-717.

Fasfous, I., & Dawoud, J. (2012). Uranium(VI) Sorption by Multiwalled Carbon Nanotubes from Aqueous Solution. *Applied Surface Science*, 433-440.

Felmy, A., Rai, D., & Mason, M. (1991). T*he Solubility of Hydrous Thorium(IV) Oxide in Chloride Media: Development of An Aqueous Ion-Interaction Model*. Radiochimica Acta, 177-185.

Garrels, R. (1955). *Some Thermodynamic Relations Among the Uranium Oxides and Their Relation to the Oxidation States of the Uranium Ores of the Colorado Plateaus.* Washington D.C.: U.S. Geological Survey.

Geier, R. (1979). *Purex Process Solvent Literature Review.* Washington.

Giri, R., & Nath, G. (2016). Physicochemical Study of Extractants for Extraction of Rare Earth Element. *Journal of Analytical Science and Technology*.

Godelitsas, A., & Armbruster, T. (2003). HEU-type Zeolites Modified by Transition Elements and Lead. *Microporous and Mesoporous Materials*, 3-24.

Habashi, F. (1997). *Handbook of Extractive Metallurgy.* Quebec: Wiley-VHC.

Hayes, S., Yu, P., O'Keefe, T., O'Keefe, M., & Stoffer, J. (2002). The Phase Stability of Cerium Species in Aqueous Systems I. E-pH Diagram for the Ce-HCLO4-H2O System. *Journal of the Electrochemical Society*, 623-630.

Hidayah, N., & Abidin, S. (2017). The Evolution of Mineral Processing in Extraction of Rare Earth Elements Using Solid-Liquid Extraction over Liquid-Liquid Extraction - A Review. *Minerals Engineering*, 103-113.

Honaker, R., Zhang, W., Yang, X., & Razaee, M. (2018). The conception of An Integrated Flowsheet for Rare Earth Elements Recovery from Coal Coarse Refuse. *Minerals Engineering*, 233-240.

Honaker, R., Zhang, W., & Werner, J. (2019). Acid Leaching of Rare Earth Elements from Coal and Coal Ash: Implications for Using Fluidized Bed Consumption to Assist in the Recovery of Critical Materials. Energy Fuels, 5971-5980.

Hostetler, P., & Garrels, R. (1962). Transportation and Precipitation of Uranium and Vanadium at Low Temperatures with Special Reference to Sandstone-Type Uranium Deposits. Economic Geology and the Bulletin of the Society of Economic Geologists, 137-167.

Jha, M., Kumari, A., Panda, R., Kumar, J., Yoo, K., & Lee, J. (2016). Review on Hydrometallurgical Recovery of Rare Earth Metals. *Hydrometallurgy*, 2-26.

Jorjani, E., & Shahbazi, M. (2016). The Production of Rare Earth Elements Group via Tributyl Phosphate Extraction and Precipitation Stripping Using Oxalic Acid. *Arabian Journal of Chemistry*, 1532-1539.

Kammerer, J., Carle, R., & Kammerer, D. (2011). Adsorption and Ion Exchange: Basic Principles and Their Application in Food Processing. *Journal of Agricultural and Food Chemistry Review*, 22-42.

Kaygun, A., & Akyil, S. (2007). Study of the Behaviour of Thorium Adsorption on PAN/Zeolite Composite Adsorbent. *Journal of Hazardous Materials*, 357-362.

Kilincarslan, A., & Akyil, S. (2005). Uranium Adsorption Characteristic and Thermodynamic Behavior of Clinoptilolite Zeolite. *Journal of Radioanalytical and Nuclear Chemistry*, 541-548.

Kini, G. (2006). *Characterization of Synthetic Zeolites Optimized for Heavy Metal Uptake from Wastewater*. Thesis, University of Florida.

Kutahyali, C., & Eral, M. (2010). Sorption Studies of Uranium and Thorium on Activated Carbon Prepared from Olive Stones: Kinetic and Thermodynamic Aspects. *Journal of Nuclear Materials*, 251-256.

Ladeira, A., & Goncalves, C. (2007). Influence of Anion Species on Uranium Separation from Acid Mine Water Using Strong Base Resins. *Journal of Hazardous Materials*, 499-504.

Langmuir, D. (1978). Uranium Solution-Mineral Equilibria at Low Temperatures with Applications to Sedimentary Ore Deposits. *Geohemica et Cosmochimica Acta*, 547-569.

Langmuir, I. (1918). The Adsorption of Gases on Plane Surfaces of Glass, Mica and Platinum. *American Chemical Society*, 1361-1368.

Li, F., Yang, Z., Weng, H., Chen, G., Lin, M., & Zhao, C. (2018). High Efficient Separation of U(VI) and Th(IV) from Rare Earth Elements in Strong Acidic Solution by Selective Sorption on Phenanthroline Diamide Functionalized Graphene Oxide. *Chemical Engineering Journal*, 340-350.

Li, Z., Chen, F., Yuan, L., Liu, Y., Zhao, Y., Chai, Z., & Shi, W. (2012). Uranium(VI) Adsorption on Graphene Oxide Nanosheets from Aqueous Solutions. *Chemical Engineering Journal*, 539-546.

Lin, R., Soong, Y., & Granite, E. (2018). Evaluation of Trace Elements in U.S. Coals Using the USGS COALQUAL Database Version 3.0. Part I: Rare Earth Elements and Yttrium (REY). *International Journal of Coal Geology*, 1-13.

Liu, H., & Pan, Z. (2011). NORM Situation in Non-Uranium Mining in China. *Annals of the ICRP*, 343-351.

Liu, X., Li, J., Wang, X., Chen, C., & Wang, X. (2015). High Performance of Phosphate Functionalized Graphene Oxide for the Selective Adsorption of U(VI) from Acidic Solution. *J. Nucl. Mater.*, 56-64.

Liu, Y., Wang, Y., Zhang, Z., Cao, X., Nie, W., Li, Q., & Hua, R. (2013). Removal of Uranium from Aqueous Solution by A Low Cost and High-Efficient Adsorbent. *Applied Surface Science*, 68-74.

Lu, Y., Wei, H., Zhang, Z., Li, Y., Wu, G., & Liao, W. (2016). Selective Extraction and Separation of Thorium from Rare Earths by a Phosphorodiamidate Extractant. *Hydrometallurgy*, 192-197.

Lu, Y., Wei, H., Zhang, Z., Li, Y., Wu, G., & Liao, W. (2016). Selective Extraction and Separation of Thorium from Rare Earths by A Phosphorodiamidate Extractant. *Hydrometallurgy*, 192-197.

Malamis, S., & Katsou, E. (2013). A Review on Zinc and Nickel Adsorption on Natural and Modified Zeolite, Bentonite, and Vermiculite: Examination of Process Parameters, Kinetics and Isotherms. *Journal of Hazardous Materials*, 428-461.

Menzies, I., & Rigby, F. (1961). Separation of Thorium from Uranium and Rare Earth Elements by Solvent Extraction with Tri-n-Butyl Phosphate-Xylene. *J. Appl. Chem.*, 104-113.

Metaxas, M., Kasselouri-Rigopoulou, V., Galiatsatou, P., Konstantopoulou, C., & Oikonomou, D. (2003). Thorium Removal by Different Adsorbents. *Journal of Hazardous Materials*, 71-82.

Misaelides, P., Godelitsas, A., Filippidis, A., Charistos, D., & Anousis, I. (1995). Thorium and Uranium Uptake by Natural Zeolitic Materials. *The Science of the Total Environment*, 237-246.

Monhemius, J. (1977). Precipitation Diagrams for Metal Hydroxides, Sulfides, Arsenates and Phosphates. *Transactions Institution of Mining and Metallurgy*, 202-206.

Monji, A., Ghoulipour, V., & Mallah, M. (2016). Selective Sorption of Uranium (IV) from Hydrochloric Acid Media by Agro-Industrial Byproducts. *Annals of Nuclear Energy*, 115-121.

Motsi, T., Rowson, N., & Simmons, M. (2009). Adsorption of Heavy Metals from Acid Mine Drainage by Natural Zeolite. *Int. J. Miner. Process.*, 42-48.

Muhling, J., Suvorova, A., & Rasmussen, B. (2014). The Occurrence and Composition of Chevkinite-(Ce) and Perrierite-(Ce) in Theoleitic Intrusive Rocks and Lunar Mare Basalt. *American Mineralogist*, 1911-1921.

Nandanwar, S., Coldsnow, K., Utgikar, V., Sabharwall, P., & Aston, D. (2016). Capture of Harmful Radioactive Contaminants from Off-Gas Stream Using Porous Solid Sorbents for Clean Environment - A Review. *Chemical Engineering Journal*, 369-381.

Nasab, M. (2014). Solvent Extraction Separation of Uranium (VI) and Thorium (IV) with Neutral Organophosphorus and Amine Ligands. *Fuel*, 595-600.

Nasab, M., Sam, A., & Milani, S. (2011). Determination of Optimum Process Conditions for the Separation of Thorium and Rare Earth Elements by Solvent Extraction. *Hydrometallurgy*, 141-147.

Navrotsky, A., Shvareva, T., & Guo, X. (2013). Thermodynamics of Uranium Minerals and Related Materials. In *Mineralogical Association of Canada Short Course 43*. Winnipeg, MB.

Orabi, A. (2013). *Determination of Uranium After Separation Using Solvent Extraction from Slightly Nitric Acid Solution and Spectrophotometric Detection*. Journal of Radiation Research and Applied Sciences, 1-10.

Palmieri, M. (1987). Separation and Determination of Trace Metal Ions Using Organic Chelating Reagents. Thesis, Iowa State University.

Parzentny, H., & Rog, L. (2019). The Role of Mineral Matter in Concentrating Uranium and Thorium in Coal and Combustion Residues from Power Plants in Poland. *Minerals*, doi:10.3390/min9050312.

Paul, J., & Campbell, G. (2011). *Investigating Rare Earth Element Mine Development in EPA Region 8 and Potential Environmental Impacts.* The United States Environmental Protection Agency.

Peiro, L., & Mendez, G. (2013). Material and Energy Requirement for Rare Earth Production. JOM, 1327-1340.

Ponou, J., Dodbiba, G., Anh, J., & Fujita, T. (2016). Selective Recovery of Rare Earth Elements from Aqueous Solution Obtained from Coal Power Plant Ash. *Journal of Environmental Chemical Engineering*, 3761-3766.

Pourbaix, M. (1974). *Atlas of Electrochemical Equilibria in Aqueous Solutions.* Brussels: Cebelcor.

Qi, D. (2018). Extractants Used in Solvent Extraction-Separation of Rare Earths: Extraction Mechanism, Properties, and Features. In *Hydrometallurgy of Rare Earths-Separation and Extraction* (pp. 187-389).

Rand, M., Fuger, J., Grenthe, I., Neck, V., & Rai, D. (2008). Chemical Thermodynamics of Thorium. Oxford.

Regenspurg, S., Margot-Roquier, C., Harfouche, M., Froidevaux, P., Steinmann, P., Junier, P., & Bernier-Latmani, R. (2010). Speciation of Naturally-Accumulated Uranium In An Organic-Rich Soil of An Alpine Region (Switzerland). *Geochimica et Cosmochimica Act*a , 2082-2098.

Sani, A., Bandegharaei, A., Hosseini, S., Kharghani, K., Zarei, H., & Rastegar, A. (2015). Kinetic, Equilibrium and Thermodynamic Studies on Sorption of Uranium and Thorium from Aqueous Solutions by A Selective Impregnated Resin Containing Carminic Acid. *Journal of Hazardous Materials*, 152-163.

Seo, E., Cheong, Y., Yim, G., Min, K., & Geroni, J. (2017). Recovery of Fe, Al and Mn in Acid Coal Mine Drainage by Sequential Selective Precipitation with Control of pH. *Catena*, 11-16.

Silva, R. G., De Morais, C. A., & Teixeria, L. V. (2018). Selective Removal of Impurities from Rare Earth Sulphuric Liquor Using Different Reagents. *Minerals Engineering*, 238-246.

Srinivas, C., Venkatesh, K., Wattal, P., Theyyunni, T., Kartha, P., & Tripathi, S. (1994). *Alkaline Hydrolysis Process for Treatment and Disposal of Purex Solvent Waste.* Bombay, India: Bhabha Atomic Research Centre.

Thakur, N. (2000). Separation of Rare Earths by Solvent Extraction. Mineral Processing and Extractive Metallurgy Review, 277-306.

Thommes, M., Kaneko, K., Niemark, A., Olivier , J., Rodriguez-Reinoso, F., Rouquerol, J., & Sing, K. (2015). Physisorption of Gases, With Special Reference to the Evaluation of Surface Area and Pore Size Distribution. *Pure Applied Chemistry*.

Tomazic, B., Branica, M., & Tezak, B. (1962). Precipitation and Hydrolysis of Uranium(VI) in Aqueous Solutions: Uranyl Nitrate-Potassium Hydroxide-Neutral Electrolyte. *Croatica Chemica Acta*, 41-50.

Torapava, N., Persson, I., Eriksson, L., & Lundberg, D. (2009). Hydration and Hydrolysis of Thorium (IV) in Aqueous Solution and the Structures of Two Crystalline Thorium(IV) Hydrates. *Inorganic Chemistry*, 11712-11723.

Wang, Y., Zhang, Z., Liu, Y., Cao, Z., Liu, Y., & Li, Q. (2012). Adsorption of U(VI) from Aqueous Solution by the Carboxyl-Mesoporous Carbon. *Chemical Engineering Journal*, 246-253.

Xie, F., Zhang, T., Dreisinger, D., & Doyle , F. (2014). A Critical Review on Solvent Extraction of Rare Earths from Aqueous Solutions. *Minerals Engineering*, 10-28.

Xiong, X., Tao, Y., Yu, Z., Yang, L., Sun, L., Fan, Y., & Luo, F. (2020). Selective Extraction of Thorium from Uranium and Rare Earth Elements Using Sulfonated Covalent Organic Framework and Its Membrane Derivative. *Chemical Engineering Journal*, 123240.

Zendelska, A., Golomeova, M., Blazev, K., Krstev, B., Golomeov, B., & Krstev, A. (2015). Adsorption of Copper Ions from Aqueous Solutions on Natural Zeolite. *Environmental Protection Engineering*, 17-36.

Zhang, J., & Zhao, B. (2016). *Separation Hydrometallurgy of Rare Earth Elements.* Saskatoon: Springer.

Zhang, J., Zhao, B., & Schreiner, B. (2016). *Separation Hydrometallurgy of Rare Earth Elements.* Saskatoon: Springer.

Zhou, H., Wang, Y., Guo, X., Dong, Y., Su, X., & Sun, X. (2018). The Recovery of Rare Earth by A Novel Extraction and Precipitation Strategy using Functional Ionic Liquids. *Journal of Molecular Liquids*, 414-420.

Zhou, L., Shang, C., Liu, Z., Huang, G., & Adesina, A. (2012). Selective Adsorption of Uranium(VI) from Aqueous Solutions Using the Ion-Imprinted Magnetic Chitosan Resins. *Journal of Colloid and Interface Science*, 165-172.

Zhu, Z., Pranolo, Y., & Cheng, C. (2015). Separation of Uranium and Thorium from Rare Earths for Rare Earth Production - A Review. *Minerals Engineering*, 185-196.

Zou, W., Zhao, L., & Han, R. (2009). Removal of Uranium (VI) by Fixed Bed Ion-Exchange Column Using Natural Zeolite Coated with Manganese Oxide. *Chinese Journal of Chemical Engineering*, 585-593.

APPENDIX A - PROJECT MANAGEMENT PLAN

PHASE 2: PILOT-SCALE TESTING OF AN INTEGRATED CIRCUIT FOR THE EXTRACTION OF RARE EARTH MINERALS AND ELEMENTS FROM COAL AND COAL BYPRODUCTS USING ADVANCED SEPARATION TECHNOLOGIES

For AOI2

University Members

University of Kentucky
Virginia Tech
West Virginia University

Corporate Members

Minerals Refining Company
Alliance Coal
Blackhawk Mining
Mineral Separations Tech

Project Management Plan

DE-FE0027035

SUBMITTED BY

University of Kentucky
Department of Mining Engineering
230 Mining & Mineral Resources Engineering
Lexington, Kentucky 40506-0107

PRINCIPAL INVESTIGATOR

Dr. Rick Honaker
Phone Number: +859-257-1108
Fax Number: +859-323-1962
E-Mail: rick.honaker@uky.edu

SUBMITTED TO

U.S. Department of Energy
National Energy Technology Laboratory
Contracting Officer: Charles Miller

October 31, 2017

1. EXECUTIVE SUMMARY

Analysis of the U.S. Geological Survey's Coal Quality Database showed that the U.S. has 10.9 million tons of rare earths resource in the coal deposits located in just five western and four eastern states. It is, therefore, proposed to design, construct, and test a ¼-ton/hour mobile pilot plant that can be used to economically extract rare earth minerals (REMs) and rare earth elements (REEs) from the non-conventional resource, which is six-times larger than the U.S. rare earth reserve. The mobile pilot plant will consist of a circuit consisting of both physical and chemical separation processes that are currently available for deployment. The results of the proposed work will be useful for U.S. coal companies to construct optimally-designed commercial rare earth recovery plants that can produce concentrates assaying >2% REEs at high recoveries in an environmentally friendly manner. The utilization of coal byproducts as a source of REEs is beneficial in improving the project economics by excluding mining costs. Meeting the goals and objectives of the proposed work will be a significant step toward creating a domestic supply chain for the critical materials needed for national security, advanced manufacturing, and renewable energy, while at the same time helping the U.S. coal companies to be more competitive and retain high-paying jobs.

In Phase I, qualified feedstocks for the mobile pilot plant have been identified. One is the byproduct stream from the Leatherwood coal preparation plant operated by the Blackhawk Mining, LLC., in which the Fire Clay coal seam is being processesed. This coal is well known for its high rare earth contents due to exposure to volcanic deposition. It has been found that the coarse refuse stream assays 324 ppm REEs on average on a whole mass basis, while the spiral middlings assay 315 ppm REEs on a whole mass basis. Channel samples taken from the Fire Clay coal seam show that the roof material and the coal segments assay 490 and 460 ppm REEs, respectively, on whole mass basis, of which nearly 40% of the REEs belong to the group of critical materials identified by U.S. DOE. Another qualified rare earths source is the byproduct from the Dotiki preparation plant operated by Alliance Coal, LLC., which mines the West Kentucky No. 13 coal seam. The coarse refuse generated from its coal cleaning operation assays 312 ppm REEs on a whole mass basis. A sample of a claystone parting that occurs throughout the seam contains 930 ppm REEs, of which 25% was neodymium (Nd) and yttrium (Y). In addition, the natural leachate generated from the coarse refuse pile contains 420 ppm REEs in the simple precipitate formed from the leachate. The precipitate has high scandium (Sc) and heavy rare earth elements (HREEs).

The first step in processing the coarse refuse will be to obtain middlings material from the coarse refuse with a specific gravity (SG) less than 2.2, which will be subsequently crushed and ground to a top size of 170 microns to improve the liberation of coal and mineral matter. The ground material will then be subjected to the hydrophobic-hydrophilic separation (HHS) process first to produce a salable coal with low ash and low moisture contents, and then to produce a REM concentrate. A hydrophobizing agent such as potassium octyl hydroxamate (KOH) or a fatty acid is added to render the REMs selectively hydrophobic. In a preliminary test, an REM concentrate assaying 17,000 ppm REE (ash-basis) was obtained from a byproduct from a Fire Clay coal. An additional cleaning step would have readily increased the grade further.

The tailings stream generated from the HHS process will be subjected to chemical leaching, followed by solvent extraction (SX). In general, REE recoveries from the middlings materials collected are substantially higher than those obtained with other byproduct streams. It has been shown that sulfuric acid leaching at pH = 0, for example, can achieve an 80% recovery at 75°C after two hours. It has been demonstrated also that the REEs present in the leach liquor can be separated from other ions by following a series of SX steps, which include loading, scrubbing,

and stripping to produce a rare earth oxide (REO) concentrate. From preliminary work, REO concentrates assaying 51% and 8.5% REEs have been obtained on a dry, whole mass basis from the Fire Clay and Kentucky No. 13 middlings, respectively. The REO concentrations from these two byproducts contain high concentrations of Sc and HREEs – higher concentration than obtainable from the conventional resources such as the Mountain Pass and Bayan Obo ores.

For Phase II, the project team proposes to construct and test a ¼-tph mobile pilot plant for the recovery REEs at two different test sites, where the Fire Clay and West Kentucky No. 13 coals are processed. The project team consists of three institutions: University of Kentucky (lead institute), West Virginia University, and Virginia Tech. They have a long history of cooperative R&D, including pilot-scale and in-plant tests and successful commercialization. The Blackhawk Mining and Alliance Coal companies will provide test sites, provide power and water, and work with the team to judiciously handle waste disposal and management. Minerals Refining Company and Mineral Separation Technologies will provide pilot-scale units of their respective separation technologies. Precipitation tanks will be employed to pre-concentrate the REEs in naturally occurring leachate produces at the mine site. Process will be tested to remove any potential issues associated with thorium or other undesirable elements. Finally, filter presses will concentrate and neutralize any solids residual prior to disposal.

The mobile pilot plant will be designed to be flexible, so that it can be used to use different types of feed stocks, including coarse refuse, ultrafine thickener underflow and naturally occurring coarse waste leachate. The coarse refuse will be screened first and then subjected to sorting using advanced sensors that can discriminate particles according to their SGs and/or chemical make-ups. The proposed plant layout will include crushers and grinding mills to improve liberation. A pilot-scale HHS unit will be used to simultaneously recover and dewater coal and subsequently produced REM concentrates. A countercurrent leaching system and SX system consisting of 10 mixer-settlers will be used for producing desired REO concentrates. Precipitation tanks will be used to extract REEs from GOB pile leachates and to address potential environmental issues associated with handling thorium (Th) and other undesirable elements.

The primary objective of this investigation is to develop, design and demonstrate a mobile pilot-scale processing system for the efficient, low-cost and environmentally benign recovery of high-value rare earth elements (REEs) from coal and coal byproducts. The proposed system integrates both physical and chemical (ion exchange and solvent extraction) separation processes that are commercially available and environmentally acceptable. The innovative enabling technology utilized in the proposed system includes an advanced froth flotation process and a novel hydrophobic-hydrophilic separation process. Both these enabling technologies were developed previously under DOE sponsorship by the project investigators working within the Center for Advanced Separation Technologies (CAST). The proposed pilot-scale circuit is expected to have a dry solids feed capacity of 1/4 ton per hour and be capable for producing up to 0.1-1.0 kilograms per hour of combined concentrates with purity levels of at least 2% REEs by weight. Upon completion, the project is expected to provide critical data as to the equipment, conditions and know-how necessary to design, construct and operate a state-of-the-art processing facility for the production of REEs from various coal and coal byproduct streams.

2. PROJECT TEAM

The project team has a long history of working together as part of the Center for Advanced Separation Technologies (CAST) and developing many advanced separation technologies that are in commercial use. The team includes the University of Kentucky, West Virginia University, and Virginia Tech and several industrial participants. These include Blackhawk Mining, Alliance Coal, Mineral Separation Technologies, Minerals Refining Company (MRC), and Outotec. As indicated by their commitment letters, the two coal companies are providing significant support for the project by hosting the two test sites, making modifications as needed to the facilities to ensure project success, assigning manpower to secure permits that may be required, supplying water and power, and transporting feedstock and waste materials when requested. The two remaining team members are technology companies. Mineral Separation Technologies (MST) is a leader in ore sorting technologies, while MRC is the licensee of the hydrophobic-hydrophilic separation (HHS) process, which has the potential to recover micron size or smaller particles. The HHS process has been developed at CAST under funding from NETL and has been tested successfully at proof-of-concept (POC) and is currently under pilot-scale testing. MST and MRC have committed the use of their pilot-scale units to the project for a period of 12 months in addition manpower support for equipment start-up. SX Kinetics is another processing equipment company who will provide their expertise and equipment in leaching and solvent extraction to assist the efforts of the project team. The team membership includes three National Academy of Engineering (NAE) members, with outstanding scientific accomplishments and ample experience in technology commercialization.

The proposed work will be managed by a professional team that has demonstrated experience in managing large interdisciplinary R&D. A schematic illustrating the overall management structure for the project is provided in Figure 1 along with the individuals responsible for overseeing the successful completion of each project task in budget periods 1 (BP1) and 2 (BP2). Dr. Rick Honaker, professor and chair of the Department Mining Engineering at the University of Kentucky (UK) will serve as the Principal Investigator for the overall project. Dr. Honaker has significant experience in managing large research and educational programs. His administrative responsibilities for the proposed project will focus on project organization, team coordination, data management, technical/administrative/financial reporting, and other activities necessary for the successful completion of this project. Fiscal controls for this project will be managed by the University of Kentucky's Office of Sponsored Projects (OSP). A Contract Administrator assigned to the project award, will coordinate fiscal management and cost reporting. Dr. Honaker will communicate directly with UK's OSP to ensure that proper expenditure controls are maintained. He will also act as the liaison between OSP and other participants to ensure compliance with financial and technical reporting requirements.

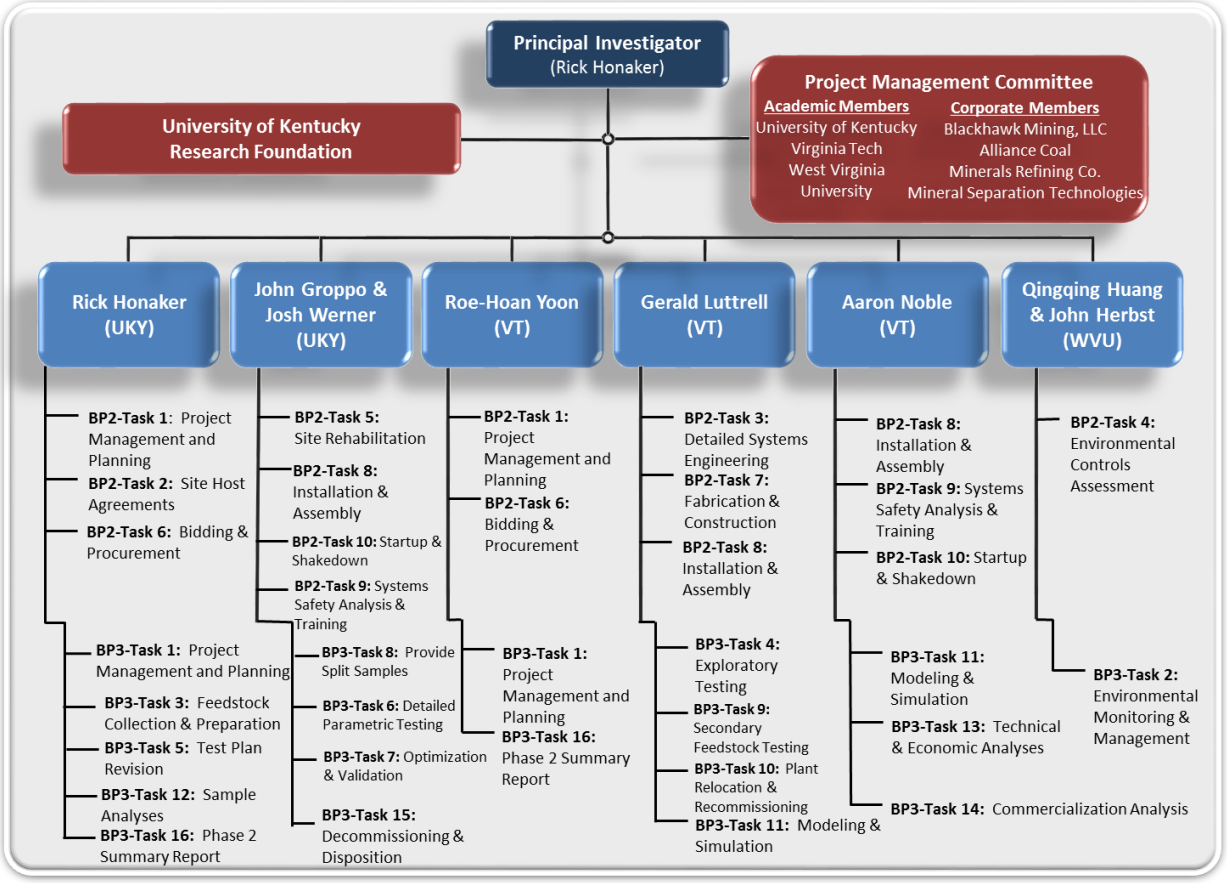

Figure 1. Project organizational diagram and assigned responsibilities.

The key members of the project team will meet by video conference on a weekly basis to update the status of assigned project tasks. A list of key team members along with their associations and contact information are provided in Table 1.

Table 1: Listing of Key Personnel and Contact Information

Personnel	Business Association	Primary Contact E-Mail
Rick Honaker	University of Kentucky	honaker@uky.edu
John Groppo	University of Kentucky	john.groppo@uky.edu
Josh Werner	University of Kentucky	jmwe256@uky.edu
Roe-Hoan Yoon	Virginia Tech	ryoon@vt.edu
Gerald Luttrell	Virginia Tech	luttrell@vt.edu
Aaron Noble	Virginia Tech	noble54@vt.edu
Qingqing Huang	West Virginia University	qingqing.huang@mail.wvu.edu
John Herbst	West Virginia University	john.herbst@mail.wvu.edu
Hunter Davis	Alliance Coal	Hunter.Davis@arlp.com
Kevin Varney	Blackhawk Mining	kvarney@blackhawkmining.com
Stan Suboleski	Mineral Refining Company	ssuboleski@evanenergy.com
Charles Roos	Mineral Separation Technologies	charles@mineralseparationtechnologies.com

The Virginia Tech team led by Dr. Roe-Hoan Yoon (NAE member) will provide support for the construction, operation and testing of the pilot-scale REE recovery plant. Dr. Yoon along with Drs. Gerald Luttrell (NAE member) and Aaron Noble provide significant expertise in technology development as well as process modeling, technical and economic analyses. A number of technologies including the Microcel flotation column and the HHS process, have been successful commercialized by the Virginia Tech researchers through funding, in part, provided by NETL.

Drs. John Herbst (NAE member) and Qingqing Huang are professors at West Virginia University who have expertise in extractive metallurgy. They will lead the environmental research and management tasks in the project with special emphasis on developing and testing methods and processes to remove thorium and other elements of environmental concern from the leachate solutions.

3. RISK MANAGEMENT PLAN

3.1 Risk Management Matrix

Upon notification of project award, the *Project Management Committee* will develop a detailed *Risk Management Plan* for the proposed project. The plan will be submitted to the DOE Contracting Officer within 60 days after the project award. The plan will identify specific risks at each stage of the project, will offer strategies for risk impact assessment, and will outline potential mitigation actions. The plan will be periodically updated and expanded throughout the project life as the work activities increase in complexity and potential risks become defined in greater detail. The plan will make use of a risk management matrix that will prioritize the potential technical, resource, and management risks. A preliminary draft of the risk management matrix compiled on a task-by-task level is provided in Table 2. As shown, the matrix includes (i) a description of specific risks and possible consequences, (ii) a percentage probability value for the likelihood that an issue may arise, (iii) a 1 to 5 scaled ranking of the expected adverse impact of a specific risk, (iv) a priority ranking determined by multiplying the probably by the impact, and (v) a listing of mitigation steps to reduce and possibility eliminate a specific risk.

3.2 Quality Assurance and Control

One risk element that must be addressed early in the project and continually monitored is the quality assurance/quality control of the data generated from the proposed work. To reduce risk associated with the collection and reporting of such data, a *Quality Assurance/Quality Control (QA/QC) Plan* will be implemented that includes both quality control and quality assessment protocols. The quality control protocols will focus on the formulation of standard operating procedures that are needed to provide reliable data, while the quality assessment protocols will audit the effectiveness of the quality control protocols. The program will address sample integrity (collection, analysis, tracking, archiving), laboratory analysis procedures, bench-scale testing procedures, equipment and process operating protocols, and data management and documentation. For the case of sample analyses, detailed written procedures, based on ASTM/ISO/EPA standards, will be prepared and provided applicable project participants.

3.3 Problem Identification and Resolution Protocols

The proposed *Statement of Project Objectives (SOPO)* is believed to be sufficiently well conceived to minimize any significant technical, resource and management issues that may impact project success. However, in order to rapidly identify and respond to any unanticipated future difficulties that may arise, the Principal Investigator (PI) will stay informed of all such issues that may affect the project via weekly Webex calls that will include all key members of the management team. Once an impediment is identified, the PI will put in place the necessary manpower and actions required to solve the problem. If it is ascertained that the problem is serious enough to jeopardize the project, DOE will be notified and kept informed of the progress in overcoming the impediment. A log of the Webex calls and corresponding minutes from each session will be recorded.

Table 2. Risk Management Matrix

	Description of Risk/Consequence	Probability (0-100%)	Impact (1-5)	Priority (PxI)	Recommended Mitigation Response
01	Rare earth element grade in final product does not meet the 2 percent requirement.	10	5	0.5	Investigate reasons, identify contaminates and refine the flowsheet design
02	Poor leachability	20	4	0.8	Change sources or leaching conditions
03	Subcontractors not delivering on time	50	4	2.0	Weekly contacts with subcontractors for progress reports.
04	Partners backing out of site agreement	20	3	0.6	Project moved to another site and/or material transported by truck to the REE plant location.
05	Site partners not providing adequate infrastructure	30	3	0.9	Project moved to another site and/or material transported by truck to the REE plant location.
06	Flowsheet design delays	50	4	2.0	Expedite the equipment construction with vendors; implement deadlines for final system design.
07	Loss of subcontractor	10	3	0.3	Seek an alternative subcontractor
08	Significant injury	10	5	0.5	Strict implementation of the Health, Safety and Environmental Plan.
09	REE recovery system has a negative impact on the total reject disposal system	20	4	0.8	Engineer an appropriate solution
10	Undesirable radioactive element concentration	50	4	2.0	Re-evaluate processes and flowsheet design followed by additional testing
11	Coal and REE markets do not support economic recovery.	30	5	1.5	Focus on lowering capital and operating costs which may require flowsheet adjustments
12	Capital and operating cost do not support economic recovery	30	5	1.5	Seek additional byproducts that could add value revenue and impact economic viability

4. PROJECT SCHEDULE

4.1 Project Timeline

Figure 1 shows the anticipated schedule for the proposed scope of work. As shown, the 31 month project has been subdivided into two consecutive budget periods with durations of 10 and 21 months, respectively. The first budget period runs from project award through commissioning, while the second budget period runs from testing through project completion. In total, the project includes 26 primary tasks involving planning, engineering, bidding, procurement, fabrication, construction, installation, training, experimentation, data analysis, technical/economic analysis, market analysis, environmental assessment, and reporting. A narrative description of the work elements included in each task and subtask is provided the *Statement of Project Objectives* (SOPO). Additional subtasks described in the SOPO will be added to the project schedule if an award is received but has been omitted at this time for brevity sake.

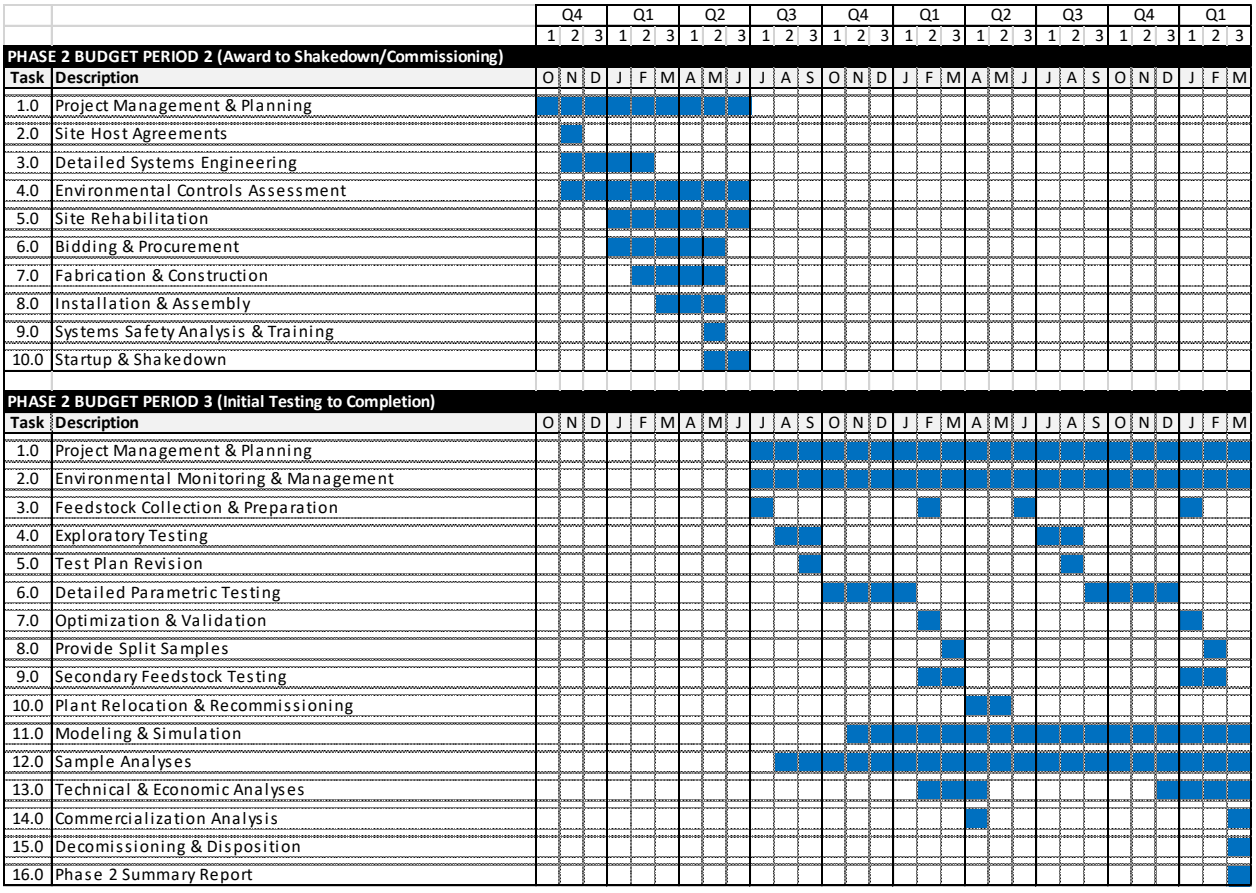

Figure 2. Proposed Project Schedule for Budget Period 2 (Award through Commissioning) and Budget Period 3 (Testing through Project Completion).

4.2 Project Milestones

Major and minor milestones for Phase II of the project are summarized in Tables 3 and 4 for Budget Periods 2 and 3, respectively. The work breakdown has been coordinated such that the end point

of each primary task represents a significant project milestone. Minor milestones associated with the completion of additional subtasks described in the *Statement of Project Objectives* (SOPO) will be added to the milestone log if the award is received, but has been omitted from this document for brevity sake. During project performance, the milestone status will be updated in quarterly *Research Performance Progress Reports* prescribed by DOE's Reporting Requirements Checklist. The update will include (i) actual status and progress, (ii) specific progress made towards milestones, and (iii) any proposed changes in the schedule or milestones.

Table 3. Listing of Significant Project Milestones for Budget Period #2 (Project Award through Startup/Commissioning).

Budget Period 1 Milestone	Completion of Task or Subtask …	Completion Date	Major or Minor?
BP1-A	1.0 - Project Management & Planning	6/30/2018	Major
BP1-B	2.0 – Site Host Agreements	11/30/2017	Major
BP1-C	3.0 – Detailed Systems Engineering	2/28/2018	Major
BP1-D	4.0 – Environmental Controls Assessment	6/30/2018	Major
BP1-E	5.0 – Site Rehabilitation	6/30/2018	Major
BP1-F	6.0 – Bidding & Procurement	5/30/2018	Major
BP1-G	7.0 – Fabrication & Construction	5/30/2018	Major
BP1-H	8.0 – Installation & Assembly	5/30/2018	Major
BP1-I	9.0 – Systems Safety Analysis & Training	5/30/2018	Major
BP1-J	10.0 – Startup & Shakedown	6/30/2018	Major

Table 4. Listing of Significant Project Milestones for Budget Period #3 (Testing through Project Completion).

Budget Period 2 Milestone	Completion of Task or Subtask …	Completion Date	Major or Minor?
BP2-A	1.0 - Project Management & Planning	3/31/2020	Major
BP2-B	2.0 – Environmental Monitoring & Management	2/28/2020	Major
BP2-C1	3.0 – Feedstock Collection & Preparation (Site 1)	7/31/2018	Major
BP2-C2	3.0 – Feedstock Collection & Preparation (Site 2)	6/30/2019	Major
BP2-D1	4.0 – Exploratory Testing (Site 1)	9/30/2018	Major
BP2-D2	4.0 – Exploratory Testing (Site 2)	8/30/2019	Major
BP2-E1	5.0 – Test Plan Revision (Site 1)	9/30/2018	Major
BP2-E2	5.0 – Test Plan Revision (Site 2)	8/30/2019	Major
BP2-F1	6.0 – Detailed Parametric Testing (Site 1)	1/31/2019	Major
BP2-F2	6.0 – Detailed Parametric Testing (Site 2)	12/30/2019	Major
BP2-G1	7.0 – Optimization & Validation (Site 1)	2/28/2019	Major
BP2-G2	7.0 – Optimization & Validation (Site 2)	1/31/2020	Major
BP1-H1	8.0 – Provide Sample Splits (Site 1)	3/31/2019	Major
BP1-H2	8.0 – Provide Sample Splits (Site 2)	2/28/2020	Major
BP2-I1	9.0 – Secondary Feedstock Testing (Site 1)	3/30/2019	Major
BP2-I2	9.0 – Secondary Feedstock Testing (Site 2)	2/28/2020	Major
BP2-J	10.0 – Plant Relocation & Recommissioning	5/31/2019	Major
BP2-K	11.0 – Modeling & Simulation	3/31/2020	Major
BP2-L	12.0 – Sample Analysis	3/31/2020	Minor
BP2-M	13.0 – Technical & Economic Analyses	3/31/2020	Major
BP2-N	14.0 – Commercialization Analysis	3/31/2020	Major
BP2-O	15.0 – Decommissioning & Disposition	3/31/2020	Minor
BP2-P	16.0 – Phase 2 Summary Report	3/31/2020	Major

5. SUCCESS CRITERIA AT DECISION POINTS

Tables 5 and 6 provide listings of important milestones and success criteria for budget periods 1 and 2, respectively.

Table 5. Listing of Success Criteria at Decision Points in Budget Period 1 (Award through Commissioning).

Milestone ID	Description of Success Criteria …
BP1-A	Project progresses in accordance with timeline/ budget. All reports submitted on time. NEPA documentation completed, submitted and approved.
BP1-B	Site host agreements successfully prepared, negotiated and executed for both industrial test locations. Completion of Task 2 in Budget Period 1.
BP1-C	Representative samples of at least 5 grams each collected under optimized conditions from each test site and shipped to DOE for REE analysis. Completion of Task 3 in Budget Period 1.
BP1-D	Successful completion of detailed systems engineering for the six required process bays. Completion of Task 4 in Budget Period 1.
BP1-E	Submission of Environmental Analysis report and receipt of final operating permits. Completion of Task 5 in Budget Period 1.
BP1-F	Completion of site rehabilitation activities for each of the two pilot-plant locations. Completion of Task 6.0 in Budget Period 1.
BP1-G	Bidding documents prepared/offered and procurement activities executed. Completion of Task 7 in Budget Period 1.
BP1-H	Field activities associated with pilot-plant fabrication and construction completed per the detailed systems design specifications. Completion of Task 8 in Budget Period 1.
BP1-I	Field activities associated with pilot-plant installation and assembly completed per the detailed systems design specifications. Completion of Task 9 in Budget Period 1.
BP1-J	Systems safety analysis, including a fatal flaw review by key participants, completed. Site personnel training completed. Completion of Task 10 in Budget Period 1.

Table 6. Listing of Success Criteria at Decision Points in Budget Period 2 (Testing through Project Completion).

Milestone ID	Description of Success Criteria …
BP2-A	Project progresses in accordance with timeline/ budget. All reports submitted on time.
BP2-B	Environmental monitoring and management plan completed including SPCC, SWPP and RCM plans. Completion of Task 2 in Budget Period 2.
BP2-C	All samples successfully collected at mine sites and prepared for testing. Feed samples must meet required >300 ppm TREE content on a whole sample basis. Completion of Task 3 in Budget Period 2.
BP2-D	Exploratory testing of both feedstocks in pilot-plant facility completed. Completion of Task 4 in Budget Period 2.
BP2-E	Test plans revised and vetted for both pilot-plant test sites based on information collected from shakedown and exploratory testing. Completion of Task 5 in Budget Period 2.
BP2-F	Detailed parametric testing of both feedstocks in pilot-plant facility completed. Completion of Task 6 in Budget Period 2.
BP2-G	Long-duration optimization and validation tests of both feedstocks in pilot-plant facility completed. Completion of Task 7 in Budget Period 2. (*Optimum sample splits provided to DOE for analysis of REE contents per Task 3 in Budget Period 1*).
BP2-H	Testing of secondary samples, such as precipitants from mine influenced waters, initiated and completed. Completion of Task 8 in Budget Period 2.
BP2-I	The relocation of recommissioning of the pilot-scale facility initiated and completed. Completion of Task 9 in Budget Period 2.
BP2-J	Mathematical models refined and simulator updated based on experimental findings. Simulations conducted for each site. Completion of Task 10 in Budget Period 2.
BP2-K	All sample analyses, including coal analyses and elemental analyses, completed per ASTM specifications. Completion of Task 11 in Budget Period 2.
BP2-L	Technical and economic analyses initiated and completed. Techno-Economic Assessment submitted to DOE. Completion of Task 12 in Budget Period 2.
BP2-M	Technology transfer completed and commercialization plan developed and implemented. Completion of Task 13 in Budget Period 2.
BP2-N	Plan for facility decommissioning and equipment transfer/disposition completed and initiated. Completion of Task 14 in Budget Period 2.

6. FUNDING AND COSTING PROFILE

The organizational funding profile and quarterly costing profile for the proposed project are summarized in Tables 7 and 8, respectively.

Table 7. Project Funding Profile (Phase 2 Only)

Recipient Organization	6.1 Phase 2 Only		
	DOE Funds	**Non-Federal Cost-Share**	**Total**
Recipient: **University of Kentucky (UK)**	$3,300,000	$334,803	$3,634,803
UK Subrecipient: Blackhawk	$0	$321,583	$321,583
UK Subrecipient: Alliance	$0	$212,000	$212,000
UK Subrecipient: West Virginia University	$200,000	$50,278	$250,278
UK Subrecipient: Virginia Tech	$2,233,495	$341,000	$2,574,495
VT Subrecipient: Minerals Refining Company	$104,505	$120,336	$224,841
VT Subrecipient: **Outotec USA**	$98,000	$0	$98,000
VT Subrecipient: Mineral Separation Technologies	$44,000	$120,000	$164,000
VT Subrecipient: Bratton Engineering	$20,000	$0	$20,000
Total ($)	$6,000,000	$1,500,000	$7,500,00

Table 8. Project Costing Profile (Phase 2 Only) DOE Funding Requirements by Calendar Quarter

Funding Quarter	**CY 2017 ($)**	**CY 2018 ($)**	**CY 2019 ($)**	**CY 2020 ($)**
Q1 (Jan – Mar)		$1,017,037	$549,581	$250,424
Q2 (Apr – Jun)		$436,558	$432,851	
Q3 (Jul – Sep)	$1,221,520	$499,536	$488,078	
Q4 (Oct – Dec)	$320,623	$405,915	$377,879	
Total ($)	$1,542,142	$2,359,045	$1,848,389	$250,424

7. HEALTH, SAFETY AND ENVIRONMENTAL MANAGEMENT

7.1 Statement of Objective

The purpose of this Health Safety and Environmental plan is to outline the major components necessary to execute the project without any environmental excursions or injuries. This represents a significant statement of project policy to ensure good environmental and social stewardship. To accomplish these objectives major health, safety and environmental risks have been identified and are discussed. In addition, the projects HSE management plant will be presented.

7.2 Environmental Risks

The major sources of environmental risks identified at this time are:

1. Modification of Feed Materials
2. Concentration of Radioactive Materials
3. Release of Reagents
4. Water Quality Impact
5. Air Quality Impact

Although not an exhaustive list of potential environmental impacts, this subset will contain the vast majority of potential environmental risks to this project.

Modification of Feed Materials

The first concern focuses on the modification of leachability of coal byproducts as a result of further processing. It is a well-known fact that coal byproducts are susceptible to natural leaching through exposure to rain and ground water. These occur at rates and with elements intrinsic to each process and coal source. The potential environmental impact is manifest in negatively impacting the natural leaching of coals in ways that either enhance the leachability of undesirable elements or increase the rate of leaching. To understand these risks TCLP (Toxicity characteristic leaching procedure) tests will be conducted to understand the changes in leachability of the coal byproducts. This data will be used to identify potential issues created by coal byproduct processing and address as needed.

Concentration of Radioactive Materials

By nature, the project entails leaching and concentration of REEs from coal and coal byproducts. Because of this there is a concern that radioactive elements which are found in coal and coal byproducts will also be subject to concentration due to similar processing characteristics of REEs. In addition, these same techniques namely leaching and solvent extraction have been utilized in the past to extract Uranium and Thorium. Because of these concerns it is necessary as part of this project to quantify and understand the risks presented by these elements. The general approach will be:

1. Attempt to prevent the concentration of these elements where possible.
2. If concentrated, dilute the stream as part of tailings thus retuning occurrence to background levels.
3. If dilution with tailings is not possible due to changing the mobility of radioactive ions due to processing, dilution and capture through alternate means will be considered.

By approaching the concentration of radioactive elements in this manner an economic and safe processing arrangements will be carried out to return the material to like and kind state post processing. Further, if concentration of undesirable radioactive elements proves to be unavoidable before abatement, University of Kentucky HSE will be contacted to provide oversite and as needed monitoring of personnel.

Release of Reagents

Inadvertent release of reagents will be controlled in a number of methods both procedurally and operationally. The most likely mode of occurrence of inadvertent release of reagents will be through leaks and spills. To prevent these occurrences a number of methods will be utilized. The first of these will be the utilization of secondary containment. As appropriate, all storage of chemicals and reagents will have secondary containment. This may

include for example containment pallets for 55-gallon drums and spill containment for all liquid reagents. For modular processing bays secondary containment will be site specific which will include banks and sumps where if drips and spills occur they may be contained and cleaned without spillage to the surrounding area. These secondary containments will be sized appropriately to the containers, or tank and in-flow rates so that overflow of containment is improbable. Procedural methods of preventing leaks and spills may include, but are not limited to:

- Never leaving a filling tank unattended;
- Filling and transferring reagents over secondary containment;
- Housekeeping procedures producing a clean and sanitary environment where drips, spills and leaks are easily identifiable;
- Spill kits and adsorptive pigs for containment and cleanup.

Water Quality Impact

It is anticipated that water quality will be maintained at the processing site by treatment and neutralization of process water to match water inherent to the site. The locations of the pilot plant will be located at mine sites where the treatment of water from mine disturbed areas and from drainage from coal byproducts is permitted and well established. It is anticipated that waste water disposal will be treated to integrate in a non-intrusive way to the sites existing water treatment infrastructure. Monitoring of pilot plant effluent will be included as part of the project.

Air Quality Impact

The primary concern of this project with regard to impacting air quality will occur from process ventilation. This will likely include two constituents, acid mists from leaching and VOC (volatile organic compounds) related to the kerosene. For the acid it may be necessary to provide additional neutralization or wet scrubbing as part of the ventilation system prior to atmospheric venting. Appropriate environmental regulations will be consulted as part of the operation of the air handling system.

7.3 Health and Safety Risks

Due to the nature of construction, commissioning and operation of the REE processing pilot plant the type and nature of Health and Safety risks significantly change through the various phases of the project. For the purpose of categorizing risk types, four distinct phases will be discussed. These are:

1. Construction
2. Startup and Shakedown
3. Operation
4. Decommissioning

Construction

The construction phase carries unique and often changing risks due to an evolving construction environment. Risks involved in the construction phase include:

- Risks due to constantly changing workplace;

- Slips trips and falls due to construction;
- Struck by hazards from moving equipment;
- Cuts and burns from fabrication activities;
- Utilization of subcontractors unfamiliar with site or processes which poses an increased risk of injury.

To mitigate this risk simple techniques will be utilized such as:

- Appropriate MSHA training;
- OSHA JHAs (Job Hazard Analysis);
- Requirements of equipment specific training (i.e. Forklift);
- Shift start safety and correlation meetings;
- Lift planning (for equipment placement);
- Subcontractor check in with site foreman;
- Establishment of site specific rules, SOPs (standard operating procedures) and PPE.

Startup and Shakedown

Risks encountered during startup are varied, but primarily center around two principles. These are untested equipment/processes and operators un-familiar with process operation. To address these needs of safely testing equipment and training personnel this phase will be characterized by emphasis on the following:

- SOP Development;
- Specific operational and readiness tests and checklists to certify equipment operability;
- Certification of operators;
- Organization of appropriate MSDS sheets and Chemical Inventory;
- Emergency response drills as needed;
- Training of mine site personnel on how to respond to emergencies, such a fire.

Operation

The operation phase is characterized by risks occurring due to opportunity frequency and familiarity. For safety in this phase the focus will be:

- Audits of and continued training to SOPs;
- Training of new operators as needed;
- Periodic maintenance and safety review meetings where incidents and near misses are reviewed and reported.

Decommissioning

The last phase of the project is decommissioning. This project phase is characterized by similar hazards as the construction phase, but with added chemical exposure risks due to used equipment. Additionally, vigilance will be needed at this stage of the project as funds and time are often short and the general tendency to move swiftly and efficiently are the highest. Care will need to be exercised from the management team to continue in diligence during this phase of the project.

7.4 HSE (Health, Safety and Environment) Management Plan

The HSE management plan is based on the Six Sigma principles of Control Plans and FMEAs (Failure modes and effects analysis). This type of methodology is common with projects in manufacturing and ISO 9001 standards. In terms of this project, the FMEA defines:

1. Possible failure modes of the process;
2. Likely outcomes of those failures;
3. Likelihood of occurrence;
4. Possibility of detection;
5. Severity of the occurrence.

An example of a FEMA is shown in Figure 3 for a leach tank which depicts the processing steps and the specific characteristics of the failures of each step. A RPN (risk priority number) is given by multiplying the failure severity by the occurrence and detection. A higher the number reflects a greater degree of severity, frequency of occurrence and difficulty to detect. The scale ranges from 1 to 10, with 10 being reserved for significant safety excursions resulting in lost time injuries or fatalities. Not meeting specification for example would rank 7 in terms of severity. For those failures resulting in a RPN number that is too high, corrective actions are assigned and tracked via the recommended actions.

FMEA Number:	FMEA Plan Owner / Phone:	Date Original:	Date Revised:
001-Plant Operation	Josh Werner (509)995-6697	10/31/2017	NA
Process:	Team:	Revision Note	
Plant	Rick Honaker, Josh Werner, Jack Groppo		
Description:	Approval Date:		
Operation of Pilot Plant	Rick Honaker 11/4/2017		

Process Number	Process Name/ Description	Tank, Device, Equipment	Characteristics			Potential Failure Mode	Potential Effect(s) of Failure	Severity	Potential Cause of Failures	Occurrence	Current Process Controls Prevention	Current Process Controls Detection	Detection	R. P. N.	Recommended actions	Responsibility & Target Date	Actions Taken & Completion Date	Severity	Occurrence	Detection	R. P. N.
			No.	Inputs	Output																
1	Leaching	Leach Tank	1A	Impeller Speed		Too Fast	None	1	Improper Start up	3	SOP	Operator	3	9	None						
						Too Slow	Not enough Leaching	7	Improper Start up	3	SOP	Operator	3	63	Non operator Control	Rick H. 11/29/2017					
			1B	Temperature		Too Hot	Evaporation	3	Process Drift	1	PID Controller	Thermocouple	1	3	None						
						Too Cold	Not enough Leaching	7	Process Drift	1			1	7	None						

Figure 3. Example of FMEA for a REE leaching tank.

The FMEA is designed to work in concert with the Control Plan. Whereas the FMEA explores and defines potential failures and their effects, the Control Plan defines the methods that the process controls. Figure 4 shows an example Control Plan associated with the FMEA in Figure 3. Control plans form the foundation of SOP development and risk mitigation for this project. As shown in Figure 3, every processing step is defined with the step inputs and outputs. All variables for that step are defined and categorized as CTQ (critical to quality) or not. This document further defines the correct operational specifications for each process step, how quality is maintained for input/outputs and a how to react to out of specification or tolerance. As shown in Figure 4, many of these controls will be specified in relevant SOPs which will need to be developed per the Control plan.

Another useful feature of the Control Plans and FEMAs is that, in this project, they will be used to control not only the pilot plant, but be used to analyze and control operator/safety activities. To achieve this objective, the phases identified in Health and Safety Risks will be treated as processes and evaluated using these methods. Control plans and FMEAs will be used in conjunction with JHAs to fulfill the mandate of this project for a safe and environmentally benign operation.

Utilization of Control Plans and FMEAs as part of our project management process will ensure adequate controls and documentation for successful project implementation.

Control Plan			
Control Plan Number: 001-Plant Operation	Control Plan Owner / Phone: Josh Werner (509)995-6697	Date Original: 10/31/2017	Date Revised: NA
Process: Plant	Team: Rick Honaker, Josh Werner, Jack Groppo	Revision Note	
Description: Operation of Pilot Plant	Approval Date: Rick Honaker 11/4/2017		

Process Number	Process Name/ Description	Tank,Device, Equpipement	Characteristics			CTQ	Methods					Reaction Plan
			No.	Inputs	Output		Product/Process Specification/Tolerance	Evaluation/ Measurement	Sample Size	Sample Freq.	Control Method	
1	Leaching	Leach Tank	1A	Impeller Speed		N	400-600 RPM	Digital Readout		1x per shift	Knob	Adjust
			1B	Temperature		Y	30-40c	Digital Readout		cont.	PLC	Adjust
			1C	% Solids		N	30-40%	Density	10ml	3X per Shift	SPC	Adjust
			1D	Size		Y	70-150 micron	Dry and Screen	100g	1x per shift	Screen and Weigh	See SOP
			1E		% Extracted	Y	70% minimum	See Assay SOP		1x per shift	ICP-OES	See SOP
2	Solvent Loading	SX loading Mixers	2A	O:A Ratio		Y	1:01	See SOP		1x per shift	SPC	See SOP
			2B	Impeller Speed		N	600-800 rpm	Digital Readout		1x per shift	Knob	Adjust

Figure 4. Example control plan associated with the FMEA for a REE leaching tank.

APPENDIX B - HEALTH, SAFETY & ENVIRONMENTAL PLAN

PHASE 2: PILOT-SCALE TESTING OF AN INTEGRATED CIRCUIT FOR THE EXTRACTION OF RARE EARTH MINERALS AND ELEMENTS FROM COAL AND COAL BYPRODUCTS USING ADVANCED SEPARATION TECHNOLOGIES

For AOI2

University Members

University of Kentucky
Virginia Tech
West Virginia University

Corporate Members

Minerals Refining Company
Alliance Coal
Blackhawk Mining
Mineral Separations Tech

Health, Safety & Environmental Plan

DE-FE0027035

SUBMITTED BY

University of Kentucky
Department of Mining Engineering
230 Mining & Mineral Resources Engineering
Lexington, Kentucky 40506-0107

PRINCIPAL INVESTIGATOR

Dr. Rick Honaker
Phone Number: +859-257-1108
Fax Number: +859-323-1962
E-Mail: rick.honaker@uky.edu

SUBMITTED TO

U.S. Department of Energy
National Energy Technology Laboratory
Program Manager: Charles Miller

April 12, 2018

Statement of Objective

The purpose of this Health Safety and Environmental plan is to outline the major components necessary to execute the project without any environmental excursions or injuries. This represents a significant statement of project policy to ensure good environmental and social stewardship. To accomplish these objectives major health, safety and environmental risks have been identified and are discussed. In addition, the projects HSE management plant will be presented.

Environmental Risks

The major sources of environmental risks identified at this time are:

1. Modification of Feed Materials
2. Concentration of Radioactive Materials
3. Release of Reagents
4. Water Quality Impact
5. Air Quality Impact

Although not an exhaustive list of potential environmental impacts, this subset will contain the vast majority of potential environmental risks to this project.

Modification of Feed Materials

The first concern focuses on the modification of leachability of coal byproducts as a result of further processing. It is a well-known fact that coal byproducts are susceptible to natural leaching through exposure to rain and ground water. These occur at rates and with elements intrinsic to each process and coal source. The potential environmental impact is manifest in negatively impacting the natural leaching of coals in ways that either enhance the leachability of undesirable elements or increase the rate of leaching. To understand these risks TCLP (Toxicity characteristic leaching procedure) tests will be conducted to understand the changes in leachability of the coal byproducts. This data will be used to identify potential issues created by coal byproduct processing and address as needed.

Concentration of Radioactive Materials

By nature, the project entails leaching and concentration of REEs from coal and coal byproducts. Because of this there is a concern that radioactive elements which are found in coal and coal byproducts will also be subject to concentration due to similar processing characteristics of REEs. In addition, these same techniques namely leaching and solvent extraction have been utilized in the past to extract Uranium and Thorium. Because of these concerns it is necessary as part of this project to quantify and understand the risks presented by these elements. The general approach will be:

1) Attempt to prevent the concentration of these elements where possible.
2) If concentrated, dilute the stream as part of tailings thus retuning occurrence to background levels.
3) If dilution with tailings is not possible due to changing the mobility of radioactive ions due to processing, dilution and capture through alternate means will be considered.

By approaching the concentration of radioactive elements in this manner an economic and safe processing arrangements will be carried out to return the material to like and kind state post processing. Further, if concentration of undesirable radioactive elements proves to be unavoidable before abatement, University of Kentucky HSE will be contacted to provide oversite and as needed monitoring of personnel.

Release of Reagents

Inadvertent release of reagents will be controlled in a number of methods both procedurally and operationally. The most likely mode of occurrence of inadvertent release of reagents will be through leaks and spills. To prevent these occurrences a number of methods will be utilized. The first of these will be the utilization of secondary containment. As appropriate all storage of chemicals and reagents will have secondary containment. This may include for example containment pallets for 55-gallon drums and spill containment for all liquid reagents. For modular processing bays secondary containment will be site specific which will include banks and sumps where if drips and spills occur they may be contained and cleaned without spillage to the surrounding area. These secondary containments will be sized appropriately to the containers, or tank and in-flow rates so that overflow of containment is improbable. Procedural methods of preventing leaks and spills may include, but are not limited to:

- Never leaving a filling tank unattended.
- Filling and transferring reagents over secondary containment.
- Housekeeping procedures producing a clean and sanitary environment where drips, spills and leaks are easily identifiable.
- Spill kits and adsorptive pigs for containment and cleanup.

Water Quality Impact

It is anticipated that water quality will be maintained at the processing site by treatment and neutralization of process water to match water inherent to the site. The locations of the pilot plant will be located at mine sites where the treatment of water from mine disturbed areas and from drainage from coal byproducts is permitted and well established. It is anticipated that waste water disposal will be treated to integrate in a non-intrusive way to the sites existing water treatment infrastructure. Monitoring of pilot plant effluent will be included as part of the project.

Air Quality Impact

The primary concern of this project with regard to impacting air quality will occur from process ventilation. This will likely include two constituents, acid mists from leaching and VOC (volatile organic compounds) related to the kerosene. For the acid it may be necessary to provide additional neutralization or wet scrubbing as part of the ventilation system prior to atmospheric venting. Appropriate environmental regulations will be consulted as part of the operation of the air handling system.

Health and Safety Risks

Due to the nature of construction, commissioning and operation of the REE processing pilot plant the type and nature of Health and Safety risks significantly change through the various phases of the project. For the purpose of categorizing risk types, four distinct phases will be discussed. These are:

1. Construction
2. Startup and Shakedown
3. Operation
4. Decommissioning

Construction

The construction phase carries unique and often changing risks due to the ever-changing construction environment. Risks involved in the construction phase include:

- Risks due to constantly changing workplace.
- Slips trips and falls due to construction.
- Struck by hazards from moving equipment.
- Cuts and burns from fabrication activities.
- Utilization of subcontractors unfamiliar with site or processes which poses an increased risk of injury.

To mitigate this risk simple techniques will be utilized such as:

- Appropriate MSHA training.
- OSHA JHAs (Job Hazard Analysis).
- Requirements of equipment specific training (i.e. Forklift).
- Shift start safety and correlation meetings.
- Lift planning (for equipment placement).
- Subcontractor check in with site foreman.
- Establishment of site specific rules, SOPs (standard operating procedures) and PPE.

Startup and Shakedown

Risks encountered during startup are varied, but primarily center around two principles. These are untested equipment/processes and operators un-familiar with process operation. To address these needs of safely testing equipment and training personnel this phase will be characterized by emphasis on the following:

- SOP Development.
- Specific operational and readiness tests and checklists to certify equipment operability.
- Certification of operators.
- Organization of appropriate MSDS sheets and Chemical Inventory.
- Emergency response drills as needed.
- Training of mine site personnel on how to respond to emergencies, such a fire.

Operation

The operation phase is characterized by risks occurring due to opportunity frequency and familiarity. For safety in this phase the focus will be:

- Audits of and continued training to SOPs.

- Training of new operators as needed.
- Periodic maintenance and safety review meetings where incidents and near misses are reviewed and reported.

Decommissioning

The last phase of the project is decommissioning. This project phase is characterized by similar hazards as the construction phase, but with added chemical exposure risks due to used equipment. Additionally, vigilance will be needed at this stage of the project as funds and time are often short and the general tendency to move swiftly and efficiently are the highest. Care will need to be exercised from the management team to continue in diligence during this phase of the project.

HSE (Health Safety and Environment) Management Plan

The HSE management plan is based on the Six Sigma principles of Control Plans and FMEAs (Failure modes and effects analysis). This type of methodology is common with projects in manufacturing and ISO 9001 standards. In terms of this project the FMEA defines:

1) Possible failure modes of the process.
2) The likely outcomes of those failures.
3) The likelihood of occurrence.
4) The possibility of detection.
5) The severity of the occurrence.

An example of this can be found in Figure 1. This figure shows the processing steps and the specific characteristics of the failures of each step. A RPN (risk priority number) is given by multiplying the failure severity by the occurrence and detection. The higher the number the more severe, more often occurring and harder to detect a potential risk or failure will be. The scale ranges from 1 to 10, with 10 being reserved for significant safety excursions resulting in lost time injuries or fatalities. Not meeting specification for example would rank 7 in terms of severity. For those failures resulting in a RPN number that is too high corrective actions are assigned and tracked via the recommended actions portion.

FMEA Number:	FMEA Plan Owner / Phone:	Date Original:	Date Revised:
001-Plant Operation	Josh Werner (509)995-6697	10/31/2017	NA
Process: Plant	Team: Rick Honaker, Josh Werner, Jack Groppo	Revision Note	
Description: Operation of Pilot Plant	Approval Date: Rick Honaker 11/4/2017		

Process Number	Process Name/ Description	Tank, Device, Equipment	Characteristics			Potential Failure Mode	Potential Effect(s) of Failure	Severity	Potential Cause of Failures	Occurrence	Current Process Controls Prevention	Current Process Controls Detection	Detection	R. P. N.	Recommended actions	Responsibility & Target Date	Actions Taken & Completion Date	Severity
			No.	Inputs	Output													
1	Leaching	Leach Tank	1A	Impeller Speed		Too Fast	None	1	Improper Start up	3	SOP	Operator	3	9	None			
						Too Slow	Not enough Leaching	7	Improper Start up	3	SOP	Operator	3	63	Non operator Control	Rick H. 11/29/2017		
			1B	Temperature		Too Hot	Evaporation	3	Process Drift	1	PID Controller	Thermocouple	1	3	None			
						Too Cold	Not enough Leaching	7	Process Drift	1			1	7	None			

Figure 1. Example of FMEA for a REE leaching tank.

The FMEA is designed to work in concert with the Control Plan. Whereas the FMEA explores and defines potential failures and their effects the Control Plan is to define the methods that the process will be controlled. Figure 2 shows and example Control Plan associated with the FMEA in Figure 1. Control plans form the foundation of SOP development and risk mitigation for this project. As shown in Figure 1 every processing step is defined with the step inputs and outputs. All variables for that step are defined and categorized as CTQ (critical to quality) or not. This document further defines the correct operational specifications for each process step,

how quality is maintained for input/outputs and a how to react to out of specification or tolerance. As shown in Figure 2 many of these controls will be specified in relevant SOPs which will need to be developed per the Control plan.

Another useful feature of the Control Plans and FEMAs is that in this project they will be used to control not only the pilot plant, but be used to analyze and control operator/safety activities. To do this the phases identified in Health and Safety Risks will be treated as processes and evaluated using these methods. Control plans and FMEAs will be used in conjunction with JHAs to fulfill the mandate of this project for safe and environmentally benign operation.

Control Plan

Control Plan Number:	Control Plan Owner / Phone:	Date Original:	Date Revised:
001-Plant Operation	Josh Werner (509)995-6697	10/31/2017	NA
Process: Plant	Team: Rick Honaker, Josh Werner, Jack Groppo	Revision Note	
Description: Operation of Pilot Plant	Approval Date: Rick Honaker 11/4/2017		

Process Number	Process Name/ Description	Tank,Device, Equpipement	Characteristics			CTQ	Methods					Reaction
			No.	Inputs	Output		Product/Process Specification/Tolerance	Evaluation/ Measurement	Sample		Control Method	
									Size	Freq.		
1	Leaching	Leach Tank	1A	Impeller Speed		N	400-600 RPM	Digital Readout		1x per shift	Knob	Adju
			1B	Temperature		Y	30-40c	Digital Readout		cont.	PLC	Adju
			1C	% Solids		N	30-40%	Density	10ml	3X per Shift	SPC	Adju
			1D	Size		Y	70-150 micron	Dry and Screen	100g	1x per shift	Screen and Weigh	See S
			1E		% Extracted	Y	70% minimum	See Assay SOP		1x per shift	ICP-OES	See S
2	Solvent Loading	SX loading Mixers	2A	O:A Ratio		Y	1:01	See SOP		1x per shift	SPC	See S
			2B	Impeller Speed		N	600-800 rpm	Digital Readout		1x per shift	Knob	Adju

Figure 2. Example of FMEA for a REE leaching tank.

Utilization of Control Plans and FMEAs as part of our project management process will ensure adequate controls and documentation for successful project implementation.

APPENDIX C- SYSTEM TESTING, OPERATION & SAMPLING/ANALYSIS PLAN

PHASE 2: PILOT-SCALE TESTING OF AN INTEGRATED CIRCUIT FOR THE EXTRACTION OF RARE EARTH MINERALS AND ELEMENTS FROM COAL AND COAL BYPRODUCTS USING ADVANCED SEPARATION TECHNOLOGIES

For AOI2

University Members

University of Kentucky
Virginia Tech
West Virginia University

Corporate Members

Minerals Refining Company
Alliance Coal
Blackhawk Mining
Mineral Separations Tech

System Testing, Operation & Sampling/Analysis Plan

DE-FE0027035

SUBMITTED BY

University of Kentucky
Department of Mining Engineering
230 Mining & Mineral Resources Engineering
Lexington, Kentucky 40506-0107

PRINCIPAL INVESTIGATOR

Dr. Rick Honaker
Phone Number: +859-257-1108
Fax Number: +859-323-1962
E-Mail: rick.honaker@uky.edu

SUBMITTED TO

U.S. Department of Energy
National Energy Technology Laboratory
Program Manager: Charles Miller

June 20, 2018

1. EXECUTIVE SUMMARY

The *primary objective* of this continuation Phase 2 project is to successfully complete the engineering development and field demonstration of pilot-scale circuitry for recovering high-value rare earth elements (REEs) from coal and coal byproducts in a cost effective and environmentally benign manner.The project team will construct and test a ¼-tph mobile pilot plant for the recovery REEs at two different test sites where the Fire Clay and West Kentucky No. 13 coals are processed. The project team consists of three institutions: University of Kentucky (lead institute), West Virginia University, and Virginia Tech. The Blackhawk Mining and Alliance Coal companies will provide test sites, provide power and water, and work with the team to judiciously handle waste disposal and management. Minerals Refining Company and Mineral Separation Technologies will provide pilot-scale units of their respective separation technologies. Precipitation tanks will be employed to pre-concentrate the REEs in naturally occurring leachate produces at the mine site. Process will be tested to remove any potential issues associated with thorium or other undesirable elements. Finally, filter presses will concentrate and neutralize any solids residual prior to disposal.

The mobile pilot plant is designed to be flexible so that it can be used for different types of feed stocks, including coarse refuse, ultrafine thickener underflow and naturally occurring coarse waste leachate. The coarse refuse will be screened first and then subjected to sorting using advanced sensors that can discriminate particles according to their SGs and/or chemical make-ups. The proposed plant layout will include crushers and grinding mills to improve liberation. A pilot-scale HHS unit will be used to simultaneously recover and dewater coal and subsequently produced REM concentrates. A countercurrent leaching system and SX system consisting of 10 mixer-settlers will be used for producing desired REO concentrates. Precipitation tanks will be used to extract REEs from GOB pile leachates and to address potential environmental issues associated with handling thorium (Th) and other undesirable elements.

The objective of this document is to identify the test procedures, specific sampling and analytical procedures, and ASTM standards that will be used during the REE pilot-scale test program.

2. CIRCUIT TEST PROCEDURES

2.1 Water Testing

At the completion of construction, startup tests will be conducted to resolve operational problems that often arise during the commissioning of pilot-scale processes. Mock operator training exercises will be conducted to ensure that all parties are familiar with standard operating and emergency shutdown procedures. Initial "water only" test runs will be conducted to ensure that pumping capacities, pipe/tubing sizes, electrical supplies, control systems, instrumentation, etc., are adequate. After completing start-up activities, shakedown tests will be initiated using actual feedstocks and staged dosing of reagents/acids/bases to validate the structural integrity of the process circuitry and to confirm the design capacities of the various unit operations used in the pilot-plant circuitry are within established norms.

2.2 Solvent Extraction and Selective Precipitation Testing

The solvent extraction circuit will receive an acidic solution produced from a coal source. The leachate will have a relative low concentration of REEs and a high content of contaminant ions such as iron, aluminum and calcium. The concentrations generally do not change significantly between coal sources. As such, the testing and optimization of the solvent extraction circuit will be isolated from the rest of the plant by using the natural mine acid water as the feedstock prior to attempting the processing of solid material sources through the physical separation and acid leaching bays. The natural mine acid water produced at Alliance Coal's Dotiki preparation plant is a result of pyrite oxidation in the coarse refuse storage area which produces a leachate having a pH value in the range of 2.2 and 3.0. The solvent extraction test program will be initiated shortly after the completion of the water-shakedown tests. The circuit evaluation will be conducted in various phases as described in the following section.

2.2.1 Shake-Down Testing

The solvent extraction circuit will be loaded with water and kerosene at a ratio of 1:1 and the circuit operated continuously prior to feed the REE leachate solution. Level controls and control valves will be adjusted to achieve the desired phase levels in each mixer-settler. Operators will be trained on the process control mechanisms and adjustments that may be needed to achieve the desired results.

Afterwards, the extractant will be loaded into the kerosene and the REE leachate added to the circuit at a predetermined volumetric flow rate. When treating the acid water, 100% of the raffinate generated from the loading stages of the solvent extraction unit will pumped to the water treatment tank where the water will be neutralized before being discharged. The aqueous phase generated from the scrubbing and stripping stages will be recirculated back to the feed with a bleed stream being extracted from the recirculated stream as shown in Figure 1. The configuration reduces acid consumption and maximizes grade from the stripping step. Initial tests will be conducted to fine tune the volumetric flow rate of the bleed streams. To achieve this task, the bleed stream of the stripping step will be reduced until the REEs begin to report in the exiting organic phase. The volumetric flow rate of the bleed stream will then be slightly increased to avoid the loss

of REEs while maximizing the purity of the final concentrate. Stability of the two phases will also be assessed and a phase modifier added if needed.

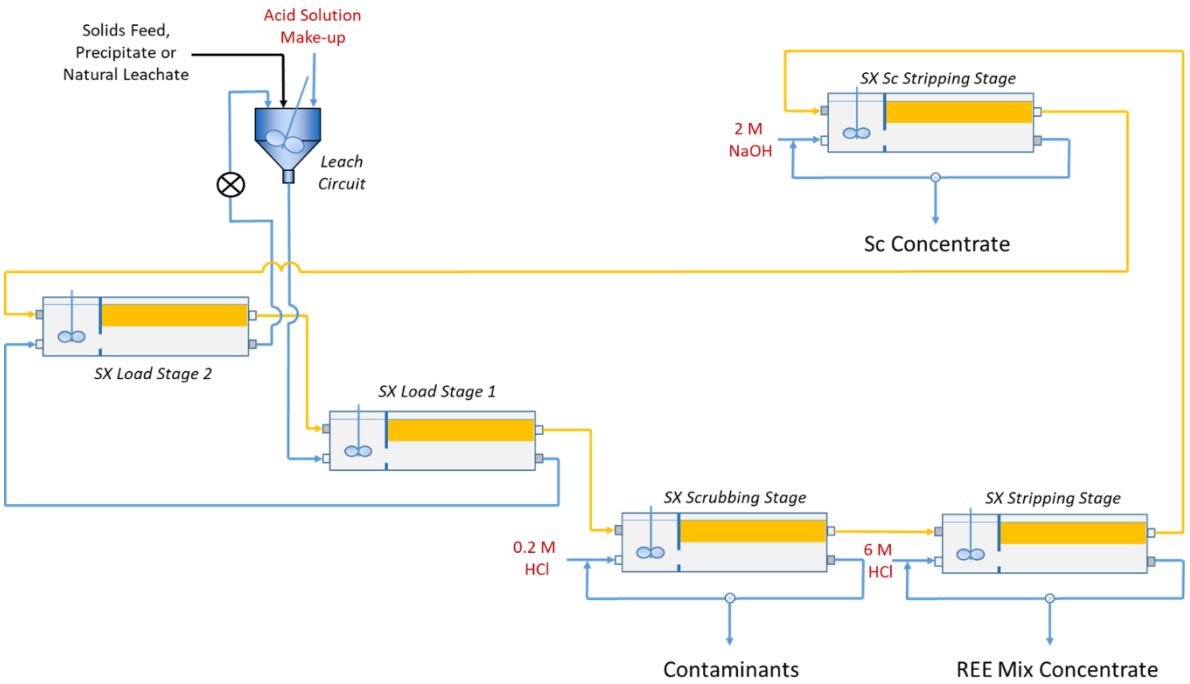

Figure 1. Rougher circuit used in the solvent extraction bay to recovery and concentrate the REEs existing in leachate solution generated from coal sources.

2.2.2 Solvent Extraction Optimization

The purpose of the test program is to maximize the purity of the final concentrate while minimizing the cost of production on a per unit mass of REE mix produced. REE grade and cost will be response variables used to optimize the settings of several operating parameter

values including: 1) volumetric feed flow rate, 2) pH value of the leachate fed to the circuit, 3) acid concentrations used in the scrubbing and stripping stages and 4) the number of stripping stages. A three-level statistically-designed test program will be conducted and the results used to develop empirical models describing the final REE grade and cost per kg of REE mix produced as a function of the parameter values. An optimization routine will be utilized to identify the conditions that provides the highest purity at the lowest cost.

2.2.3 Cleaner Circuit Optimization

A cleaner circuit will be used to produce the final REE concentrate which is needed due to the large amount of contaminant ions existing in the original leachate relative to the REE content. The circuit will be similar to Figure 1 minus the scrubbing step. The initial pH for the cleaner circuit will be selected to maximize the rejection of contaminants. An optimization program similar to the one described in section 2.2.2 will be utilized for this effort.

2.2.4 Selective Precipitation

Selective precipitation using oxalic acid will be utilized to produce the final REE mix concentrate using oxalic acid. A test program will be conducted to optimize the solution pH and oxalic acid dosage while maintaining the operating parameters of the solvent extraction system at their optimum values. Both final purity of the REE product and cost of production will be used to identify the optimum pH and chemical dosage values.

2.3 Physical Separation and Leaching Circuit Testing

After optimizing the solvent extraction and selective precipitation circuit, middlings material collected from the coarse refuse stream at Alliance Coal's Dotiki preparation plant will be recovered using a sorter systems and fed to the REE pilot plant. The sorter will be calibrated to achieve a density separation of around 1.80 SG. The middlings material will be crushed and ground to a top size of around 177 microns. Typical collector and frother dosages will be utilized in a flotation column to remove carbonaceous material and produce and clean coal concentrate. The tailings of the primary flotation column will be conditioned with a collector (hydroxamate) and then fed to a second flotation column to remove alkali earth minerals that are acid consumers. Standard operating conditions for a column flotation cell will be utilized. The tailings of the second column will be thickened and filtered to produce a feed stock for the

leaching circuit. The grinding step through the flotation columns and dewatering operations will be conducted continuously.

A detailed experimental program will be performed with the primary objective of fully evaluating the performance of all key unit operations employed in the pilot-scale test facility using parametric testing techniques (i.e., statistical design of experiments). A Box-Behnken style, 3-level test design will be performed which requires 54 individual test runs to be conducted for each grouping of six process variables. The emphasis of the parametric testing will be (i) to optimize the performance of the REE extraction circuitry in terms of recovery, grade and profitability and (ii) to collect additional operating data and scale-up information necessary to complete the engineering design of future full-scale production units. This task will be repeated for each of the two primary test sites. Operating parameters that will be studies as part of the test program include volumetric feed rate, solids concentration, leaching temperature, acid concentration and the percentage of the raffinate from the loading stage of the solvent extraction circuit that can be recycled to the acid leaching circuit. A preliminary economic evaluation of the circuit showed that raffinate recycle is a major economic parameter for REE recovery from coal-based solid sources.

2.4 Testing of the HHS Process

The test plan calls for the HHS module to be used to treat three different process streams available within the physical separation circuits. The first stream to be tested is the froth overflow from the decarbonization flotation column. The objective for treating this stream is to demonstrate the ability of the HHS process to produce a low-ash, low-moisture coal product that is highly marketable. If successful, the costs for operations upstream of this unit can potentially be covered by the sale of the coal product. This would allow the underflow stream from the decarbonization column to be available for downstream REE processing at no cost to the REE circuitry. When operating in this mode, the tailings from the HHS process will reenter the rare earth production system by being pumped back to the decarbonization thickener.

The second stream to be treated by the HHS process is underflow from the decarbonization flotation column. This stream will be reagentized using appropriate collectors (fatty acid, hydroxomate, etc.) so as to make ultrafine rare earth minerals (REMs) hydrophobic and recoverable as a concentrate via the HHS process. The objective for treating this stream is to demonstrate that the HHS process can produce a REM concentrate at a grade of 2% total REEs

or higher from the decarbonization flotation waste stream. This treatment step also simultaneously removes alkaline minerals with the REM concentrate so as to reduce acid demands for the downstream acid leaching circuitry. When operating as a rare earth mineral recovery unit, the tailings from the HHS process will be pumped back to the dealkalinization thickener. As such, the HHS process is essentially just treating bypass and/or slip streams from the existing circuitry. The REM concentrate will be collected and evaluated to determine the best approach for extracting REEs from the REM concentrate (i.e., acid and/or alkaline cracking). The cracking step will be performed off-site for safety reasons since high pressure/temperature equipment is utilized for cracking.

The third stream to be treated by the HHS process is the froth concentrate from the dealkalinization flotation column. This test is very similar to that described above, except that the feed to be purified by the HHS process will be preconcentrated by the dealkalinization flotation column. Initial test work suggests that this flotation rougher/HHS cleaner approach may be more attractive from an operational perspective. Please note that the HHS module could not be incorporated into the internal structure of the pilot-plant test facility for safety and regulatory reasons due to limitations on volumes of flammable liquids allowed in enclosed structures. In fact, the HHS process is an "open air" processing circuit similar to other hydrocarbon processing plants used in the petroleum and chemical industries.

The number of test parameters that need to be examined when evaluating the HHS process is small due to the relatively narrow range of acceptable operating limits for most of the unit operations used within the process. As such, the primary test variables to be examined during the evaluation will largely focus on feed slurry rate, solvent dosage rate and collector dosage. These three variables will be examined as a three-level, three-parameter test matrix. Other operating variables, such as mixer speeds, stripper temperature, filter presser, etc., will only be adjusted for cases in which standard operating levels have been exceeded to ensure safe equipment operation.

3. Sampling Plan

3.1 Sampling Methods

NI 43-101 standards stress the importance of sample quality control and require adequacy of sample preparation, security, and analytical procedures (Ontario Securities Commission,

2011). To mitigate sampling bias and ensure representative samples, standard protocols and ASTM procedures will be employed through sample collection, preparation, and analysis. Relevant ASTM standards for coal characterization include: gross material sampling (ASTM D2234/D2234M-10), sample preparation (D2013/D2013M-12), proximate analysis (D3172), washability analysis (D4371-06(2012)), size analysis (D4749-87(2012)), trace element analysis (D657-11), and grindability (D409/D409M-12). The standard also specifies full stream cut versus stationary sampling effects and the sampling device characteristics.

In addition to mitigating sampling bias, the sampling program must be designed to ensure that sufficient material is collected to minimize fundamental sampling error. As a result, minimum sample masses will be determined using Gy's method (1979) as is standard for mineral processing quality control applications. For example, considering dilute REE samples and conservative material properties, preliminary calculations show that, approximately 20 grams of -60 mesh material are needed produce an REE assay of 300 PPM +/- 10 PPM with a confidence of 95%.

The project will require the laboratory analysis of a large number of solid and liquid streams collected under steady-state conditions from each test run. The coal analyses will, unless otherwise specified, be limited to the determinations of total moisture, ash and total sulfur for each solid sample. Selected product samples, such as those with potential to be sold into the coal market, may be analyzed for other parameters influencing marketability such as particle size, volatile matter, chlorine, heating value, etc. ASTM procedures and standards will be employed for all determinations. Samples subjected to analyses will include representative splits collected around the various unit operations in the pilot-scale circuitry. Samples of the process water, make-up water and reagents will also be collected for each unit operation in order to obtain a complete material balance around the entire facility.

Mass and liquid flow rates from most streams will be directly measured using flow meters and a Marcy density scale along with direct measurement of solids concentration. The mass and liquid flow rate of any stream which cannot be directly measured will be calculated from sample assays using the two-product formula. All test data will be analyzed using a material balance program and adjusted to obtain a consistent and reliable set of test data. Data that cannot be satisfactorily reconciled with a mass balance will be considered as unreliable and

will be eliminated from the data set. Samples deemed to be reliable based on the material balance will then be subjected to elemental analyses.

Environmental management will also require representative sampling of the waste streams produced by the pilot plant. The pH value of the waste water will be monitored and controlled on-line using an automated system to meter the amount of caustic solution needed to maintain the pH value in the range of 7.5 to 8.0. Representative water samples will be collected every four hours of operation and analyzed for conductivity and elemental content. The results will be used to determine if additional water treatment measures are required to meet the mine permit requirements prior to disposal. Representative samples of the solid residues will also be collected and subjected to a TCLP test to determine if additional solids treatment is needed prior to disposal.

3.2 Sampling Points

The mobile ¼-ton per hour facility contains seven modules to provide the different functions needed to recover and concentrate the REEs from various coal feedstocks. The modules include: 1) pre-concentration, 2) size reduction and liberation, 3) physical separation, 4), acid leaching, 5) solvent extraction and precipitation, and 6) chemical storage and 7) rare earth mineral concentration. Other than bay 6, all bays will have sample points that will be used to obtain the representative samples needed to characterize the process streams and provide the data needed for mass and volumetric flow balances.

The first bay involves the extraction of a component existing within an active process stream or stored reject material at a coal preparation plant using x-ray transmission sorting technology. The maximum particle size that can be effectively sorted by the technology being used in the pilot plant is 50 mm and the minimum is 6 mm. As such, Figure 2 shows the pre-concentration bay receiving feed that is obtained from a sweep belt sampler located on the coarse refuse belt. The material is first screened using a double-deck vibrating screening unit to remove any material coarser than 50 mm and finer the 6 mm. Three sample points located at the feed (sample point 1-1) and discharge streams will be periodically sampled to allow a determination of the mass flow distributions. Sample point 1-3 is the feed stream to the sorter unit and sample points 1-4 and 1-5 are located at the discharge of the sorter product streams. Sampling at these locations will indicate the amount of rare earth element pre-concentration achievable by the

sorter, quantify the quality data for the feed to the next process bay and provide the data needed for a mass balance determination as well as elemental recovery values. Samples from each location will be taken on a daily basis. Experimental tests focused on the sorter performance will require sampling from points 1-3, 1-4 and 1-5 during each test condition.

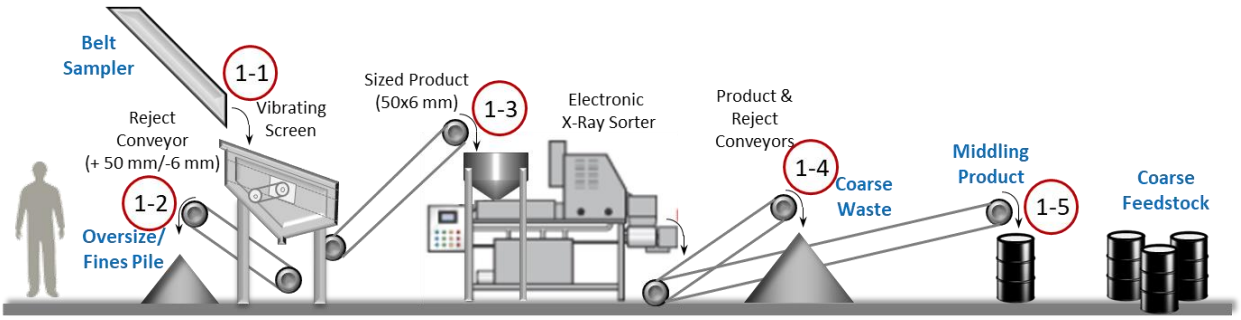

Figure 2. Sample point locations for the Pre-concentration module (Bay 1).

The purpose of Bay 2 is to reduce the particle size of the middling product generated from Bay 1 to a predetermined top size and to liberate the rare earth minerals present in the coal source. The particle size distribution feeding Bay 2 is known by the sample taken at location 1-5 shown in Figure 2. There are four sample locations identified in Bay 2 (Figure 3) which will provide the necessary information needed for mass balancing although other locations are accessible for sampling slurry streams for pulp density and solids content measurement and physically measuring the volumetric flow rate using a stop watch and a calibrated container. Samples will be taken frequently at location 2-4 to provide control of the top particle size that will feed the downstream process bays. The other locations will be sampled periodically to obtain the data needed for controlling the circuit and conducting the techno-economic study.

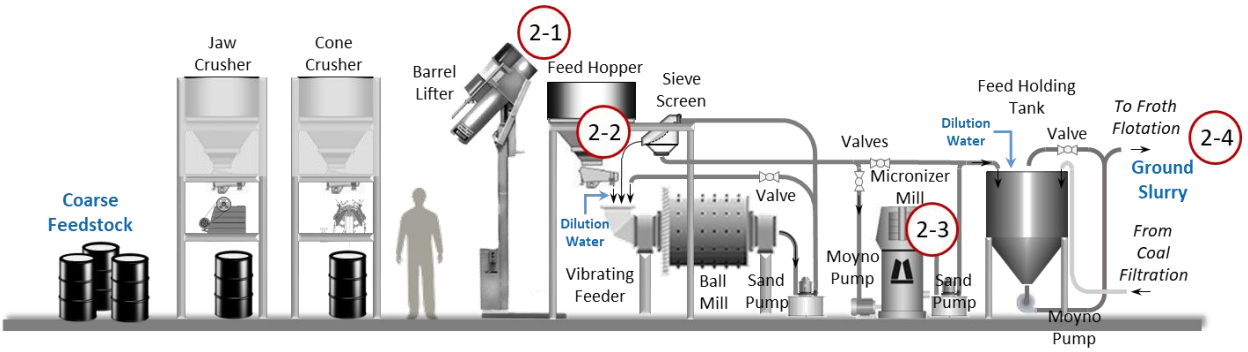

Figure 3. Sample point locations for the size reduction/liberation module (Bay 2).

Bay 3 is the physical separation bay which produces a clean coal concentrate and remove the alkali earth minerals prior to the leaching circuit using two column flotation cells as shown in

Figure 4. The physical separation bay receives feed slurry from a feed holding tank in Bay 2 and the sample collected at 2-4 has the characteristics and elemental composition that can be used to assess the performance of Bay 3 and the decarbonization flotation column. Sample locations 3-1 and 3-2 shown in Figure 4 will provide representative materials and associated composition data needed to determine the potential quality of the clean coal concentration, mass yield to the flotation concentrate and tailing streams and component recovery values to each stream. The representative sample collected at 3-2 has the same mineral and elemental composition as the feed to the dealkalinization column. As such, only samples at locations 3-3 and 3-4 are needed to obtain mass and volumetric flow information and element recovery values. Samples location 3-5 provides a material with the same elemental content as the sample obtained from 3-4. The only need for a sample from location 3-5 is to determine the solids content which is needed to achieve the desired solids concentration in the leach circuit feed.

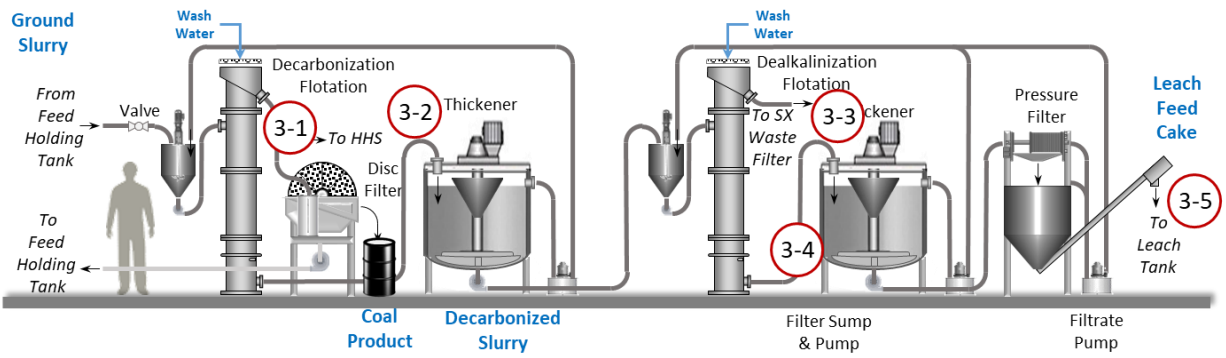

Figure 4. Sample point locations for the physical separation module (Bay 3).

The acid leaching circuit which is referred to as Bay 4 is comprised of a number of mixed tanks and thickeners as shown in Figure 5. The sample location 3-5 represents the feed and the products of Bay 4 are represented at sample locations 4-1, 4-2 and 4-3. Sample location 4-1 is the leachate solution containing the recovered REEs that reports to the solvent extraction circuit (Bay 5). Sample location 4-2 is the solid residuals remaining after leaching and 4-3 is the sample location of the circuit waste water that will be treated prior to disposal. Representative samples from these three streams will be collected throughout each test condition and operating period at a minimum of one per hour. The samples will be analyzed for elemental composition using ICP-OES and other characteristic contents needed for a mass and volume balance.

Sample locations 4-4 through 4- 8 represent internal process streams that are critical for process control and circuit modeling. Sample locations 4-5, 4-6 and 4-7 are centered around the thickener responsible for separating the solids from the leachate that will be subsequently treated by solvent extraction to concentrate the REEs. Sampling around the unit will provide mass and volume flow balances. Sample location 4-8 is the process stream containing the solid residuals after the leaching process and thus will be analyzed for elemental content for recovery calculations and percent solids to assist in the operation of the downstream filter press.

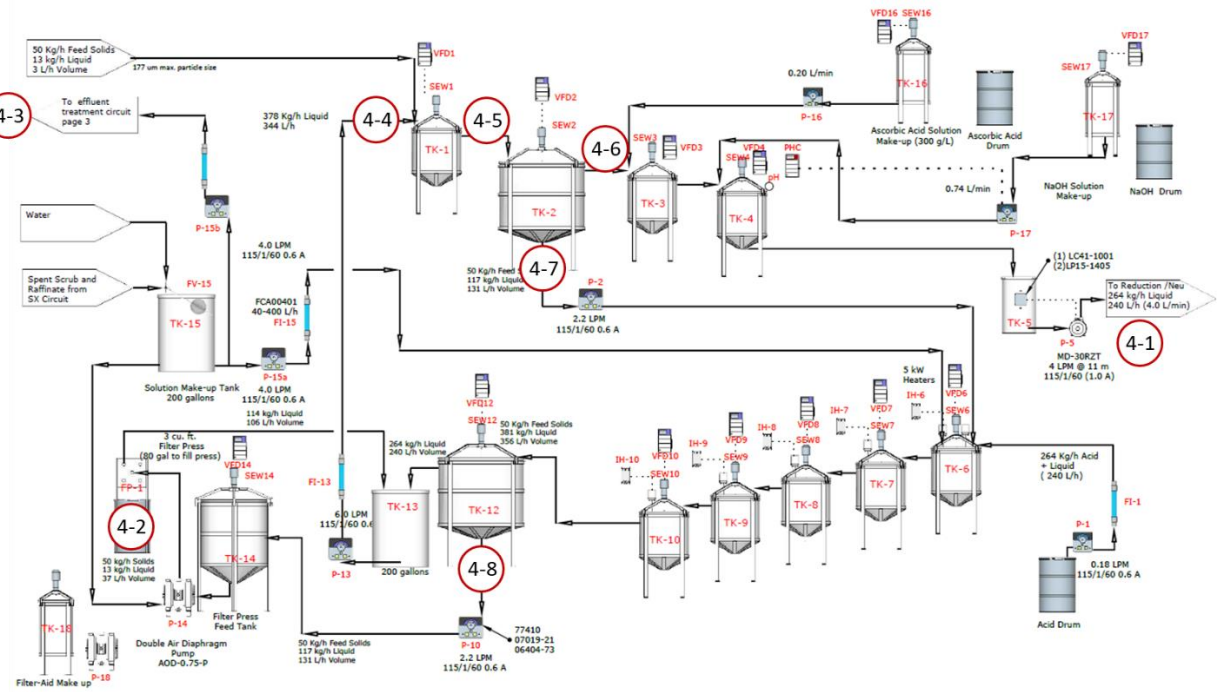

Figure 5. Sample point locations for the acid leaching module (Bay 4).

Bay 5 is the solvent extraction and selective precipitation circuit used to concentrate the REEs contained in the leachate solution (4-1) generated by the acid leach circuit. Sample location 5-1 shown in Figure 6 is the process stream containing the final rare earth element concentrate. Sample location 5-2 is the solid material generated from precipitating the contaminate ions from the process water and thus contains the large majority of the contaminants that reported in the circuit feed stream (4-1). Sample 5-3 is the waste water stream generated from the circuit comprising Bay 5. Obtaining a sample at 5-4 will allow isolation of the solvent extraction performance prior to being treated by selective precipitation using oxalic acid.

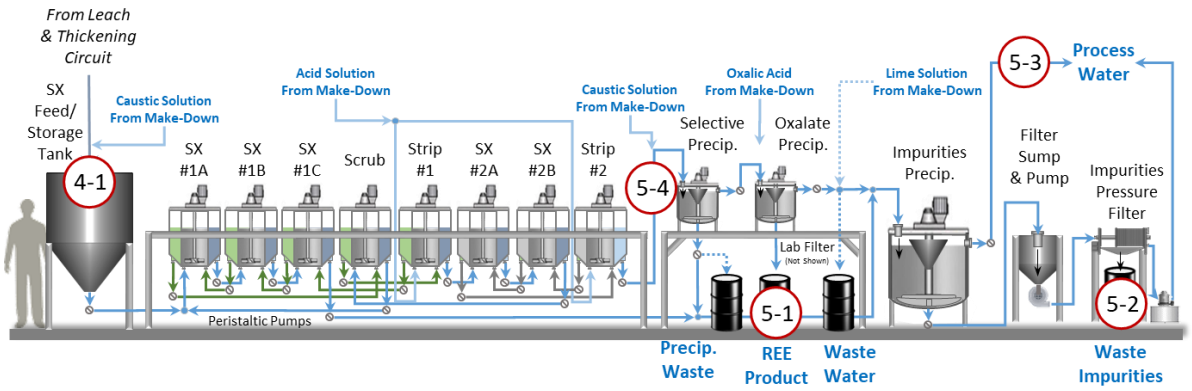

Figure 6. Sample point locations for the solvent extraction and selective precipitation module (Bay 5).

Bay 7 consists of the process equipment incorporated into the hydrophobic-hydrophilic separation (HH) process (see Figure 7). As described earlier, this mobile processing platform is designed to treat various process streams within the physical separation circuitry. The HHS process will initially be tested using feed from the grinding circuits to demonstrate the ability of the technology to produce a high-quality dry coal product. Representative samples to be collected when operating in this mode include the coal module circuit feed (7-1), the clean coal filter product (7-2) and the coal module circuit tails (7-3). After completing this work, the HHS process will then be used to treat the decarbonized tails stream to directly generate a rare earth mineral (REM) concentrate. In this case, representative samples to be collected from the REM module circuit feed (7-3), the REM filter product (7-4) and the REM circuit tails (7-5). As described elsewhere in this document, standard coal and REM analyses will be conducted on each solid sample in order to obtain a full mass balance for the concentration process. In addition, a separate group of sealed samples will be collected and subjected to quantitative gas/liquid chromatography/mass spectroscopy so that consumption rates and full material balances can be obtained for the solvent(s) used in the HHS process.

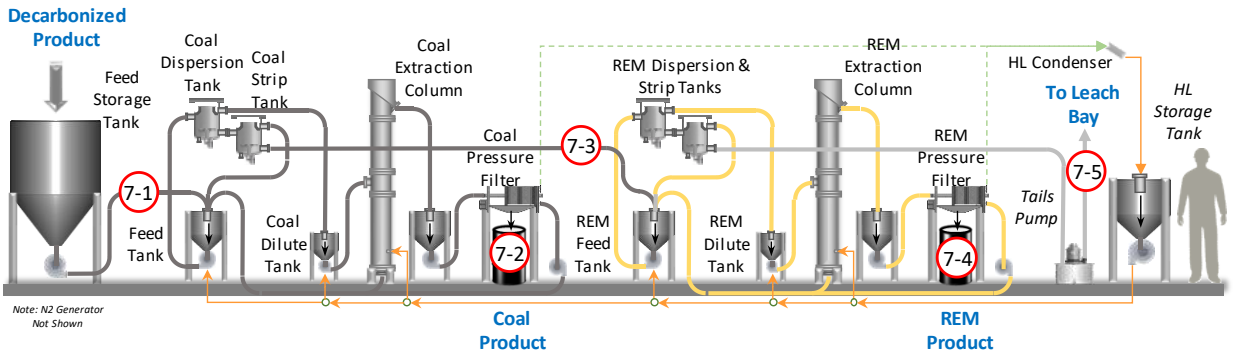

Figure 7. Sample point locations for the hydrophobic-hydrophilic separation (HHS) module (Bay 7).

3.3 NETL Sample

The project team will provide NETL with a single sample that reflects the highest achieved REE concentration generated during conduct of project effort for each major feedstock used in the test program. The quantity of material to be provided to NETL shall be no less than 5 grams. Material Safety Data Sheets (MSDS) will accompany material supplied to NETL. DOE/NETL employees or agents will be provided the opportunity to witness the sampling and splitting. It is understood that the results of any analysis arranged by DOE/NETL will be documented in a Publicly Releasable Report accessible on the NETL website.

4. ANALYTICAL ANALYSIS PLAN

4.1 Elemental Analyses

The selected solid samples and all liquid samples collected in the hydrometallurgy circuit (i.e., leaching, solvent extraction and selective precipitation units) will be analyzed for rare earth content as well as other elements of interest using an inductively coupled plasma-optical emission spectrometer (ICO-OES). The ICP-OES will be located at the pilot plant facility to allow relatively quick turnaround of the analytical results. Unless otherwise specified, the concentrations of the following elements will be determined for all samples: Cerium (58), Dysprosium (66), Erbium (68), Europium (63), Gadolinium (64), Holmium (67), Lanthanum (57), Lutetium (71), Neodymium (60), Praseodymium (59), Scandium (21), Samarium (62), Terbium (65), Thulium (69), Yttrium (39) and Ytterbium (70). Other critical elements such as cobalt, vanadium, magnesium, manganese and germanium will also be included in the analysis. Selected samples will also be analyzed for contents of environmentally sensitive elements (e.g., Thorium (90) and uranium (92)) as well as other elements of commercial interest (e.g., Iridium (77), Lithium (3), etc.). Standard REE analysis procedures will be used for all determinations.

Elemental content of a solid material requires complete digestion using an acid mix and analysis of the resultant solution using an Inductively Coupled Plasma Mass Spectrometer (ICP-MS). The sample preparation procedure that will be used follows the ASTM D6357 method for ashing and digestion of coal and refuse samples with modifications made for

digestion using a digestion block apparatus. Two standard samples with known elemental compositions as supplied by NIST will be included in one out of every 20 samples to assess the quality of both the digestion process and the ICP-OES analysis. In addition, a duplicate from a given solid sample will be included every 40 samples. The REE recovery of these check standards must be +/- 10% RSD before the results from the analyses of a batch of samples are accepted. Lastly, to isolate the analytical results provided by the ICP-OES unit, two liquid standards having known rare earth element contents will be analyzed every 50 samples. The same recovery criteria (i.e., +/- 10% RSD) will be used to accept or reject a set of data obtained from a given batch of samples.

4.2 Mineralogy Analyses

In some cases, it will be necessary to evaluate the mineralogy of the solids material existing in various parts of the pilot plant. For the coal-rich material, the carbon will be removed prior to the analysis using low temperature (110°C), oxygen-enriched plasma ashing which prevents a change in the mineral chemical structures while removing the carbon components (Bond and Giroux, 2013). X-ray diffraction (XRD) analyses will be conducted using an Advance D8 instrument produced by the Bruker company. The scanning will be performed from 10° to 70° with a stepwise increase of 0.02° and a scanning speed of 0.5°/min. The XRD spectra will be analyzed to estimate concentrations of major mineral components using the EVA software developed by the Bruker company.

4.3 HHS Solvent Analyses

The HHS process utilizes non-polar solvents that are recycled and reused by the process. In order to accurately determine the final consumption rates, selected sealed samples will be collected and analyzed for solvent content. The concentrations of these solvents, which are typically reported in ppm levels, will be determined using a standard mass spectroscopy. In this procedure, 100 mg of solid material is heated to a temperature that is sufficient to evaporate all of the solvent (i.e., 50°C for pentane solvent) while the off-gas is subjected to gas/liquid chromatography/mass spectroscopy. The resultant peak area from the chromatogram is then compared to standard chromatograms to quantitatively determine the total mass of solvent present in the total sample.

4.4 HHS REM Analyses

The concentrated samples of rare earth minerals (REMs) generated by the HHS process will be subjected to “cracking” tests in which a pressurized high-temperature reactor is utilized to dissolve the REE-bearing minerals present in the concentrates. At present, the team intents to have this procedure be performed as a contractual service by an outside commercial laboratory. As such, it is not expected that this laboratory will be able to generate a sufficient amount of digested concentrate for testing in the pilot-scale solvent extraction module. Instead, this sample will be treated in a laboratory solvent-extraction test to establish the expected performance of the downstream hydrometallurgical processes.

APPENDIX D – Environmental monitoring and management supplementary data

Figure *59* The PANanalytical XRD used throughout the study.

(A)

(B)

Figure 60 Instrument used for the SEM analysis of various solid samples. (A) Hitachi S4700 SEM-EDX (B) Denton Desk V Sputter and Carbon Coater.

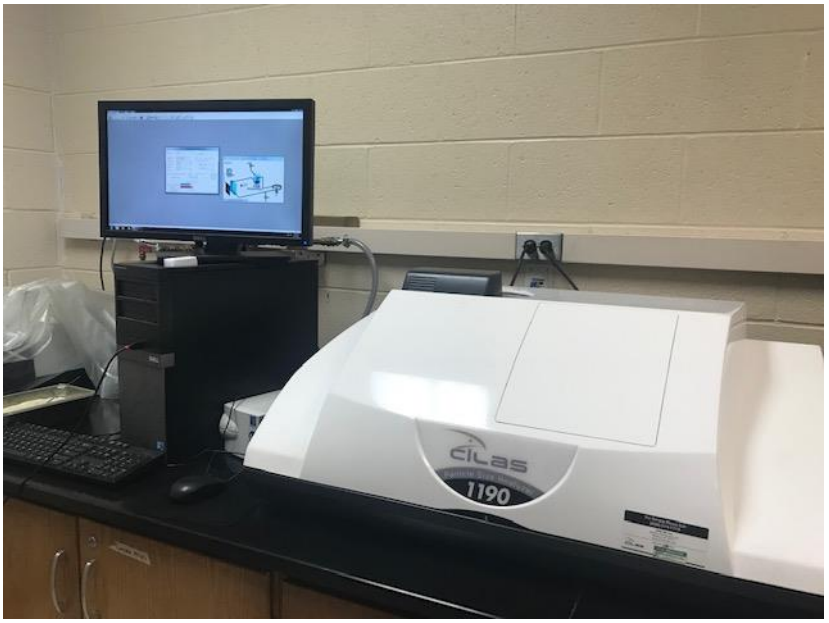

Figure 61 The CILAS particle size analyzer used throughout the study.

Figure 62 The Vanta handheld XRF used throughout the study.

Figure 63 BET nitrogen adsorption instrument used for the characterization of zeolite samples.

Table 18 Individual rare earth elements, thorium, and uranium concentrations (mg/L) in the filtrates at various pH values during the preliminary selective precipitation tests.

Element/pH	4.66	5	6.17	6.55	8	8.15	8.42	9.4	9.8
Sc	0.001	0.001	0.001	0.001	0.002	0.000	0.000	0.000	0.000
Y	0.674	0.547	0.517	0.389	0.008	0.003	0.006	0.001	0.025
La	0.433	0.409	0.389	0.35	0.032	0.013	0.02	0.004	0.018
Ce	3.287	2.857	2.745	2.386	0.083	0.039	0.049	0.039	0.126
Pr	0.468	0.415	0.373	0.291	0.025	0.025	0.025	0.025	0.025
Nd	1.967	1.701	1.562	1.200	0.029	0.009	0.018	0.009	0.073
Sm	0.663	0.524	0.454	0.308	0.036	0.041	0.047	0.04	0.064
Eu	0.107	0.084	0.067	0.042	0.004	0.004	0.004	0.004	0.004
Gd	0.443	0.354	0.302	0.210	0.006	0.006	0.006	0.006	0.011
Tb	0.015	0.015	0.015	0.015	0.015	0.015	0.015	0.015	0.015
Dy	0.18	0.137	0.103	0.061	0.005	0.005	0.005	0.005	0.006
Ho	0.024	0.019	0.016	0.009	0.003	0.003	0.003	0.003	0.003
Er	0.076	0.058	0.047	0.031	0.012	0.012	0.012	0.012	0.012
Tm	0.000	0.000	0.000	0.001	0.002	0.002	0.003	0.004	0.001
Yb	0.03	0.014	0.014	0.005	0.000	0.000	0.000	0.000	0.000
Lu	0.003	0.001	0.002	0.001	0.001	0.001	0.001	0.001	0.001
Th	0.005	0.000	0.000	0.000	0.000	0.000	0.000	0.000	0.000
U	0.150	0.040	0.003	0.001	0.001	0.002	0.001	0.001	0.008

Table 19 Individual rare earth elements, thorium, and uranium precipitation (%) at various pH values during the preliminary selective precipitation tests.

Element/pH	4.66	5.00	6.17	6.55	8.00	8.15	8.42	9.40	9.80
Sc	79.09	80.20	79.09	100.00	100.00	100.00	100.00	100.00	100.00
Y	14.44	34.25	34.36	58.76	99.13	99.68	99.24	99.87	96.99
La	12.75	21.96	21.61	39.26	94.28	97.74	95.97	99.19	96.56
Ce	16.81	31.53	30.52	48.28	98.15	99.15	98.76	99.01	96.98
Pr	18.84	31.85	35.30	55.67	96.07	96.19	95.66	95.66	95.89
Nd	17.50	32.44	34.47	56.75	98.92	99.68	99.24	99.62	97.10
Sm	11.00	33.39	39.04	63.74	95.63	95.17	93.69	94.62	91.85
Eu	19.35	40.05	49.49	68.54	96.91	97.00	96.98	96.98	97.14
Gd	15.15	35.80	42.15	67.04	99.03	99.06	98.85	98.85	98.00
Tb	15.21	19.71	15.21	42.50	40.72	42.50	15.21	15.15	19.71
Dy	18.07	40.95	53.11	74.28	97.83	97.89	97.72	97.72	97.41
Ho	18.38	38.82	45.58	66.66	88.89	88.89	89.79	89.78	90.33
Er	19.11	41.54	49.97	71.47	88.62	88.96	87.22	87.21	87.89
Tm	0.00	0.00	0.00	0.00	0.00	0.00	0.00	0.00	0.00
Yb	21.57	65.34	63.39	88.82	100.00	100.00	100.00	100.00	100.00
Lu	33.95	79.15	55.96	59.74	58.50	59.74	77.98	77.96	79.15
Th	95.49	99.83	99.99	99.99	99.99	99.99	99.99	99.99	99.99
U	28.67	82.18	98.45	99.59	99.40	99.90	99.82	99.37	96.52
TREEs	16.32	32.46	33.95	54.44	97.71	98.49	97.89	98.36	98.37

Table 20 Precipitation (%) of heavy, light, critical, and uncritical rare earth elements at various pH values during the preliminary selective precipitation tests.

Element/pH	4.66	5	6.17	6.55	8	8.15	8.42	9.4	9.8
TREEs	16.32	32.46	33.95	54.44	97.71	98.49	97.89	98.36	98.37
HREEs	15.93	36.96	41.32	64.67	97.45	97.76	97.18	97.45	96.05
LREEs	16.38	31.41	32.25	52.11	97.70	98.66	98.05	98.56	96.44
CREEs	17.18	33.35	35.96	58.12	98.14	98.72	98.23	98.57	96.59
UCREEs	15.72	31.83	32.53	51.87	97.41	98.33	97.65	98.21	96.21

Table 21 Extraction recovery (%) of total rare earths, thorium, and uranium during the exploratory solvent extraction tests.

Element/Recovery (%)	One-Stage	Double-Stage
TREEs	86.97	96.59
Thorium	92.76	93.80
Uranium	51.46	42.74

Table 22 Extraction recovery (%) individual rare earth elements during the exploratory solvent extraction tests.

Element/Recovery (%)	One-Stage	Double-Stage
Sc	63.76	62.54
Y	94.92	96.24
La	91.40	96.50
Ce	87.74	96.67
Pr	91.11	96.62
Nd	90.27	96.67
Sm	91.76	96.76
Eu	90.27	96.74
Gd	90.69	96.27
Tb	94.15	95.42
Dy	89.83	96.64
Ho	91.79	96.39
Er	96.03	96.35
Tm	78.70	92.49
Yb	92.49	95.94
Lu	98.37	94.94
Th	92.76	93.80
U	51.46	42.74

Table 23 Extraction recovery (%) of heavy, light, critical, and uncritical rare earth elements during the exploratory solvent extraction tests.

Element/Recovery (%)	One-Stage	Double-Stage
TREEs	89.97	95.59
HREEs	92.79	96.31
LREEs	89.31	96.66
CREEs	91.32	96.57
UCREEs	89.01	96.66

Table 24 Precipitation (%) of total rare earth elements, thorium, uranium, and major metals during the one-stage modified experimental protocol.

Element/pH	TREEs	Thorium	Uranium	Major Metals
4.85	19.32	99.90	47.89	24.57

Table 25 Individual rare earth elements and uranium extraction recovery (%) into the final rare earth product stream based on solely solvent extraction circuit during the first subset of solvent extraction tests.

Element/Test	1	2	3	4	5	6	7	8	9	10	11	12	13	14	15
Sc	0.00	0.00	0.00	0.00	0.00	0.00	0.00	0.00	0.00	0.00	0.00	0.00	0.00	0.00	0.00
Y	99.43	97.7	100.0	98.54	99.34	99.51	100.0	100.0	89.7	93.9	95.0	92.4	93.3	97.68	96.17
La	96.76	98.7	99.41	97.09	98.89	96.78	94.12	98.39	90.2	95.5	95.9	93.1	94.9	97.76	97.59
Ce	97.95	95.9	99.55	97.82	98.38	99.08	92.74	100.0	89.6	94.3	95.1	92.5	93.7	96.65	96.33
Pr	94.88	88.8	98.49	94.09	98.62	95.03	100.0	97.98	91.8	87.2	87.6	87.1	87.1	93.22	82.67
Nd	97.64	95.8	98.00	96.36	97.45	95.43	97.13	96.95	89.7	94.4	95.3	92.6	93.7	96.84	97.08
Sm	97.39	94.9	97.76	95.82	96.94	94.85	94.03	97.04	90.9	93.7	93.9	93.5	93.5	95.05	91.00
Eu	98.70	94.6	100.0	96.63	100.0	100.0	93.02	100.0	91.9	92.3	92.5	92.1	92.0	95.83	88.68
Gd	98.23	94.6	98.74	97.62	98.83	97.40	93.79	99.18	91.6	94.3	96.5	93.1	92.6	96.79	97.09
Tb	92.31	84.6	77.14	81.81	78.95	84.21	60.53	70.73	76.4	62.7	62.7	64.4	63.6	77.14	54.72
Dy	100.0	96.7	100.0	100.0	100.0	100.0	96.40	100.0	90.9	94.6	97.0	93.3	93.3	98.73	99.38
Ho	100.0	92.8	100.0	100.0	100.0	100.0	94.12	100.0	80.0	66.6	68.0	66.6	66.6	80.00	58.62
Er	100.0	94.4	100.0	96.88	100.0	100.0	93.44	100.0	88.8	80.7	81.4	80.4	80.4	89.61	74.47
Tm	0.00	0.00	0.00	0.00	0.00	0.00	0.00	0.00	0.00	0.00	0.00	0.00	0.00	0.00	0.00
Yb	100.0	94.1	100.0	100.0	100.0	100.0	90.48	100.0	89.2	93.1	96.5	92.8	89.2	100.0	100.0
Lu	0.00	0.00	0.00	0.00	0.00	0.00	0.00	0.00	0.00	0.00	0.00	0.00	0.00	0.00	0.00
U	66.67	33.3	23.53	17.65	17.65	29.41	11.76	5.86	46.1	11.6	34.5	69.0	20.1	89.36	17.07
TREEs	97.83	95.5	98.85	97.09	98.12	97.41	94.79	98.62	89.9	93.5	94.3	92.0	92.8	96.35	94.58

Table 26 Individual rare earth elements and uranium concentrations (mg/L) in the final rare earth product stream based on solely solvent extraction circuit during the first subset of solvent extraction tests.

Element/Concentration	1	2	3	4	5	6	7	8	9	10	11	12	13	14	15
Sc	0.00	0.47	0.00	0.00	0.00	0.00	0.00	0.00	0.00	0.00	0.00	0.00	0.00	0.00	0.00
Y	0.52	0.32	0.55	0.54	0.61	0.61	0.53	0.62	0.60	0.65	0.65	0.62	0.63	0.63	0.65
La	0.33	2.39	0.34	0.33	0.36	0.36	0.34	0.37	0.37	0.40	0.41	0.38	0.39	0.39	0.41
Ce	2.53	0.22	2.67	2.60	2.91	2.92	2.39	2.97	2.79	3.06	3.04	2.88	2.96	2.94	3.04
Pr	0.24	1.36	0.26	0.26	0.29	0.29	0.26	0.29	0.41	0.44	0.46	0.43	0.43	0.44	0.46
Nd	1.45	0.59	1.57	1.53	1.68	1.69	1.52	1.72	1.73	1.88	1.89	1.79	1.82	1.81	1.86
Sm	0.06	0.07	0.70	0.69	0.76	0.77	0.65	0.79	0.57	0.60	0.63	0.58	0.58	0.60	0.61
Eu	0.08	0.26	0.09	0.09	0.10	0.10	0.08	0.10	0.09	0.10	0.10	0.10	0.09	0.09	0.09
Gd	0.28	0.02	0.31	0.33	0.34	0.34	0.29	0.36	0.38	0.40	0.42	0.39	0.39	0.39	0.40
Tb	0.02	0.12	0.03	0.03	0.03	0.03	0.02	0.03	0.03	0.03	0.03	0.03	0.03	0.03	0.03
Dy	0.13	0.01	0.15	0.15	0.16	0.16	0.13	0.16	0.15	0.16	0.17	0.16	0.15	0.16	0.16
Ho	0.01	0.05	0.02	0.02	0.02	0.02	0.02	0.02	0.01	0.02	0.02	0.02	0.02	0.02	0.02
Er	0.06	0.00	0.06	0.06	0.07	0.07	0.06	0.07	0.06	0.07	0.07	0.07	0.07	0.07	0.07
Tm	0.00	0.02	0.00	0.00	0.00	0.00	0.00	0.00	0.00	0.00	0.00	0.00	0.00	0.00	0.00
Yb	0.02	0.00	0.02	0.02	0.03	0.03	0.02	0.03	0.03	0.03	0.03	0.03	0.03	0.03	0.03
Lu	0.00	0.00	0.00	0.00	0.00	0.00	0.00	0.00	0.00	0.00	0.00	0.00	0.00	0.00	0.00
U	0.02	0.01	0.04	0.03	0.03	0.05	0.02	0.01	0.05	0.01	0.03	0.07	0.02	0.04	0.01
TREEs	6.31	5.88	6.77	6.64	7.34	7.39	6.29	7.52	7.23	7.83	7.90	7.46	7.58	7.58	7.83

Table 27 Overall extraction recovery (%) of total rare earth elements and uranium during the first subset of solvent extraction tests.

Test Number	Extraction Recovery (%) of TREEs	Extraction Recovery (%) of Uranium
1	78.93	34.68
2	77.09	17.34
3	79.75	12.24
4	78.33	9.18
5	79.16	9.18
6	78.59	15.30
7	76.48	6.12
8	79.57	3.05
9	72.60	23.93
10	75.45	5.72
11	76.14	17.69
12	74.25	35.89
13	74.93	10.40
14	77.74	46.49
15	76.31	8.88

Table 28 Individual rare earths and uranium extraction recovery (%) into the final rare earth product stream based solely on the solvent extraction circuit during the second subset of solvent extraction tests.

Element/Test	1	2	3	4	5	6	7	8	9	10	11	12	13	14	15
Sc	0.00	0.00	0.00	0.00	0.00	0.00	0.00	0.00	0.00	0.00	0.00	0.00	0.00	0.00	0.00
Y	98.79	96.7	97.55	98.15	98.48	92.87	93.17	94.23	95.84	96.30	95.32	98.100	70.21	95.38	95.7
La	98.53	97.8	97.52	97.92	98.04	96.15	95.89	94.21	95.53	95.94	95.24	98.04	75.99	96.47	98.9
Ce	97.82	96.0	96.00	97.19	95.87	90.94	90.11	92.31	93.60	93.50	93.20	95.57	76.37	96.10	96.5
Pr	96.65	92.5	87.86	96.85	88.17	87.33	85.00	84.89	84.61	86.56	87.55	78.97	84.11	95.87	95.0
Nd	97.98	96.0	96.69	97.28	96.14	91.32	91.32	92.44	93.90	94.19	93.41	95.91	78.28	94.81	96.2
Sm	93.24	86.3	92.40	92.72	91.63	81.97	80.71	91.99	90.58	89.01	91.93	90.12	86.82	95.55	97.1
Eu	98.06	90.0	96.15	98.17	92.79	87.76	90.14	90.98	91.30	91.11	91.75	91.67	73.63	95.18	96.0
Gd	98.14	93.3	96.77	97.66	95.96	88.65	91.23	92.36	93.38	93.72	93.22	95.48	72.80	96.30	95.3
Tb	88.24	77.1	78.95	88.89	65.96	61.91	60.64	58.62	60.98	60.98	62.79	61.90	55.56	96.58	50.0
Dy	98.32	89.7	98.31	98.94	98.90	89.02	90.57	94.60	97.37	97.31	97.52	98.73	71.91	96.44	97.6
Ho	90.00	80.9	82.61	90.91	70.37	65.22	67.89	67.57	65.22	63.64	66.67	66.67	61.29	95.61	78.9
Er	94.94	89.4	90.48	95.24	82.80	80.00	80.64	78.75	79.75	79.49	80.73	80.73	72.15	96.30	89.7
Tm	0.00	0.00	0.00	0.00	0.00	0.00	0.00	0.00	0.00	0.00	0.00	0.00	0.00	0.00	20.0
Yb	100.0	82.1	100.0	100.0	100.0	83.33	100.0	100.0	100.0	100.0	100.00	100.00	56.53	98.84	86.2
Lu	0.00	20.0	100.0	100.0	100.0	100.0	100.0	100.0	0.00	0.00	100.00	100.00	41.09	95.95	20.0
U	62.47	4.28	42.92	59.39	57.22	12.00	29.95	3.42	23.33	31.68	10.00	22.58	5.14	30.00	5.46
TREEs	97.57	94.6	95.37	97.09	94.83	89.61	80.23	91.00	92.94	92.87	92.79	94.00	81.53	94.22	95.7

Table 28 continued

Element/Test	16	17	18	19	20	21	22	23	24	25	26	27
Sc	20.00	20.00	14.29	33.33	20.00	23.53	20.00	20.00	20.00	33.33	14.28	14.28
Y	96.15	96.81	97.22	95.92	97.35	95.94	95.87	96.05	94.18	93.25	96.13	96.20
La	98.93	98.93	98.45	97.57	98.91	98.11	97.96	97.66	96.41	94.95	96.47	96.47
Ce	95.40	95.88	95.23	95.41	96.28	94.85	94.97	95.29	93.05	93.15	95.29	95.00
Pr	94.71	94.66	92.69	95.50	94.68	93.80	94.97	94.82	92.72	95.14	92.56	93.72
Nd	95.17	95.63	95.44	95.29	96.05	94.70	95.08	95.22	93.38	92.63	94.45	93.92
Sm	93.61	95.77	95.81	95.08	97.33	96.04	95.64	95.15	93.67	96.31	96.18	96.10
Eu	95.87	95.83	94.18	96.81	95.83	96.70	95.96	95.79	93.75	94.57	93.94	96.55
Gd	94.72	95.19	95.83	94.63	96.08	95.15	94.90	95.16	93.29	95.95	93.75	95.10
Tb	47.83	47.83	39.40	63.64	46.67	51.85	48.94	47.83	48.94	63.64	39.98	48.99
Dy	97.48	97.50	96.44	96.84	97.47	98.00	97.59	97.50	95.65	96.13	96.38	98.25
Ho	78.95	78.95	71.43	87.50	77.78	82.20	78.95	77.78	77.78	86.67	71.43	80.77
Er	89.33	89.19	85.19	94.21	89.19	91.28	89.33	88.89	88.89	93.85	84.62	92.18
Tm	20.00	20.00	14.28	33.33	20.00	23.53	20.00	20.00	20.00	33.33	14.28	14.28
Yb	86.21	86.21	81.25	92.31	85.72	88.50	85.19	84.62	84.00	91.30	78.57	91.69
Lu	20.00	20.00	14.28	33.33	20.00	23.53	20.00	20.00	20.00	33.33	14.28	14.28
U	22.58	11.87	12.73	36.77	43.33	40.43	13.73	60.78	21.57	50.98	7.27	37.26
TREEs	94.65	95.20	94.43	95.16	95.64	94.63	94.61	94.70	92.80	93.41	93.92	94.93

Tab le 29 Individual rare earth elements and uranium concentrations (mg/L) in the final rare earth product stream based solely on solvent extraction unit during the second subset of solvent extraction tests.

Element/Concentration	1	2	3	4	5	6	7	8	9	10	11	12	13	14	15
Sc	0.00	0.00	0.00	0.00	0.00	0.00	0.00	0.00	0.00	0.00	0.00	0.00	0.00	0.00	0.00
Y	0.65	0.62	0.64	0.69	0.65	0.60	0.59	0.78	0.60	0.57	0.61	0.62	0.71	0.60	0.63
La	0.40	0.40	0.39	0.42	0.40	0.40	0.41	0.49	0.39	0.38	0.40	0.40	0.44	0.40	0.39
Ce	3.09	2.99	3.00	3.36	3.06	2.79	2.78	3.71	2.87	2.73	2.93	2.98	3.33	3.00	3.12
Pr	0.46	0.45	0.46	0.49	0.48	0.44	0.48	0.56	0.42	0.41	0.45	0.44	0.51	0.45	0.46
Nd	1.95	1.85	1.90	2.08	1.94	1.81	1.85	2.35	1.76	1.69	1.81	1.83	2.08	2.00	1.87
Sm	0.65	0.60	0.64	0.70	0.67	0.58	0.60	0.76	0.56	0.55	0.59	0.58	0.68	0.62	0.62
Eu	0.10	0.09	0.10	0.11	0.10	0.09	0.10	0.12	0.08	0.08	0.09	0.09	0.11	0.10	0.10
Gd	0.42	0.39	0.42	0.45	0.43	0.38	0.45	0.51	0.37	0.36	0.39	0.38	0.44	0.41	0.41
Tb	0.03	0.03	0.03	0.03	0.03	0.03	0.03	0.03	0.03	0.03	0.03	0.03	0.03	0.02	0.02
Dy	0.18	0.16	0.18	0.19	0.18	0.15	0.20	0.21	0.15	0.15	0.16	0.16	0.18	0.16	0.16
Ho	0.02	0.02	0.02	0.02	0.02	0.02	0.02	0.03	0.02	0.01	0.02	0.02	0.02	0.02	0.02
Er	0.08	0.07	0.08	0.08	0.08	0.06	0.06	0.09	0.06	0.06	0.07	0.07	0.08	0.07	0.07
Tm	0.00	0.00	0.00	0.00	0.00	0.00	0.00	0.00	0.00	0.00	0.00	0.00	0.00	0.00	0.00
Yb	0.03	0.02	0.03	0.03	0.03	0.02	0.02	0.03	0.02	0.02	0.02	0.02	0.03	0.03	0.03
Lu	0.00	0.00	0.00	0.00	0.00	0.00	0.00	0.00	0.00	0.00	0.00	0.00	0.00	0.00	0.00
U	0.12	0.01	0.08	0.11	0.10	0.02	0.02	0.00	0.01	0.01	0.00	0.01	0.00	0.00	0.00
TREEs	8.15	7.69	7.89	8.64	8.06	7.35	7.61	9.66	7.30	7.04	7.57	7.61	8.63	7.88	7.91

Table 29 continued

Element/Concentration	16	17	18	19	20	21	22	23	24	25	26	27
Sc	0.00	0.00	0.00	0.00	0.00	0.00	0.00	0.00	0.00	0.00	0.00	0.00
Y	0.60	0.61	0.63	0.59	0.59	0.63	0.60	0.58	0.58	0.55	0.60	0.60
La	0.37	0.37	0.38	0.36	0.36	0.38	0.38	0.38	0.38	0.36	0.38	0.38
Ce	2.90	2.93	3.06	2.85	2.85	3.03	3.02	2.91	2.92	2.76	2.97	3.00
Pr	0.43	0.43	0.46	0.42	0.43	0.45	0.45	0.44	0.43	0.41	0.45	0.45
Nd	1.74	1.75	1.83	1.70	1.70	1.81	1.82	1.75	1.75	1.65	1.79	1.80
Sm	0.59	0.59	0.62	0.58	0.58	0.61	0.61	0.59	0.59	0.57	0.61	0.61
Eu	0.09	0.09	0.10	0.09	0.09	0.10	0.10	0.09	0.09	0.09	0.09	0.09
Gd	0.39	0.40	0.41	0.39	0.39	0.40	0.41	0.39	0.39	0.38	0.41	0.40
Tb	0.02	0.02	0.02	0.02	0.02	0.02	0.02	0.02	0.02	0.02	0.02	0.02
Dy	0.16	0.16	0.16	0.15	0.15	0.16	0.16	0.16	0.15	0.15	0.16	0.16
Ho	0.02	0.02	0.02	0.01	0.01	0.02	0.02	0.01	0.01	0.01	0.01	0.01
Er	0.07	0.07	0.07	0.07	0.07	0.07	0.07	0.06	0.06	0.06	0.07	0.07
Tm	0.00	0.00	0.00	0.00	0.00	0.00	0.00	0.00	0.00	0.00	0.00	0.00
Yb	0.03	0.03	0.03	0.02	0.02	0.03	0.02	0.02	0.02	0.02	0.02	0.02
Lu	0.00	0.00	0.00	0.00	0.00	0.00	0.00	0.00	0.00	0.00	0.00	0.00
U	0.02	0.01	0.01	0.03	0.03	0.03	0.00	0.03	0.01	0.03	0.00	0.02
TREEs	7.40	7.45	7.76	7.26	7.28	7.68	7.69	7.42	7.41	7.04	7.58	7.63

Table 30 Overall extraction recovery (%) of total rare earth elements and uranium during the first subset of solvent extraction tests.

Test Number	Extraction Recovery (%) of TREEs	Extraction Recovery (%) of Uranium
1	77.11	31.84
2	74.76	2.18
3	75.37	21.87
4	76.71	30.25
5	74.94	29.16
6	70.82	6.12
7	63.41	15.26
8	71.92	1.74
9	73.45	11.89
10	73.40	16.14
11	73.33	5.10
12	74.29	11.51
13	64.43	2.62
14	74.46	15.29
15	75.65	2.78
16	74.80	11.51
17	75.24	6.05
18	74.63	6.49
19	75.20	18.74
20	75.58	22.02
21	74.79	20.60
22	74.77	6.77
23	74.84	30.97
24	73.34	11.00
25	73.82	25.98
26	74.22	3.71
27	75.02	18.99

Table 31 RE Oxide precipitation at various pH values.

Element/pH	4.6	5.5	7.0	7.5	8	8.5	9.5	10.0
TREEs	11.48	15.83	36.24	37.00	74.80	81.08	99.65	99.74
Thorium	95.01	100.00	100.00	100.00	100.00	100.00	100.00	100.00

Table 32 Adsorption recovery of total rare earths, thorium, and uranium during zeolite adsorption tests

Test Number	TREEs	Thorium	Uranium
1	45.88	98.81	98.46
2	76.88	99.86	91.29
3	73.33	99.88	94.35
4	67.33	98.28	96.75
5	90.67	99.89	94.28
6	77.71	99.13	98.46
7	83.64	99.97	96.60
8	91.76	99.20	93.17
9	21.36	98.79	50.40
10	73.20	99.94	97.59
11	20.43	99.17	89.60
12	92.00	99.90	94.06
13	84.21	99.33	80.09
14	53.64	99.61	91.02
15	38.92	99.96	97.31
16	0.03	99.33	0.00
17	14.09	99.61	37.64
18	73.75	99.96	98.65
19	89.00	99.28	92.42
20	94.00	99.86	93.11
21	49.29	99.92	90.87
22	96.00	86.71	77.38
23	2.67	36.67	0.00
24	89.58	99.80	87.32
25	92.00	98.83	81.55
26	10.19	82.43	0.00
27	1.01	72.52	0.00

Table 33 Individual rare earth elements, thorium and uranium concentrations (mg/L) in the aqueous filtrate after zeolite adsorption tests

Element/Concentration	1	2	3	4	5	6	7	8	9	10	11	12	13	14	15
Sc	0.00	0.00	0.00	0.00	0.00	0.00	0.00	0.00	0.00	0.00	0.00	0.00	0.00	0.00	0.00
Y	0.49	0.22	0.27	0.26	0.10	0.13	0.12	0.07	0.74	0.18	0.62	0.05	0.19	0.37	0.55
La	0.39	0.22	0.24	0.27	0.11	0.23	0.16	0.11	0.45	0.24	0.41	0.08	0.17	0.34	0.37
Ce	2.35	0.91	1.10	1.43	0.37	1.06	0.61	0.32	3.33	1.21	2.90	0.24	0.64	1.95	2.48
Pr	0.33	0.10	0.13	0.19	0.06	0.12	0.08	0.06	0.49	0.12	0.41	0.06	0.09	0.27	0.36
Nd	1.35	0.35	0.47	0.70	0.14	0.43	0.25	0.15	2.01	0.51	1.72	0.10	0.31	1.08	1.45
Sm	0.35	0.08	0.13	0.18	0.07	0.11	0.08	0.05	0.65	0.12	0.55	0.05	0.10	0.28	0.45
Eu	0.05	0.01	0.01	0.02	0.01	0.01	0.01	0.01	0.10	0.01	0.09	0.01	0.01	0.04	0.07
Gd	0.25	0.06	0.09	0.12	0.03	0.06	0.04	0.02	0.44	0.08	0.37	0.02	0.05	0.20	0.31
Tb	0.03	0.03	0.03	0.03	0.03	0.03	0.03	0.03	0.03	0.03	0.03	0.03	0.03	0.03	0.03
Dy	0.09	0.02	0.03	0.04	0.01	0.01	0.01	0.01	0.18	0.02	0.15	0.01	0.02	0.06	0.13
Ho	0.01	0.01	0.01	0.01	0.01	0.01	0.01	0.01	0.03	0.01	0.02	0.02	0.01	0.01	0.02
Er	0.04	0.02	0.02	0.02	0.02	0.02	0.02	0.02	0.08	0.02	0.07	0.01	0.02	0.03	0.05
Tm	0.00	0.00	0.00	0.00	0.01	0.01	0.01	0.00	0.00	0.00	0.00	0.00	0.00	0.00	0.00
Yb	0.01	0.00	0.00	0.00	0.00	0.00	0.00	0.00	0.03	0.00	0.03	0.00	0.00	0.01	0.02
Lu	0.00	0.00	0.00	0.00	0.00	0.00	0.00	0.00	0.00	0.00	0.00	0.00	0.00	0.00	0.00
Th	0.00	0.00	0.00	0.00	0.00	0.00	0.00	0.00	0.00	0.00	0.00	0.00	0.00	0.00	0.00
U	0.00	0.02	0.01	0.01	0.01	0.00	0.01	0.02	0.13	0.01	0.02	0.01	0.05	0.02	0.01

Table 33 continued

Element/Concentration	16	17	18	19	20	21	22	23	24	25	26	27
Sc	0.00	0.00	0.00	0.00	0.00	0.00	0.00	0.00	0.00	0.00	0.00	0.00
Y	0.80	0.69	0.18	0.06	0.03	0.44	0.01	0.64	0.13	0.02	0.79	0.84
La	0.56	0.44	0.26	0.11	0.04	0.35	0.00	0.54	0.08	0.03	0.52	0.56
Ce	3.93	3.12	1.15	0.34	0.11	1.95	0.07	3.93	0.35	0.08	3.35	3.78
Pr	0.54	0.49	0.16	0.06	0.06	0.30	0.06	0.52	0.06	0.06	0.53	0.57
Nd	2.37	2.00	0.56	0.14	0.05	1.22	0.01	2.37	0.16	0.03	2.03	2.31
Sm	0.77	0.67	0.14	0.08	0.01	0.35	0.05	0.75	0.08	0.05	0.76	0.82
Eu	0.14	0.10	0.01	0.01	0.01	0.05	0.01	0.13	0.01	0.01	0.14	0.15
Gd	0.61	0.44	0.08	0.02	0.03	0.24	0.01	0.59	0.03	0.01	0.59	0.64
Tb	0.03	0.03	0.03	0.03	0.01	0.03	0.03	0.03	0.03	0.03	0.03	0.03
Dy	0.25	0.18	0.02	0.01	0.01	0.08	0.01	0.25	0.01	0.01	0.25	0.27
Ho	0.03	0.03	0.01	0.01	0.02	0.01	0.01	0.03	0.01	0.01	0.03	0.04
Er	0.11	0.08	0.02	0.02	0.01	0.04	0.02	0.11	0.01	0.02	0.11	0.12
Tm	0.00	0.00	0.00	0.00	0.00	0.00	0.01	0.00	0.02	0.01	0.00	0.00
Yb	0.05	0.03	0.00	0.00	0.00	0.01	0.00	0.05	0.01	0.00	0.05	0.05
Lu	0.00	0.00	0.00	0.00	0.00	0.00	0.00	0.00	0.00	0.00	0.00	0.00
Th	0.00	0.00	0.00	0.00	0.00	0.00	0.02	0.08	0.00	0.00	0.02	0.04
U	0.30	0.14	0.00	0.02	0.01	0.02	0.05	0.30	0.03	0.04	0.20	0.30

Table 34 Adsorption kinetics

Elements/Time (min)	5	10	15	30	45	60	120	180
TREEs	0.00	3.04	11.28	11.28	19.56	20.13	20.16	21.55
Thorium	86.47	86.76	87.48	87.48	89.70	90.60	91.02	93.41
Uranium	0.00	0.22	2.22	2.50	4.10	5.76	6.83	7.88

APPENDIX E: WKY No. 13 Core Hole Analysis Results

Location Information:

- Alliance Core
- WC-18-28
- Nebo Quad.
- Webster Co., KY
- N: 2061940.1288
- E: 1076243.0548
- Surface: 398.4753
- NAD83 SP South
- Lat: 37.475135N
- Long: 87.694287W

Table 1. Lithology analysis results and profile of the core within the vertical segment associated with the West Kentucky No. 13 coal seam.

KGS ID	Lithology	From (ft)	To (ft)	Thickness (ft)	Thickness (in)	Thickness (cm)
4155	*Roof Shale*	*710.55*	*710.75*	*0.20*	*2.40*	*6.10*
missing	*core*	*710.75*	*711.15*	*0.40*	*4.80*	*12.19*
4156	*Roof Shale*	*711.15*	*711.30*	*0.15*	*1.80*	*4.57*
4157	Coal	711.30	711.60	0.30	3.60	9.14
4158	Coal	711.60	711.86	0.26	3.12	7.92
4159	Coal	711.86	712.21	0.35	4.20	10.67
4160	*Parting*	*712.21*	*712.39*	*0.18*	*2.16*	*5.49*
4161	Coal	712.39	712.57	0.18	2.16	5.49
4162	Coal	712.57	712.87	0.30	3.60	9.14
4163	*Parting*	*712.87*	*713.06*	*0.19*	*2.28*	*5.79*
4164	*Parting*	*713.06*	*713.56*	*0.50*	*6.00*	*15.24*
4165	*Parting*	*713.56*	*714.06*	*0.50*	*6.00*	*15.24*
4166	*Parting*	*714.06*	*714.56*	*0.50*	*6.00*	*15.24*
4167	*Parting*	*714.56*	*715.06*	*0.50*	*6.00*	*15.24*
4168	*Parting*	*715.06*	*715.71*	*0.65*	*7.80*	*19.81*
4169	*Parting*	*715.71*	*716.14*	*0.43*	*5.16*	*13.11*
4170	*Parting*	*716.14*	*716.34*	*0.20*	*2.40*	*6.10*
4171	Coal	716.34	716.54	0.20	2.40	6.10
4172	Coal	716.54	716.96	0.42	5.04	12.80
4173	Coal	716.96	717.54	0.58	6.96	17.68
4174	Coal	717.54	718.09	0.55	6.60	16.76
4175	Coal	718.09	718.59	0.50	6.00	15.24
4176	Coal	718.59	719.13	0.54	6.48	16.46
4177	Coal	719.13	719.63	0.50	6.00	15.24
4178	Coal	719.63	719.93	0.30	3.60	9.14
4179	*Parting*	*719.93*	*720.03*	*0.10*	*1.20*	*3.05*
4180	Coal	720.03	720.23	0.20	2.40	6.10
4181	Coal	720.23	720.50	0.27	3.24	8.23
4182	Coal	720.50	720.75	0.25	3.00	7.62
4183	Coal	720.75	721.05	0.30	3.60	9.14
4184	Coal	721.05	721.36	0.31	3.72	9.45
4185	Coal	721.36	721.67	0.31	3.72	9.45
4186	*Seat Rock*	*721.67*	*722.13*	*0.46*	*5.52*	*14.02*
4187	*Seat Rock*	*722.13*	*722.53*	*0.40*	*4.80*	*12.19*

Table 2. Proximate analysis results of samples taken from each vertical segment associated with the West Kentucky No. 13 coal seam.

Sample ID	Lithology	Carbon (%), db	Sulfur (%), db	Moisture (%)	Ash (%), db	Volatiles (%), db	Fixed Carbon (%), db
4155	*Roof Shale*	1.56	1.29	1.18	92.85	7.91	0.00
4156	*Roof Shale*	15.62	1.82	2.18	75.15	15.26	9.59
4157	Coal	70.87	2.92	3.12	15.76	37.77	46.47
4158	Coal	76.42	5.44	2.87	6.34	41.46	52.20
4159	Coal	78.72	2.70	3.17	5.73	40.31	53.96
4160	*Parting*	6.54	0.83	2.66	85.40	10.83	3.77
4161	Coal	65.90	10.64	3.32	18.02	35.85	46.13
4162	Coal	63.07	11.03	3.42	20.02	35.17	44.81
4163	*Parting*	10.94	6.01	2.76	72.47	17.41	10.12
4164	*Parting*	2.16	2.00	2.60	89.93	9.66	0.41
4165	*Parting*	0.74	1.36	1.89	91.63	8.35	0.02
4166	*Parting*	0.90	1.80	1.40	92.01	8.29	0.00
4167	*Parting*	0.45	1.13	1.36	92.81	7.13	0.06
4168	*Parting*	0.30	1.17	1.74	92.75	7.20	0.05
4169	*Parting*	0.26	0.77	2.97	91.44	8.51	0.05
4170	*Parting*	1.21	0.66	2.63	90.02	9.83	0.15
4171	Coal	33.92	6.83	2.17	54.37	19.00	26.63
4172	Coal	69.77	6.58	3.04	13.62	36.97	49.41
4173	Coal	76.01	3.08	3.20	8.22	38.80	52.98
4174	Coal	78.58	2.10	3.12	7.73	40.15	52.12
4175	Coal	80.24	1.84	3.29	5.26	38.56	56.18
4176	Coal	79.57	1.64	3.49	4.22	40.36	55.42
4177	Coal	74.13	1.84	3.38	9.51	37.06	53.43
4178	Coal	74.45	3.38	3.53	9.68	37.58	52.74
4179	*Parting*	36.60	26.58	2.71	40.14	27.78	32.08
4180	Coal	75.47	2.40	3.79	9.04	37.30	53.66
4181	Coal	73.57	2.94	3.80	9.92	38.00	52.08
4182	Coal	63.42	9.03	3.23	19.09	35.02	45.89
4183	Coal	74.49	6.03	3.77	9.59	36.73	53.68
4184	Coal	54.21	5.23	3.25	34.50	29.38	36.12
4185	Coal	42.90	9.76	2.92	43.75	27.57	28.68
4186	*Seat Rock*	3.01	3.55	2.55	88.13	10.11	1.76
4187	*Seat Rock*	0.96	1.45	2.30	93.39	6.68	0.00

Table 3. REE analysis results of samples taken from each vertical segment associated with the West Kentucky No. 13 coal seam (dry, ash basis).

Sample ID	Lithology	Sc	Y	La	Ce	Pr	Nd	Sm	Eu	Gd	Tb	Dy	Ho	Er	Tm	Yb	Lu	total	*Th*
4155	*Roof Shale*	16.53	23.88	46.77	98.46	10.73	48.30	10.12	0.75	7.90	0.08	5.62	0.28	4.36	0.10	2.57	0.20	**276.65**	*28.85*
4156	*Roof Shale*	19.16	19.38	64.17	128.50	12.80	53.21	8.74	0.66	5.20	0.00	4.11	0.56	3.85	0.47	2.80	0.00	**323.58**	*36.47*
4157	Coal	38.26	39.49	31.03	66.34	8.53	37.86	10.00	0.69	7.80	1.52	7.07	0.00	5.80	0.02	5.23	1.82	**261.47**	*26.61*
4158	Coal	22.73	64.81	11.92	24.43	15.70	22.39	32.07	1.30	11.61	7.74	0.00	0.00	4.28	0.00	11.16	13.16	**243.29**	*24.51*
4159	Coal	78.80	110.96	95.48	200.62	28.07	108.78	29.61	4.99	24.71	5.52	18.72	0.00	11.58	2.18	13.28	5.95	**739.27**	*56.62*
4160	*Parting*	16.85	47.14	57.28	128.95	12.26	60.93	12.61	1.71	14.38	0.37	11.91	1.85	6.34	0.66	2.94	0.00	**376.17**	*38.00*
4161	Coal	30.69	21.72	17.21	29.27	13.83	22.44	26.77	0.76	5.76	6.65	0.00	0.00	0.94	0.00	7.80	11.40	**195.24**	*25.05*
4162	Coal	39.06	56.04	16.04	32.80	15.20	39.36	29.27	2.91	13.53	8.14	0.70	0.00	4.14	0.00	10.73	10.31	**278.23**	*25.85*
4163	*Parting*	18.59	45.62	107.47	263.79	34.59	132.91	43.20	5.49	26.80	3.75	8.08	0.00	4.02	1.26	5.01	5.24	**705.83**	*59.87*
4164	*Parting*	21.63	40.27	59.23	120.12	12.84	56.39	14.05	1.81	13.48	1.16	10.34	0.98	5.48	0.63	3.47	0.27	**362.16**	*37.84*
4165	*Parting*	19.98	33.33	43.71	95.95	10.72	46.99	10.38	0.96	8.94	0.58	8.04	0.60	4.65	0.20	3.03	0.08	**288.14**	*31.06*
4166	*Parting*	20.15	31.85	41.58	97.93	12.46	51.13	12.16	2.18	10.39	1.48	7.71	1.29	4.90	1.03	4.22	1.12	**301.58**	*14.80*
4167	*Parting*	19.79	28.20	44.24	107.71	12.24	49.06	11.11	2.00	9.19	1.12	7.00	1.37	4.55	1.20	3.96	0.80	**303.54**	*15.87*
4168	*Parting*	21.65	30.94	56.39	141.59	14.83	56.92	12.79	2.42	10.43	1.06	8.91	1.76	5.11	1.61	4.43	0.78	**371.64**	*18.75*
4169	*Parting*	23.27	27.28	46.73	109.86	11.26	45.84	10.14	2.13	9.23	1.30	8.26	2.11	5.01	1.38	4.40	0.45	**308.64**	*23.08*
4170	*Parting*	23.73	20.57	177.20	448.57	43.69	149.99	20.21	2.69	8.99	0.00	6.60	3.27	5.98	3.82	4.11	0.62	**920.04**	*35.27*
4171	Coal	43.64	36.42	54.81	154.40	21.50	84.20	22.39	3.87	15.00	2.92	9.63	0.76	4.49	1.40	7.10	2.80	**465.33**	*20.95*
4172	Coal	43.22	87.36	22.01	44.84	17.72	46.61	24.51	2.97	13.87	7.94	8.78	0.00	5.39	0.55	15.96	10.19	**351.94**	*10.91*
4173	Coal	21.22	80.31	37.17	93.65	16.25	50.46	21.32	2.58	15.28	4.99	10.86	0.00	7.69	1.11	10.17	6.46	**379.52**	*17.32*
4174	Coal	41.98	70.22	34.30	58.25	14.16	47.93	16.47	2.79	24.17	4.11	11.02	0.00	5.72	1.03	6.91	4.66	**343.72**	*16.35*
4175	Coal	30.27	75.07	58.62	120.91	18.41	61.25	20.51	3.10	19.23	4.19	11.01	0.00	6.42	1.38	8.23	5.57	**444.17**	*24.36*
4176	Coal	23.18	64.36	41.85	110.03	18.49	57.19	20.42	2.83	14.81	3.24	6.61	0.00	6.13	2.03	6.93	5.55	**383.64**	*15.56*
4177	Coal	20.99	36.30	43.94	104.89	14.16	48.37	14.10	2.14	10.72	1.60	4.37	0.22	5.08	1.07	4.67	2.91	**315.53**	*16.85*
4178	Coal	19.20	44.51	40.31	100.80	18.28	49.87	19.86	2.28	12.41	3.28	1.33	0.00	4.16	1.05	5.99	6.40	**329.72**	*13.48*
4179	*Parting*	2.82	6.33	8.43	20.06	19.28	14.20	29.00	0.23	4.34	5.82	0.00	0.00	0.00	0.00	7.13	15.38	**133.01**	*3.10*
4180	Coal	27.45	44.61	31.76	61.69	11.82	39.34	12.47	1.71	12.32	2.35	3.35	0.00	4.91	1.22	5.59	4.33	**264.93**	*13.19*
4181	Coal	20.84	56.45	38.96	94.23	15.73	47.45	17.03	2.12	12.81	2.59	4.31	0.00	5.59	1.42	6.13	5.49	**331.14**	*13.71*
4182	Coal	12.94	51.83	32.60	88.96	20.88	49.43	27.13	2.19	13.64	4.46	0.00	0.00	4.15	0.57	7.48	9.63	**325.89**	*10.97*
4183	Coal	19.27	77.09	26.33	69.45	21.91	45.28	30.73	2.57	15.70	6.09	1.96	0.00	7.41	1.61	13.54	12.44	**351.38**	*9.69*
4184	Coal	23.60	55.74	73.53	150.99	19.28	65.55	19.16	3.34	15.70	2.51	11.30	0.86	7.86	1.25	8.54	3.82	**463.02**	*24.14*
4185	Coal	23.07	46.21	46.49	86.23	16.50	48.63	19.19	3.01	14.16	3.82	7.93	0.00	6.33	0.83	8.61	5.80	**336.83**	*19.92*
4186	*Seat Rock*	19.08	23.25	137.01	322.82	37.58	150.46	32.96	4.36	12.30	0.00	5.75	1.49	4.73	0.57	4.36	2.29	**759.04**	*25.65*
4187	*Seat Rock*	20.70	15.43	59.49	119.45	11.74	38.95	6.70	1.22	5.02	0.00	3.44	1.48	4.21	0.57	3.25	0.67	**292.31**	*18.31*

Table 4. REE analysis results of samples taken from each vertical segment associated with the West Kentucky No. 13 coal seam (dry, whole mass).

Lithology	Total REE (whole basis, ppm)																
	Total	Sc	Y	La	Ce	Pr	Nd	Sm	Eu	Gd	Tb	Dy	Ho	Er	Tm	Yb	Lu
Roof Shale	256.87	15.34	22.17	43.42	91.42	9.96	44.85	9.40	0.69	7.33	0.08	5.21	0.26	4.05	0.09	2.38	0.19
Roof Shale	243.17	14.40	14.56	48.22	96.57	9.62	39.99	6.57	0.49	3.91	0.00	3.09	0.42	2.89	0.35	2.10	0.00
Coal	41.21	6.03	6.22	4.89	10.45	1.35	5.97	1.58	0.11	1.23	0.24	1.11	0.00	0.91	0.00	0.82	0.29
Coal	15.42	1.44	4.11	0.76	1.55	1.00	1.42	2.03	0.08	0.74	0.49	0.00	0.00	0.27	0.00	0.71	0.83
Coal	42.36	4.52	6.36	5.47	11.50	1.61	6.23	1.70	0.29	1.42	0.32	1.07	0.00	0.66	0.13	0.76	0.34
Parting	321.25	14.39	40.26	48.91	110.12	10.47	52.04	10.77	1.46	12.28	0.32	10.17	1.58	5.42	0.56	2.51	0.00
Coal	35.18	5.53	3.91	3.10	5.27	2.49	4.04	4.82	0.14	1.04	1.20	0.00	0.00	0.17	0.00	1.41	2.05
Coal	55.70	7.82	11.22	3.21	6.57	3.04	7.88	5.86	0.58	2.71	1.63	0.14	0.00	0.83	0.00	2.15	2.06
Parting	511.52	13.47	33.06	77.89	191.17	25.07	96.32	31.31	3.98	19.42	2.72	5.86	0.00	2.91	0.92	3.63	3.80
Parting	325.69	19.45	36.22	53.27	108.02	11.54	50.71	12.64	1.62	12.13	1.04	9.30	0.88	4.92	0.56	3.12	0.25
Parting	264.02	18.31	30.54	40.05	87.92	9.82	43.06	9.51	0.88	8.19	0.53	7.36	0.55	4.26	0.18	2.77	0.07
Parting	277.49	18.54	29.30	38.26	90.11	11.46	47.04	11.19	2.00	9.56	1.36	7.09	1.19	4.51	0.95	3.89	1.03
Parting	281.72	18.37	26.17	41.06	99.97	11.36	45.53	10.31	1.86	8.53	1.04	6.49	1.27	4.22	1.11	3.68	0.74
Parting	344.70	20.08	28.70	52.31	131.33	13.75	52.80	11.86	2.24	9.68	0.98	8.26	1.63	4.74	1.50	4.11	0.73
Parting	282.22	21.27	24.95	42.73	100.45	10.29	41.92	9.27	1.95	8.44	1.19	7.55	1.93	4.58	1.26	4.02	0.41
Parting	828.22	21.36	18.52	159.52	403.80	39.33	135.02	18.19	2.42	8.10	0.00	5.94	2.94	5.38	3.44	3.70	0.55
Coal	253.00	23.73	19.80	29.80	83.95	11.69	45.78	12.17	2.10	8.16	1.59	5.24	0.41	2.44	0.76	3.86	1.52
Coal	47.93	5.89	11.90	3.00	6.11	2.41	6.35	3.34	0.41	1.89	1.08	1.20	0.00	0.73	0.08	2.17	1.39
Coal	31.20	1.74	6.60	3.06	7.70	1.34	4.15	1.75	0.21	1.26	0.41	0.89	0.00	0.63	0.09	0.84	0.53
Coal	26.57	3.25	5.43	2.65	4.50	1.09	3.70	1.27	0.22	1.87	0.32	0.85	0.00	0.44	0.08	0.53	0.36
Coal	23.36	1.59	3.95	3.08	6.36	0.97	3.22	1.08	0.16	1.01	0.22	0.58	0.00	0.34	0.07	0.43	0.29
Coal	16.19	0.98	2.72	1.77	4.64	0.78	2.41	0.86	0.12	0.62	0.14	0.28	0.00	0.26	0.09	0.29	0.23
Coal	30.01	2.00	3.45	4.18	9.98	1.35	4.60	1.34	0.20	1.02	0.15	0.42	0.02	0.48	0.10	0.44	0.28
Coal	31.92	1.86	4.31	3.90	9.76	1.77	4.83	1.92	0.22	1.20	0.32	0.13	0.00	0.40	0.10	0.58	0.62
Parting	53.39	1.13	2.54	3.38	8.05	7.74	5.70	11.64	0.09	1.74	2.33	0.00	0.00	0.00	0.00	2.86	6.17
Coal	23.95	2.48	4.03	2.87	5.58	1.07	3.56	1.13	0.15	1.11	0.21	0.30	0.00	0.44	0.11	0.51	0.39
Coal	32.85	2.07	5.60	3.87	9.35	1.56	4.71	1.69	0.21	1.27	0.26	0.43	0.00	0.55	0.14	0.61	0.54
Coal	62.21	2.47	9.89	6.22	16.98	3.99	9.44	5.18	0.42	2.60	0.85	0.00	0.00	0.79	0.11	1.43	1.84
Coal	33.70	1.85	7.39	2.52	6.66	2.10	4.34	2.95	0.25	1.51	0.58	0.19	0.00	0.71	0.15	1.30	1.19
Coal	159.74	8.14	19.23	25.37	52.09	6.65	22.61	6.61	1.15	5.42	0.87	3.90	0.30	2.71	0.43	2.95	1.32
Coal	147.36	10.09	20.22	20.34	37.72	7.22	21.28	8.40	1.32	6.19	1.67	3.47	0.00	2.77	0.36	3.77	2.54
Seat Rock	668.94	16.81	20.49	120.75	284.51	33.12	132.60	29.05	3.84	10.84	0.00	5.07	1.32	4.17	0.51	3.84	2.02
Seat Rock	272.99	19.33	14.41	55.56	111.56	10.96	36.37	6.26	1.14	4.68	0.00	3.21	1.38	3.94	0.53	3.03	0.63

Table 5. Percent distribution of the rare earth elements relative to the total REE content of samples taken from each vertical segment associated with the West Kentucky No. 13 coal seam.

Lithology	PERCENT OF TOTAL REE																	Total REE
	Total	Sc	Y	La	Ce	Pr	Nd	Sm	Eu	Gd	Tb	Dy	Ho	Er	Tm	Yb	Lu	(ppm)
Roof Shale	100.00	5.97	8.63	16.91	35.59	3.88	17.46	3.66	0.27	2.86	0.03	2.03	0.10	1.58	0.04	0.93	0.07	256.87
Roof Shale	100.00	5.92	5.99	19.83	39.71	3.95	16.44	2.70	0.20	1.61	0.00	1.27	0.17	1.19	0.14	0.86	0.00	243.17
Coal	100.00	14.63	15.10	11.87	25.37	3.26	14.48	3.82	0.27	2.98	0.58	2.70	0.00	2.22	0.01	2.00	0.70	41.21
Coal	100.00	9.34	26.64	4.90	10.04	6.45	9.20	13.18	0.53	4.77	3.18	0.00	0.00	1.76	0.00	4.59	5.41	15.42
Coal	100.00	10.66	15.01	12.92	27.14	3.80	14.71	4.01	0.67	3.34	0.75	2.53	0.00	1.57	0.30	1.80	0.81	42.36
Parting	100.00	4.48	12.53	15.23	34.28	3.26	16.20	3.35	0.46	3.82	0.10	3.17	0.49	1.69	0.18	0.78	0.00	321.25
Coal	100.00	15.72	11.12	8.81	14.99	7.09	11.49	13.71	0.39	2.95	3.41	0.00	0.00	0.48	0.00	4.00	5.84	35.18
Coal	100.00	14.04	20.14	5.77	11.79	5.46	14.15	10.52	1.05	4.86	2.93	0.25	0.00	1.49	0.00	3.86	3.71	55.70
Parting	100.00	2.63	6.46	15.23	37.37	4.90	18.83	6.12	0.78	3.80	0.53	1.15	0.00	0.57	0.18	0.71	0.74	511.52
Parting	100.00	5.97	11.12	16.36	33.17	3.54	15.57	3.88	0.50	3.72	0.32	2.86	0.27	1.51	0.17	0.96	0.08	325.69
Parting	100.00	6.93	11.57	15.17	33.30	3.72	16.31	3.60	0.33	3.10	0.20	2.79	0.21	1.61	0.07	1.05	0.03	264.02
Parting	100.00	6.68	10.56	13.79	32.47	4.13	16.95	4.03	0.72	3.45	0.49	2.56	0.43	1.62	0.34	1.40	0.37	277.49
Parting	100.00	6.52	9.29	14.57	35.49	4.03	16.16	3.66	0.66	3.03	0.37	2.31	0.45	1.50	0.40	1.31	0.26	281.72
Parting	100.00	5.83	8.33	15.17	38.10	3.99	15.32	3.44	0.65	2.81	0.29	2.40	0.47	1.38	0.43	1.19	0.21	344.70
Parting	100.00	7.54	8.84	15.14	35.59	3.65	14.85	3.29	0.69	2.99	0.42	2.67	0.68	1.62	0.45	1.43	0.14	282.22
Parting	100.00	2.58	2.24	19.26	48.76	4.75	16.30	2.20	0.29	0.98	0.00	0.72	0.36	0.65	0.41	0.45	0.07	828.22
Coal	100.00	9.38	7.83	11.78	33.18	4.62	18.09	4.81	0.83	3.22	0.63	2.07	0.16	0.96	0.30	1.53	0.60	253.00
Coal	100.00	12.28	24.82	6.25	12.74	5.04	13.24	6.97	0.85	3.94	2.26	2.49	0.00	1.53	0.16	4.53	2.90	47.93
Coal	100.00	5.59	21.16	9.79	24.68	4.28	13.30	5.62	0.68	4.03	1.31	2.86	0.00	2.03	0.29	2.68	1.70	31.20
Coal	100.00	12.21	20.43	9.98	16.95	4.12	13.94	4.79	0.81	7.03	1.19	3.21	0.00	1.66	0.30	2.01	1.36	26.57
Coal	100.00	6.81	16.90	13.20	27.22	4.14	13.79	4.62	0.70	4.33	0.94	2.48	0.00	1.45	0.31	1.85	1.25	23.36
Coal	100.00	6.04	16.78	10.91	28.68	4.82	14.91	5.32	0.74	3.86	0.85	1.72	0.00	1.60	0.53	1.81	1.45	16.19
Coal	100.00	6.65	11.50	13.93	33.24	4.49	15.33	4.47	0.68	3.40	0.51	1.38	0.07	1.61	0.34	1.48	0.92	30.01
Coal	100.00	5.82	13.50	12.22	30.57	5.54	15.12	6.02	0.69	3.76	1.00	0.40	0.00	1.26	0.32	1.82	1.94	31.92
Parting	100.00	2.12	4.76	6.34	15.08	14.50	10.68	21.80	0.17	3.26	4.37	0.00	0.00	0.00	0.00	5.36	11.56	53.39
Coal	100.00	10.36	16.84	11.99	23.29	4.46	14.85	4.71	0.65	4.65	0.89	1.26	0.00	1.85	0.46	2.11	1.63	23.95
Coal	100.00	6.29	17.05	11.77	28.46	4.75	14.33	5.14	0.64	3.87	0.78	1.30	0.00	1.69	0.43	1.85	1.66	32.85
Coal	100.00	3.97	15.90	10.00	27.30	6.41	15.17	8.32	0.67	4.18	1.37	0.00	0.00	1.27	0.17	2.29	2.96	62.21
Coal	100.00	5.49	21.94	7.49	19.77	6.23	12.89	8.74	0.73	4.47	1.73	0.56	0.00	2.11	0.46	3.85	3.54	33.70
Coal	100.00	5.10	12.04	15.88	32.61	4.16	14.16	4.14	0.72	3.39	0.54	2.44	0.19	1.70	0.27	1.85	0.82	159.74
Coal	100.00	6.85	13.72	13.80	25.60	4.90	14.44	5.70	0.89	4.20	1.13	2.35	0.00	1.88	0.25	2.56	1.72	147.36
Seat Rock	100.00	2.51	3.06	18.05	42.53	4.95	19.82	4.34	0.57	1.62	0.00	0.76	0.20	0.62	0.08	0.57	0.30	668.94
Seat Rock	100.00	7.08	5.28	20.35	40.87	4.02	13.32	2.29	0.42	1.72	0.00	1.18	0.50	1.44	0.19	1.11	0.23	272.99

Table 6. Mineralogy analysis results from X-ray Diffraction performed on samples obtained from each vertical segment associated with the West Kentucky No. 13 coal seam.

Lithology	SiO2 (%)	Al2O3 (%)	Fe2O3 (%)	CaO (%)	MgO (%)	MnO (%)	Na2O (%)	K2O (%)	P2O5 (%)	TiO2 (%)	BaO (%)	SrO (%)	SO3 (%)	Total (%)
Roof Shale	58.18	21.57	6.57	0.56	1.60	0.09	0.58	3.71	0.14	1.00			3.01	97.00
Roof Shale	43.80	22.21	4.89	0.36	1.32	0.02	0.53	3.60	0.08	0.97			6.77	84.55
Coal	54.51	23.58	15.61	0.60	1.42	0.02	0.61	3.40	0.07	1.06	0.21	0.03	0.39	101.52
Coal	9.73	8.27	75.42	1.53	0.19	0.02	0.15	0.39	0.07	0.31	0.04	0.03	0.73	96.88
Coal	35.13	20.58	36.35	2.91	0.54	0.02	0.40	1.15	0.75	1.50	0.06	0.17	1.04	100.60
Parting	53.33	24.79	2.78	0.53	1.01	0.01	0.65	2.69	0.58	1.37			3.37	91.11
Coal	16.51	9.75	69.50	0.45	0.32	0.04	0.05	0.85	0.05	0.54	0.07	0.02	0.30	98.45
Coal	23.90	10.98	62.10	0.54	0.52	0.04	0.19	1.45	0.15	0.60	0.02	0.02	0.23	100.75
Parting	35.31	16.68	15.32	0.56	0.80	0.01	0.40	2.01	0.51	0.70			7.23	79.52
Parting	54.71	25.11	5.20	0.41	1.08	0.06	0.63	3.20	0.11	1.07			4.45	96.02
Parting	57.32	24.76	5.51	0.33	1.13	0.07	0.55	3.52	0.04	1.00			2.91	97.14
Parting	57.18	23.67	6.03	0.29	1.25	0.05	0.50	3.65	0.04	1.01			3.67	97.33
Parting	58.63	23.57	5.12	0.27	1.27	0.04	0.50	3.67	0.04	0.98			2.34	96.42
Parting	58.20	24.41	4.53	0.25	1.24	0.03	0.57	3.72	0.04	0.97			2.36	96.33
Parting	54.70	28.31	3.55	0.28	0.91	0.02	0.72	2.58	0.04	1.08			1.58	93.77
Parting	54.98	28.97	2.37	0.27	0.58	0.00	0.68	1.85	0.10	1.62			1.41	92.83
Coal	53.00	23.84	18.10	0.72	0.72	0.01	0.26	2.47	0.05	1.08	0.04	0.02	0.63	100.94
Coal	27.43	12.63	53.01	0.86	0.43	0.04	0.14	1.19	0.05	0.67	0.02	0.02	0.52	97.01
Coal	38.60	19.00	36.24	0.93	0.57	0.02	0.14	1.58	0.07	0.94	0.21	0.03	0.56	98.88
Coal	31.39	16.67	23.23	14.17	0.79	0.08	0.14	1.33	0.10	0.69	1.39	0.05	7.91	97.95
Coal	36.19	21.49	27.53	5.03	0.64	0.03	0.42	1.41	0.12	0.83	0.03	0.05	5.04	98.81
Coal	45.39	19.11	28.33	1.86	0.62	0.02	0.36	1.59	0.21	0.85	0.03	0.05	1.21	99.62
Coal	54.41	22.09	16.83	1.15	1.05	0.02	0.32	2.70	0.39	1.03	0.04	0.03	0.63	100.68
Coal	40.60	16.32	35.19	1.70	0.79	0.02	0.23	2.07	0.56	0.78	0.03	0.03	0.94	99.27
Parting	8.74	3.26	87.59	0.41	0.18	0.02	0.00	0.48	0.11	0.27	0.00	0.01	0.28	101.34
Coal	45.45	17.07	23.17	5.30	0.93	0.04	0.34	2.11	0.29	0.79	0.03	0.03	4.20	99.75
Coal	47.91	17.20	26.14	2.19	0.99	0.02	0.34	2.39	0.61	0.82	0.21	0.03	1.03	99.87
Coal	32.92	11.66	46.92	1.80	0.64	0.02	0.17	1.64	0.69	0.66	0.03	0.02	0.91	98.08
Coal	21.90	9.04	65.39	1.98	0.36	0.02	0.10	0.87	0.53	0.45	0.18	0.03	1.09	101.94
Coal	51.13	22.09	19.38	1.40	1.04	0.01	0.49	3.14	0.41	0.90	0.04	0.05	0.85	100.93
Coal	43.01	19.51	28.70	1.38	0.99	0.03	0.38	3.23	0.27	0.71	0.04	0.04	0.99	99.29
Seat Rock	55.26	21.81	6.91	0.32	1.10	0.03	0.92	3.62	0.37	0.81			10.55	101.70
Seat Rock	61.83	22.47	3.53	0.27	1.27	0.01	0.89	4.24	0.05	0.94			2.93	98.43

Table 7. Trace element contents of samples obtained from each vertical segment associated with the West Kentucky No. 13 coal seam.

Lithology	Ba (PPM)	Ce (PPM)	Co (PPM)	Cr (PPM)	Cu (PPM)	Ga (PPM)	La (PPM)	Mo (PPM)	Nb (PPM)	Ni (PPM)	Pb (PPM)	Rb (PPM)	Sr (PPM)	Th (PPM)	U (PPM)	V (PPM)	Y (PPM)	Zn (PPM)	Zr (PPM)
Roof Shale	544		17	84	19		37	0	17	39	17	187	219	9	15	134	36	103	192
Roof Shale	447		14	110	44		26	7	14	89	29	234	274	12	35	153	35	139	183
Coal	1515	50	38	103	75	28	60		16	11	386	134	174	12	4	200	55	619	170
Coal	352	15	91	69	99	41	90		4	0	1979	4	115	9	5	192	39	324	89
Coal	588	159	68	556	181	56	104		31	42	395	35	968	15	7	739	83	774	269
Parting	601		8	89	37		20	3	3	80	26	180	974	12	37	136	28	34	363
Coal	622	0	94	202	102	32	81		9	0	359	13	57	13	0	357	18	60	104
Coal	232	0	78	139	65	28	80		6	0	322	25	47	13	0	593	43	186	130
Parting	415		33	103	85		88	0	0	73	28	129	284	0	0	126	28	130	106
Parting	510		14	112	57		31	0	20	82	27	233	195	10	20	170	31	64	174
Parting	522		15	102	33		36	0	20	60	24	207	140	10	15	158	33	63	153
Parting	545		17	100	24		36	0	21	58	23	193	115	8	11	155	35	94	167
Parting	545		15	95	25		32	0	21	56	21	201	119	10	15	147	34	108	172
Parting	539		14	101	40		31	0	21	69	25	221	140	11	20	154	33	113	160
Parting	451		11	126	54		26	0	23	106	30	176	150	12	9	178	37	71	181
Parting	429		8	124	27		18	8	18	120	34	124	557	11	12	133	43	30	325
Coal	372	121	50	148	75	17	71		16	90	164	127	100	13	11	322	49	82	197
Coal	215	17	79	104	48	33	83		12	10	115	27	57	12	10	456	73	68	146
Coal	1448	57	52	88	59	23	79		13	8	138	55	151	13	3	162	69	75	130
Coal	8960	46	39	78	65	14	46		11	35	82	48	275	11	6	132	58	86	127
Coal	265	97	45	101	79	17	75		12	27	115	55	296	13	3	155	58	104	140
Coal	258	81	48	106	71	20	72		14	25	109	73	325	9	0	155	57	140	140
Coal	361	76	27	104	59	16	61		15	37	77	149	218	11	2	161	49	102	106
Coal	280	71	49	83	31	18	72		12	0	149	67	150	11	0	129	44	83	76
Parting	86	0	80	25	0	21	79		6	0	164	6	6	9	0	5	6	20	9
Coal	296	47	34	86	47	16	54		14	24	118	92	211	8	3	129	44	101	91
Coal	1825	62	40	80	49	18	61		12	17	131	91	202	11	0	126	55	89	87
Coal	269	55	65	66	24	19	78		8	0	129	34	91	11	3	84	43	43	55
Coal	1393	24	77	68	33	27	76		8	0	215	15	114	9	0	131	47	47	43
Coal	426	116	30	98	108	17	74		13	42	133	140	345	11	9	195	58	62	102
Coal	341	64	46	96	95	19	70		12	24	257	107	209	10	11	224	51	131	91
Seat Rock	498		18	98	42		54	19	0	112	35	205	1230	5	35	96	32	35	299
Seat Rock	445		10	92	27		29	14	16	45	23	314	232	14	42	146	34	44	172